PH

Volu

Information for Contributors

Manuscripts

Send manuscripts to ... Brookhaven National Laboratory, Upton, Long Island, New York.

Each article submitted ... of (a) textual material ... to be set in type, and ... graphs from which ... tones will be made. ... of an abstract, the ... material, references, ... this material must be ... (except mathematical ... with wide margins (for ... the printer) on ... letter size. The original ... should be submitted.

For general style, ... form, recent issues ... consulted.

The prime requisite ... clear to the typesetter ... nor a mathematician.

Abstracts

An abstract must ... should be adequate ... mary. As an index, ... major and minor, ... tion is presented. ... the conclusions of the ... results of general ...

Mathematical Expressions

All but the simplest ... should be carefully ... to distinguish between ... Indicate clearly ... inverted carets and ... complicated superscripts ... repetition of a complicated ... representing it by some ... the margin Greek letters ... Use fractional exponents ... Use the solidus (/) ... will save vertical space.

References

References should be ... bered consecutively ... thus:

[1] A. B. Smith, ... (1962).
[2] C. Lamb, *Hydrodynamics* ... Teddington, England, ... pp. 673, 675.

Tables

All but the simplest ... material should be organized ... rather than as a part of the running text. Tables ... written on sheets separate from the ... with indications in the margin of the ... where the table is to be inserted. Each table ... have a caption which will make the data ... table intelligible without reference to the ... Avoid complicated column headings; if ... sary, use symbols which are explained in ... table caption.

Figures

Wherever possible figures should be ... for the width of a column of the *Physical ...* (3 inches). A convenient reduction ratio is ... 2:1 or 3:1. The original drawings or photo... should therefore be in general about 4 to 9 ... wide and the lettering and symbols should ... large enough on the original that when ... they shall not be less than about $\frac{1}{16}$ in. (... mm). If the reduction is 3:1, the original let... ing should be not less than $\frac{1}{12}$ in. high.

The process of making zinc etchings or co... halftones is a black and white photographic ... Therefore line drawings must be in ... white paper or tracing cloth. Coordinate pa... not desirable but if used must be blue lined ... the coordinate lines which are to show ... inked over.

Photographs should have maximum black ... white contrast.

Plan figures to use space efficiently. Avoid ... wasting space, particularly at the top or bot...

Identify on the black or other suitable ... each original drawing or photograph with ... author's name and the figure number. Figures ... should be numbered consecutively and the ... proximate position indicated in the margin of the ... running text. Figure captions should be ... and included with the manuscript (not on ... of the figure).

Avoid round and oval photographs.

Alterations

Take great care that each manuscript is ... graphically accurate. A limited number of ... tions in proof are unavoidable, but the ... making extensive alterations after the art... been set in type will be charged to the au...

Proof and all correspondence concerning ... in the process of publication should be ad... to the Publication Manager, American ... of Physics, 57 East 55 Street, New York ... York.

THE PHYSICAL REVIEW

A journal of experimental and theoretical physics established by E. L. Nichols in 1893

VOLUME 83

Second Series

JULY 1–SEPTEMBER 15, 1951

Published for the

AMERICAN PHYSICAL SOCIETY

by the

AMERICAN INSTITUTE OF PHYSICS

Incorporated

THE PHYSICAL REVIEW

A journal of experimental and theoretical physics established by E. L. Nichols in 1893

Published by the American Institute of Physics for the

AMERICAN PHYSICAL SOCIETY

Officers

President

C. C. LAURITSEN
California Institute of Technology
Pasadena, California

Vice-President

J. H. VAN VLECK
Harvard University
Cambridge, Massachusetts

Secretary

K. K. DARROW
Bell Telephone Laboratories
Office:
Columbia University
New York 27, New York

Treasurer

G. B. PEGRAM
Columbia University
New York 27, New York

Local Secretary for the Pacific Coast

J. KAPLAN
University of California at Los Angeles
Los Angeles, California

Managing Editor

S. A. GOUDSMIT
Brookhaven National Laboratory
Upton, Long Island
New York

BOARD OF EDITORS

Editor

S. A. GOUDSMIT

Assistant Editor

S. PASTERNACK

Associate Editors

J. BARDEEN, T. BONNER, R. G. HERB, W. E. LAMB, JR., A. J. F. SIEGERT, W. E. STEPHENS, HARVEY BROOKS, R. F. CHRISTY, C. L. CRITCHFIELD, M. DEUTSCH, T. H. JOHNSON, BRUNO ROSSI, M. GOLDHABER, R. HOFSTADTER, A. W. LAWSON, A. PAIS, R. SERBER, C. H. TOWNES

Manuscripts for publication should be submitted to S. A. GOUDSMIT, Brookhaven National Laboratory, Upton, Long Island, New York. The authors' institutions are requested to pay a publication charge of $8 per page which, if honored, entitles them to 100 free reprints. Instructions will be sent with galley proofs.

Proof and all correspondence concerning papers in the process of publication should be addressed to the Publication Manager, American Institute of Physics, 57 East 55 Street, New York 22, New York.

Subscription Price

United States and Canada $25.00
Elsewhere $27.00

Back Numbers [1]

Yearly back number rate when complete year is available:
Prior to 1949: $20.00
Thereafter: $27.00
Single copies: $2.00 each, prior to July, 1929;
$1.00 each, July, 1929–December, 1941;
$2.00 each, January, 1942–December, 1946;
$1.00 each, January, 1947–December, 1948;
$1.25 each, thereafter.
General index, 1893–1920: $4.00.

Subscriptions, renewals, and orders for back numbers should be addressed to the American Institute of Physics, 57 East 55 Street, New York 22, New York.

Changes of address in the case of members of the American Physical Society should be addressed to the Treasurer; in the case of other subscribers to the American Institute of Physics.

[1] For Series 1 inquire of Physics Department, Cornell University, Ithaca, New York.

The Physical Review is published semi-monthly at Prince and Lemon Streets, Lancaster, Pennsylvania.

Entered as second-class matter March 6, 1947, at the Post Office at Lancaster, Pennsylvania, under the Act of March 3, 1879.

Acceptance for mailing at special rate of postage provided for in paragraph (d-2), section 34.40, P. L. & R. of 1948, authorized January 27, 1933.

THE
PHYSICAL REVIEW

A journal of experimental and theoretical physics established by E. L. Nichols in 1893

SECOND SERIES, VOL. 83, NO. 1 JULY 1, 1951

The Analysis of π-Meson Production in Nucleon-Nucleon Collisions*†

KENNETH M. WATSON AND KEITH A. BRUECKNER
Radiation Laboratory, Physics Department, University of California, Berkeley, California
(Received February 27, 1951)

A phenomenological analysis of meson production in nucleon-nucleon collisions is proposed. On the basis of an hypothesis that the production takes place for collisions whose impact parameters tend to be less than the range of nuclear forces, a partial wave analysis of the scattering matrix is given. The theory seems capable of describing the experimental results in a simple manner. It is shown, on the assumption that the π-meson is pseudoscalar, that angular momentum and parity considerations play an important role in interpreting the experimental results. If processes involving mesons are related to nuclear forces, then the hypothesis of charge symmetry in nuclear phenomena should receive a crucial test in experiments concerning meson production.

I. INTRODUCTION

THE data which has at present been obtained on the production of π-mesons in the collisions of two nucleons is very incomplete, yet it is sufficient to establish a number of interesting features of these processes. Indeed, there seems to be enough quantitative information to warrant the development of a systematic and unified interpretation of the phenomena of meson production in nucleon collisions, and it is the purpose of the present paper to sketch the outline of such a means of interpretation on the basis of a phenomenological theory. Although this type of analysis is less satisfying than one based on a fundamental theory of elementary particles, the lack of any satisfactory form of a basic theory makes it necessary to fall back on a phenomenological approach in the hope of obtaining a unified picture of the processes under consideration. The theory developed here should also be of assistance in the study of meson production in complex nuclei (which is not considered in the present paper) and in the comparison with the inverse processes of meson absorption.

Some of the qualitative experimental information on meson production which has been obtained at this laboratory is given in Table I. From these results, with the corresponding cross sections, it is possible to deduce approximately the nucleon-nucleon cross sections for meson production; see Table II.

We shall present in Sec. II a formalism for giving a partial wave analysis of the experiments on meson production in terms of a partial wave analysis of the scattering matrix. Such a study establishes naturally relationships between the energy spectrum of the mesons, their angular distribution, and the excitation function for the cross section. It is particularly useful, as shown by Brueckner, Serber, and Watson,[1] in the study of the inverse processes of meson absorption. In this section the requirements of conservation of parity and angular momentum and of charge symmetry are also considered and are shown to be very effective in introducing simplifications into the analysis.

It has been pointed out by Brueckner, Chew, and

TABLE I. Qualitative experimental results for processes involving production of charged and neutral mesons by nucleons bombarding free nucleons or complex nuclei.

A. Free nucleons	B. Complex nuclei
(1) $P+P\rightarrow\pi^+$ (allowed)[a]	(1) $P+(P,N)\rightarrow\pi^+$ (allowed)[a]
(2) $P+N\rightarrow\pi^+$ (unobserved)	(2) $P+(P,N)\rightarrow\pi^-$ (allowed)[a]
(3) $N+N\rightarrow\pi^-$ (unobserved)	(3) $P+(P,N)\rightarrow\pi^0$ (allowed)[b]
(4) $N+P\rightarrow\pi^-$ (unobserved)	(4) $N+(P,N)\rightarrow\pi^+$ (allowed)[d]
(5) $N+N\rightarrow\pi^0$ (unobserved)	(5) $N+(P,N)\rightarrow\pi^-$ (allowed)[d]
(6) $N+P\rightarrow\pi^0$ (unobserved)	(6) $N+(P,N)\rightarrow\pi^0$ (unobserved)
(7) $P+P\rightarrow\pi^0$ (forbidden)[b]	

[a] Cartwright, Richman, Whitehead, and Wilcox, Phys. Rev. **78**, 823 (1950).
[b] Bjorkland, Crandall, Moyer, and York, Phys. Rev. **77**, 213 (1950).
[c] C. Richman and H. A. Wilcox, Phys. Rev. **78**, 496 (1950).
[d] Bradner, O'Connell, and Rankin, private communication.

* This work was performed under the auspices of the AEC.
† This work was reported at the February 9, 1951, meeting of the American Physical Society. Phys. Rev. **82**, 336 (1951).

[1] Brueckner, Serber and Watson, Phys. Rev. **81**, 575 (1951).

TABLE II. Nucleon-nucleon cross sections for production of charged and neutral mesons. The experimental results given in Table I, from which the cross sections are deduced, are indicated in column II.

I. Process		II. Experiment	III. Total cross sections ($\times 10^{28}$ cm^2) Complex nuclei	Free
(1) $P+P\to\pi^+$	allowed	$A(1)$, $B(1)$	3.3 ± 1.0	3.0 ± 1.0[a]
(3) $P+P\to\pi^0$	forbidden	$A(7)$	?	0.1 ± 0.1
(3) $N+P\to\pi^+$	allowed	$B(4)$, $B(1)$	0.8 ± 0.4	?
(4) $N+P\to\pi^-$	allowed	$B(2)$	0.8 ± 0.4	?
(5) $N+P\to\pi^0$	allowed	$A(7)$, $B(3)$	1.7 ± 0.9	?
(6) $N+N\to\pi^-$	possible	$B(5)$	?	?
(7) $N+N\to\pi^0$	unobserved		?	?

[a] Deduced from the cross section in the forward direction with the angular distribution found in Sec. IV.

Hart[2] that the production of mesons in nucleon-nucleon collisions is strongly dependent on the interactions of the nucleons in the final state. In the course of applying the theory of the present paper, the calculations of these authors have been extended. These considerations are discussed in Sec. III.

Cross sections deduced from the preceding development are given in Sec. III, and in Sec. IV these are compared with and fitted to the experimental results on the production of π^+ mesons in proton-proton collisions. A summary of the results obtained in the present paper is presented in the final section.

II. FORMAL CONSIDERATIONS

A. Introduction of General Transition Matrix

Above the threshold for meson production, the study of nuclear collisions is complicated by the interdependence of the elastic and the inelastic (meson production) scattering. This fact leads to characteristic difficulties in the use of the Schrödinger equation to describe high enery nuclear scattering events. To escape these difficulties, we propose the application of the scattering matrix in the analysis of meson production. In so doing we lose some insight into the mechanism of these phenomena, but are left on a sounder theoretical footing for the description of the rather complex experimental results.

The considerations are most easily carried out in the center-of-mass coordinate system. We may then partially characterize the collision by the relative momentum $\mathbf{p}$ of the incoming nucleons, which collide to produce a meson with momentum $\mathbf{q}$, and the final relative momentum $\mathbf{p}'$ of the nucleons after the meson is produced. In particular, we introduce a transition matrix

$$R=(\mathbf{q},\mathbf{p}'|R|\mathbf{p}) \tag{1}$$

(which also depends upon spin and isotopic spin variables of the particles in question) describing the transition from the initial to the final state accompanied by the production (or absorption) of a meson.

We suppose the two incoming nucleons in the initial state to have a wave function ψ_I, the two final nucleons to be in a state ψ_F, and the produced meson to be in a state ϕ_q. The probability amplitude for the transition is described by

$$(F|R|I)=(\psi_F\phi_q, R\psi_I). \tag{2}$$

We can expect that to a fairly good approximation ψ_I can be represented by a plane wave, but this approximation is not necessary in our analysis, since we can define a new R' as $R'=R\psi_I$. Using R' in Eq. (2), we must consider the new ψ_I to be a plane wave. We assume that ϕ_q represents a plane wave for the outgoing meson. However, considerable physical insight is gained by calculating ψ_F explicitly, so we do this in the next section.

The cross section is then given as (we use as units $\hbar=c=1$)

$$d\sigma=(2\pi)^4(dJ/v_R)\sum(F|R|I)^2, \tag{3}$$

where v_R is the relative velocity of the incoming nucleons, dJ is the volume in phase space accessible to the particles in the final state, and $\sum$ means a sum and average over the final and initial spin states, respectively.

B. Partial Wave Analysis

A few physical considerations can be employed to introduce considerable simplifications of the general expression (2). For energies available from present accelerators, the greater part of the center-of-mass energy of the incident nucleons goes into the rest mass of the meson, leaving relatively little for the kinetic energies of the three final particles (a total of about 20 Mev for the Berkeley cyclotron). This loss of kinetic energy is necessarily accompanied by large momentum transfers, which in turn suggests that the collision producing a meson takes place at close distances of approach for the two nucleons. This can be interpreted as representing a short range of interaction for producing mesons—roughly of order $\hbar/P$ (where P is the momentum transfer), which is considerably less than the range of nuclear forces. In view of this evidence of a short range of interaction and the relatively small kinetic energies of the final particles, it seems natural to attempt a partial wave analysis of the final state. Indeed, we may very well expect the process to lead predominantly to one angular momentum state for the relative motion of the two nucleons (s-state) and to another for the angular momentum of the meson relative to the two nucleons. We must, however, expect small admixtures of other angular momentum states.

The pronounced peak of high energy mesons which is observed experimentally is rather conclusive evidence that the final nucleon state is predominantly an s-state (zero relative angular momentum), since this peak corresponds to small relative energies for the two nucleons

[2] K. A. Brueckner, Phys. Rev. **82**, 598 (1951). (In particular, see Appendix.)

(this point is developed in greater detail in Secs. III and IV). On the other hand, calculations of the meson energy spectrum, as described in the next section, indicate that most of the mesons have an angular momentum of $l=0$ or 1.

We now make more explicit use of our hypothesis of a short range interaction. Since the de Broglie wavelengths of the particles in the final state are appreciably greater that $\hbar/P$, our deduced range of interaction, we can with little error introduce a zero range approximation. In particular, this means that for S-states we can replace $\psi(\mathbf{r})$ by $\psi(0)$, and for P-states, which vanish at the origin, we can replace $\psi(\mathbf{r})$ by grad$\psi(0)$. If in addition we assume that for P-states we can use a plane wave approximation, the gradient operator can be replaced by $i\mathbf{P}$, where $\mathbf{P}$ is the momentum of the particle. This means, for instance, that for final nucleon S-states the dependence of Eq. (2) on $\psi_F(r)$ will be given by the multiplicative factor $(2\pi)^{\frac{1}{2}}\psi_F(0)$.

Then, in the approximation that we need consider only final nucleon S-states, the quantity $\sum|(F|R|I)|^2$ in Eq. (3) can be decomposed into the product of two factors, one of which is just

$$(2\pi)^3|\psi_F(0)|^2. \tag{4}$$

The other depends upon the meson angular momentum state. For meson S- and P-states (taken as plane waves),[3] we have for this factor

$$s: \quad \Gamma^2(p)g_{FI}, \tag{5}$$

$$p(\text{sym}): \quad \Gamma^2(p)g_{FI}q^2, \tag{6}$$

$$p(\cos^2\theta): \quad \Gamma^2(p)g_{FI}q^2\cos^2\theta, \tag{7}$$

where θ is the angle between the vectors $\mathbf{q}$ and $\mathbf{p}$. The symbol "s" means a meson S-state; p(sym) means a meson P-state with a symmetrical angular distribution; $p(\cos^2\theta)$ means a meson P-state with a $\cos^2\theta$ angular distribution. The quantities $\Gamma^2(p)$ are numerical functions of the initial momentum, p, of the nucleons and are constant for a given beam energy. The g_{FI} are numerical quantities depending upon initial and final spin and isotopic spin states.

To include the possibility of some nucleon P-state admixture, we have two more permissible terms (since for nucleon P-states, the plane wave approximation for final states is satisfactory, we replace the factor $(2\pi)^3\psi_F^2(0)$ used above by p'^2 in this case),

$$(p, s): \quad \Gamma^2(p)g_{FI}p'^2, \tag{8}$$

$$(p, p): \quad \Gamma^2(p)g_{FI}p'^2q^2, \tag{9}$$

[3] There is evidence of a nonvanishing nucleon-meson elastic scattering cross section, which implies that the wave function for the outcoming mesons is not rigorously that for a plane wave. This effect would be expected to modify only the low energy end of the spectrum of produced mesons. No evidence for this has been observed experimentally; however, this may well be due to the difficulty of detecting low energy mesons. A further discussion of this point is given by Brueckner, Serber, and Watson (reference 1).

TABLE III. Transitions allowed by Pauli principle, conservation of angular momentum, and conservation of parity for production of pseudoscalar mesons in nucleon-nucleon collisions. The final nucleons are assumed to be in S-states. The columns (a) indicate the corresponding matrices required by charge symmetry as calculated in Sec. II D.

	Meson in S-state	(a)	Meson in P-state	(a)
PP, π^+ NN, π^-	$^3P_0\rightarrow{}^1S_0$	M_1	$^1S_0\rightarrow{}^3S_1$ $^1D_2$	M_3
	$^3P_1\rightarrow{}^3S_1$	M_3		
PP, π^0 NN, π^0	$^3P_0\rightarrow{}^1S_0$	M_1	forbidden	M_1
NP, π^+ NP, π^-	$^3P_0\rightarrow{}^1S_0$	M_1	$^3S_1\rightarrow{}^1S_0$ $^3D_1$	M_3
NP, π^0	$^3P_0\rightarrow{}^1S_0$	0	$^3S_1\rightarrow{}^3S_1$ $^3D_{1,2}$	0
	$^3P_1\rightarrow{}^3S_1$	M_3	$^3S_1\rightarrow{}^1S_0$ $^3D_1$	M_3
	$^1P_1\rightarrow{}^3S_1$	0	$^1S_0\rightarrow{}^3S_1$ $^1D_2$	M_3

referring, respectively, to meson S- and p-states for a final nucleon p-state. We might also include a $\cos^2\theta$ factor in the last term. There will be no terms linear in p', as we are interested only in cross sections for which an integration has been performed over the angular distribution of the final nucleons. We also need consider no terms linear in $\cos\theta$, if we restrict ourselves to the consideration of proton-proton collisions.

The choice of any one of these factors [expressions (5) to (9)] permits us to calculate the cross section for meson production uniquely, except for a numerical factor to be used in fitting the results to the experimental magnitude of the cross section. In general we must expect to use a suitably chosen linear combination of these terms in obtaining the experimental cross section.

A more formal development of the ideas developed in this section is given in the Appendix.

C. Parity and Angular Momentum Requirements

We can introduce considerable simplification by restricting ourselves to the consideration of pseudoscalar mesons. At the time of writing this seems to be the most reasonable choice since it is known that the π^0 meson cannot have spin one[4] and since the experiments on the absorption of π^- mesons in deuterium indicate that the charged π-meson is not scalar.[1,5,6] If further experimental results should lead to contrary evidence, an analysis such as that given here can be made for any given spin and parity of the meson.

Then, on the assumption that the π-meson is pseudoscalar, we can enumerate all possible transitions to produce π-mesons which are consistent with the Pauli

[4] Steinberger, Panofsky, and Steller, Phys. Rev. 78, 802 (1950).
[5] Panofsky, Aamodt, and Hadley, Phys. Rev. 81, 565 (1951).
[6] S. Tamor, Phys. Rev. 82, 38 (1951).

principle, parity and angular momentum conservation, and the assumption that the final nucleons are emitted primarily into s-states—i.e., our deductions will not be valid for the (small) part of the cross section corresponding to nucleons in higher angular momentum final states. The permissible transitions are given in Table III. Of course, under actual experimental conditions, the initial state will be a statistically weighted combination of those listed in the table.

It is clear that if the hypothesis that the meson is pseudoscalar is to be maintained, the experimental results must be consistent with Table III. For example, if the (pp, π^+) process leads to mesons in p-states, the final neutron and proton must be in a triplet state only. Again, if the production of mesons into p-states represents a universal type of coupling for all production processes in nucleon-nucleon collisions, reference to Table III indicates the existence of a general selection rule prohibiting the (pp, π^0) process.

D. Further Symmetry Requirements

If we are to assume that the meson is a pseudoscalar, then the transition matrix R must be invariant under spatial rotations but change sign under a coordinate reflection. The consequences of the hypothesis of charge independence of nuclear forces are also of interest, since we here have the possibility of greater uniqueness to test this hypothesis than is afforded by elastic nuclear scattering.

Because of the considerable interest in this latter hypothesis we shall develop in detail its consequences for meson production. In particular, charge independence of nuclear forces implies invariance with respect to rotations in charge space.‡ We may thus impose this condition of invariance on the transition matrix, R. Presumably meson production is not independent of nuclear forces.

The rotation operator in charge space consists of two parts, one of which is

$$\mathbf{T}=\tfrac{1}{2}(\boldsymbol{\tau}^{(1)}+\boldsymbol{\tau}^{(2)}), \tag{10}$$

where $\boldsymbol{\tau}^{(1)}$ and $\boldsymbol{\tau}^{(2)}$ are the isotopic spin matrices of the two nucleons. This is, of course, the analog of the usual spin angular momentum. We define an orbital angular momentum as the rotation operator, $\mathbf{L}$, for the meson wave functions in charge space. This can be easily done by constructing three-dimensional vector operators $\mathbf{U}$ and $\mathbf{U}^+$ which destroy and create mesons; i.e.,

$$[U_i, U_j^+]=\delta_{ij}, \quad (i, j=1, 2, 3), \tag{11}$$

all other combinations commuting. An invariant is $\boldsymbol{\tau}\cdot\mathbf{U}$. Then

$$\mathbf{L}=i\mathbf{U}\times\mathbf{U}^+. \tag{12}$$

The infinitesimal rotations about an axis $\hat{a}$ are generated by $\hat{a}\cdot\mathbf{J}$, where

$$\mathbf{J}=\mathbf{T}+\mathbf{L}. \tag{13}$$

Invariance of R about the axis $\hat{a}$ implies $[\hat{a}\cdot\mathbf{J}, R]=0$, or, since we assume complete symmetry,

$$[\mathbf{J}, R]=0. \tag{14}$$

The eigenvalues of $Q\equiv 1-J_3$ give the total charge of the system in units of the proton charge.

To develop the consequences of Eq. (14), we choose the following representation. For $\boldsymbol{\tau}$, we decompose the isotopic spin states into a singlet state, s, and three triplet states t^+, t^0, t^-, as usual (t^+ corresponds to a state consisting of two neutrons, etc.). For the representation of $\mathbf{L}$, we note that

$$\mathbf{L}\omega(0)=0, \tag{15}$$

where $\omega(0)$ is a state containing no mesons, or a state of zero "orbital angular momentum." The states $\omega(1^+)$, $\omega(1^0)$, $\omega(1^-)$—that is, states containing one positive, one neutral, and one negative meson, respectively—correspond to an orbital angular momentum of unity ($l=1$). Since

$$\begin{aligned} L_3\omega(1^+)&=-\omega(1^+),\\ L_3\omega(1^0)&=0,\\ L_3\omega(1^-)&=\omega(1^-), \end{aligned} \tag{16}$$

we conclude that these states transform as the three spherical harmonics of order one. We may thus use the usual angular momentum matrix elements for $\mathbf{L}$ in the ω-representation.

It then follows that the eigenstates of $J^2=j(j+1)$ for the final state containing two nucleons and a meson correspond to one set for $j=2$, two sets for $j=1$, and one set for $j=0$. Since the initial state containing two nucleons only corresponds to $j=1$ and $j=0$, we conclude that all transitions to final states with $j=2$ are forbidden. This then leaves us with only *three independent* matrices, R, corresponding to the two representations with $j=1$ and the one with $j=0$.

The explicit relationships can easily be obtained from Eq. (14) by evaluating the matrix of the commutator between a state with no meson and one with one meson of a given charge. The matrix elements of R are written as $(1^-t^0|R|t^+)$, etc., as designating a transition from a nucleon t^+ state to a nucleon t^0 state to produce a negative meson. Similarly $(1^-s|R|t^+)$ designates the same transition, except that the final nucleons are in a singlet isotopic spin state. R also depends on the nucleon spin and momentum coordinates, but this dependence is not explicitly written for the present.

Rotations about the "3" axis give us just charge conservation from Eq. (14). Those about the "1" and

‡ We are indebted to Professor D. L. Falkoff for calling our attention to a paper by W. Heitler, Proc. Roy. Irish Acad. **51A**, 33 (1946), in which similar considerations are applied to the scattering of mesons by nucleons.

"2" axes give us the following relations:

$$\begin{aligned} M_1 &= (1^+t^+|R|t^0) = (1^+t^0|R|t^-) \\ &= (1^0t^+|R|t^+) = -(1^0t^-|R|t^-) \\ &= -(1^-t^0|R|t^+) = -(1^-t^-|R|t^0), \\ M_2 &= (1^+t^+|R|s) = (1^-t^-|R|s) = -(1^0t^0|R|s), \\ M_3 &= (1^0s|R|t^0) = (1^+s|R|t^-) = (1^-s|R|t^+), \\ & (1^0t^0|R|t^0) = (1^0s|R|s) = 0. \end{aligned} \quad (17)$$

All other matrices vanish by the requirement of charge conservation. We thus find three sets of matrices, as asserted above.

We can now combine the results of the requirements of the charge symmetry hypothesis with the requirements of conservation of angular momentum and parity. The matrices M_1, M_2, and M_3 corresponding to the allowed transitions given in Table III are listed in columns (a) of that table. We see that if the meson is emitted into an s-state, then the smallness of the (PP, π^0) process (Tables I and II) also requires the smallness of the (NP, π^+) and (NP, π^-) processes in contradiction with experiment. This would also require that the (PP, π^+) cross section be twice the (NP, π^0) cross section (because of the difference of the normalization of the wave functions).

If the meson is emitted into a P-state, then the only restriction is that $\sigma(NP, \pi^0)$ be equal to $\sigma(NP, \pi^+)$ plus $\frac{1}{2}\sigma(PP, \pi^+)$, which is consistent with the present rather inaccurate experimental data. It is interesting to observe that this assumption for the final meson angular momentum state automatically gives a selection rule inhibiting the (PP, π^0) process.

We conclude that to give agreement with the approximate magnitudes of the experimental cross sections it must be assumed that the meson, if pseudoscalar, is emitted predominantly into p-states, while the final nucleons are in s-states. We shall make a more detailed analysis of these conclusions in the following sections.

III. CALCULATED CROSS SECTIONS

If the energy of the final nucleons were sufficiently high, we could take $(2\pi)^3|\psi_F(0)|^2$ as unity. In actual fact, for the energies presently available this quantity is effectively much larger than unity and must be calculated on the basis of some assumed force for the two nucleon system. In particular, we need only the partial wave of zero angular momentum. Also, if the final state is a neutron-proton system with some triplet spin state present, there is a large probability that a deuteron will be formed.

When the nucleons in the final state are not bound, the wave function is a function of their relative momentum p', which is related to the meson kinetic energy, T.

Unfortunately, $\psi_F(0)$ depends more strongly upon the assumed shape of the two nucleon potential than does the low energy scattering data. Calculations have thus been made for both square well and exponential potentials (tensor forces have not been included) whose parameters were chosen to fit the low energy scattering. The n-p (neutron-proton) triplet scattering length and effective range were taken from Christian and Hart.[7] In accordance with an assumed charge symmetry (at low energies) of nuclear forces, the n-n (neutron-neutron), p-p (proton-proton), and n-p singlet potentials were assumed to be the same and were taken from Jackson's and Blatt's work.[8] The effect of the coulomb interaction in the p-p case was included for the square well, but not for the exponential well, and amounted to only a 10 percent reduction in the total cross section for 340-Mev collisions (laboratory frame of reference).

TABLE IV. Values of the arbitrary constants $\Gamma^2 g$, adjusted to give a total cross section (neglecting deuteron formation) at 343 Mev of $2.60(10)^{-28}$ cm^2. The notation (Triplet, S), etc., refers to the spin state of the final nucleons and the orbital angular momentum state of the meson [Eqs. (5), (6), (7)].

	(Triplet, S)	(Singlet, S)	(Triplet, P-sym)
$\Gamma^2 g$	$1.94(10)^{-44}\frac{\text{cm}^2}{(\text{Mev})^5}$	$2.01(10)^{-44}\frac{\text{cm}^2}{(\text{Mev})^5}$	$4.90(10)^{-42}\frac{\text{cm}^2}{(\text{Mev}^7)}$
	(Singlet, P-sym)	(Triplet, P-cosθ)	(Singlet, P-cosθ)
$\Gamma^2 g$	$4.36(10)^{-43}\frac{\text{cm}^2}{(\text{Mev})^7}$	$1.47(10)^{-47}\frac{\text{cm}^2}{(\text{Mev})^7}$	$1.31(10)^{-47}\frac{\text{cm}^2}{(\text{Mev})^7}$

The results for square and exponential wells were in only fair agreement—although the discrepancies were within present experimental errors. For instance, for a final n-p triplet state, the ratio of number of neuterons formed to number of unbound particles agreed to within about 5 percent. Also the cross section for forming a deuteron using an exponential well agreed to within a few percent with that calculated using the wave function of Chew and Goldberger.[9]

The exponential well, as being the more reasonable physically, was chosen for the calculations presented here, and it is felt that the results are sufficiently reliable until much more accurate and complete experimental results are available than at present. Eventually, meson production may provide a means of probing nuclear forces at close distances.

With the values of $|\psi_F(0)|^2$ we are in a position to evaluate the partial cross sections corresponding to the expressions (5) to (9). Giving the constants $\Gamma^2 g$ of these expressions fixed numerical values, we need consider only three types of final states: final unbound triplet and singlet states of the nucleons, and final states with a deuteron formed. The values of $\Gamma^2 g$ were arbitrarily chosen to normalize the total cross sections (disregarding deuteron formation) to $2.60(10)^{-28}$ cm^2. These values are listed in Table IV.

The cross sections are designated as follows:

$$d\sigma(\text{Triplet, } P\text{-sym}) = \sigma_0(\text{Triplet, } P\text{-sym})(\theta, T)d\Omega_\epsilon dT, \quad (18)$$

[7] R. Christian and E. Hart, Phys. Rev. **77**, 441 (1950).
[8] J. D. Jackson and J. M. Blatt, Revs. Modern Phys. **22**, 77 (1950).
[9] G. F. Chew and M. L. Goldberger, Phys. Rev. **75**, 1637 (1949).

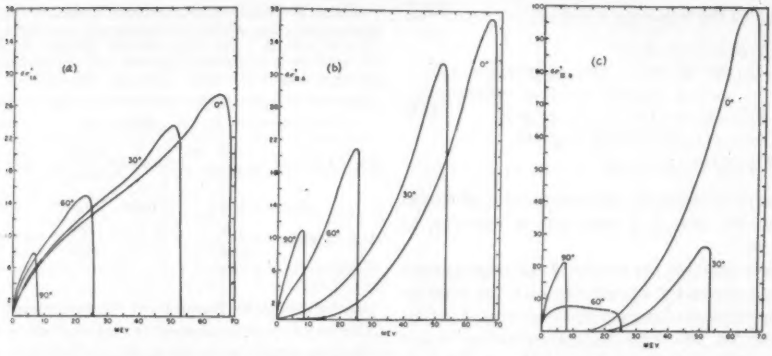

FIG. 1. Differential cross section for meson production in the laboratory system in units of 10^{-31} cm² per Mev per unit solid angle [designated as σ_0 in Eq. (18)] at an initial nucleon energy of 343 Mev and for a meson rest-mass energy of 140 Mev. The final nucleons are assumed to be in a triplet spin state. The energy scale in Mev refers to the meson kinetic energy; the angles indicated are the angles between the meson and incident nucleon momenta. (a) is for (S) type coupling; (b) is for P(sym) type coupling; (c) is for $P(\cos^2\theta)$ type coupling [this notation is defined by Eqs. (5), (6), and (7)].

where the spin state of the final nucleons (triplet or singlet) and the type of meson p-state (symmetrical or $\cos^2\theta$) are indicated. Here T is the meson kinetic energy, $d\Omega_q$ is an element of solid angle into which the meson is emitted, and θ is the angle between the meson and beam directions. If a deuteron is formed, the mesons have a fixed energy, T_0, and we have a cross section (symmetrical or $\cos^2\theta$)

$$d\sigma(\text{deuteron, } P\text{-sym}) = \sigma_0(\text{deuteron, } P\text{-sym})(\theta)d\Omega_q dT, \quad (19)$$

where

$$\sigma_0(\text{deuteron, } P\text{-sym})(\theta) = \sigma_0(\text{triplet, } P\text{-sym})(\theta, T_0)\delta(T-T_0). \quad (20)$$

To facilitate comparison with experiment, the differential cross sections of Eq. (18) have been transformed to the laboratory system and are plotted in Figs. 1 and 2 for a beam energy of 343 Mev. Cross sections with the final nucleons in P-states are also given in Fig. 3 to show the marked contrast with the processes in which the final nucleons are in S-states. The quantities are plotted in units of cm² (Mev-steradian)$^{-1}$. The corresponding cross sections for deuteron formation, i.e., σ_0(deuteron, sym)(θ) and σ_0(deuteron, $\cos^2\theta$)(θ) of Eq. (19) have also been transformed to the laboratory system and are given in Table V. For the numerical results, the values of $\Gamma^2 g$ given in Table IV have been used.

TABLE V. Differential cross section, $d\sigma/d\Omega$, in units of 10^{-28} cm² per unit solid angle for production of a positive π-meson and a deuteron in a 343-Mev p–p collision. θ is the angle between the directions of the initial nucleon beam and meson momenta in the laboratory system. The notation is the same as that used in Table IV.

θ	(Triplet, S)	(Triplet, P-sym)	(Triplet, P-cos²θ)	Meson energy (Mev)
0°	1.75	2.87	8.61	73
30°	1.42	2.32	2.38	56
60°	0.82	1.34	0.32	28
90°	0.28	0.46	0.83	11

The rather striking peak in the curves of Figs. 1 and 2 is due to the rapid increase of $|\psi_F(0)|^2$ with increasing meson energy.

Since the quantities $\Gamma^2(p)$ presumably vary much less rapidly with energy than do the other factors in the cross section, it is instructive to observe the variation of total cross section with beam energy on the assumption that these quantities are constant. This variation is given in Figs. 4 and 5. Deuteron formation has been included for final triplet states.

IV. COMPARISON WITH THE EXPERIMENTAL DATA ON (PP, π^+) PRODUCTION

The most detailed experimental data avaiable is for (PP, π^+) production with a beam energy of 341±2 Mev. The experiments of Richman, Cartwright, and Whitehead[10] and of Cartwright, Richman, Whitehead, and Wilcox[11] give the meson energy spectrum at zero degrees (±3°) with respect to the beam direction. Further results concerning the energy spectrum at 30° have been obtained by Peterson[12] and at 18° by Peterson, Iloff, and Sherman.[13]

The experimental energy spectrum at zero degrees is given by the points in Fig. 6. To fit this data, we are restricted to final nucleon triplet states (see Table III), since we concluded in Sec. II that the mesons were emitted predominantly into p-states.

[10] Richman, Cartwright, and Whitehead, private communication.
[11] Cartwright, Richman, Whitehead, and Wilcox, Phys. Rev. **78**, 823 (1950).
[12] V. Z. Peterson, private communication.
[13] Peterson, Iloff, and Sherman, Phys. Rev. **81**, 647A (1951).

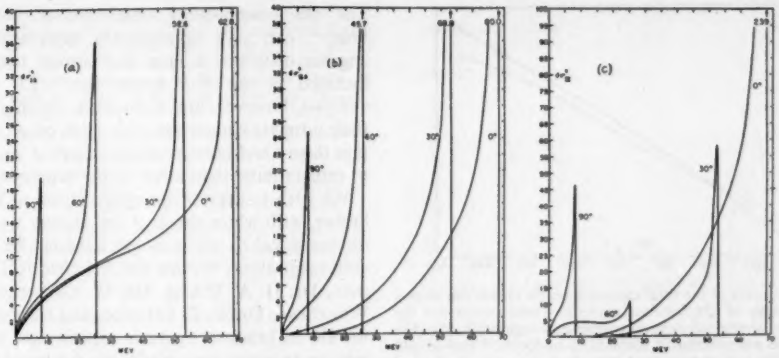

FIG. 2. Differential cross section for meson production with a beam energy of 343 Mev. The final nucleons are assumed to be in a singlet spin state, but otherwise the notation is the same as for Fig. 1.

The corresponding cross section, calculated from the (p-) type coupling of Eqs. (6) and (7) and folded into the experimental energy resolution,[14] is given in Fig. 6. The agreement seems to be quite satisfactory. A small amount of meson s-state could be included to raise the low energy end of the spectrum if this turns out to be necessary.

The angular distribution of the mesons is also of particular interest. Designating the production cross section per steradian at an angle θ' with respect to the beam direction (laboratory frame of reference) by $\sigma(\theta')$, i.e., the area under the meson energy spectrum curve, we have the experimental results given in the first column of Table VI. It is quite apparent that a spherically symmetric angular distribution is incompatible with the experimental results. On the other hand, the $\cos^2\theta$ type cross section lies within the experimental error. We thus conclude that the predominant term in the cross section is of the form (p-$\cos^2\theta$) of Eq. (7), giving additional support to the conclusion of Sec. II that the meson is emitted into p-states.

The experimental error given in Table VI is consistent with a maximum of about 40 percent spherically symmetric contribution to the total cross section at 341 Mev, although, of course, the contribution may be much less. Experiments are now in progress to measure the cross section at 60 degrees. At this angle the $\cos^2\theta$ contribution is quite small ($\cong 1/20$ its value in the forward direction), so deviations from the $\cos^2\theta$ distribution should be readily detectable.

V. SUMMARY OF RESULTS

We have shown that the analysis of the production of mesons in nucleon-nucleon collisions near threshold can be greatly simplified by use of the requirements of angular momentum and parity conservation and of charge symmetry. Further simplification is introduced if the meson is assumed to be pseudoscalar, in conformity with other experimental evidence.

Analysis of the experimental data indicates that the pseudoscalar meson is emitted predominantly into p-states, since this assumption allows prediction of (1) small (PP, π^0) cross section; (2) large ratio of (NP, π^0) and (NP, π^+) to (PP, π^0); (3) approximate $\cos^2\theta$ angular distribution of π^+ mesons produced in PP collisions; (4) predominance of final NP triplet states in (PP, π^+) process and consequent large probability of deuteron formation.

The consequences of the hypothesis of charge symmetry are also of particular interest for the processes of meson production, as is apparent from an examination of Table III. Since experimental evidence indicates that the predominant final state in the production process is a nucleon s-state and a meson p-state, it also

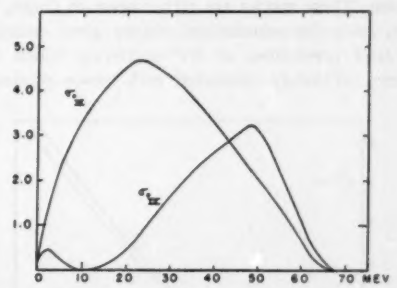

FIG. 3. Differential cross section (in the laboratory system) in the direction of the beam for producing mesons in 343-Mev nucleon collisions when the nucleons in the final state are in p-states. The energy scale refers to the meson kinetic energy; the ordinate is given in arbitrary units. The cross section σ_{III} and σ_{IV} refer to the respective couplings of expressions (8) and (9). The lack of high energy peak is readily apparent from a comparison with Figs. 1 and 2. *Note added in proof:* The labels on the cross sections in the figure are incorrect. For "III" read "(p,s)"; for "IV" read "(p,p)."

[14] Richman, Cartwright, and Whitehead (to be published soon). A similar spectrum, with equivalent energy resolution, has been obtained by Peterson, Iloff, and Sherman (private communication) at 18°.

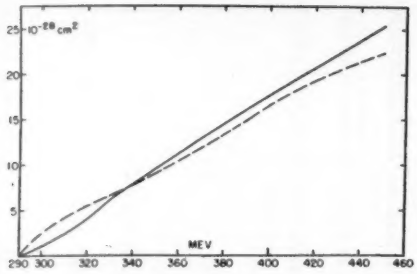

FIG. 4. Variation of the total cross section for meson production with the energy of the incident nucleon. These curves are the consequences of the (S) type of coupling of expression (5). The cross sections are arbitrarily normalized to 8×10^{-28} cm² at 340 Mev. The solid curve is for a final nucleon singlet state, the dashed curve is for a final nucleon triplet state and includes the possibility of deuteron formation.

follows that

$$\sigma(NP, \pi^0)=\sigma(NP, \pi^+)+\tfrac{1}{2}\sigma(PP, \pi^+). \qquad (21)$$

In addition, a comparison of the energy spectrum of π^+ and π^- mesons produced in NP collisions will give a direct comparison of NN and PP singlet potentials through the dependence of the cross sections on $|\psi_F(0)|^2$ [Eq. (2)]. Further information concerning the properties of nuclear forces at close distances may very well be obtained from such experiments.

The relation of these results to meson theory is of some interest. This is so, in particular, since pseudoscalar meson theory has in many cases given reasonable qualitative agreement with experiment. Brueckner[2] found that pseudoscalar theory with pseudovector coupling predicted correctly the $\cos^2\theta$ angular distribution (for proper choice of the coupling constants), the predominance of final nucleon triplet states in (PP, π^+) production, and the smallness of the (PP, π^0) cross section. These results are rather open to doubt, however, since the pseudoscalar theory gives completely incorrect predictions of NP scattering which is, of course, intimately connected with meson production.

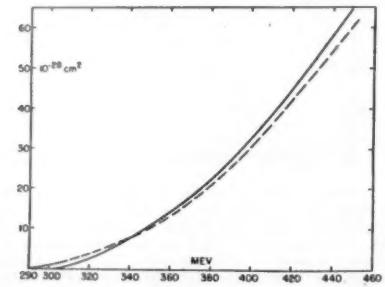

FIG. 5. Variation of the total cross section for meson production. The definitions and symbols are the same as for Fig. 4 except that here the (p-) type coupling of expressions (6) and (7) is assumed.

The phenomenological treatment of Marshak and Foldy[15] can give approximate agreement with the angular distribution only if a strong tensor force is included in the N-P interaction. Such methods of analysis, however, are of doubtful validity because of their intimate connection with weak coupling perturbation theory and because of the failure of any one model to explain more than a few of the experimental results.

We wish to express our appreciation to Professor R. Serber, with whom much of the present work has been discussed and to whom we are indebted for many valuable suggestions. We are also indebted to Dr. C. Richman, Dr. H. A. Wilcox, Mr. W. Cartwright, Miss M. Whitehead, Dr. V. Z. Peterson, and their collaborators for aid in interpreting their experiments and for permission to quote their results in advance of publication. Further appreciation is expressed to Mr. D. Clark and Mr. W. Noh for their considerable assistance with the numerical calculations.

APPENDIX

We now consider a more detailed development of the ideas developed in Sec. II.

In Eq. (1) we introduced the transition matrix, $(\mathbf{q}, \mathbf{p}'|R|\mathbf{p})$ for the description of meson production. This was defined in the center-of-mass coordinate system, and $\mathbf{p}$ was considered to be the relative momentum of the initial nucleons, $\mathbf{p}'$ that for the final nucleons, and $\mathbf{q}$ the relative momentum of the meson and the center-of-mass of the two nucleons. The partial wave analysis of the final state is most easily effected by such an expansion of R:

$$(\mathbf{q}, \mathbf{p}'|R|\mathbf{p})=(q, p'|R_1|\mathbf{p})+q_i(q, p'|R_2|\mathbf{p})_i + (q_iq_j-\tfrac{1}{3}q^2\delta_{ij})(q, p'|R_3|\mathbf{p})_{ij}+p_i'(q, p'|R_4|\mathbf{p})_i+\cdots \qquad (A\text{-}1)$$

(a summation over repeated indices is implied), where the various R_i ($i=1, 2, \cdots$) are functions of the magnitude only of the vectors $\mathbf{q}$ and $\mathbf{p}'$. The short range hypothesis developed in Sec. II implies that the R_i depend only weakly on the quantities q and p'. The zero range approximation used implies that we neglect any dependence of the R_i on q and p'. Then, neglecting for the present, those terms which depend on factors of p' (i.e., we keep only nucleon s-states), we can put R into the form

$$R=\Sigma_i\,\Gamma_i(p)O_i(\boldsymbol{\sigma}, \boldsymbol{\tau}, \mathbf{q}, \mathbf{p}). \qquad (A\text{-}2)$$

Here the $\Gamma_i(p)$ are real numerical functions of p only—i.e., the beam energy—and the O_i are homogeneous polynomials in both $\mathbf{q}$ and $\mathbf{p}$, multiplied by various combinations of the vector matrices of spin and isotopic spin, $\boldsymbol{\sigma}$ and $\boldsymbol{\tau}$, respectively.

Then the transition matrix $(F|R|I)$ [Eq. (2)] will be given by

$$(F|R|I)=\Sigma_i\,\Gamma_i(p)(F|O_i|I)(2\pi)^{\frac{1}{2}}\psi_F^*(0), \qquad (A\text{-}3)$$

where $(F|O_i|I)$ is obtained from that of Eq. (A-2) by evaluating the matrix elements of $\boldsymbol{\sigma}$ and $\boldsymbol{\tau}$, and $\psi_F(0)$ is the final nucleon wave function, $\psi_F(r)$, evaluated at $r=0$ (because of the zero range hypothesis).

It is the quantities $(F|O_i|I)$ that determine the detailed nature of the cross sections—i.e., lead to cross sections of the type represented by expressions (5), etc. It is therefore of interest to see the symmetry restrictions that can be placed on these quantities.

These requirements can be easily discussed in terms of the operators $O_i(\boldsymbol{\sigma}, \boldsymbol{\tau}, \mathbf{q}, \mathbf{p})$ of Eq. (A-2). On the assumption that the meson is pseudoscalar, these must be invariant under rotations and change signs upon coordinate reflections. Thus, the following

[15] R. Marshak and L. Foldy, Phys. Rev. **75**, 1493 (1949).

TABLE VI. The angular distribution for (pp, π^+) mesons is analyzed on the basis of experimental data (see references 10–14) at 0°, 18°, and 30° with respect to the beam direction. In the second column are given the experimental ratios of cross sections. The calculated ratios for center-of-mass spherical symmetry and $\cos^2\theta$ angular distribution are given [notation is that of Eqs. (6) and (7)] in the remaining two columns.

Ratio	Experimental	(P-sym)	(P-$\cos^2\theta$)
$\sigma(0°)/\sigma(30°)$	3.5±0.7	1.25	4.14
$\sigma_d(0°)/\sigma_d(18°)$[a]	1.6±0.3	1.08	1.54

[a] By σ_d we mean just the cross section for meson production with deuteron formation. Experimentally, this is the area under the high energy peak in the meson spectrum.

combinations of the vectors $\boldsymbol{\sigma}$, $\mathbf{q}$, and $\mathbf{p}$ are possible:

$$\begin{aligned}
A_1(1) &= (p\cdot q)^{n-1}\boldsymbol{\sigma}^{(1)}\cdot\mathbf{p},\\
A_2(1) &= (p\cdot q)^{n}(\boldsymbol{\sigma}^{(1)}\cdot\mathbf{q}),\\
A_3(1) &= (p\cdot q)^{n-2}\boldsymbol{\sigma}^{(1)}\cdot\mathbf{p}\boldsymbol{\sigma}^{(2)}\cdot(\mathbf{p}\times\mathbf{q}),\\
A_4(1) &= (p\cdot q)^{n-1}\boldsymbol{\sigma}^{(1)}\cdot\mathbf{q}\boldsymbol{\sigma}^{(2)}\cdot(\mathbf{p}\times\mathbf{q}),\\
A_5(1) &= \tfrac{1}{2}(p\cdot q)^{n-1}\boldsymbol{\sigma}^{(1)}\times\boldsymbol{\sigma}^{(2)}\cdot\mathbf{p},\\
A_6(1) &= \tfrac{1}{2}(p\cdot q)^{n}\boldsymbol{\sigma}^{(1)}\times\boldsymbol{\sigma}^{(2)}\cdot\mathbf{q},
\end{aligned} \tag{A-4}$$

(where n is a positive integer). The superscript "1" refers to one nucleon, "2" refers to the other. Similar quantities $A(2)$ can be defined by interchanging "1" and "2" and replacing $\mathbf{p}$ by $-\mathbf{p}$ (i.e., interchanging the nucleons). The quantities O_i must be invariant with respect to interchanging the nucleons.

Evaluation of the spin matrices in Eqs. (A-4) for a given process when combined with the results of Eqs. (17) leads immediately to numerical values for the quantities g_{Ti} of expressions (5), etc. —that is, to the structure of the $(F|O_i|I)$ of Eq. (A-3). We thus find by a suitable choice of the A's of Eq. (A-4) and by the hypothesis of charge symmetry an almost complete specification of the cross sections—we have then only two arbitrary numerical factors with which to adjust the absolute magnitude of the total cross sections, one for M_2 and one for M_3 of Eqs. (17).

The characteristics of the leading term in the (pp, π^+) cross section determine this choice of the A's uniquely to the approximation that the cross section is represented by the leading $\phi(\cos^2\theta)$ term—for the matrices M_3, at least. This is a linear combination

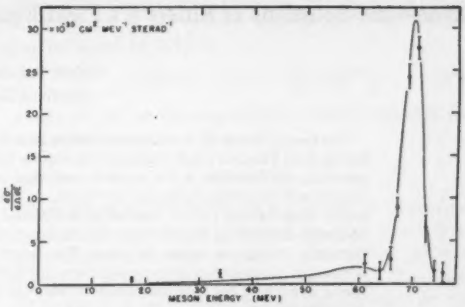

FIG. 6. Differential cross section for meson production in the direction of the beam at 341 Mev. The solid curve is calculated from the (ϕ-) type coupling of expressions (6) and (7), i.e., for mesons emitted into ϕ-states and a final triplet state for the neutron and proton. This curve has been "folded" into the experimental energy resolution. The experimental points are those of Cartwright, Richman, and Whitehead (reference 10).

of A_1 and A_3 with $n=2$. This linear combination does not lead to further ambiguity (i.e., introduce new arbitrary parameters) however, since these terms differ only by factors of the spin singlet and triplet projection operators. This distinction is not significant, as M_2 and M_3 are resolved into spin eigenstates. We can thus consider just the term A_1; although we are strictly justified in assigning it to M_3 only, since the (np, π^+) cross section has not been measured as yet.

If charge symmetry is not assumed, it is easy to enumerate the few possible combinations of τ-operators possible in the $O_i(\boldsymbol{\sigma}, \boldsymbol{\tau}, \mathbf{q}, \mathbf{p})$. This leads to more numerical parameters than we had before, which can be used, if necessary, to adjust to the experimental cross sections.

We have concentrated largely on the leading term in the cross section. When experimental evidence warrants the use of correction terms, it will be necessary to consider others of the A's in Eqs. (A-4).

Nonstatic Solutions of Einstein's Field Equations for Spheres of Fluids Radiating Energy

P. C. VAIDYA*
Vallabh Vidyanagar, Anand, India
(Received December 28, 1950)

The energy tensor for a mixture of matter and outflowing radiation is derived, and a set of equations following from Einstein's field equations are written down whose solutions would represent nonstatic radiating spherical distributions. A few explicit analytical solutions are obtained, which describe a distribution of matter and outflowing radiation for $r \leq a(t)$, an ever-expanding zone of pure radiation for $a(t) \leq r \leq b(t)$ and empty space beyond $r = b(t)$. Since $db(t)/dt$ is almost equal to 1 and $da(t)/dt$ is negative, the solutions obtained represent contracting distributions, but the contraction is not gravitational because m/r is a constant on the boundary $r = a(t)$, m being the mass. The contraction is a purely relativistic effect, the corresponding newtonian distributions being equilibrium distributions. It is hoped that the scheme developed here will be useful in working out solutions which would help in a clear understanding of the initial or the final stages of stellar evolution.

I. INTRODUCTION

IT is well known that during the initial stages of stellar evolution, and during the final stages when the thermonuclear sources of energy are exhausted, the conditions within the interior of the star are such that the general relativistic corrections to the newtonian theory become important. So a description of the stellar interior based on the relativistic gravitational theory would provide a clearer picture of the processes during these stages of stellar evolution. Taking appropriate static solutions of Einstein's field equations, Oppenheimer and Volkoff[1] have found that equilibrium configurations of massive neutron cores do not exist for masses greater than $0.7\odot$. Therefore, for description, of the final evolutionary stages of heavier stars nonstatic solutions of the field equations have to be considered. Oppenheimer and Snyder[2] have succeeded in getting a nonstatic solution representing the continued gravitational contraction of a stellar body after all its sources of thermonuclear energy are exhausted. But in obtaining this solution the radial pressure of the stellar matter and the gravitational effect of any escaping radiation were neglected. The importance of nonstatic solutions in understanding certain aspects of the earlier stages of stellar evolution has been recently emphasized by Klein.[3] Thus it appears that a study of the field equations of general relativity with a view to getting solutions representing nonstatic spherically symmetric distributions is a necessary first step toward a clear understanding of the problems of the earlier and the later stages of stellar evolution.

A nonstatic distribution would be radiating energy, and so it would be surrounded by an ever-expanding zone of radiation. If this radiating distribution together with its radiation is to form an isolated system, beyond the zone of pure radiation we must have empty space given by the Schwarzschild's exterior solution. In the following we shall develop a scheme for working out solutions of Einstein's field equations which will sustain the above picture of a nonstatic distribution. Using a line-element we have

$$ds^2 = -e^{\lambda}dR^2 - R^2(d\theta^2 + \sin^2\theta d\varphi^2) + e^{\nu}dT^2, \qquad \lambda = \lambda(R, T), \quad \nu = \nu(R, T). \tag{1.1}$$

We shall work out solutions which will describe (1) a "mixture" of matter and outflowing radiation for $R \leq R_i(T)$, (2) a zone of pure outflowing radiation for $R_i(T) \leq R \leq R_e(T)$, and (3) empty space for $R \geq R_e(T)$, the line-element being then given by the well-known Schwarzschild's exterior solution,

$$ds^2 = -(1-2M/R)^{-1}dR^2 - R^2(d\theta^2 + \sin^2\theta d\varphi^2) + (1-2M/R)dT^2, \tag{1.2}$$

M, a constant, being the total mass of the distribution and the radiated energy. We shall call the solution for $R \leq R_i(T)$ the interior solution and the one holding good for $R_i(T) \leq R \leq R_e(T)$ the exterior solution. In this notation the boundary $R = R_i(T)$ will be called the interior boundary and $R = R_e(T)$ will be called the exterior boundary. We begin with the method of finding the interior solution.

II. THE ENERGY-TENSOR FOR THE INTERIOR FIELD

Following Tolman[4] we express the energy-momentum tensor for the combined field of matter and radiation in the form

$$T^{\mu\nu} = T^{\mu\nu}{}_{(me)} + T^{\mu\nu}{}_{(em)}. \tag{2.1}$$

Here $T^{\mu\nu}{}_{(me)}$ stands for the mechanical energy tensor, i.e., the tensor due to matter. $T^{\mu\nu}{}_{(em)}$ stands for the electromagnetic tensor, i.e., the tensor due to radiation. The matter comprising the distribution may be regarded as a perfect fluid so that

$$T^{\mu\nu}{}_{(me)} = (p+\rho)v^{\mu}v^{\nu} - pg^{\mu\nu}; \tag{2.2}$$

$$v^{\mu}v_{\mu} = 1; \tag{2.3}$$

* Springer Research Scholar, University of Bombay, Bombay, India.
[1] J. R. Oppenheimer and G. M. Volkoff, Phys. Rev. **55**, 374 (1939).
[2] J. R. Oppenheimer and H. Snyder, Phys. Rev. **56**, 455 (1939).
[3] O. Klein, Arkiv Mat. Astron. Fysik **34A**, 19 (1947).
[4] R. C. Tolman, *Relativity Thermodynamics and Cosmology* (Oxford University Press, New York, 1934), p. 261.

and for the directional flow of radiation in empty space, the author has proved elsewhere[5] the formula

$$T^{\mu\nu}{}_{(em)}=\sigma w^\mu w^\nu, \tag{2.4}$$

$$w^\mu w_\mu=0, \quad (w^\mu)_{,\nu}w^\nu=0, \tag{2.5}$$

σ being the density of the flowing radiation. This simple formula can obviously be taken over to the case of radiation flowing through a medium; the presence of the medium will affect only the law of variation of the scalar σ. Thus we can write the final expression for the energy tensor (2.1) as

$$T^{\mu\nu}=(p+\rho)v^\mu v^\nu-pg^{\mu\nu}+\sigma w^\mu w^\nu, \tag{2.6}$$

with the further Eqs. (2.3) and (2.5) for the vectors v^μ and w^μ.

We shall now work out the consequences of the fundamental equations

$$(T_\mu{}^\nu)_{,\nu}=0. \tag{2.7}$$

For this purpose we choose a co-moving frame of reference, i.e., a frame of reference relative to which the fluid comprising the distribution is at rest. In such a reference-frame the line-element showing spherical symmetry cannot be of the form (1.1) but has to be of the general form

$$\begin{gathered}ds^2=-e^\alpha dr^2-r^2e^\beta(d\theta^2+\sin^2\theta d\varphi^2)+e^\gamma dt^2,\\ \alpha=\alpha(r,t), \quad \beta=\beta(r,t), \quad \gamma=\gamma(r,t).\end{gathered} \tag{2.8}$$

Using this line-element and the form (2.6) of the energy tensor with the additional restrictions

$$v^1=v^2=v^3=0, \quad v^4=e^{-\gamma/2} \tag{2.9}$$

due to the co-moving nature of the reference-frame, Eqs. (2.7) lead to

$$-p'-\tfrac{1}{2}(p+\rho)\gamma'+(\sigma w^\nu)_{,\nu}w_1=0 \tag{2.10}$$

and

$$\dot\rho+(p+\rho)(\dot\beta+\dot\alpha/2)+(\sigma w^\nu)_{,\nu}w_4=0. \tag{2.11}$$

Here a prime denotes a differentiation with regard to r, while an overhead dot denotes that with regard to t. On elimination of σ between these two equations we find

$$p'+\tfrac{1}{2}(p+\rho)\gamma'-e^{(\alpha-\gamma)/2}[\dot\rho+(p+\rho)(\dot\beta+\dot\alpha/2)]=0. \tag{2.12}$$

Equation (2.12) replaces the familiar equation

$$p'+(p+\rho)\gamma'/2=0$$

for the static distributions. We shall now show that (2.11) leads, at the newtonian level of approximation, to the well-known equation expressing the equilibrium of a stellar configuration[6]

$$p'+p_r{}'=-G\rho M(r)/r^2, \tag{2.13}$$

p_r being the radiation pressure; while Eq. (2.11) will be a purely relativistic equation having no newtonian counterpart. It has already been proved that[7] in space not occupied by matter

$$\sigma w_\mu w^\nu=-F_{\mu\alpha}F^{\nu\alpha}+\tfrac{1}{4}\delta_\mu{}^\nu F_{\alpha\beta}F^{\alpha\beta}, \tag{2.14}$$

where $F^{\mu\nu}$ is the skew-symmetric electromagnetic field tensor, so that

$$(\sigma w^\nu)_{,\nu}=0.$$

When the radiation traverses a medium, it is weakened by absorption and so (2.14) will not hold good. If σ is the density of flowing radiation after it has traversed a length s of the medium and σ_0 the density that would be obtained if there were no medium present, we may write

$$\sigma=\sigma_0e^{-f}$$

so that

$$\sigma w_\mu w^\nu=e^{-f}[-F_{\mu\alpha}F^{\nu\alpha}+\tfrac{1}{4}\delta_\mu{}^\nu F_{\alpha\beta}F^{\alpha\beta}], \tag{2.15}$$

where $f=f(r,t)$ may be regarded as the "optical depth" of the medium[8] which is connected with its mass absorption coefficient κ through

$$df/ds\equiv w^1(\partial f/\partial r)+w^4\partial f/\partial t=\kappa\rho.$$

With this law of absorption of the medium, (2.10) immediately transforms to

$$-p'-\tfrac{1}{2}(p+\rho)\gamma'-\kappa\rho\sigma w_1=0.$$

Again, for quasi-static processes, writing

$$p_r{}'=-\kappa\rho L(r)/4\pi r^2$$

we can finally get

$$p'+p_r{}'=-(p+\rho)\gamma'/2, \tag{2.16}$$

where $L(r)=-4\pi r^2\sigma w_1$ measures the luminosity of the distribution at the newtonian level of approximation. Equation (2.16) readily gives the familiar equation (2.13). We are thus able to recover the newtonian equation of stellar equilibrium from our energy-momentum tensor (2.6). This gives an increased confidence in the form (2.6) of the energy tensor for a mixture of matter and radiation.

III. GENERAL METHOD OF FINDING THE INTERIOR SOLUTION

Using the co-moving frame of reference introduced in the last section we write the line-element as

$$\begin{gathered}ds^2=-e^\alpha dr^2-r^2e^\beta(d\theta^2+\sin^2\theta d\varphi^2)+e^\gamma dt^2,\\ \alpha=\alpha(r,t), \quad \beta=\beta(r,t), \quad \gamma=\gamma(r,t).\end{gathered} \tag{3.1}$$

The components of $T_\mu{}^\nu$ can now be calculated in terms of the functions α, β, γ with the help of the field equa-

[5] P. C. Vaidya, Proc. Indian Acad. Sci., to be published.

[6] S. Chandrasekhar, *Introduction to the Study of Stellar Structure* (Chicago University Press, Chicago, 1939), pp. 213, 214.

[7] V. V. Narlikar and P. C. Vaidya, Nature **159**, 642 (1947).

[8] See reference 6, p. 191. For simplicity we are considering here the case of homogeneous radiation.

tions of Einstein. We find these components to be

$$8\pi T_1{}^1=-e^{-\alpha}\left[\frac{\beta'^2}{4}+\frac{\beta'\gamma'}{2}+\frac{\beta'+\gamma'}{r}+\frac{1}{r^2}\right]+\frac{e^{-\beta}}{r^2}+e^{-\gamma}\left[\frac{\partial^2\beta}{\partial t^2}+\frac{3}{4}\dot{\beta}^2-\frac{\dot{\beta}\dot{\gamma}}{2}\right]; \quad (3.2)$$

$$8\pi T_2{}^2=8\pi T_3{}^3=-e^{-\alpha}\left[\frac{\beta''}{2}+\frac{\gamma''}{2}+\frac{\beta'^2}{4}+\frac{\gamma'^2}{4}-\frac{\alpha'\beta'}{4}+\frac{\beta'\gamma'}{4}-\frac{\alpha'\gamma'}{4}-\frac{\alpha'}{2r}+\frac{\beta'}{r}+\frac{\gamma'}{2r}\right]+e^{-\gamma}\left[\frac{\partial^2\alpha/\partial t^2}{2}+\frac{\partial^2\beta/\partial t^2}{2}+\frac{\dot{\alpha}^2}{4}+\frac{\dot{\beta}^2}{4}+\frac{\dot{\alpha}\dot{\beta}}{4}-\frac{\dot{\alpha}\dot{\gamma}}{4}-\frac{\dot{\beta}\dot{\gamma}}{4}\right]; \quad (3.3)$$

$$8\pi T_4{}^4=-e^{-\alpha}\left[\beta''+\frac{3}{4}\beta'^2-\frac{\alpha'\beta'}{2}+\frac{3\beta'}{r}-\frac{\alpha'}{r}+\frac{1}{r^2}\right]+\frac{e^{-\beta}}{2}+e^{-\gamma}\left[\frac{\dot{\alpha}\dot{\beta}}{2}+\frac{\dot{\beta}^2}{4}\right]; \quad (3.4)$$

$$8\pi T_1{}^4=-e^{-\gamma}\left[\dot{\beta}'-\frac{\dot{\beta}\gamma'}{2}+(\dot{\beta}-\dot{\alpha})\frac{\beta'}{2}+(\dot{\beta}-\dot{\alpha})\frac{1}{r}\right]. \quad (3.5)$$

But the form (2.6) of the tensor $T_\mu{}^\nu$, *viz.*

$$T_\mu{}^\nu=(p+\rho)v_\mu v^\nu-pg_\mu{}^\nu+\sigma w_\mu w^\nu \quad (3.6)$$

with

$$v^1=v^2=v^3=0, \quad v^4=e^{-\gamma/2} \quad (3.7)$$

and

$$w^2=w^3=0, \quad w_\mu w^\mu=0, \quad (w^\mu)_{,\nu}w^\nu=0, \quad (3.8)$$

gives

$$T_1{}^1=-p+\sigma w_1w^1, \quad T_2{}^2=T_3{}^3=-p, \quad T_4{}^4=\rho+\sigma w_4w^4, \quad T_1{}^4=\sigma w_1w^4. \quad (3.9)$$

Hence we can find the physical quantities p, ρ, σ, v^μ, and w^μ in terms of the functions α, β, and γ:

$$p=-T_2{}^2; \quad \rho=T_1{}^1+T_4{}^4-T_2{}^2; \quad (3.10)$$

$$\sigma=-e^{(3\alpha-\gamma)/2}(w^1)^2T_1{}^4; \quad (3.11)$$

$$w^4=e^{(\alpha-\gamma)/2}w^1;$$

$$\frac{\partial w^1}{\partial r}+e^{(\alpha-\gamma)/2}\frac{\partial w^1}{\partial t}+w^1\left[\frac{\alpha'+\gamma'}{2}+e^{(\alpha-\gamma)/2}\dot{\alpha}\right]=0. \quad (3.12)$$

The last equation (3.12) follows from (3.8). Once α, β, γ are known as functions of r and t, Eqs. (3.2) to (3.6) determine the components of $T_\mu{}^\nu$ as functions of r and t and then (3.10), (3.11), and (3.12) determine the march of the physical variables ρ, p, σ, etc., through the distribution at any time t. Equations (3.9) lead to the following relation between the components of $T_\mu{}^\nu$:

$$T_1{}^1-T_2{}^2=e^{(\gamma-\alpha)/2}T_1{}^4. \quad (3.13)$$

Substituting the values of $T_1{}^1$, $T_2{}^2$ and $T_1{}^4$ from (3.2), (3.3), and (3.5) we find that (3.13) gives

$$\frac{\beta''}{2}+\frac{\gamma''}{2}+\frac{\gamma'^2}{4}-\frac{\alpha'\beta'}{4}-\frac{\beta'\gamma'}{4}-\frac{\gamma'\alpha'}{4}-\frac{\alpha'}{2r}-\frac{\gamma'}{2r}-\frac{1}{r^2}+\frac{e^{\alpha-\beta}}{r^2}+e^{\alpha-\gamma}\left[\frac{\partial^2\beta/\partial t^2}{2}-\frac{\partial^2\alpha/\partial t^2}{2}-\frac{\dot{\alpha}^2}{4}+\frac{\dot{\beta}^2}{2}-\frac{\dot{\alpha}\dot{\beta}}{4}-\frac{\dot{\beta}\dot{\gamma}}{4}+\frac{\dot{\alpha}\dot{\gamma}}{4}\right]+e^{(\alpha-\gamma)/2}\left[\dot{\beta}'-\frac{\dot{\beta}\gamma'}{2}+(\dot{\beta}-\dot{\alpha})\frac{\beta'}{2}+(\dot{\beta}-\dot{\alpha})\frac{1}{r}\right]=0. \quad (3.14)$$

It may be noted that this relation is identical with Eq. (2.13) of the last section. Equation (3.14) is one relation between the three functions α, β, and γ. This relation, it will be remembered, is a consequence of the co-moving nature of the coordinate system used. Two more relations are necessary in order to determine the three functions α, β, and γ. These relations are not supplied by the gravitational theory but are given by the physical nature of the distributions under consideration. They are: (1) the equation of state of the material of the distribution usually expressed as a relation between p and ρ; (2) the law of energy generation within the distribution. Given these two relations we must use (3.14) with them and determine the forms of the three functions α, β, and γ; and then, as stated above, the complete march of the physical variables within the distribution can be determined. This is then the general scheme of working out the internal solution.

But even in the static case (where $\sigma=0$) the problem treated in this direct way presents a formidable mathematical task and explicit solutions are not known for any but the simplest equations of state ($\rho=0$ and $\rho=a$ constant). We therefore adopt the indirect procedure suggested by Tolman[9] of solving (3.14) together with two assumed relations between α, β, and γ and then seeing what equation of state and what type of energy-generating system the solution so obtained possesses. But there is one important point to be noted in applying Tolman's method to our case. The interior boundary is obtained by finding the first value of r at which the fluid pressure p vanishes. But as the coordinates in use are co-moving, the radius of the interior boundary must be constant so that the two assumed relations between α, β, and γ must be such as would make the resulting p vanish for a constant value of r. This considerably limits the choice of the two relations to be assumed. In the

[9] R. C. Tolman, Phys. Rev. **55**, 364 (1939).

TABLE I. Relations among the constants in the nine mutually independent interior solutions.

Solution	p and m	u and l	n	$s+1$	Ck	D^2
I	$p=s$ $m=n$	$u=s+1$ $l=n$	1	—	$2(s+1-q)$	$-2(s+1)(s+1-2q)$
II	$p=s$ $m=n$	$u=s+1$ $l=n$	0	—	—	$2(s+1)(s+1-Ck)$
III	$p=s$ $m=n$	$u=s+1$ $l=n-1$	—	$q(2n^2-1)/n$	$2nqB$	$2q^2(1-2n^2)/n^2$
IV	$p=s-2q$ $m=n-1$	$u=s+1$ $l=n-1$	—	0	$Bq(3-4n)/(n-1)$	$4q^2(2n^2-1)$
V	$p=s-q$ $m=n-\frac{1}{2}$	$u=s+1$ $l=n$	$(3\pm\sqrt{5})4$	—	$s+1-q$	$2q[(4n-1)q-(2n-1)(s+1)]$
VI	$p=s-q$ $m=n-\frac{1}{2}$	$u=s+1$ $l=n$	$(3\pm\sqrt{5})/4$	0	—	$8n^2q^2+4Cknq$
VII	$p=s$ $m=n-\frac{1}{2}$	$u=s+1-2q$ $l=n-1$	1	—	$s+1-q$	$2B(s+1)^2-4Bq^2$
VIII	$p=s$ $m=n-\frac{1}{2}$	$u=s+1-2q$ $l=n-1$	—	$2nq$	$(1-2n)q$	$4Bq^2(2n^2-1)$
IX	$p=s$ $m=n-\frac{1}{2}$	$u=s+1-2q$ $l=n-1$	—	0	$(1-2n)q$	$-4Bq^2$

next section we show that a large number of solutions of Eq. (3.14) can be obtained by choosing particular forms of the functions α, β, and γ:

IV. PARTICULAR INTERIOR SOLUTIONS

We try to solve Eq. (3.14) with the following forms of the functions α, β, and γ:

$$e^{-\alpha}=A^2e^{2kt}r^{-2s}(B+r^{2q})^{2n}; \tag{4.1}$$

$$e^{-\beta}=A^2D^2e^{2kt}r^{-2p}(B+r^{2q})^{2m}; \tag{4.2}$$

$$e^{-\gamma}=A^2C^2e^{2kt}r^{-2u}(B+r^{2q})^{2l}. \tag{4.3}$$

All the twelve new symbols introduced here stand for constants whose values are to be suitably determined.[10] When these forms of α, β, γ are used in the differential equation (3.14), it will be found that, in general, seven restrictions are imposed on these twelve parameters so that seven of them get determined in terms of the rest. Now it happens that Eq. (3.14) leaves a fairly wide choice of the seven constants to be determined by it and as many as 39 different solutions of that equation can be obtained by this method. But some of these solutions are mutually transformable by simple transformations of the radial coordinate. The accompanying table gives the nine sets of relations between these constants representing the nine mutually independent solutions of (3.14). In Table I the second and the third columns give the values of the four parameters p, m, u, and l and the last four columns give the values of the other four parameters n, $s+1$, Ck, and D^2. As only seven parameters are determined by (3.14), there is always one dash in one of the last four columns for every solution. The physical contents of all these solutions have been investigated and it is found that they can be grouped together into four different groups. We put on record here one solution of each of these four physically distinct types.

[10] There will be no occasion for any confusion between the parameter p introduced in (4.2) and the fluid pressure p.

Solution III

We have

$$e^{\alpha}=\frac{e^{-2kt}r^{2s}}{A^2(B+r^{2q})^{2n}},\quad e^{\beta}=\frac{e^{\alpha}}{D^2},\quad e^{\gamma}=r^2(B+r^{2q})^2\frac{e^{\alpha}}{C^2},$$

with $s+1=q(2n^2-1)/n$, $Ck=2nqB$, $n^2D^2=2q^2(1-2n^2)$. We then have

$$8\pi p=\frac{e^{-\alpha}q^2(1-2n)}{r^2n^2}\cdot\frac{(1-2n)r^{2q}+(1+2n)B}{r^{2q}+B},$$

$$8\pi\rho=\frac{e^{-\alpha}q^2}{r^2n^2}\cdot\frac{(1-4n^2)r^{2q}+(1+4n^2)B}{r^{2q}+B},$$

$$8\pi T_1^4=-\frac{e^{-\alpha}4CBq^2}{r^3}\cdot\frac{(2n-1)r^{2q}+(2n^2-1)B}{(r^{2q}+B)^2},$$

$$w^1=Ee^{(-\alpha-\gamma)/2},$$

E is an arbitrary constant. This solution can give a finite constant radius of the interior boundary where p will vanish. If $r=a$ is to be the interior boundary, the

solution will be of physical significance only if

$$\text{(i)}\quad p=0 \text{ for } r=a; \tag{4.4}$$

$$\text{(ii)}\quad p>0 \text{ for } r<a; \tag{4.5}$$

$$\text{(iii)}\quad \rho>0 \text{ for } r\leq a. \tag{4.6}$$

These restrictions are satisfied by this solution if $B=-a^{2q}(1-2n)/(1+2n)$, q is negative, and $0<n<\frac{1}{2}$. For $\frac{1}{4}\leq n<\frac{1}{2}$, $\rho-3p$ will be nonnegative for $r\leq a$. It is now found that T_1^4 is negative for $r\leq a$ so that the product σw^1 is positive and we find

$$8\pi\sigma=\frac{e^{\frac{1}{2}(\gamma-\alpha)}4CBq^2}{E^2r^3}\cdot\frac{(2n-1)r^{2q}+(2n^2-1)B}{(r^{2q}+B)^3},$$

so that $\dot{\sigma}=0$. This last property is common to all our solutions.

Solution VIII

We have

$$e^\alpha=\frac{e^{-2kt}r^{2s}}{A^2(B+r^{2q})^{2n}},\quad e^\beta=(B+r^{2q})\frac{e^\alpha}{D^2},$$

$$e^\gamma=r^{2-4q}(B+r^{2q})^2e^\alpha/C^2$$

with $s+1=2nq$, $Ck=(1-2n)q$, $D^2=4Bq^2(2n^2-1)$.

We then have

$$8\pi p=4q^2(1-n)\frac{e^{-\alpha}}{r^2}\cdot\frac{nr^{2q}+(1-n)B}{r^{2q}+B},$$

$$8\pi\rho=4q^2(n-1)\frac{e^{-\alpha}}{r^2}\cdot\frac{3nr^{2q}+(n+1)B}{r^{2q}+B},$$

$$8\pi T_1^4=-\frac{4q^2(1-2n)(n-1)CBe^{-\alpha}}{r^{3-4q}(B+r^{2q})^3},$$

$$w^1=Ee^{-(\alpha+\gamma)/2}.$$

This solution can give a finite constant radius $r=a$ of the interior boundary; and the conditions (4.4), (4.5), (4.6) are satisfied if $B=na^{2q}/(n-1)$, q is positive, and n does not lie in the range $(-1, +1)$. It is now found that T_1^4 is positive for $r\leq a$. This makes σw^1 negative; and since we have begun with w^1 positive, this means that the solution gives negative values of σ within the sphere $r=a$. It appears, therefore, that the solution has no physical significance. But then, as given by the differential equation (3.12), w^1 always gets determined with an arbitrary multiplying constant and so the negative sign of the product σw^1 can as well be attributed to w^1 making σ positive. Of course, once we accept a negative value of w^1, the whole problem of solving Einstein's field equations has to be studied afresh. The distribution then would not be radiating energy, but it would be absorbing energy. The results of this paper will no longer hold because an absorbing distribution will not be isolated. This particular solution leads to quite new types of distributions—radiation absorbing distributions—allowed by the gravitational theory of Einstein. These new types of distributions are at present being investigated.[11]

Solution IX

We have

$$e^\alpha=\frac{e^{-2kt}}{A^2r^2(B+r^{2q})^{2n}},\quad e^\beta=(B+r^{2q})\frac{e^\alpha}{D^2},$$

$$e^\gamma=r^{2-4q}(B+r^{2q})^2e^\alpha/C^2,$$

with $Ck=(1-2n)q$, $D^2=-4q^2B$.

We then have

$$8\pi p=\frac{e^{-\alpha}}{r^2}\cdot\frac{4q^2B}{r^{2q}+B},$$

$$8\pi\rho=-\frac{e^{-\alpha}\cdot 4q^2B}{r^2(B+r^{2q})},$$

$$8\pi T_1^4=\frac{e^{-\alpha}4Cq^2(1-2n)}{r^{3-4q}}\cdot\frac{nr^{2q}+B}{(r^{2q}+B)^3}.$$

Here we have $\rho+p=0$. If the cosmological constant Λ is introduced, it will be found that DeSitter's static cosmological solution is a particular case of this solution obtained by putting $n=\frac{1}{2}$ here.

Solution IV

We have

$$e^\alpha=\frac{e^{-2kt}}{A^2r^2(B+r^{2q})^{2n}},\quad e^\beta=(B+r^{2q})^2r^{-4q}\frac{e^\alpha}{D^2},$$

$$e^\gamma=r^2(B+r^{2q})^2e^\alpha/C^2,$$

with $Ck=B(3-4n)q/(n-1)$, $D^2=4q^2(2n^2-1)$.

We then have

$$8\pi p=\frac{4q^2e^{-\alpha}}{r^2(B+r^{2q})^2}[(n-1)^2r^{4q}+Br^{2q}$$
$$-B^2(2n-1)(6n-5)/4(n-1)^2],$$

$$8\pi\rho=\frac{4q^2e^{-\alpha}}{r^2(B+r^{2q})^2}[(n^2-1)r^{4q}+Br^{2q}(1-6n)$$
$$+3B^2(2n-1)(6n-5)/4(n-1)^2],$$

$$8\pi T_1^4=\frac{4Cq^2e^{-\alpha}}{r^3(B+r^{2q})^3}B(3-4n)r^{2q}.$$

This solution can give a finite boundary $r=a$ and the conditions (4.4), (4.5), (4.6) are satisfied by (1) q is

[11] P. C. Vaidya, Nature **166**, 565 (1950).

negative, (2) $B=a^{2q}/x$ or $B=-a^{2q}/y$, where

$$x, y=\tfrac{1}{2}[(12n^2-16n+6)^{\frac{1}{2}}\mp 1]/(n-1)^2,$$

and (3) $1<n\leq 2$ when B is negative and $1<n\leq z$ when B is positive, where z is that root of the cubic

$$45z^3-123z^2+106z-31=0$$

which lies between 1 and 2. Under these conditions we have $\rho-3p\geq 0$ for $r\leq a$.

It is found that when B is positive, T_1^4 is negative, so that w^1 is positive and the distribution is a radiating one. It is further found that in this case $\rho-3p$ does not strictly decrease from $r=0$ to the value of ρ on the boundary, but that it attains a non-negative minimum value at a point within the distribution. When B is negative, T_1^4 is positive, so that the solution then represents a radiation-absorbing distribution.

V. THE EXTERIOR SOLUTION

The exterior solution of a radiating star describing a distribution of pure outflowing radiation has already been completely discussed elsewhere,[12] and we put down here the results of this solution that are useful for our present work. The line-element describing this field is

$$ds^2=\frac{-1}{1-2m/R}dR^2-R^2(d\theta^2+\sin^2\theta d\varphi^2)+\frac{\dot{m}^2}{f^2}\left(1-\frac{2m}{R}\right)dT^2, \quad (5.1)$$

where $m=m(R, T)$, $\dot{m}=\partial m/\partial T$, and $f=f(m)$ is an arbitrary function of m given by

$$(\partial m/\partial R)(1-2m/R)=f(m). \quad (5.2)$$

This solution is true for $R_i(T)\leq R\leq R_e(T)$, and it is continuous at $R=R_e(T)$ with the Schwarzschild's exterior solution

$$ds^2=-(1-2M/R)^{-1}dR^2-R^2(d\theta^2+\sin^2\theta d\varphi^2)+(1-2M/R)dT^2.$$

The continuity of $g_{\mu\nu}$ at $R=R_e(T)$ determines the function $R_e(T)$ and the arbitrary function $\varphi(T)$ of T which occurs when (5.2) is solved as a differential equation for m. It is found that $R_e(T)$ is given by

$$(dR_e/dT)=1-2M/R_e. \quad (5.3)$$

The function $f(m)$ is left arbitrary and will be determined by the conditions at the interior boundary $R=R_i(T)$. The energy-momentum tensor describing this zone of pure radiation is given by

$$T_\mu^\nu=\sigma w_\mu w^\nu, \quad w_\mu w^\mu=0, \quad (w^\mu)_{,\nu}w^\nu=0$$

and we have

$$\sigma=F(m)/4\pi r^2, \quad w^1=[f(m)/F(m)]^{\frac{1}{2}}, \quad (5.4)$$

$F(m)$ being another arbitrary function of m.

[12] P. C. Vaidya, Current Sci. (India) 12, 183 (1943); see reference 5. See also H. Mineur, Ann. école normale supér. Sér. 3, 5, 1 (1933).

Equation (5.2) for the function $m(R, T)$ can be readily solved in the particular case

$$f(m)=f=\text{a constant}.$$

If $f<\frac{1}{8}$ we find that

$$(m-xR)^j(m-yR)^k=\varphi(T) \quad (5.5)$$

satisfies (5.2) if

$$x, y=\tfrac{1}{4}(1\pm(1-8f)^{\frac{1}{2}}), \quad j, k=\tfrac{1}{2}(1\mp(1-8f)^{-\frac{1}{2}}).$$

The continuity of $g_{\mu\nu}$ at the exterior boundary determines $\varphi(T)$ to be

$$\varphi(T)=(M-xR_e)^j(M-yR_e)^k.$$

We are now ready to make the connection of our interior solution with this exterior solution over the boundary.

VI. CONNECTION BETWEEN THE INTERIOR AND THE EXTERIOR SOLUTIONS

Our interior solutions have been obtained with reference to the co-moving coordinates characterized by the line-element

$$ds^2=-e^\alpha dr^2-r^2e^\beta(d\theta^2+\sin^2\theta d\varphi^2)+e^\gamma dt^2, \quad (6.1)$$

while the exterior solution is developed in the coordinates (R, T) of the line-element,

$$ds^2=-e^\lambda dR^2-R^2(d\theta^2+\sin^2\theta d\varphi^2)+e^\nu dT^2. \quad (6.2)$$

The first problem then is to transform the coordinates (r, t) of (6.1) to the coordinates (R, T) of (6.2). As the general features of all the radiating distributions obtained here are the same, we illustrate the method of making the connection by taking a particular case of Solution III and connecting it with the exterior solution.

Detailed Consideration of a Particular Case of Solution III

We shall choose $n=\frac{1}{4}$ so that $\rho_c/p_c=3$, ρ_c being the central density and p_c being the central pressure. The solution then is

$$e^\alpha=\frac{e^{-2kt}\cdot r^{-7q}}{A^2r^2(B+r^{2q})^{\frac{1}{2}}}, \quad e^\beta=\frac{e^\alpha}{28q^2}, \quad e^\gamma=\frac{e^\alpha r^2(B+r^{2q})^2}{C^2}.$$

$$8\pi p=\frac{12q^2}{r^2}e^{-\alpha}\cdot\frac{r^{2q}-a^{2q}}{3r^{2q}-a^{2q}},$$

$$8\pi\rho=\frac{4q^2}{r^2}e^{-\alpha}\cdot\frac{9r^{2q}-5a^{2q}}{3r^{2q}-a^{2q}}, \quad (6.3)$$

$$8\pi\sigma=\frac{q^2a^{2q}}{18E^2C^2}(12r^{2q}-7a^{2q}),$$

$$v^1=v^2=v^3=0, \quad v^4=e^{-\gamma/2},$$

$$w^2=w^3=0, \quad w^1=Ee^{-(\alpha+\gamma)/2}, \quad w^4=Ee^{-\gamma}, \quad Ck=-qa^{2q}/6.$$

B is given in terms of the boundary radius by $B=-a^{2q}/3$ and we must take q to be negative.

It will be noted that the solution corresponds to a sphere of fluid of infinite density and pressure at the center, having at that point the ratio which would hold for disordered radiation or for particles of such high kinetic energy that their rest mass may be neglected in comparison with their total mass. Other ratios could of course be obtained with a different choice for the parameter n. The constant B is negative. As B approaches zero through negative values, the ratio of the pressure and the density approach $\frac{1}{3}$ throughout, the constant k approaches zero, and the sphere tends to be static and larger without limit.

We now transform this solution to the line-element (6.2). Let the equations of transformation be

$$R=R(r, t), \quad T=T(r, t).$$

The law of transformation of the tensor $g^{\mu\nu}$ leads to

$$e^{-\lambda}=R'^2e^{-\alpha}-\dot{R}^2e^{-\gamma}, \tag{6.4}$$

$$R^2=r^2e^{\beta}, \tag{6.5}$$

$$e^{-\nu}=-T'^2e^{-\alpha}+\dot{T}^2e^{-\gamma}, \tag{6.6}$$

$$0=-R'T'e^{-\alpha}+\dot{R}\dot{T}e^{-\gamma}. \tag{6.7}$$

Equation (6.5) immediately gives $R(r, t)$. Equation (6.7) can be integrated to find $T(r, t)$. It gives

$$(3)^{-7}r^{36q}(24r^{2q}-7a^{2q})^8(28A^2q^2)^{14}R^{28}\Psi(T)=1, \tag{6.8}$$

$\Psi(T)$ being an arbitrary function of T. The boundary $R=R_i(T)$ of the distribution is now easily obtained by putting $r=a$ in (6.8). We then find

$$(3)^{-7}(17)^8(28A^2q^2)^{14}a^{112q}R_i^{28}\Psi(T)=1, \tag{6.9}$$

so that

$$(1/\Psi)(\partial\Psi/\partial T)+(28/R_i)(\partial R_i/\partial T)=0. \tag{6.10}$$

The transformations of coordinates can now be completed. We find that

$$e^{\lambda}=7(3r^{2q}-a^{2q})/3(4r^{2q}-a^{2q}),$$

$$e^{\nu}=[112(3r^{2q}-a^{2q})^2a^{-4q}+e^{\lambda}](\partial\psi/\partial T)^2(R/28\psi)^2,$$

$$8\pi p=(9-14e^{-\lambda})/7R^2, \quad 8\pi\rho=(11-14e^{-\lambda})/7R^2,$$

$$8\pi\sigma=\frac{q^2a^{4q}}{18E^2C^2}\,\frac{16-21e^{-\lambda}}{7e^{-\lambda}-4}, \quad w^1=-\frac{3}{7q}\,\frac{EC}{a^{2q}}\,\frac{7e^{-\lambda}-4}{R},$$

$$v^1=-(7e^{-\lambda}-4)/2(28)^{\frac{1}{2}}.$$

Over the boundary $R=R_i(T)$ we have

$$e^{-\lambda}=9/14, \quad e^{\nu}=(448+14/9)(dR_i/dT)^2, \quad p=0,$$
$$8\pi\rho=2/7R_i^2, \quad 8\pi\sigma=5q^2a^{4q}/18E^2c^2, \quad v^1=-1/4(28)^{\frac{1}{2}}.$$

As v^1 is negative, it is clear that dR_i/dT is negative and so the distribution is a contracting one. We now connect this solution with the exterior solution (5.1). The connection is made through the continuity of $g_{\mu\nu}$, p, and σ at $R=R_i(T)$. The continuity of p is already obtained by making $p=0$ on $R=R_i$. The continuity of e^{λ} gives

$$m_i/R_i=5/28 \quad \text{or} \quad m(R_i, T)=(5/28)R_i, \tag{6.11}$$

so that m/R is a constant on the boundary. Equation (6.11) is an equation to determine $\Psi(T)$ once the form of the function $m(R, T)$ is known. The continuity of e^{ν} gives

$$[1/f(m_i)](\partial m/\partial T)_i=(14\times17/9)(dR_i/dT). \tag{6.12}$$

We now show that (6.11) and (6.12) together determine $f(m)$ as a constant. For that purpose we determine $(\partial m/\partial T)_i$, i.e., the value of $\partial m/\partial T$ when $R=R_i$, by differentiating (6.11) with regard to T:

$$(\partial m/\partial R_i)(dR_i/dT)+(\partial m/\partial T)_i = (5/28)(dR_i/dT). \tag{6.13}$$

But on using (5.2) we find that

$$\partial m/\partial R_i=(\partial m/\partial R)_i=(14/9)f(m_i),$$

and therefore (6.13) gives

$$f(m_i)=5/(28)^2.$$

Now m_i is not a constant, but $f(m_i)$ is a constant. This is possible only if the arbitrary function $f(m)$ is a constant. To complete the process of using the continuity of $g_{\mu\nu}$ at $R=R_i(T)$ we must now determine $m(R, T)$ of the exterior solution so that (6.11) may determine the arbitrary function $\Psi(T)$. As $f(m)$ is a constant $=5/(28)^2$, the form of the function $m(R, T)$ is the one given by (5.4). We find that

$$(m-xR)^i(m-yR)^h=(M-xR_e)^i(M-yR_e)^h; \quad x, y=\tfrac{1}{4}(1\pm(93/98)^{\frac{1}{2}}); \quad j, h=\tfrac{1}{4}(1\mp(98/93)^{\frac{1}{2}}). \tag{6.14}$$

M is a constant and $R_e=R_e(T)$ is the exterior boundary determined by

$$dR_e/dT=1-2M/R_e.$$

On the internal boundary $R=R_i(T)$ (6.14) and (6.11) give

$$R_i(5-28x)^i(5-28y)^h=28(M-xR_e)^i(M-yR_e)^h,$$

so that the arbitrary function $\Psi(T)$ now gets determined by

$$\Psi(T)=K(M-xR_e)^{-28i}(M-yR_e)^{-28h},$$
$$K=(3)^7(28)^{14}(17)^{-8}(Aq)^{-28}a^{-112q}(5-28x)^{28i}(5-28y)^{28h}.$$

Thus the continuity of $g_{\mu\nu}$ across $R=R_i(T)$ determines the function $f(m)$ of the exterior solution and the function $\Psi(T)$ of the interior solution. The only arbitrary function left undetermined in the scheme of our solutions is the function $F(m)$ of (5.4). This is now determined by the continuity of σ, the density of the flowing radiation across $R=R_i(T)$. For this continuity leads to

$$F(m_i)/4\pi R_i^2=5q^2a^{4q}/144\pi E^2c^2,$$

which is readily satisfied by

$$F(m)=[(14qa^{2q})^2/45E^2c^2]m^2.$$

This completes the connection of the solutions at the interior boundary.

VII. CONCLUSION

Here we have given the first complete nonstatic solution, holding from $R=0$ to $R=\infty$, representing an isolated spherically symmetric nonstatic distribution radiating out energy. There are two boundaries, the interior one and the exterior one, but we have been able to give a line-element whose coefficients are continuous throughout from $R=0$ to $R=\infty$. It has already been proved by the author[5] that in the case of a distribution with the line-element

$$ds^2=-e^{\lambda}dR^2-R^2(d\theta^2+\sin^2\theta d\varphi^2)+e^{\nu}dT^2,$$

the continuity of $g_{\mu\nu}$ alone is sufficient to insure that the total mass of the isolated distribution is conserved.

The solution discussed in detail in the last section shows that the corresponding material distribution is contracting, dR_i/dT being negative. But m_i/R_i is a constant, m_i being the mass of the distribution as observed from its external gravitational field. So the newtonian gravitational potential energy of the interior distribution remains constant and the contraction therefore is not gravitational. It seems to be a purely relativistic effect. The radiating distribution loses energy and so its mass decreases. But if m_i/R_i is to remain a constant, then R_i must also decrease. This may explain the contraction.

Some of the particular solutions derived here have suggested the existence of a new class of solutions of Einstein's field equation. These solutions would represent non-isolated spherically symmetric distributions absorbing energy from the cosmos. These are at present being investigated.

PHYSICAL REVIEW VOLUME 83, NUMBER 1 JULY 1, 1951

On the Ionization Yields of Fission Fragments*†

R. B. LEACHMAN‡
Institute for Atomic Research, Iowa State College, Ames, Iowa
(Received September 13, 1950)

The disagreement between the distributions in fission fragment mass and ionization is attributed to a variation in ionization yield with fragment mass and to a dispersion arising from such effects as neutron recoil and instrumental errors of ionization measurement. After the effects of dispersion in the available data of fragments from U^{235} slow neutron fission are taken into account, the variation in ionization yield is estimated from the remaining disagreement in distributions. For the most probable fission asymmetry, the energy-ionization ratio of light fragments is found to be approximately 3.7 percent less than for heavy fragments.

I. INTRODUCTION

A RECENT analysis[1] of the ionization produced by slow, heavy particles indicates that appreciable kinetic energy is lost to recoiling gas atoms having a reduced ionization efficiency. The resulting increase in the energy-ionization rate dE/dI as the heavy particle is stopped accounts for the ionization defect, the difference between the actual energy of the particle and the energy determined from the total ionization on the basis of $w=dE/dI$ of fast particles. Since the ionization defect increases with the mass of the particle, it is expected that w_H, the energy-ionization ratio obtained for complete stopping of a heavy fission fragment, is greater than w_L of a light fragment.

Any direct measure of w_L and w_H would require measurements of both the ionization and energy of individual fragments. Because fission fragments do not all have the same kinetic energy, mass and effective charge, energy measurements of individual fragments by such means as calorimetry, magnetic deflection or electrostatic deflection have not been feasible. From the momentum condition of fission and the measured mass distribution,[2] however, the distribution in the *relative* kinetic energies of the complementary light and heavy fragments can be determined quite accurately. In this investigation, a comparison of this energy ratio distribution with the corresponding ionization ratio distribution[3,4] is used to determine indirectly w_L/w_H for the slow neutron fission of U^{235}.

II. COMPARISON OF DISTRIBUTIONS

Method

Using double "back-to-back" ionization chambers, both Brunton and Hanna[3] and Deutsch and Ramsey[4] have made coincidence measurements of the number of ion pairs I_L and I_H (subscripts L and H always refer

* Work performed in the Ames Laboratory of the AEC.
† Details of this analysis are contained in ISC 98.
‡ Now at Los Alamos Scientific Laboratory, Los Alamos, New Mexico.
[1] Knipp, Leachman, and Ling, Phys. Rev. **80**, 478 (1950).
[2] Plutonium Project, Revs. Modern Phys. **18**, 513 (1946).
[3] D. C. Brunton and G. C. Hanna, Can. J. Research **A28**, 190 (1950).
[4] M. Deutsch and M. Ramsey, MDDC 945 (1946) (unpublished).

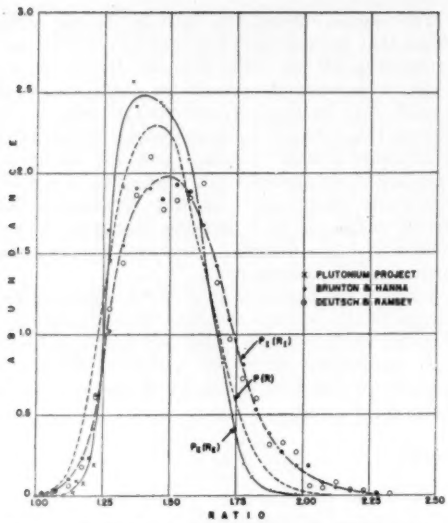

FIG. 1. Ratio distributions for fragments from U^{235} slow neutron fission. The ionization and energy ratio distributions, $P_I(R_I)$ and $P_E(R_E)$, are based on experimental data; the ionization energy ratio distribution $P(R)$ is calculated.

to the complementary light and heavy fragments) formed as fission fragments are stopped in a gas mixture of argon plus a few percent of carbon dioxide. From these data is obtained the distribution $P_I(R_I)$ in the ionization ratio $R_I=I_L/I_H$ shown in Fig. 1. Ionization data in this form can be compared directly with the only available energy data, the distribution $P_E(R_E)$ obtained from the fission momentum relation $R_E=E_L/E_H=m_H/m_L$. Although m_L and m_H are the fragment masses before neutron emission, the distribution in m_H/m_L can be obtained from the distribution in the measured[2] final masses (masses after neutron emission) by correcting for the mass of the emitted neutrons. Using the assumption that 1.25 neutrons are emitted from each fragment, an assumption that is later seen to give only a small error, together with representative points from the mass yield curve, we obtain the approximate $P_E(R_E)$ shown in Fig. 1.

The considerable difference between the ionization ratio data $P_I(R_I)$ and the corresponding energy ratio data $P_E(R_E)$, a difference much larger than the experimental uncertainties of the measurements,[5] is assumed to be due to, first, a broadening of $P_E(R_E)$ by the energy dispersion arising from instrumental errors of ionization measurement and from recoil due to the emission of prompt neutrons and, second, an expansion of this dispersed energy ratio distribution into an ionization ratio distribution of higher ratios due to a decrease of w_L/w_H with mass ratio.

In the quantitative determinations of the dispersion and of the decrease of w_L/w_H with mass, it is important to distinguish between the energy distributions and the ionization distribution being compared. The *ionizations* I_L and I_H are experimental data and so include the effects of dispersion. As such, they are representative of the *ionization energies* w_LI_L and w_HI_H. The ionization energies are distinguished from the *initial energies* E_L and E_H by the effect of dispersion, an initial energy being deviated into a larger or smaller ionization energy by the dispersion. Correspondingly, the distribution $P(R)$ in the ionization energy ratio $R=w_LI_L/w_HI_H$ differs from $P_E(R_E)$ by the effect of dispersion and from $P_I(R_I)$ by the variation in w_L/w_H. Since in this paper all distributions and dispersions are normalized to unity, the relation between $P_E(R_E)$ and $P(R)$ is

$$P(R)=\int_0^\infty dR_E D_r(R_E, R)P_E(R_E), \qquad (1)$$

and between $P(R)$ and $P_I(R_I)$ is

$$P_I(R_I)=P(R)[(w_L/w_H)+\alpha R_I] \qquad (2)$$

or

$$\int_1^{R_I} dR_I P_I(R_I)=\int_1^R dRP(R), \qquad (3)$$

where in Eq. (1) $D_r(R_E, R)$ is the distribution in the energy ratio deviation $(R-R_E)$ and in Eq. (2) $\alpha=[d(w_L/w_H)/dR_I]$. Equation (2) follows from the relations $P_I(R_I)dR_I=P(R)dR$ and $R=(w_L/w_H)R_I$.

The treatment of the distributions consists of, first, a calculation of $P(R)$ using an estimated dispersion $D_r(R_E, R)$ in Eq. (1) and, second, a determination of w_L/w_H by a comparison of $P(R)$ and $P_I(R_I)$ by Eqs. (2) or (3).

The Dispersion Width

The determination of the dispersion function $D_r(R_E, R)$ is aided by a comparison of $P_E(R_E)$ and $P_I(R_I)$ in the region of symmetrical fission, where the slight difference in complementary fragment masses minimizes the effect of the variations in w_L and w_H. In this region, it is to be expected[6] that the energy-ionization ratio is a slowly varying function of the fission asymmetry, such that w_L/w_H as a function of R_I linearly approaches unity as R_I approaches unity. On this basis, we require

$$w_L/w_H=1+\alpha(R_I-1), \quad \alpha=\text{constant}, \qquad (4)$$

in the region of symmetrical fission, where the dependence of w_L/w_H on such other factors as the total energy $E=E_L+E_H$ and the nuclear charge division is neglected. It is seen that the requirements on $D_r(R_E, R)$ are that it disperse $P_E(R_E)$ by Eq. (1) into a $P(R)$

[5] The points in the peak of the Brunton and Hanna ionization ratio distribution represent $1.2(10^6)$ observations. According to M. S. Freedman and E. P. Steinberg (CC 3420), most of the points of the Plutonium Project yield curve have a precision of about five percent.

[6] N. Bohr, Kgl. Danske Vid. Sels. Math.-Fys. Medd. **18**, No. 8 (1948).

which, when compared with $P_I(R_I)$ by Eqs. (2) or (3), satisfies the symmetrical fission requirements on w_L/w_H stated in Eq. (4).

Since the limited available data and the lack of sensitivity of this method make a completely analytical determination of $D_r(R_E, R)$ impractical, the method is used only to estimate the width of an assumed dispersion function. While it is not simple to anticipate directly the form of $D_r(R_E, R)$, it does seem reasonable that the form of the energy dispersions $D_L(E_L, w_L I_L)$ and $D_H(E_H, w_H I_H)$ in the light and heavy fragments should each be nearly gaussian. As illustrated in Fig. 2, these fragment energy dispersions combine into an energy ratio dispersion $D_r(R_E, R)$ and a total energy dispersion $D_T(E, w_L I_L + w_H I_H)$ through the geometric combination of the fragment energy deviations $e_L = w_L I_L - E_L$ and $e_H = w_H I_H - E_H$ into the energy ratio deviation $r = R - R_E$ and the total energy deviation $e = w_L I_L + w_H I_H - E$. By this analysis it can be shown that gaussian energy dispersions having energy deviations e_L and e_H negligible compared to E_L and E_H combine into a gaussian ratio dispersion and a gaussian total energy dispersion.

Various trial values of the ratio dispersion width δr (all widths are full widths at half maximum) have been used in Eq. (1) with the gaussian dispersion

$$D_r(R_E, R) \propto \exp[-(4)(0.69)\{(R_E - R)/\delta r\}^2]$$

to obtain the trial $P(R)$ distributions shown for the region of symmetrical fission in Fig. 3. In order to determine the most suitable dispersion width, these trial ionization energy ratio distributions $P(R)$ were compared with $P_I(R_I)$ by Eq. (2). The width $\delta r = 0.10$ was found to be too narrow; α fluctuated from a large positive value near symmetrical fission to negative values at greater ratios. The width $\delta r = 0.18$ was found to be too broad; α was a large negative value near symmetrical fission but small at greater ratios. The width $\delta r = 0.14$ with its consequent $\alpha \cong -0.10$ was found to give the least fluctuation. The disagreement at 1.025 in Fig. 3 is either due to inadequate data or to the use of a dispersion function with too large a tail.

Variation of w_L/w_H

In order to apply $D_r(R_E, R)$ to all degrees of asymmetry, its change in width with fission asymmetry must be determined. An estimate of the possible extremes of this asymmetry dependence is possible by assuming that the dispersion is predominantly due to either (1) instrumental errors or (2) neutron recoil. The characteristics of the true dispersion is expected to be between these extremes. With the extreme (1), the widths of the fragment energy dispersions D_L and D_H are expected to be nearly equal and constant. It can be shown that under these conditions δr varies as $(R_E^2+1)^{\frac{1}{2}}(R_E+1)/E$. On the other hand, the effect of the recoil of an isotropic emission of neutrons from the moving fragments increases the width of D_L as $(R_E)^{\frac{1}{2}}$ and decreases the width of D_H as $(R_E)^{-\frac{1}{2}}$. On this basis, δr varies as $(2R_E)^{\frac{1}{2}}(R_E+1)/E$ for the extreme (2). These extremes result in $P(R)$ distributions that differ insignificantly.

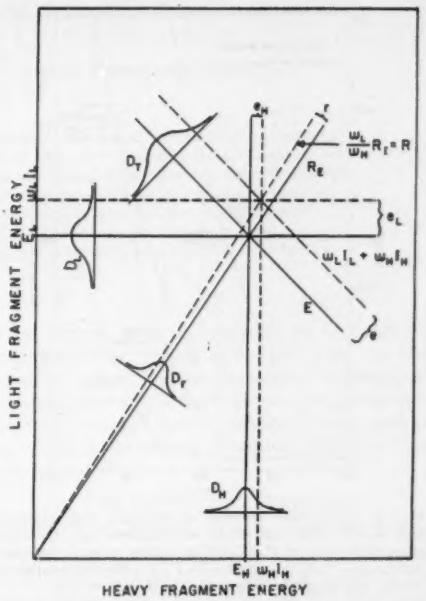

FIG. 2. Illustration of the energy quantities associated with two complementary fragments. Deviations change the initial energy quantities (solid lines) into ionization energy quantities (dotted lines). Possible dispersion functions of deviations are sketched.

When the symmetrical fission gaussian dispersion width $\delta r = 0.14$ varying within the above extremes is used in Eq. (1), the $P(R)$ distribution in Fig. 1 is obtained. When compared with $P_I(R_I)$ by Eq. (3), this calculated $P(R)$ results in the approximate variation of w_L/w_H shown in Fig. 4.

III. DISCUSSION

The variation of w_L/w_H in Fig. 4 can be used with the assumption that the ionization defects Δ_L and Δ_H vary roughly as the fragment mass to obtain an estimate of the ionization defect. From the definition of the ionization defects

$$\Delta_L = w_L I_L - wI_L, \quad \Delta_H = w_H I_H - wI_H$$

it follows that

$$\frac{w_L}{w_H} = \frac{1+(\Delta_L/wI_L)}{1+(\Delta_H/wI_H)},$$

from which it is found that the total ionization defect

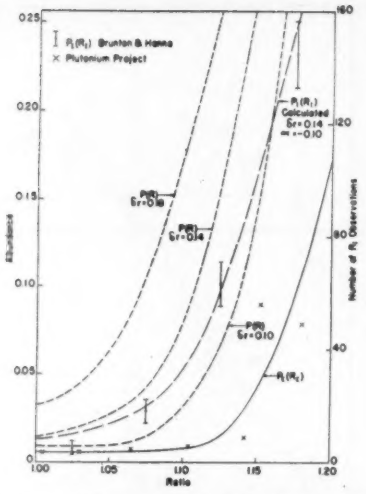

FIG. 3. Comparison of ratio distributions near symmetrical fission of U^{235}. The trial $P(R)$ distributions were obtained by various dispersions of $P_E(R_E)$. Comparison is made between the experimental $P_I(R_I)$ points and the $P_I(R_I)$ distribution calculated from the best determination of $D_r(R_E, R)$ and w_L/w_H.

for the most probable fission asymmetry is about 6 or 7 Mev. Since this essentially is energy unobserved as ionization, it should be added to the 155.8-Mev ionization chamber measurement[3] of the average kinetic energy of fission, bringing it into better agreement with the 165±8-Mev calorimetric measurement.[7] This estimate of the total ionization defect should be compared with the value of 6.7 Mev calculated[1] from properties of the recoil gas atoms.

Other estimates of the magnitude of the components of the dispersion are in reasonable agreement with the width determined here by distribution comparison. The width $\delta r = 0.14$ corresponds to an 8.1-Mev symmetrical fission dispersion width of D_L and D_H. These fragment energy dispersions are composed of the 2.5- and 5-Mev channel widths used by Brunton and Hanna, the several other additional ionization chamber instru-

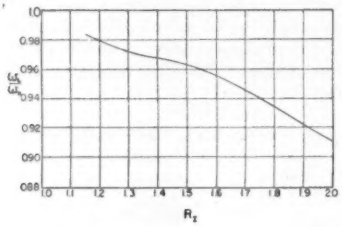

FIG. 4. Curve of the relative energy ionization ratio for light and heavy fragments.

[7] M. C. Henderson, Phys. Rev. **58**, 774 (1940).

TABLE I. Comparison of the energy distribution widths including dispersion with energy widths (without dispersion) calculated on the basis of the estimated dispersion being due predominantly to either (1) instrumental errors or (2) neutron recoil. Data are for the slow neutron fission of U^{235}.

	Width observed by Brunton-Hanna	Calculated energy width from dispersion (1)	Calculated energy width from dispersion (2)
Light fragment energy	12 Mev	8.8 Mev	7.0 Mev
Heavy fragment energy	20	18.3	18.8
Total energy at $R_I=1.2$	30	27.7	27.7
Total energy at $R_I=1.5$	20	16.4	16.1
Total energy at $R_I=2.0$	15	9.6	8.3

mental errors of less than 2-Mev width and the contribution of neutron recoil. On the basis of the average neutron energy found by Wilson,[8] the recoil energies of the fragments are $\pm 2.4(R_E)^{\frac{1}{2}}$ Mev and $\pm 2.4(R_E)^{-\frac{1}{2}}$ Mev for the backward and forward emission of a neutron from the light and heavy fragments, respectively. The combination of these estimated components results in a composite energy dispersion width somewhat less than that obtained by distribution comparison.

Although the determination of the dispersion by distribution comparison is not precise, it is interesting to note that the energy distributions observed by ionization are appreciably narrowed when this dispersion is removed by calculation. The calculated energy widths (widths without dispersion) in Table I are based on the approximation that all dispersions and distributions are gaussian in form.

Any explanation of the difference between $P_E(R_E)$ and $P_I(R_I)$ based on the assumption of a unity value of w_L/w_H for asymmetric fission requires the use of a decidedly asymmetric dispersion function. This possibility seems very unlikely in view of the nature of the instrumental errors and the measurements of DeBenedetti *et al.*,[9] which show that neutron emission from the moving fragments is not strongly preferential in direction. Actually, since any variation in the number of neutrons emitted per fragment tends to broaden the true $P_E(R_E)$ into the approximate distribution based on fragment mass measurements, the true difference between $P_E(R_E)$ and $P_I(R_I)$ can be slightly larger than indicated by the approximate $P_E(R_E)$ in Fig. 1. By taking 0.5 as a reasonable estimate of the dispersion width in the number of neutrons emitted per fragment, we find that the resulting mass ratio dispersion width of 0.01 broadens the true $P_E(R_E)$ by an amount small compared to the estimated energy dispersion width of 0.14.

The author is very grateful to Professor J. K. Knipp for many valuable suggestions and criticisms on this paper.

[8] R. R. Wilson, Phys. Rev. **72**, 189 (1947).
[9] DeBenedetti, Francis, Preston, and Bonner, Phys. Rev. **74**, 1645 (1948).

On the Nucleon Cascade with Ionization Loss

H. MESSEL
School of Theoretical Physics, Dublin Institute for Advanced Studies, Dublin, Ireland
(Received October 25, 1950)

The fundamental equations for a nucleon cascade including ionization loss are given. Solutions satisfying the exact boundary conditions are found in a manner similar to that used by Bhabha and Chakrabarty for the electron-photon cascade. However, in the present treatment, second-order equations are not resorted to and all four cases (protons producing protons and neutrons; neutrons producing protons and neutrons) are treated simultaneously. The results are given in tabular and graphic form and can be adapted easily to any specific problem. A number of examples showing the effect of ionization loss have been computed and the ratio of neutrons to protons given. The calculations are carried out using the cross section formulated by Heitler and Jánossy.

I. INTRODUCTION

IN a series of recent papers[1-5] the theory of the nucleon cascade has been developed and compared with experiment. In the cited papers adequate treatments have been given for the deduction of the expressions for average numbers and the fluctuations to be expected from the average, both for homogeneous nuclear matter and inhomogeneous matter. However, so far no detailed treatment of the problem has been given when ionization losses are taken into consideration.

In the present paper the cascade equations are given for protons and neutrons taking into account ionization losses, and exact solutions are found satisfying the correct boundary conditions. We retain the assumptions regarding the form of the cross section, made in the papers mentioned above. Since little is still known regarding the exact behavior of the nucleon cross sections at low energies, the solutions found will in all probability be out by a large factor in this region.

When the nucleon cascade is considered as a proton-neutron cascade with ionization loss, then the problem immediately becomes analogous to that for the electron-photon cascade. It is natural therefore to treat the problem of the nucleon cascade in a manner analogous to that which Bhabha and Chakrabarty[6,7] used for the electron-photon cascade. There have appeared a number of criticisms of the Bhabha-Chakrabarty solution;[8,9] however, we feel that these criticisms deal with minor points only and apply at most to the low energy region where no theory so far can claim success.

Though the solution of the electron-photon cascade with ionization loss obtained by Bhabha and Chakrabarty is elegant in many respects, we feel that the extreme simplicity underlying its derivation has been somewhat obscured. We give a treatment which appears to be straightforward, without resorting to second-order equations. Numerical results and several examples are given, showing the effects of taking ionization losses into account.

II. THE DIFFUSION EQUATIONS

Let $S^{(i,k)}(E,\theta)dE$ be the average number of protons or neutrons (depending on the suffix k) in the energy range E, $E+dE$ at a depth θ in inhomogeneous matter, due to a primary particle of energy E_0. The suffix $i=1,2$ refers to the primary particle and $k=1,2$ to the secondary. The number 1 always refers to a proton and 2 to a neutron. The ionization loss β is assumed to be independent of energy and is taken to be equal to 130 Mev per 65 g/cm² air throughout the problem.

We define $V(E/E')dE/E'$ as the probability that a nucleon of energy E' falling on a nucleus gives rise to one or more nucleons, and that one of the emerging nucleons has an energy in the interval E, $E+dE$. The function $V(E/E')$ has been determined by Jánossy and Messel[3] and we use their result. The fundamental equations can now be written as

$$\frac{\partial}{\partial\theta}S^{(i,k)}(E,\theta)+S^{(i,k)}(E,\theta)=\tfrac{1}{2}\int_0^\infty\{S^{(i,k)}(E',\theta)+S^{(i,3-k)}(E',\theta)\}\times V(E/E')\frac{dE'}{E'}+\delta_{1,k}\beta\frac{\partial}{\partial E}S^{(i,k)}(E,\theta). \quad (1)$$

We take the Mellin transform of (1) with respect to (E/E_0), and in order to keep the transform dimensionless we let

$$P^{(i,k)}(s,\theta)=\int_0^\infty(E/E_0)^{s-1}S^{(i,k)}(E,\theta)dE. \quad (2)$$

There then results

$$\frac{\partial}{\partial\theta}P^{(i,k)}(s,\theta)+A(s)P^{(i,k)}(s,\theta)+B(s)P^{(i,3-k)}(s,\theta)=-\delta_{1,k}(\beta/E_0)(s-1)P^{(i,k)}(s-1,\theta), \quad (2a)$$

[1] W. Heitler and L. Jánossy, Proc. Phys. Soc. (London) A62, 374 (1949).
[2] H. Messel, Proc. Roy. Irish Acad. A 54, 125 (1951).
[3] L. Jánossy and H. Messel, Proc. Roy. Irish Acad. A 54, 245 (1951).
[4] H. Messel and D. M. Ritson, Proc. Phys. Soc. (London) (1950) A 63, 1359 (1950).
[5] P. Budini and N. Dallaporta, Nuovo Cimento 7, 3 (1950).
[6] H. J. Bhabha and S. K. Chakrabarty, Proc. Roy. Soc. A181, 267 (1943).
[7] H. J. Bhabha and S. K. Chakrabarty, Phys. Rev. 74, 1352 (1948).
[8] I. E. Tamm and S. Belenky, Phys. Rev. 70, 660 (1946).
[9] H. S. Snyder, Phys. Rev. 76, 1563 (1949).

where

$$\left.\begin{aligned} V(s)&=\int_0^\infty u^{s-1}V(u)du, \\ V(s)&=2[1-(1+D_A\alpha_s)\exp(-D_A\alpha_s)]/(D_A\alpha_s)^2 \end{aligned}\right\} \quad (2b)$$

$$A(s)=1-\tfrac{1}{2}V(s), \quad B(s)=-\tfrac{1}{2}V(s), \quad (2c)$$

$$\alpha_s=\int_0^\infty\int_0^\infty (1-\epsilon_1^{s-1}-\epsilon_2^{s-1})w(\epsilon_1,\epsilon_2)d\epsilon_1 d\epsilon_2, \quad (2d)$$

$$w(\epsilon_1,\epsilon_2)=15\epsilon_2^2(1-\epsilon_1). \quad (2e)$$

[See the references given in Sec. I for details of the cross section given in (2d) and (2e).]

In (2b) D_A is the number of collisions suffered by a nucleon on traversal of a nucleus (of atomic weight A) along the nuclear diameter; D_A was taken equal to 2.41 for air in the previous publications mentioned above. The solution of (2a) is immediately given by

$$P^{(i,k)}(s,\theta)=P_0^{(i,k)}(s,\theta)-(\beta/E_0)(s-1)\times\int_0^\theta P_0^{(1,k)}(s,\theta-\theta')P^{(i,1)}(s-1,\theta')d\theta', \quad (3)$$

where $P_0^{(i,k)}(s,\theta)$ is the solution of the homogeneous part of (2a), i.e., of

$$\frac{\partial}{\partial\theta}P^{(i,k)}(s,\theta)+A(s)P^{(i,k)}(s,\theta)+B(s)P^{(i,3-k)}(s,\theta)=0. \quad (4)$$

From (2), (4), and the initial condition

$$S^{(i,k)}(E,0)=\begin{cases}\delta(E-E_0) & \text{for } i=k\\ 0 & \text{for } i\neq k,\end{cases}$$

it is easily shown that

$$P_0^{(i,k)}(s,\theta)=\tfrac{1}{2}\{\exp[-(1-V(s))\theta]\pm\exp(-\theta)\}\begin{matrix}\text{plus sign for } i=k\\ \text{minus sign for } i\neq k.\end{matrix} \quad (5)$$

That (3) is a solution of (2a) is most readily seen by substituting (3) directly into (2a) and seeing that (2a) is satisfied.

Next let us write

$$P^{(i,k)}(s,\theta)=\sum_{n=0}^\infty P_n^{(i,k)}(s,\theta)(-\beta/E_0)^n. \quad (6)$$

We substitute (6) into (3), equate equal powers of (β/E_0) and find the recursion formula

$$P_n^{(i,k)}(s,\theta)=(s-1)\int_0^\theta P_0^{(1,k)}(s,\theta-\theta')P_{n-1}^{(i,1)}(s-1,\theta')d\theta'. \quad (7)$$

Keeping in mind definition (2), we invert the Mellin transform and find

$$S^{(i,k)}(E,\theta)=\frac{1}{2\pi i}\frac{1}{E_0}\int_C\left(\frac{E_0}{E}\right)^s\times\left\{\sum_{n=0}^\infty P_n^{(i,k)}(s,\theta)(-\beta/E_0)^n\right\}ds. \quad (8)$$

The $(n+1)$th term of (8) is given by

$$\frac{1}{2\pi i}\frac{1}{E_0}\int_C\left(\frac{E_0}{E}\right)^s P_n^{(i,k)}(s,\theta)(-\beta/E_0)^n ds=\frac{1}{2\pi i}\frac{1}{E_0}(-\beta)^n\int_C\frac{E_0^{s-n}}{E^s}P_n^{(i,k)}(s,\theta)ds. \quad (9)$$

Replacing $s-n$ by s and shifting back the path of integration, we find the $(n+1)$th term is given by the expression

$$\frac{1}{2\pi i}\frac{1}{E_0}(-\beta/E)^n\int_C\left(\frac{E_0}{E}\right)^s P_n^{(i,k)}(s+n,\theta)ds. \quad (10)$$

Hence (8) can be written as

$$S^{(i,k)}(E,\theta)=\frac{1}{2\pi i}\frac{1}{E_0}\int_C\left(\frac{E_0}{E}\right)^s\times\left\{\sum_{n=0}^\infty(-\beta/E)^n P_n^{(i,k)}(s+n,\theta)\right\}ds. \quad (11)$$

We omit here the detailed mathematical proof that (11) is absolutely and uniformly convergent for $E>\beta\theta$, since the proof is entirely ananlogous to that given both by Iyengar[10] and Bhabha and Chakrabarty.[7]

For convenience we now write (11) as

$$S^{(i,k)}(E,\theta)=\frac{1}{2\pi i}\frac{1}{E_0}\int_C\left(\frac{E_0}{E}\right)^s\times\left\{\sum_{n=0}(-\beta/E)^n\frac{\Gamma(s+n)}{\Gamma(s)}Q_n^{(i,k)}(s,\theta)\right\}ds, \quad (12)$$

where

$$[\Gamma(s+n)/\Gamma(s)]Q_n^{(i,k)}(s,\theta)=P_n^{(i,k)}(s+n,\theta). \quad (12a)$$

Now let us define

$$g^{(i,k)}(s,\theta)=Q_1^{(i,k)}(s,\theta)/Q_0^{(i,k)}(s,\theta) \quad (13)$$

and

$$f_n^{(i,k)}(s,\theta)=\left\{Q_0^{(i,k)}(s,\theta)\frac{[g^{(i,k)}(s,\theta)]^n}{n!}-Q_1^{(i,k)}(s,\theta)\frac{[g^{(i,k)}(s,\theta)]^{n-1}}{(n-1)!}+\cdots\right\}. \quad (14)$$

[10] K. S. K. Iyengar, Proc. Indian Acad. Sci. **A15**, 195 (1942).

We write the integrand of (12) as follows:

$$E_0^s \sum_{n=0}^{\infty} (-\beta)^n \frac{\Gamma(s+n)}{\Gamma(s)} \frac{Q_n^{(i,k)}(s,\theta)}{\{(E+\beta g^{(i,k)}(s,\theta))-\beta g^{(i,k)}(s,\theta)\}^{n+s}}$$

and expand

$$\{(E+\beta g^{(i,k)}(s,\theta))-\beta g^{(i,k)}(s,\theta)\}^{n+s}$$

in powers of

$$\beta g^{(i,k)}(s,\theta)/(E+\beta g^{(i,k)}(s,\theta)).$$

Rearranging the resultant double series (this can be done since the double series is absolutely convergent) yields

$$S^{(i,k)}(E,\theta)=\frac{1}{2\pi i}\frac{1}{E_0}\int_C \left(\frac{E_0}{E+\beta g^{(i,k)}(s,\theta)}\right)^s \times\left\{\sum_{n=0}^{\infty}\left(\frac{\beta}{E+\beta g^{(i,k)}(s,\theta)}\right)^n \frac{\Gamma(s+n)}{\Gamma(s)} f_n^{(i,k)}(s,\theta)\right\} ds. \quad (15)$$

The solution (15) is now entirely analogous to that given by Bhabha and Chakrabarty for the electron-photon cascade; however, in the present development the complete four cases are covered (proton-proton, proton-neutron, neutron-neutron and neutron-proton). In order to find the expression for integral spectra we integrate (15) from E to E_0 and find

$$N^{(i,k)}(E,\theta)=\sum_{n=0}^{\infty} N_n^{(i,k)}(E,\theta) \quad (16)$$

with

$$N_n^{(i,k)}(E,\theta)=\frac{1}{2\pi i}\int_C \frac{1}{s+n-1}\left(\frac{E_0}{\beta}\right)^{s-1} \times\left(\frac{\beta}{E+\beta g^{(i,k)}(s,\theta)}\right)^{s+n-1} \frac{\Gamma(s+n)}{\Gamma(s)} f_n^{(i,k)}(s,\theta) ds. \quad (17)$$

The integration of (17) is carried out along a line parallel to the imaginary axis running from $s_0-i\infty$ to $s_0+i\infty$ with $s_0>1$.

The solution is now complete and appears in the form of a series. However, as was shown by Bhabha and Chakrabarty, it suffices for all practical purposes to take the first two terms of the series, and for many cases where we are considering particles above a given energy E, which is not too small, the first term suffices. It should be noted that at present we are not justified in considering particles with energies which are very low, because it is precisely in this region that we know little of the true behavior of a nucleon cross section.

III. DETERMINATION OF $g^{(i,k)}(s,\theta)$ AND $f_n^{(i,k)}(s,\theta)$

From the definitions (13) and (14) and the recurrence relation (7) explicit expressions for the $g^{(i,k)}(s,\theta)$ can easily be obtained. We give here only the results of the integration.

$$g^{(i,k)}(s,\theta)=\left\{\pm\theta\exp(-\theta)+\sum_{\nu=0}^{2} A_\nu^{(i,k)}(s)\exp[(u_\nu(s)\theta)]\right\} \times\{P_0^{(i,k)}(s,\theta)\}^{-1} \quad \begin{matrix}\text{plus sign for } i=k\\ \text{minus sign for } i\neq k,\end{matrix} \quad (18)$$

where

$$\left.\begin{aligned} u_0(s)&=-1,\\ u_1(s)&=-(1-V(s)),\\ u_2(s)&=-(1-V(s+1)),\end{aligned}\right\} \quad (18a)$$

$$\left.\begin{aligned} A_0^{(2,2)}(s)&=-A_0^{(1,1)}(s)=\frac{V(s)+V(s+1)}{4V(s)V(s+1)},\\ A_1^{(2,1)}(s)&=A_1^{(1,1)}(s)=\frac{2V(s)-V(s+1)}{4V(s)[V(s)-V(s+1)]},\\ A_2^{(1,2)}(s)&=A_2^{(1,1)}(s)\\ &=\frac{V(s)-2V(s+1)}{4V(s+1)[V(s)-V(s+1)]},\\ A_0^{(2,1)}(s)&=-A_0^{(1,2)}(s)=\frac{V(s)-V(s+1)}{4V(s)V(s+1)},\\ A_1^{(2,2)}(s)&=A_1^{(1,2)}(s)=\frac{V(s+1)}{4V(s)[V(s)-V(s+1)]},\\ A_2^{(2,2)}(s)&=A_2^{(2,1)}(s)\\ &=\frac{-V(s)}{4V(s+1)[V(s)-V(s+1)]}.\end{aligned}\right\} \quad (18b)$$

For real s greater than 0.1 the terms proportional to $\exp(-\theta)$ are negligible for all except very small θ; hence to a good approximation the first two terms of (18) can be dropped. Using this simplifying approximation we find

$$g^{(i,k)}(s,\theta)=2\{A_1^{(i,k)}(s)+A_2^{(i,k)}(s) \times\exp(-[V(s)-V(s+1)]\theta)\}. \quad (19)$$

The values of $f_n^{(i,k)}(s,\theta)$ can also be easily obtained by simply using the recursion relations. The work involved in finding $f_1^{(i,k)}(s,\theta)$ is not as great as would appear since one can readily utilize the numerical work completed in finding $Q_1^{(i,k)}(s,\theta)$. We do not carry out the evaluation for the second term of the series, since at present we do not feel that such a refinement is justified.

IV. EVALUATION AND NUMERICAL RESULTS

In Tables I and II we have tabulated the functions $g^{(1,1)}(s,\theta)$ and $g^{(1,2)}(s,\theta)$ for a wide range of s-values

TABLE I. The quantity $g^{(1,1)}(s, \theta)$ as a function of s for various constant values of the depth in air, θ. θ is measured in units of 65 g/cm².

$s \backslash \theta$	1	2	4	6	8	10	15	20
0.1	0.318	0.308	0.307	0.307	0.307	0.307	0.307	0.307
0.2	0.462	0.467	0.458	0.458	0.458	0.458	0.458	0.458
0.3	0.587	0.654	0.640	0.638	0.637	0.637	0.637	0.637
0.4	0.682	0.847	0.850	0.844	0.843	0.843	0.843	0.843
0.5	0.752	1.024	1.083	1.069	1.073	1.072	1.072	1.072
0.6	0.802	1.177	1.325	1.328	1.326	1.325	1.325	1.325
0.7	0.839	1.303	1.565	1.595	1.598	1.599	1.600	1.600
0.8	0.867	1.405	1.791	1.864	1.882	1.889	1.895	1.895
0.9	0.889	1.488	1.998	2.130	2.174	2.192	2.209	2.212
1.0	0.905	1.556	2.185	2.385	2.464	2.501	2.538	2.548
1.1	0.918	1.611	2.350	2.627	2.749	2.809	2.879	2.901
1.2	0.929	1.656	2.496	2.850	3.024	3.113	3.226	3.268
1.3	0.937	1.694	2.625	3.056	3.286	3.407	3.574	3.644
1.4	0.944	1.726	2.737	3.243	3.534	3.689	3.920	4.026
1.5	0.950	1.752	2.836	3.414	3.768	3.959	4.258	4.409
1.6	0.955	1.775	2.923	3.569	3.986	4.213	4.586	4.790
1.7	0.959	1.794	3.000	3.709	4.191	4.454	4.905	5.165
1.8	0.963	1.811	3.068	3.837	4.381	4.680	5.210	5.531
1.9	0.966	1.826	3.128	3.952	4.559	4.892	5.501	5.887
2.0	0.969	1.839	3.182	4.057	4.724	5.090	5.778	6.231
2.1	0.971	1.850	3.230	4.153	4.879	5.276	6.041	6.563
2.2	0.973	1.860	3.273	4.240	5.023	5.450	6.290	6.880
2.3	0.975	1.869	3.312	4.319	5.157	5.613	6.525	7.184
2.4	0.976	1.876	3.347	4.392	5.283	5.766	6.749	7.474
2.5	0.978	1.884	3.379	4.459	5.401	5.909	6.958	7.751
2.6	0.979	1.890	3.409	4.520	5.512	6.045	7.165	8.014
2.7	0.981	1.896	3.434	4.576	5.615	6.170	7.343	8.264
2.8	0.982	1.901	3.459	4.629	5.713	6.289	7.520	8.502
2.9	0.983	1.906	3.480	4.677	5.805	6.401	7.687	8.727
3.0	0.984	1.910	3.501	4.721	5.891	6.506	7.844	8.941

TABLE II. The quantity $g^{(1,2)}(s, \theta)$ as a function of s for various constant values of the depth in air, θ. θ is measured in units of 65 g/cm².

$s \backslash \theta$	1	2	4	6	8	10	15	20
0.1	0.033	0.032	0.031	0.031	0.031	0.031	0.031	0.031
0.2	0.062	0.069	0.065	0.065	0.065	0.065	0.065	0.065
0.3	0.095	0.118	0.118	0.117	0.117	0.117	0.117	0.117
0.3	0.130	0.179	0.193	0.191	0.190	0.190	0.190	0.190
0.5	0.162	0.243	0.287	0.289	0.288	0.288	0.287	0.287
0.6	0.192	0.306	0.393	0.409	0.411	0.410	0.410	0.410
0.7	0.219	0.366	0.505	0.545	0.557	0.558	0.559	0.559
0.8	0.244	0.420	0.615	0.690	0.720	0.727	0.733	0.733
0.9	0.265	0.469	0.720	0.837	0.896	0.916	0.931	0.935
1.0	0.285	0.513	0.819	0.983	1.077	1.113	1.151	1.161
1.1	0.302	0.552	0.910	1.122	1.257	1.317	1.387	1.409
1.2	0.317	0.588	0.993	1.253	1.433	1.522	1.635	1.677
1.3	0.331	0.619	1.069	1.375	1.602	1.723	1.890	1.960
1.4	0.343	0.647	1.137	1.488	1.762	1.917	2.147	2.253
1.5	0.355	0.673	1.199	1.592	1.911	2.102	2.402	2.553
1.6	0.365	0.696	1.255	1.687	2.050	2.278	2.651	2.854
1.7	0.374	0.716	1.306	1.774	2.180	2.443	2.894	3.154
1.8	0.382	0.735	1.352	1.854	2.299	2.597	3.128	3.449
1.9	0.389	0.752	1.394	1.927	2.408	2.741	3.351	3.737
2.0	0.396	0.767	1.432	1.993	2.510	2.876	3.563	4.017
2.1	0.402	0.782	1.467	2.055	2.603	3.001	3.765	4.287
2.2	0.408	0.794	1.498	2.111	2.689	3.116	3.955	4.546
2.3	0.413	0.806	1.528	2.163	2.768	3.223	4.135	4.794
2.4	0.418	0.817	1.555	2.210	2.840	3.323	4.307	5.031
2.5	0.422	0.827	1.580	2.254	2.908	3.416	4.464	5.257
2.6	0.427	0.837	1.603	2.295	2.970	3.503	4.623	5.472
2.7	0.430	0.845	1.623	2.332	3.027	3.582	4.754	5.675
2.8	0.434	0.853	1.644	2.368	3.081	3.656	4.888	6.869
2.9	0.437	0.860	1.661	2.400	3.130	3.726	5.012	6.052
3.0	0.440	0.867	1.679	2.429	3.176	3.790	5.129	6.226

and eight different values of the depth θ. The evaluation for small depths was carried out using the exact expression (18); however, for $\theta \geq 10$ we used the simplified expression given by (19). It will be noted from (18), (18a) and (18b) that the value of $g^{(i,k)}(s, \theta)$ remains finite for all positive s and θ values.

In order to evaluate $N^{(i,k)}(E, \theta)$ we may use a single saddle integration on the $N_n{}^{(i,k)}(E, \theta)$, yielding:

$$N_n{}^{(i,k)}(E, \theta) = [-2\pi J''(s_n, \theta)]^{-\frac{1}{2}} \exp[-J(s_n, \theta)], \quad (20)$$

where

$$-J(s, \theta) = (s-1)\ln(E_0/\beta) + (s+n-1)\ln[\beta/E+\beta g^{(i,k)}(s, \theta)] - \ln(s+n-1) + \ln\Gamma(s+n) - \ln\Gamma(s) + \ln[f_n(i, k)(s, \theta)], \quad (21)$$

and

$$J''(s_n, \theta) = \{\partial^2 J(s, \theta)/\partial s^2\}_{s=s_n}. \quad (21a)$$

The saddle point, s_n, is determined by the relation

$$\partial J(s, \theta)/\partial s = 0 \quad (22)$$

i.e., from

$$\ln(E_0/\beta) - \frac{1}{s+n-1} + \frac{\partial}{\partial s}[\ln\Gamma(s+n) - \ln\Gamma(s)] + \frac{\partial}{\partial s}\ln[f_n{}^{(i,k)}(s, \theta)] + \left\{\ln\frac{\beta}{E+\beta g^{(i,k)}(s, \theta)} - (s+n-1)\frac{\beta}{E+\beta g^{(i,k)}(s, \theta)}\frac{\partial}{\partial s}g^{(i,k)}(s, \theta)\right\} = 0. \quad (23)$$

In carrying out the evaluation of (23) it will be noted that for $E \gg \beta$ the second term in the last set of brackets in (23) can be neglected without appreciable error; however, for E equal to or of the order of β, it cannot be neglected. This difficulty is remedied by noting that the saddle point, s_n, varies only very slowly with E and thus

$$\{\beta/[E+\beta g^{(i,k)}(s, \theta)]\}^{s+n-1}$$

can be treated as a slowly varying factor (in comparison with $f_n{}^{(i,k)}(s, \theta)$). It can thus be removed from the expression for $J(s, \theta)$ and treated as a purely multiplicative factor, evaluated at the points $s = s_n$, where s_n

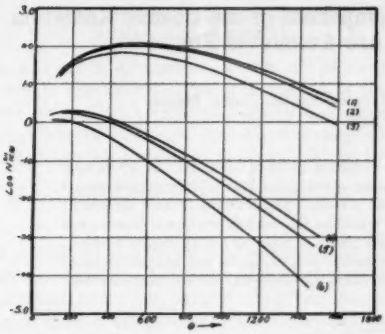

Fig. 1. The logarithm of the average number of protons above a given energy E at an atmospheric depth of θ g/cm² due to an incident primary proton of energy E_0. In curve (1), $E_0/E=10^6$, $\beta=0$; curve (2), $E_0/E=10^6$, $E_0=13\times10^{13}$ ev, $E=10\beta$; curve (3), $E_0/E=10^6$, $E_0=13\times10^{12}$ ev, $E=\beta$; curve (4), $E_0/E=10^3$, $\beta=0$; curve (5), $E_0/E=10^3$, $E_0=13\times10^{10}$ ev, $E=10\beta$; curve (6), $E_0/E=10^3$, $E_0=13\times10^9$ ev, $E=\beta$.

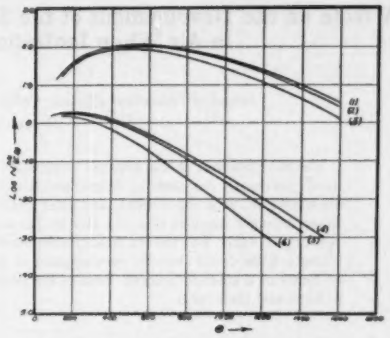

FIG. 2. The logarithm of the average number of neutrons above a given energy E at an atmospheric depth of θ g/cm² due to an incident primary proton of energy E_0. In curve (1), $E_0/E=10^6$, $\beta=0$; curve (2), $E_0/E=10^6$, $E_0=13\times10^{13}$ ev, $E=10\beta$; curve (3), $E_0/E=10^6$, $E_0=13\times10^{12}$ ev, $E=\beta$; curve (4), $E_0/E=10^3$, $\beta=0$; curve (5), $E_0/E=10^3$, $E_0=13\times10^{10}$ ev, $E=10\beta$; curve (6), $E_0/E=10^3$, $E_0=13\times10^9$ ev, $E=\beta$.

is now determined from (23) by neglecting the factor in the curly brackets.

As was mentioned in Sec. II, for all practical purposes it suffices to take the first two terms of the series for $N^{(i,k)}(E,\theta)$ and if we do not consider energies less than the ionization loss β, then a fair approximation to $N^{(i,k)}(E,\theta)$ is provided by $N_0{}^{(i,k)}(E,\theta)$.

Thus for $E\approx\beta$, $E_0\gg\beta$,

$$N^{(i,k)}(E,\theta)\approx\left\{\frac{\beta}{E+\beta g^{(i,k)}(s,\theta)}\right\}^{s-1}\frac{1}{2\pi i}\times\int_C\left(\frac{E_0}{\beta}\right)^{s-1}f_0{}^{(i,k)}(s,\theta)\frac{ds}{s-1}. \quad (24)$$

(Note that on the right we now simply have a correction factor multiplying the solution neglecting ionization loss.)

In Figs. 1, 2, and 3 we have given the results of a calculation using (24).[11] Several different primary energies were chosen and the values of E considered were $E=\beta$ and $E=10\beta$. We have considered the cases $i=1$ and $k=1$ and 2.

V. DISCUSSION OF RESULTS

In Fig. 1 we have plotted the average numbers of protons above a given energy E in a cascade developing in a finite absorber, due to a primary proton of energy E_0, both when ionization losses are neglected and when they are taken into account. Various values of the primary energy E_0 and of the energy E were chosen, in order to show how the effect of ionization loss varies according to the energy range in which we are interested. Similarly, in Fig. 2 the average numbers of neutrons due to a primary proton for the same energy ranges are plotted. Finally, in Fig. 3 the ratio of neutrons to protons is given.

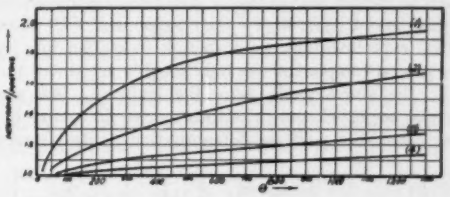

FIG. 3. The ratio of the number of neutrons to protons above a given energy E, at an atmospheric depth of θ g/cm² due to an incident primary proton of energy E_0. In curve (1), $E_0/E=10^6$, $E_0=13\times10^9$ ev, $E=\beta$; curve (2), $E_0/E=10^6$, $E_0=13\times10^{12}$ ev, $E=\beta$; curve (3), $E_0/E=10^3$, $E_0=13\times10^{10}$ ev, $E=10\beta$; curve (4), $E_0/E=10^6$, $E_0=13\times10^{13}$ ev, $E=10\beta$.

It is seen from Figs. 1, 2, and 3 that the effect of ionization is by no means negligible when $E=\beta$; however, with increasing energy E, the effect readily falls off and already for $E=10\beta$ is practically negligible.

Comparison of the theory (with ionization loss) and experimental data is being made in a subsequent paper.

My thanks are due to Professor E. Schrödinger for encouragement to carry on with the above research and to Professor L. Jánossy for many stimulating discussions. I would like to express my thanks to the National Research Council of Canada for provision of a Special Scholarship and to the School of Theoretical Physics at the Dublin Institute for Advanced Studies for the provision of a Research Scholarship.

[11] At small depths the calculation is out by a small factor due to the neglect in the numerical work of the second exponential occurring in $f_0{}^{(i,k)}(s,\theta)$. Due to this fact $N^{(1,1)}(E,\theta)$ is slightly greater and $N^{(1,2)}(E,\theta)$ slightly smaller than given by the curves for depths $\theta=0$ to 200 g/cm². As a consequence the ratio of neutrons to protons in the same depth range is exaggerated.

A Note on the Development of the Nucleon Component of the Cosmic Radiation in Air When Ionization Losses Are Accounted For

H. MESSEL
School of Theoretical Physics, Dublin Institute for Advanced Studies, Dublin, Ireland
(Received November 8, 1950)

The development of the nucleon component of the cosmic radiation in air is considered in terms of a model previously discussed by Messel and Ritson, with the inclusion of ionization losses. The results obtained are compared with experiment, and good qualitative agreement is found. The good qualitative agreement found strongly suggests that the Heitler-Jánossy assumptions regarding the nucleon-nucleon collision cross section are valid. But from a quantitative standpoint it appears that a number of points require revision. There is little doubt that the development of the nucleonic component can in fact be well accounted for in in terms of a cascade process. Results are presented in graphic form for neutrons, protons, neutrons plus protons and their ratio.

I. INTRODUCTION

RECENTLY Messel and Ritson[1] discussed the development of the nucleonic component of the cosmic radiation in air using a model which was formulated by Messel[2] and which had been suggested by the work of Heitler and Jánossy.[3] The results obtained by Messel and Ritson were in fair agreement with those found experimentally even though ionization loss by the proton component was only roughly accounted for.

In the above work, since the ionization loss was largely neglected, only the total nucleonic component was considered and no differentiation made between protons and neutrons. Lately, however, the theory of the nucleon cascade has been treated more exhaustively by Messel.[4] Ionization loss was taken into consideration, protons distinguished from neutrons, and a solution satisfying the correct boundary conditions given which should be valid down to energies at which little is known regarding the cross section for nucleon-nucleon collisions. This work has verified that the effect of ionization loss at large depths is by no means negligible, and that its neglect does in fact lead to serious errors in any problem dealing with energies of the order of the ionization loss.

There has also appeared lately[5–7] an overwhelming amount of experimental evidence supporting the hypothesis that the development of the nucleon component of the cosmic radiation must be described in terms of a cascade process. In view of the above, we have felt justified in investigating the application of the same model as previously[1] to the interpretation of experimental results on the nucleon component, but in this instance we have considered the effect of ionization loss and distinguished protons from neutrons.

The results given below are obtained using the Heitler-Jánossy assumptions regarding the cross section for nucleon-nucleon collisions. It may be countered that their assumptions are open to serious objections, that the form of the cross section obtained from their theory is not even approximately correct. We believe the answer to the above lies in the results obtained below. These results do show that the theory using the Heitler-Jánossy form of cross section can account, from a qualitative point, for the observed experimental results on cosmic-ray nucleons. That complete quantitative agreement is not found does not prove that the assumptions with regard to the nucleon-nucleon cross section are wrong, but may only point to the fact that the actual values of constants appearing in the cross section are not correct.

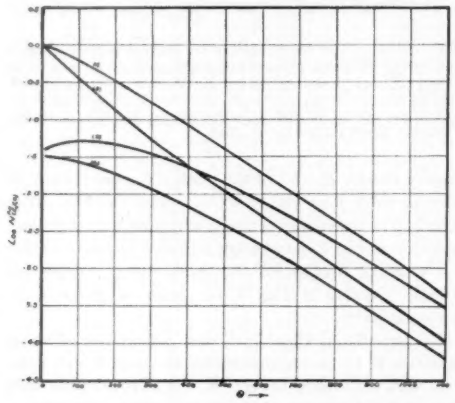

FIG. 1. Logarithm of the vertical intensity of protons with energies greater than E at an atmospheric depth of θ g/cm^2 due to an incident porton power law spectrum given by (4). In curve (1), $E=266$ Mev, $E_c=2000$ Mev, the cut-off energy corresponding to northern latitudes; curve (2), $E=2000$ Mev, $E_c=2000$ Mev; curve (3), $E=266$ Mev, $E_c=15{,}000$ Mev, the cut-off energy corresponding to the geomagnetic equator; curve (4), $E=2000$ Mev, $E_c=15{,}000$ Mev. The results have been normalized to an intensity of "one" proton at northern latitudes and $(2/15)^{1.7}$ protons at the geomagnetic equator.

[1] H. Messel and D. M. Ritson, Proc. Phys. Soc. (London) **A63**, 1359 (1950).
[2] H. Messel, Proc. Roy. Irish Acad. **A54**, 125 (1951).
[3] W. Heitler and L. Jánossy, Proc. Phys. Soc. (London) **A63**, 374 (1949).
[4] H. Messel, Phys. Rev. **83**, 21 (1950).
[5] M. Conversi, Phys. Rev. **79**, 749 (1950).
[6] Cocconi, Cocconi, Tongiorgi, and Widgoff, Phys. Rev. **79**, 768 (1950).
[7] Bernardini, Cortini, and Manfredini, Phys. Rev. **79**, 952 (1950).

II. THE MODEL, EVALUATION AND NUMERICAL RESULTS

For a detailed discussion of the model used see reference 1. The cross section was defined as follows. In a process in which a nucleon of energy E_0 loses energy and also gives rise to a recoil nucleon, it is assumed that the probability for a collision to occur is given by

$$w(E_0; E_1, E_2)dE_1dE_2 = w(E_1/E_0, E_2/E_0)dE_1dE_2/E_0^2 = \sigma\epsilon_2^{\delta}(1-\epsilon_1)^{\alpha}d\epsilon_1 d\epsilon_2, \quad (1)$$

where $\sigma=15$, $\delta=2$, and $\alpha=1$. The model also incorporates an interaction mean free path of 65 g/cm², and an absorption mean free path of 130 g/cm² in air. The ionization loss β is assumed to remain constant throughout the course of the work. This assumption is reasonably correct for the energy region we shall be considering. Below a few hundred million electron volts β is no longer independent of the energy. In the work below β is taken to equal 130.10^6 ev per 65 g/cm² air. The depth θ is measured in units of 65 g/cm².

Using the above model it has been shown[4] that the number of particles $N^{(i,k)}(E_c, E, \theta)$ with energies greater than E at a depth θ in inhomogeneous matter (E_c is the cut-off energy) is given by the expression[7a]

$$N^{(i,k)}(E_c, E, \theta) = \sum_{n=0}^{\infty} N_n{}^{(i,k)}(E_c, E, \theta), \quad (2)$$

(the suffix $i=1, 2$ refers to the primary particle and $k=1, 2$ to the secondary and the number "one" always refers to a proton and "two" to a neutron) where

$$N_n{}^{(i,k)}(E_c, E, \theta) = \frac{1}{2\pi i}\int_{s_0-i\infty}^{s_0+i\infty}\left(\frac{E_c}{\beta}\right)^{s-1}\frac{\gamma}{\gamma-s+1}\left(\frac{\beta}{E+\beta g^{(i,k)}(s,\theta)}\right)^{s+n-1} \times\frac{\Gamma(s+n)}{\Gamma(s)}f_n{}^{(i,k)}(s,\theta)\frac{ds}{s+n-1} \quad (3)$$

$$(\gamma+1>s_0)$$

with

$$N^{(i)}(E_c, E, 0) = \begin{cases}(E/E_c)^{-\gamma} & E>E_c \quad \gamma=1.7\\ 1 & E<E_c.\end{cases} \quad (4)$$

For the definitions of $g^{(i,k)}(s, \theta)$ and $f_n{}^{(i,k)}(s, \theta)$ we refer the readers to reference 4, as the expressions are rather too lengthy to be given here in full. It was also shown there that, to a fair approximation for $E\approx\beta$ and $E_c\ll\beta$, one obtains

$$N^{(i,k)}(E_c, E, \theta)\approx\left(\frac{\beta}{E+\beta g^{(i,k)}(s,\theta)}\right)^{s-1}\frac{1}{2\pi i} \times\int_{s_0-i\infty}^{s_0+i\infty}\left(\frac{E_c}{\beta}\right)^{s-1}\frac{\gamma}{\gamma-s+1}f_0{}^{(i,k)}(s,\theta)\frac{ds}{s-1}. \quad (5)$$

[7a] The proof was given for a single incident particle; however, it may readily be shown by an almost identical proof that (2) holds when we consider an incident power law spectrum.

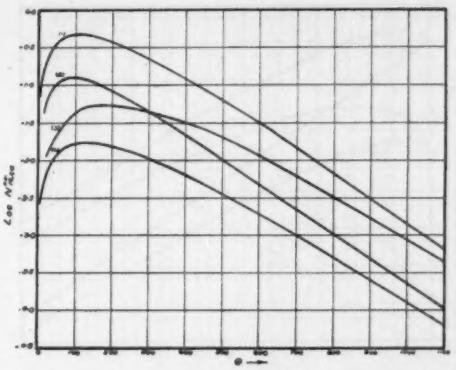

FIG. 2. Logarithm of the vertical intensity of neutrons with energies greater than E at an atmospheric depth of θ g/cm² due to an incident proton power law spectrum given by (4). In curve (1), $E=266$ Mev, $E_c=2000$ Mev, the cut-off energy corresponding to northern latitudes; curve (2), $E=2000$ Mev, $E_c=2000$ Mev; curve (3), $E=266$ Mev, $E_c=15{,}000$ Mev, the cut-off energy corresponding to the geomagnetic equator; curve (4), $E=2000$ Mev, $E_c=15{,}000$ Mev. The results have been normalized to an intensity of "one" proton at northern latitudes and $(2/15)^{1.7}$ protons at the geomagnetic equator.

Using (5) we have evaluated the curves giving the numbers of protons and neutrons with energies greater than $E=266$ Mev and $E=2000$ Mev for the incident proton power law spectrum given by (4). The values of the cut-off chosen were $E_c=2000$ Mev and $E_c=15{,}000$ Mev corresponding roughly to the cut-off energy at "northern" latitudes and the geomagnetic equator.

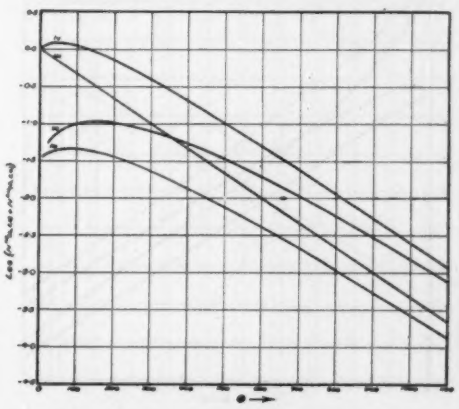

FIG. 3. Logarithm of the vertical intensity of neutrons plus protons with energies greater than E at an atmospheric depth of θ g/cm² due to an incident proton power law spectrum given by (4). In curve (1), $E=266$ Mev, $E_c=2000$ Mev, the cut-off energy corresponding to northern latitudes; curve (2), $E=2000$ Mev, $E_c=2000$ Mev; curve (3), $E=266$ Mev, $E_c=15{,}000$ Mev, the cut-off energy corresponding to the geomagnetic equator; curve (4), $E=2000$ Mev, $E_c=15{,}000$ Mev. The results have been normalized to an intensity of "one" proton at northern latitudes and $(2/15)^{1.7}$ protons at the geomagnetic equator.

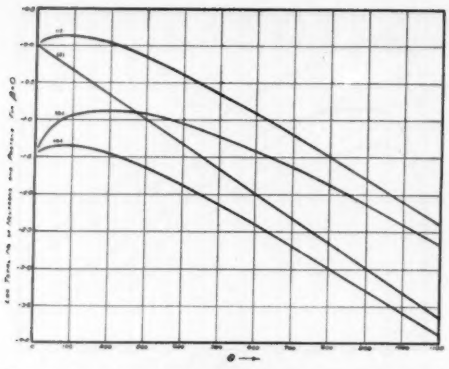

FIG. 4. Logarithm of the vertical intensity of neutrons plus protons with energies greater than E at an atmospheric depth of θ g/cm^2 due to an incident proton power law spectrum given by (4). In this case we assume the ionization loss β equal to zero. In curve (1), $E=266$ Mev, $E_c=2000$ Mev, the cut-off energy corresponding to northern latitudes; curve (2), $E=2000$ Mev, $E_c=2000$ Mev; curve (3), $E=266$ Mev, $E_c=15{,}000$ Mev, the cut-off energy corresponding to the geomagnetic equator; curve (4), $E=2000$ Mev, $E_c=15{,}000$ Mev. The results have been normalized to an intensity of "one" proton at northern latitudes and $(2/15)^{1.7}$ protons at the geomagnetic equator.

Figures 1, 2, and 3 give the vertical intensities of protons, neutrons and protons plus neutrons for the various energies above. For the sake of comparison we have reproduced[1] in Fig. 4 the curves giving the vertical intensity of protons plus neutrons when ionization

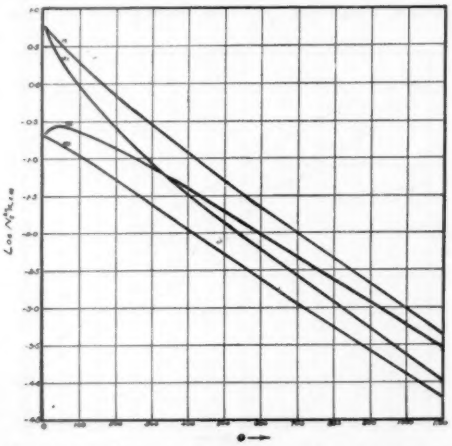

FIG. 5. Logarithm of the "total" intensity of protons with energies greater than E at an atmospheric depth of θ g/cm^2 due to an incident proton power law spectrum given by (4). In curve (1), $E=266$ Mev, $E_c=2000$ Mev, the cut-off energy corresponding to northern latitudes; curve (2), $E=2000$ Mev, $E_c=2000$ Mev; curve (3), $E=266$ Mev; $E_c=15{,}000$ Mev, the cut-off energy corresponding to the geomagnetic equator; curve (4), $E=2000$ Mev, $E_c=15{,}000$ Mev. The results have been normalized to an intensity of 2π protons at northern latitudes and $2\pi(2/15)^{1.7}$ protons at the geomagnetic equator.

losses were neglected. It will be noted that the errors due to the neglect of ionization loss are indeed considerable for the case of $E=266$ Mev.

An inverse Gross transformation was also carried out in order that we be able to compare our results with experimental data, which are practically all of a non-directional variety. The results of the transformation are given in Figs. 5, 6, and 7. Finally, in Fig. 8 we have plotted the ratio of neutrons to protons for the various energies.

III. COMPARISON OF THEORETICAL RESULTS WITH EXPERIMENT

(a) Latitude Effect

In Tables I and II we give the latitude effect both for the vertical and total intensity of protons (P) and neutrons (N) above an energy $E=266$ Mev. The results in all cases show an increasing latitude effect

TABLE I. Predicted latitude effect for the vertical intensity of the proton and neutron component of the cosmic radiation, between northern latitudes $E_c=2$ Bev and the geomagnetic equator $E_c=15$ Bev. The particles have energies greater than $E=266$ Mev.

Atmospheric depth in g/cm^2	200		310		650		1030	
	P	N	P	N	P	N	P	N
$E=266$ Mev	7.1	6.8	4.7	4.6	2.2	2.4	1.7	1.6

TABLE II. Predicted latitude effect for the total intensity of the proton and neutron component of the cosmic radiation betwen northern latitudes and the geomagnetic equator. Only particles with energies greater than 266 Mev are considered.

Atmospheric depth in g/cm^2	200		310		650		1030	
	P	N	P	N	P	N	P	N
$E=266$ Mev	5.1	5.1	3.5	3.5	2.1	2.1	1.6	1.6

with increasing altitude. The results of Simpson,[8] Yagoda,[9] and Yuan[10] on the slow neutron component of the cosmic radiation indicate an increasing latitude effect with increasing altitude. Their results indicate a value of 3.5 for this effect at an atmospheric depth of 312 g/cm^2 and 2.3 at 600 g/cm^2. These results appear to be in good agreement with those predicted in Table II. It should be noted, however, that the above authors were dealing with neutron energies considerably smaller than ours, and hence one would expect to find the experimental values higher than the predicted values of Table II.

The work of Conversi[5] on protons with energies of the order of 500 Mev gives a latitude effect of 3.2 ± 0.5 between the latitudes 0° and 60°N, at an atmospheric

[8] S. A. Simpson, Proc. Echo Lake Conf., p. 175 (1949) (unpublished).

[9] H. Yagoda, Proc. Echo Lake Conf., p. 169 (1949) (unpublished).

[10] L. Yuan, Proc. Echo Lake Conf., p. 181 (1949) (unpublished).

depth of 312 g/cm². McMahon *et al.*[11] working with ionization chambers give a latitude effect of 1.17±0.04 for protons with energies of the order of 5 Bev and 1.96 ±0.18 for protons with energies of the order of 0.4 Bev, at an atmospheric depth of 300 g/cm², between latitudes 55°N and 20°N. The results of Conversi[5] and McMahon *et al.*[11] appear to be in general agreement, but the values predicted above appear too high in comparison with theirs, especially for protons with energies greater than 2 Bev. (See Figs. 1 and 5, curves (2) and (4).) The work of the above authors also indicates a decrease in latitude effect for the protons with greater energies, at small atmospheric depths. It should be noted that our model shows only a slight variation in latitude effect for particles of different energies. Winckler *et al.*[12] give a latitude effect of 6.3 between 0° and 50°N at an atmospheric depth of 15 g/cm² for the vertical flux, which can quite safely be assumed equal to the primary vertical flux. In agreement with Winckler *et al.*, Whyte,[13] from ionization chamber observations on bursts at high altitudes, finds a latitude effect of 6.0 at 20 g/cm² and 3.0 at 200 g/cm² between latitudes 0° and 52°. These values are much smaller than those given in Figs. 1-7.

TABLE III. Predicted values for the AMFP in g/cm² air at the geomagnetic equator and northern latitudes, for the vertical intensity of the proton and neutron component of the cosmic radiation. Only particles with energies greater than 266 Mev are considered.

Atmospheric depth in g/cm²	200–400		500–700	
	P	*N*	*P*	*N*
Geomagnetic equator	275	360	172	171
Northern latitudes	145	176	135	135

TABLE IV. Predicted values for the AMFP in g/cm² at the geomagnetic equator and northern latitudes, for the total intensity of the proton and neutron component of the cosmic radiation. Energies larger than 266 Mev are considered.

Atmospheric depth in g/cm² air	200–400		500–700	
	P	*N*	*P*	*N*
Geomagnetic equator	159	175	143	135
Northern latitudes	108	115	125	123

TABLE V. Predicted values for the AMFP in g/cm² air at the geomagnetic equator and northern latitudes for the total nucleon intensity. Energies greater than 266 Mev are considered.

Atmospheric depth in g/cm²	200–400	500–700
Geomagnetic equator	157	143
Northern latitudes	109	123

[11] McMahon, Rossi, and Burdett, Phys. Rev. **80**, 157 (1950).
[12] Winckler, Stix, Dwight, and Sabin, Phys. Rev. **79**, 656 (1950).
[13] G. N. Whyte, Phys. Rev. **82**, 204 (1951).

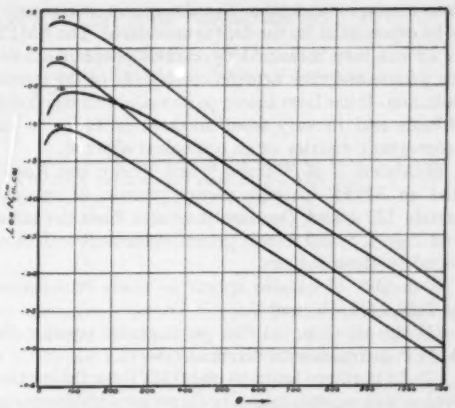

FIG. 6. Logarithm of the "total" intensity of neutrons with energies greater than E at an atmospheric depth of θ g/cm² due to an incident proton power law spectrum given by (4). In curve (1), $E=266$ Mev, $E_c=2000$ Mev, the cut-off energy corresponding to northern latitudes; curve (2), $E=2000$ Mev, $E_c=2000$ Mev; curve (3), $E=266$ Mev, $E_c=15{,}000$ Mev, the cut-off energy corresponding to the geomagnetic equator; curve (4), $E=2000$ Mev, $E_c=15{,}000$ Mev. The results have been normalized to an intensity of 2π protons at northern latitudes and $2\pi(2/15)^{1.7}$ protons at the geomagnetic equator.

(b) Absorption Mean Free Path (AMFP)

In Tables III, IV, and V, we have collected the values of the predicted AMFP for the vertical and total proton and neutron and total nucleon intensity, between va-

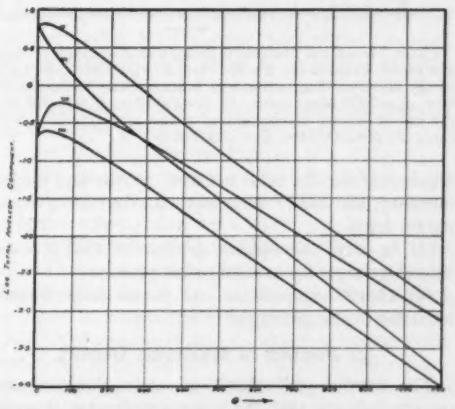

FIG. 7. Logarithms of the "total" intensity of neutrons plus protons with energies greater than E at an atmospheric depth of θ g/cm² due to an incident proton power law spectrum given by (4). In curve (1), $E=266$ Mev, $E_c=2000$ Mev, the cut-off energy corresponding to northern latitudes; curve (2), $E=2000$ Mev, $E_c=2000$ Mev; curve (3), $E=266$ Mev, $E_c=15{,}000$ Mev, the cut-off energy corresponding to the geomagnetic equator; curve (4), $E=2000$ Mev, $E_c=15{,}000$ Mev. The results have been normalized to an intensity of 2π protons at northern latitudes and $2\pi(2/15)^{1.7}$ protons at the geomagnetic equator.

rious atmospheric depths. The absorption was assumed to be exponential for the depths considered. The AMFP in air has been measured by various people, both for the proton and slow neutron component of the cosmic radiation. It has been shown to increase with increasing altitude and to vary from northern latitudes to the geomagnetic equator at an equivalent altitude.

McMahon *et al.*,[11] Tinlot,[14] and Bridge and Rossi[15] find an AMFP for high energy protons, of approximately 125 g/cm². Our results as seen from the tables and Figs. 1, 5, and 7 are in general agreement with those found by these authors.

A number of features appear on closer examination of Tables III, IV, and V.

(1) In all cases, at the geomagnetic equator the AMFP decreases with decreasing depth.

(2) At northern latitudes the AMFP for the vertical proton and neutron intensity decreases with decreasing

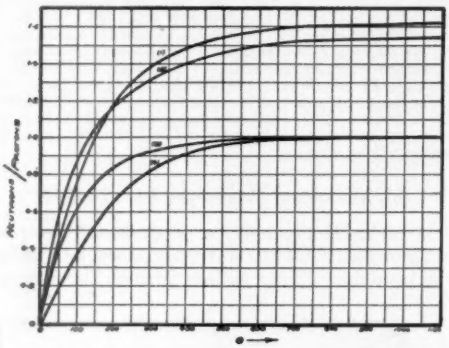

FIG. 8. The ratio of neutrons to protons at an atmospheric depth of θ g/cm². In curve (1), $E=266$ Mev, $E_c=2000$ Mev, the cut-off energy corresponding to northern latitudes; curve (2), $E=2000$ Mev, $E_c=2000$ Mev; curve (3), $E=266$ Mev, $E_c=15{,}000$ Mev, the cut-off energy corresponding to the geomagnetic equator; curve (4), $E=2000$ Mev, $E_c=15{,}000$ Mev.

depth, but for the total neutron, proton and nucleon intensity, the AMFP increases with decreasing atmospheric depth.

(3) At small atmospheric depths the AMFP is considerably larger for neutrons than protons.

(4) AMFP increases as one passes from northern latitudes to the geomagnetic equator.

(c) Position of Maximum Density

The results of Staker[16] on atmospheric neutron density indicate that the maximum density of atmospheric neutrons occurs at a greater absorption depth the closer to the geomagnetic equator the measurements are made. His results give a maximum density at 110 g/cm² for 30.4°N and at 100 g/cm² at 54.7°N. These results appear to be in good agreement with those predicted theoretically. From Fig. 2 it will be seen that the maximum density does occur at a greater absorption depth, the closer to the geomagnetic equator the measurements are made. A maximum neutron density at 100 g/cm² for northern latitudes, and at 170 g/cm² at the geomagnetic equator, is predicted. (See curves (1) and (3).)

Whyte's[13] results on bursts appear to behave similarly. He finds that the position of the maximum for the burst producing component of the cosmic radiation varies with latitude. At the geomagnetic equator he finds that the maximum intensity occurs at an atmospheric depth of 100 g/cm², while at northern latitudes a small maximum (if any) occurs at 50 g/cm². This type of behavior is also indicated by our theoretical results (see Fig. 7). A very small maximum for northern latitudes at 25 g/cm² and a pronounced maximum at 80 g/cm² for the geomagnetic equator is predicted, for nucleons with energies greater than 266 Mev.

(d) Neutron-Proton Ratio

Measurements with the photographic plate by Page[17] and by Brown *et al.*,[18] and measurement with counters by Cocconi *et al.*,[6] give an indication of the proton-neutron ratio in the cosmic radiation.

Cocconi *et al.*, dealing with very high energy nucleons, find a neutron-proton ratio varying from about 1 to 2. The measurements by means of the photographic plate indicate a neutron-proton ratio of approximately 4 for the energies we are concerned with. It will be noted that these values are much higher than those indicated by our theory. Figure 8 shows a maximum neutron-proton ratio of 1.7.

IV. CONCLUSION

The results above appear to leave little room for doubt that the observed experimental behavior of the nucleon component of the cosmic radiation can be accounted for in terms of a nucleon cascade. The quantitative agreement between theory and experiment is still not entirely satisfactory, even for the limited energy range we have been considering. Recent experimental results strongly indicate a much smaller power law exponent than that which we have been using. A revision of the actual cross section used is therefore required.

Lately we have reformulated our model and it is hoped to present the results shortly. Much stronger quantitative agreement is indicated.

My thanks are due Professor E. Schrödinger for encouragement to carry on with the above research, to Professor C. B. A. McCusker, Dr. E. P. George, and Mr. D. D. Millar for helpful discussion. I would also like to express may thanks to the School of Theoretical Physics at the Dublin Institute for Advanced Studies for the provision of a Research Scholarship.

[14] J. Tinlot, Phys. Rev. **73**, 1476 (1948); **74**, 1197 (1948).
[15] H. Bridge and B. Rossi, Phys. Rev. **75**, 810 (1949).
[16] W. P. Staker, Phys. Rev. **80**, 52 (1950).
[17] N. Page, Proc. Phys. Soc. (London) **A63**, 250 (1950).
[18] Brown, Camerini, Fowler, Heitler, King, and Powell, Phil. Mag. **40**, 862 (1949).

Energy Level at 31 Kev in Al^{28} from $Al^{27}(d, p)Al^{28}$ Reaction*†

H. Enge,‡ W. W. Buechner, A. Sperduto, and D. M. Van Patter
Physics Department and Laboratory for Nuclear Science and Engineering, Massachusetts Institute of Technology, Cambridge, Massachusetts

(Received March 13, 1951)

The proton group previously assigned to the ground state of Al^{28} from the $Al^{27}(d, p)Al^{28}$ reaction has been found to be a doublet, the low energy member of which is ascribed to an excited state at 31.2±2.0 kev. The Q-value corresponding to the Al^{28} ground state has been measured as 5.494±0.010 Mev. The Q-value corresponding to the ground state of Mg^{25} in the $Al^{27}(d, \alpha)Mg^{25}$ reaction is 6.694±0.010 Mev, and the first excited level in Mg^{25} is at 0.584±0.006 Mev.

I. INTRODUCTION

ELEMENT number 13, aluminum, exists in nature as a single isotope with mass number 27. Bombardment of aluminum targets with deuterons leads to formation of Al^{28} through the reaction $Al^{27}(d, p)Al^{28}$. Al^{28} decays through β^- emission to Si^{28}.

The $Al^{27}(d, p)Al^{28}$ reaction was first observed by Lawrence and Livingston[1] in 1934. McMillan and Lawrence[2] subsequently observed five proton and two alpha-particle groups from aluminum targets bombarded with 2.2-Mev deuterons. Livingston and Bethe[3] recalculated the Q-values from these observations and found 5.79 Mev for the Q-value corresponding to the Al^{28} ground state. A number of papers on this reaction has followed, reporting ground-state Q-values of about 5.5 Mev. Range measurements have been used throughout for determining the proton energy, the quoted errors being ±50 kev or higher.

Quite recently, Kinsey, Bartholomew, and Walker[4] have reported a Q-value of 7.72±0.02 Mev for the transition to the ground state in the $Al^{27}(n, \gamma)Al^{28}$ reaction. Mobley and Laubenstein[5] have measured the binding energy of the deuteron to be 2.226±0.003 Mev. Combining these two results gives 5.49±0.02 Mev for the Q-value corresponding to the ground state in the $Al^{27}(d, p)Al^{28}$ reaction.

The proton groups emitted from aluminum targets bombarded with deuterons have been studied, using the M.I.T. magnetic spectrograph to analyze the proton energy. In order to obtain an accurate determination of the Q-values, very thin targets, of the order of 10 kev or less, have been used. The proton peak assigned to the ground state in the first measurements had a configuration in the $H\rho$ diagram that indicated that the group might be a doublet. By improving the resolution of the apparatus, we have been able to separate the two peaks. We assign the upper of these to the Al^{28} ground state and the lower to a low-lying excited state in Al^{28}. Other possibilities are ruled out by measurements to be described in the following section.

II. EXPERIMENTAL ARRANGEMENTS

The apparatus and experimental techniques are essentially the same as those that have been described in a previous paper.[6] Deuterons accelerated in the field of an electrostatic generator are focused and deflected 90 degrees through a magnetic analyzer. After passing a defining slit, the beam hits the target which is placed between the pole pieces of an annular magnet. This annular magnet provides the homogeneous magnetic field for a 180-degree, single-focusing spectrograph. Protons leaving the target at 90 degrees to the incident beam are analyzed in the spectrograph. As recorders, Eastman Kodak NTA nuclear-track plates are used. The tracks are counted under a microscope in strips of 0.23 or 0.50 millimeter in width, and the number of tracks in each strip is plotted *versus* strip distance from the target or *versus* $H\rho$.

As in previous experiments in this Laboratory, polonium alpha-particles were used to calibrate the fluxmeter of the annular magnet. For this purpose, the target was replaced by a silver wire coated with polonium. The value of $H\rho$ for polonium alpha-particles used as an absolute standard was computed from Briggs' value[7] for the $H\rho$ of RaC′ alpha-particles and from Lewis and Bowden's value[8] for the ratio of velocities of RaC′ alpha-particles and polonium alpha-particles. From these measurements, the value of $H\rho$ for polonium alpha-particles is 3.3159×10^5 gauss-cm (absolute emu), accurate to 1 part in 5000.

The incident energy of the deuterons was calculated from the observed energy of deuterons elastically scattered from the C^{12} nuclei in a thin Formvar target.

* This work has been supported by the joint program of the ONR and AEC.

† This work was reported at the meeting of the American Physical Society in Chicago, in November, 1950. Phys. Rev. **81**, 317 (1951).

‡ On leave from the University of Bergen, Bergen, Norway.

[1] E. O. Lawrence and M. S. Livingston, Phys. Rev. **45**, 220 (1934).

[2] E. McMillan and E. O. Lawrence, Phys. Rev. **47**, 343 (1935).

[3] M. S. Livingston and H. A. Bethe, Revs. Modern Phys. **9**, 329 (1937).

[4] Kinsey, Bartholomew, and Walker, Phys. Rev. **78**, 481 (1950).

[5] R. C. Mobley and R. A. Laubenstein, Phys. Rev. **80**, 309 (1950).

[6] Buechner, Strait, Stergiopoulos, and Sperduto, Phys. Rev. **74**, 1569 (1948).

[7] G. H. Briggs, Proc. Roy. Soc. (London) **A157**, 183 (1936).

[8] W. B. Lewis and B. V. Bowden, Proc. Roy. Soc. (London) **A145**, 250 (1934).

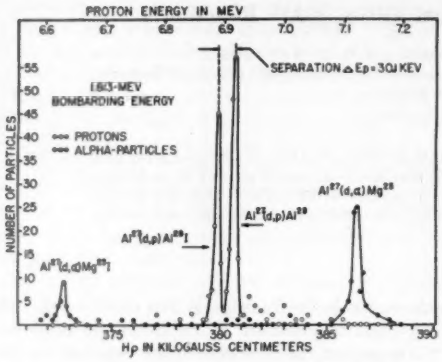

FIG. 1. Proton and alpha-particle groups from thin aluminum target bombarded with 1.813-Mev deuterons.

The aluminum targets employed in these experiments were prepared by evaporating aluminum onto platinum sheets or onto Formvar films supported by nickel-wire frames. Aluminum foils have also been used which were approximately 15 kev thick and were prepared by evaporating aluminum onto Formvar and then dissolving the Formvar in ethylene dichloride. These targets, however, were extremely fragile and were difficult to use.

To improve the resolution of the apparatus, an extra slit of 0.3-mm width was placed in the deuteron beam immediately in front of the target. The resolution obtained was about $\Delta(H\rho)/(H\rho)=7\times10^{-4}$, where $\Delta(H\rho)$ is the half-width of the peak.

III. RESULTS AND DISCUSSION

Preliminary measurements[9] in this Laboratory with a comparatively thick target yielded a fairly accurate determination of the Q-value corresponding to the ground state of Al^{28} but did not disclose the double structure of the proton group.

More than twenty different exposures have now been made with twelve different thin targets in the proper $H\rho$ region for the ground state at 1.2-, 1.5-, 1.8-, and 2.0-Mev bombarding energy. Figure 1 gives $H\rho$ diagrams of the proton and alpha-particle groups on one of these plates. The target for this particular run had a platinum backing, and the bombarding energy employed was 1.813 Mev. The proton doublet shown in the middle of Fig. 1 is consistent on all plates.

The most obvious interpretation of the data is that the right-hand peak in the doublet is associated with the ground state of Al^{28}, and the left-hand peak is due to a low-lying excited level. Other possibilities are:

1. The ground-state peak shows as a doublet because of peculiarities in the target, nonhomogeneous deuteron beam, or other instrumental errors; and

2. One of the peaks in the doublet is caused by aluminum; the other, by some contaminant in the target.

It is believed that sources of error of the type listed in item No. 1 may be ruled out by the appearance of the two alpha-particle groups found on the same plates. The two alpha-particle peaks shown in Fig. 1 have been assigned to the Mg^{25} ground state and to the first excited state from the $Al^{27}(d,\alpha)Mg^{25}$ reaction. As far as can be judged with the present resolution of the apparatus, there is no structure in either of these groups. Since they arise from the same target and were recorded simultaneously with the protons and at nearly the same $H\rho$, this lack of structure indicates that the two proton groups are due to nuclear rather than to instrumental effects. As a further control against aberration in the spectrograph, some of the plates were exposed with different settings of the field strength, thereby varying the position of the peaks on the plates. No change in either the appearance or the Q-values of the groups was observed.

In order to rule out the possibility that one of the proton groups arose from a contaminant in the target, accurate energy measurements were made on the proton groups at incident deuteron energies of 1.514 and 1.809 Mev. Wide plots of the proton doublet at the two different bombarding energies are given in Fig. 2.

Assuming that the right-hand member is the ground-state peak and the left-hand member is caused by a low-lying excited level in Al^{28}, the energy of the level has been calculated. From the 1.514-Mev plate, the energy is $E=31.4\pm0.5$ kev; from the 1.809-Mev plate, it is $E=31.0\pm0.6$ kev. Inasmuch as the values check well within the limits of error, these results do not contradict the assumption that both groups are associated with Al^{28}.

Aside from negligibly small correction terms due to relativistic effects and to the fact that the angle of observation is not precisely 90 degrees, a change of ΔE_{in} in the bombarding energy causes a change

$$\Delta E_{out}=\frac{M_{res}-M_{in}}{M_{res}+M_{out}}\Delta E_{in}$$

in the energy of the emitted particle. M_{res}, M_{in}, and M_{out} are the masses of the residual nucleus and incoming and outgoing particles. Using this formula and the separation between the peaks at 1.514-Mev bombarding energy, the separation to be expected at 1.809-Mev bombarding energy has been calculated on the assumption that the right-hand peak is due to Al^{27} and the left-hand peak to P^{31} as target nuclei. The same calculation has been made for Na^{23}, and the expected positions of the left-hand peak for the two cases given in Fig. 2. From these calculations, it is concluded that, if one of the peaks is due to Al^{27}, the other cannot be due to any nucleus with a mass number outside the region $24\lesssim M\lesssim30$. The same experiments and calcula-

[9] K. Huang, B.S. thesis, M. I. T. (June, 1950).

tions have been made using an aluminum-on-Formvar target; the conclusion is the same.

In this mass region, only magnesium, aluminum, and silicon have stable isotopes. Finally, to rule out magnesium and silicon, a search was made for proton groups from such targets in the position of the doublet, but no such groups were found. Special measurements were taken to insure that the yields from the magnesium and silicon targets used were higher than those from the magnesium and silicon contamination in the aluminum targets.

The voltage shift and the test runs have proved that, if one of the peaks in the doublet is due to aluminum, both of them are. From the measurements, it is concluded that Al^{28} has an excited level at 31.2 ± 2.0 kev. The proton yield from the $Al^{27}(d, p)Al^{28}$ reaction assigned to this level is about 55 percent of the ground-state yield and does not vary much with deuteron energies from 1.2 to 1.8 Mev. The Q-value corresponding to the Al^{28} ground state in this reaction was measured as 5.494 ± 0.010 Mev, in good agreement with the value of 5.49 ± 0.02 Mev obtained from the combination of the results obtained by Kinsey, *et al.*, and by Mobley and Laubenstein.

Several attempts have been made to verify this excited state using other means. Measurements have been made on the $Si^{30}(d, \alpha)Al^{28}$ reaction, using SiO_2 targets enriched in the Si^{30} isotope. (This enriched material was made available by the Stable Isotopes Division, AEC, Oak Ridge.) While the highest energy alpha-particle group observed from this reaction had a greater half-width than would be expected from the appearance of the proton groups from the same target, for reasons of intensity no conclusive measurements have thus far been possible. Also, attempts have been made in collaboration with Mr. N. S. Wall to detect the low energy gamma-rays from this level. These attempts have not been successful because of the high background of radiation from the decay of the other states of Al^{28}.

In addition to this unexpectedly low excited state,

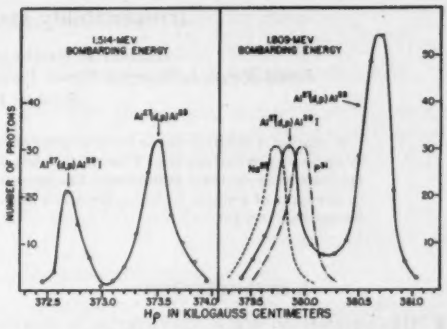

FIG. 2. Proton doublet at two different bombarding energies.

evidence has been found for a large number of other levels in Al^{28}. These appear to have a complicated structure, and considerable further work at the highest resolution will be necessary to establish their locations.

From the alpha-particle groups observed in these experiments, it is calculated that the Q-value corresponding to the ground state of Mg^{25} in the $Al^{27}(d, \alpha)Mg^{25}$ reaction is 6.694 ± 0.010 Mev, and the first excited level in Mg^{25} is at 0.584 ± 0.006 Mev. The relative yield for the alpha-particle group assigned to this excited state is about 38 percent of the ground-state yield at 1.5-Mev and 1.8-Mev bombarding energy.

This work was carried out while one of the authors (Harald Enge) was at the Laboratory under the auspices of the 1950 Foreign Student Summer Project at MIT. We wish to express our appreciation to the Student Committee in charge of the program and to the various organizations which collaborated with them in making the program possible. We are also indebted to our colleagues in the High Voltage Laboratory who have collaborated in various stages of this work. We wish to thank Mrs. Cecilia Bryant, Mr. W. A. Tripp, and Mrs. Clara Stucky for their assistance in connection with the reading of the photographic plates.

Irreversibility and Generalized Noise*

HERBERT B. CALLEN AND THEODORE A. WELTON†
Randal Morgan Laboratory of Physics, University of Pennsylvania, Philadelphia, Pennsylvania
(Received January 11, 1951)

A relation is obtained between the generalized resistance and the fluctuations of the generalized forces in linear dissipative systems. This relation forms the extension of the Nyquist relation for the voltage fluctuations in electrical impedances. The general formalism is illustrated by applications to several particular types of systems, including Brownian motion, electric field fluctuations in the vacuum, and pressure fluctuations in a gas.

I. INTRODUCTION

THE parameters which characterize a thermodynamic system in equilibrium do not generally have precise values, but undergo spontaneous fluctuations. These thermodynamic parameters are of two classes: the "extensive" parameters,[1] such as the volume or the mole numbers, and the "intensive" parameters[2] or "generalized forces," such as the pressure or chemical potentials.

An equation relating particularly to the fluctuations in voltage (a "generalized force") in linear electrical systems was derived many years ago by Nyquist,[3] and such voltage fluctuations are generally referred to as Nyquist or Johnson "noise." The voltage fluctuations are related, not to the standard thermodynamic parameters of the system, but to the electrical resistance. The Nyquist relation is thus of a form unique in physics, correlating a property of a system in *equilibrium* (i.e., the voltage fluctuations) with a parameter which characterizes an irreversible process (i.e., the electrical resistance). The equation, furthermore, gives not only the mean square fluctuating voltage, but provides, in addition, the frequency spectrum of the fluctuations. The proof of the relation is based on an ingenious union of the second law of thermodynamics and a direct calculation of the fluctuations in a particular simple system (an ideal transmission line).

It has frequently been conjectured that the Nyquist relation can be extended to a general class of dissipative systems other than merely electrical systems. Yet, to our knowledge, no proof has been given of such a generalization, nor have any criteria been developed for the type of system or the character of the "forces" to which the generalized Nyquist relation may be applied. The development of such a proof and of such criteria is the purpose of this paper (Secs. II, III, and IV). The general theorem thus establishes a relation between the "impedance" in a general linear dissipative system and the fluctuations of appropriate generalized "forces."

Several illustrative applications are made of the general theorem. The viscous drag of a fluid on a moving body is shown to imply a fluctuating force, and application of the general theorem immediately yields the fundamental result of the theory of Brownian motion. The existence of a radiation impedance for the electromagnetic radiation from an oscillating charge is shown to imply a fluctuating electric field in the vacuum, and application of the general theorem yields the Planck radiation law. Finally, the existence of an acoustic radiation impedance of a gaseous medium is shown to imply pressure fluctuations, which may be related to the thermodynamic properties of the gas. The theorem thus correlates a number of known effects under one general principle and is able to predict a class of new relations.

In the final section of the paper, we discuss an intuitive interpretation of the principles underlying the theorem.

It is felt that the relationship between equilibrium fluctuations and irreversibility which is here developed provides a method for a general approach to a theory of irreversibility, using statistical ensemble methods. We are currently investigating such an approach.

II. THE DISSIPATION

A system may be said to be dissipative if it is capable of absorbing energy when subjected to a time-periodic perturbation (as an electrical resistor absorbs energy from an impressed periodic voltage). The system may be said to be linear if the power dissipation is quadratic in the magnitude of the perturbation. For a linear dissipative system, an impedance may be defined, and the proportionality constant between the power and the square of the perturbation amplitude is simply related to the impedance [in the electrical case, Power $=(\text{voltage})^2 \cdot R/|Z|^2$].

In the present section we treat the applied perturbation by the usual quantum mechanical perturbation

* This work was supported in part by the ONR.
† Now at Oak Ridge National Laboratory, Oak Ridge, Tennessee.

[1] For the theory of fluctuations of extensive parameters see Fowler, *Statistical Mechanics* (Cambridge University Press, London, 1936), second edition; or Tolman, *Principles of Statistical Mechanics* (Oxford University Press, London, 1938). A recent development of the theory is given by M. J. Klein and L. Tisza, Phys. Rev. 76, 1861 (1949).

[2] A statistical mechanical theory of fluctuations of intensive parameters will be given in a subsequent paper by R. F. Greene and H. B. Callen.

[3] H. Nyquist, Phys. Rev. 32, 110 (1928). A very neat derivation and an interesting discussion is given by J. C. Slater, Radiation Laboratory Report; "Report on Noise and the Reception of Pulses," February 3, 1941, unpublished.

methods and thus relate the power dissipation to certain matrix elements of the perturbation operator. We thereby show that for small perturbations, a system with densely distributed energy levels is dissipative and linear, and we obtain certain pertinent information relative to the impedance function.

Let the hamiltonian of the system in the absence of the perturbation be H_0, a function of the coordinates $q_1 \cdots q_K \cdots$ and momenta $p_1 \cdots p_K \cdots$ of the system. In the presence of the perturbation, the hamiltonian is

$$H = H_0(\cdots q_K \cdots p_K \cdots) + VQ(\cdots q_K \cdots p_K \cdots). \quad (2.1)$$

where Q is a function of the coordinates and momenta, and V is a function of time which measures the instantaneous magnitude of the perturbation.

Again invoking the electrical case as a clarifying example, we may have V as the impressed voltage and $Q = \sum e_i x_i / L$, where e_i is the charge on the ith particle, x_i is its distance from one end of the resistor, and L is the total length of the resistor.

If the applied perturbation varies sinusoidally with time, we have

$$V = V_0 \sin \omega t. \quad (2.2)$$

We may now employ standard time-dependent perturbation theory to compute the power dissipation. Let $\psi_1, \psi_2 \cdots \psi_n \cdots$ be the set of eigenfunctions of the unperturbed hamiltonian H_0, so that

$$H_0 \psi_n = E_n \psi_n, \quad (2.3)$$

and let the true wave function be ψ. Expanding ψ in terms of the ψ_n,

$$\psi = \sum_n a_n(t) \psi_n, \quad (2.4)$$

and substituting into the Schroedinger equation for ψ,

$$H_0 \psi + V_0 \sin \omega t Q \psi = i\hbar \partial \psi / \partial t, \quad (2.5)$$

one obtains a set of first-order equations for the coefficients $a_n(t)$, which may readily be integrated. If the energy levels of the system are densely distributed, one thus finds that the total induced transition probability of a system initially in the state ψ_n is

$$\tfrac{1}{2}\pi V_0^2 \hbar^{-1} \{ |\langle E_n + \hbar\omega | Q | E_n \rangle|^2 \rho(E_n + \hbar\omega) + |\langle E_n - \hbar\omega | Q | E_n \rangle|^2 \rho(E_n - \hbar\omega) \}, \quad (2.6)$$

where the symbol $\langle E_n + \hbar\omega | Q | E_n \rangle$ indicates the matrix element of the operator corresponding to Q between the state with eigenvalue $E_n + \hbar\omega$ and the state with eigenvalue E_n. The symbol $\rho(E)$ indicates the density-in-energy of the quantum states in the neighborhood of E, so that the number of states between E and $E + \delta E$ is $\rho(E)\delta E$.

Each transition from the state ψ_n to the state with eigenvalue $E_n + \hbar\omega$ is accompanied by the absorption of energy $\hbar\omega$, and each transition from ψ_n to the state with eigenvalue $E_n - \hbar\omega$ is accompanied by the emission of energy $\hbar\omega$. Thus the rate of absorption of energy by a system initially in the nth state is

$$\tfrac{1}{2}\pi V_0^2 \omega \{ |\langle E_n + \hbar\omega | Q | E_n \rangle|^2 \rho(E_n + \hbar\omega) - |\langle E_n - \hbar\omega | Q | E_n \rangle|^2 \rho(E_n - \hbar\omega) \}. \quad (2.7)$$

To predict the behavior of a real thermodynamic system, we must average over-all initial states, weighting each according to the Boltzmann factor $\exp(-E_n/kT)$. Let the weighting factor be $f(E_n)$, so that

$$f(E_n + \hbar\omega)/f(E_n) = f(E_n)/f(E_n - \hbar\omega) = \exp(-\hbar\omega/kT). \quad (2.8)$$

The power dissipation is, then,

$$\text{Power} = \tfrac{1}{2}\pi V_0^2 \omega \sum_n \{ |\langle E_n + \hbar\omega | Q | E_n \rangle|^2 \rho(E_n + \hbar\omega) - |\langle E_n - \hbar\omega | Q | E_n \rangle|^2 \rho(E_n - \hbar\omega) \} f(E_n). \quad (2.9)$$

The summation over n may be replaced by an integration over energy

$$\sum_n (\ \ ) \rightarrow \int_0^\infty (\ \ ) \rho(E) dE, \quad (2.10)$$

whence

$$\text{Power} = \tfrac{1}{2}\pi V_0^2 \omega \int_0^\infty \rho(E) f(E) \times \{ |\langle E + \hbar\omega | Q | E \rangle|^2 \rho(E + \hbar\omega) - |\langle E - \hbar\omega | Q | E \rangle|^2 \rho(E - \hbar\omega) \} dE. \quad (2.11)$$

We thus find that a small periodic perturbation applied to a system, the eigenstates of which are densely distributed in energy, leads to a power dissipation quadratic in the perturbation. For such a linear system it is possible to define an impedance $Z(\omega)$, the ratio of the force V to the response $\dot{Q}$, where all quantities are now assumed to be written in standard complex notation,

$$V = Z(\omega) \dot{Q}. \quad (2.12)$$

The instantaneous power is $V\dot{Q}R/|Z|$, and the average power is

$$\text{Power} = \tfrac{1}{2} V_0^2 R(\omega) / |Z(\omega)|^2, \quad (2.13)$$

where $R(\omega)$, the resistance, is the real part of $Z(\omega)$.

If the applied perturbation is not sinusoidal, but some general function of time $V(t)$, and if $v(\omega)$ and $\dot{q}(\omega)$ are the fourier transforms of $V(t)$ and $\dot{Q}(t)$, the impedance is defined in terms of the fourier transforms:

$$v(\omega) = Z(\omega) \dot{q}(\omega). \quad (2.14)$$

In this notation we then obtain, for the general linear dissipative system,

$$R/|Z|^2 = \pi\omega \int_0^\infty \rho(E) f(E) \{ |\langle E + \hbar\omega | Q | E \rangle|^2 \rho(E + \hbar\omega) - |\langle E - \hbar\omega | Q | E \rangle|^2 \rho(E - \hbar\omega) \} dE. \quad (2.15)$$

III. THE FLUCTUATION

We have, in the previous section, considered a system to which is applied a force V, eliciting a response $\dot{Q}$. We now consider the system to be left in thermal equilibrium, with no applied force. We may expect, even in this isolated condition, that the system will exhibit a spontaneously fluctuating $\dot{Q}$, which may be associated with a spontaneously fluctuating force. We shall see, in this section, that such a spontaneously fluctuating force does in fact exist, and we shall find its magnitude.

Let $\langle V^2\rangle$ be the mean square value of the spontaneously fluctuating force, and let $\langle\dot{Q}^2\rangle$ be the mean square value of the spontaneously fluctuating $\dot{Q}$. Although we shall be primarily interested in $\langle V^2\rangle$, we shall find it convenient to compute $\langle\dot{Q}^2\rangle$ and to obtain $\langle V^2\rangle$ from Eq. (2.14).

Consider that the system is known to be in the nth eigenstate. The hermitian property of H_0 causes the expectation value of $\dot{Q}$, $\langle E_n|\dot{Q}|E_n\rangle$, to vanish. The mean square fluctuation of $\dot{Q}$ is therefore given by the expectation value of $\dot{Q}^2$ or $\langle E_n|\dot{Q}^2|E_n\rangle$. Then

$$\begin{aligned}\langle E_n|\dot{Q}^2|E_n\rangle&=\textstyle\sum_m\langle E_n|\dot{Q}|E_m\rangle\langle E_m|\dot{Q}|E_n\rangle\\&=\hbar^{-2}\textstyle\sum_m\langle E_n|H_0Q-QH_0|E_m\rangle\\&\qquad\times\langle E_m|H_0Q-QH_0|E_n\rangle\\&=\hbar^{-2}\textstyle\sum_m(E_n-E_m)^2|\langle E_m|Q|E_n\rangle|^2.\end{aligned}\tag{3.1}$$

Introducing a frequency ω by

$$\hbar\omega=|E_n-E_m|,\tag{3.2}$$

the summation over m may be replaced by two integrals over ω (one for $E_n<E_m$ and one for $E_n>E_m$):

$$\begin{aligned}\langle E_n|\dot{Q}^2|E_n\rangle&=\hbar^{-2}\int_0^\infty(\hbar\omega)^2|\langle E_n+\hbar\omega|Q|E_n\rangle|^2\\&\qquad\times\rho(E_n+\hbar\omega)\hbar d\omega+\hbar^{-2}\int_0^\infty(\hbar\omega)^2\\&\qquad\times|\langle E_n-\hbar\omega|Q|E_n\rangle|^2\rho(E_n-\hbar\omega)\hbar d\omega.\\&=\int_0^\infty\hbar\omega^2\{|\langle E_n+\hbar\omega|Q|E_n\rangle|^2\rho(E_n+\hbar\omega)\\&\qquad+|\langle E_n-\hbar\omega|Q|E_n\rangle|^2\rho(E_n-\hbar\omega)\}d\omega.\end{aligned}\tag{3.3}$$

The fluctuation actually observed in a real thermodynamic system is obtained by multiplying the fluctuation in the nth state by the weighting factor $f(E_n)$, and summing

$$\begin{aligned}\langle\dot{Q}^2\rangle=\textstyle\sum_n f(E_n)\int_0^\infty&\hbar\omega^2\{|\langle E_n+\hbar\omega|Q|E_n\rangle|^2\rho(E_n+\hbar\omega)\\&+|\langle E_n-\hbar\omega|Q|E_n\rangle|^2\rho(E_n-\hbar\omega)\}d\omega.\end{aligned}\tag{3.4}$$

As in Eq. (2.10), the summation over n may be replaced by an integration over the energy spectrum if we introduce the density factor $\rho(E)$. Thus we finally obtain

$$\begin{aligned}\langle\dot{Q}^2\rangle=\int_0^\infty\hbar\omega^2\Big[\int_0^\infty&\rho(E)f(E)\{|\langle E+\hbar\omega|Q|E\rangle|^2\rho(E+\hbar\omega)\\&+|\langle E-\hbar\omega|Q|E\rangle|^2\rho(E-\hbar\omega)\}dE\Big]d\omega,\end{aligned}\tag{3.5}$$

or, utilizing the definition (2.14) of the impedance,

$$\begin{aligned}\langle V^2\rangle=\int_0^\infty|Z|^2\hbar\omega^2\Big[\int_0^\infty&\rho(E)f(E)\\&\times\{|\langle E+\hbar\omega|Q|E\rangle|^2\rho(E+\hbar\omega)\\&+|\langle E-\hbar\omega|Q|E\rangle|^2\rho(E-\hbar\omega)\}dE\Big]d\omega.\end{aligned}\tag{3.6}$$

IV. THE GENERALIZED NYQUIST RELATION

In the two previous sections we have computed $R/|Z|^2$ and $\langle V^2\rangle$. These quantities involve the constructs

$$\begin{aligned}\int_0^\infty&\rho(E)f(E)\{|\langle E+\hbar\omega|Q|E\rangle|^2\rho(E+\hbar\omega)\\&\pm|\langle E-\hbar\omega|Q|E\rangle|^2\rho(E-\hbar\omega)\}dE,\end{aligned}\tag{4.1}$$

the negative sign being associated with $R/|Z|^2$ and the positive sign with $\langle V^2\rangle$. We shall now see that the two values of (4.1) are simply related, and thus establish the desired relation between $\langle V^2\rangle$ and $R(\omega)$.

Consider first the value of (4.1) corresponding to the negative sign, which we denote by $C(-)$.

$$\begin{aligned}C(-)=\int_0^\infty&f(E)|\langle E+\hbar\omega|Q|E\rangle|^2\rho(E+\hbar\omega)\rho(E)dE\\&-\int_0^\infty f(E)|\langle E-\hbar\omega|Q|E\rangle|^2\rho(E)\rho(E-\hbar\omega)dE.\end{aligned}\tag{4.2}$$

In the second integral we note that $\langle E-\hbar\omega|Q|E\rangle$ vanishes for $E<\hbar\omega$, and making the transformation $E\rightarrow E+\hbar\omega$ in the integration variable, we obtain

$$\begin{aligned}C(-)=\int_0^\infty&|\langle E+\hbar\omega|Q|E\rangle|^2\rho(E+\hbar\omega)\rho(E)f(E)\\&\times\{1-f(E+\hbar\omega)/f(E)\}dE.\end{aligned}\tag{4.3}$$

By Eq. (2.8) this becomes

$$\begin{aligned}C(-)=\{1-\exp(-\hbar\omega/kT)\}\int_0^\infty&|\langle E+\hbar\omega|Q|E\rangle|^2\\&\times\rho(E+\hbar\omega)\rho(E)f(E)dE.\end{aligned}\tag{4.4}$$

If $C(+)$ denotes the value of (4.1) corresponding to the positive sign, we obtain, in an identical fashion,

$$C'(+)=\{1+\exp(-\hbar\omega/kT)\}\int_0^\infty |\langle E+\hbar\omega|Q|E\rangle|^2 \times\rho(E+\hbar\omega)\rho(E)f(E)dE. \quad (4.5)$$

With these alternative expressions for (4.1), we can write, from Eq. (2.15),

$$R(\omega)/|Z(\omega)|^2=\pi\omega\{1-\exp(-\hbar\omega/kT)\} \times\int_0^\infty |\langle E+\hbar\omega|Q|E\rangle|^2\rho(E+\hbar\omega)\rho(E)f(E)dE, \quad (4.6)$$

and from Eq. (3.6),

$$\langle V^2\rangle=\int_0^\infty |Z|^2\hbar\omega^2\{1+\exp(-\hbar\omega/kT)\} \times\int_0^\infty |\langle E+\hbar\omega|Q|E\rangle|^2\rho(E+\hbar\omega)\rho(E)f(E)dEd\omega. \quad (4.7)$$

Comparison of these equations yields directly our fundamental theorem:

$$\langle V^2\rangle=(2/\pi)\int_0^\infty R(\omega)E(\omega, T)d\omega, \quad (4.8)$$

where

$$E(\omega, T)=\tfrac{1}{2}\hbar\omega+\hbar\omega[\exp(\hbar\omega/kT)-1]^{-1}. \quad (4.9)$$

It may be recognized that $E(\omega, T)$ is, formally, the expression for the mean energy at the temperature T of an oscillator of natural frequency ω.

At high temperatures, $E(\omega, T)$ takes its equipartition value

$$E(\omega, T)\simeq kT, \quad (kT\gg\hbar\omega) \quad (4.10)$$

and the generalized Nyquist relation takes its most familiar form

$$\langle V^2\rangle\simeq(2/\pi)kT\int R(\omega)d\omega. \quad (4.11)$$

To reiterate then, a system with a generalized resistance $R(\omega)$ exhibits, in equilibrium, a fluctuating force given by Eq. (4.8) or, at high temperature, by Eq. (4.11).

We shall now consider a few specific applications of this theorem. The application to the electrical case is obvious, the general Eq. (4.8) being identical with the Nyquist relation if the force V is interpreted as the voltage. The content of the general theorem is, however, clarified by considering certain less trivial applications.

V. APPLICATION TO BROWNIAN MOTION

The fundamental result of the theory of the Brownian motion of a small particle immersed in a fluid is that the particle moves in response to a randomly fluctuating force $F(t)$ (with components F_x, F_y, F_z) such that

$$\langle F_x^2\rangle=(2/\pi)kT\eta\int d\omega. \quad (5.1)$$

Here η is a frictional constant, so defined that the viscous drag on a particle moving with velocity v is

$$\text{Frictional force}=-\eta v. \quad (5.2)$$

(If, in particular, the particle is spherical, η is known by Stokes' law as $6\pi\cdot$(viscosity)$\cdot$(radius).)

It is interesting to recall briefly the rather complicated and circuitous chain of reasoning by which the above result is obtained. One first makes the *assumption* that the particle moves in response to a randomly fluctuating force which has a *constant*, but unknown, spectral density. (The spectral density is, in actuality, not constant, and Eq. (5.1) is not valid at high frequencies.) By application of the theory of stochastic processes, one is then able to predict the distribution functions for either the displacement or the velocity of the particle.[4] The distribution function for displacement yields the diffusion constant, which in turn may be related by the Einstein relation[5] to the frictional constant η, thus evaluating the spectral density.[6] Alternatively, the distribution function for velocity yields the energy, which is known by the equipartition theorem and which therefore evaluates the spectral density, yielding Eq. (5.1).

We now apply our general formalism to the Brownian motion. We assume the existence of a viscous force as given by Eq. (5.2). The system of a particle in a fluid, the particle being acted on by an external force, is then dissipative and linear. The real part of the impedance is simply η (the inertial mass of the particle giving a pure reactance of $m\omega$). We conclude immediately, in accordance with Eq. (4.8), that a particle in a fluid is acted upon by a spontaneously fluctuating force for which

$$\langle F_x^2\rangle=(2/\pi)\eta\int_0^\infty E(\omega, T)d\omega. \quad (5.3)$$

For high temperatures or low frequencies, ($\hbar\omega\ll kT$); this reduces to Eq. (5.1).

VI. ELECTRIC DIPOLE RADIATION RESISTANCE AND ELECTRIC FIELD FLUCTUATIONS IN THE VACUUM

An oscillating electric charge radiates energy, leading to a radiation resistance. We shall see that this radiation resistance implies a fluctuating electric field as given by the Planck radiation law.

[4] See M. C. Wang and G. E. Uhlenbeck, Revs. Modern Phys. **17**, 323 (1945); and J. L. Doob, Ann. Math. **43**, 351 (1942).

[5] See A. Einstein, *Investigations on the Theory of the Brownian Movement* (Dutton and Company, New York); or A. Einstein, Ann. Physik **17**, 549 (1905).

[6] A similar analysis has been applied to the flow of heat by L. S. Ornstein and J. M. W. Milatz, Physica **6**, 1139 (1939).

Consider a dipole, of charge e, displacement x, and dipole moment $p=ex$. Let one charge be fixed and let the other oscillate so that

$$P=P_0 \sin\omega t. \tag{6.1}$$

It is well known that the electric dipole radiation leads to a dissipative force[7]

$$F_d=-\tfrac{2}{3}e^2c^{-3}d^2v/dt^2, \tag{6.2}$$

where v is the velocity of the moving charge. The equation of motion of this charge is

$$m dv/dt+m\omega_0^2x+F_d=F, \tag{6.3}$$

where F is the applied force, and ω_0 is the natural frequency associated with the intra-dipole binding force. Inserting (6.1) in (6.3) we get

$$F=mP_0e^{-1}(\omega_0^2-\omega^2)\sin\omega t+\tfrac{2}{3}e\omega^3c^{-3}P_0\cos\omega t. \tag{6.4}$$

One may note that the average rate of radiation of energy $\langle Fv\rangle$ is

$$\langle Fv\rangle=\tfrac{1}{2}(\tfrac{2}{3}e\omega^3c^{-3}P_0)(\omega P_0e^{-1})=\tfrac{1}{3}\omega^4c^{-3}P_0^2. \tag{6.5}$$

The real part of the impedance is obtained by taking the ratio of the in-phase component of F to v. Thus

$$R(\omega)=(\tfrac{2}{3}e\omega^3c^{-3}P_0)/(\omega P_0e^{-1})=\tfrac{2}{3}e^2c^{-3}\omega^2. \tag{6.6}$$

According to our general theorem, we now deduce that there exists a randomly fluctuating force $e\mathcal{E}_x$ on the charge, and hence a randomly fluctuating electric field $\mathcal{E}_x$, such that

$$\langle e^2\mathcal{E}_x^2\rangle=(2/\pi)\int_0^\infty E(\omega, T)\tfrac{2}{3}e^2c^{-3}\omega^2 d\omega,$$

or

$$\langle \mathcal{E}_x^2\rangle=(4/3)\pi^{-1}c^{-3}$$
$$\times\int_0^\infty\{\tfrac{1}{2}\hbar\omega+\hbar\omega[\exp(\hbar\omega/kT)-1]^{-1}\}\omega^2 d\omega. \tag{6.7}$$

This conclusion can be put into a more familiar form by utilizing the fact that the energy density in an isotropic radiation field is simply

$$\text{Energy density}=\langle\mathcal{E}^2\rangle/4\pi=3\langle\mathcal{E}_x^2\rangle/4\pi \tag{6.8}$$

whence

Energy density

$$=\pi^{-2}c^{-3}\int_0^\infty\{\tfrac{1}{2}\hbar\omega+\hbar\omega[\exp(\hbar\omega/kT)-1]^{-1}\}\omega^2 d\omega. \tag{6.9}$$

The first term in this equation gives the familiar infinite "zero-point" contribution, and the second term gives the Planck radiation law.[8]

[7] W. Heitler, *The Quantum Theory of Radiation* (Oxford University Press, London, 1936).

[8] The interaction of free electron and radiation field has been discussed from a somewhat different point of view by W. Pauli, Z. Physik 18, 272 (1923); A. Einstein and P. Ehrenfest, Z. Physik 19, 301 (1923).

VII. ACOUSTIC RADIATION RESISTANCE AND PRESSURE FLUCTUATIONS IN A GAS

We now consider the acoustic radiation from a small oscillating sphere in a gaseous medium. This radiation leads to a radiation impedance which, in accordance with our general theorem, implies a fluctuating pressure in the gas.

The wave equation for the propogation of pressure waves in the gas is

$$\nabla^2P=c^{-2}\partial^2P/\partial t^2, \tag{7.1}$$

where c is the velocity of sound in the gas. Let the radius of the sphere be a, and let

$$a=a_0+e^{-i\omega t}\delta a \tag{7.2}$$

so that the sphere expands and contracts sinusoidally. The boundary condition to be satisfied by the pressure waves at $r=a_0$ is

$$\rho\partial^2a/\partial t^2=-\partial P/\partial r \quad \text{at} \quad r=a_0, \tag{7.3}$$

where ρ is the equilibrium value of the density. The solution of these equations is readily found to be

$$P=r^{-1}P_0\exp(iKr-i\omega t), \tag{7.4}$$

where

$$K=\omega/c \tag{7.5}$$

and

$$P_0=-\rho\omega^2a_0^2\delta a[1+iKa_0]\cdot[1+(Ka_0)^2]^{-1}$$
$$\times\exp(-iKa_0). \tag{7.6}$$

Thus, the compressive force acting on the surface of the sphere is

$$F=4\pi a_0P_0\exp(iKa_0-i\omega t), \tag{7.7}$$

and defining the radiation impedance as the ratio of complex force to complex velocity, we find

$$\begin{aligned} Z&=F/[-i\omega\exp(-i\omega t)\delta a] \\ Z&=[4\pi a_0^2\rho c(Ka_0)^2-i4\pi a_0^2\rho cKa_0]/[1+(Ka_0)^2]. \end{aligned} \tag{7.8}$$

The generalized Nyquist relation now states that a sphere immersed in a gas will experience a fluctuating compressive force, such that

$$\langle F^2\rangle=(2/\pi)\int E(\omega, T)4\pi a_0^2\rho c(\omega a_0/c)^2$$
$$\times[1+(\omega a_0/c)^2]^{-1}d\omega. \tag{7.9}$$

The fluctuating pressure is the compressive force per unit area on a vanishingly small sphere.

$$\langle P^2\rangle=\lim_{a_0\to 0}\langle F^2\rangle/(4\pi a_0^2)^2, \tag{7.10}$$

or

$$\langle P^2\rangle=\tfrac{1}{2}\pi^{-2}c^{-1}\rho\int E(\omega, T)\omega^2 d\omega. \tag{7.11}$$

This result may be checked by a direct computation paralleling the standard derivation of the Planck radiation law for the electromagnetic modes in a

vacuum. The number of acoustic modes with frequency between ω and $\omega+d\omega$ is $\frac{1}{2}\pi^{-2}c^{-3}\omega^2 d\omega$, and the acoustic energy density is

$$\text{Energy density}=\int E(\omega, T)\tfrac{1}{2}\pi^{-2}c^{-3}\omega^2 d\omega. \quad (7.12)$$

Employing the relation that the acoustic energy density is proportional to the mean square excess pressure

$$\text{Energy density}=\rho^{-1}c^{-2}\langle P^2\rangle, \quad (7.13)$$

we again obtain Eq. (7.11).

It is interesting to compare the above result with the pressure fluctuations at a boundary of the gas. The proximity to the boundary, and the shape of the boundary, may be expected to influence the radiation impedance and hence the pressure fluctuations. We consider the pressure fluctuations immediately contiguous to a plane rigid boundary, and we shall find that for this simple case, the mean square pressure fluctuation is just twice that in the volume of the gas.

Consider a plane wall bounding a semi-infinite region containing the gas. If the wall contains a circular piston of radius a_0, the radiation resistance is[9]

$$R=\pi a_0^2\rho c[1-ca_0^{-1}\omega^{-1}J_1(2\omega a_0/c)], \quad (7.14)$$

where J_1 indicates the first order bessel function. The fluctuating force acting on a circular area in a plane boundary is therefore

$$\langle F^2\rangle=(2/\pi)\int E(\omega, T)\pi a_0^2\rho c \times[1-ca_0^{-1}\omega^{-1}J_1(2\omega a_0/c)]d\omega, \quad (7.15)$$

and the fluctuating pressure is

$$\langle P^2\rangle=\lim_{a_0\to 0}\langle F^2\rangle/(\pi a_0^2)^2 \quad (7.16)$$

or

$$\langle P^2\rangle=\rho\pi^{-2}c^{-1}\int E(\omega, T)\omega^2 d\omega. \quad (7.17)$$

Thus the mean square fluctuating wall pressure, as given by (7.17), is just twice the mean square fluctuating volume pressure, as given by (7.11). This factor of two clearly arises from the fact that the pressure waves in the gas must have velocity nodes at the wall. Fluctuations in the neighborhood of the wall may be found by treating the radiation from an oscillating sphere near a reflecting boundary.

Finally, it will be noted that the above equations for pressure fluctuations involve the velocity of sound in the gas, which is not a usual thermodynamic parameter. This quantity may, however, be expressed in terms of standard thermodynamic quantities. Thus for frequencies which are sufficiently high that the compressions in the acoustic waves may be considered to be adiabatic, we have[9]

$$c^2=C_P C_V^{-1}\rho^{-1}\mathfrak{K}_T^{-1}, \quad (7.18)$$

where C_P and C_V are the specific heats at constant pressure and volume, ρ is the density, and $\mathfrak{K}_T$ is the isothermal compressibility. For these frequencies, the pressure fluctuations in the volume of the gas are thus given by

$$\langle P^2\rangle=\tfrac{1}{2}\pi^{-2}\rho^2\mathfrak{K}_T C_V C_P^{-1}\int E(\omega, T)\omega^2 d\omega. \quad (7.19)$$

VIII. CONCLUSION

The generalized Nyquist relation establishes a quantitative correlation between dissipation, as described by the resistance, and certain fluctuations. It seems to be possible to give an intuitive interpretation of such a connection.

A dissipative process may be conveniently considered to involve the interaction of two systems, which we characterize as the "source system" and the "dissipative system." The dissipative system, explicitly considered in Secs. II and III, is necessarily a system with densely distributed energy levels and is capable of absorbing energy when acted upon by a periodic force. The source system is the system which provides this periodic force and which delivers energy to the dissipative system.

Assume the source system to be first isolated from the dissipative system and to be given some internal energy. If the source system is a simple dynamical system, its subsequent dynamics will be periodic (as, for instance, the oscillations of a pendulum or of a polyatomic molecule). The system may be thought of as possessing a sort of internal coherence. If, now, the source system is allowed to act on the dissipative system, this internal coherence is destroyed, the periodic motion vanishes and the energy is sapped away, and the source system is left at last with only the random disordered energy ($\simeq kT$) characteristic of thermal equilibrium. This loss of coherence within the source system may be thought of as being *caused* by the random fluctuations generated by the dissipative system and acting on the source system. The dissipation thus appears as the macroscopic manifestation of the disordering effect of the Nyquist fluctuations and, as such, is necessarily quantitatively correlated with the fluctuations.

An analogy which is perhaps useful is provided by the historical development of the theory of spontaneous radiation from excited atoms. After the initial development of quantum mechanics, it was found impossible to compute the spontaneous transition probabilities for an isolated excited atom, and this dissipative process appeared to be outside the existing structure of dynamics. With the development of quantum electrodynamics, however, the dissipation could be computed,

[9] P. M. Morse, *Vibration and Sound* (McGraw-Hill Book Company, Inc., New York, 1936).

and it was found that the "spontaneous" transitions could be consistently considered to be induced by the random fluctuations of the electromagnetic field in the vacuum. In this case, of course, the excited atom plays the role of the source system, and the "vacuum" plays the role of the dissipative system.

It would thus appear that a reasonable approach to the development of a theory of linear irreversible processes is through the development of the theory of fluctuations in equilibrium systems. Certain results in this connection will be given in subsequent papers by Richard F. Greene and one of the authors (H.B.C.).

PHYSICAL REVIEW VOLUME 83, NUMBER 1 JULY 1, 1951

The Disintegration of Nd^{147}

W. S. EMMERICH AND J. D. KURBATOV
Ohio State University, Columbus, Ohio
(Received March 12, 1951)

Three groups of monochromatic electrons corresponding to gamma-rays of 91.5±1.0 kev, 320±3 kev, and 534±4 kev have been identified in the disintegration of Nd^{147}. These gamma-rays are ascribed to transitions in Pm^{147}. Evidence has been obtained for a complex beta-spectrum of Nd^{147}. On the basis of coincidences, a partial scheme of disintegration for Nd^{147} is proposed. The total energy decrease from the ground state of Nd^{147} to the ground state of Pm^{147} nuclei is 1.425±0.015 Mev.

I. INTRODUCTION

SINCE the original observation of an 11-day period radioactive neodymium[1] several papers have been published on the radiations emitted by this species.[2–5] When fission products became available, it was possible to identify the 11-day period as mass number 147. By absorption technique, the beta-emission was found to be 0.9 Mev and ~0.4 Mev with intensities of 60 and 40 percent, respectively.[4] Low energy electrons, x-rays, and gamma-rays of ~0.58 Mev with an intensity of 40 percent were also observed. Coincidences were obtained between high energy betas and x-rays, also between lower energy betas and gammas. In a recent letter[5] beta-energies of 780 kev and 175 kev were reported, complex beta-gamma-coincidences were found, and the absence of gamma-gamma-coincidences noted.

II. PROCEDURE

For the present study, commercially supplied neodymium in the form of neodymium oxide was irradiated with neutrons at the Oak Ridge National Laboratory. The activated material was aged to allow for the decay of 12-min Pm^{151} and 47-hr Pm^{149}. Corrections were applied in various phases of this investigation for the growth of 0.22-Mev beta-rays of the daughter product, Pm^{147}. Spectrometer sources were prepared on Cellophane tape. They were not covered, and a radiogram showed that the distribution of the activity was practically uniform. Since neutron-activated material was used, inert neodymium was present, and a method of obtaining a correction for scattering in the source (at low energies) is mentioned below in connection with the correction for counter window absorption. Sources for the coincidence counter were mounted on Cellophane and covered with zapon.

TABLE I. Internal conversion electrons in Nd^{147}.

Energy of electrons (kev)	Estimated intensity	Conversion shell	Energy of gamma-ray (kev)
46.0±0.5	strong	*K*	
84.5±0.5	strong	*L*	91.5
89.9±0.5	medium	*M*	
275 ±3	weak	*K*	
315 ±4	very weak	*L*	320
489 ±4	medium	*K*	
528 ±5	weak	*L*	534

Measurements were carried out with the aid of a permanent magnet electron spectrograph, a thick lens beta-spectrometer, and coincidence counters.

The electron spectrograph is of the semicircular type using photographic plates as detectors. Although large sources had to be used to attain sufficient intensity for the measurement of internal conversion electrons in this instrument, a resolution of ~ one percent could be obtained for energies over 100 kev. The magnetic field strength between the pole pieces was determined with internal conversion electrons of I^{131} and Cs^{137}.

The ring focusing was efficiently attained in the beta-spectrometer by using a coil that extends along the total path length of the electrons. The position of the defining baffle was found from electron trajectories as determined by the empirically measured magnetic field distribution inside the coil. Additional baffles were installed to minimize scattering from the walls and to eliminate the higher order focusing of slow electrons. A 2-mg/cm² mica window G-M counter was used as detector. The spectrometer was operated with a resolution of ~4

[1] Law, Pool, Kurbatov, and Quill, Phys. Rev. **59**, 936 (1941).
[2] W. Bothe, Z. Naturforsch. **1**, 179 (1946).
[3] Cork, Shreffler, and Fowler, Phys. Rev. **74**, 240 (1948).
[4] Marinsky, Glendenin, and Coryell, J. Am. Chem. Soc. **69**, 2781 (1947).
[5] C. E. Mandeville and E. Shapiro, Phys. Rev. **79**, 391 (1950).

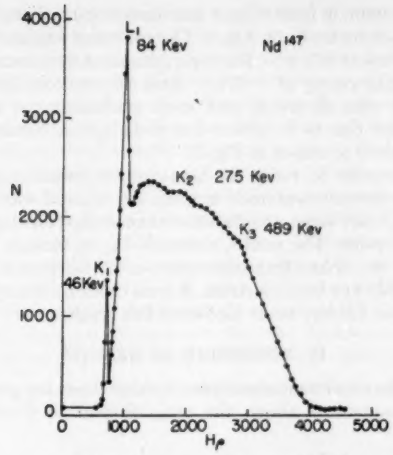

FIG. 1. Spectrometer reading for Nd^{147}.

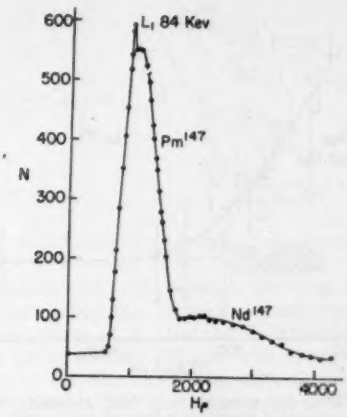

FIG. 2. Spectrometer reading for Pm^{147} grown from Nd^{147}. (Nd decayed about eight half-lives.)

percent. The calibration constant was found by using the internal conversion electrons of Cs^{137} and Au^{198}. The relativistic approximation of the Fermi function given by Bethe and Bacher[6] was applied in the calculations of the Fermi plot. Since Pm^{147} appears as the decay product of Nd^{147}, and is known to have a beta-spectrum of the allowed shape,[7,8] the original source of Nd could be used after sufficient aging to give at once an experimental correction for window absorption and source scattering. Window absorption was also checked with the allowed beta-spectrum of Co^{60}.

The coincidence work was done with a Rossi circuit having a resolving time of 5×10^{-7} second. The source was placed at the center of a 4-mm aperture in an aluminum shield between two mica window G-M counters facing each other. The resolving time was measured with Sr^{90} under identical geometric conditions. Co^{60} was used to determine the efficiency of the counters.

III. EXPERIMENTAL RESULTS

Table I gives the energies of internal conversion electrons determined by the spectrographic method and the gamma-energies as calculated on the basis of the transitions in Pm. For the 91-kev transition, the momentum interval between K-conversion and L-conversion electrons is sufficiently well resolved to verify experimentally that the transition is in Pm. Because comparatively strong sources are required to operate the spectrograph, reliable measurements were confined to little more than one half-life. Nine days after freshly irradiated material had been exposed for 72 hours, a second exposure of 72 hours was taken. It was noted that the electron lines listed in Table I had decreased in intensity. Immediately afterwards, an exposure of 160 hours was taken. In this plate, the lines appeared with approximately the same intensity as in the first plate.

Relative intensity measurements were carried out on the K and L lines of the 91-kev transition and the K/L-ratio was found to be $\sim$2.5 with this method.

Because of the high sensitivity of the magnetic lens spectrometer, the measurements of the beta-spectrum could be extended through a period covering five half-lives. Uncorrected spectrometer readings taken at the beginning and at the end of this time are shown in Fig. 1 and Fig. 2. These indicate: (1) the comparatively high intensity of the internal conversion electrons of the 91-kev transition as compared to the 320-kev and 534-kev transition, considering that window absorption is appreciable in the region below 100 kev; (2) the rapid growth of the 0.22-Mev beta-emission of Pm^{147}; and (3) the absence of long-life metastable states in Pm^{147} above 50 kev. A half-life of 11.1 ± 0.5 days was obtained for electrons in several energy ranges above 0.23 Mev

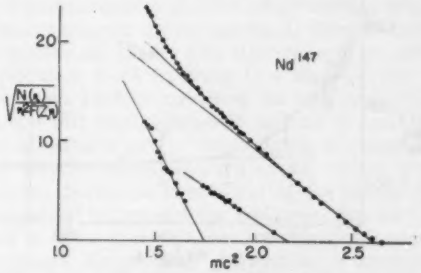

FIG. 3. Fermi plot for Nd^{147}.

[6] H. A. Bethe and R. F. Bacher, Revs. Modern Phys. 8, 82 (1936).
[7] Lidofsky, Macklin, and Wu, Phys. Rev. 76, 1888 (1949).
[8] Langer, Motz, and Price, Phys. Rev. 77, 798 (1950).

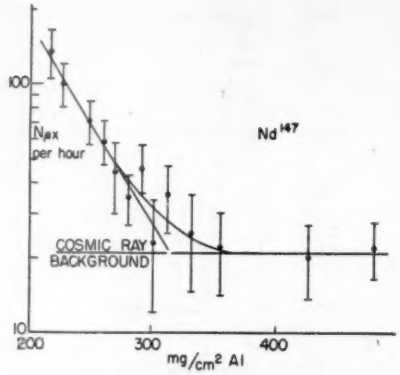

FIG. 4. Beta-x-ray coincidences in Nd^{147} obtained with equal amounts of aluminum in front of each counter.

from the spectrometer readings throughout this period. A Fermi plot is shown in Fig. 3. Assuming allowed shapes, three superimposed beta-spectra are apparent, having end points of 825±15 kev, 600±30 kev, and 380±30 kev. The precise energy determination is made difficult by interference from internal conversion electrons. The relative intensity of the components has been calculated on this basis as being approximately 60:15:25 in the order of decreasing energy. Using window corrected data, the K/L-ratio of the 91-kev transition was found to be ~2.9.

It was the aim of the coincidence measurements to establish a genetic relationship between the various radiations found in Nd^{147}. It was stated by previous workers[5] that no gamma-gamma-coincidences exist. In the present work, this result has been confirmed. The total experimental coincidence rate between the principal electromagnetic radiations, i.e., ~38-kev x-rays and gammas, was found to be not more than five percent of the experimentally observed coincidences between the two gamma-rays of Co^{60} under the same geometrical conditions. Strong coincidences were obtained between high energy betas and x-rays. In order to find the upper energy of the betas, absorption with equal amounts of aluminum in front of each counter was carried out. The results are shown in Fig. 4. The end point was found to be close to 825 kev. The x-rays involved were found to have an energy of ~38 kev. Beta-electron coincidences were also observed, and upon subtraction of beta-counts due to 0.22-Mev Pm radiation, a curve was obtained as shown in Fig. 5.

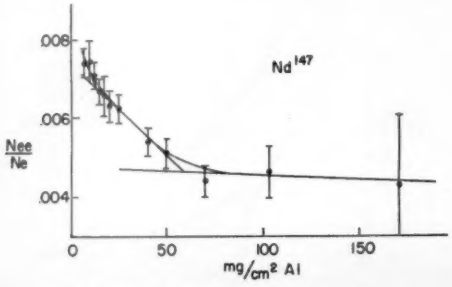

FIG. 5. Beta-electron coincidences in Nd^{147}.

In order to verify the beta-electron coincidences, a measurement was made in which one channel was open to 825-kev betas, and the other channel used for electron absorption. The results, shown in Fig. 6, indicate that it is the 91-kev transition which is in coincidence with the 825-kev beta-spectrum. A cross check by absorption on the 825-kev betas confirmed this result.

IV. DISCUSSION OF RESULTS

The experimental evidence obtained from the present measurements allows the establishment of a partial

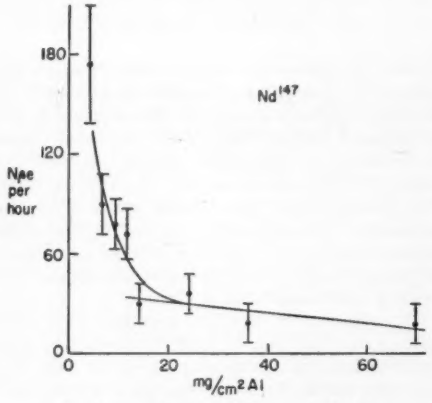

FIG. 6. Beta-electron coincidences with high energy betas in Nd^{147}.

decay scheme shown in Fig. 7. In this scheme the most abundant photons are included. Likewise, beta-spectra of the highest abundance are considered. The total energy difference between the ground states of the Nd^{147} and Pm^{147} nuclei appears to be 1.425±0.015 Mev. This scheme is supported by observation of coincidences between the 825-kev beta-spectrum and the 91-kev gamma-transition. Considering the presence of conversion electrons due to gamma-rays of 320 kev and 534 kev, the Fermi plot obtained may be used to obtain qualitative information on the complexity of the Nd^{147} beta-spectrum. By subtraction of the 825-kev component, the two other spectra of 600 kev and 380 kev are indicated, which are less certain. These energies, in conjunction with the gamma-rays of 320 kev and 534 kev, respectively, are added in the decay scheme. Independent supporting evidence is obtained from the decay measurements of internal conversion lines in the spec-

trograph, from the coincidences observed between the 600-kev beta-spectrum and conversion electrons of the 320-kev gamma-ray, and from the absence of gamma-gamma coincidences. A search for long-life metastable states has yielded negative information. A ground to ground beta-transition has not been observed experimentally in the present measurements. On the basis of relative intensities, the *ft* value for the 825-kev beta-transition is $\sim 3\times 10^7$, for the 600-kev transition $\sim 4\times 10^7$, and for the 380-kev transitions $\sim 5\times 10^6$.

Of the three gamma-rays, most information is available on the 91-kev transition. Although it appears to be highly converted, and has a K/L-ratio of about 2.5,* the mean life is expected to be less than 5×10^{-7} second, since coincidences are observed. In the case of the 320-kev and the 534-kev gamma-rays, K-conversion lines are considerably more intense than L-conversion lines.

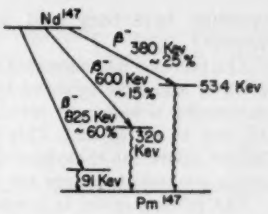

FIG. 7. Partial decay of Nd^{147}.

The authors wish to thank Mr. C. McWhirt and the crew of the machine shop for the construction of equipment, and Messrs. E. B. Dale and P. Zeldes for assistance in taking readings. We also wish to express our gratitude to the Ohio State University Development Fund for grants to carry on this research.

* Self-absorption in the source may account for the low experimental value of this ratio.

PHYSICAL REVIEW VOLUME 83, NUMBER 1 JULY 1, 1951

The Proton Component of the Cosmic Radiation at Sea Level*

E. L. GOLDWASSER† AND T. C. MERKLE, JR.
Department of Physics, University of California, Berkeley, California

(Received March 19, 1951)

The range spectra of mesons and protons in the sea-level cosmic radiation have been investigated with a cloud chamber that had within its volume a total of 10 cm, of lead equivalent absorbing material. Measurements were made with absorbers equivalent to 2, 7, 17, and 48 cm of lead above the apparatus. The masses of stopping particles were determined by observing the momentum and range of each particle. One hundred and sixty-one mesons (mass $=205\pm 2m_e$) and 72 protons (mass $=1900\pm 44m_e$) were observed. No evidence was found for the existence of any particles with intermediate mass. Data obtained under each of the four thicknesses of moderating absorber were used to give four points on the differential range spectra for mesons and protons. The meson spectrum has a peak occurring in the range between 17 cm and 30 cm of lead. The observed proton component can be interpreted either as the residual of a flux of protons which is incident on top of the moderator and degraded in energy with passage through the moderator, or as a flux of protons produced in the moderator by an incident neutral radiation, probably neutrons. The proton range spectrum fits an exponential absorption law with a mean free path of 12 cm of lead. This is just the order of attenuation to be expected from nuclear interactions of protons or neutrons. Thus, if the protons are incident on the moderator, their differential range spectrum would have to have been flat in the region between 8 and 54 cm range in lead. This implication, together with the behavior of the proton component in the lead absorber plates observed in the cloud chamber, points to the incident neutron hypothesis as the more probable explanation of the observed protons.

I. INTRODUCTION

IN the experiment of Merkle, Goldwasser, and Brode[1] it was found that the penetrating component of the cosmic radiation with ranges between 4 and 13 cm of lead consisted of approximately equal numbers of mesons and protons. The observed flux of stopping protons amounted to about 1 percent of the total penetrating component. The experimental observations reported in this paper were undertaken to determine the nature of the proton component and its source.

The apparatus used was the same as that used in the previous experiment with a few minor modifications. A schematic diagram is shown in Fig. 1. The momentum of a particle was measured by observation of the radius of curvature of its trajectory in a magnetic field of 4500 gauss. Particles traversing the momentum cloud chamber with residual ranges of less than 11 cm of lead were observed to stop in one of a series of copper and lead absorber plates mounted in the second cloud chamber. Numerical integrations of the energy loss equation for copper and for lead were then used in order to calculate masses from the observed momenta and ranges. Recent direct observations of range and velocity of high energy protons made in the 184-in.

* Assisted by the joint program of the ONR and the AEC.
† Westinghouse Fellow, now at the University of Illinois, Urbana, Illinois.
[1] Merkle, Goldwasser, and Brode, Phys. Rev. **79**, 926 (1950).

cyclotron have been used to determine the mass values.[2,3]

The previous measurements under the equivalent of 2 cm of lead were extended by the use of additional moderating absorbers to permit observations under 7, 17, and 48 cm of lead. This absorbing material was located above the three-tube Geiger counter telescope which was used to trigger the apparatus.

The limiting factor in accurate mass determination was again found to be the turbulence in the momentum cloud chamber. A study of the no-field tracks revealed a mean residual curvature of $+0.016$ reciprocal meters, with a probable error of ± 0.016 reciprocal meters. Each momentum calculation was corrected for the observed mean no-field curvature.

II. MASS DATA

In this experiment 8500 events were photographed of which 1400 were without a magnetic field. The mean values for the data obtained here, together with that previously reported,[1] involve 161 stopping mesons and 72 stopping protons. For the mesons the mean mass is found to be $m=205\pm 2\, m_e$. For the protons $m=1900 \pm 44\, m_e$. The mean value of the meson masses measured under 7, 17, and 48 cm of lead is $208\pm 2\, m_e$. This is significantly higher than that obtained in the previous experiment with the same apparatus, but with no lead above it. The mean mass values for the 64 positive mesons and 49 negative mesons under 7, 17, and 48 cm of lead agree within the probable errors assigned. The observed mass shift cannot, therefore, be explained by a consistent change of the mean turbulent curvature.

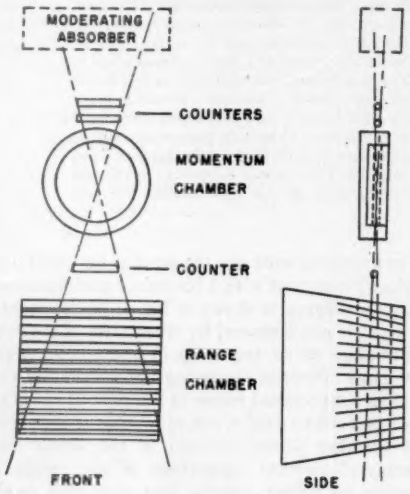

FIG. 1. Schematic diagram of apparatus.

[2] C. J. Bakker and E. Segrè, Phys. Rev. **81**, 489 (1951).
[3] E. Segrè and R. L. Mather, private communication.

A change in the calibration of the magnetic field would account for the shifts, but the field was checked with a flux meter, which in turn was calibrated by the use of the proton resonance. The comparison of the mean masses from the different groups of measurements seems to indicate that there is present some unknown source of systematic fluctuations which makes the values of the probable errors relatively meaningless. It is possible that a small contamination of pi-mesons and deuterons is present and is dependent on the amount of absorber placed over the apparatus.

III. RANGE DATA

Table I shows the significant data obtained under 7, 17, and 48 cm of lead moderator and under 2 cm of lead equivalent during the previous work.

Using these data, differential range spectra for mesons and protons are presented in Fig. 2.

IV. MESON COMPONENT

The meson spectrum shows the expected peaked shape, but the peak is much more pronounced than that which has been found by most other workers.[4,5] It should be noted that counter experiments and cloud chamber work which do not specifically identify the particles whose ranges are observed, may lump the proton stopping rate with that of the mesons. Doing this with the data of the current experiment gives a spectrum which is relatively flat in the low range region and then drops off at ranges greater than 25 cm of lead. There is one remaining important discrepancy between this explanation and existing experimental results. This lies in the results of counter experiments by Sands[6] which tag the stopping mesons by observation of the delayed coincidences of the decay electrons. The spectrum obtained in this way was also much less peaked than that shown for mesons in Fig. 2. This may be due in part to an inaccuracy of the operating time under 2 cm of lead equivalent in the first part of this experiment. During that part of the experiment the dead time of the apparatus fluctuated considerably, but the time given is believed to be within 10 percent of the correct value.

V. PROTON COMPONENT

In order to calculate the flux of protons in various prospective range intervals, as they are present in the atmosphere above the moderating absorber, it is necessary to correct the observed flux of stopping particles by a factor consistent with the rate of removal of protons through nuclear interaction processes in the moderating absorber. Although no exact value for this cross section is known, most of the available data points to the geometrical cross section of the nucleus as a

[4] For a summary, see B. Rossi, Revs. Modern Phys. **20**, 537 (1948).
[5] L. S. Germain, Phys. Rev. **80**, 616 (1950).
[6] M. Sands, Phys. Rev. **77**, 180 (1950).

TABLE I. Observed range data.

Mean Pb equiv. traversed (cm)	Hours operating time	No. of stopped mesons	No. of stopped protons	Stopping mesons per hr	Stopping protons per hr	Mean meson mass	Mean proton mass
8	518	48	53	0.09	0.102	194	1875
13	220	43	14	0.20	0.064	214	1989
23	142	35	4	0.26	0.028	207	1799
54	230	35	1	0.15	0.004	201	2625

reasonable approximation throughout the energy region under investigation. Thus if the protons were incident on the moderator in some arbitrary energy spectrum, from consideration of ionization losses only, there would exist a prospective differential range spectrum for the protons in the air above the moderator, and this can be represented as:

$$(dN/dR)_0 = f(R). \tag{1}$$

To investigate this spectrum, the stopping rate under several thicknesses, R_i, of absorber must be observed. But in R_i centimeters of absorber, nuclear interactions occur to the extent that the observed stopping rate would be:

$$(dN/dR_i)_{R_i} = f(R_i)\exp(-R_i/L_{\text{Pb}}), \tag{2}$$

where L_{Pb} is the mean free path of the protons for nuclear interaction, $L=1/n\sigma$ where n=number of nuclei per cc of absorber and σ is the cross section per nucleus.

The proton spectrum of Fig. 2 is replotted on semi-logarithmic coordinates in curve 1 of Fig. 3. The experimental points are found to be consistent with an exponential attenuation, $e^{-R/L}$. The slope of the straight line shown gives $L \simeq 12$ cm of lead. But, using the geometric cross section of the lead nucleus, $\sigma=\pi(1.5)\times10^{-26}\times A^{\frac{2}{3}}=2.47\times10^{-24}$ cm^2, gives $L_{\text{Pb}}=12$ cm. This means that in Eq. (3), $f(R)$ must be a constant, and thus Eq. (1) now becomes

$$(dN/dR)_0 = \text{constant}$$

in the region investigated. In other words, if the stopping protons observed are, indeed, a part of a proton flux incident above the moderator, then this differential spectrum $(dN/dR)_0$, is constant between 8 and 54 cm of lead. From this assumption, one would be forced to the conclusion that protons constitute an appreciable portion of the sea-level radiation. In the first part of the experiment, with 8 cm average range, it was found that the numbers of stopping mesons and protons were roughly equal. The question of possible selectivity of the apparatus has been investigated. The magnetic field across the momentum cloud chamber constitutes a momentum selector which can prevent low momentum particles from entering the range chamber. Calculations of this effect have been carried out, and they show that the effective solid angle of the apparatus for the detection of mesons is about two-thirds of that for the detection of protons. The assumption that the flux of protons at sea level with prospective ranges between 8 and 54 cm is constant leads to the improbable conclusion that 25 percent of the penetrating particles in this range interval are protons.

There is another possible interpretation of the observed proton component. If it is assumed that at sea level there is a neutron component with energies in the neighborhood of 200 Mev, then these neutrons may be expected to interact with the nuclei of any absorbing medium. Some of these interactions will have the nature of stars of several prongs. Others will have the nature of knock-on or charge exchange processes. Protons originating from such interactions will have all energies up to that of the incident neutrons. Since the cross section for neutrons is about equal to that for protons, the attenuation which is observed under increasing thicknesses of moderator is just what would be expected due to the attenuation of the neutron flux in the moderator. The protons observed to stop are then mainly produced either in the absorber or in the atmosphere within one mean free path of the top counters. The minimum neutron flux required at sea level would be about 1 percent of the total hard component, but the requirement is strongly dependent on the relative frequencies of various kinds of interactions.

If the protons observed in this experiment are the penetrating portion of an incident flux of protons, then the attenuation of protons observed within the range chamber in all parts of the experiment should merely be a continuous part of the attenuation observed when operating under various thicknesses of absorber. To test this, the range chamber was divided for the purpose

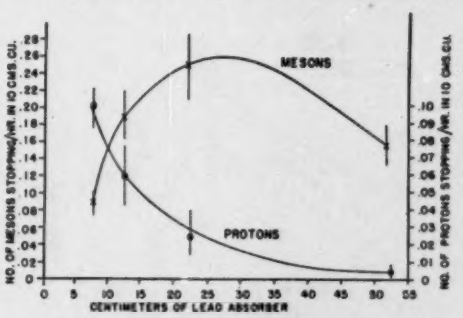

FIG. 2. Differential range spectra for mesons and protons obtained by adding moderating absorber above apparatus.

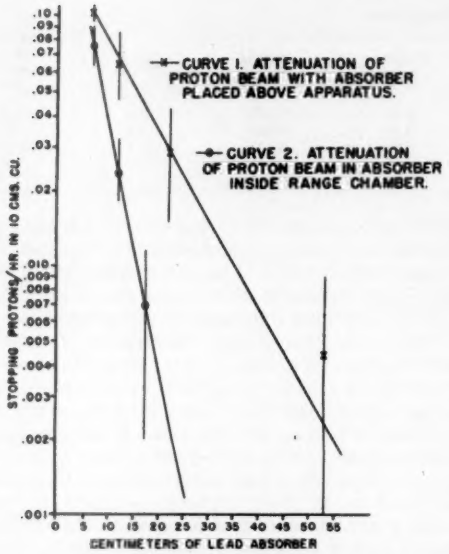
CURVE 1. ATTENUATION OF PROTON BEAM WITH ABSORBER PLACED ABOVE APPARATUS.
CURVE 2. ATTENUATION OF PROTON BEAM IN ABSORBER INSIDE RANGE CHAMBER.
STOPPING PROTONS/HR. IN 10 CMS. CU.
CENTIMETERS OF LEAD ABSORBER

FIG. 3. Semi-logarithmic plot of differential range spectra for protons: 1. with moderating absorber added above apparatus; 2. with increasing absorber inside range chamber.

of statistics into two 4.5 cm range intervals. The flux of protons stopping in the top 4.5 cm and the flux stopping in the bottom 4.5 cm, when operating under 2 cm and 7 cm effective lead moderator, are plotted as curve 2 in Fig. 3. The flux under 7 cm moderator has been normalized to that under 2 cm so as to make the common points at 11.5 cm coincide. The results can be interpreted as a true proton attenuation only if there is no important instrumental attenuation from the top to the bottom of the range chamber. The observed meson stops occurred with essentially equal probabilities in the top and bottom of the chamber. Thus it can be safely assumed that there is no significant instrumental attenuation.

The slope of this new curve gives $L \simeq 4$ cm. The difference between the slopes of these two lines is believed to be significant. The results thus appear to be inconsistent with the incident proton hypothesis.

According to the incident neutron hypothesis, the curve for an absorber placed above the counters shows essentially the attenuation of the primary neutrons; while the attenuation observed within the range chamber merely represents the range spectrum of the secondary protons. This depends on the spectrum of neutrons and on the probabilities of various types of interaction. The fact that curve 2 in Fig. 3 is steeper than curve 1, means simply that short range secondaries are more probable than long range ones.

The observations reported in this paper appear to support the hypothesis that most of the protons observed coming from the atmosphere and from lead absorbers up to 54 cm in thickness are secondary particles from neutron reactions. The proton flux observed in this work is in excess of that observed by other workers both in this laboratory and elsewhere. Experiments are now being undertaken to resolve this discrepancy and to check the neutron reaction hypothesis.

The authors are pleased to have this opportunity to express their gratitude to Professors R. B. Brode and W. B. Fretter for many helpful discussions and invaluable advice. We also wish to express our thanks to Messrs. J. Lipson and G. Plummer, who processed all of the film for the experiment, and Messrs. A. Villaire and J. Ballam, who assisted in the maintenance of the apparatus and the reading of film.

Excitation Functions for Proton Reactions with Sodium and Magnesium*

J. W. MEADOWS AND R. B. HOLT
Nuclear Laboratory, Harvard University, Cambridge, Massachusetts
(Received March 6, 1951)

Proton bombardment at energies up to 120 Mev have been carried out on the Harvard University cyclotron using targets of $Na^{23}NO_3$, $Mg^{25}O$, $Mg^{26}O$, and ordinary MgO. A stacked sample and absorber technique was employed, using the formation of C^{11} from interleaved polyethylene foils as a monitor. The internal scattered beam at about 180° from the scatterer and 1 inch below the median plane was employed to give better energy resolution. Absolute excitation curves have been obtained for the reactions yielding F^{18} and Na^{24} from Mg^{25} and Mg^{26}, F^{18} from Mg^{24}, and F^{18} and Na^{22} from Na^{23}.

I. INTRODUCTION

A SYSTEMATIC study of a considerable number of reactions between protons with energies up to 120 Mev and fairly light nuclei is in progress, using the Harvard University 95-in. cyclotron. Our interest in these reactions arises from the fact that the ordinary compound nucleus theory begins to fail in this energy range and in this portion of the periodic table. This paper presents results obtained to date on Na^{23}, Mg^{24}, Mg^{25}, and Mg^{26}.

II. EXPERIMENTAL METHOD

Since it has been found[1] that the energy spread in the primary beam of the Harvard cyclotron is of the order of 10 Mev, it was necessary to use an internal scattered beam (above or below the median plane) with the target to be bombarded located at approximately 180° from the scatterer in order to obtain good energy resolution. This arrangement provides focusing of particles of a given energy scattered at all small azimuthal angles, with various energies spread radially. The energy resolution is determined by the width of the target. The experimental arrangement[2] is shown in Fig. 1.

The stacked "foil" technique was used. The targets consisted of pellets of $NaNO_3$, natural MgO, and MgO enriched[3] in Mg^{25} and Mg^{26}. The pellets were $\frac{5}{16}$ in. in diameter and had a surface density of 20 to 40 mg/cm². These were placed in Lucite holders and stacked between $\frac{7}{16}$-in. diameter disks of copper or aluminum. A polyethylene foil of the same diameter was placed with each pellet. The $C^{12}(p, pn)C^{11}$ cross section[4] was used to monitor the beam. The excitation curve of this reaction was re-run as a check on our energy values. The samples were counted with a mica end window Geiger counter, and the decay curves were resolved to determine the amounts of the different activities present. All samples were counted, as nearly as possible, under the same geometry and mounting arrangements. Experimental corrections were made for the effect of sample thickness. The absolute values of the cross sections given are probably accurate to ±20 percent. The activities were identified by their half-lives and ranges in aluminum.

III. EXPERIMENTAL RESULTS AND CONCLUSIONS

The excitation function curves for Mg^{26} to form Na^{24} and F^{18} are shown in Fig. 2. The threshold (corrected to the laboratory system) of the $Mg^{26}(p, pd)Na^{24}$ reaction is 21.8 Mev, and that of the $Mg^{26}(p, 2pn)Na^{24}$ is 24.9 Mev. The observed threshold of approximately 20 Mev is in reasonable agreement with the first reaction shown. The curve does not show the pronounced maximum characteristic of compound nucleus formation, which indicated that other processes, such as direct knockout, etc., are probably relatively important. The large number of possible mechanisms for this reaction would lead one to expect a relatively smooth excitation function curve; our method does not provide the necessary information for deciding relative contributions of these mechanisms.

The lowest threshold energy for the formation of F^{18} from Mg^{26} is 24.6 Mev via the reaction $Mg^{26}(p, 2\alpha n)F^{18}$. The measured threshold is between 20 and 30 Mev. Other probable reactions have thresholds in excess of 40 Mev. The lack of pronounced structure of the curve

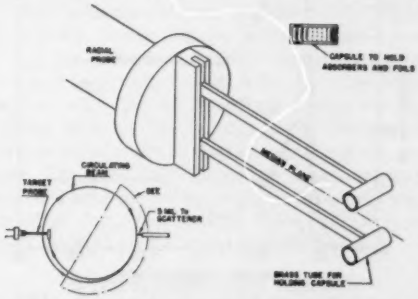

FIG. 1. Position of scatterer and target in the cyclotron tank and diagram of target holder.

* Supported by the joint program of the ONR and AEC.
[1] N. Bloembergen and P. J. Van Heerden, Phys. Rev. 82, 316A (1951).
[2] This method was developed by N. M. Hintz and N. F. Ramsey and reported in Phys. Rev. 82, 304A, 342A (1951).
[3] This material was obtained from Oak Ridge National Laboratory, Oak Ridge, Tennessee.
[4] Aamodt, Peterson, and Phillips, UCRL-526 (1949) (unpublished).

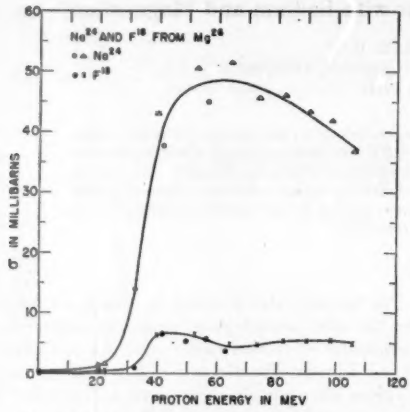

FIG. 2. Excitation functions for the formation of F^{18} and Na^{24} from Mg^{26}.

at higher energies suggests that the higher threshold reactions are relatively important.

The excitation curves for the formation of Na^{24} and F^{18} from Mg^{25} (see Fig. 3) both show pronounced maxima, indicating the importance of the formation of compound nuclei in these reactions. The $Mg^{25}(p, 2p)Na^{24}$ reaction with a threshold of 11.6 Mev is the only possible one for the formation of Na^{24}. The observed threshold is in good agreement with the above value. The three possible mechanisms (formation of compound nuclei of Mg^{26} or Al^{26} or direct knock-out) are probably all important. The general shape of this curve agrees very well with the shape calculated[5] for the $C^{12}(n, 2n)C^{11}$ reaction. The reason for the sharp peak is the low threshold for the reaction, which favors compound nucleus formation.

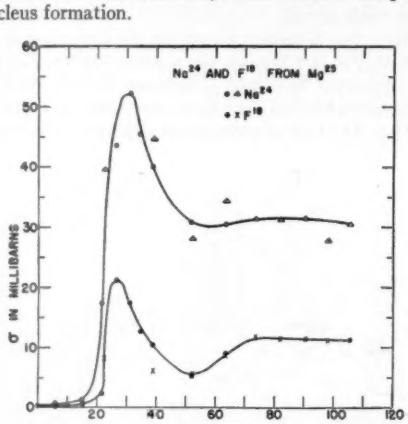

FIG. 3. Excitation functions for the formation of F^{18} and Na^{24} from Mg^{25}.

[5] W. Hecrotte and P. Wolff, Phys. Rev. **73**, 265 (1948).

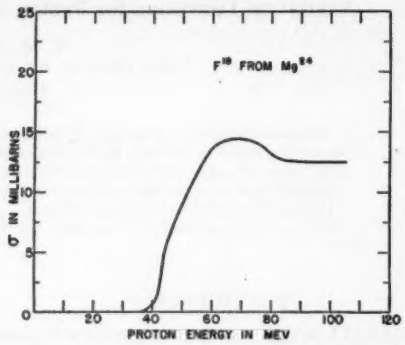

FIG. 4. Excitation function for the formation of F^{18} from Mg^{24}.

The $Mg^{25}(p, 2\alpha)F^{18}$ reaction, with a threshold of 12.0 Mev, is the lowest energetically possible reaction. The next energetically possible reaction has a threshold of about 35 Mev, which means that the reaction in the energy range between 12 and 35 Mev can proceed only by the formation of the Al^{26} compound nucleus and the "boiling off" of two α-particles. This is evident from the shape of the curve obtained in this energy range. At higher energies, the cross section again begins to rise, as reactions with higher thresholds become important.

The excitation function for the formation of F^{18} from Mg^{24} was obtained by bombarding natural MgO (78.6 percent Mg^{24}) and subtracting out the known contributions of the Mg^{25} and Mg^{26} present. The resulting curve is Fig. 4. The initial reaction (at relatively low energies) is probably $Mg^{24}(p, pad)F^{18}$ with a threshold of 32.8 Mev or $Mg^{24}(p, He^3\alpha)F^{18}$ with a threshold of 26.5 Mev.

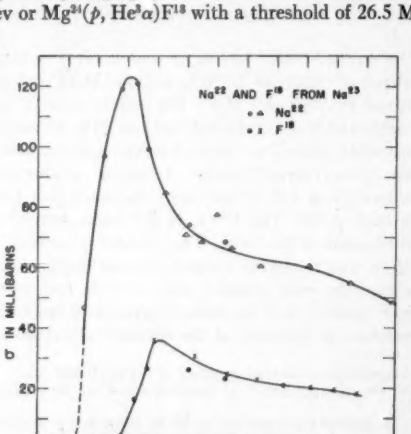

FIG. 5. Excitation functions for the formation of F^{18} and Na^{22} from Na^{23}.

The method of subtraction used makes the observed threshold somewhat inaccurate, but it is certainly less than 40 Mev.

Results obtained with Na^{22} are shown in Fig. 5. Na^{22} may be formed by the (p, d) or the (p, pn) reaction with thresholds of 11.6 and 13.8 Mev, respectively. The observed curve seems to be in agreement with the lower value. The pronounced maxima indicates the formation of a compound nucleus, and its breadth indicates that both possible modes of decay are important. At higher energies mechanisms other than the formation of the compound nucleus become important. The general shape of the curve is in fair agreement with the one calculated[6] for the $C^{12}(p, pn)C^{11}$ reaction. However, this does not account for the decline of the cross section above 100 Mev.

The $Na^{23}(p, \alpha d)F^{18}$ and $Na^{23}(p, pn\alpha)F^{18}$ with thresholds at 20.3 and 22.5 Mev, respectively, are probably the reactions by which F^{18} is formed initially. The maxima at approximately 40 Mev indicates the formation of a compound nucleus as the principal reaction at the lower energies. In the vicinity of 50 Mev other reactions such as $(p, 3p3n)$ become energetically possible and may account for the slow decline of the cross section at higher energies.

[6] W. Hecrotte and P. Wolff, Phys. Rev. 73, 264 (1948).

PHYSICAL REVIEW VOLUME 83, NUMBER 1 JULY 1, 1951

The Origin of Bombardment-Enhanced Thermionic Emission

J. B. JOHNSON
Bell Telephone Laboratories, Murray Hill, New Jersey
(Received March 21, 1951)

Measurements on bombardment-enhanced thermionic emission from oxide cathodes show that (a) the effect is not related to normal fading and recovery of thermionic emission; (b) the emitted electrons have energies in the thermal range rather than in the secondary range. Calculations indicate that the electron bombardment releases more than enough internal secondaries to account for the effect as increased thermionic emission. A more comprehensive theory is needed for explaining why the observed effect is not even larger.

I. INTRODUCTION

A THERMIONIC emitter of (BaSr)O has its emission temporarily increased when bombarded by electrons.[1] In addition to the normal thermionic emission and to the secondary emission which normally accompanies the bombardment, there is a gradual increase of current during the first few microseconds of bombardment and a corresponding gradual decrease when the bombarding pulse is over. The persistence of the added emission after the end of the bombardment led to the belief that the emission is of thermionic rather than secondary origin. As a possible source of the bombardment-enhanced thermionic emission was suggested either a reduction of work function or an increase in the density of conduction electrons in the bombarded target. The experiments reported here deal with the energy distribution of the emitted electrons, and with the relation of the enhanced emission to the phenomenon of fading. They give further proof of the thermionic origin of the increased current, and support the view that change of electron density rather than of surface conditions is the principal cause of this current.

II. METHOD

The experiments were done with equipment similar to that described earlier. The target of activated (BaSr)O on Ni, a collector electrode and an electron gun are enclosed in a gettered and sealed-off tube. A pulsed electron beam bombards the target, with the collector negative or positive for measuring the primary or secondary current. The current of the target circuit actuates a video amplifier and is displayed on an oscilloscope. Typical results are shown in Fig. 1, which has two sets of oscillograms, (a) and (b), each of three traces, two displaced slightly from the axis which is the central trace. (The vertical strokes have been dotted in for clearness.) In the lower trace of each set the 1250-volt beam was pulsed on for 10 μsec while the collector was negative, and the trace records primary beam current. The upper trace, with the beam similarly pulsed, was made with the collector positive (with amplifier gain reduced). In Fig. 1(a) the target temperature was low and the thermionic current negligible, and the flat-topped upper trace records well-behaved secondary current. In Fig. 1(b) the thermionic current was high, but being dc it was blocked out in the coupling condensers of the circuit and does not appear in the oscillogram. The upper trace in this set shows clearly the variation of emission during and after the beam current pulse when thermionic current flows, and it is this variable emission that is under discussion.

III. EXPERIMENTS ON FADING

When temperature-limited thermionic current is drawn suddenly from an active oxide cathode there is

[1] J. B. Johnson, Phys. Rev. 73, 1058 (1948).

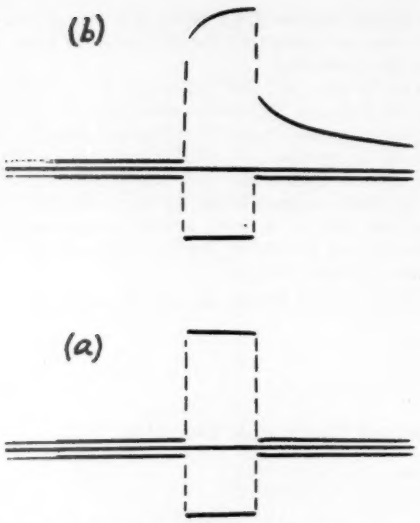

FIG. 1. Rise of enhanced emission with temperature. (a) 520°C, $I_{th}=10\ \mu a$; (b) 670°C, $I_{th}=1500\ \mu a$. $V_p=1250$ v, $V_c=-22$ or $+64$. Pulse 10 μsec. $i_p=31\ \mu a$. Tube 499355. Lower trace primary current i_p, upper trace secondary current.

usually a decrease in current with time,[2] with recovery of activity when current is not drawn. This fading process is believed to be caused by a change in the surface composition of the cathode, due to material coming either electrolytically from the interior of the cathode or by evaporation from the anode.

A typical oscillogram of the fading is shown in Fig. 2. Above the line of the x-axis the current is seen to start from an ill-defined high value when the anode voltage is applied, and to have decayed by a substantial fraction within a millisecond, as indicated by the 2500-cps calibration trace below the axis. These traces were made with single sweeps. Figure 3 shows results for a different target under different conditions. The collector voltage was applied in repetitive 145-microsecond pulses

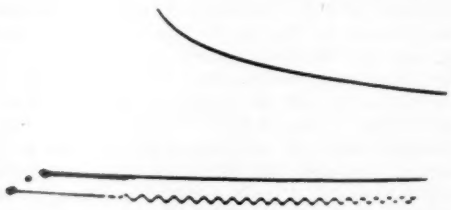

FIG. 2. Fading of thermionic emission in millisecond range. Timing trace 2500 cps. Tube LS 12.

[2] R. L. Sproull, Phys. Rev. **67**, 166 (1945); Kalaschnikov, Kubetski, and Oscher, J. Techn. Phys. USSR **16**, 1369 (1946); E. A. Coomes, J. Appl. Phys. **17**, 647 (1946); D. A. Wright, Proc. Phys. Soc. (London) **B62**, 398 (1949); G. R. Feaster, J. Appl. Phys. **20**, 415 (1949).

and fading in this time is seen. (The upper trace is electrically parallel to the axis on the 'scope.)

It seemed possible that the enhanced thermionic emission is related to this phenomenon in the following way. When the beam of primary electrons is turned on while the collector is positive, for measuring the secondary current, then the cathode has already been delivering thermionic current for a second or more and it might be in a state of reduced activity. If now bombardment by electrons could bring about a partial return of activity, there would be a growth of thermionic current when the beam is turned on and fading at the end of the bombardment.

Two types of experiments were done to see whether this might explain the observed enhanced emission. In one series the positive dc collector voltage was replaced by short positive pulses;[3] in the other were used targets with different fading rates.

In the measurements with pulsed positive collector the negative collector voltage was applied dc as usual, for measuring the primary beam current. At intervals there was superimposed on the negative bias a positive

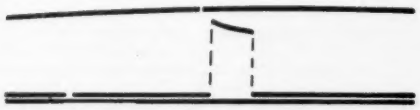

FIG. 3. Fading of thermionic current in microsecond range. 600°C, $I_{th}=430\ \mu a$, $V_c=100$ v pulsed 145 μsec. Tube MN 74.

pulse that brought the collector voltage to about $+30$ volts for some number of microseconds. The target would then emit its full thermionic current, overloading the amplifier at the input in the direction of positive deflection. For preventing the overload the thermionic current pulse was balanced out by applying the collector pulse to an inverter circuit to give a small adjustable negative replica of the voltage pulse, which was applied directly to the input of the amplifier. This canceled the thermionic current pulse except for short spikes at the beginning and end of the pulse and for changes in the thermionic current during the pulse. Fading thus was seen even though the main component of thermionic current was canceled out by the bucking circuit. Within the collector pulse the shorter beam current pulse was applied, and then the secondary and enhanced current was seen in its proper size superimposed on the canceled-out thermionic current.

Applying this technique to targets which exhibited fading, it was found that the change in current during the 10 microsecond beam pulse was always greater than the fading of thermionic emission during even the 145-microsecond collector pulse applied as in Fig. 3. This is strong evidence that the fading and recovery process is not responsible for the changes in current on bombardment.

[3] A similar procedure was used by T. J. Jones, Nature **161**, 846 (1948). Here no enhancement was found.

This point was followed further in connection with a tube that showed no fading under any of the experimental conditions. The tube had parts made of very clean nickel that could be well outgassed. In particular, it had a dummy anode that was used during the pumping, activation, and aging. Only when the process was complete was the well-cleaned anode slid in place.

Results for this tube are shown in Fig. 4. The temperature was 640°C, the thermionic emission about 0.5 ma. The lowest oscillogram, Fig. 4(a), gives the thermionic emission during 145-microsecond pulses of collector voltage, with no evidence of fading in this time. Figure 4(b) records the primary beam current and secondary yield in a 10-μsec beam pulse, both positive and negative collector voltage being dc. The enhanced emission is evident. The amplifier gain was reduced by a factor 4 for the positive pulse, so that the secondary yield δ is about 6. The more complicated procedure for the positive pulsed collector is shown in the top oscillogram, Fig. 4(c). The axis and 10-μsec primary pulse are recorded as before. The positive collector pulse was 40 μsec long, and the flat-topped trace of this length shows the thermionic current during this pulse, without the electron beam, and with reduced gain. There is no fading. The 10-μsec positive pulse is the secondary and enhanced thermionic emission. The main thermionic current is bucked out, the spikes at the ends of the pulse representing uncompensated capacity coupling between target and collector. The rise of the positive pulse as well as the tail at the end are essentially the same for the pulsed as for the dc collector. Fading, if present at all, is certainly less in the long pulse of collector voltage than the change in current during the short bombarding pulse. If there were any significant but undetected fading, it would surely be widely different for the two operating conditions of pulsed and dc collector voltage. We conclude that the fading phenomenon is not responsible for the added emission during the electron bombardment.

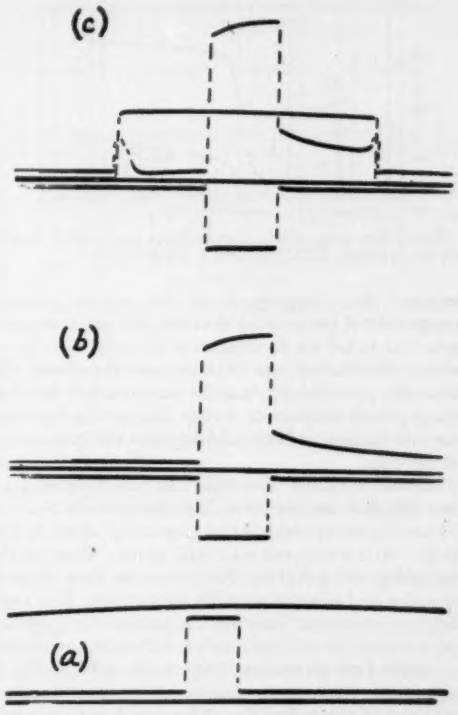

FIG. 4. Comparison of enhancement for pulsed and dc collector voltage. (a) Fading, $V_c = 100$ v, pulsed 145 μsec. (b) Enhancement, $V_c = 64$ v dc. (c) Enhancement, $V_c = 64$ v pulsed 40 μsec. Trace 1, i_p; trace 2, i_s with I_{1b} bucked out; trace 3, I_{1b} alone. 640°C, $I_{1b} \sim 0.5$ ma, i_p pulse 10 μsec. $V_p = 1250$ v. Tube 499355.

IV. INITIAL VELOCITY DISTRIBUTION

If the positive collector voltage is not high enough to collect the full emitted current, then the variable enhanced current appears suppressed more than the normal secondary current. This selective suppression is shown in Fig. 5. Here the target was bombarded for 10 μsec during a 35-μsec collector pulse, the normal thermionic current being balanced out by the bucking pulse. The successive exposures were made with various collector voltages, −22 volts for the lowest trace, 0 for the next, and on to +43 volts for the highest. The first to show a rise in current during the pulse was at +26 volts. The shape of the curves is here evidently altered by a combination of space charge and initial velocities. Before more quantitative results are presented, the arrangement of the collector and target of this particular tube will need description.[4]

[4] See reference 1, Fig. 1, for more detailed electrode structure.

The flat coated part of the target, about 0.3 cm² in area, is the thermionic and secondary emitter. The central part of it, perhaps 0.03 cm², is bombarded by the electron beam. The collector is not plane but presents a flat internal cone to the target, with the spacing at the outside edge about 0.4 mm and greater at the center. The structure is therefore not the planar one

FIG. 5. Space charge limitation of secondary current. I_{1b} dc, $< I_s$ pulsed. 415°C, $V_p = 350$ v. V_c pulse 40 μsec; i_p pulse 10 μsec. $V_c = -22, 0, 4.5, 9, 18, 26, 29, 33, 43$ volts. Tube MN 74.

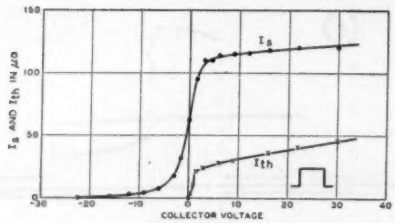

FIG. 6. Retarding potential curve without space charge. $I_{th}<I_s$, I_{th} dc, I_s pulsed. 415°C, $V_p=350$ v. Tube MN 74.

required for measurement of the normal velocity component of the emitted electrons, nor the concentric spherical called for in measuring the total velocity or energy distribution, but is in between these two. The retarding-potential curves to be presented are therefore not a proper measure of energy distribution, but they can still be used to distinguish between different groups of electrons.

Results obtained with this tube will be shown for two different temperatures. The bombarding beam of 34 μa was set at 350 volts to give a δ of about 4. The height of the response was read on the 'scope at the beginning and end of the 20-μsec pulses, for a range of negative and positive dc collector voltages. The pulse heights, measured from the bottom of the negative pulse when the collector was at -22 volts, are plotted in terms of microamperes. They are labeled I_s in Fig. 6, and in Fig. 7 I_{s1} and I_{s2} corresponding to the beginning and end of the pulse. The difference $I_{s2}-I_{s1}$ is again the enhancement under discussion. The thermionic current I_{th} was measured with a dc meter.

In the run of Fig. 6 the target temperature, 415°C, was so low that the thermionic current was less than the secondary current, and there was no appreciable space charge limitation of either. More detailed measurements on the thermionic current showed that the contact potential made the collector 0.7 volt negative with respect to the target. It saturated at about 1.5 volts, showing thereafter the gradual rise usual with oxide cathodes. At negative collector voltages the curve I_s makes a reasonable retarding-potential curve for secondary electrons, showing the presence of electrons with energy of a few volts, in contrast with the thermal energies of the thermionic electrons. The curve still rises for positive collector voltages, reaching a saturation at about 5 volts. This region of "negative energies" has often been observed in secondary emission but never clearly explained. It may be related to surface roughness or to internal fields of the target or more probably to patch fields at the collector. There was no enhancement seen in any part of this curve.

The results with the target at higher temperature, 660°C, are shown in Fig. 7. The thermionic current is now much larger than the current of the secondary pulses and is clearly limited by space charge at the lower collector voltages. For negative collector, the secondary curve is almost identical with that of Fig. 6 where the temperature was lower, so that the amount and energy distribution of the main part of the secondary current is relatively unchanged by the temperature. At high positive collector potentials the secondary pulse is again about as high as at the lower temperature of Fig. 6, but now shows the enhancement during the pulse in the region where the thermionic emission is approximately saturated. Here the enhancement amounts to about 3 percent of the thermionic current from the bombarded area. An interesting change is seen in the region from 0 to +15 volts. Here the pulse height is limited, over a range of almost 10 volts, to a fraction of the total secondaries. Other temperatures and thermionic currents gave the same results, the difference being only in the voltage range of the flat depressed portion of the curve. The explanation[5] seems to be that the secondaries, when they flow, add to the space charge of the thermionic current, and the new and lower potential minimum prevents the flow of an additional small fraction of the thermionic current. The effect disappears with remarkable sharpness when at some voltage, here 12 volts, the potential minimum is no longer maintained. The enhanced emission appears fully developed only at the right of the point where the potential minimum disappears, never at the left in the region of true secondaries. The significance of this is that the electrons involved in the enhanced emission have energies all in the region of thermal energies. They must be thermal rather than secondary in origin.

V. SOURCE OF THE ENHANCED THERMIONIC EMISSION

The thermionic emission generated by electron bombardment has been shown to be unrelated to the fading process, which involves a change in work function. It is too large to be explained by temperature rise of the surface due to bombardment.[1] A different way of accounting for the increased emission is to assume that the bombardment raises the density of conduction electrons available for thermionic emission near the surface of the target.[1] A rough calculation makes this hypothesis seem plausible.

In the experiment of Fig. 7 the oxide target was bombarded for 20 μsec by a 34-μa beam of 350-volt electrons. When particles bombard a semiconductor or insulator, they raise a number of electrons from filled energy bands to the conduction band, and produce an equal number of mobile positive holes in the filled bands. In comparison with other substances,[6,7] an electron-hole pair

[5] Suggested by Dr. C. Herring in discussion. A similar increase in space charge by secondary electrons emitted from the anode causes current depression in screen-grid tubes and has been observed in triodes and diodes as reported by R. K. Matheson and L. S. Nergaard at the meeting of the Division of Electron Physics of the American Physical Society on January 31, 1951 [Phys. Rev. 82, 373 (1951)].

[6] Robert Hofstadter, Nucleonics 4, No. 4, 29 (1949).

[7] K. G. McKay, Phys. Rev. 74, 1606 (1948); 77, 816 (1950).

for each 10 ev of the primary particle seems reasonable for the oxide target, or here 35 per incident electron. From the shape of curves such as that of Fig. 1(b) it seems probable that the free lifetime of these carriers is not short compared with 10 μsec. Suppose half of them are left at the end of 20 μsec. The number of new conduction electrons and holes left at the end of the pulse is then $N=7.5\times10^{10}$. The distance over which the excess electron density spreads is governed principally by the ambipolar diffusion of the holes, since beyond the Debye distance electrical neutrality is maintained. It is much greater than the penetration of the primary electrons and may be estimated as follows. The Einstein relation between mobility μ and diffusion coefficient D gives for the latter $D=\mu kT/e$. The diffusion distance over which the carriers spread on the average in a time τ is given by $d=(D\tau)^{\frac{1}{2}}=(\mu\tau kT/e)^{\frac{1}{2}}$. The mobility of the holes is thought to be of the order 1 cm^2/volt sec; and using this value the diffusion distance for 20 μsec is $d=1.4\times10^{-3}$ cm, probably greater than the grain size of the oxide. The depth and the area then give a value for the volume Ω occupied by the N electrons, and the density of added electrons becomes $\Delta n=N/\Omega=1.8\times10^{15}$/cm^3. This calculated increase in density is to be justified as a reasonable source of the observed enhancement.

The total density n of conduction electrons in the oxide-target can be estimated as to order of magnitude from conductivity measurements made on very similar coatings by Hannay, MacNair, and White.[8] These authors found the conductivity remarkably reproducible, and at the temperature of our target, 940°K, obtained approximately the value $\sigma=2.0\times10^{-4}$ ohm^{-1} cm^{-1}. Combining with this the same mobility for electrons as was used previously for holes, we get a value for the density of conduction electrons, $n=\sigma/\mu e=1.25\times10^{15}$/cm^3. If this were the original density of electrons in our target and the bombardment increased it in the same ratio as observed for the emission, 3 percent, then a rise in electron density $\Delta n=3.75\times10^{13}$/cm^3 would

[8] Hannay, MacNair, and White, J. Appl. Phys. **20**, 669 (1949).

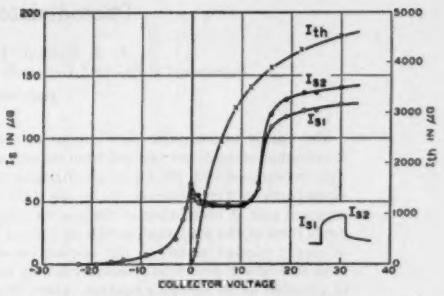

FIG. 7. Retarding potential curve with space charge. $I_{th}\gg I_s$, I_{th} dc, I_s pulsed. 660°C, $V_p=350$ v. Tube MN 74.

just account for the observed enhancement. The value calculated from bombardment considerations is about 50 times greater than this. A series of similar computations for other experimental conditions gives a mean factor of about 30.

Considering the wide difference of approach and the very rough assignment of values to mobility and conductivity for the targets tested, this seems at first sight a reasonable accord. The difference is not trivial, however. It does not seem possible to bring the results into agreement by choosing other values of μ and σ that lie within reasonable ranges. Even adding elementary considerations of trapping and recombination of charges does not bring the results sufficiently into line. The mechanism must be more complicated than that assumed. For the present the result that the predicted enhancement is even larger than the observed value makes very plausible the hypothesis that the bombardment-enhanced thermionic emission has its origin in the increase in density of conduction electrons by the bombardment.

This work has been stimulated by frequent discussions with N. B. Hannay, C. Herring, K. G. McKay, and A. H. White, and greatly facilitated by electronic circuits designed by R. W. Hull and maintained by H. V. Matthews.

Photodisintegration of Copper*

P. R. BYERLY, JR.,† AND W. E. STEPHENS
Department of Physics,‡ University of Pennsylvania, Philadelphia, Pennsylvania
(Received March 21, 1951)

The energy and angular distributions of the protons, deuterons, and alpha-particles and the energy distribution of neutrons emitted from copper nuclei irradiated with the x-rays from a 24-Mev betatron were determined with the use of photographic emulsions. The yields of neutrons, protons, deuterons, and alpha-particles were observed to be 3.6, 1.07, 0.34, and 0.04×10^{8} particles, respectively, per mole per roentgen unit. A comparison of the neutron:proton yields and the energy distribution with the theoretical predictions of the statistical models and direct photoelectric action indicate that the photodisintegration of copper consists mainly in the evaporation of nuclear particles from the excited nuclei. However, the large numbers of deuterons observed can only be explained by a different mechanism such as the "pick up" of a proton by an emerging neutron. About 10 percent of the neutrons and protons have energies greater than expected from evaporation. These are ascribed to a direct photoelectric effect. The observed angular anisotropy of these high energy protons supports this interpretation.

I. INTRODUCTION

MEASUREMENTS[1] of photodisintegration cross sections in the middle weight nuclei, where the photoreaction leads to a radioactive isotope, indicate photoproton to photoneutron yield ratios considerably larger than theoretical calculations[2] based on the evaporation of nuclear particles from an excited nucleus. Explanations[3–5] for this discrepancy differ with regard to the details of the emitted particles. Initial observation from experiments[6] on the angle and energy distribution of the photoprotons from magnesium were consistent with an evaporation process. We then started to examine the photoneutrons from copper by proton recoils in nuclear emulsions. In the course of this work, it became evident that a large number of photoprotons were also being emitted. It proved possible to determine the numbers and energy distributions of both the neutrons and the charged particles emitted in the photonuclear process. Some results of these experiments have been published.[7] Meanwhile, other research has been published[8–10] which indicates the occurrence of direct photoelectric effects in nucleii. Several theoretical discussions of the photonuclear process have been published.[11,12]

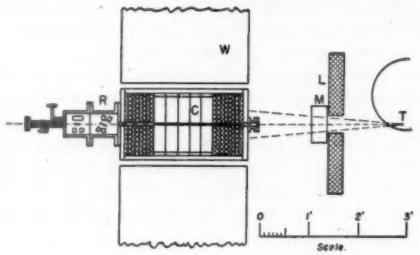

FIG. 1. Experimental arrangement showing betatron target T, lead wall L, monitor M, evacuated collimator C, concrete wall W, evacuated double camera T, foils F.

TABLE I. Details of various exposures.

Run	1	2a	2b	3	4
		Double proton camera			
Camera	Single proton	front section	rear section	Single proton	Neutron
Foil thickness (mg/cm²)	9.1	9.1	9.1	none	
Inches	0.0004	0.0004	0.0004		½
Angle to beam	0°	30°	0°		0°
Betatron energy	24 Mev	24	24	24	24
Roentgens at foil	8150	9125	9125	3800	8290
Emulsion	Ilford C-2	Ilford C-2	Ilford C-2 and NTC-3 Exp.	Ilford C-2	Ilford C-2
Thickness	100μ	200μ	200μ and 100μ	200μ	100μ
Size (in.)	½×1	½×1	½×1 and 1×1	½×1	1×3
Area scanned (mm²)	521	242 total	52	52	98
Distance from froil to start of scan (in.)	½	1	½	1	1½
Purpose	preliminary energy distribution	angular and energy distribution	grain counting	background	neutron energy
Total tracks measured	1000	1796	200	6	1000 recoils

* This paper contains essential portions of a thesis by P. R. Byerly, Jr., presented to the Faculty of the Graduate School of the University of Pennsylvania in partial fulfillment of the requirements for the Ph.D. degree.

† Now at the Radiation Laboratory, University of California, Berkeley, California.

‡ Supported in part by the joint program of the ONR and AEC; also aided by a grant from the Committee to Aid Research of the University of Pennsylvania.

[1] O. Hirzel and H. Wäffler, Helv. Phys. Acta **20**, 374 (1947).
[2] V. F. Weisskopf and D. H. Ewing, Phys. Rev. **57**, 472, 935 (1940).
[3] L. I. Schiff, Phys. Rev. **73**, 1311 (1948).
[4] E. D. Courant, Phys. Rev. **74**, 1226 A (1948); and private communication.
[5] P. Jensen, Naturwiss. **35**, 190 (1948).
[6] Toms, Halpern, and Stephens, Phys. Rev. **77**, 753 A (1950).
[7] P. R. Byerly, Jr. and W. E. Stephens, Phys. Rev. **81**, 473 (1951).
[8] B. C. Diven and G. M. Almy, Phys. Rev. **79**, 242 A (1950); **80**, 407 (1950).
[9] Curtis, Hornbostel, Lee, and Salant, Phys. Rev. **77**, 290 (1950).
[10] H. L. Poss, Phys. Rev. **79**, 539 (1950).
[11] M. Goldhaber and E. Teller, Phys. Rev. **74**, 1046 (1948).
[12] J. S. Levinger and H. A. Bethe, Phys. Rev. **78**, 115 (1950).

II. EXPERIMENTS

A. Detection of Deuterons

A collimated beam of x-rays from a 24-Mev betatron was used to irradiate targets of pure copper, and the photoparticles were observed in nuclear emulsions. The experimental arrangement is shown in Fig. 1. The setup was similar to that described previously[13] with the addition of a lead wall, L, and a concrete wall, W, to improve the shielding. The monitor, M, was calibrated against a 100 R Victoreen thimble chamber in a three-inch prestwood box for betatron energies from 15 Mev to 25 Mev. In order to check the alignment of the x-ray beam, the collimator, and the camera, plugs were made to hold x-ray film along the axis of the beam at the entrance and exit holes of the camera. Adjustments were made until the beam and apparatus were aligned to better than 1/64 in.

Preliminary runs with copper to look for neutron recoils in the emulsions had indicated an abundance of photoprotons from the copper. Then the first run was made to explore the energy distribution of these photoprotons. A foil of 0.4-mil copper (9.1 mg/cm²) was placed at a small angle to the x-ray beam, and several Ilford C-2 nuclear emulsion plates, cut to ½ in.×1 in., were placed alongside the foil with their surfaces tangent to the bottom of the beam. (Table I gives the details of the various exposures.) Now 521 square mm of these plates were scanned for tracks that enter the surface of the emulsion and come from the foil. These tracks were required to have a dip angle between 0° and 15° and a horizontal angle of 90°±15° to the beam direction. Here 1000 tracks satisfied these criteria, and their lengths were measured.

About 20 percent of the otherwise good tracks did not end in the emulsion. To correct for these, the geometric probability that a track of a given length would go through the emulsion was calculated on the assumption that the protons were ejected uniformly in the irradiated portions of the foil. The observed tracks which did not leave the emulsion were corrected by this factor. Half the equivalent foil thickness was added to the observed range, and this total range changed to proton energy by the range-energy curve for Ilford emulsions.[14] Figure 2 gives the resulting energy distribution. The extra peak at 2.5 Mev and the low energy, 1.9 Mev, of the low energy protons appeared anomalous for copper.

In order to check the possibility that deuterons were producing these anomalies, a run (Table I, 2b) was arranged to allow grain counting on the tracks to identify the particle mass. The rear section of the double camera was used for the grain counting experiment. As in run 1, the copper foil was set at 0° to the beam, and the plates set close alongside. On one side

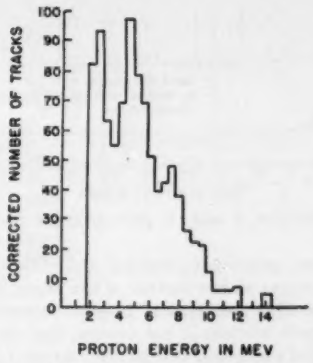

FIG. 2. Corrected energy distribution of photoprotons in run 1.

were set two, ¼-in.×1-in., Ilford C-2, 200μ plates and on the other side, a 1-in.×1-in., Eastman NTC-3 Exp., 100μ plate. Run number 2a using the front section of the camera was arranged to give an angular distribution of the protons at the same time. The emulsion thickness was increased to 200μ to reduce the probability that a long-range proton would go through the emulsion. In the front section of the double proton camera was mounted a 0.4-mil copper foil at an angle of 30° to the beam. Ten, ¼-in.×1-in., Ilford C-2, 200μ nuclear plates were set at angles of 30°, 60°, 90°, 120°, and 150° to the beam. All the front corners were placed about ⅜-in. from the axis of the ½-in. diameter beam. The plates

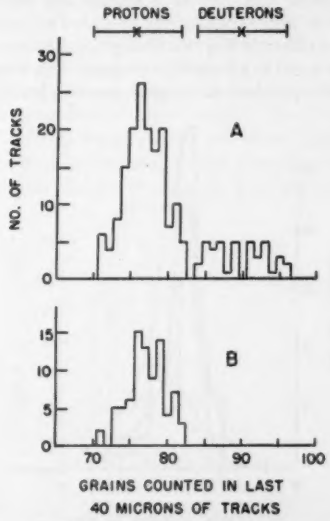

FIG. 3. A. Number of tracks entering surface (photoparticles) as a function of grains counted in the last 40μ of track. B. Number of tracks originating inside emulsion (recoil protons) as a functions of grains counted in last 40μ of track. Faded Ilford C-2 200μ emulsion (selected for flat tracks).

[13] M. E. Toms and W. E. Stephens, Phys. Rev. **82**, 709 (1951).
[14] Lattes, Fowler, and Cuer, Proc. Roy. Soc. (London) **59**, 883 (1947).

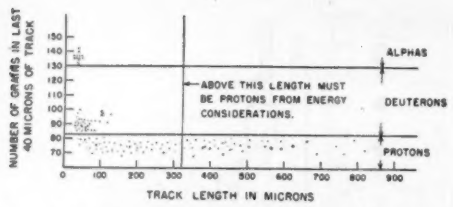
NUMBER OF GRAINS IN LAST 40 MICRONS OF TRACK
ALPHAS
ABOVE THIS LENGTH MUST BE PROTONS FROM ENERGY CONSIDERATIONS.
DEUTERONS
PROTONS
TRACK LENGTH IN MICRONS

FIG. 4. Distribution of tracks in grain count and track length.

were aligned pointing to the foil and with their top surfaces tangent to the bottom of the beam. After an exposure of 9125 roentgens of 24-Mev bremsstrahlung x-rays in both sections of the camera, the plates were removed and processed. One of the rear section Ilford C-2 plates was allowed to fade for one week and then developed normally by a temperature change method. The second Ilford plate was developed immediately with an amidol-sodium sulfite developer. (25 grams sodium sulphite (anhydrous) plus 3 grams amidol to 1 liter of water instead of D-19.) The Eastman NTC-3 Exp. was developed strongly. All of these plates allowed grain counting on the proton tracks.

The faded Ilford plate was the most satisfactory, and Fig. 3 shows the numbers of tracks as a function of grains in the last 40μ of the track. Figure 3A shows the results of grain counting tracks which entered the surface of the emulsion in a direction from the foil, ended in the emulsion, and had small enough dip so that the last 40μ of the track were all in focus. This latter criterion was only to eliminate the need for a correction in grain spacing due to dip. Two groups of tracks are evident in Fig. 3A. One group has an average of 77 grains and is ascribed to protons. This identification is confirmed by similarly grain counting tracks which originated inside the emulsion and which must certainly have been recoil protons. Figure 3B shows the numbers of these recoil protons as a function of grains in the last 40μ, in agreement with the lower peak in Fig. 3A. The second group of tracks in Fig. 3A has an average of 90 grains in the last 40μ of track and is ascribed to deuterons. According to Lattes *et al.*,[15] the grain counts vary as the 0.289 power of the mass. This relation would predict a ratio of 1.22 for the grain count of deuterons compared to protons. The observed value of 1.17 seems in agreement with this.

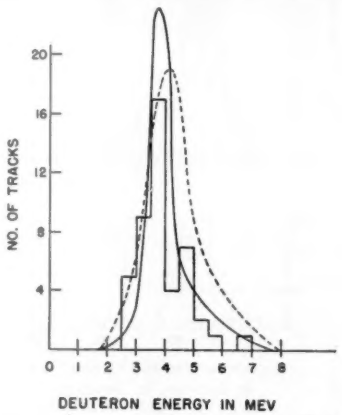

FIG. 5. Energy distribution of deuterons. The histogram indicates the observed tracks identified by grain counting as deuterons. The solid curve is the distribution calculated on the statistical model. The dashed curve is based on Schiff's model.

As a check on this assignment, grain counting was also done on the amidol developed plate. Two groups were also evident with a grain count ratio of 1.26. The grain counts on the phototracks from the faded plate are plotted in Fig. 4 as a function of the track length. All tracks over 330μ must be protons from considerations of the maximum photon energy and the deuteron binding energy in copper. Also on this plot are a few tracks identified as alpha-particles because of their high grain count. The distinction between protons, deuterons, and alpha-particles is clearly evident. It also seems clear that most of the low energy peak of Fig. 2 is due to deuterons, as had been suspected.

Since it is possible that the selection of tracks on the criterion of flatness of the last 40μ of track might discriminate between protons and deuterons, the grain counting was repeated and all the phototracks in a selected region were counted for the number of grains in the last 10μ. These tracks were separated into protons and deuterons on the basis of this count. We found 149 protons and 46 deuterons, giving the ratio of protons to deuterons as 3.24 to 1 with an uncertainty of about 30 percent. The deuteron ranges were changed to an energy scale, and the distribution in energy is shown in the histogram of Fig. 5.

B. Protons and Neutrons

The angular distribution plates in the front section of the proton camera in exposure 2a were developed by temperature development in D-19. It was not found possible to avoid surface fogging in the development of these 200μ emulsions. Consequently, several grain layers were wiped off the emulsions with cotton after washing. This allowed the tracks to be followed to the surface and it is believed affects the true length by less than 1μ. Different areas were scanned on the 30°, 60°, 90°, 120°, and 150° plates, as shown in Table II. Since these areas were at different distances from the foil, the effective solid angles were measured by a separate experiment in which the copper foil was replaced by a similar polonium alpha-source. Similar nuclear emulsions were exposed and the alpha-particles counted in equivalent scanned areas. The source was calibrated in a flow counter and the solid angle determined for the regions scanned on the plates. The criteria for selection

[15] Lattes, Occhialini, and Powell, Proc. Phys. Soc. (London) **61**, 173 (1948).

TABLE II. Angular distribution of tracks in run 2a.

Angle	Area scanned (mm^2)	Solid angle per mm^2	Tracks observed	Correction factor	Corrected number
30°	86	1.65×10^{-6}	175	3.35	586
60°	39	10.5×10^{-6}	423	1.17	495
90° right	26	9.2×10^{-6}	270	1	559
90° left	26	9.2×10^{-6}	289		
120°	39	10.5×10^{-6}	481	1.17	564
150°	86	1.65×10^{-6}	158	3.35	530

of tracks were: track must start on the surface of the emulsion and end in the emulsion; the initial direction must be from the foil both in horizontal angle (±7°) and dip (0° to 15°). The measured range of the track was increased by the equivalent half-thickness of the foil (13μ to 15μ). This is also the uncertainty in energy of the particles and varies from ±⅓ Mev for 3-Mev protons to ±0.15 Mev for 10-Mev protons.

Figure 6 shows the observed numbers of tracks, corrected for solid angle scanned, plotted as a function of angle. In addition to the totals, the angular distribution is given for groups of energies: 1.6 to 3.6 Mev (which is mostly deuterons), 3.6 to 10 Mev, and above 10 Mev. In order to avoid any distortion, the "above 10 Mev" group includes also the 33 tracks which did not end in the emulsion. These were all over 10 Mev, so no correction of length was necessary.

The energy distribution of the tracks measured in the angular distribution is shown in Fig. 7. The energy distributions observed at separate angles are similar but less significant statistically. The energy distributions observed on opposite 90° plates are quite similar and check the alignment of the beam, foil, and plates.

The background was determined in several ways. Run number 3 was similar to the front section of run 2 with the foil omitted. Only six tracks were observed at 90°. This corresponds to 15 out of the 559 tracks observed at 90° in run 2 or to 2.7 percent. In run 2, all the tracks entering the surface of the emulsions in the wrong direction were plotted as a function of angle from the foil direction. They were quite isotropic and if ascribed to protons scattered from the walls would give an additional correction of 8 out of 1796 or 0.6 percent. The tracks that went through the emulsion were 1.8 percent. Consequently, the total correction is negligible except for the high energy portion of the spectrum.

In order to check the possibility of an (n,p) reaction producing protons by the background neutrons in the x-ray beam, we attempted to activate phosphorus in the collimated beam at the same time a copper foil was activated. No activity was detected in the phosphorus when copper was activated to 500 counts per second. From this we deduce less than 0.1 percent of the protons are from an (n,p) reaction.

In run 2 a large number of alpha-particles were observed and measured. Although many of these are

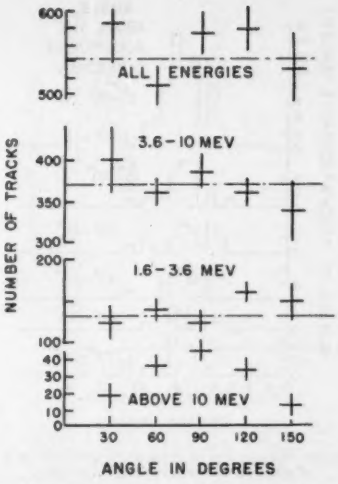

FIG. 6. Angular distribution of tracks for various energy groups.

contamination alpha-particles, when they were plotted against angle about the acceptable direction from the foil, as in Fig. 8, a surplus was evident in the acceptable direction. These alpha-particles appear at all angles from the beam and are isotropic although the statistical uncertainty is as great as 30 percent at 30° and 150°. The energy distribution of these photo alpha-particles is given in Fig. 9. The ratio of the numbers of alpha-particles to protons is 1 to 24.3.

In run 4 a smaller camera was substituted for the proton camera. In this neutron camera, the target was a copper slug ¼ in. in diameter and ¼ in. long. Neutrons ejected from the copper were detected by proton recoils in nuclear emulsions placed nearby. The 1-in.×3-in., Ilford C-2, 100μ plates were set in a plane perpendicular to the beam with the leading edge ⅜ in. from the center of the copper. Proton recoils were measured which had

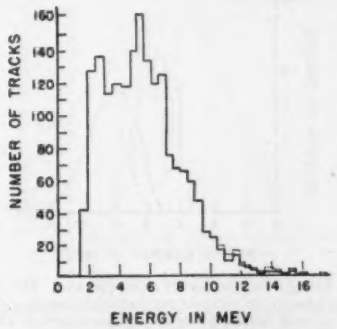

FIG. 7. Energy distribution of tracks measured at all angles. The dotted lines indicate those tracks which passed out of the emulsion.

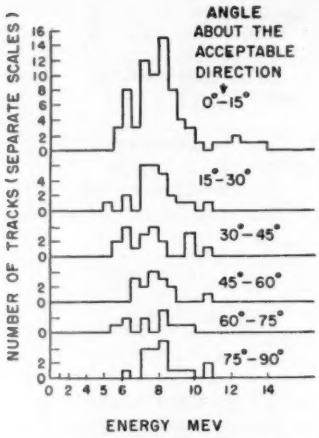

FIG. 8. Energy distribution of total alpha-particles as a function of angle from the acceptable direction.

angles within ±15° to the direction from the center of the copper. The procedure described by Richards[16] was followed in making geometric corrections for wall effects, acceptance ratios, etc. Run number 3 was used for background determination. There were too few recoils in the acceptable direction in run 3 to give good statistics, so all the recoils were measured and a background estimated for run 4. Table III shows the background and observed good recoils. Figure 10 gives the energy distribution of the good neutron recoils corrected for background, acceptance ratios, and neutron-proton scattering cross section. This plot, then, should give the energy distribution of the photoneutrons emitted from the copper. Because of the presence of occasional clusters of background developed grains, tracks shorter than 3μ were not measured. This puts a lower limit of 0.3 Mev to the neutron energy detected.

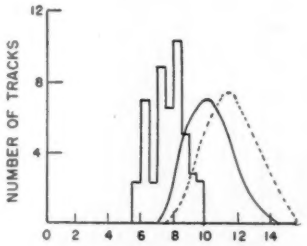

FIG. 9. Energy distribution of alpha-particles. The histogram gives the alpha-tracks ascribed to photodisintegration of copper. The solid curve is calculated on the statistical model. The dashed curve is calculated on Schiff's model.

[16] H. T. Richards, Phys. Rev. **59**, 796 (1941).

TABLE III. Neutron recoils and background.

Energy interval (Mev)	Recoils observed in run 3	Calculated background for run 4	Good recoils observed in run 4
0.3 to 0.8	75	60	236
0.8 to 1.3	51	41	286
1.3 to 1.8	26	21	166
1.8 to 2.3	7	5	96
greater than 2.3	5	4	216

C. Yields

The yields of the protons, deuterons, and alpha-particles could be determined from the solid angles and tracks observed. The neutron yields were determined both from the number of proton recoils and also by the radioactivity produced in the (γ,n) reactions. The yield of photoparticles is defined as

$$Y=Ly=nL/ANtR\omega,$$

where n is the number of photoparticles observed in an area "a" which subtends a solid angle ω at the foil, A is the area of the beam which intercepts the foil, N is the number of nuclei/cc, t is the thickness of the foil in the direction of the beam, R is the number of roentgen units delivered at the foil, ω is the fractional solid angle which the scanned area subtends at the foil, y is the yield per nucleus per roentgen unit, L is Avogadro's number, and Y is the yield per mole per roentgen unit.

In run number 2a at 90°, $R=9125$ roentgens, $Nt=1.72\times10^{20}$ nuclei/cm² in direction of beam, $A=0.317$ cm², $\omega=4.78\times10^{-4}$ for 52 mm² scanned and $n=559$ tracks observed in 52 mm² scanned, giving $Y=1.41\times10^{6}$ particles per mole roentgen unit. Since this includes both protons and deuterons, we can separate this into $Y_p=1.07\times10^{6}$ protons/mole/r and $Y_d=0.34\times10^{6}$ deuterons/mole/r.

In run number 4

$$n/\omega=n'/\sigma'N't'\omega k.$$

Here n is the number of neutrons entering the region in emulsion scanned for recoil protons, n' is the observed number of "good" recoil protons, σ' is the n-p scattering cross section, N' is the number of hydrogen nuclei/cc in the emulsion, t' is the distance along the neutron path in the scanned region, ω is the fractional solid angle subtended by the region scanned at the copper slug, and k is the fraction of recoils observed as "good" recoils (for ±15°). Then $N'=3.38\times10^{22}$ hydrogen nuclei/cc, $t'\omega=1.01\times10^{-4}$ for 98 mm² scanned of 100μ emulsion, $k=0.087$, and $n'/\sigma'=300\times10^{24}$ averaged over the energy spectrum, giving $n/\omega=1.0\times10^{9}$ neutrons; and $A=0.317$ cm², $Nt=5.35\times10^{22}$ copper nuclei/cm² in $\frac{1}{4}$-in. slug, $R=8290$ roentgen units, giving $y_n=0.70\times10^{-17}$ neutrons/nucleus/r or $Y_n=4.2\times10^{6}$ neutrons/mole/r.

This value is uncertain mainly due to the difficulty of selecting recoils within exactly the ±15° angle. In

order to determine this neutron yield independently, we have measured the radioactivity produced in the $Cu^{65}(\gamma,n)Cu^{64}$ and $Cu^{63}(\gamma,n)Cu^{62}$ transmutations. During run 2, an 8-mil copper foil was activated at the exit of the double camera for three hours of the run. This foil was counted for several days, and the saturated activities of Cu^{62} and Cu^{64} were determined as 6900 counts/min and 550 counts/min. The counter was calibrated against a radium D plus E source[17] which determined the saturated disintegrations per minute of Cu^{62} to be 3.12×10^4 and of Cu^{64} to be 2.98×10^4. Using other data from run 2 gives $Y_{63}=2.6\times10^6$ neutron/mole of Cu^{63}/r and $Y_{65}=5.8\times10^6$ n/mole of Cu^{65}/r, combining to give $Y_n=3.56\times10^6$ neutrons/mole of copper/r. In addition, the excitation curve of Cu^{62} was taken by varying the betatron energy and observing the radioactivity produced. The cross-section curve was calculated from this excitation curve and the x-ray photon energy distribution.[18] A peak cross section of 0.10 barn was observed at 17.5 Mev, as shown in Fig. 11.

III. DISCUSSION

The yields of photoparticles from copper with 24-Mev x-rays can be summarized as:

$Y_p=1.07\times10^6$ protons/mole/r,
$Y_d=0.34\times10^6$ deuterons/mole/r,
$Y_\alpha=0.04\times10^6$ alphas/mole/r,
$Y_n=3.56\times10^6$ neutrons/mole/r from radioactivity,
or $=4.2\times10^6$ neutrons/mole/r from recoils.

The uncertainties in these yields is of the order of 50 percent. The relative values are perhaps somewhat better.

The proton yield is in good agreement with results of Mann and Halpern who give 1×10^6 protons/mole/r from copper in their scintillation detector survey.[19] The photoemission of protons has also been observed by Chastel[20] with the lithium gamma-rays. His cross section of 10^{-27} cm^2 is somewhat lower than the value inferred from our work. From the radioactivity produced and the threshold (γ,d) and (γ,α) reactions have been observed by the Saskatchewan group.[21] Their integrated cross sections for $S^{32}(\gamma,d)$ and $Rb^{87}(\gamma,\alpha)$ are somewhat lower than the values inferred from our yields. There are a number of values of the yields of (γn) reactions in copper. Price and Kerst[22] measured the total neutron yield by slowing the neutrons down and absorbing them in rhodium. Their value of 2.5×10^6 neutrons/mole/r is for 22-Mev x-rays. Estimating it to 2.8×10^6 n/M/r at 24 Mev still leaves it appreciably smaller than our value. However, the Saskatchewan

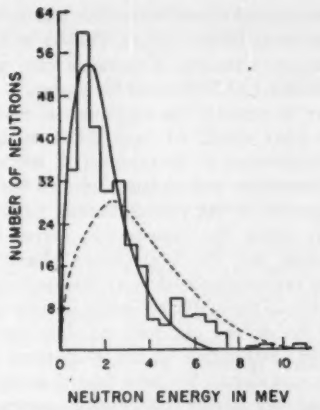

FIG. 10. Energy distribution of the neutrons. The histogram shows the distribution of recoil proton tracks corrected for background, acceptance ratio, and n-p cross section to give photoneutron energy distribution. The solid curve is calculated on the statistical model. The dashed curve is calculated on Schiff's model.

group[21] has carefully measured the radioactivity produced, and from their results a yield of $.375\times10^6$ n/M/r can be calculated. These results on Cu^{63} are confirmed by Rosenfeld, Marshall, and Wright,[23] and others.[8,24]

If we take $Y_n=3.8\times10^6$ n/M/r and add the others, we get a total photoyield of 5.24×10^6 particles/M/r or 8.7×10^{-18} particles/nucleus/r. This can be changed to an integrated cross section with reasonable assumptions as to shape of the cross-section curves. The total integrated cross section is estimated to be 1.4 Mev-barns. This can be compared with the value predicted by Goldhaber and Teller[11] of 0.91 Mev-barn. Levinger and Bethe[12] calculate a total integrated cross section

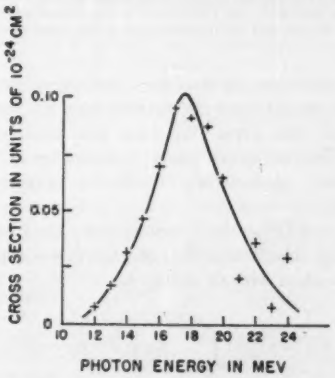

FIG. 11. Calculated cross section for $Cu^{63}(\gamma,n)Cu^{62}$ determined from the excitation curve of Cu^{62}.

[17] B. P. Burtt, Nucleonics **5**, No. 8, 28 (1949).
[18] Johns, Katz, Douglas, and Haslam, Phys. Rev. **80**, 1062 (1950).
[19] A. K. Mann and J. Halpern, Phys. Rev. **81**, 318 A (1951).
[20] R. Chastel, Compt. rend. **230**, 2020 (1950).
[21] Harrington, Katz, Haslam, and Johns, Phys. Rev. **81**, 660 A (1951); R. N. H. Haslam and H. M. Skarsgard, Phys. Rev. **81**, 479 L (1951).
[22] G. A. Price and D. W. Kerst, Phys. Rev. **77**, 806 (1950).
[23] Rosenfeld, Marshall, and Wright, Phys. Rev. **82**, 301A (1951).
[24] A. C. Helmholz and K. Strauch, Phys. Rev. **78**, 86 (1950).

for a more general dipole interaction and include the effect of exchange forces. Using a Yukawa well, $r_0=1.5\times10^{-13}$ cm, and a fraction of exchange force of $\frac{1}{2}$, they would calculate 1.32 Mev-barns for copper.

In order to compare the experimental results with theory in more detail, we have calculated both the energy distributions to be expected of the neutrons, protons, deuterons, and alphas, and also the relative yields expected on the various nuclear models. Since we do not know the cross-section curves for each transmutation nor the total photon absorption, we start from the experimental (γ,n) cross-section curves. On the basis of the statistical model nucleus of Weisskopf and Ewing,[2] we can then calculate the number and energy distribution of the evaporated protons, deuterons, and alphas. We have done these separately, normalizing the energy distribution curves to the

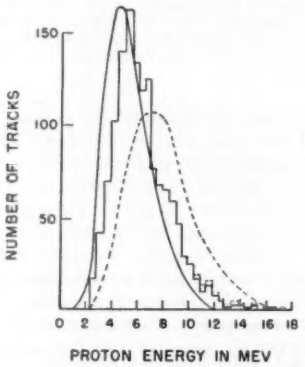

FIG. 12. Energy distribution of the photoprotons. The histogram represents the experimental results from run 2a with the deuterons subtracted. The dotted lines indicate those tracks which did not end in the emulsion. The solid curve is the normalized statistical model prediction and the dashed curve is the Schiff model.

experimental ones, so that the distribution comparison with experiment need not depend upon accurate yield data and vice versa. We have also considered the regular level excitation model proposed by Schiff[3] and the direct photoelectric interaction suggested by Courant.[4]

Almy and Diven[5] have written down the formula for the energy distribution $F(\epsilon)$ of a particle b evaporated from a nucleus with an energy ϵ.

$$F(\epsilon)=\epsilon S_b(\epsilon)\int_0^{E_{\max}} K\omega_R(E-B_b-\epsilon)dE,$$

where ϵ is the energy of an emitted particle b, $S_b(\epsilon)$ is the penetration factor,[2] ω_R is the level density of the resultant nucleus, E is the photon energy, B_b is the binding energy of the particle b; and

$$K=N(E,E_{\max})\sigma(\gamma,n)/C,$$

$$C=\int_0^{\epsilon_{n\,\max}}\epsilon_n\omega_R(E-B_n-\epsilon_n)d\epsilon_n,$$

where N is the number of photons of energy E, σ is the (γ,n) cross section as a function of E, ϵ_n is the emitted neutron energy, B_n is the neutron binding energy, and $\epsilon_{n\,\max}=E-B_n$. The total emission of particle b is the integral of F with respect to ϵ from 0 to $\epsilon_{\max}=E-B_b$. The level density can be described by the normal statistical model[2] as

$$\omega_R(\mathcal{E})=\exp(a\mathcal{E})^{\frac{1}{2}} \quad \text{with} \quad a=1.6(A-40)^{\frac{1}{2}}$$

or by Schiff's regular level excitation[3]

$$\omega_R(\mathcal{E})=(a/4)\ln(a\mathcal{E}/4+1).$$

The coefficient C can be calculated from these to be

$$C_{WE}=(2/a)[(D-6/a)+\exp(aD)^{\frac{1}{2}}\times\{2(D+3/a)-(6/a)(aD)^{\frac{1}{2}}\}],$$

$$C_S=(a/8)(D+4/a)^2[\ln2(D+4/a)-3/2]+(D+3/a),$$

where $D=E-B$, and $\mathcal{E}=E-B_b-\epsilon$. The bremsstrahlung distribution N was taken from the calculations of the Saskatchewan group.[18] The binding energies were calculated from the empirical mass equation, checked with experimental values where possible, and are shown in Table IV. The (γ,n) cross section for Cu^{63} was taken from Fig. 11 and is close to the Saskatchewan curve.[18] The $Cu^{65}(\gamma,n)$ cross-section curve was assumed to be similar in magnitude but shifted down 0.7 Mev. This is somewhat different from the Saskatchewan curve,[18] which was not available at the time the calculations were made. A partial recalculation using the Saskatchewan curve does not materially change the values.

The energy distribution $F(\epsilon)$ was calculated for each level density formula and for each isotope of copper. The isotopic curves were combined and normalized to the experimental curves. Figures 10, 12, 5, and 9 show the comparison between the observed energy distributions of the neutrons, protons, deuterons, and alpha-particles, and the calculated distributions. In each case the histogram shows the experimental results, the solid curve represents the statistical model, and the dashed curve gives the results of Schiff's assumptions (also normalized to the observed number). Table V gives the results of integrating the energy distributions to get total calculated yields.

The agreement between experiment and the statistical model for the evaporation of neutrons seems quite good (Fig. 10 and Table V). There are, however, about 10 percent of the neutrons which have energies higher than expected on the Weisskopf and Ewing evaporation model.

It is possible that a larger energy level density at low excitations of the resultant nucleus, or an effect similar to Schiff's proposed selective excitation, might account for some of this discrepancy. However, in view of the fact that a similar high energy excess appears in the proton energy distribution curve, Fig. 12, and that these high energy protons have a non-isotropic distribution with a maximum at 90°, Fig. 6, it seems probable that these high energy neutrons and protons are the result of a direct photoelectric effect of a photon on a nucleon. These results are in good agreement with similar data for the photoprotons from silver reported by Almy and Diven.[8]

None of the theoretical calculations of the photon interaction have, so far, been extended to the calculation of these details. However, it would seem that a process of absorption of the photon by a nucleon, such as the dipole interaction discussed by Levinger and Bethe, could result in most of the observed phenomena. In a few cases the proton or neutron which has absorbed the photon could escape from the nucleus without further interaction, especially if the proton or neutron were on the surface. These particles would retain the photon energy minus the binding energy and would have a non-isotropic distribution with a maximum at 90° if they had no angular momentum in the nucleus.[4] Those particles which absorb a photon and make a collision within the nucleus might be expected to make further collisions and lose the absorbed energy to the nucleus as a whole. This excited nucleus would then evaporate a neutron or proton according to the statistical model. Although the number of directly ejected protons may be only a small fraction of the photon absorption and consequently difficult to observe in low atomic number elements where the low coulomb barrier permits appreciable proton evaporation in competition with neutron evaporation, it may nevertheless be a major fraction of the photoprotons from higher atomic number elements. Here the high coulomb barrier prevents appreciable proton evaporation in competition with neutron evaporation. Consequently, such a direct ejection of protons may account for the observation in heavy elements of larger (γ,p) cross sections than predicted by evaporation models.

The theoretical calculations on the statistical model seem to predict a larger number of low energy protons than were observed in Fig. 12. Since the neutron curves show good agreement in the low energy region, the discrepancy may be ascribed either to experimental error (the low energy shape was determined by subtracting the deuterons from the total curve, Fig. 7, and is uncertain due to the small numbers involved) or to errors in the coulomb barrier penetration factors.

The alpha-particles observed seem most probably to be evaporated from the compound nucleus (Fig. 9 and Table V). It seems reasonable to account for any discrepancies in numbers or energy between theory and experiment on the basis of some uncertainty in the experimental results, caused by the small numbers, and some uncertainty in the theoretical calculations. However, the alphas ejected in cosmic-ray stars are also of lower energy than expected.[25]

None of these concepts, however, seem able to account for the large numbers of deuterons observed. All of the evaporation models predict several orders of magnitude too small a yield for evaporated deuterons (assuming preformed deuterons), despite the facts that the energy spectrum is consistent with a statistical model evaporation and that the angular distribution (as evidenced by the 1.6- to 3.6-Mev group in Fig. 6) seems isotropic. A calculation of the direct photoelectric[4] yield of preformed deuterons also gives much too small a number. Consequently, we are forced to postulate some other mechanism for this effect. The "pick-up" process[25] by which an outgoing "evaporated" neutron or proton picks up an apposite particle seems likely. In fact, the probability that an outgoing particle with velocity corresponding to its excitation temperature will happen to find another particle going in a similar direction with a similar velocity might be greater for these energies than for the high energies Chew and Goldberger[26] consider. On the other hand, it will be less probable that this "deuteron" will escape over the barrier at these lower energies. York[27] has observed that 1/12 of the 90-Mev neutrons which interacted

TABLE IV. Particle binding energies in copper.

	Cu^{63}		Cu^{65}	
	Calc. (Mev)	Exp. (Mev)	Calc. (Mev)	Exp. (Mev)
neutron	11.0	10.9	10.1	10.2
proton	6.1	6.2*	7.4	7.7*
deuteron	14.6		14.7	
alpha-particle	6.3		5.7	

* Determined from (γ,n) threshold and beta-ray energy.

TABLE V. Relative yields of photoparticles (in units of 10^6 particles/mole/r).

	Neutrons	Protons	Deuterons	Alphas
Observed				
Cu^{63}	2.6			
Cu^{65}	5.8			
Normal copper	3.6	1.07	0.34	0.04
Calculated with statistical model of Weisskopf and Ewing				
Cu^{63}	(3.0)*	1.07	0.0002	
Cu^{65}	(5.6)*	0.37	0.0005	
Normal copper	(3.8)*	0.86	0.0003	0.006
Calculated with Schiff model				
Normal copper	(3.6)*	2.0	0.0013	0.040
Calculated with formulae of Le Couteur				
Normal copper	(3.6)*	1.1	0.0023	0.015

* Assumed values.

[25] Bernardini, Cortini, and Manfredini, Phys. Rev. **79**, 952 (1950).
[26] G. F. Chew and M. L. Goldberger, Phys. Rev. **77**, 470 (1950).
[27] H. York, Phys. Rev. **75**, 1467 A (1949).

with a carbon nucleus "picked up" a proton and escaped as a deuteron. The present observation of 1/14 as many deuterons as neutrons and protons may be the result of such a "pick-up" process at low energies. If this interpretation were true, one might expect to observe a few tritons also emerging from copper. However, the binding energy of a triton to its residual nucleus is large, so that its probability of escape would be small.

Some of the initial photographic techniques and the nuclear emulsion camera used in this work were developed by Miss M. Elaine Toms.

PHYSICAL REVIEW VOLUME 83, NUMBER 1 JULY 1, 1951

The Radiations from Hafnium

S. B. Burson, K. W. Blair, H. B. Keller, and S. Wexler
Argonne National Laboratory, Chicago, Illinois
(Received March 12, 1951)

The 70-day, 45-day, 5.5-hour, and 19-second activities of Hf have been investigated by spectrometric, spectrographic, absorption, and coincidence methods. From activation experiments on the separated Hf isotopes, the following assignments have been made: 70-day—$_{72}Hf^{176}$; 19-second—$_{72}Hf^{179*}$; 5.5-hour—$_{72}Hf^{180*}$; 45-day—$_{72}Hf^{181}$.

70-day period.—The photographic spectrograms of the internal conversion electrons associated with the 70-day period in $_{72}Hf^{176}$ indicated the presence of four gamma-rays. The association of Lu work functions with the various lines confirmed the hypothesis of K electron capture in $_{72}Hf^{176}$ leading to an excited state of $_{71}Lu^{176}$.

45-day period.—An investigation of the internal conversion electron spectrum in the Argonne 180° beta-ray spectrometer indicated the presence of one beta-ray of 0.42 ± 0.01 Mev and five gamma-rays. An upper limit of 1 percent may be placed on any more energetic beta-ray. Single and coincidence absorptions in lead and aluminum showed the three strongest gamma-rays and the single beta-ray. Delayed coincidence absorption indicated that the 0.42-Mev beta-ray leads directly to the 22-microsecond metastable state of $_{73}Ta^{181}$. No delayed gamma-coincidences were found. Thus, all gamma-rays appear to follow the 22-microsecond state. Additional coincidence measurements showed internal conversion electron groups corresponding to three of the gamma-rays. The decay scheme proposed by Chu and Wiedenbeck, as modified by Cork *et al.* was confirmed.

5.5-hour period.—Activation of extremely pure Hf samples showed an activity of 5.5 hours in addition to the 45-day period. The assignment of this activity to Hf was confirmed by chemical methods. No delayed coincidences were observed. Internal conversion electron groups corresponding to five gamma-rays were resolved; absorption in lead indicated three of the photon components. Aluminum absorptions indicated coincidences between internal conversion electron groups from at least two of the gamma-rays. Activation of separated isotopes shows that this activity is one of an isomeric state of $_{72}Hf^{180}$.

19-second period.—A photographic spectrogram of the internal conversion electrons showed the presence of a single gamma-ray; the association of Hf work functions with the four lines observed verified the hypothesis of an isomeric state in $_{72}Hf^{179}$.

INTRODUCTION

EXTENSIVE experiments have been carried out by several investigators[1–15] on the 45-day activity of $_{72}Hf^{181}$. A longer activity of 70 days has also been reported[16] and assigned to $_{72}Hf^{175}$. The results of the spectrographic measurements are generally in good agreement; but many of the coincidence measurements seem to be in conflict and at times have led to anomalous conclusions. The high intensity of the internal conversion electron groups from the many gamma-rays present make the interpretation of both single and coincidence absorption curves extremely difficult. We have taken advantage of the 22-microsecond isomeric state of $_{73}Ta^{181}$ to separate the primary beta-ray from the internal conversion electron spectrum, thereby facilitating careful inspection of each independently.

After the completion of many of these experiments using normal Hf, the separated isotopes were obtained from the Isotopes Division of the Oak Ridge National Laboratory. In the subsequent discussion, all references to Hf indicate normal Hf, the separated isotopes being referred to explicitly. These isotopes made possible the definite isotopic assignment of the activities. Accurate gamma-ray energy determinations were made by measurement of the internal conversion electron groups associated with each isotope. The details of the techniques and instrumentation employed in these measurements will be discussed in a subsequent publication.[17]

[1] H. Neuert, Z. Naturforsch. **2a**, 432 (1947).
[2] L. Madansky and M. L. Wiedenbeck, Phys. Rev. **72**, 185 (1947).
[3] M. L. Wiedenbeck and K. Y. Chu, Phys. Rev. **72**, 1164 (1947).
[4] S. DeBenedetti and F. K. McGowan, Phys. Rev. **74**, 728 (1948); Phys. Rev. **70**, 569 (1946).
[5] Cork, Schreffler, and Fowler, Phys. Rev. **72**, 1209 (1947).
[6] Bunyan, Lundby, Ward, and Walker, Proc. Phys. Soc. (London) **61**, 300 (1948).
[7] Benes, Ghosh, Hedgran, and Hole, Nature **162**, 261 (1948).
[8] A. F. Voight and B. J. Thamer, Phys. Rev. **74**, 1264 (1948).
[9] Mandeville, Scherb, and Keighton, Phys. Rev. **75**, 221 (1949).
[10] K. Y. Chu and M. L. Wiedenbeck, Phys. Rev. **75**, 226 (1949).
[11] Arne Lundby, Phys. Rev. **76**, 1809 (1949).
[12] Erling Jensen, Phys. Rev. **76**, 958 (1949).
[13] Cork, Stoddard, Rutledge, Branyan, and LeBlanc, Phys. Rev. **78**, 299 (1950).
[14] M. Deutsch and A. Hedgran, Phys. Rev. **79**, 400 (1950).
[15] W. C. Barber, Phys. Rev. **78**, 641 (1950).
[16] G. Wilkinson and H. Hicks, Phys. Rev. **75**, 696 (1949).
[17] H. B. Keller and J. M. Cork, to be published.

THE SOURCES

The samples of normal HfO_2 were prepared through the courtesy of J. J. Katz and the Chemistry Division of the Argonne Laboratory. All sources used in these experiments were activated by neutron bombardment in the heavy water moderated nuclear reactor of this laboratory with the exception of the 45-day Hf source used in the beta-ray spectrometer, which was activated in the Oak Ridge reactor. The activated powder was placed on Scotch tape previously arranged on the source holders.

COINCIDENCE CIRCUITS

Two concidence circuits were used. The first circuit measured only direct coincidences and had a resolving time of 0.48 μsec. The second circuit had a resolving time variable from 1.25 to 10 μsec in five steps. In addition, this circuit was equipped with a trigger-pair type delay circuit in one of the channels. This allowed a variable delay from 0 to 30 μsec with six intervening positions. The counters used were of the end window type having mica windows of 2 mg/cm^2.

A lead shield $\frac{1}{4}$-in. thick not only served as a support for the source and holder, but also reduced the probability of spurious coincidences due to either beta- or Compton scattering.

70-DAY ACTIVITY

By proton and deuteron bombardment of Lu, Wilkinson, and Hicks[16] have produced an activity of 70±2 days which they have attributed to $_{72}Hf^{175}$. From our decay curves of each of the separated Hf isotopes, we are able to confirm their conclusion as to the assignment of this activity. The spectrographic data on the gamma-ray energies for this period are set forth in Table I.

The best agreement among the gamma-ray energies computed from the various conversion electron lines was obtained when fitted with Lu work functions, confirming the hypothesis of K electron capture. This conclusion was further born out by the relatively high intensity of the Auger lines, being due to the K x-rays of high intensity. As this type of photographic data does not lend itself readily to intensity determinations, no effort was made to determine relative intensities of the lines.

Four gamma-rays have been resolved. A tentative level scheme is presented (Fig. 1). Placing the 0.0891-Mev gamma-ray above rather than below the 0.3423-Mev gamma-ray is arbitrary; none of our experiments yielded evidence which would resolve this question.

45-DAY ACTIVITY

Photon Radiations

The values of the energies of the gamma-rays were determined by an examination of the internal conversion electron spectrum of $_{72}Hf^{181}$ in both the 180° beta-ray spectrometer and the 180° internal conversion electron spectrograph. The values are given in Tables II and III, respectively. The energy values have been assigned from the more accurate photographic measurements on the activated enriched $_{72}Hf^{180}$.

Absorption of the photon radiations in Pb indicated three components (Fig. 2) that agree reasonably well with the spectrographic determinations of the three strongest groups. Finally, the photon spectrum was examined by covering the spectrometer source with an Al cap and a 40-mg Pb/cm^2 foil and observing the photoelectron spectrum. The results were in substantial

TABLE I. Gamma-ray energies from internal conversion electron spectrogram of $_{72}Hf^{175}$.

Electron energy	Proposed interpretation	Energy sum (Mev)	Gamma-energy (Mev)
0.0257	K	0.0891	
0.0782	L_I	0.0891	
0.0864	M	0.0889	
0.0885	N	0.0890	0.0891
0.0500	K	0.1134	
0.1025	L_I	0.1134	
0.1110	M	0.1135	0.1134
0.1650	K	0.2284	0.2284
0.2789	K	0.3423	
0.3314	L_I	0.3423	
0.3400	M	0.3425	0.3423
0.0427	Auger L_{II}		α_1
0.0440	L_{III}, L_{II}		α_1; α_2
0.0500	M		α_1
0.0511	M, N		α_2; α_1
0.0532	M		α_2

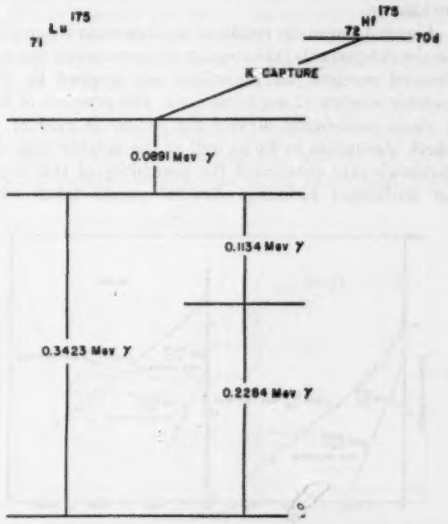

FIG. 1. Proposed decay scheme for $_{72}Hf^{175}$ (70-day).

TABLE II. Gamma-ray energies from internal conversion electron lines measured in the 180° beta-ray spectrometer for $_{72}Hf^{181}$ (normal).

Electron energy	Proposed interpretation	Energy sum (Mev)	Gamma-energy (Mev)
0.0730	L	0.084	0.084[a]
0.0662	K	0.133	0.133
0.1228	L	0.134	
0.1316	M	0.134	
0.693	K	0.136	0.136
0.1240	L	0.135	
0.1334	M	0.136	
0.275	K	0.342	0.342[a]
0.279	K	0.346	0.346
0.333	L	0.345	
0.420	K	0.487	0.488
0.478	L	0.489	
0.554	K	0.621	0.621
0.611	L	0.622	

[a] To be identified with $_{72}Hf^{175}$ (70 day).

TABLE III. Gamma-ray energies from internal conversion electron spectrogram for $_{72}Hf^{181}$ (activated enriched $_{72}Hf^{180}$).

Electron energy	Proposed interpretation	Energy sum (Mev)	Gamma-energy (Mev)
0.0655	K	0.1329	
0.1217	$L_{I,II}$	0.1329	
0.1230	L_{III}	0.1329	
0.1303	M	0.1330	
0.1322	N	0.1328	0.1329
0.0685	K	0.1359	
0.1245	$L_{I,II}$	0.1357	
0.1335	M	0.1362	0.1358
0.2773	K	0.3447	
0.3330	$L_{I,II}$	0.3442	
0.3408	M	0.3435	0.3441
0.4135	K	0.4809	
0.4696	$L_{I,II}$	0.4808	
0.4780	M	0.4807	0.4808
0.5438	K	0.6112	0.6112

agreement with those of the internal conversion electron spectrum.

Delayed Coincidence Measurements

Since the counting rate for delayed coincidences increases with resolving time, it is desirable to increase the latter to a point as high as possible consistent with a tolerable accidental background. To this end a value of 7.25 μsec was selected in conjunction with a delay of 8.5 μsec. This is sufficiently greater than the resolving time to prevent the recording of any prompt coincidences.

Figure 3 shows the results of an aluminum absorption on the delayed side; the counter whose response was not delayed received all radiations not stopped by the counter window (2 mg mica/cm²). The presence of but a single component of 10.5 mg Al/cm² is evident. A check absorption in Be as well as the notably high coincidence rate eliminated the possibility of this being an uncharged radiation. Several points taken with thicker absorbers than are shown indicated no harder component and apparently a complete absence of coincidences involving delayed gamma-rays. The conclusions from these experiments are that the 22-μsec metastable state follows directly upon a beta-decay from $_{72}Hf^{181}$ to $_{73}Ta^{181}$, and that the energy of the beta-ray is about 0.4 Mev. Thus, all gamma-ray transitions follow the 22-μsec metastable state to lower states in $_{73}Ta^{181}$.

Figure 4 shows the results of a similar absorption on the undelayed side. The thinness of the source and counter windows accentuated the characteristic shape of the monoenergetic electron groups, permitting a relatively good estimation of their ranges. The electron group energies as assigned in Table IV agree quite well with the three strongest gamma-rays previously discussed. In obtaining the energy values of the electron groups from our calibration curves the 2-mg mica/cm² counter window was assumed to have the same absorption characteristics as aluminum.

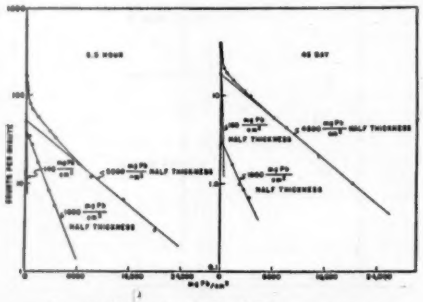

FIG. 2. Absorption in Pb of Hf gamma-rays.

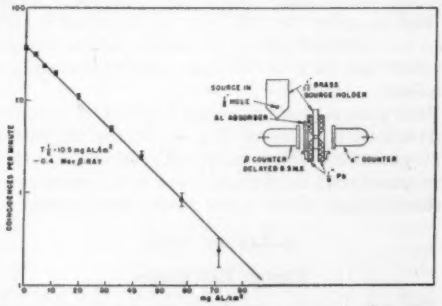

FIG. 3. Absorption in Al of $_{72}Hf^{181}$ (45-day) β, ϵ^- coincidences with β-counter delayed 8.5 microseconds. Absorption on delayed side, $\tau = 7.25$ microseconds.

TABLE IV. Analysis of electron group energies.

Component	Range (mg Al/cm²) (corrected)	Electron energy (Mev)	Shell in Ta	Energy sum (Mev)	Probable γ-ray (Mev)
A	14	0.090	*K*	0.157	0.1329
B	31	0.150	*L*	0.161	0.1329
C	75	0.300	*K*	0.367	0.3441
D	96	0.350	*L*	0.361	0.3441
E	115	0.395	*K*	0.467	0.4808

Prompt Coincidences

With no filter before the 2-mg mica/cm² window of one counter, an absorption in aluminum on the second counter yielded a curve for prompt coincidences (resolving time 0.48 μsec) that shows three electron groups, which from their ranges probably correspond to the gamma-rays of 0.4808, 0.3441, and 0.1329, and/or 0.1358 Mev. The structure of this curve (Fig. 5) indicates that most of the prompt coincidences are between internal conversion electrons.

When a filter of 15.6 mg Al/cm² (which with the Scotch tape source backing gave an effective filter thickness of about 23.4 mg Al/cm²) was placed before the first counter, the absorption curve showed the intensities of the two harder components to be reduced to ~5 percent relative to the softer group, which alone remained clearly distinguishable (Fig. 6). From this one may conclude that relatively few of the coincidences are ones between two electrons of high energy.

Furthermore, if an undelayed beta-ray branch of energy comparable to that of the delayed branch represented any appreciable fraction of the disintegrations, it would have stood out clearly when the filter was inserted, for the low resolving time of the coincidence circuit suppressed the delayed coincidence rate to approximately 0.8 percent of the integrated rate.

One further experiment was done in an attempt to find an undelayed branch. A source was placed in coincidence geometry with a filter of 1.885 g Pb/cm² between the source and one counter. This filter reduced to a negligible intensity the soft gamma-rays

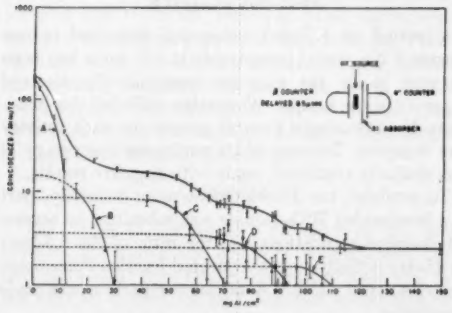

FIG. 4. Absorption in Al of $_{73}Hf^{181}$ (45-day) β, ϵ^- coincidences with β-counter delayed 8.5 microseconds. Absorption on undelayed side, $\tau = 7.25$ μsec.

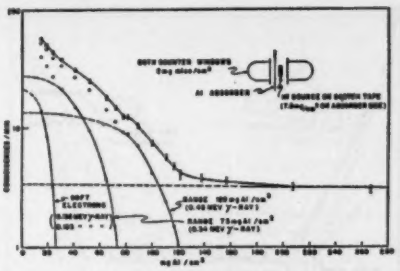

FIG. 5. Absorption in Al of $_{73}Hf^{181}$ (45-day) $\epsilon^- - \epsilon^-$ coincidences.

and x-rays and attenuated the 0.3441-Mev gamma-ray to 50 percent and the 0.4808-Mev gamma-ray to 77 percent. Between the source and the other counter a composite filter was placed. This filter consisted of the Scotch tape source mounting, 10.8 mg Ta/cm², and 6.9 mg Al/cm². The entire filter was approximately equivalent to 30 mg Al/cm², which was sufficient to eliminate the soft conversion electrons from the 0.1329- and 0.1358-Mev gamma-rays. The Ta was included to preferentially remove the *L* x-rays. This arrangement would permit coincidences to be recorded only if they were between one of the two harder gamma-rays and beta-rays or electrons with sufficient energy to penetrate the filter. The filter reduced the beta-ray associated with the delayed state to about 12 percent. Since a beta-ray associated with the undelayed branch would be probably expected to have as much energy as the delayed beta-ray, this arrangement was quite sensitive to prompt beta-gamma-coincidences, especially considering that the short resolving time of the circuit (1.25 μsec) already suppressed the delayed coincidences to 4 percent. After determining the coincidence rate with no delay, the beta-counter was delayed 1.75 μsec and the coincidence counting rate due to the delayed branch determined. Correction for *X*-gamma- and gamma-gamma-coincidences (determined with a thick Al filter before the beta-counter) allowed all beta-gamma-coincidences observed in the nondelayed condi-

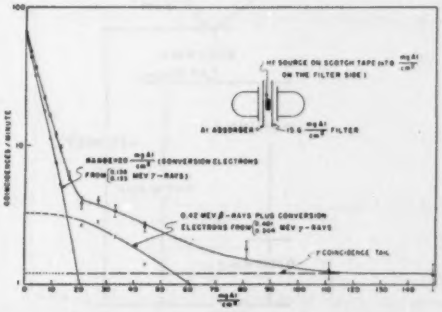

FIG. 6. Absorption in Al of $_{73}Hf^{181}$ (45-day) $\epsilon^- - \epsilon^-$ coincidences.

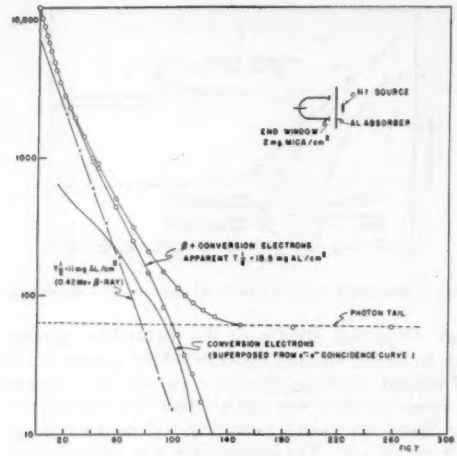

FIG. 7. Absorption in Al of $_{72}Hf^{181}$ (45-day) β-rays.

tion to be attributed to the delayed branch. The low counting rate did not permit good statistics to be obtained; hence the experiment permits us only to place an upper limit of about 5 percent on a possible undelayed branch.

Beta-Spectrum

The presence of internal conversion electrons in the neighborhood of the beta-end point prevented an exact determination of the beta-ray energy in the 180° spectrometer. However, an extrapolation of a Fermi-Kurie plot of the beta-ray continuum measured in the spectrometer gave a beta-ray end point of 0.420±0.010 Mev. No harder beta-ray was observed. The sensitivity of the spectrometer would have allowed the detection of a harder beta-ray component of intensity >1 percent of the 0.420-Mev beta-ray.

A careful single beta-ray absorption in aluminum was made (Fig. 7). By attributing about 5 percent of the radiation to internal conversion electrons from the combined 0.3441- and 0.4808-Mev gamma-rays and by superimposing the $\epsilon^- - \epsilon^-$ coincidence curve to obtain an approximation to the shape of the electron groups, the absorption reduced to a single beta-ray of 11 mg Al/cm² half-thickness, which corresponds to the delayed 0.4-Mev beta-ray.

Decay Scheme

The decay scheme for $_{72}Hf^{181}$ as originally proposed by Chu and Wiedenbeck[10] and modified by Cork *et al.*[13] and by Barber[15] is confirmed. It is shown in Fig. 8. The energy levels assigned to $_{73}Ta^{181}$ show excellent internal consistency, the maximum deviation of any sum being about 0.3 percent.

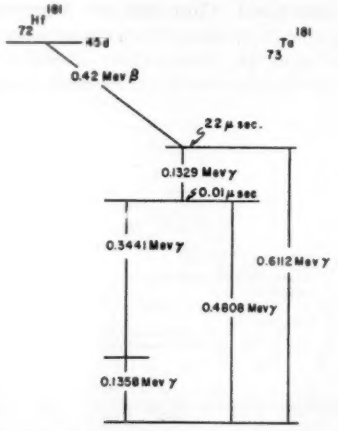

FIG. 8. Proposed decay scheme for $_{72}Hf^{181}$ (45-day).

TABLE V. Gamma-ray energies from internal conversion electron spectrogram for $_{72}Hf^{180}$ (5.5-hr) (activated enriched $_{72}Hf^{179}$).

Electron energy	Proposed interpretation	Energy sum (Mev)	Gamma-energy (Mev)
0.0460	$L_{I,II}$	0.0568	
0.0473	L_{III}	0.0569	
0.0542	M	0.0568	0.0568
0.0277	K	0.0931	
0.0824	$L_{I,II}$	0.0932	
0.0837	L_{III}	0.0933	
0.0906	M	0.0932	
0.0926	N	0.0931	0.0932
0.1485	K	0.2139	
0.2032	$L_{I,II}$	0.2140	
0.2116	M	0.2142	0.2140
0.2649	K	0.3303	
0.3196	$L_{I,II}$	0.3304	0.3304
0.3763	K	0.4417	
0.4317	$L_{I,II}$	0.4425	0.4420

5.5-HOUR ACTIVITY

A period of 5.5±0.1 hours was identified in our sources.[18] No period comparable to 5.5 hours has been reported in Zr, the only spectrographically detected impurity in the sample. We further excluded this possibility by activating a pure Zr sample; no such activity was observed. Because of its analogous chemistry, Ti was similarly examined, again with negative results.

To establish the Z assignment more definitely, part of a bombarded HfO_2 sample was submitted to several Hf chemical separations and the ratio of the 5.5-hour to 45-day activity in the separated fraction determined from its decay curve.[19] A similar comparison was made

[18] This activity, earlier designated ~6 hours, was first observed in this Laboratory by C. O. Muehlhause.

[19] See Appendix.

on the remaining portion of the originally activated sample. The observed 5.5 hr/45 day ratio for the separated fraction was 1.57±0.05 and for the fraction of the original 1.55±0.03. The chemical procedure was highly specific for Hf, so that it would be very unlikely that the ratios of the activities would remain constant unless both periods were in the same element. Finally, upon activation of the various separated isotopes the ratio of the 5.5-hr to 45-day periods was found to be greatly increased upon bombardment of enriched $_{72}Hf^{179}$; the period was thus assigned to $_{72}Hf^{180}$.

Photon Radiations

All of the internal conversion electron lines found to be associated with the 5.5-hr activity yielded the best energy agreement when fitted with Hf work functions. Five gamma-rays were identified, and the spectrographic results are tabulated in Table V. The associa-

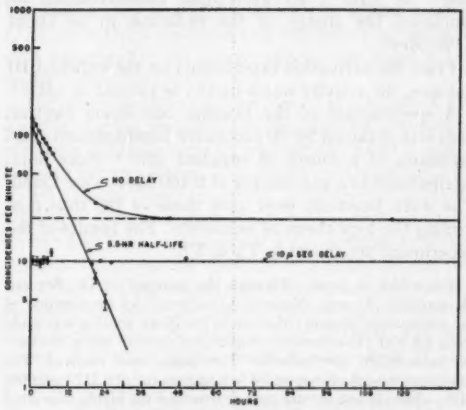

FIG. 9. Decay of Hf σ^-–β-coincidences (with and without 10 μsec delay).

tion of Hf work functions with these gamma-rays leads to the conclusion that the 5.5-hr activity is an isomeric state of $_{72}Hf^{180}$. In the lead absorption curve, Fig. 2, three of the gamma-rays have been resolved. Prior to the time when the enriched isotopes became available, the striking similarity between this curve and the corresponding lead absorption for the 45-day photon radiations led to considerable difficulty regarding the isotopic assignment of the activity.

Coincidences

The decay of the beta-σ^- coincidences (no filters between the source and counters) was followed under two conditions: with neither channel delayed and with one channel delayed 10 μsec. Figure 9 shows that only prompt coincidences were found to be associated with the 5.5-hour activity.

An absorption in Al of the prompt gamma-σ^- coin-

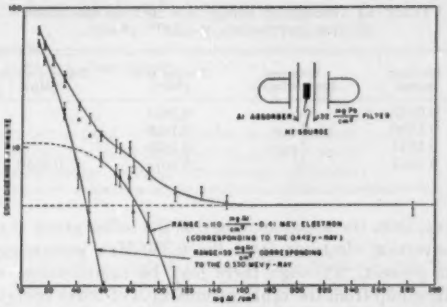

FIG. 10. Absorption in Al of $_{72}Hf^{180}$ (5.5-hr) $\gamma-\sigma^-$ coincidences.

cidences was made using a fixed filter of 32 mg Pb/cm² between the source and one of the counters. This filter not only suppressed all internal conversion electrons except those from the hardest gamma-ray, but also served to further accentuate the counter sensitivity to it by acting as a radiator for the unconverted gamma-rays. The filter was thin enough so that, aside from *L* x-rays, none of the other uncharged radiations was appreciably attenuated. The resulting absorption curve in Fig. 10 is resolved into two components. The more energetic component appears to be an electron group with an approximate range of 110 mg Al/cm², which corresponds to the *K* shell internal conversion electrons from the 0.442-Mev gamma-ray. Note the excellent agreement between the range of this component as observed in the coincidence curve and the corresponding component as observed in the single aluminum absorption (Fig. 11). This component evidently represents coincidences of the *K* conversion electrons from the 0.442-Mev gamma-ray with related *K* x-rays or other gamma-rays associated with the same disintegration. The low relative intensity of the component (about 10 percent) relative to the softer group is consistent with this view, especially when the much lower sensitivity of the counter for uncharged radiation is considered. The accuracy of the points does not permit further detailed analysis of the curve. It is clear, how-

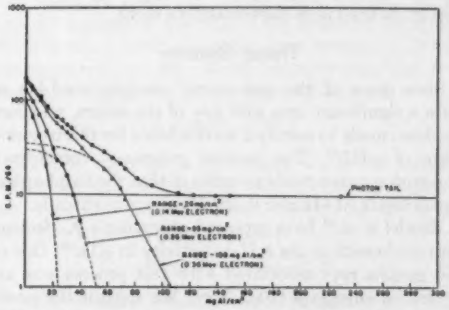

FIG. 11. Absorption in Al of $_{72}Hf^{180}$ (5.5-hr) radiations.

TABLE VI. Gamma-ray energy from internal conversion electron spectrogram of $_{72}Hf^{179}$ (19-sec).

Electron energy	Proposed interpretation	Energy sum (Mev)	Gamma energy (Mev)
0.0957	K	0.1611	
0.1500	$L_{I,II}$	0.1608	
0.1512	L_{III}	0.1608	
0.1587	M	0.1613	0.1610

ever, from the apparent range of the softer group that conversion electrons from the 0.330-Mev gamma-ray are present. Although there may be contributions to this group from the other gamma-rays of lower energy, their resolution would not be possible. It is fairly safe to conclude that the 0.442 and 0.330 gamma-rays are in coincidence.

Single Absorption in Al

A careful absorption in Al (Fig. 11) of the charged component of the radiations using the enriched $_{72}Hf^{179}$ resolved into three components. The statistical errors of all points were less than 0.5 percent and the counter sensitivity was frequently checked with a standard during the run. The source was mounted on a backing of 0.7 mg/cm² to minimize back-scattering. The accuracy and large number of points permit a reasonably reliable analysis. The range (~108 mg Al/cm²−0.36-Mev electron group) of the most energetic electron group, distinguishable as such by its characteristic shape, is in good agreement both with the corresponding portion of the coincidence curve (Fig. 10), and with the range one would expect to observe for the K shell conversion of the 0.442-Mev gamma-ray. Because of the extrapolations necessary, the succeeding analysis is, of course, not as reliable. The two groups which have been resolved (Fig. 11) are in good agreement with the groups identified in the spectrographic plates which correspond to the K shell conversion lines from the 0.330-Mev and the 0.214-Mev gamma-rays.

This analysis would not of itself present a convincing argument in support of the hypothesis of an isomeric transition, but the fact that an analysis is possible which is consistent with the remaining body of information gives the curve substantiative merit.

Decay Scheme

Since none of the gamma-ray energies combine to form a significant sum with any of the others, no effort has been made to specify a level scheme for this isomeric state of $_{72}Hf^{180}$. The prompt gamma-e^- coincidence absorption curve tends to indicate that the two hardest components (0.442 and 0.330 Mev) are in cascade.

Bendel *et al.*[20] have reported observing a K electron capture branch in the 8.15-hr activity in $_{73}Ta^{180}$. One of the gamma-rays associated with this process was assigned an energy of 0.092 Mev. We suggest the possibility that this radiation is identical with the 0.0932-Mev gamma-ray present in the 5.5-hr activity of $_{72}Hf^{180}$. Their failure to observe any of the other gamma-rays which we have assigned to this activity may indicate that the $_{73}Ta^{180}$ nucleus decays to one of the lower energy levels of $_{72}Hf^{180}$, rather than to the 5.5-hr state. If these hypotheses are correct, we would be inclined to place the 0.0932-Mev gamma-ray at or near the bottom of the level scheme.

It is also worthy of note that the assignment of this activity to an isomeric state of $_{72}Hf^{180}$ is in violation of the general rule of Mattauch which states that isomeric states are not in general found in isotopes with both even atomic number and even mass number.

[20] Bendel, Brown, and Becker, Phys. Rev. **81**, 300 (1951).

19-SECOND ACTIVITY

In 1940, Flammersfeld[21] reported a 19-sec activity in Hf which he deduced to be an isomeric state of either $_{72}Hf^{177}$ or $_{72}Hf^{179}$. By absorption measurements, he concluded the energy of the radiation to be about 0.190 Mev.

From the activation experiments on the enriched Hf isotopes, the activity was found to be present in $_{72}Hf^{179}$.

A spectrogram of the internal conversion electron lines was obtained by 50 successive bombardments and exposures of a source of enriched $_{72}Hf^{179}$. Four lines, attributable to a gamma-ray of 0.160 Mev, were found. The work functions used were those of Hf, thus confirming the hypothesis of isomerism. The results of the experiment are shown in Table VI.

Note added in proof:—Through the courtesy of Dr. Bernard Hamermesh (Argonne National Laboratory) an examination of the unconverted photon radiations of the 19-sec activity was made using his NaI (Tl-activated) proportional counter and a 20-channel pulse-height discriminator. Two peaks were resolved. The more intense peak corresponded to a gamma-ray of 0.217 (±0.005) Mev, while the less intense peak represented the highly converted 0.160-Mev component. The former value is in excellent agreement with that reported by der Mateosian and Goldhaber.[22] These authors have also recently reported evidence indicating coincidences between the two gamma-rays.

For their helpful suggestions in the early phases of the work, we wish to thank Dr. C. O. Muehlhause, Dr. M. Goldhaber, and Mr. E. der Mateosian.

[21] A. Flammersfeld, Naturwiss. **32**, 68 (1944).

[22] E. der Mateosian and M. Goldhaber, Phys. Rev. **82**, 115 (1951).

APPENDIX

Chemical Procedure

Several mg of very pure activated HfO_2 were dissolved in HF and the excess fumed off with H_2SO_4. The solution was diluted to 10 ml, 10-mg inactive Hf added as carrier, $Hf(OH)_4$ precipitated with 6M NH_4OH, and the hydroxide washed several times with dilute NH_4OH. The precipitate was dissolved in 10 ml of 10 percent H_2SO_4, 8 ml of 10 percent $(NH_4)_2HPO_4$ and 1 ml conc. H_2SO_4 added, and the solution heated to 40–50°C to effect precipitation of $HfO(H_2PO_4)_2$. The latter was centrifuged, washed with cold 5 percent NH_4NO_3, and ignited at 1200°C for a short time.

Theory of Grain Boundary Motion*

R. SMOLUCHOWSKI
Carnegie Institute of Technology, Pittsburgh, Pennsylvania
(Received March 12, 1951)

The mobility of grain boundaries in metals is considered from a point of view similar to that used by Mott in his theory of viscosity of grain boundaries. By introducing a factor dependent on surface tension of the grain boundary and inserting the experimental activation energy, one obtains satisfactory agreement with experiment.

AMONG the various theories and atomic models of grain boundaries, there are two which seem to allow an interpretation of most of the experimental facts. One of them is the dislocation model, proposed sometime ago by Burgers,[1] and recently described in a more quantitative way by Shockley and Read.[2] Briefly, the grain boundary is upposed to be an array of dislocations which allow two grains to meet at any angle. For small angles, the dislocations are far apart (roughly $1/(\sin\alpha)$ lattice constants) and the theory agrees well with experiment; for larger angles, one expects the model to break down.

The other theory we owe to Mott.[3] It is based on the idea that a grain boundary can be pictured as a sequence of islands of good atomic fit separated by areas of misfit between the two grains. This theory is particularly well suited to large angles where the dislocation model fails. Studies of grain boundary diffusion performed recently[4] for the first time on individual grain boundaries throw important light on the question of applicability of the two theories. They indicate that there is a rather drastic change in the behavior of grain boundaries in columnar copper at around 20 degrees angle between the two grains. For lower angles there is very little if any preferential grain boundary diffusion; for higher angles, on the other hand, the diffusion increases rapidly, reaching a maximum around 45 degrees. This seems to be in agreement with the following interpretation: At small angles, the grain boundary can be pictured as made up of dislocations reasonably far apart and the atomic mobility along such a grain boundary is not much different from that inside of the grain. At angles around 20 degrees, where the dislocations would overlap and lose their identity, the grain boundary is better described in terms of islands of fit and misfit. In such grain boundaries the state of disorder is high, and at low temperatures the diffusion is much faster than the volume diffusion in accord with a lower activation energy.

The present paper is concerned not so much with the mobility of the individual atoms along grain boundaries as with their collective movement associated with the migration of grain boundaries as a whole. On the dislocation model one expects the mobility of a grain boundary to be determined by the mobility of an array of dislocations as it was considered by Shockley. Although a dislocation can move with great ease in its plane of slip, it has to rely on a slow mechanism of atomic diffusion for a motion in a direction perpendicular to that plane. At very small angles of the order of 10^{-4} radian, as, for instance, for mosaic boundaries, the mobility is very high as shown by Guinier.[5] Most experimental determinations of the velocity of motion of true grain boundaries are based on measuring the largest grains, and thus presumably they correspond to grain boundaries with large atomic mobility. It is for that reason that the theory here developed is based on Mott's model.

The basic mechanism of motion of a grain boundary is thus a transfer of a group of atoms from the lattice of one grain to the disordered state at the grain boundary and a transfer of a group of atoms from the disordered boundary layer to the crystalline lattice of the other grain. The two processes are somewhat analogous to melting and solidifying. However, as pointed out by Mott, a literal interpretation of the viscosity of the grain boundary as an extension of a liquid condition to low temperatures is not very tenable in view of the much more rapid temperature dependence of the viscosity of grain boundaries as compared with viscosity of the same metal in liquid state.

In order to make the theory more specific, let us consider a group of n atoms in the lattice of one grain which forms a layer along the grain boundary. In his theory of viscous slip, Mott assumed that the free energy for disordering such a group of atoms is

$$F=nL(1-T/T_m),$$

where L is the heat of fusion and T_m is the melting point. We shall assume that this free energy depends also upon the specific surface energy σ of the grain boundary in the following manner:

$$F=nL(1-T/T_m)-\sigma nvT/T_m, \qquad (1)$$

* This work was sponsored by an AEC contract.

[1] J. M. Burgers, Proc. Phys. Soc. (London) **52**, 23 (1940).

[2] W. Shockley, Phys. Rev. **78**, 275 (1950). T. H. van der Merwe, Proc. Phys. Soc. (London) **63**, 616 (1950).

[3] N. F. Mott, Proc. Phys. Soc. (London) **60**, 391 (1948).

[4] M. R. Achter and R. Smoluchowski, Phys. Rev. **76**, 470 (1949); Proc. Nat. Res. Council Conference on "Lattice Imperfections," Pocono Manor, October, 1950. M. R. Achter, Carnegie Institute of Technology, thesis, 1950.

[5] A. Guinier and J. Tennevin, *Progress in Metal Physics*, Vol. 2 (1950).

TABLE I. Observed and calculated mobilities of grain boundaries.

	Q cal/mole	V_0(obs)cm/sec	V_0(calc)cm/sec
Ag	28000	2×10^2	1.5×10^4
Al	71–85000	10^{18}–10^{19}	1.3×10^{20}
Brass	55000	10^8–10^9	1.6×10^{10}

where v is the area of the layer per atom. Thus the higher the surface energy, the easier it is to disorder the group. This seems to be in accord with the fact that mobility of grain boundaries is strongly dependent upon such crystallographic factors as orientation of the grains and of the grain boundary itself. At the melting point the first term in (1) vanishes; the second term does not vanish, but it is very small, since σ is proportional to the shear modulus G which itself reaches small values at T_m. However, in view of the relatively limited temperature range over which experimental data exist, we can put $\sigma=0$ at $T=T_m$. The general character of the underlying assumptions does not seem to justify a more elaborate consideration of that point.

In a stationary grain boundary the number of atoms ordering and disordering on each side of the boundary is the same. However, a driving force, such as

$$\tau_s=2\sigma/r \tag{2}$$

or

$$\tau_c=\sigma/r, \tag{3}$$

caused by a spherical or cylindrical radius of curvature r of the grain boundary, can cause its migration. If we say that the force displaces the atoms on the average by a fraction f of the atomic diameter a, then the work done is

$$\tau nfav.$$

The rate of motion of the boundary is then, according to the usual rate theory,

$$V=va\exp(-F+\tau nfav)/kT-va\exp(-F-\tau nfav)/kT$$
$$=2va\exp(-F/kT)\sinh(\tau nfav/kT)$$

or approximately

$$V\cong(2v\tau a^2nfv/kT)\exp(-F/kT),$$

where v is the atomic frequency. Inserting the expressions for τ and F we have for a spherical grain of radius r

$$V=V_0\exp(-Q/kT) \tag{4}$$

with

$$V_0=(4va^2\sigma nfv/rkT)\exp[(nL+\sigma nv)/kT_m] \tag{5}$$

and

$$Q=nL. \tag{6}$$

There are several sets of experimental data vailable which permit a comparison with theory: Alexander and co-workers[6] on silver, Beck and co-workers[7] on aluminum and brass, and Walker[8] and Burke[9] on brass. Their data (in certain cases replotted in the form $\ln V$ *versus* $1/T$) give the heats of activation shown in Table I. With $L=2.73$, 2.52, and 3.0 for Ag, Al, and brass, one obtains from (6) for n the values 10, 29–35, and 18 atoms, respectively. There is not enough information available to distinguish among the surface energies σ for each of the three metals. It is assumed thus that for all of them $\sigma=400$ erg/cm^2, which is a typical value observed for copper by Hollomon and Turnbull.[10] Also there are not enough quantitative data available to consider in detail the influence of grain orientation and boundary orientation on σ. The grain radii in the three sets of measurements were approximately 0.05, 0.05, and 0.005 cm. The factor f, which plays very little role in the quantitative check of the theory, was arbitrarily put equal to 0.5. The other values were as follows: $v=10^{12}$ sec^{-1}, $a=10^{-8}$ cm, and $T=500$°C, all the experiments being made in proximity of that temperature. The last two columns of Table I permit the comparison of the theoretical and experimental values of V_0. It should be stressed here that a relatively small change in Q affects the V_0 a great deal and so, in general, an agreement better than within one or two orders of magnitude should be considered fortuitous. Such factors as stress magnifications, cold work, etc., have not been considered at all.

It is interesting to note the strong dependence of mobility on surface tension σ indicated by formula (4). As shown by numerous investigators,[11] in a given metal grain boundary energies can vary from zero to a maximum value. If, instead of putting $\sigma=400$ erg/cm^2, we have assumed $\sigma=100$ erg/cm^2, then the V_0 would come out 25 times lower. For twin boundaries, which according to various estimates have an energy of the order of a few percent of the maximum value, the mobility is 1000 times lower. This is in basic agreement with observation.

The theory here developed indicates the need for quantitative studies of mobility of grain boundaries as a function of grain orientation, and for more information on the corresponding orientation dependence of the grain boundary energies. It would be particularly interesting to study the effects at lower angles between the grains where the dislocation model is applicable, and at intermediate angles where the island model becomes more fruitful.

[6] Alexander, Baluffi, Dawson, Kling, and Rossi, Sylvania Electric Products Company Report NYO-663.

[7] Beck, Holzworth, and Hu, Phys. Rev. **73**, 526 (1948).

[8] H. L. Walker, University of Illinois Eng. Exp. Stat., Bulletin 359 (1945).

[9] J. E. Burke, Trans. Am. Inst. Mining Met. Engrs. **180**, 73 (1949).

[10] J. H. Hollomon and D. Trumbull, General Electric Company, Report RL-398.

[11] C. G. Dunn and F. Lionetti, J. Metals **1**, 125 (1949). Dunn, Daniels, and Bolton (to be published). K. T. Aust and B. Chalmers, Proc. Roy. Soc. (London) **201**, 210 (1950); **204**, 359 (1950). B. Chalmers, Proc. Roy. Soc. (London) **196**, 64 (1949).

The Solution of the Schrödinger Equation for an Approximate Atomic Field*

EDWARD H. KERNER
Department of Physics, Wayne University, Detroit, Michigan
(Received October 6, 1950)

An approximate atomic potential having an "effective nuclear charge for potential," that is, bilinear in the radial distance from the nucleus, is discussed and shown to approximate reasonably well to Hartree or Fermi-Thomas potentials. The Schrödinger equation with the approximate potential is solved as a series of hydrogenic wave functions and as a power series in $Ar/(1+Ar)$ (A being a parameter of the potential). Some illustrative numerical results pertaining to the mercury atom are presented.

1. THE APPROXIMATE POTENTIAL

THE atomic potentials[1] $-Z_p(r)/r$ of Hartree and Fermi-Thomas may be represented adequately for many purposes through the simple formula for Z_p,

$$Z_{pA}=Z/(1+Ar).$$

Figure 1 gives a comparison of the different potentials for the mercury atom.[2]

Figure 2 tests the formula by showing $A(r)=(Z/Z_p-1)/r$ as a function of r for different atoms, Z_p being that given by Hartree.[3] It is seen that Z_{pA} is quite satisfactory out to radii for which Z_p is from 10 to 20 percent of Z, and is certainly too big beyond these radii. An analysis of the curves in the regions where they are flat shows that a good average value for A is $1.525Z^{\frac{1}{3}}$. The approximate potential may of course be improved substantially by adding terms with higher powers of r in the denominator of Z_{pA}; usually a quadratic and a cubic term suffice to give high accuracy over essentially the whole range of r. However, the cost of this in extra mathematical complexity is too great for any but the simplest of atomic calculations.

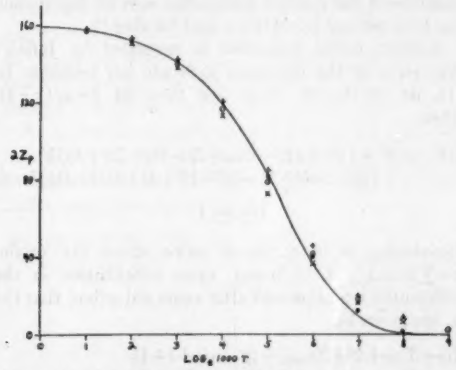

FIG. 1. Comparison of Z_p's for mercury. Smooth curve: Hartree $2Z_p$; ●=Fermi-Thomas $2Z_p$; ×=$2Z_{pA}$ for $A=8$; ○=$2Z_{pA}$ for $A=7$; +=$2Z_{pA}$ for $A=6$.

The Fermi-Thomas φ function, satisfying $x^{\frac{1}{2}}\varphi''=\varphi^{\frac{1}{2}}$ with $r=0.88534x/Z^{\frac{1}{3}}=bx$, is given by $\varphi_A=(1+Abx)^{-1}$ in our approximation. Figure 2 gives $Ab=(\varphi^{-1}-1)/x$ (φ being that for a neutral atom) as a function of x. A comparison of the expansions of φ and φ_A near the origin shows that $A(Z)\simeq 1.79Z^{\frac{1}{3}}$, while direct substitution of φ_A in the Fermi-Thomas equation shows that $A\simeq 1.34Z^{\frac{1}{3}}$ for x near $2^{\frac{1}{3}}/3=0.42$. The solutions φ_0 of the Fermi equation corresponding to positive ions, i.e., those which are zero at a finite x, say, x_0, may be simply and precisely approximated for all x by $\varphi_q=(1-x/x_0)/(1+qx)$, where q depends (although insensitively) on x_0. This is tested in Fig. 2, where $q=(1-x/x_0-\varphi_0)/(\varphi_0 x)$ is plotted against x for a few x_0's. The parameter q could be calculated from the Fermi-Thomas boundary condition $x_0\varphi'(x_0)=(N-Z)/Z$, N being the number of electrons in the ion, but this gives a spurious q value because φ_q does not have the right slope at x_0. The φ_q has an accuracy comparable to that of the relatively complicated Sommerfeld[4] approximate solution of the Fermi equation. Also, the error in φ_q as a representation of φ_0 is mainly in the

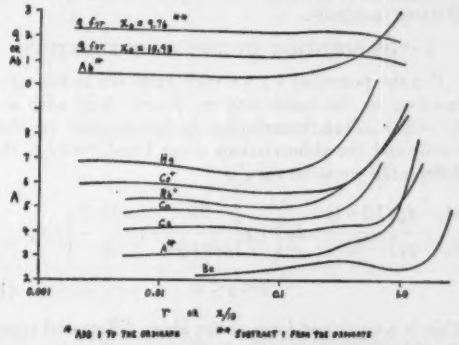

FIG. 2. The upper two curves show q as a function of $x/10$; x is the Fermi-Thomas variable and x_0 is the ionic radius. The next curve shows Ab as a function of $x/10$ using the Fermi-Thomas function φ for neutral atoms. The lower seven curves show A as a function of r for different atoms, using values of Z_p given by Hartree.

* Some of this work was a part of the author's doctoral thesis at Cornell University.

[1] Atomic units will be used throughout the discussion.

[2] D. R. Hartree, Phys. Rev. 46, 743 (1934); Proc. Roy. Soc. (London) 149, 210 (1935).

[3] D. R. Hartree, Proc. Cambridge Phil. Soc. 24, 89 (1928); Proc. Roy. Soc. (London) 143, 506 (1934) and 166, 450 (1938).

[4] A. Sommerfeld, Z. Physik, 78, 283 (1932).

direction of making it more "Hartree-like" if q is given a value which makes φ_0 and φ_q agree at smaller r, since then φ_q is somewhat smaller than φ_0 for large r while φ_0 is somewhat larger than the Hartree function for such r.

Our final potential for an ion is now

$$-V_a=\frac{Z(1-r/r_0)}{r(1+ar)}+\frac{Z-N}{r_0} \qquad r<r_0$$
$$=(Z-N)/r \qquad r>r_0,$$

where r_0 is the ionic radius and $a=q/b\sim Z^{\frac{1}{3}}$. In the special case where r_0 is large we get the potential $-V_A(r)=Z/r(1+Ar)$. For the present, we shall principally discuss V_A as a generator of Schrödinger wave functions, postponing a consideration of Dirac functions as well as a more extensive treatment of V_a and of various atomic calculations for a later report. Since V_A is close to the Hartree potential over a range of r where most wave functions have their largest amplitudes, we may expect V_A to yield a set of useful functions for electrons in the atomic core but not in the outermost shells. Without too serious consequences we will not distinguish between separate potentials for separate electron groups and the approximate potential itself. Our wave functions therefore will be orthogonal. Some evaluation of the accuracy of wave functions calculated with V_A is provided by a work of Slater,[5] who has shown that empirical approximations (correct to within about one percent) to Hartree functions are generated by potentials which, compared with the Hartree potentials, are very poor at large r and for r in the vicinity of the roots of his functions, sometimes being off by a factor of two or more and having the wrong sign as well. It is to be presumed that the wave functions arising from V_A are in many cases sufficiently close to Hartree functions.

2. THE SOLUTION OF THE WAVE EQUATION

For the potential V_A we may write the radial wave function in the usual way as $R=r^le^{-\epsilon r}g(r)$ with $\epsilon=+(-2E)^{\frac{1}{2}}$. Then, introducing the independent variable $x=Ar$ and the abbreviations $\alpha=\epsilon/A$ and $\beta=Z/A$, the differential equation for g is

$$\frac{d^2g}{dx^2}+\frac{dg}{dx}\left\{\frac{2(l+1)}{x}-2\alpha\right\}+g\left\{\frac{2\beta}{x(1+x)}-\frac{2\alpha(l+1)}{x}\right\}=0,$$
$$0\leq x\leq\infty \qquad (1)$$

This is a confluent form of the Heun differential equation,[6] having regular singularities at $x=0$ and $x=-1$, and an irregular singularity at infinity. In the case that $\alpha=0$, (1) is a hypergeometric equation. If $l=0$, (1) may be reduced by the transformations $g=e^{\alpha x}(1+x)f(x)$, $z=1+2x$ to a case of the spheroidal wave equation studies in detail by Chu and Stratton.[7] A confluent Heun equation arises also in the hydrogen molecule ion problem,[8] which is mathematically closely related to the present one. It will be observed that for either of the potentials V_A or V_a the integrals of the WKB approximation may be evaluated in terms of the standard elliptic integrals, since the integrand is a rational function of r and the square root of a quartic polynomial in r.[9]

The eigensolutions to (1) may be conveniently expanded in hydrogenic functions, as in perturbation theory. This has the advantage that the largest terms can often be picked out. Instead of the Laguerre polynomials proper, we will use the equivalent confluent fluent hypergeometric polynomials. Setting

$$g=\sum_{\nu=0}^{\infty}c_\nu F(-\nu, 2l+2, 2\alpha x),$$

and using the recurrence formulas for the F functions, it is found that the c_ν are given by the recurrence relation

$$c_{\nu+1}(\nu+1)(\nu+l+2)/2+c_\nu\{\beta-\alpha(l+\nu+1)-(l+\nu+1)^2\}+c_{\nu-1}(\nu+l)(\nu+2l+1)/2 \quad \nu=0, 1, 2, \cdots; c_{-1}=0. \qquad (2)$$

A more general potential, involving higher powers of r in Z_{pA} as mentioned before, may be treated similarly through repeated application of the recurrence formulas for the F functions; each successive additional power of r beyond the first, in either the numerator or denominator of Z_{pA}, gives two extra terms in the recurrence formulas for the c_ν. The convergence of expansions of the present kind, when α is an eigenvalue, has been proven by McCrea and Newing.[10]

Another useful expansion is suggested by Jaffe's[11] discussion of the hydrogen molecule ion problem. In (1), let $g=(1+x)^{-l-1}h(x)$ and then let $\xi=x/(x+1)$. Then

$$\xi(1-\xi)^2h''+\{2(l+2)\xi^2-2(\alpha+2l+3)\xi+2(l+1)\}h'+\{2\beta-2\alpha(l+1)-2(l+1)^2+(l+1)(l+2)\xi\}h=0,$$
$$0\leq\xi\leq 1.$$

Developing h in a power series about the origin, $h=\sum_{\nu=0}^{\infty}a_\nu\xi^\nu$, it is found, upon substitution in the differential equation and after some reduction, that the a_ν are given by

$$\tfrac{1}{2}(\nu+1)(\nu+2l+2)a_{\nu+1}+\{\beta-\alpha(\nu+l+1)-(\nu+l+1)^2\}a_\nu+\tfrac{1}{2}(\nu+l)(\nu+l+1)a_{\nu-1}=0,$$
$$\nu=0, 1, 2, \cdots; \quad a_{-1}=0.$$

[5] J. C. Slater, Phys. Rev. **42**, 33 (1932).
[6] E. L. Ince, *Ordinary Differential Equations* (Longmans, Green and Company, London, 1927), p. 394.
[7] L. J. Chu and J. A. Stratton, J. Math. Phys. **20**, 259 (1941).
[8] W. G. Baber and H. R. Hasse, Proc. Cambridge Phil. Soc. **31**, 564 (1935).
[9] E. T. Whittaker and G. N. Watson, *Modern Analysis* (The Macmillan Company, New York, 1943), article 22.7.
[10] McCrea and Newing, Proc. London Math. Soc. **37**, 520 (1934).
[11] G. Jaffe, Z. Physik **87**, 535 (1935).

If now one sets $a_\nu = b_\nu f(\nu)$ and determines $f(\nu)$ so that $f(\nu+1)/f(\nu) = (\nu+l+2)/(\nu+2l+2)$, i.e., so that

$$f(\nu) = \binom{l+\nu+1}{\nu} \Big/ \binom{2l+\nu+1}{\nu},$$

then b_ν satisfies just the same difference equation as the c_ν of Eq. (2). As in the hydrogen molecule ion problem, the series is convergent for all ξ in $0 \leq \xi \leq 1$. Thus, the evaluation of *one* set of expansion coefficients provides *two* representations of the wave function.

The solutions to (1) may also be expanded in series of bessel functions, in powers of $(1+Ar)^{-1}$, and in other ways. For the potential V_a, an expansion of the wave function R in powers of $(1-r/r_0)/(1+ar)$ (for $r<r_0$) is convenient, since the boundary conditions of a smooth junction of R at r_0 with the hydrogenic solution beyond r_0 is easily met by specifying the first two expansion coefficients.

In a three-term recurrence formula such as (2), the eigenvalues of α must be found before the formula can be used to compute the c_ν. Formulas of this type are ordinarily handled by a method of continued fractions first used by Ince[12] in connection with Mathieu's equation. The method was improved by Bouwkamp[13] for use with the spheroidal wave equation. Although applicable in principle to most second-order difference equations, this method turns out to be uncommonly awkward in practice for Eq. (2). Alternatively, (2) may be looked upon as an infinite set of linear equations in the c_ν. For the self-consistency of the equations, the determinant Δ of the coefficients of the c_ν must be zero. Then $\Delta(\alpha)=0$ is a transcendental equation in α whose roots are the eigenvalues. Since c_{n-l-1} may be expected to be among the largest c_ν, n meaning the principal quantum number, the determinant can be conveniently written around the "main term" $\beta-\alpha n-n^2$.

As a zeroth approximation to $\Delta=0$, one may take $\beta-\alpha n-n^2=0$, so that $\epsilon_0 = Z/n-nA$. In the limit $A=0$ we have then the hydrogenic value for ϵ. A much better approximation would be

$$\begin{vmatrix} \beta-\alpha(n-1)-(n-1)^2, & n(n-1-l)/2, & 0 \\ (n-1)(n+l)/2, & \beta-\alpha n-n^2, & (n-l)(n+1)/2 \\ 0, & n(n+l+1)/2, & \beta-\alpha(n+1)-(n+1)^2 \end{vmatrix} = 0. \quad (3)$$

This mode of expanding the determinant is like that used for the infinite determinant for characteristic values arising from Hill's differential equation.[14] An approximate root of (3) is found explicitly by introducing $\alpha_0 = \epsilon_0/A$ into the corner terms of the determinant. The result is

$$\epsilon_1 = \frac{Z}{n} - nA + \frac{A^2}{4}\frac{(n+l+1)(n-l)(n+1)}{(Z/n)+(n+1)A} - \frac{A^2}{4}\frac{(n-l-1)(n+l)(n-1)}{(Z/n)+(n-1)A}. \quad (4)$$

Equations (3) and (4) are useful for quickly obtaining approximate eigen-ϵ.

The roots of the infinite determinant may be calculated with arbitrary accuracy with the following technique. First, rewrite (2) for simplicity as

$$c_{\nu-1}d_{\nu,\nu-1} + c_\nu d_{\nu\nu} + c_{\nu+1} = 0,$$

$$d_{\nu,\nu-1} = \frac{(\nu+l)(\nu+2l+1)}{(\nu+1)(\nu+l+2)},$$

$$d_{\nu\nu} = \frac{2[\beta-\alpha(\nu+l+1)-(\nu+l+1)^2]}{(\nu+1)(\nu+l+2)},$$

so that the characteristic equation for α is

$$\Delta = \begin{vmatrix} d_{00} & 1 & 0 & \cdots & & & & \\ d_{10} & d_{11} & 1 & 0 & \cdots & & & \\ 0 & d_{21} & d_{22} & 1 & \cdots & & & \\ \cdots & \cdots & \cdots & \cdots & \cdots & \cdots & \cdots & \\ & \cdots & 0 & d_{m,m-1} & d_{mm} & 1 & 0 & \cdots \\ & & \cdots & \cdots & \cdots & \cdots & \cdots & \cdots \end{vmatrix} = 0.$$

The determinant of the $(m+1)$th order, Δ_{m+1}, equal to Δ with all rows and columns beyond the mth omitted, may be expanded in minors starting at the lower right-hand corner where d_{mm} is situated:

$$\Delta_{m+1} = d_{mm}\Delta_m - d_{m,m-1}\Delta_{m-1}. \quad (5)$$

With the conventions $\Delta_0 = 1$, $\Delta_1 = d_{00}$, (5) permits the computation in succession of the determinants Δ_m up to any order desired. Let α_0 be an approximate root of Δ. Performing a variation of (5) with respect to α, one has

$$\delta\Delta_{m+1} = \Delta_m\delta d_{mm} + d_{mm}\delta\Delta_m - d_{m,m-1}\delta\Delta_{m-1}$$

$$\delta d_{mm} = \frac{-2(l+m+1)}{(m+1)(m+l+2)}\delta\alpha. \quad (6)$$

With the approximate α_0, the Δ_m and $\delta\Delta_m$ may be found in succession, and for sufficiently large m it can be required that

$$\Delta_{m+1}(\alpha_0+\delta\alpha) = \Delta_{m+1}(\alpha_0) + \frac{\delta\Delta_{m+1}}{\delta\alpha}\delta\alpha = 0,$$

which determines a correction $\delta\alpha$ to α_0. The $\delta\alpha$ deduced in this way turn out to be remarkably independent of m beginning at relatively low m (see Table I), so that a good value for α can be found with little

[12] E. L. Ince, Phil. Mag. **6**, 547 (1928).
[13] C. J. Bouwkamp, J. Math. Phys. **26**, 79 (1947).
[14] Reference 9, §19.42.

TABLE I. Example of calculation of eigenvalues and expansion coefficients; $Z=80$, $1S$ state, $A=1/.145$, $\beta=11.6$.

Initial $\alpha=10.673$ m	$d_{m,m}$	Δ_{m+1}	$\delta\Delta_{m+1}/\delta\alpha$	$\delta\alpha$	$d_{m+1,m}$	$2/m+2$
0	−0.0730	−0.0730	−1.0		$0.3\overline{3}$	1.0
1	−4.5820	$0.0011526\overline{6}$	$4.630\overline{6}$		0.5	$0.6\overline{6}$
2	$-4.9031\overline{6}$	0.03084828	−22.205506	$+1.3892\times10^{-3}$	0.6	0.50
3	−4.70920	−0.14596234	101.77943	$+1.4341\times10^{-3}$	$0.6\overline{6}$	0.40
4	−4.4510	0.62911285	−438.16792	$+1.4358\times10^{-3}$	0.71428571	$0.3\overline{3}$
5	$-4.211\overline{3}$	−2.5451451	1772.3918	$+1.4360\times10^{-3}$	0.750	0.28571428
6	−4.0039643	9.7188354	−6767.3314	$+1.4361\times10^{-3}$	$0.7\overline{7}$	$0.25\overline{0}$
7	$-3.827\overline{3}$	−35.217665			0.8	$0.2\overline{2}$
			$\delta\alpha=+1.44\times10^{-4}$			
New $\alpha=10.67444$					$\delta\Delta_{m+1}$	Δ_{m+1} corr.
0	−0.07444	−0.07444	−1.0		$+5.02432\times10^{-6}$	-7.443498×10^{-3}
1	−4.582960	0.007822209	4.6325867		-2.32756×10^{-5}	$+7.798933\times10^{-3}$
2	-4.903886	−0.001139227	−22.221591		$+1.11648\times10^{-4}$	-1.027578×10^{-3}
3	−4.7097760	0.0006721776	101.87962	-6.5978×10^{-6}	-5.11876×10^{-4}	$+1.60301\times10^{-4}$
4	−4.4514800	−0.002232700	−438.70092	-5.0893×10^{-6}	$+2.20426\times10^{-3}$	-2.8434×10^{-5}
5	−4.2117448	0.008923438	1774.9258	-5.0275×10^{-6}	-8.91780×10^{-3}	$+5.634\times10^{-6}$
6	−4.0043243	−0.034057814	−6778.3550	-5.0245×10^{-6}	+0.0340566	-1.15×10^{-5}
7	−3.8276533	0.12342105	24564.703	-5.0243×10^{-6}	−0.12342	$+0\times10^{-5}$
			$\delta\alpha=-5.0243\times10^{-6}$			
Final $\alpha=10.674434976$						

labor. With obvious modifications this method could be applied to any three-term recurrence relation like (2). The similarity to Bouwkamp's method will be evident. It follows from Eqs. (2) and (5) that $c_\nu=(-1)^\nu\Delta_\nu$; hence the calculations may be performed directly with the c_ν.

The approximate c_ν (or Δ_ν) computed with the approximate α can be easily corrected after $\delta\alpha$ has itself been determined. An illustrative example is given in Table I for the $1S$ state of mercury assuming $A=1/0.145=6.896$ and $\beta=Z/A=11.6$. As in the example, one characteristically finds that the Δ_m diverge in opposite senses for α which are slightly above or below the correct value. This provides a good check on the calculations. Another check comes from the fact that $\delta\alpha$ may be found at every step, and for a good initial α is observed to converge rapidly to a limit. If the initial α is poor, this convergence is poor, and it is best to correct α before going too far and to start over. Not more than one or two such iterations, depending on the accuracy sought, provides both an eigenvalue and a set of expansion coefficients having many significant digits in most cases. An hour with a desk calculator suffices to determine an α correct to within one part in a million, frequently better than this.

TABLE II. Comparison of eigenvalues of ϵ for $Z=80$.

		From Eq. (4)		From infinite determinant	
n,l	Hartree	$A=6.986$	$A=6$	$A=6.896$	$A=6$
$1S$	74.48	73.61	74.39	73.62	74.40
$2S$	30.41	29.23	30.40	29.44	30.46
$2P$	29.87	28.56	29.86	28.72	29.98
$3S$	14.76	12.97	14.40	14.23	15.29
$3P$	14.19	12.39	13.91	13.35	14.73
$3D$	13.08	11.24	12.93	12.16	13.57
$4S$	6.87	4.72	5.47	7.22	8.08
$4P$	6.34	3.29	5.09	6.69	7.61
$4D$	5.27	2.43	4.34	5.61	6.69
$4F$	3.09	1.15	3.20	3.91	5.18

In practice, it is usually not necessary to go beyond $m=10$ or 20, except for states with the largest quantum numbers corresponding to optical states. For example, some fifty or sixty terms must be computed for the $n=5$ states of mercury before the divergence of the c_ν is evident (although only about fifteen are needed for the $n=4$ states). Neither the approximate potential nor the expansions that have been used for the wave functions are suitable for such states.

The evaluation of the c_ν is completed by an examination of their behavior for large ν. In (2), let $c_\nu=k_\nu/(l+\nu+1)$. Then

$$\tfrac{1}{2}(\nu+1)k_{\nu+1}+k_\nu\{[\beta/(l+\nu+1)]-(\alpha+l+\nu+1)\}+\tfrac{1}{2}k_{\nu-1}(\nu+2l+1)=0. \quad (7)$$

In the limit of large ν, $\beta/(l+\nu+1)$ is negligible in comparison with $\alpha+l+\nu+1$, and (7) becomes a difference equation of hypergeometric type[15] with the asymptotic solutions

$$k(\nu)=\exp[\pm 2(2\alpha)^{\frac{1}{2}}(\nu+2l+1)^{\frac{1}{2}}]\times(\nu+2l+1)^{l+\frac{1}{4}}\{1\pm O(1/\nu^{\frac{1}{2}})\}.$$

The $\pm$ signs correspond to the independent solutions of the difference equation, the minus sign giving convergent expansions of the wave functions.

A few results obtained with the aforementioned procedures are given in Table II and Fig. 3. Table II shows eigen-ϵ computed from (4) and from the infinite determinant in comparison with Hartree's values, for $Z=80$. Figure 3 shows how the $2S$ and $2P$ levels split as the non-coulomb potential $-Z_{pA}/r$ is turned on

[15] P. M. Batchelder, *Linear Difference Equations* (Harvard University Press, Cambridge, 1927), p. 175. The difference equation is of the "irregular" type, having a characteristic equation with equal roots.

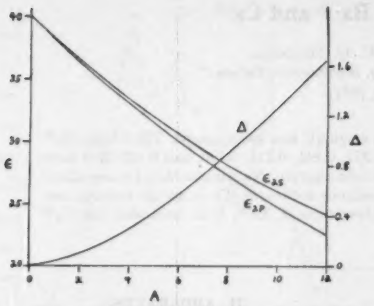

FIG. 3. ϵ as a function of A for Z fixed at 80 and for the $2S$ and $2P$ states. $\Delta=\epsilon_{2S}-\epsilon_{2P}$ shows the splitting of the states as the non-coulomb character of the potential is amplified through increasing A.

through increasing A. Normalization factors for the wave functions may be easily found in terms of the c_r by making use of the orthogonality of the F functions and the recurrence formulas for them. Such quantities as transition probabilities are also computed in a straightforward way from tables of c_r and one may see the separate hydrogenlike contributions to the final value.

An example of the use of the approximate potential directly is the calculation of the scattering amplitude $f(\theta)$ for a fast electron in the potential. In the Born approximation,

$$f(\theta)=\frac{8\pi^2m}{h^2}\int_0^\infty\frac{\sin Kr}{Kr}\frac{Z}{r(1+Ar)}r^2dr$$
$$=\frac{8\pi^2mZ}{h^2A^2}\left\{\frac{\sin(K/A)\mathrm{Ci}(K/A)+\cos(K/A)[\pi/2-\mathrm{Si}(K/A)]}{K/A}\right\}$$
$$=\frac{8\pi^2mZ}{h^2A^2}\varphi\left(\frac{K}{A}\right), \tag{8}$$

where $K=(4\pi mv/h)\sin(\theta/2)$, mv being the incident electron momentum and θ the scattering angle. In the limit of small K/A, $\varphi(x)$ diverges as $[x\log(1.781x)+\frac{1}{2}\pi-x]/x$, reflecting the fact the approximate potential is too large at large r so that the incident electron is affected too much in a distant collision. If one cuts off the potential at $r=R$, then (8) is replaced by

$$f(\theta)=\frac{8\pi^2mZ}{h^2A^2}\left\{\frac{\sin(K/A)[\mathrm{Ci}(K/A)-\mathrm{Ci}((1+AR)K/A)]+\cos(K/A)[\mathrm{Si}((1+AR)K/A)-\mathrm{Si}(K/A)]}{K/A}\right\}$$
$$=\frac{8\pi^2mZ}{h^2A^2}\Phi\left(\frac{K}{A}\right).$$

For small K/A, $\Phi(K/A)=AR-\log(1+AR)$. The functions φ, Φ, and that $f(\theta)$, f_{FT}, arising from the Fermi-Thomas potential[16] may be conveniently compared on a log-log graph. This is done in Fig. 4, where f_{FT} is plotted against $Z^{-\frac{1}{3}}v\sin(\theta/2)$ and φ and Φ (for $AR=26$) are plotted against K/A. It is seen that φ and Φ are indistinguishable except at small K/A, and that Φ and f_{FT} agree satisfactorily.

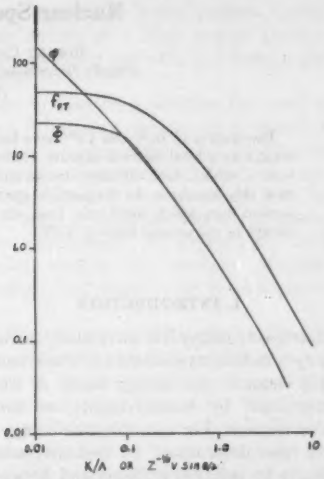

FIG. 4. Comparison of scattering amplitudes in Born approximation. φ is calculated directly with the approximate potential $-Z_{eA}/r$. Φ is calculated with the potential cut-off at R for the case that $AR=26$. f_{FT} is the Fermi-Thomas scattering amplitude.

In conclusion, the writer wishes to thank Professors Richard P. Feynman and Hans A. Bethe for friendly discussion and criticism.

[16] N. F. Mott and H. S. W. Massey, *The Theory of Atomic Collisions* (Oxford University Press, New York, 1949).

Nuclear Spectroscopy of Ba^{131} and Cs^{131}

ROBERT CANADA AND ALLAN C. G. MITCHELL
*Physics Department, Indiana University, Bloomington, Indiana**
(Received March 19, 1951)

The spectra of Ba^{131} and Cs^{131} have been investigated in a magnetic lens spectrograph. The 12-day Ba^{131} decays by orbital electron capture. Gamma-rays at 0.497, 0.371, 0.241, 0.213, 0.196, and 0.122 Mev have been observed. Cs^{131} (10-day) decays entirely by orbital electron capture. No gamma-rays are associated with this transition. In the particle spectrum only Auger electrons are found. There are no internal conversion lines which could arise from the 0.080- and 0.163-Mev states of Xe^{131}. It is concluded that Cs^{131} decays to the ground state of Xe^{131}.

I. INTRODUCTION

IN nuclear spectroscopy it is particularly advantageous to study a radioactive substance whose end product is a stable element, the energy levels of which have been ascertained by measurements on some other radioactive element. For example, the energy levels of Te^{124} have been determined[1] by measurements on I^{124}, which decays by positron emission and K-capture, and also by measurements[2,3] on Sb^{124}, which decays by the emission of beta-rays. The levels of Te^{124}, determined in these two ways, agree. Numerous other examples are known.[4] If, in addition, the product nucleus is known to have a metastable state, certain conclusions about the configurations of the various states involved may be obtained with the help of the shell model of nuclear structure.[5] This is true since the shell model has been particularly helpful in explaining regions of isomerism and in predicting the configurations of ground states and metastable states.

With this in mind we have made a study of the radiations of Cs^{131}. Cs^{131} goes to Xe^{131} by orbital electron capture. The levels of Xe^{131} are known from a study[4] of I^{131}. Furthermore, a metastable state of 12-day half-life is known[6,6a] in Xe^{131}. Since Ba^{131} is the parent of Cs^{131}, this nuclide was also studied.

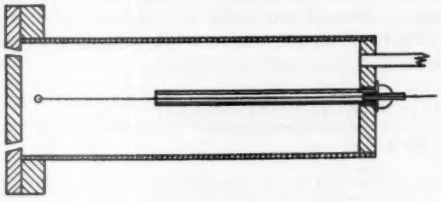

FIG. 1. Diagram of counter with annular opening allowing the use of thin film windows with ring type focusing.

II. APPARATUS

The measurements were made with a magnetic lens type spectrometer which has been described[7] previously and which has been modified to use ring focusing. The position of the ring focus was located in the following manner. Three cones of electrons were defined by placing a baffle with three annular slits at the central plane of the lens. Essentially a "point source," 1.3 mm in diameter, of thorium active deposit was used to produce a line of internal conversion electrons. When the coil current was set to focus the "F" line from ThC ($H\rho$ = 1385 gauss-cm), sharp patterns of concentric circles were obtained on an electron sensitive film exposed at positions near the counter end of the spectrometer chamber. Six such exposures were made, from which it was possible to plot the trajectories of electrons from the inner, outer, and center regions of the acceptance zone. The crossing of these trajectories located the position of the ring focus. The annulus of best focus was found to be 3.76 cm in diameter and located 9.2 cm from the plane of axial focus. The width of the annulus was found to be 3 mm when the usual sized sources were used.

In order to have ring focusing and still be able to use thin film counter windows, a 5.08 cm diameter counter was constructed so that an annular counter window could be employed to define the focus ring. Zapon films laid down on the window plate provided a window which held without leaking and transmitted electrons having energies down to 11 kev. The counter is shown in Fig. 1.

III. EXPERIMENTS ON Ba^{131}

Ba^{131} has a half-life of 12 days and can be formed by neutron capture in barium. The properties of the radiations from Ba^{131} were first investigated by Yu, Gideon, and Kurbatov[8] using absorption and cloud-chamber techniques. These investigations showed that Ba^{131} emits no positrons but decays by orbital electron capture accompanied by gamma-rays and internal conversion electrons. The energy of the gamma-rays have been measured by absorption experiments in lead by

* Supported by the joint program of the ONR and AEC.
[1] Mitchell, Mei, Maienschein, and Peacock, Phys. Rev. **76**, 1450 (1949).
[2] Kern, Zaffarano, and Mitchell, Phys. Rev. **73**, 1142 (1948).
[3] C. S. Cook and L. M. Langer, Phys. Rev. **73**, 1149 (1948).
[4] A. C. G. Mitchell, Revs. Modern Phys. **22**, 36 (1950).
[5] M. Goeppert-Mayer, Phys. Rev. **78**, 16 (1950).
[6] Brosi, DeWitt, and Zeldes, Phys. Rev. **75**, 1615 (1949).
[6a] I. Bergstrom, Phys. Rev. **80**, 114 (1950).
[7] Bunker, Canada, and Mitchell, Phys. Rev. **79**, 610 (1950).
[8] Yu, Gideon, and Kurbatov, Phys. Rev. **71**, 382 (1947).

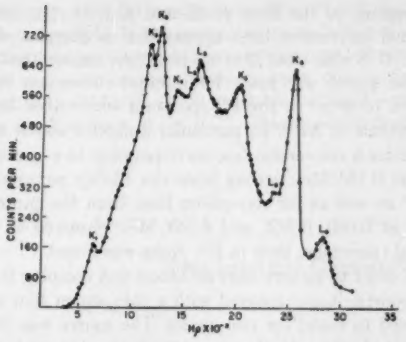

FIG. 2. Spectrum of secondary electrons ejected from lead by gamma-rays of Ba^{131}. (K_1—0.122 Mev); (K_2 and L_2—0.196 Mev); (K_3 and L_3—0.213 Mev); (K_4—0.241 Mev); (K_5 and L_5—0.371 Mev); (K_6 and L_6—0.497 Mev).

the above-mentioned authors and by Katcoff[9] who found gamma-rays at approximately 0.26, 0.5, and 1.2 Mev. In addition Katcoff measured the absorption of the electrons in aluminum and found two groups at energies of 0.42 and 0.24 Mev. Finally, Dale *et al.*[10] and Zimmerman *et al.*[11] have measured the spectrum of the gamma-rays and have found two lines—one at 0.496 and the other at 0.213 Mev.

Ba^{131} was prepared by neutron bombardment of barium in the Oak Ridge pile. The sample, in the form of $Ba(NO_3)_2$ was dissolved in water and Cs carrier added. The barium was then precipitated with $(NH_4)_2CO_3$ from a hot solution. The $BaCO_3$ was then dissolved in dilute HNO_3 and, after the addition of other alkaline earth carriers, was precipitated as the nitrate with fuming nitric acid.

The specific activity of the source was quite low. In order to get a sufficient counting rate, the source was packed into a large cylindrical capsule, made of copper, approximately 1 cm in diameter by 1 cm deep. A lead radiator of surface desity 20 mg/cm² covered the ends of the capsule. The spectrum of the photoelectrons ejected from the lead radiator was measured in the lens. The counting rate was quite low, so that long counts for each point had to be taken.

The results are shown in Fig. 2 in which the number of counts per minute is plotted against the magnetic rigidity in gauss-cm. The following photoelectric peaks are to be seen: a K peak for a gamma-ray of 0.122 Mev; K and L for 0.196 Mev; K and L for 0.213 Mev; K for 0.241 Mev; K and L for 0.371 Mev; and K and L for 0.497 Mev. It will be seen that the curve does not go to the background immediately beyond the line for the 0.497 gamma-ray. Presumably, a low intensity, high energy gamma-ray is also present. Cuffey[12] determined the energy of a high energy gamma-ray, by coincidence counting methods, and found a gamma-ray of 0.82 Mev.

In order to determine whether the peak of lowest energy is a K line for a gamma-ray of energy 0.12 Mev or an L line for some gamma-ray of lower energy, a beta-ray source was examined. Since the specific activity of the material was extremely low, the source had to be thick in order to obtain any counting rate above the background. An experiment, taking very long counts, showed two internal conversion lines corresponding to K and L lines from a gamma-ray at 0.120 Mev.

It is difficult to estimate the relative intensity of the various gamma-rays from the results shown in Fig. 2 on account of the low specific activity of the source. A rough estimate was made, using Gray's[13] empirical formula, and the results are shown in Table I. It is possible that the estimate of the intensity of the line at 0.122 Mev is too low since this line is internally converted. At the present time it is not possible to give a complete disintegration scheme for Ba^{131}. From energy considerations it appears likely that the lines of energy 0.122 and 0.371 Mev are in series, and both are in parallel with the line at 0.497 Mev.

While these experiments were in progress a similar investigation was carried out by Kondaiah[14] who found lines at 0.122, 0.206, 0.372, and 0.494 Mev. The present experiments confirm the lines at 0.122, 0.371, and 0.497 Mev, but, in addition, show a line at 0.241 Mev and indicate that the line reported by Kondaiah at 0.206 Mev is really two lines at 0.196 and 0.213 Mev.

IV. EXPERIMENTS ON Cs^{131}

Cs^{131}, the daughter of Ba^{131}, has a half-life of 10 days. This substance has been investigated by Yu, Gideon, and Kurbatov,[8] Katcoff,[9] and Yaffe *et al.*[15] Yu, Gideon, and Kurbatov, on the one hand, and Yaffe *et al.* on the other, find x-rays of xenon and in addition internal conversion electrons for a gamma-ray of energy 0.145 Mev. Katcoff finds only x-rays and Auger electrons.

Cs^{131} grows from Ba^{131} and can be prepared by separating cesium from the parent Ba^{131}. The chemical

TABLE I. Relative intensities of gamma-rays of Ba^{131}.

E_γ (Mev)	Relative intensity
0.497	1.00
0.371	0.12
0.241	0.014
0.213	0.053
0.196	0.044
0.122	0.013

[9] S. Katcoff, Phys. Rev. **72**, 1160 (1947).
[10] Dale, Richert, Redfield, and Kurbatov, Phys. Rev. **80**, 763 (1950).
[11] Zimmerman, Dale, Thomas, and Kurbatov, Phys. Rev. **80**, 908 (1950).
[12] W. H. Cuffey, Phys. Rev. **82**, 461 (1951).
[13] L. H. Gray, Proc. Cambridge Phil. Soc. **27**, 103 (1931).
[14] E. Kondaiah, Ark. Fysik **2**, 295 (1950).
[15] Yaffe, Kirsch, Standil, and Grunland, Phys. Rev. **75**, 699 (1949).

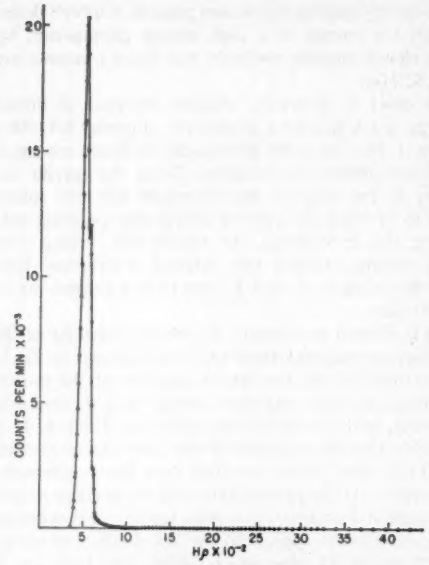

FIG. 3. Electron spectrum of Cs^{131} showing Auger electrons from xenon K_α x-rays.

procedure was carried out in the following way. The filtrates from the barium precipitation were united, additional alkaline earth carrier added, and the alkaline earths were reprecipitated by the addition of $(NH_4)_2CO_3$ and $(NH_4)_2C_2O_2$. The filtrate contained the active cesium and the cesium carrier which had been added, any alkali impurities, together with ammonium salts. The ammonium salts were destroyed with aqua regia and the solution evaporated nearly to dryness. The solution was then made 0.2*N* in HCl and placed in an ion exchange column. The column was eluted with 0.2*N* HCl and counts taken on aliquots of the effluent solution at frequent intervals. The curve, showing counting rate per cubic centimeter of the effluent against the time, exhibited three maxima. The first two maxima were quite small, probably arising from potassium and rubidium impurities, and the third one contained most of the activity. That part of the solution corresponding to the cesium peak was then evaporated to a small volume and used in the preparation of sources.

A very thin beta-ray source was mounted on a Zapon film and measured in the magnetic lens. The results are shown in Fig. 3, in which the number of counts per minute is plotted as a function of the magnetic rigidity in gauss-cm. From an inspection of Fig. 3 it will be seen that only Auger lines appear. Two of these lines are at 24.0 and 27.5 kev, respectively, with an indication of a third at 31 kev. The two strong Auger lines found correspond to the lines *K*-2*L* and *K*-*L*-*M*. No other internal conversion lines appear out to energies of 1 Mev. It is also clear that no positrons are emitted. A careful search was made for internal conversion lines known to occur in the I^{131} spectrum which arise from transitions in Xe^{131}. In particular a careful search was made for a conversion line corresponding to a gamma-ray at 0.163 Mev arising from the 12-day metastable Xe^{131} as well as for conversion lines from the gamma-rays at 0.080, 0.282, and 0.363 Mev observed as internal conversion lines in I^{131}. None was found.

In order to be sure that no xenon was escaping from the source, it was covered with a thin zapon film and allowed to stand for two weeks. The source was then examined again in the spectrometer and no internal conversion lines were found. It is, therefore, clear that Cs^{131} goes by orbital electron capture to the ground state of Xe^{131}.

In order to be sure that no high energy gamma-rays were present, the source was tested with a lead lined Geiger-Müller counter (insensitive to soft x-rays) and no counts above the background were obtained. It is probable that the gamma-ray of energy 0.145 Mev found by some investigators[9,15] is an impurity.

V. DISCUSSION

The behavior of the transition $Cs^{131} \rightarrow Xe^{131}$ is, at first sight, to some extent surprising. The levels of Xe^{131} are now quite well known from the study of I^{131}. Excited states of Xe^{131} are found at 80, 163, 363, and 717 kev. The fact that none of the low-lying states of Xe^{131} is excited when Cs^{131} decays by orbital electron capture has two possible explanations. In the first place the mass of Cs^{131} may not be sufficiently greater than that of Xe^{131} to allow transitions to any states higher than the ground state of Xe^{131}. This would fix the mass of Cs^{131} with respect to that of Xe^{131} to within 80 kev.

Another possible explanation may arise if one assumes that transitions to any of the low-lying states of Xe^{131} are forbidden by selection rules. While the energy levels of Xe^{131} are now quite well established and the internal conversion coefficients for the three low energy lines have been measured,[16] it turns out to be impossible to make self-consistent assignments of spin and parity to the three levels involved. The shell model predicts the configuration $d_{3/2}$ for the ground state of Xe^{131}, which agrees with the known spin of 3/2. The half-life and energy of the gamma-ray of the 12-day metastable state[6a] of Xe^{131} is in good agreement with the assumption that this transition is characterized as magnetic 2^4 pole radiation. The configuration of the state at 163 kev is probably $h_{11/2}$. The configuration of the state at 80 kev is not known from experiment. The shell model

[16] Kern, Mitchell, and Zaffarano, Phys. Rev. **76**, 94 (1949).

predicts $g_{7/2}$ for the configuration of Cs^{131} but $d_{3/2}$ may also be possible. If the configuration of Cs^{131} is $g_{7/2}$ and enough energy is available, one would expect the transition to $h_{11/2}$ to be more probable than that to $d_{3/2}$. If slightly less than 80 kev is available for the K capture process, the value of log $ft \sim 5$. This would indicate an allowed transition and would suggest $d_{3/2}$ as the configuration of the ground state of Cs^{131}.

The authors are indebted to Mr. A. Lessor for help in the chemical separations and to Messrs. A. Smith, C. M. Huddleston, and W. H. Cuffey for help with the measurements.

PHYSICAL REVIEW VOLUME 83, NUMBER 1 JULY 1, 1951

The Internal Conversion Coefficients. I: The K-Shell*

M. E. Rose, G. H. Goertzel,† and B. I. Spinrad,‡ *Oak Ridge National Laboratory, Oak Ridge, Tennessee*

and

J. Harr and P. Strong, *The Computation Laboratory of Harvard University, Cambridge, Massachusetts*

(Received February 26, 1951)

The internal conversion coefficients for electric and magnetic multipole radiation have been computed for the K-shell in the relativistic case with the unscreened coulomb field acting on the electron. The numerical results, which are obtained to four-significant-figure accuracy, were computed on the automatic sequence relay calculator (Mark I) and are given here for 12 values of Z in the range $10 \leqslant Z \leqslant 96$ and 6 gamma-ray energies (between 0.3 mc^2 and 5.0 mc^2) for the first five electric and first five magnetic multipoles.

I. INTRODUCTION

THE results of the calculation of the K-shell internal conversion coefficient (defined as the ratio of conversion electrons to quanta) which are presented herein were very briefly described in a previous communication.[1] Subsequent to May, 1949, tables of these coefficients together with an extensive interpolation were circulated privately. Inasmuch as plans for the calculation of the L-shell coefficients were instituted very soon after the completion of the K-shell work, publication of the present material was held up in the hope of presenting all of the numerical results together. This does not seem to be feasible, and this paper is written in the interest of making the K-shell results more readily available.

At the time of completion of this work the only existing accurate calculations of the K-shell internal conversion coefficients were those of Hulme[2] (for electric dipole, $Z=84$), of Taylor and Mott[3] (electric quadrupole, $Z=84$) and of Fisk and Taylor[4] (magnetic dipole, quadrupole, and octupole, $Z=84$). Shortly afterward, Griffith and Stanley[5] made calculations of the K-shell electric dipole coefficients for five values of Z in the range 69–89. Subsequently, the coefficients for electric dipole, quadrupole, and magnetic dipole for Cu, In, Po, and U at low energies were obtained by Reitz.[6] Here screening was taken into account by numerical integration of the Dirac radial equations with a Thomas-Fermi-Dirac potential. In the present work where $k \gtrsim 0.3$ (kmc^2 is the gamma-ray energy) no effect of screening is considered. Comparison with Reitz's results where our calculations overlap fully justifies this procedure. Calculations of the L_I-shell coefficients with unscreened wave functions have been carried out by Gellman *et al.*[7] for the same multipoles, and the same Z and k-values as appear in Reitz's work. However, these results are primarily of orientation value, since the neglect of screening cannot be justified in this case. In fact, in the calculation of the L-shell coefficients[8] (including all sub-shells) which are now under way, screening is taken into account in the same manner as was done by Reitz. In addition, low energy K-shell coefficients for all important multipoles and for essentially the same range of values of Z as in the K-shell work are being carried out with screened wave functions in parallel with the L-shell computation.

Until the L-shell and low energy K-shell results become available, it is necessary to supplement the present values of the coefficients with low energy extrapolations based on a comparison of these values and those obtained from the nonrelativistic formulas of Uhlenbeck and Hebb[9] and the essentially nonrelativistic

* This document is based on work performed for the AEC at the Oak Ridge National Laboratory.

† Now at New York University, Washington Square College, New York, New York.

‡ Now at Argonne National Laboratory, Chicago, Illinois.

[1] Rose, Goertzel, Spinrad, Harr, and Strong, Phys. Rev. **76**, 184A, 1883 (1949).

[2] H. R. Hulme, Proc. Roy. Soc. (London) **A138**, 643 (1932).

[3] H. M. Taylor and N. F. Mott, Proc. Roy. Soc. (London) **A138**, 665 (1932).

[4] J. B. Fisk and H. M. Taylor, Proc. Roy. Soc. (London) **A143**, 674 (194); **A146**, 178 (1934); H. M. Taylor, Proc. Cambridge, Phil. Soc. **32**, 291 (1936).

[5] B. A. Griffith and J. P. Stanley, Phys. Rev. **75**, 534, 1110 (1949).

[6] J. R. Reitz, Phys. Rev. **77**, 10 (1950).

[7] Gellman, Griffith, and Stanley, Phys. Rev. **80**, 866 (1950).

[8] M. E. Rose and G. Goertzel (to be published).

[9] M. H. Hebb and G. E. Uhlenbeck, Physica **5**, 605 (1938). See also S. M. Dancoff and P. Morrison, Phys. Rev. **55**, 122 (1939).

TABLE I. Internal conversion coefficients. The power of ten by which the entries should be multiplied is given by the number in parentheses.

Z	k	α_1	α_2	α_3	α_4	α_5	β_1	β_2	β_3	β_4	β_5
10	0.3	9.041 (−4)	8.549 (−3)	6.822 (−2)	5.173 (−1)	3.845 (0)	4.465 (−4)	3.321 (−3)	2.461 (−2)	1.829 (−1)	1.364 (0)
	0.5	1.804 (−4)	1.112 (−3)	5.866 (−3)	2.947 (−2)	1.451 (−1)	1.356 (−4)	6.709 (−4)	3.282 (−3)	1.606 (−2)	7.865 (−2)
	1.0	2.476 (−5)	8.837 (−5)	2.803 (−4)	8.544 (−4)	2.558 (−3)	2.993 (−5)	9.132 (−5)	2.728 (−4)	8.105 (−4)	2.404 (−3)
	1.8	6.361 (−6)	1.521 (−5)	3.360 (−5)	7.221 (−5)	1.531 (−4)	9.379 (−6)	2.051 (−5)	4.379 (−5)	9.259 (−5)	1.949 (−4)
	3.0	2.552 (−6)	4.646 (−6)	8.051 (−6)	1.368 (−5)	2.301 (−5)	3.791 (−6)	6.595 (−6)	1.124 (−5)	1.895 (−5)	3.175 (−5)
	5.0	1.224 (−6)	1.823 (−6)	2.645 (−6)	3.786 (−6)	5.377 (−6)	1.685 (−6)	2.462 (−6)	3.545 (−6)	5.057 (−6)	7.169 (−6)
20	0.3	5.617 (−3)	4.892 (−2)	3.576 (−1)	2.486 (0)	1.700 (1)	4.313 (−3)	3.159 (−2)	2.265 (−1)	1.629 (0)	1.176 (1)
	0.5	1.183 (−3)	6.850 (−3)	3.392 (−2)	1.599 (−1)	7.395 (−1)	1.245 (−3)	6.139 (−3)	2.940 (−2)	1.406 (−1)	6.737 (−1)
	1.0	1.721 (−4)	5.941 (−4)	1.817 (−3)	5.340 (−3)	1.541 (−2)	2.584 (−4)	8.028 (−4)	2.385 (−3)	7.006 (−3)	2.052 (−2)
	1.8	4.522 (−5)	1.084 (−4)	2.371 (−4)	5.020 (−4)	1.047 (−3)	7.685 (−5)	1.743 (−4)	3.755 (−4)	7.935 (−4)	1.662 (−3)
	3.0	1.808 (−5)	3.391 (−5)	5.944 (−5)	1.013 (−4)	1.701 (−4)	2.965 (−5)	5.409 (−5)	9.415 (−5)	1.602 (−4)	2.692 (−4)
	5.0	8.542 (−6)	1.327 (−5)	1.973 (−5)	2.870 (−5)	4.116 (−5)	1.261 (−5)	1.937 (−5)	2.870 (−5)	4.166 (−5)	5.970 (−5)
30	0.3	1.518 (−2)	1.194 (−1)	7.852 (−1)	4.919 (0)	3.042 (1)	1.857 (−2)	1.341 (−1)	9.187 (−1)	6.292 (0)	4.322 (1)
	0.5	3.362 (−3)	1.804 (−2)	8.285 (−2)	3.627 (−1)	1.562 (0)	5.101 (−3)	2.503 (−2)	1.165 (−1)	5.400 (−1)	2.508 (0)
	1.0	5.175 (−4)	1.717 (−3)	5.044 (−3)	1.424 (−2)	3.955 (−2)	9.937 (−4)	3.132 (−3)	9.204 (−3)	2.661 (−2)	7.663 (−2)
	1.8	1.393 (−4)	3.343 (−4)	7.233 (−4)	1.510 (−3)	3.100 (−3)	2.796 (−4)	6.563 (−4)	1.420 (−3)	2.986 (−3)	6.206 (−3)
	3.0	5.552 (−5)	1.075 (−4)	1.907 (−4)	3.263 (−4)	5.476 (−4)	1.024 (−4)	1.964 (−4)	3.477 (−4)	5.949 (−4)	9.999 (−4)
	5.0	2.583 (−5)	4.198 (−5)	6.417 (−5)	9.488 (−5)	1.375 (−4)	4.134 (−5)	6.730 (−5)	1.025 (−4)	1.511 (−4)	2.183 (−4)
40	0.3	2.949 (−2)	2.042 (−1)	1.180 (0)	6.518 (0)	3.569 (1)	5.865 (−2)	4.131 (−1)	2.645 (0)	1.681 (1)	1.070 (2)
	0.5	6.850 (−3)	3.352 (−2)	1.410 (−1)	5.672 (−1)	2.255 (0)	1.544 (−2)	7.465 (−2)	3.329 (−1)	1.474 (0)	6.536 (0)
	1.0	1.116 (−3)	3.538 (−3)	9.954 (−3)	2.698 (−2)	7.211 (−2)	2.834 (−3)	8.975 (−3)	2.585 (−2)	7.302 (−2)	2.052 (−1)
	1.8	3.083 (−4)	7.407 (−4)	1.589 (−3)	3.275 (−3)	6.632 (−3)	7.540 (−4)	1.818 (−3)	3.920 (−3)	8.161 (−3)	1.675 (−2)
	3.0	1.227 (−4)	2.457 (−4)	4.426 (−4)	7.613 (−4)	1.278 (−3)	2.614 (−4)	5.253 (−4)	9.405 (−4)	1.610 (−3)	2.696 (−3)
	5.0	5.621 (−5)	9.603 (−5)	1.513 (−4)	2.277 (−4)	3.332 (−4)	9.938 (−5)	1.723 (−4)	2.689 (−4)	4.009 (−4)	5.820 (−4)
54	0.3	5.640 (−2)	3.082 (−1)	1.414 (0)	6.252 (0)	2.776 (1)	2.317 (−1)	1.520 (0)	8.376 (0)	4.518 (1)	2.429 (2)
	0.5	1.401 (−2)	5.830 (−2)	2.123 (−1)	7.487 (−1)	2.643 (0)	5.831 (−2)	2.672 (−1)	1.086 (0)	4.360 (0)	1.751 (1)
	1.0	2.479 (−3)	7.323 (−3)	1.943 (−2)	5.001 (−2)	1.277 (−1)	9.973 (−3)	3.685 (−2)	8.461 (−2)	2.270 (−1)	6.059 (−1)
	1.8	7.136 (−4)	1.725 (−3)	3.682 (−3)	7.508 (−3)	1.500 (−2)	2.467 (−3)	6.013 (−3)	1.269 (−2)	2.570 (−2)	5.123 (−2)
	3.0	2.848 (−4)	6.026 (−4)	1.115 (−3)	1.938 (−3)	3.259 (−3)	7.906 (−4)	1.666 (−3)	2.984 (−3)	5.057 (−3)	8.345 (−3)
	5.0	1.277 (−4)	2.366 (−4)	3.910 (−4)	6.040 (−4)	8.964 (−4)	2.732 (−4)	5.160 (−4)	8.245 (−4)	1.237 (−3)	1.793 (−3)
64	0.3	7.931 (−2)	3.456 (−1)	1.283 (0)	4.663 (0)	1.735 (1)	5.753 (−1)	3.441 (0)	1.613 (1)	7.280 (1)	3.257 (2)
	0.5	2.072 (−2)	7.485 (−2)	2.435 (−1)	7.808 (−1)	2.547 (0)	1.417 (−1)	6.019 (−1)	2.215 (0)	8.036 (0)	2.914 (1)
	1.0	3.910 (−3)	1.099 (−2)	2.824 (−2)	7.075 (−2)	1.766 (−1)	2.332 (−2)	6.848 (−2)	1.777 (−1)	4.519 (−1)	1.145 (0)
	1.8	1.165 (−3)	2.856 (−3)	6.133 (−3)	1.248 (−2)	2.475 (−2)	5.520 (−3)	1.311 (−2)	2.680 (−2)	5.259 (−2)	1.017 (−1)
	3.0	4.676 (−4)	1.041 (−3)	1.974 (−3)	3.464 (−3)	5.834 (−3)	1.679 (−3)	3.553 (−3)	6.271 (−3)	1.044 (−2)	1.693 (−2)
	5.0	2.069 (−4)	4.113 (−4)	7.067 (−4)	1.112 (−3)	1.666 (−3)	5.401 (−4)	1.064 (−3)	1.706 (−3)	2.547 (−3)	3.664 (−3)
72	0.3	9.882 (−2)	3.425 (−1)	1.037 (0)	3.143 (0)	9.969 (0)	1.186 (0)	6.344 (0)	2.488 (1)	9.204 (1)	3.349 (2)
	0.5	2.699 (−2)	8.579 (−2)	2.555 (−1)	7.651 (−1)	2.361 (0)	2.892 (−1)	1.116 (0)	3.697 (0)	1.206 (1)	3.930 (1)
	1.0	5.384 (−3)	1.468 (−2)	3.718 (−2)	9.186 (−2)	2.258 (−1)	4.650 (−2)	1.268 (−1)	3.098 (−1)	7.451 (−1)	1.789 (0)
	1.8	1.656 (−3)	4.161 (−3)	9.044 (−3)	1.841 (−2)	3.628 (−2)	1.070 (−2)	2.411 (−2)	4.739 (−2)	8.991 (−2)	1.683 (−1)
	3.0	6.703 (−4)	1.572 (−3)	3.054 (−3)	5.400 (−3)	9.087 (−3)	3.138 (−3)	6.456 (−3)	1.113 (−2)	1.814 (−2)	2.880 (−2)
	5.0	2.941 (−4)	6.255 (−4)	1.112 (−3)	1.776 (−3)	2.673 (−3)	9.565 (−4)	1.895 (−3)	3.010 (−3)	4.444 (−3)	6.320 (−3)
78	0.3	1.136 (−1)	3.196 (−1)	8.102 (−1)	2.095 (0)	5.732 (0)	2.075 (0)	9.877 (0)	3.254 (1)	9.856 (1)	2.906 (2)
	0.5	3.215 (−2)	9.242 (−2)	2.594 (−1)	7.417 (−1)	2.190 (0)	5.030 (−1)	1.756 (0)	5.272 (0)	1.557 (1)	4.596 (1)
	1.0	6.712 (−3)	1.810 (−2)	4.575 (−2)	1.121 (−1)	2.716 (−1)	7.989 (−2)	2.005 (−1)	4.630 (−1)	1.058 (0)	2.421 (0)
	1.8	2.120 (−3)	5.499 (−3)	1.211 (−2)	2.463 (−2)	4.819 (−2)	1.808 (−2)	3.812 (−2)	7.212 (−2)	1.325 (−1)	2.409 (−1)
	3.0	8.659 (−4)	2.135 (−3)	4.233 (−3)	7.516 (−3)	1.261 (−2)	5.190 (−3)	1.016 (−2)	1.706 (−2)	2.721 (−2)	4.238 (−2)
	5.0	3.783 (−4)	8.549 (−4)	1.562 (−3)	2.518 (−3)	3.795 (−3)	1.528 (−3)	2.952 (−3)	4.616 (−3)	6.724 (−3)	9.447 (−3)
83	0.5	3.669 (−2)	9.721 (−2)	2.615 (−1)	7.184 (−1)	2.022 (0)	8.171 (−1)	2.556 (0)	6.957 (0)	1.862 (1)	4.979 (1)
	1.0	7.980 (−3)	2.163 (−2)	5.485 (−2)	1.332 (−1)	3.171 (−1)	1.289 (−1)	2.946 (−1)	6.430 (−1)	1.399 (0)	3.054 (0)
	1.8	2.584 (−3)	6.970 (−3)	1.554 (−2)	3.153 (−2)	6.109 (−2)	2.888 (−2)	5.617 (−2)	1.022 (−1)	1.820 (−1)	3.217 (−1)
	3.0	1.065 (−3)	2.768 (−3)	5.584 (−3)	9.931 (−3)	1.659 (−2)	8.179 (−3)	1.497 (−2)	2.441 (−2)	3.809 (−2)	5.821 (−2)
	5.0	4.646 (−4)	1.115 (−3)	2.083 (−3)	3.379 (−3)	5.093 (−3)	2.354 (−3)	4.328 (−3)	6.630 (−3)	9.514 (−3)	1.320 (−2)
88	0.5	4.138 (−2)	1.020 (−1)	2.643 (−1)	6.900 (−1)	1.813 (0)	1.373 (0)	3.726 (0)	9.029 (0)	2.149 (1)	5.111 (1)
	1.0	9.409 (−3)	2.613 (−2)	6.661 (−2)	1.594 (−1)	3.698 (−1)	2.156 (−1)	4.356 (−1)	8.900 (−1)	1.829 (0)	3.784 (0)
	1.8	3.132 (−3)	8.929 (−3)	2.016 (−2)	4.063 (−2)	7.762 (−2)	4.804 (−2)	8.362 (−2)	1.452 (−1)	2.493 (−1)	4.265 (−1)
	3.0	1.306 (−3)	3.625 (−3)	7.432 (−3)	1.321 (−2)	2.189 (−2)	1.349 (−2)	2.234 (−2)	3.512 (−2)	5.340 (−2)	7.982 (−2)
	5.0	5.697 (−4)	1.468 (−3)	2.805 (−3)	4.568 (−3)	6.868 (−3)	3.824 (−3)	6.454 (−3)	9.613 (−3)	1.353 (−2)	1.848 (−2)
92	0.5	4.516 (−2)	1.066 (−1)	2.675 (−1)	6.590 (−1)	1.601 (0)	2.152 (0)	5.057 (0)	1.098 (1)	2.339 (1)	4.976 (1)
	1.0	1.068 (−2)	3.083 (−2)	7.878 (−2)	1.850 (−1)	4.172 (−1)	3.379 (−1)	6.003 (−1)	1.153 (0)	2.250 (0)	4.435 (0)
	1.8	3.640 (−3)	1.102 (−2)	2.507 (−2)	5.008 (−2)	9.423 (−2)	7.514 (−2)	1.162 (−1)	1.929 (−1)	3.204 (−1)	5.323 (−1)
	3.0	1.535 (−3)	4.551 (−3)	9.435 (−3)	1.670 (−2)	2.745 (−2)	2.104 (−2)	3.119 (−2)	4.731 (−2)	7.020 (−2)	1.028 (−1)
	5.0	6.709 (−4)	1.851 (−3)	3.595 (−3)	5.860 (−3)	8.775 (−3)	5.932 (−3)	9.028 (−3)	1.306 (−2)	1.805 (−2)	2.429 (−2)
96	0.5	4.890 (−2)	1.129 (−1)	2.713 (−1)	6.142 (−1)	1.341 (0)	3.529 (0)	6.901 (0)	1.319 (1)	2.466 (1)	4.596 (1)
	1.0	1.206 (−2)	3.706 (−2)	9.438 (−2)	2.156 (−1)	4.684 (−1)	5.547 (−1)	8.356 (−1)	1.496 (0)	2.752 (0)	5.137 (0)
	1.8	4.222 (−3)	1.383 (−2)	3.156 (−2)	6.216 (−2)	1.147 (−1)	1.235 (−1)	1.635 (−1)	2.578 (−1)	4.123 (−1)	6.629 (−1)
	3.0	1.804 (−3)	5.799 (−3)	1.212 (−2)	2.130 (−2)	3.461 (−2)	3.461 (−2)	4.421 (−2)	6.428 (−2)	9.274 (−2)	1.327 (−1)
	5.0	7.913 (−4)	2.370 (−3)	4.664 (−3)	7.589 (−3)	1.130 (−2)	9.769 (−3)	1.286 (−2)	1.796 (−2)	2.427 (−2)	3.211 (−2)

results of Drell.[10] A convenient set of graphs for this purpose has been prepared by Axel and Goodrich.[11] As has been emphasized elsewhere, the direct use of these nonrelativistic formulas leads to considerable error for all but rather small Z and k. The same remark applies to the Born approximation results of Dancoff and Morrison,[9] which applies with sufficient accuracy only for very small Z and large k, or more specifically, for $e^2Z/\hbar v \ll 1$, where v is the velocity of the conversion electron in the continuum. From the results of the Toronto group[7] it also appears that the ratio of K to L conversion coefficients as calculated by Hebb and Nelson[12] (electric) and by Tralli and Lowen[13] (mag-

[10] S. D. Drell, Phys. Rev. **75**, 132 (1949).
[11] P. Axel and R. F. Goodrich, ONR report (unpublished).
[12] M. H. Hebb and E. Nelson, Phys. Rev. **58**, 486 (1940).
[13] N. Tralli and I. S. Lowen, Phys. Rev. **76**, 1541 (1949).

netic) is subject to surprisingly large errors because of the approximations made.

II. RESULTS AND DISCUSSION

The parameters chosen for the machine computation, which was performed on the automatic sequence relay calculator (Mark I) at the Computation Laboratory of Harvard University, were: 12 values of Z in the range $10 \leqslant Z \leqslant 96$ and 6 values of k in the range $0.3 \leqslant k \leqslant 5.0$ For $Z \geqslant 83$ it was necessary to drop the value $k=0.3$, and five values in the range $0.5 \leqslant k \leqslant 5.0$ were used. In each case the first five electric and first five magnetic multipoles were computed. The calculations were originally carried out for $Z \geqslant 40$, based on the expectation that the approximative results would be sufficiently accurate for $Z<40$. In this range the values of Z chosen were such as to obtain an approximately uniform scale in Z^3 since one expected, very roughly, a Z^3 dependence of the conversion coefficient. The extension of the computations to $Z<40$ was made at a later stage when the original expectations proved to be too optimistic.

The restriction to $k \geqslant 0.3$ was made for the following reasons. The computations involve the evaluation of a large number of series (hypergeometric functions) which become slowly convergent in this region ($k \approx 0.3$). More rapid convergence could be obtained by transforming to functions of the reciprocal argument on the other side of the radius of convergence. However, in this region of the $k-Z$ plane the effect of screening is important, and it did not appear worth while to invest the necessary effort in such unscreened calculations in view of the plans for making screened calculations. The hypergeometric series which occur [see Appendix, Eq. (28)] were evaluated term by term up to the point where the first term neglected had an absolute value less than 10^{-6}, the first term being equal to unity, of course. The gamma-functions of real and complex argument (see Appendix) were obtained by a Taylor series representation of Sterling's formula wherein the first term neglected made a relative error of less than 10^{-6}. The 680 values of the internal conversion coefficients obtained in this way are accurate to at least four significant figures. While this accuracy is far better than present experimental needs require, it is necessary for the purpose of interpolation to values of the conversion coefficient at $Z-k$ values other than those which appear in the machine calculations. Interpolations were carried out to obtain coefficients for 26 values of Z and 16 values of k representing a total of 4020 values of the conversion coefficients. For this purpose it is convenient to interpolate the ratio of the values given below in the tables to the Dancoff-Morrison Born approximation formulas,[9] since this ratio is much less sensitive with Z and k than are the computed coefficients themselves. The interpolated results checked with other calculations where overlap occurred.[2,3,5]

The analytical basis of the calculation is given in the Appendix. For reasons of space limitation only the machine computed coefficients are given in Table I below. In this table α_l and β_l are the conversion coefficients for electric and magnetic 2^l-pole radiation, respectively. More extensive tables including the interpolated values appear separately.[14] A limited number of interpolated values can be obtained from the curves given in Figs. 1–10, which represents only a part of the numerical results. Although it is not to be expected that many cases will arise which involve multipole orders with $l>5$, reasonably accurate values for $l=6$ can be obtained as follows. While α_l and β_l are sensitively dependent on l, the ratios α_{l+1}/α_l and β_{l+1}/β_l are fairly insensitive. Consequently, a one-step extrapolation gives α_6 and β_6 with an error of about 5 percent. Figure 11 illustrates this extrapolation for electric multipoles.

A considerable amount of experimental data on internal conversion coefficients now exists, and the numerical results given here have been used by many investigators to make assignments of angular momentum and parity to nuclear levels. It would seem certain that the theoretical basis of these calculations is sound, but it is worth while to note that in many cases the assignments made are in agreement with other nuclear spectroscopic data. For example, the assignments based on internal conversion measurements[15] in the decay of Co^{60} and Cs^{134} are in agreement with the results of angular correlation measurements.[16] However, in some instances discrepancies exist. Notable cases are those in which assignments are based on the rough theoretical estimates of radiation lifetime. A compilation of the internal conversion data as well as experimental results obtained by other methods of nuclear spectroscopy is now being made. It seems too early to draw any conclusions from such comparisons, in view of the uncertainty of many of the proposed decay schemes and the possibility of more accurate measurements of internal conversion coefficients. One conclusion which seems to be valid concerns the apparent scarcity of electric cipole lines. Out of a total of 89 cases where assignments can be made, 84 are fairly definitely not electric dipole and in the remaining cases the assignment as electric dipole is not certain by any means.

The authors take pleasure in expressing their appreciation to Professor H. H. Aiken of the Harvard Computation Laboratory and to Dr. A. M. Weinberg of the Oak Ridge National Laboratory through whose efforts the Mark I calculator was made available to us. The assistance of all members of the Oak Ridge Mathematics Panel, led by Dr. A. S. Householder, as well as

[14] M. E. Rose and G. H. Goertzel, AEC report (to be published).
[15] Waggoner, Moon, and Roberts, Phys. Rev. 80, 420 (1950).
[16] E. L. Brady and M. Deutsch, Phys. Rev. 74, 1541 (1948); 78, 558 (1950). F. Metzger and M. Deutsch, Phys. Rev. 78, 551 (1950).

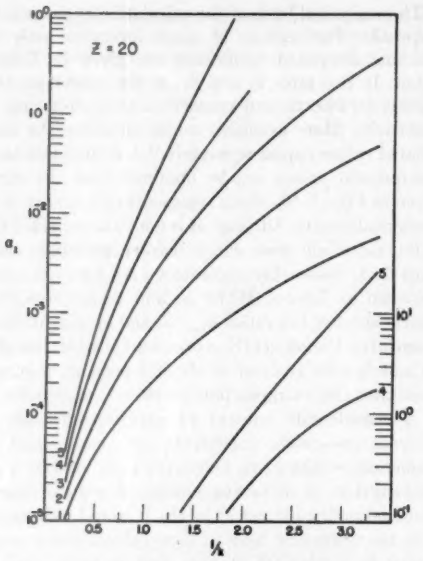

FIG. 1. The electric multipole conversion coefficients (K-shell) for $Z=20$ as a function of $1/k=(\text{gamma-energy}/mc^2)^{-1}$. The numbers attached to the curves give the value of l. The ordinate scale at the right refers to the low energy portion of the curves for 2^4 and 2^5 poles.

that rendered by Drs. N. Tralli, S. D. Drell, and G. B. Arfken was invaluable.

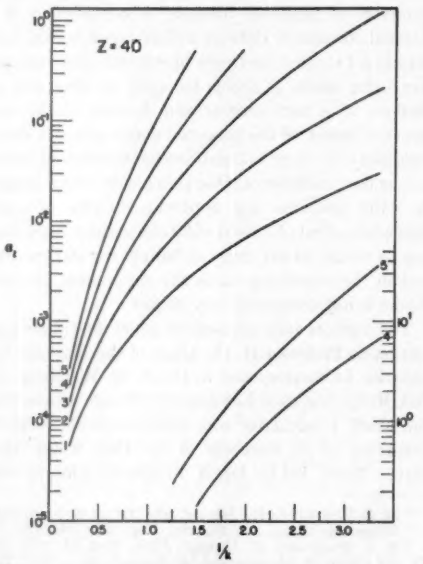

FIG. 2. Same as Fig. 1 for $Z=40$.

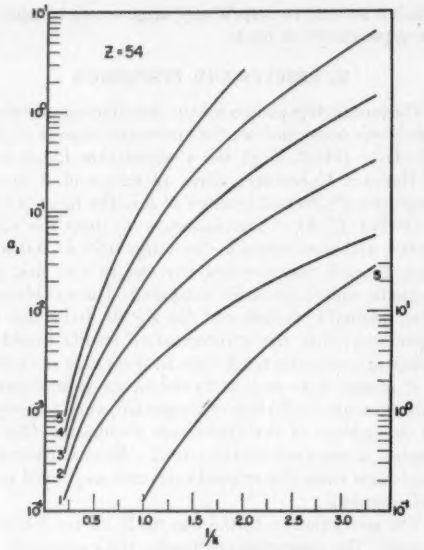

FIG. 3. Same as Fig. 1 for $Z=54$.

APPENDIX

The number of conversion electrons per unit time is found by the usual perturbation procedure to be

$$N_e=2\pi\alpha n\sum|(\psi_f|\phi+\boldsymbol{\alpha}\cdot\mathbf{A}|\psi_i)|^2, \qquad (1)$$

where ψ_f, the final state wave function, is normalized

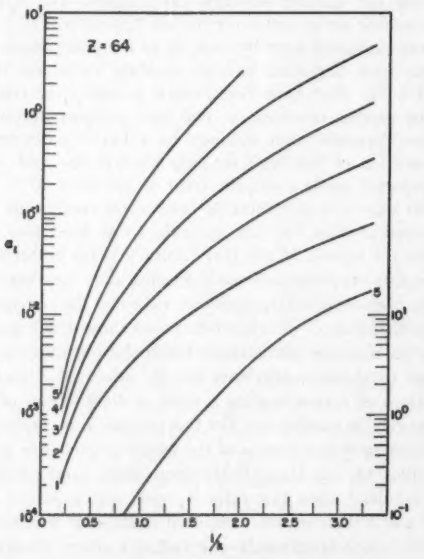

FIG. 4. Same as Fig. 1 for $Z=64$.

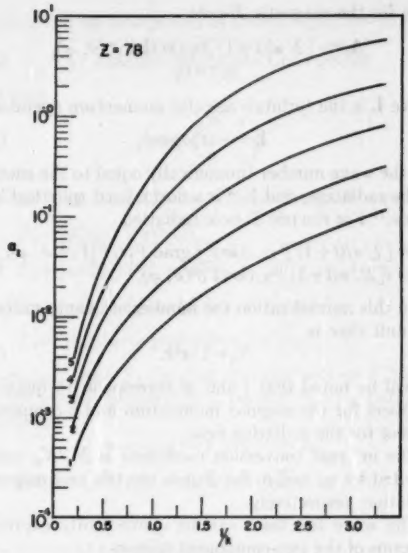

FIG. 5. Same as Fig. 1 for $Z=78$.

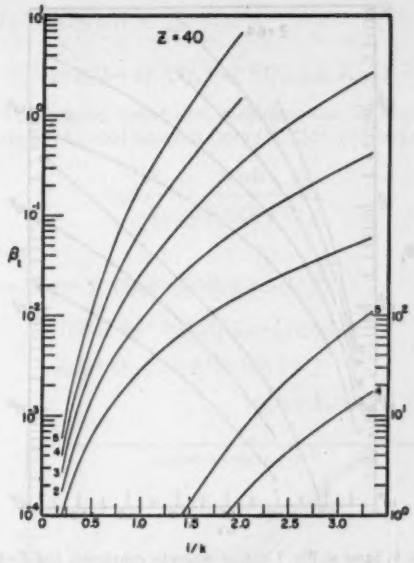

FIG. 7. Same as Fig. 1 but for magnetic conversion and $Z=4$

to unit energy range[17] and ψ_i, the initial state wave function, is normalized to unity in all configuration space. A sum over all final states, including magnetic substates, and an average over initial magnetic substates is implied by the sum sign. In (1) α is the Dirac matrix vector, α the fine structure constant, n is the number of electrons in the initial state, while ϕ and $\mathbf{A}$ are the scalar and vector potentials of the radiation field (see (3) below).

It is most convenient to use the following representa-

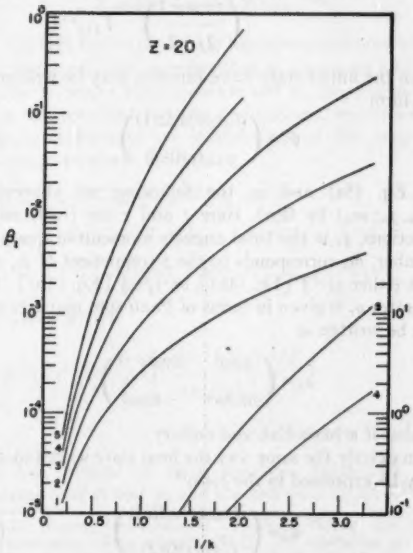

FIG. 6. Same as Fig. 1 but for magnetic multipole conversion.

[17] M. E. Rose, Phys. Rev. **51**, 484 (1937).

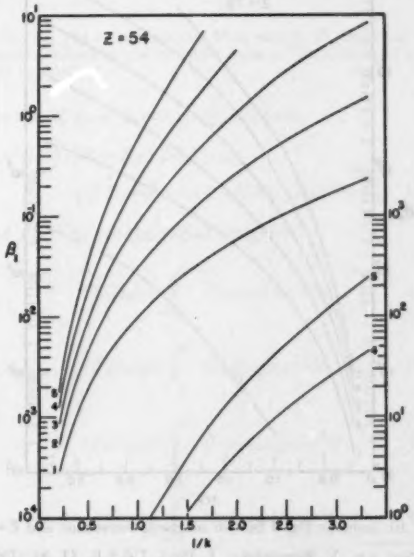

FIG. 8. Same as Fig. 1 but for magnetic conversion and $Z=54$.

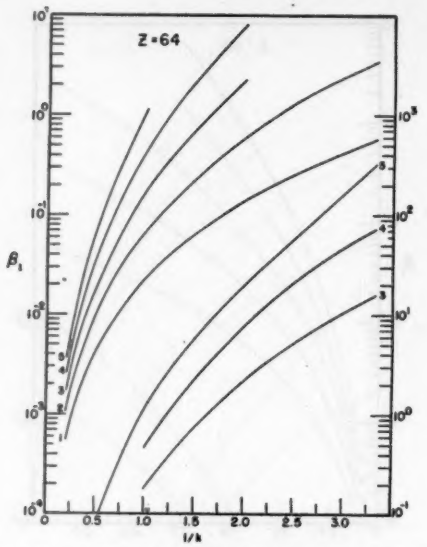

FIG. 9. Same as Fig. 1 but for magnetic conversion and $Z=64$.

tion of the multipole fields.[18] Designating the spherical hankel function by

$$\chi_l(x)=(\pi/2x)^{\frac{1}{2}}H_{l+\frac{1}{2}}^{(1)}(x), \tag{2}$$

where $H^{(1)}$ is the hankel function of the first kind, we have for the magnetic 2^l-pole

$$\mathbf{A}_l^m=[2/\pi l(l+1)]^{\frac{1}{2}}\chi_l(kr)\mathbf{L}Y_l^m(\vartheta,\varphi), \quad \phi_l^m=0, \tag{3a}$$

where $\mathbf{L}$ is the (orbital) angular momentum operator

$$\mathbf{L}=-i\mathbf{r}\times\text{grad}, \tag{3b}$$

k is the wave number (numerically equal to the energy) of the radiation, and Y_l^m is a normalized spherical harmonic.[17] For electric 2^l-pole radiation

$$\mathbf{A}_l^m=[2/\pi l(l+1)]^{\frac{1}{2}}\chi_{l-1}(kr)[r\ \text{grad}+l\mathbf{r}/r]Y_l^m(\vartheta,\varphi), \quad \phi_l^m=i[2l/\pi(l+1)]^{\frac{1}{2}}\chi_l(kr)Y_l^m(\vartheta,\varphi). \tag{3c}$$

With this normalization the number of quanta radiated per unit time is

$$N_q=1/\pi^2k. \tag{3d}$$

It will be noted that l and m correspond to quantum numbers for the angular momentum and z-component thereof for the radiation field.

The internal conversion coefficient is N_e/N_q, and is denoted by α_l and β_l for 2^l-pole electric and magnetic radiation, respectively.

The wave functions can be conveniently expressed in terms of the two-component spinors

$$\Omega(j-\tfrac{1}{2},j;\mu)=\begin{pmatrix}(j+\mu/2j)^{\frac{1}{2}} & Y_{j-\frac{1}{2}}^{\mu-\frac{1}{2}}\\ -(j-\mu/2j)^{\frac{1}{2}} & Y_{j-\frac{1}{2}}^{\mu+\frac{1}{2}}\end{pmatrix} \tag{4a}$$

and

$$\Omega(j+\tfrac{1}{2},j;\mu)=\begin{bmatrix}\left(\dfrac{j-\mu+1}{2j+2}\right)^{\frac{1}{2}} & Y_{j+\frac{1}{2}}^{\mu-\frac{1}{2}}\\ \left(\dfrac{j+\mu+1}{2j+2}\right)^{\frac{1}{2}} & Y_{j+\frac{1}{2}}^{\mu+\frac{1}{2}}\end{bmatrix}. \tag{4b}$$

Then the initial state wave function may be written in the form

$$\psi_j=\begin{pmatrix}if_{l_1j_1}(r)\sigma_r\Omega(1)\\ g_{l_1j_1}(r)\Omega(1)\end{pmatrix}. \tag{5a}$$

In Eq. (5a) and in the following we abbreviate $\Omega(l_n,j_n;m_n)$ by $\Omega(n)$. Here f and g are (real) radial functions, j_1 is the total angular momentum quantum number, m_1 corresponds to the z-component of j_1, and l_1 is either $j_1-\frac{1}{2}$ [Eq. (4a)], or $j_1+\frac{1}{2}$ [Eq. (4b)]. The operator σ_r is given in terms of Pauli spin matrices and can be written as

$$\sigma_r=\begin{pmatrix}\cos\vartheta & \sin\vartheta e^{-i\varphi}\\ \sin\vartheta e^{i\varphi} & -\cos\vartheta\end{pmatrix}, \tag{6}$$

so that it is hermitian and unitary.

In exactly the same way the final state wave function may be expressed in the form[19]

$$\psi_f=\begin{pmatrix}iF_{l_2j_2}(r)\sigma_r\Omega(2)\\ G_{l_2j_2}(r)\Omega(2)\end{pmatrix} \tag{5b}$$

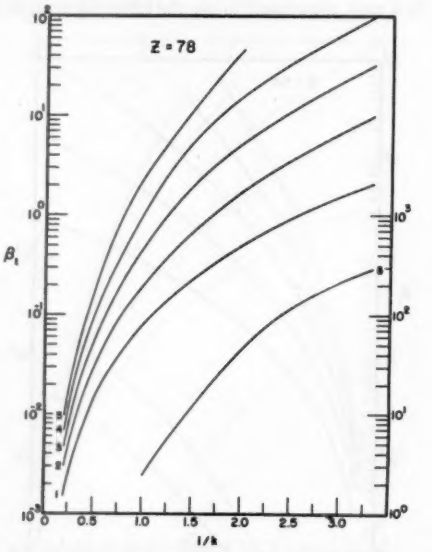

FIG. 10. Same as Fig. 1 but for magnetic conversion and $Z=78$.

[18] See, e.g., V. Berestetzky, J. Phys. U.S.S.R. **11**, 85 (1947); also W. Heitler, Proc. Cambridge Phil. Soc. **32**, 112 (1936).

[19] The (real) radial functions F and G are denoted by f and g, respectively, in reference 17.

with j_s and m_2 interpreted as above; again $l_2 = j_2 \pm \frac{1}{2}$.

(a) Electric Multipole Conversion

Using

$$\alpha = \begin{pmatrix} 0 & \sigma \\ \sigma & 0 \end{pmatrix}$$

we find that the following angular integrals appear:

$$T_1 = (\Omega(2) | Y_l^m | \Omega(1)), \tag{7a}$$

$$T_2 = (\sigma_r \Omega(2) | Y_l^m | \sigma_r \Omega(1)), \tag{7b}$$

$$T_3 = (\sigma_r \Omega(2) | (r \operatorname{grad} + l\mathfrak{r}/r) Y_l^m | \cdot \sigma \Omega(1)), \tag{7c}$$

$$T_4 = (\Omega(2) | \boldsymbol{\sigma} \cdot (r \operatorname{grad} + l\mathfrak{r}/r) Y_l^m | \sigma_r \Omega(1)), \tag{7d}$$

where in T_3 and T_4 the grad operator acts on Y_l^m only. By the unitary property of σ_r we find $T_2 = T_1$. Using the relations

$$r\sigma_r \boldsymbol{\sigma} \cdot \operatorname{grad} = \mathbf{r} \cdot \operatorname{grad} - \boldsymbol{\sigma} \cdot \mathbf{L},$$

$$\boldsymbol{\sigma} \cdot \mathbf{L} \Omega(i) = [j_i(j_i+1) - l_i(l_i+1) - \tfrac{3}{4}] \Omega(i), \quad i = 1, 2 \tag{8}$$

we find

$$T_3 = T_1[l + j_1(j_1+1) - l_1(l_1+1) - j_2(j_2+1) + l_2(l_2+1)], \tag{9a}$$

$$T_4 = T_1[l + j_2(j_2+1) - l_2(l_2+1) - j_1(j_1+1) + l_1(l_1+1)]. \tag{9b}$$

The evaluation of T_1 can be carried out in a straightforward manner. We have

$$T_1 = Q(l; l_2 j_2; l_1 j_1) S_{j_2 m m_1}^{(l j_1)}. \tag{10}$$

In Eq. (10) the $S_{l_2 m m_1}^{(l l_1)}$ are transformation coefficients for vector addition corresponding to the vector addition of l and l_1 with z components m and m_1, respectively, to give the resultant l_2 with z component $m_2 = m + m_1$.[20] The Q coefficients are independent of the magnetic quantum numbers. In fact,

$$Q(l; l_2 j_2; l_1 j_1) = [S_{j_2, 0, \frac{1}{2}}^{(l_2 \frac{1}{2})} S_{j_1, 0, \frac{1}{2}}^{(l_1 \frac{1}{2})} \times (Y_{l_2}^0 | Y_l^0 | Y_{l_1}^0) S_{j_1, 1, -\frac{1}{2}}^{(l_1 \frac{1}{2})} S_{j_2, 1, -\frac{1}{2}}^{(l_2 \frac{1}{2})} \times (Y_{l_2}^1 | Y_l^0 | Y_{l_1}^1)] \{S_{j_2, 0, \frac{1}{2}}^{(l j_1)}\}^{-1}. \tag{11}$$

We make use of

$$(Y_{l_2}^{m_2} | Y_l^m | Y_{l_1}^{m_1}) = \left[\frac{(2l+1)(2l_1+1)}{4\pi(2l_2+1)}\right]^{\frac{1}{2}} \times S_{l_2, 0, 0}^{(l l_1)} S_{l_2, m, m_1}^{(l l_1)} \tag{11a}$$

for the integral of three spherical harmonics. The average over m and m_1 and the sum over m_2 gives[20]

$$(2l+1)^{-1}(2j_1+1)^{-1} \sum_{m m_1 m_2} |T_1|^2 = (2j_2+1)(2l+1)^{-1}(2j_1+1)^{-1}[Q(l; l_2 j_2; l_1 j_1)]^2. \tag{12}$$

The internal conversion coefficient can be obtained in terms of radial integrals from (1), (3d), (9), and (12):

$$\alpha_l = \frac{N_e}{N_\gamma} = \frac{2\pi a k l}{(l+1)(2l+1)} U_l, \tag{13}$$

where

$$U_l = (2\pi/l^3) \sum_{l_2 j_2} (2j_2+1)[Q(l; l_2 j_2; l_1 j_1)]^2 \times |l(R_1 + R_2 - R_3 + R_4)_{l_2 j_2} + [j_2(j_2+1) - l_2(l_2+1) - j_1(j_1+1) + l_1(l_1+1)] \times (R_3 + R_4)_{l_2 j_2}|^2. \tag{13a}$$

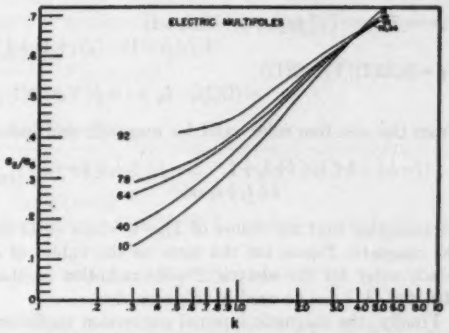

FIG. 11. The ratio of electric 2^s to electric 2^s conversion coefficients obtained by extrapolating α_l/α_{l+1}. The attached numbers refer to Z values.

For the K shell ($l_1 = 0$, $j = \frac{1}{2}$) we have

$$U_l = (l+1) | R_1 + R_2 + 2R_4 |_{l, l+\frac{1}{2}}^2 + l | R_1 + R_2 - (2 + 1/l) R_3 - R_4/l |_{l, l-\frac{1}{2}}^2, \tag{13b}$$

and $R_1 \cdots R_4$ are the radial integrals

$$(R_1)_{l_2 j_2} = \int_0^\infty F_{l_2 j_2} \chi_l f_{l_1 j_1} r^2 dr, \tag{13c}$$

$$(R_2)_{l_2 j_2} = \int_0^\infty G_{l_2 j_2} \chi_l g_{l_1 j_1} r^2 dr, \tag{13d}$$

$$(R_3)_{l_2 j_2} = \int_0^\infty F_{l_2 j_2} \chi_{l-1} g_{l_1 j_1} r^2 dr, \tag{13e}$$

$$(R_4)_{l_2 j_2} = \int_0^\infty G_{l_2 j_2} \chi_{l-1} f_{l_1 j_1} r^2 dr. \tag{13f}$$

In (13b) the values of $l_2 j_2$ for which the integrals must

[20] E. Wigner, *Gruppentheorie* (Friedrich Vieweg und Sohn, Braunschweig, 1931), Chapter XVII. The tabulation of these coefficients given in E. U. Condon and G. H. Shortley, *Theory of Atomic Spectra* (Cambridge University Press, Cambridge, 1935), pp. 76–77, suffices for all cases considered here. In the latter reference the coefficients are denoted by $(l l_1 m m_1 | l_2 j_2 m_2)$.

be evaluated have been written as subscripts outside the absolute value signs. The selection rules giving the values of l_2 and j_2 over which the sum in (1) must be taken are

$$|l-l_1|\leqslant l_2\leqslant l+l_1, \quad |l-j_1|\leqslant j_2\leqslant l+j_1, \quad l+l_1+l_2 \text{ even}, \tag{14}$$

where the last is the parity selection rule.

(b) Magnetic Multipoles

The calculation for the magnetic multipole proceeds in similar fashion. The angular matrix elements which appear are

$$T_5=(\sigma,\Omega(2)|\,\mathbf{L}Y_l^m|\cdot\boldsymbol{\sigma}\Omega(1)) \tag{15a}$$

and

$$T_6=(\Omega(2)|\,\mathbf{L}Y_l^m|\cdot\boldsymbol{\sigma}\sigma,\Omega(1)), \tag{15b}$$

which can be transformed to a common form

$$T_5=-T_6=-T_1'[j_2(j_2+1)-l_2(l_2+1)+j_1(j_1+1)-l_1(l_1+1)+\tfrac{1}{2}],$$
$$T_1'=(\sigma,\Omega(2)|\,Y_l^m|\,\Omega(1))=(\Omega(2j_2-l_2,\,j_2;\,m_2)|\,Y_l^m|\,\Omega(1)).$$

From the selection rules valid for magnetic multipoles

$$|l-l_1|-1\leqslant l_2\leqslant l+l_1+1, \quad |l-j_1|\leqslant j_2\leqslant l+j_1, \quad l+l_1+l_2 \text{ odd} \tag{16}$$

we recognize that the values of $2j_2-l_2$ which enter for the magnetic 2^l-pole are the same as the values of l_2 which enter for the electric 2^l-pole radiation so that (10) and (11) can be used in this case also.

Finally, the magnetic internal conversion coefficient is given by

$$\beta_l=\frac{2\pi\alpha kl}{(l+1)(2l+1)}U_l', \tag{17}$$

where

$$U_l'=(2\pi/l^2)\sum_{l_2j_2}(2j_2+1)[j_2(j_2+1)-l_2(l_2+1)+j_1(j_1+1)-l_1(l_1+1)+\tfrac{1}{2}]^2\times[Q(l;\,2j_2-l_2,\,j_2;\,l_1,\,j_1)]^2|R_3'+R_4'|^2{}_{l_2j_2} \tag{17a}$$

and

$$(R_3')_{l_2j_2}=\int_0^\infty F_{l_2j_2\chi_l}g_{l_1j_1}r^2dr, \tag{17b}$$

$$(R_4')_{l_2j_2}=\int_0^\infty G_{l_2j_2\chi_l}f_{l_1j_1}r^2dr. \tag{17c}$$

For the K-shell

$$U_l'=(l+1)|R_3'+R_4'|^2{}_{l+1,\,l+\frac{1}{2}}+(l+1)^2/l|R_3'+R_4'|^2{}_{l-1,\,l-\frac{1}{2}}. \tag{18}$$

(c) Radial Integration and Transformation of Results

The radial integrations are carried out exactly as in Hulme's calculation.[9] For the hankel function we use the series representation

$$H_{l+\frac{1}{2}}^{(1)}(x)=(-i)^{l+1}\left(\frac{\pi x}{2}\right)^{-\frac{1}{2}}e^{ix}\sum_{\nu=0}^{l}\frac{(l+\nu)!}{\nu!(l-\nu)!}\left(\frac{i}{2x}\right)^\nu, \tag{19}$$

and for the radial functions of the final state wave function the integral representations[17] are employed. The radial functions for the ground state are

$$f=-(1-\gamma)^{\frac{1}{2}}Dr^{\gamma-1}e^{-\alpha Zr}, \quad g=(1+\gamma)^{\frac{1}{2}}Dr^{\gamma-1}e^{-\alpha Zr}, \tag{20}$$

where

$$\gamma=(1-\alpha^2Z^2)^{\frac{1}{2}} \tag{20a}$$

is the total energy (including rest energy) in the K-shell and

$$D=(2\alpha Z)^{\gamma+\frac{1}{2}}[2\Gamma(2\gamma+1)]^{-1} \tag{20b}$$

is a normalization factor.

We introduce the following notation for quantities occurring in the final state wave function:

$$\gamma'=[(j_2+\tfrac{1}{2})^2-\alpha^2Z^2]^{\frac{1}{2}}, \tag{21a}$$

$$N_{j_2}{}^2=\frac{e^{\pi\xi}(p/2)^{2\gamma'}}{4\pi p|\,\Gamma(\gamma'+i\xi)\,|^2}, \tag{21b}$$

$$\xi=\alpha ZW/p, \tag{21c}$$

where $p(>0)$ is the final state momentum and $W=(p^2+1)^{\frac{1}{2}}$ is the final state energy (including rest energy). Then we find for the electric multipole conversion (omitting common factors of modulus unity)

$$(R_1)_{l,\,l\pm\frac{1}{2}}=-i(W-1)^{\frac{1}{2}}(1-\gamma)^{\frac{1}{2}}DN_{l\pm\frac{1}{2}}\times[K_{l,\,l\pm\frac{1}{2}}-\exp(-2i\eta_\pm)K^*{}_{l,\,l\pm\frac{1}{2}}], \tag{22a}$$

$$(R_2)_{l,\,l\pm\frac{1}{2}}=(W+1)^{\frac{1}{2}}(1+\gamma)^{\frac{1}{2}}DN_{l\pm\frac{1}{2}}\times[K_{l,\,l\pm\frac{1}{2}}+\exp(-2i\eta_\pm)K^*{}_{l,\,l\pm\frac{1}{2}}], \tag{22b}$$

$$(R_3)_{l,\,l\pm\frac{1}{2}}=-(W-1)^{\frac{1}{2}}(1+\gamma)^{\frac{1}{2}}DN_{l\pm\frac{1}{2}}\times[K_{l-1,\,l\pm\frac{1}{2}}-\exp(-2i\eta_\pm)K^*{}_{l-1,\,l\pm\frac{1}{2}}], \tag{22c}$$

$$(R_4)_{l,\,l\pm\frac{1}{2}}=-i(W+1)^{\frac{1}{2}}(1-\gamma)^{\frac{1}{2}}DN_{l\pm\frac{1}{2}}\times[K_{l-1,\,l\pm\frac{1}{2}}+\exp(-2i\eta_\pm)K^*{}_{l-1,\,l\pm\frac{1}{2}}], \tag{22d}$$

and for the magnetic conversion

$$(R_3')_{l',\,l'\pm\frac{1}{2}}=-(W-1)^{\frac{1}{2}}(1+\gamma)^{\frac{1}{2}}DN_{l'\mp\frac{1}{2}}\times[K_{l,\,l'\mp\frac{1}{2}}-\exp(-2i\eta_\pm)K^*{}_{l,\,l'\mp\frac{1}{2}}], \tag{22e}$$

$$(R_4')_{l',\,l'\pm\frac{1}{2}}=-i(W+1)^{\frac{1}{2}}(1-\gamma)^{\frac{1}{2}}DN_{l'\mp\frac{1}{2}}\times[K_{l,\,l'\mp\frac{1}{2}}+\exp(-2i\eta_\pm)K^*{}_{l,\,l'\mp\frac{1}{2}}], \tag{22f}$$

where the $\pm$ in the second subscript in R_3', R_4' goes with $l'=l\mp1$. Note that for both values of l', $2j-l'=l$. In (22) we have introduced

$$\exp(-2i\eta_\pm)=\frac{\gamma'+i\xi}{\pm(j+\frac{1}{2})+i\alpha Z/p} \tag{23}$$

and the value to be used for j is the same as the second subscript in K. Also K^* is obtained from K by changing the sign of p in the formulas given below:

$$K_{\lambda,j}=\sum_{\nu=0}^{\lambda}\frac{(\lambda+\nu)!}{(\lambda-\nu)!}E_{j\nu}, \tag{24a}$$

$$K_{\lambda,j}^*=\sum_{\nu=0}^{\lambda}\frac{(\lambda+\nu)!}{(\lambda-\nu)!}E_{j\nu}^*, \tag{24b}$$

and the $E_{j\nu}$, $E_{j\nu}^*$ are defined by

$$\begin{pmatrix}E_{j\nu}\\E_{j\nu}^*\end{pmatrix}=\left(-\frac{p}{2k\zeta}\right)^{\nu}\frac{\Gamma(\gamma+\gamma'-\nu)}{\nu!\Gamma(2\gamma'+1)}$$
$$\times\frac{2^{2\gamma'}}{k}\left(\frac{\zeta}{ip}\right)^{\gamma+\gamma'}|\Gamma(\gamma'+i\xi)|^2$$
$$\times\begin{pmatrix}(\gamma'+i\xi)F(\gamma'+\gamma-\nu,\gamma'+1+i\xi;2\gamma'+1;2\zeta)\\(\gamma'-i\xi)F(\gamma'+\gamma-\nu,\gamma'+i\xi;2\gamma'+1;2\zeta)\end{pmatrix}, \tag{25}$$

where

$$\zeta=ip/[\alpha Z+i(p-k)] \tag{25a}$$

and F is the hypergeometric function

$$F(a,b;c;z)=\frac{\Gamma(c)}{\Gamma(a)\Gamma(b)}\sum_{n=0}^{\infty}\frac{\Gamma(a+n)\Gamma(b+n)}{\Gamma(c+n)}\frac{z^n}{n!}. \tag{25b}$$

In (25) we have used the relations

$$F(a,b;c;z)=(1-z)^{-a}F(a,c-b;c;z/(z-1)) \tag{25c}$$

and with

$$\zeta^*=-ip/[\alpha Z-i(k+p)]$$

we have

$$2\zeta^*/(2\zeta^*-1)=2\zeta. \tag{25d}$$

The result (25) applies only in the circle of convergence: $|2\zeta|<1$. Applying the conservation of energy

$$k+\gamma=W \tag{26}$$

it is seen that the region $|2\zeta|<1$ applies only in a narrow band of the $Z-k$ plane near the K-threshold. For all cases considered in the numerical work the analytic continuation of (25) is required; that is, we use

$$\frac{\Gamma(a)\Gamma(b)}{\Gamma(c)}F(a,b;c;z)$$
$$=\frac{\Gamma(a)\Gamma(a-b)}{\Gamma(a-c)}(-z)^{-a}F(a,1-c+a;1-b+a;1/z)$$
$$+\frac{\Gamma(b)\Gamma(b-a)}{\Gamma(b-c)}(-z)^{-b}F(b,1-c+b;1-a+b;1/z). \tag{27}$$

Applied to E_{j0} and E_{j0}^* this gives

$$\begin{pmatrix}E_{j0}\\E_{j0}^*\end{pmatrix}=\frac{2^{2\gamma'}}{k}\left(\frac{\zeta}{ip}\right)^{\gamma+\gamma'}\left\{(-2\zeta)^{-\gamma-\gamma'}\frac{\Gamma(\gamma'+\gamma)\Gamma(-\gamma+i\xi)\Gamma(\gamma'-i\xi)}{\Gamma(\gamma'-\gamma+1)}\begin{pmatrix}(-\gamma+i\xi)F(\gamma'+\gamma,\gamma-\gamma';\gamma-i\xi;1/2\zeta)\\(\gamma'-i\xi)F(\gamma'+\gamma,\gamma-\gamma';\gamma+1-i\xi;1/2\zeta)\end{pmatrix}\right.$$
$$\left.+(-2\zeta)^{-\gamma'-i\xi}\Gamma(\gamma'+i\xi)\Gamma(\gamma-1-i\xi)\begin{pmatrix}(\gamma'+i\xi)(-2\zeta)^{-1}F(\gamma'+1+i\xi,1-\gamma'+i\xi;2-\gamma+i\xi;1/2\zeta)\\(\gamma-1-i\xi)F(\gamma'+i\xi,-\gamma'+i\xi;1-\gamma+i\xi;1/2\zeta)\end{pmatrix}\right\}, \tag{28}$$

where we require $|2\zeta|>1$, $|\arg(-2\zeta)|<\pi$ and

$$|\arg(\zeta/ip)|<\pi/2.$$

The task of obtaining $E_{j\nu}$ and $E_{j\nu}^*$ for $\nu\neq0$ is greatly simplified by the use of recurrence relations. With the aid of

$$(c-a)F(a-1,b;c;z)$$
$$=b(1-z)F(a,b+1;c;z)+(c-b-a)F(a,b;c;z)$$

and

$$(c-a)F(a-1,b+1;c;z)$$
$$=(b-a+1)(1-z)F(a,b+1;c;z)+(c-b-1)F(a,b;c;z)$$

we find the following recurrence relation which we write in matrix form:

$$\begin{pmatrix}E_{j,\nu+1}\\E_{j,\nu+1}^*\end{pmatrix}=\frac{(-p/2k\zeta)}{(\nu+1)(\gamma+\gamma'+\nu-1)(\gamma'-\gamma+\nu+1)}$$
$$\times\begin{pmatrix}\nu+1-\gamma+i\xi & \gamma'+i\xi\\ \gamma'-i\xi & \nu+1-\gamma-i\xi\end{pmatrix}\begin{pmatrix}(1-2\zeta)E_{j\nu}\\E_{j\nu}^*\end{pmatrix}. \tag{29}$$

For all cases considered $|2\zeta|>1$ so that (28) and (29) determine all the $E_{j\nu}$, $E_{j\nu}^*$ and from (13), (17), (18), (22), and (24) the internal conversion coefficients are obtained. Some further simplification may be made by introducing the transformations discussed by Gellman *et al.*[7]

The Structure of Ammonium Chloride by Neutron Diffraction

G. H. GOLDSCHMIDT* AND D. G. HURST
Atomic Energy Project, National Research Council of Canada, Chalk River, Ontario, Canada
(Received February 13, 1951)

From the intensities of powder diffraction lines the positions of the deuterons in ND_4Cl have been determined at liquid nitrogen and room temperatures. The experimental results confirm at low temperature the space group T_d^1 and the tetrahedral structure of the ammonium ion with an $N-D$ separation 1.03A. At room temperature the T_d^1 space group persists. Neither free rotation nor disordered orientations of the ammonium ions have been observed. Details concerning deuteron vibrations are discussed.

INTRODUCTION

ANOMALIES in the behavior of ammonium chloride were first observed by Simon[1] who detected a sharp transition at −30°C in the specific heat at constant pressure. X-ray investigations[2] showed that the nitrogen and chlorine atoms were arranged in a lattice of the CsCl type and that a change of 1 percent in the lattice constant accompanied the transition, but these investigations gave no information about the hydrogen atoms. Pauling[3] suggested that onset of free rotation of the ammonium ion might account for the change in specific heat. Quanitative details of the onset of rotation for dipole interactions were discussed by Fowler[4] and in a somewhat different form by Kirkwood.[5] Eucken[6] pointed out that the rotational heat required for the ammonium ion above the critical temperature was not in agreement with experiment. In the meantime, Frenkel[7] had suggested an order-disorder transition for the ammonium ion, detailed mathematical treatment being given by Nagamiya.[8]

Concurrently experimental evidence in support of both the rotation and order-disorder theories accumulated. Hettich[9] observed the disappearance of the piezoelectric effect at the transition temperature and attributed it to rotation. Menzies and Mills[10] reported that below −30°C the Raman line of 183 cm^{-1} was clearly visible, but that it was absent in the room temperature phase, while Krishnan[11] found that the line persisted in that phase but with much less intensity. Menzies and Mills, although favoring rotation, stated that a possible explanation for their results was onset of a simple torsional oscillation of the ammonium ion, while Couture and Mathieu[12] deduced rotation about a threefold axis from Raman polarization measurements. Similar differences occurred among the infrared results, where Beck[13] observed rotational structure on at least one vibrational band, while Wagner and Hornig[14] found evidence for the order-disorder theory. Solid state experiments by Bridgman,[15] and Lawson,[16] and electron diffraction measurements by Laschkarew[17] did not lead to conclusive results.

Since the difficulties arose from ignorance of the positions and behavior of the hydrogen atoms, it was decided to study ammonium chloride by neutron diffraction methods so that by comparison of experimental and calculated structure factor the correct distribution of the hydrogen atoms could be determined. Measurements by the powder method at liquid nitrogen and room temperature are reported in the present paper and it is shown that they establish the structures. For experimental reasons[18] deuterated ammonium chloride was used, and because the physical properties of deuterated and ordinary ammonium chloride are similar[14,19] the results of the structure determination may be expected to apply qualitatively to the ordinary chloride.

APPARATUS AND PROCEDURE

The general design of the spectrometer, the counting equipment, and the monitor of the neutron intensity have been previously discussed[20] and the collimation of the primary neutron beam has been described.[21] The monochromatic beam was selected from the primary beam by a sodium chloride crystal placed in the transmission position; diffraction by diamond powder gave the wavelength as 1.07A.

The spectrometer arm, carrying the main neutron counter and a defining collimator (0.5×1.5×19 inches long), was driven by a reversible synchronous motor and moved between two limit switches at the rate of

* Now at Imperial College, London, England.
[1] F. Simon, Ann. Physik (4) **68**, 241 (1922).
[2] F. Simon and C. v. Simson, Naturwiss. **14**, 880 (1926).
[3] L. Pauling, Phys. Rev. **36**, 430 (1930).
[4] R. H. Fowler, Proc. Roy. Soc. (London) (A) **149**, 1 (1935).
[5] J. Kirkwood, J. Chem. Phys. **8**, 205 (1940).
[6] A. Eucken, Z. Elektrochem. **45**, 126 (1939).
[7] J. Frenkel, Acta Physicochimica **3**, 23 (1935).
[8] T. Nagamiya, Proc. Phys. Math. Soc. Japan **24**, 137 (1942).
[9] A. Hettich, Z. physik Chem. (A) **168**, 353 (1934).
[10] A. C. Menzies and H. R. Mills, Proc. Roy. Soc. (London) (A) **148**, 407 (1935).
[11] R. S. Krishnan, Proc. Indian Acad. Sci. (A) **26**, 432 (1947).
[12] L. Couture and J. P. Mathieu, Proc. Indian Acad. Sci. (A) **28**, 401 (1948).
[13] C. Beck, J. Chem. Phys. **12**, 71 (1944).
[14] E. L. Wagner and D. F. Hornig, J. Chem. Phys. **18**, 296 (1950).
[15] P. W. Bridgman, Phys. Rev. **38**, 182 (1931).
[16] A. W. Lawson, Phys. Rev. **57**, 417 (1940).
[17] W. E. Laschkarew and I. D. Usyskin, Z. Physik **85**, 618 (1933).
[18] Shull, Wollan, Morton, and Davidson, Phys. Rev. **73**, 842 (1948).
[19] Clusius, Kruis, and Schanzer, Z. Anorg. u. allgem. Chem. **236**, 24 (1938).
[20] D. G. Hurst and N. Z. Alcock, Can. J. Phys. **29**, 36 (1951).
[21] Hurst, Pressesky, and Tunnicliffe, Rev. Sci. Instr. **21**, 705 (1950).

approximately 1.1 degree per hour. To check automatically the progress of the spectrometer arm, a phonograph crystal cartridge which was attached to the arm had its stylus adjusted to cross every 0.1-inch graduation (1.1°) of a graduated circle. The movement of the stylus into the graduations created a pulse in the crystal, which was recorded after amplification.

The specimen table was coupled to the arm by a belt system and followed at half the angular rate. The table carried a stainless steel Dewar flask with 0.007-inch windows and a separate support for the airtight cassette containing the powder specimen. The cassette could be centered accurately on the axis of rotation of the table. The windows of the cassette were made of 0.005-inch Dural, spaced approximately 0.1 inch apart, and large enough to accommodate the neutron beam (0.5×1 inch) at all required angles. The area occupied by the powder was determined from a radiograph of the filled cassette.

A chromel-alumel thermocouple was soldered to the surface of the cassette and the temperature of the cassette was recorded. For low temperature experiments liquid nitrogen was maintained in the Dewar flash by an automatic refill system connected to a 50 liter flask; the temperature fluctuated between −170°C and −190°C.

All counts were recorded on a multiple pen recorder and analyzed by the following method. The number of counts in each fifteen minute interval was corrected for fluctuations in the intensity of the primary neutron beam. The difference between measurements with full and empty cassettes gave the effect of the powder. The resulting diffraction pattern of the powder was plotted as an integral curve against angle. An example of such a plot, which includes two diffraction peaks, is shown in Fig. 1. The incoherent background appears as straight lines and the integrated intensity of the peaks is given by the height of the steps I and I'. Because the width of each step depended on the resolution of the spectrometer, overlapping of peaks sometimes occurred even with simple cubic compounds and it was then difficult to assign the correct position and slope to the background lines. In such a case the point of minimum slope between unresolved peaks was selected and a line parallel to the nearest resolved background line was drawn through this point.

GENERAL THEORY

For a flat slab of crystalline powder whose normal makes an angle θ with the incident beam[22] the integrated intensity in a peak is

$$I_{hkl}=BP_0\frac{W\exp(-ut\sec\theta)}{\rho A\sin^2 2\theta}j_{hkl}N^2|F_{hkl}|^2, \quad (1)$$

where hkl is the reflection index, P_0 is the power in the primary beam, B is an instrumental constant determined by calibration, t is the thickness of the slab, W is the weight of powder in the cassette, A is the area of the powder, ρ is the crystalline density, u is the absorption coefficient, 2θ is the angle between incident and diffracted beams, j_{hkl} is the multiplicity factor, and N is the number of unit cells per cm³. F_{hkl} is the structure factor for the unit cell and may be written

$$F_{hkl}=\sum_n f_n R_n\exp\{-2\pi i(hx_n+ky_n+lz_n)\} \quad (2)$$

where the summation is carried out over all the atoms in the unit cell; $x_n y_n z_n$ are the fractional coordinates of nucleus n, f_n is the bound nuclear scattering length, and R_n is a correction factor for thermal and zero-point vibrations. Instead of the coherent scattering amplitude

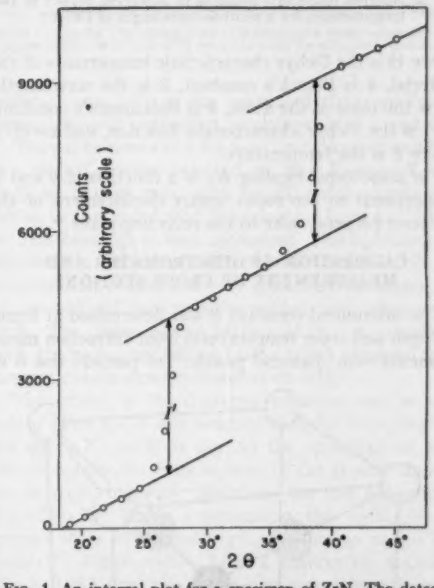

FIG. 1. An integral plot for a specimen of ZrN. The detector moved at a constant angular rate and the accumulated counts are plotted against angular position of the detector. The steps I and I' are the integrated intensities of two diffraction peaks.

f_n, it is usual to state the coherent cross section, σ_n, which is defined by

$$\sigma_n=4\pi|f_n|^2. \quad (3)$$

The factor R_n has been calculated by Debye and Waller for x-rays, and Weinstock[23] has discussed the application to neutrons. For isotropic binding

$$R_n=\exp(-K_n\sin^2\theta) \quad (4)$$

with

$$K_n=\frac{6h^2}{\lambda^2 m_n k\Theta}\left(\frac{\varphi(x)}{x}+\tfrac{1}{4}\right) \quad (5)$$

[22] E. O. Wollan and C. G. Shull, Phys. Rev. 73, 830 (1948).

[23] R. Weinstock, Phys. Rev. 65, 1 (1944).

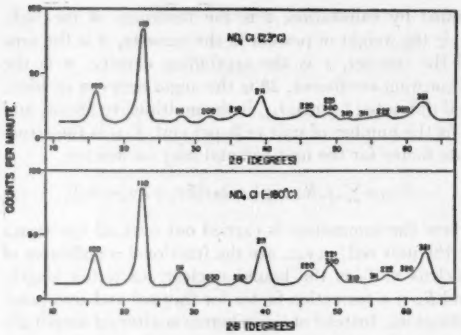

FIG. 2. Neutron diffraction patterns of powdered ND_4Cl at two temperatures, for a neutron wavelength of 1.07A.

where Θ is the Debye characteristic temperature of the material, h is Planck's constant, λ is the wavelength, m_n is the mass of the atom, k is Boltzmann's constant, $\varphi(x)$ is the Debye characteristic function, and $x=\Theta/T$ where T is the temperature.

For anisotropic binding K_n is a function of θ and is proportional to the mean square displacement of the scatterer perpendicular to the reflecting plane.[24]

CALIBRATION OF SPECTROMETER AND MEASUREMENT OF CROSS SECTIONS

The instrument constant B was determined at liquid nitrogen and room temperatures from diffraction measurements with diamond powder[22] of particle size 6 to 12 microns, the bound coherent cross section of carbon being taken as 5.52 barns.[25]

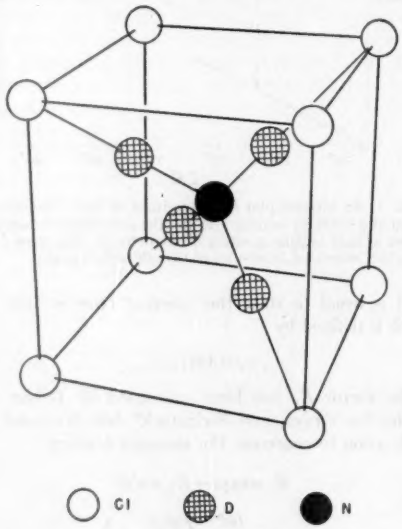

FIG. 3. The unit cell of ND_4Cl.

[24] R. W. James, *The Optical Principles of the Diffraction of X-Rays* (G. Bell and Sons, London, 1948), Chapter V.

Preliminary comparison of observed and calculated intensities for the ammonium chloride diffraction pattern at low temperature cast doubt on the values available for the coherent cross sections of chlorine and nitrogen. They were therefore redetermined from powder diffraction patterns of NaCl and ZrN at liquid air temperatures. Special precautions were taken to prepare crystals of NaCl with maximum particle size 10 microns; the ZrN was obtained commercially at 600 mesh. ZrN was used in spite of its hafnium impurity of 3 percent because no pure simple cubic nitride was available. The following values were obtained for the bound coherent cross sections:—

$$\sigma_{Cl}=11.9 \text{ barns}$$
$$\sigma_{Na}=1.63 \text{ barns}$$
$$\sigma_{Zr}=5.1 \text{ barns}$$
$$\sigma_{N}=9.1 \text{ barns.}$$

The chlorine and sodium cross sections are in fair agreement with the values of 12.8 barns and 1.51 barns published by Wollan and Shull,[22] while the high value of the nitrogen cross section shows that there is little spin incoherence, in disagreement with other results.[26] Gas scattering experiments carried out in this laboratory have also given the higher value for the nitrogen cross section. The deuterium cross section was taken to be 5.8 barns.[20]

STRUCTURE DETERMINATION OF ND_4Cl

Diffraction measurements were made at liquid nitrogen and room temperatures using deuterated ammonium chloride with a deuterium purity of 99.4 percent.[27] The diffraction patterns are shown in Fig. 2. Integrated intensities I_{hkl} were found from integral plots as previously described, and experimental structure factor moduli $|F_{hkl}|_E$ were derived by Eq. (1). These are tabulated for the low and high temperatures in Table I, column 11, and Table IV, column 4, respectively, the units being 10^{-12} cm. The errors quoted are the maximum deviations from the mean of several measurements.

The experimental moduli were compared with the moduli of structure factors calculated by Eq. (2) for models suggested by the previous experimental work. In these models several minor parameters were available for adjustment: the nitrogen deuterium distance was known to be about 1A but some variation from this was permissible; the R factors in Eq. (2), even if taken as following Eq. (4), still gave latitude because the Debye temperature was not found in the literature and because Eq. (5) may not apply accurately; and the cross sections could be varied within the experimental error of their determination.

[25] E. Melkonian, Phys. Rev. **76**, 1750 (1949).
[26] C. G. Shull and E. O. Wollan, Phys. Rev. **75**, 1302 (1949).
[27] The ND_4Cl was prepared and analyzed by the Analytical Development Section, Chemical Control Branch, Chalk River.

TABLE I. Variation of parameters in the low temperature case.

	Trial calculations								Final[a] choice	Experimental results	
	Trial 1	Trial 2	Trial 3	Trial 4	Trial 5	Trial 6	Trial 7	Trial 8			
K_{Cl}	0.36	0.36	0.36	0.20	0.20	0.20	0.20	0.20	0.15		
K_N	0.78	0.78	0.78	0.52	0.52	0.52	0.52	0.52	0.39		
K_D	5.5	5.5	3.6	3.6	3.6	2.7	2.7	2.7	2.7		
r(A)	1.00	1.10	1.00	1.00	1.05	1.05	1.04	1.03	1.03		
hkl	$\lvert F_{hkl}\rvert$	$\lvert F_{hkl}\rvert$	$\lvert F_{hkl}\rvert$	$\lvert F_{hkl}\rvert$	$\lvert F_{hkl}\rvert$	$\lvert F_{hkl}\rvert$	$\lvert F_{hkl}\rvert$	$\lvert F_{hkl}\rvert$	$\lvert F_{hkl}\rvert$	$\lvert F_{hkl}\rvert_E$	Error
100	1.32	1.13	1.37	1.37	1.28	1.31	1.34	1.35	1.38	1.39	2%
110	2.58	2.41	2.62	2.63	2.53	2.56	2.59	2.60	2.59	2.54	2%
111	1.08	1.25	1.18	1.19	1.29	1.39	1.33	1.32	1.33	1.35	4%
200	1.21	0.90	1.13	1.12	1.00				1.01	0.98	4%
210	0.44	0.64	0.49	0.48	0.55				0.53	0.55	4%
211	1.74	1.82	1.89	1.92	1.97				1.97	1.95	4%
220	1.78	1.93	1.81	1.87	1.95				1.94	1.92	4%
222	1.73	1.60	1.85	1.94	1.87				2.02	1.94	20%
321	1.68	1.72	1.78	1.85	1.88				1.93	1.94	5%

[a] For the structure factors in this column the chlorine cross section was taken as 11.5 barns. The change from 11.9 barns gave better agreement, and is within the experimental error of the measurement. (The intensities from the planes (310), (311), and (320) were too small for accurate measurement. The peaks due to (300), and (221) are coincident and are omitted from this table.)

LOW TEMPERATURE PHASE

The low temperature structure suggested by the previous experimental work is illustrated by the model shown in Fig. 3. In this model the nitrogen and chlorine atoms are in positions $(xyz)_N=000$, $(xyz)_{Cl}=\frac{1}{2}\frac{1}{2}\frac{1}{2}$. The ammonium ion is tetrahedral with the deuterium atoms on the diagonals of the unit cell at a distance r from the nitrogen atoms so that the coordinates of the four deuterium atoms are $(xyz)_D=xxx$, $x\bar{x}\bar{x}$, $\bar{x}\bar{x}x$, $\bar{x}x\bar{x}$ where $x=r/(\sqrt{3}a)$ and a is the length of the cube edge. The space group of this lattice is T_d^1, and the structure factor with R of the form given by Eq. (4) becomes

$$F_{hkl}=f_N\exp(-K_N\sin^2\theta)+(-1)^{h+k+l}f_{Cl}\times\exp(-K_{Cl}\sin^2\theta)+4f_D\exp(-K_D\sin^2\theta)\times\{\cos(2\pi hx)\cos(2\pi kx)\cos(2\pi lx)-i\sin(2\pi hx)\sin(2\pi kx)\sin(2\pi lx)\}. \quad (6)$$

Since no Debye temperature for ND_4Cl could be found in the literature, the K values in preliminary calculations were based on the Debye temperature of NaCl. This temperature is 281°K and its use was suggested by the similarity in the low temperature specific heats of ND_4Cl and NaCl[28] and by the similarity of the ionic masses. r was taken as 1A. The initial agreement was good and calculations were continued by the methods of successive approximation. The course of the calculations is summarized in Table I, where the adjustable parameters are shown at the top of the table and the corresponding $|F_{hkl}|$ below. The choice of parameters implies that the nitrogen chlorine and deuterium atoms are considered as separate units. It might be more correct to assume that the lattice is made up of chlorine and ammonium ions with the deuterons as internal constituents of the ammonium ions. However, this would introduce complexity which is not justified at present, especially as the calculated structure factors were relatively insensitive to changes in K_N and K_{Cl}.

The parameters r and K_D were first changed, and then K_N and K_{Cl} were adjusted so that $K_Nm_N=K_{Cl}m_{Cl}=K_Dm_D$ in conformity with Eq. (5). In the final calculation it was found that changing σ_{Cl} from 11.9 barns to 11.5 barns gave best agreement. The agreement of the final set of calculated structure factors with the experimental results was very good, and the number of planes was sufficient to make unlikely any other structure. The value of $r=1.03\text{A}\pm0.02\text{A}$, is consistent with the recent result[29] $r=1.025\pm0.01$A obtained from magnetic resonance experiments on NH_4Cl.

The extent of the deuteron vibration can be estimated from K_D, if it is assumed that the reduction factor $\exp(-K_D\sin^2\theta)$ is due to the spreading of each deuteron over the finite volume of the ground state of an isotropic harmonic vibration. On this assumption $K_D=(2\pi s/\lambda)^2$ where s determines the width of the ground state with density proportional to $\exp[-\{\text{radius}/s\}^2]$. For $K_D=2.7$ (Table I, column 10) the value of s is 0.28A, and this value is an upper limit because inelastic scattering was neglected.

ROOM TEMPERATURE PHASE

It was suggested by Pauling and Frenkel that the transition at −30°C in NH_4Cl marks the onset of vibrations which are large enough to lead to a disordered arrangement of the ammonium ion in the lattice. Pauling suggested that the tetrahedra rotate freely above the transition temperature, while Frenkel proposed that some ammonium ions have sufficient energy to cross the potential barrier and rotate about the {100} axis, taking up a position at 90° to the original orientation. These disordered arrangements introduced a center of symmetry into the lattice and offered an

[28] F. Seitz, *Modern Theory of Solids* (McGraw-Hill Book Company, Inc., New York, 1940), p. 57.

[29] Gutowsky, Kistiakowsky, Pake, and Purcell, J. Chem. Phys. 17, 972 (1949).

TABLE II. Comparison of $|F|$'s observed at room temperature with $|F|$'s calculated for three models.

hkl	Calculated Model (a) $\lvert F_{hkl}\rvert$	Model (b) $\lvert F_{hkl}\rvert$	Model (d) $\lvert F_{hkl}\rvert$	Experimental $\lvert F_{hkl}\rvert_E$
100	1.54	0.97	0.97	1.41
110	2.57	2.19	2.19	2.47
111	0.13	0.01	0.48	0.89
200	1.50	1.40	1.40	1.09
210	0.59	0.30	0.30	0.68
211	0.97	1.45	1.49	1.43
220	0.81	1.40	1.40	1.39
222	0.94	1.22	1.22	1.08
321	1.06	1.14	1.14	1.32

easy explanation for the disappearance of the piezoelectric effect. There was, however, not sufficient evidence to prove whether either of the two suggestions was correct, and to cover all important possibilities, four models (a), (b), (c), and (d) have been considered in the present work. These models differ in the behavior of the ammonium ion, but not in the positions of the nitrogen and chlorine atoms because these are known from x-ray studies.

In model (a), called the spherical shell model, the ammonium ion is assumed to be rotating freely. The four deuterium atoms present a thin spherical shell of radius r to the incoming neutrons, insofar as the coherent scattering is concerned. The deuterium contribution to the structure factor for this thin shell is

$$F_D = 4f_D \sin y/y, \tag{7}$$

where

$$y = (4\pi r \sin\theta)/\lambda.$$

Model (b) corresponds to Frenkel's suggestion of total disorder in the arrangement of the tetrahedra on the two sets of diagonals in each cube. For coherent scattering this is equivalent to placing one-half deuteron on each diagonal in the unit cubes and is called the half-hydrogen model. Such an arrangement would arise from a "resonance" between the two sets of diagonals.

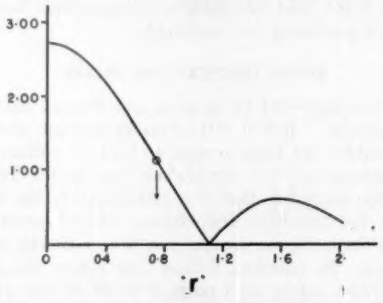

FIG. 4. The contribution to the (111) structure factor of ND_4Cl by the four deuterons, on the assumption of free rotation of a rigid ammonium ion. The variable r is the nitrogen deuterium distance and the arrow indicates the value which would be required to make this model fit the experimental result for the (111) reflection.

The structure factor is that of Eq. (6) without the imaginary term. In model (c) the ammonium ions lie in mirror image positions in neighboring cells, and the original unit cell has to be enlarged eight times to conform with the altered symmetry conditions. The resulting space group is O_h^5 with $a=7.73$A. A diffraction line whose intensity is comparable with the line marked (111) in Fig. 2 should be observed at $2\theta=14°$ and this line can be regarded as a characteristic feature of this model. Finally, in model (d), the low temperature form is assumed to persist at room temperature and the space group remains unaltered. The structure factor is given by Eq. (6) on the assumption that Eq. (4) applies.

Since no new lines were observed in the spectrum, calculations on model (c) were unnecessary, and this model was not considered further. Preliminary calculations of $|F_{hkl}|$ for each of the models (a), (b), and (d) were undertaken with $r=1.00$A and $\Theta=281°$K, and the results were tabulated with the experimental values (Table II). Although the agreement was poor, further calculations led to the choice of a satisfactory model.

The value of $|F_{111}|$ was found to be particularly sensitive to the deuterium contributions because the contributions of the chlorine and nitrogen nearly cancel, and this quantity was of primary importance in the attempts to get a fit by variation of the parameters. For agreement with the experimental value of $|F_{111}|$ the deuterium contribution must equal 1.12. For model (a) the deuterium contribution to $|F_{111}|$ was plotted as a function of the radius r for $0<r<2$A (Fig. 4). Only one radius ($r=0.74$A) gave agreement with the required value 1.12. This radius, besides being unlikely, brought $|F_{100}|$ up to 2.0 compared to the experimental value 1.41. Introducing a factor $\exp(-K_D \sin^2\theta)$ into Eq. (7), i.e., changing the thickness of the spherical shell, did not help, and further calculations clearly indicated that the spherical model had to be abandoned. It also proved impossible to adjust model (b) satisfactorily because the calculated $|F_{111}|$ was too small for all reasonable values of the nitrogen deuterium separation. In fact, the introduction of a center of symmetry, as in models (a) and (b), destroyed the strong imaginary component of the (111) structure factor. This left only unsymmetrical structures such as model (d) to be considered.

In the calculation of the structure factor of model (d) the K's and r's were varied as before. With $K_D=9.5$ fair agreement was obtained for the $|F_{hkl}|$ values (Table III). However, when the agreement for the low index plane (100) was good $|F_{200}|$ was unsatisfactory (columns 2 and 3), or when the agreement for the higher index 200 improved $|F_{100}|$ deteriorated (columns 4 and 5). This suggested that the correction factor $\exp(-K_D \sin^2\theta)$ no longer applied, and that the deuterium distribution should not be treated as isotropic in the high temperature modification.

An anisotropic distribution of the deuterium nuclei could arise from small torsional oscillations of the

ammonium ion about its center. This motion would cause each vertex of the tetrahedron to move on a spherical cap of radius 1.03A. The structure factor of this model was obtained by methods based on unpublished work of Dr. N. K. Pope. Each deuteron was considered to be spread out into a spherical cloud corresponding to the simple interpretation given above of the low temperature value of K_D. The center of this cloud was assumed to move over the spherical cap with a probability density proportional to $\exp(-u^2/l_D^2)$ where u is the distance of the center of the cloud from the appropriate diagonal of the unit cell, and l_D is a parameter. For simplicity of calculation, the curvature of the spherical cap was neglected, and the cap was treated as a flat plate perpendicular to the diagonal and at a distance r_1 from the nitrogen. The structure factor of this plate is

$$f_D \exp\{-K_D \sin^2\theta \sin^2\psi - 2\pi i(hx_1+ky_1+lz_1)\}$$

where (x_1, y_1, z_1) are the fractional coordinates of the point of intersection with the diagonal, and ψ is the angle between the normal to the plate and the direction $\{hkl\}$.

The contribution of the deuterium to the structure factor of the unit cell is the sum of four such terms corresponding to the four deuterons. The result is

$$\begin{aligned}F_D = f_D \exp(-K_D \sin^2\theta)\exp(-4\pi l_D^2 \sin^2\theta/\lambda^2)\\ \times[\{\cos 2\pi x_1(h+k+l) - i \sin 2\pi x_1(h+k+l)\}\\ \times\exp\beta(h+k+l)^2 + \{\cos 2\pi x_1(h-k-l)\\ - i \sin 2\pi x_1(h-k-l)\}\exp\beta(h-k-l)^2\\ + \{\cos 2\pi x_1(-h-k+l) - i \sin 2\pi x_1(-h-k+l)\}\\ \times\exp\beta(-h-k+l)^2 + \{\cos 2\pi x_1(-h+k-l)\\ - i \sin 2\pi x_1(-h+k-l)\}\exp\beta(-h+k-l)^2]\end{aligned}$$

where

$$x_1 = r_1/(a\sqrt{3})$$

and

$$\beta = \pi^2 l_D^2/(3a^2).$$

In the calculations of the structure factors K_N and K_{Cl} were 2.7 and 1.1 corresponding to $\Theta = 281°K$ and $T = 296°K$, K_D was 2.7, the final low temperature value, and l_D was chosen equal to 0.3A. Different values of r_1 were tried and maximum agreement was obtained for $r_1 = 0.97A$ (Table IV). Since the agreement was within experimental error, further refinement of the K values and l_D was considered meaningless. The agreement proves that the model contains the essential features of the deuterium distribution.

It seems reasonable to assume that the nitrogen deuterium distance does not change from 1.03A, and that r_1 is the apparent mean distance of the deuteron density distribution in the {111} direction. For the case of the spherical cap, this leads to an approximate amplitude of oscillation of $18 \pm 2°$ which is consistent with the l_D value.

The anisotropic distribution may also be interpreted as a motion of the deuterons around the diagonals.

TABLE III. Variation of parameters of model (d).

K_{Cl}	1.1	0.53	0.53	1.1	
K_N	2.7	1.36	1.36	2.7	
K_D	9.5	9.5	9.5	9.5	
r	0.90	0.90	1.03	1.03	
hkl	$\lvert F_{hkl}\rvert$	$\lvert F_{hkl}\rvert$	$\lvert F_{hkl}\rvert$	$\lvert F_{hkl}\rvert$	$\lvert F_{hkl}\rvert_E$
100	1.37	1.37	1.16	1.16	1.41
110	2.57	2.62	2.58	2.33	2.47
111	0.71	0.92	0.87	0.88	0.89
200	1.44	1.54	1.22	1.13	1.09
210	0.30	0.29	0.43	0.44	0.68
211	1.52	1.63	1.60	1.48	1.43
220	1.39	1.55	1.56	1.41	1.39
222	1.25	1.46	1.45	1.25	1.08
321	1.29	1.50	1.40	1.18	1.32

However, the present results cannot be used to distinguish between these fine details of deuterium behavior.

CONCLUSION

The structure of deuterated ammonium chloride has been shown to possess T_d^1 symmetry at both $-180°C$ and $23°C$. No evidence for free rotation or disorder has been found.

In the low temperature modification the nitrogen deuterium distance is $1.03 \pm 0.02A$ and the distribution of each deuteron is spherical to within the experimental resolution. This distribution is largely due to zero-point vibrations and its characteristic radius is 0.28A.

In the room temperature modification the distribution of the deuteron is spread transversely to the cube diagonal. This anisotropic distribution can be interpreted in several ways, for example, as an angular oscillation of the tetrahedron about the nitrogen as center, or as a motion of the deuterons around the diagonals. In the former the deuterium distribution has the shape of a spherical cap with radius (nitrogen deuterium distance) equal to 1.03A, and the apparent nitrogen deuterium distance along the cube diagonal is 0.97A. In the latter the center of the deuteron moves approximately in a circle in a plane which cuts the cube diagonal at 0.97A from the nitrogen. (It is of

TABLE IV. Comparison of final model with experimental results (room temperature). A value of $\sigma_{Cl} = 11.5$ barns was used for this table.

	Calculated		Experimental	
hkl	$\lvert F_{hkl}\rvert$ $r_1 = 1.00A$	$\lvert F_{hkl}\rvert$ $r_1 = 0.97A$	$\lvert F_{hkl}\rvert_E$	Error
100	1.35	1.41	1.41	2%
110	2.42	2.48	2.47	2%
111	1.03	0.95	0.89	5%
200	1.00	1.11	1.09	20%
210	0.61	0.56	0.68	20%
211	1.52	1.54	1.43	20%
220	1.28	1.25	1.39	20%
222	1.53	1.54	1.08	40%
321	1.28	1.28	1.32	5%

interest to note that electron diffraction[17] has given a value of 0.95±0.07A for the nitrogen hydrogen separation in NH_4Cl at room temperature.) Interpretations in terms of stationary tetrahedra involving angular displacement disorder are much less likely.

The disappearance of the piezoelectric effect and the absence or weakening of the Raman line, 183 cm^{-1}, above −30°C can now no longer be explained in terms of disorder or a centro-symmetric structure. However, angular oscillations of the ammonium tetrahedra may disturb the charge distribution in the lattice sufficiently to weaken the Raman line and to make the piezoelectric effect unobservable. A sudden onset of such oscillations may also be the cause of the lattice expansion at the transition temperature and the discontinuity in specific heat.

Theoretical studies are being undertaken to explain the observed behavior, and further experiments are planned to study as a function of temperature the change from the −180°C form to the room temperature form. This is of particular interest because of the existence of a magnetic resonance line width transition at −140°C.[20]

We wish to thank Dr. N. K. Pope for his help and advice regarding the theoretical aspects of the work, and Mr. W. J. Woytowich for his technical assistance.

[20] H. S. Gutowsky and G. E. Pake, J. Chem. Phys. **16**, 1164 (1948).

PHYSICAL REVIEW VOLUME 83, NUMBER 1 JULY 1, 1951

The Theory of Pressure Broadening and Its Application to Microwave Spectra

MASATAKA MIZUSHIMA
Physics Department, Faculty of Science, Tokyo University, Tokyo, Japan
(Received July 5, 1950)

In this paper the calculation of the widths of several absorption lines in the microwave region is attempted. First, the fourier integral formula for transition probability is deduced with the adiabatic assumption. Then the width and the shift of the absorption line are calculated, assuming the well type and the inverse power intermolecular potential. Applying the latter model, the width is calculated for several kinds of self-broadened microwave absorption line. A theoretical formula which gives the width of the ammonia inversion line is obtained as a function of $K/[J(J+1)]^{\frac{1}{2}}$, where K and J are the rotational quantum number. It agrees with experiment for large $K/[J(J+1)]^{\frac{1}{2}}$, and its temperature dependence is also good. In the microwave absorption of oxygen, the quadrupole interaction is shown to be responsible for the width, and our theoretical result agrees with experiment if the quadrupole moment of this molecule is 2.5 to 2.0×10^{-26}. It is also shown that the widths of the rotational lines of linear and symmetric top molecules can be explained by the dipole interaction.

I. INTRODUCTION

IT was about half a century ago that the first theory of pressure broadening was proposed by Lorentz.[1] Since then much theoretical and experimental work has been performed on this subject. In microwave spectra, the technique of which has been developed in the past few years, the width can be measured fairly accurately; and recently many interesting data have been obtained in this region. Thus, it may still be interesting and valuable to give further consideration to this subject.

In his theory Lorentz[1] assumed that the molecule is represented by a classical oscillator and that the intermolecular collisions are so strong that the oscillation process is absolutely interrupted by them. His formula which gives the intensity at circular frequency ω is

$$I(\omega)=(c/\pi)[\pi a^2\bar{V}N/\{(\omega-\omega_0)^2+(\pi a^2\bar{V}N)^2\}], \quad (1)$$

where $\bar{V}$ is the mean relative velocity of the molecules, a is the radius of the molecule, N is the number of molecules in unit volume, and c is the total intensity. At $|\omega-\omega_0|=\pi a^2\bar{V}N$ the intensity is just half of the maximum intensity, and thus this quantity gives the half-width of the spectral line. Van Vleck and Weisskopf[2] revised this formula, and Van Vleck and Margenau[3] proved that absorption and emission lines have the same shape in this model. In applying the above formula, the collision radius a was found to be very different from the kinetic collision radius; thus, a was taken as a mere parameter with whose physical meaning we are not concerned.

Kuhn,[4] Margenau,[5] and some others developed a theory in which molecules are assumed to be randomly distributed in space and simultaneously interacting with the radiating molecule. This theory is valid at high pressure and can explain the asymmetry of line shape which is observed in this region. But since we are treating the low pressure region, we cannot use this theory.

[1] H. A. Lorentz, Proc. Amst. Acad. Sci. **8**, 591 (1906).

[2] J. H. Van Vleck and V. F. Weisskopf, Revs. Modern Phys. **17**, 227 (1945).
[3] J. H. Van Vleck and H. Margenau, Phys. Rev. **76**, 1211 (1949).
[4] H. Kuhn, Proc. Roy. Soc. (London) **A18**, 987 (1934).
[5] H. Margenau, Phys. Rev. **48**, 755 (1935); H. Margenau and W. W. Watson, Revs. Modern Phys. **8**, 22 (1936).

Another theory, called the fourier integral theory, was developed by Weisskopf.[6] By the WKB method he obtained the following formula:

$$I(\omega) \propto \left| \int^{\infty} \exp\left\{ -i\omega_0 t - i\int^{t} (\Delta p/\hbar)dt + i\omega t \right\} dt \right|^2, \quad (2)$$

where Δp is the difference of the intermolecular forces in initial and final states of the radiating process. Lindholm,[7] Foley,[8] and Anderson[9] have recently developed theories of this type, and the present author[10-12] has also published some papers in this direction. In this paper we shall use the fourier integral theory.

II. DISCUSSION ON THE FOURIER INTEGRAL THEORY

The simultaneous collisions of three or more molecules are neglected throughout this paper because we are treating the extremely low pressure region.

The hamiltonian of a two-molecular system can be divided into three parts:

$$H = H_\alpha + H_\beta + H_{\alpha\beta}, \quad (3)$$

where H_α and H_β are the hamiltonians of the isolated molecules α and β, respectively, and $H_{\alpha\beta}$ is the intermolecular potential between these two molecules. If the radiation field interacts with molecule α, H_r must be added to the above hamiltonian, where

$$H_r = F\mu e^{i\omega t}, \quad (4)$$

μ is the dipole moment of molecule α, ω is the circular frequency of the field, and F is the amplitude. Since we do not take into account the simultaneous optical transition of two molecules, we do not need the hamiltonian which gives the interaction of the radiation field with molecule β. In this paper α is called the radiating molecule, and β is called the colliding molecule.

In the radiation theory it is convenient to take the basis which makes H_α and H_β diagonal. In this case the Schroedinger equation is

$$i\hbar\partial a_2^*/\partial t = \sum_i (H - i\hbar\partial/\partial t)_{2i} a_i^*, \quad (5)$$

where a_i^* is the probability amplitude of state i. The term $i\hbar\partial/\partial t$ comes from the relative motion of the molecules.[12a] In the following we shall restrict ourselves to the adiabatic case; that is, we shall neglect the effect of the motion of the molecule. The adiabatic assumption in Eq. (5) means neglecting $i\hbar\partial/\partial t$ as compared with H. In this case we obtain

$$i\hbar\dot{a}_2^* = (E_2 + v_2)a_2^* + \sum_i (H_{\alpha\beta}'' + H_r)_{2i} a_i^*, \quad (6)$$

where $\dot{a}_2^*$ is the time derivative of a_2^*, E_2 is the energy of the isolated molecule in state 2, v_2 is the eigenvalue of the diagonal part of $H_{\alpha\beta}$, and $H_{\alpha\beta}''$ is the remaining part of $H_{\alpha\beta}$. Turning to Heiseberg's representation

$$a_i^* = a_i \exp\left\{ -i\left(E_i t + \int^t v_i dt \right) \Big/ \hbar \right\}, \quad (7)$$

and neglecting all a_i except $a_1(=1)$ according to the initial condition, our equation becomes

$$i\hbar\dot{a}_2 = (H_{\alpha\beta}'' + H_r)_{21} \times \exp\left[i\left\{ (E_2 - E_1)t + \int^t (v_2 - v_1)dt \right\} \Big/ \hbar \right]. \quad (8)$$

If we neglect $H_{\alpha\beta}''$, the transition probability from 1 to 2 is obtained by integration to be

$$\mu_{21}^2 F^2 \left| \int^{\infty} \exp\left[i\left\{ (E_2 - E_1)t + \int^t (v_2 - v_1)dt \right\} \Big/ \hbar + i\omega t \right] dt \right|^2, \quad (9)$$

which is the fourier integral formula.

This procedure is generalized to include nondiagonal terms as follows. Taking the same basis as above, our Schroedinger equation in matrix form is

$$i\hbar\partial\mathbf{a}^*/\partial t = (\mathbf{H}_\alpha + \mathbf{H}_\beta + \mathbf{H}_{\alpha\beta} + \mathbf{H}_r)\mathbf{a}^*. \quad (10)$$

By a unitary transformation $\mathbf{T}$, $(\mathbf{H}_\alpha + \mathbf{H}_\beta + \mathbf{H}_{\alpha\beta})$ is diagonalized.

$$\mathbf{T}(\mathbf{H}_\alpha + \mathbf{H}_\beta + \mathbf{H}_{\alpha\beta})\mathbf{T}^{-1} = (V_i\delta_{ij}). \quad (11)$$

Transforming by $\mathbf{T}$, Eq. (10) becomes

$$i\hbar\mathbf{T}\partial\mathbf{a}/\partial t^*\mathbf{T}^{-1} = \mathbf{T}(\mathbf{H}_\alpha + \mathbf{H}_\beta + \mathbf{H}_{\alpha\beta} + \mathbf{H}_r)\mathbf{T}^{-1}\mathbf{T}\mathbf{a}^*\mathbf{T}^{-1} = \{(V_i\delta_{ij}) + \mathbf{T}\mathbf{H}_r\mathbf{T}^{-1}\}\mathbf{T}\mathbf{a}^*\mathbf{T}^{-1}. \quad (12)$$

Then, by a transformation analogous to Eq. (7), and neglecting $\partial\mathbf{T}/\partial t$ by the adiabatic assumption, we get

$$i\hbar\mathbf{T}\partial\mathbf{a}/\partial t\mathbf{T}^{-1} = \left\{ \exp\left(i\int^t V_i dt \Big/ \hbar \right)\delta_{ij} \right\}\mathbf{T}\mathbf{H}_r\mathbf{T}^{-1} \times \left\{ \exp\left(-i\int^t V_i dt \Big/ \hbar \right)\delta_{ij} \right\}\mathbf{T}\mathbf{a}\mathbf{T}^{-1}. \quad (13)$$

Finally, by the inverse transformation,

$$i\hbar\partial\mathbf{a}/\partial t = \mathbf{T}^{-1}\left\{ \exp\left(i\int^t V_i dt \Big/ \hbar \right)\delta_{ij} \right\}\mathbf{T}Fe^{i\omega t}\mu\mathbf{T}^{-1} \times \left\{ \exp\left(-i\int^t V_i dt \Big/ \hbar \right)\delta_{ij} \right\}\mathbf{T}\mathbf{a}. \quad (14)$$

When integrated this gives the generalized fourier integral formula.

[6] V. F. Weisskopf, Physik. Z. **34**, 1 (1933).
[7] E. Lindholm, Arkiv. Mat. Astron. Fysik. **32**, 17 (1945).
[8] H. M. Foley, Phys. Rev. **69**, 616 (1946).
[9] P. W. Anderson, Phys. Rev. **76**, 647 (1949).
[10] M. Mizushima, Phys. Rev. **74**, 705 (1946).
[11] M. Mizushima, J. Phys. Soc. Japan **4**, 191 (1949).
[12] M. Mizushima, Research Chem. Phys. **29**, 25 (1950).
[12a] That the term $i\hbar\partial/\partial t$ must be included in the right side of this equation was first pointed out by H. Margenau (private communication).

In cases where the intermolecular potential is so small that it can be taken into account by the second-order perturbation, the matrix $\mathbf{T}$ is approximated by the unit matrix. In this case

$$i\hbar\dot{a}_i = F\mu_{ij}\exp\left[i\left\{(E_i-E_j)t + \int^t (v_i'-v_j')dt\right\}\Big/\hbar + i\omega t\right]a_j, \quad (15)$$

where

$$V_i = E_i + v_i'.$$

By integration, Weisskopf's formula (2) is obtained.

Foley[8] has proved that Weisskopf's formula can be reduced to

$$I(\omega) = (c/\pi)[(A/\tau_0)/\{(\omega-\omega_0-B/\tau_0)^2+(A/\tau_0)^2\}], \quad (16)$$

where

$$A = \langle 1-\cos\alpha\rangle_{Av}, \quad B = \langle \sin\alpha\rangle_{Av}, \quad \alpha = \int(\Delta p/\hbar)dt,$$

and τ_0 is the mean time between collisions. His derivation of Eq. (16) is inadequate in that he replaced the sum of averages by the average of sums [Eqs. (14) and (15) in reference 8], although the recalculation with corrected order does not change the result essentially. Doing this, and avoiding the use of τ_0, we can easily obtain

$$I(\nu) = (c/\pi)[\Delta\nu/\{(\nu-\nu_0-\Delta\nu')^2+(\Delta\nu)^2\}], \quad (17)$$

which corresponds to Eq. (16), where

$$\Delta\nu = \int F(s)(1-\cos\alpha_s)ds/2\pi, \quad (18a)$$

$$\Delta\nu' = \int F(s)\sin\alpha_s ds/2\pi. \quad (18b)$$

and $F(s)ds$ is the number of collisions with collision parameters between s and $s+ds$ in unit time. In Eq. (17), $\Delta\nu$ is usually called the width parameter, and $\Delta\nu'$ gives the shift of intensity maximum by pressure.

In the case of an absorption line, to which the present consideration is limited, $F(s)ds$ can be obtained by the gas kinetic theory as

$$F(s)ds = 8\pi^{\frac{1}{2}}(m/2kT)^{\frac{3}{2}} \times \exp(-mV^2/2kT)V^3 dV\rho d\rho GN, \quad (19)$$

where m is the reduced mass, V is the relative velocity, ρ is the impact parameter of collision, G is the probability of the molecule being in a rotational state, and N is the number of molecules in unit volume. In Eq. (19), V and ρ are integrated from 0 to ∞, and G is summed over all states.

III. WELL-TYPE POTENTIAL AND THE LORENTZ FORMULA

If the intermolecular potential is such that

$$\Delta p = \gamma \text{ for } R<a, \quad \Delta p = 0 \text{ for } R>a, \quad (20)$$

then the integral α is

$$\alpha = 2(a^2-\rho^2)^{\frac{1}{2}}\gamma/(V\hbar). \quad (21)$$

Thus our formulas (18) give

$$\Delta\nu = \tfrac{1}{2}a^2\bar{V}N - 4\pi^{-\frac{1}{2}}\hbar^2(m/4kT)^{\frac{1}{2}}\int_0^\infty \varphi^{-3} \times\exp(-m/4kT\varphi^2)\{(a\varphi/2\gamma\hbar)\sin(2\gamma a\varphi/\hbar) +[\cos(2\gamma a\varphi/\hbar)-1]/4\gamma^2\}d\varphi, \quad (22a)$$

$$\Delta\nu' = 4\pi^{-\frac{1}{2}}\hbar^2(m/4kT)^{\frac{1}{2}}\int_0^\infty \varphi^{-3}\exp(-m/4kT\varphi^2) \times\{\sin(2\gamma a\varphi/\hbar)/4\gamma^2 -(a\varphi/2\gamma\hbar)\cos(2\gamma a\varphi/\hbar)\}d\varphi, \quad (22b)$$

respectively.

If the potential difference is so large that we may put $\gamma=\infty$, then we obtain Lorentz's formulas:

$$\Delta\nu = a^2\bar{V}N/2, \quad (23a)$$

$$\Delta\nu' = 0. \quad (23b)$$

Thus, we can make an interpretation of the so-called strong collision in the present theory.

V. INVERSE POWER POTENTIAL

There are many cases where Δp can be expressed as

$$\Delta p = \hbar\Delta\mu/R^n, \quad (24)$$

where R is the intermolecular distance. If the path of the molecule is straight, then by Eq. (16),

$$\alpha = \int_{-\infty}^{\infty}\Delta\mu/(\rho^2+V^2t^2)^{n/2}dt = (\Delta\mu/V\rho^{n-1})\pi\Gamma(n-1)2^{2-n}[\Gamma(n/2)]^{-2}. \quad (25)$$

Thus, our formulas which give the width and the shift of a spectral line become

$$\Delta\nu = (\pi^{(5-n)/(2n-2)}/2)(kT/2m)^{(3-n)/(2n-2)} \times\Gamma((2n-3)/(n-1))\Gamma((n-3)/(n-1)) \times[\Gamma(n-1)/\{\Gamma(n/2)\}^2]^{2/(n-1)} \times\sin\{\pi(n-3)/(2n-2)\}\langle|\Delta\mu|^{2/(n-1)}\rangle N, \quad (26a)$$

$$\Delta\nu' = \tan[\pi/(n-1)]\Delta\nu\langle\Delta\mu/|\Delta\mu|\rangle, \quad (26b)$$

where n must be larger than 2; otherwise they diverge.

For some special values of n, which we shall meet

later, these equations give

$$\Delta\nu=(\pi/2)\langle|\Delta\mu|\rangle N \text{ for } n=3, \quad (27a)$$

$$\Delta\nu=(2/\sqrt{3})\Gamma(7/4)(kT/M)^{1/4}\langle|\Delta\mu|^{\frac{1}{2}}\rangle N \text{ for } n=5, \quad (27b)$$

$$\Delta\nu=(\pi^{-1/10}/2)(kT/M)^{2/10}\Gamma(9/5)\Gamma(3/5)\times\{12/\Gamma(3)\}^{2/5}\sin(3\pi/10)\langle|\Delta\mu|^{2/5}\rangle N \text{ for } n=6, \quad (27c)$$

respectively. (In these formulas the real mass $M=2m$ is used.) The last formula agrees approximately with that of Lindholm.[7] We do not calculate the shift except for some simple cases.

If the sign of $\Delta\mu$ is common to all collisions, Eq. (26) gives Foley's relation[8]

$$|\Delta\nu'|/\Delta\nu=\tan[\pi/(n-1)]. \quad (28)$$

But in most cases of molecular spectra the above assumption does not hold, and Eq. (28) cannot be applied.

In the case of molecules, $\Delta\mu$ contains some factors which depend on angular variables. If the orientation of the molecule in space does not change in a collision, these factors may also vary with R. We shall neglect this effect throughout this paper; that is, we assume the orientation to change suitably in a collision.

VI. INVERSION SPECTRUM OF AMMONIA

There has been much theoretical and experimental work on this famous microwave absorption spectrum. The measurement of the width by Bleaney and Penrose[13] showed an interesting regularity, which we shall consider in this section. The theoretical calculation of the width was first attempted by the present author.[10,11] In these papers he succeeded in explaining Good's experimental result.[14] Margenau[15] showed by a simple calculation that the width parameter for each J, K line can be expressed by

$$\Delta\nu=34K/[J(J+1)]^{\frac{1}{2}} \text{ Mc/mm Hg}, \quad (29)$$

which agrees with the experimental result of Bleaney and Penrose. Anderson,[9] making an elaborate theoretical consideration, succeeded in explaining the relative width of these fine structure lines.

The vibrational ground state of the ammonia molecule splits into two states which are symmetric and antisymmetric with respect to the inversion. The wave functions of them are denoted by ψ_+ and ψ_-, respectively.[16]

In the two-molecule system there are four states, whose wave functions are $\psi_+(1)\psi_+(2)$, $\psi_-(1)\psi_-(2)$, $\psi_+(1)\psi_-(2)$, and $\psi_-(1)\psi_+(2)$. The rotational part may be taken into account by simply multiplying them by $\Theta_{J,K,M}(1)\Theta_{J',K',M'}(2)$, where Θ is the rotational wave function of the symmetric top rotator, and J, K, M are the rotational quantum numbers. Thus, our total wave function is

$$\begin{aligned}\Psi_{J,K,J',K'}&=\sum_{M,M'}a_{MM'}\psi_+(1)\Theta_{J,K,M}(1)\psi_+(2)\Theta_{J',K',M'}(2)\\&+\sum_{M,M'}b_{MM'}\psi_-(1)\Theta_{J,K,M}(1)\psi_-(2)\Theta_{J',K',M'}(2)\\&+\sum_{MM'}c_{MM'}\psi_+(1)\Theta_{J,K,M}(1)\psi_-(2)\Theta_{J',K',M'}(2)\\&+\sum_{M,M'}d_{MM'}\psi_-(1)\Theta_{J,K,M}(1)\psi_+(2)\Theta_{J',K',M'}(2). \quad (30)\end{aligned}$$

The main part of the intermolecular potential is the dipole-dipole interaction

$$H_{\alpha\beta}=\{\boldsymbol{\mu}_\alpha\cdot\boldsymbol{\mu}_\beta-3(\boldsymbol{\mu}_\alpha\cdot\mathbf{R})(\boldsymbol{\mu}_\beta\cdot\mathbf{R})/R^2\}/R^3. \quad (31)$$

Thus our matrix $\mathbf{H}_{\alpha\beta}$

$$\mathbf{H}_{\alpha\beta}=\begin{bmatrix}-\epsilon\mathbf{E} & \mathbf{A} & 0 & 0\\ \mathbf{A} & \epsilon\mathbf{E} & 0 & 0\\ 0 & 0 & 0 & \mathbf{A}\\ 0 & 0 & \mathbf{A} & 0\end{bmatrix}, \quad (32)$$

where ϵ is the energy difference of ψ_+ and ψ_- states of an isolated molecule and $\mathbf{A}$ is the matrix obtained by Margenau and Warren,[17]

$$\begin{aligned}&(M_jM_j'|A|M_iM_i')\\&=(\mu^2/R^3)\{KK'/[J(J+1)J'(J'+1)]\}\\&\times[-2M_iM_i'\delta(M_j,M_i)\delta(M_j',M_i')\\&\pm\tfrac{1}{2}\{(J-M_i+1)(J+M_i)(J'-M_i')(J'+M_i'+1)\}^{\frac{1}{2}}\\&\times\delta(M_j,M_i-1)\delta(M_j',M_i'+1)\\&\pm\tfrac{1}{2}\{(J+M_i+1)(J-M_i)(J'+M_i')(J'-M_i'+1)\}^{\frac{1}{2}}\\&\times\delta(M_j,M_i+1)\delta(M_j',M_i'-1)]. \quad (33)\end{aligned}$$

If $\mathbf{l}$ is a transformation matrix which diagonalizes $\mathbf{A}$, then $\mathbf{L}=\mathbf{l}+\mathbf{l}+\mathbf{l}+\mathbf{l}$ (direct sum) transforms our matrix (32) to

$$\mathbf{L}\mathbf{H}_{\alpha\beta}\mathbf{L}^{-1}=\begin{bmatrix}-\epsilon\mathbf{E} & (e_i\delta_{ij}) & 0 & 0\\ (e_i\delta_{ij}) & \epsilon\mathbf{E} & 0 & 0\\ 0 & 0 & 0 & (e_i\delta_{ij})\\ 0 & 0 & (e_i\delta_{ij}) & 0\end{bmatrix}, \quad (34)$$

which can be factorized easily. Thus it is shown that the following four-dimensional reduced matrix is sufficient for our calculation;

$${}_m\mathbf{H}_{\alpha\beta}=\begin{bmatrix}-\epsilon & e_m & 0 & 0\\ e_m & \epsilon & 0 & 0\\ 0 & 0 & 0 & e_m\\ 0 & 0 & e_m & 0\end{bmatrix}, \quad m=1,\cdots,(2J+1)(2J'+1). \quad (35)$$

[13] B. Bleaney and R. P. Penrose, Proc. Phys. Soc. (London) **59**, 424 (1947).
[14] W. Good, Phys. Rev. **70**, 213 (1946).
[15] H. Margenau, Phys. Rev. **76**, 121 (1949).
[16] G. Herzberg, *Infra-Red and Raman Spectra of Polyatomic Molecules* (D. Van Nostrand Company, Inc., New York, 1945).
[17] H. Margenau and D. J. Warren, Phys. Rev. **51**, 748 (1935).

The unitary matrix which diagonalizes this matrix is

$$ {}_m\mathbf{T}=\begin{pmatrix} a & -b & 0 & 0 \\ b & a & 0 & 0 \\ 0 & 0 & 2^{-\frac{1}{2}} & -2^{-\frac{1}{2}} \\ 0 & 0 & 2^{-\frac{1}{2}} & 2^{-\frac{1}{2}} \end{pmatrix}, \tag{36} $$

$$ a=\{(\epsilon^2+e_m^2)^{\frac{1}{2}}+\epsilon\}^{\frac{1}{2}}/(4\epsilon^2+4e_m^2)^{\frac{1}{4}}, $$

$$ b=\{(\epsilon^2+e_m^2)^{\frac{1}{2}}-\epsilon\}^{\frac{1}{2}}/(4\epsilon^2+4e_m^2)^{\frac{1}{4}}, $$

and[18]

$$ {}_m\mathbf{T}_m\mathbf{H}_{\alpha\beta m}\mathbf{T}^{-1}=\begin{pmatrix} -(\epsilon^2+e_m^2)^{\frac{1}{2}} & 0 & 0 & 0 \\ 0 & (\epsilon^2+e_m^2)^{\frac{1}{2}} & 0 & 0 \\ 0 & 0 & -e_m & 0 \\ 0 & 0 & 0 & e_m \end{pmatrix}. \tag{37} $$

From symmetry considerations, it is clear that

$$ \int \psi_+\mu\psi_+ d\tau=\int \psi_-\mu\psi_- d\tau=0, \tag{38} $$

and it was shown[19] that

$$ \int \psi_+\mu\psi_- d\tau=\mu^* \tag{39} $$

is the quantity obtained by the dielectric constant measurement as the dipole moment of this molecule. Thus our matrix $\mathfrak{y}$ is

$$ \mathfrak{y}=\mu^*\begin{pmatrix} 0 & 0 & 1 & 1 \\ 0 & 0 & 1 & 1 \\ 1 & 1 & 0 & 0 \\ 1 & 1 & 0 & 0 \end{pmatrix}. \tag{40} $$

From Eqs. (13), (36), (37), and (40), we obtain the following formula

$$ \begin{pmatrix} \dot{a}_1 \\ \dot{a}_2 \\ \dot{a}_3 \\ \dot{a}_4 \end{pmatrix}=\mu^* F e^{i\omega t}\begin{pmatrix} 0 & 0 & c^* & c^* \\ 0 & 0 & c^* & c^* \\ c & c & 0 & 0 \\ c & c & 0 & 0 \end{pmatrix}\begin{pmatrix} a_1 \\ a_2 \\ a_3 \\ a_4 \end{pmatrix}, \tag{41} $$

where

$$ c=\Big[\{(\epsilon^2+e_m^2)^{\frac{1}{2}}+\epsilon-e_m\} \times\exp\Big\{i\int^t([e_m+(\epsilon^2+e_m^2)^{\frac{1}{2}}]/\hbar)dt\Big\} +\{(\epsilon^2+e_m^2)^{\frac{1}{2}}-\epsilon+e_m\} \times\exp\Big\{i\int^t([e_m-(\epsilon^2+e_m^2)^{\frac{1}{2}}]/\hbar)dt\Big\}\Big]\Big/ (4\epsilon^2+4e_m^2)^{\frac{1}{4}}, $$

and c^* is the complex conjugate of c.

[18] This result was published independently by the present author (references 10 and 11) and Margenau [H. Margenau, Phys. Rev. 76, 1423 (1949)].

[19] M. Mizushima, J. Phys. Soc. Japan 4, 11 (1949).

Since e_m is an eigenvalue of the matrix (33), it is proportional to R^{-3}. Thus, when the intermolecular distance is smaller than some critical length, e_m is larger than ϵ. In this region, neglecting ϵ as compared with e_m, c can be approximated by

$$ c\simeq\exp\Big\{i\int^t(e_m-|e_m|)\hbar^{-1}dt\Big\}. \tag{42} $$

When the intermolecular distance is larger than this critical length, and accordingly $e_m<\epsilon$, the approximate expression for c is

$$ c\simeq\exp(i\epsilon t/\hbar). \tag{43} $$

Thus, we use

$$ c\simeq\exp\Big\{i\int^t(\epsilon+e_m-|e_m|)\hbar^{-1}dt\Big\} \tag{44} $$

as an approximation throughout these regions.

Putting

$$ e_m=\hbar\Delta\mu_m/R^3, \tag{45} $$

we obtain from Eq. (27a) the following formula for the width parameter

$$ \Delta\nu_1=(\pi/2)\langle|\Delta\mu_m|-\Delta\mu_m\rangle N. \tag{46} $$

Since Margenau and Warren[17] showed that $\langle\Delta\mu_m\rangle=0$,

$$ \Delta\nu_1=(\pi/2)\langle|\Delta\mu_m|\rangle N. \tag{47} $$

Assuming the gaussian distribution for $\Delta\mu_m$, the average may be calculated by using the root mean square of e_m given by Margenau and Warren.[17] Thus,

$$ \Delta\nu_1=(\pi/3)^{\frac{1}{2}}(\mu^{*2}/\hbar)\langle|K|/[J(J+1)]^{\frac{1}{2}}\rangle \times|K/[J(J+1)]^{\frac{1}{2}}|N. \tag{48} $$

Numerical calculations were made with $T=297°\mathrm{K}$ and $\mu^*=1.44\times10^{-18}$, and the result is

$$ \Delta\nu_1=39|K/[J(J+1)]^{\frac{1}{2}}|\ \mathrm{Mc/mm\ Hg}, \tag{49} $$

which is nearly the same as Margenau's result (29), although the method of calculation is very different.

Approximation (44) is not good at large distances, the actual intermolecular potential being much smaller when $\epsilon>e_m$. Thus, the next approximation is to cut the intermolecular potential at $R_c=(\hbar\Delta\mu_m/\epsilon)^{\frac{1}{3}}$. Using the same α as in the above calculation, but limiting the integration over ρ to $0-R_c$ instead of $0-\infty$, we easily obtain the following formula

$$ \Delta\nu_2=\Delta\nu_1-8(2\pi/3)^{\frac{1}{2}}(M/4kT)^{\frac{1}{2}}\epsilon^{\frac{1}{3}}\hbar^{-2} \times\mu^{*8/3}\langle|K/[J(J+1)]^{\frac{1}{2}}|^{4/3}\rangle \times|K/[J(J+1)]^{\frac{1}{2}}|^{4/3}N, \tag{50} $$

which, at 297°K, is

$$ \Delta\nu_2=39|K/[J(J+1)]^{\frac{1}{2}}| -13|K/[J(J+1)]^{\frac{1}{2}}|^{4/3}\ \mathrm{Mc/mm\ Hg}. \tag{51} $$

These formulas are plotted in Fig. 1 together with the experimental data of Bleaney and Penrose.[13] We see that our formula (51) agrees very well with experi-

ment at large values of $K/[J(J+1)]^{\frac{1}{2}}$. It is quite natural that the agreement is not so good for small values of $K/[J(J+1)]^{\frac{1}{2}}$, since in that region the second-order force, which is not considered in this paper, may contribute a great deal.

Howard and Smith[20] measured the width of the 3,3 line at 300°K and 195°K, and found that the width is larger at the lower temperature. The ratio of the widths at these two temperatures at constant pressure is 0.66 ± 0.03. Our theory predicts that

$$\Delta\nu_2=59.5|K/[J(J+1)]^{\frac{1}{2}}|-22|K/[J(J+1)]^{\frac{1}{2}}|^{4/3} \text{ Mc/mm Hg} \quad (52)$$

at 195°K. The ratio of Eq. (51) to Eq. (52) for the 3,3 line is 0.69, which agrees very well with the above experimental result.[21]

From $\langle\Delta\mu_m\rangle=0$ we can easily conclude that the shift of the line is zero.

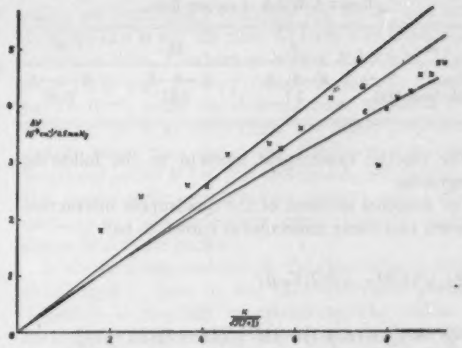

FIG. 1. Width parameters of ammonia inversion lines. ×, Bleaney and Penrose's experimental results (reference 13); a, Margenau's theoretical curve [Eq. (29)]; b, Eq. (49); c, Eq. (51).

VII. MAGNETIC ABSORPTION OF OXYGEN

Since the electronic ground state of oxygen is $^3\Sigma$, this molecule has a magnetic absorption in the microwave region, corresponding to transitions among the triplet levels. Beringer[22] observed this absorption first, and Van Vleck[23] made a theoretical consideration of it, taking the width as merely a parameter. Later, Strandberg *et al.*,[24] and Beringer and Castle[25] measured this absorption, but they could not succeed in separating the fine structure. Recently, Gordy *et al.*[26] have finally succeeded in observing the fine structure, and they have also observed the widths of some lines.[27]

In this molecule, the total angular momentum $\mathbf{J}$ is composed of the electronic spin angular momentum $\mathbf{S}$ ($|\mathbf{S}|=1$), and the ordinary rotational one $\mathbf{K}$. Thus, there are three states $J=K+1, K, K-1$ corresponding to one K, except for $K=0, 1$ states. The wave functions of these three states are obtained[28] as

$$\begin{pmatrix}\Psi_{K+1,M}\\ \Psi_{K,M}\\ \Psi_{K-1,M}\end{pmatrix}=\begin{pmatrix}\left\{\frac{(K+M)(K+M+1)}{2(2K+1)(K+1)}\right\}^{\frac{1}{2}} & \left\{\frac{(K-M+1)(K+M+1)}{(2K+1)(K+1)}\right\}^{\frac{1}{2}} & \left\{\frac{(K-M)(K-M+1)}{2(2K+1)(K+1)}\right\}^{\frac{1}{2}}\\ \left\{\frac{(K+M)(K-M+1)}{2K(K+1)}\right\}^{\frac{1}{2}} & \frac{M}{\{K(K+1)\}^{\frac{1}{2}}} & \left\{\frac{(K-M)(K+M+1)}{2K(K+1)}\right\}^{\frac{1}{2}}\\ \left\{\frac{(K-M)(K-M+1)}{2K(2K+1)}\right\}^{\frac{1}{2}} & \left\{\frac{(K-M)(K+M)}{K(2K+1)}\right\}^{\frac{1}{2}} & \left\{\frac{(K+M+1)(K+M)}{2K(2K+1)}\right\}^{\frac{1}{2}}\end{pmatrix}\begin{pmatrix}\Theta_{K,M-1}\sigma_1\\ \Theta_{K,M}\sigma_0\\ \Theta_{K,M+1}\sigma_{-1}\end{pmatrix}, \quad (53)$$

where $\Theta_{K,M}$ is the ordinary rotational wave function of a linear molecule with quantum numbers K, M; σ_m is the spin wave function, and m is its magnetic quantum number.

The energies of these three states were calculated by Kramers[29] and Schlapp;[30] but, according to Gordy *et al.*,[27] their theoretical results may be revised in some respects. Anyway, it is known that $J=K$ is the highest level, and the other two levels are a little lower and near to each other. The separations of these levels depend on K.

Magnetic absorption is allowed for $J=K-1\rightarrow K$ and $J=K+1\rightarrow K$ transitions, and thus there are two kinds of absorption lines.

There are no dipole forces between oxygen molecules. The contribution to the width by the London force seems to be small, since $K\pm1$ and K states have nearly common electronic states and the London force is nearly equal for these states.[30a] Of course, there is the magnetic dipole interaction between oxygen molecules, but this is found to be so small that it cannot explain the observed width. We shall try to calculate the width due

[20] R. Howard and W. V. Smith, Phys. Rev. **77**, 840 (1950).
[21] Anderson's theory (reference 9) could also explain the same experiment (reference 21). However, the agreement of the two theoretical results in this case is rather accidental. The temperature dependence of other lines may distinguish between these two theories.
[22] R. Beringer, Phys. Rev. **70**, 53 (1946).
[23] J. H. Van Vleck, Phys. Rev. **71**, 413 (1947).
[24] Strandberg, Meng, and Ingersoll, Phys. Rev. **75**, 1524 (1949).
[25] R. Beringer and J. G. Castle, Phys. Rev. **75**, 1963 (1949).
[26] Burkhalter, Anderson, Smith, and Gordy, Phys. Rev. **77**, 152 (1950).
[27] Burkhalter, Anderson, Smith, and Gordy, Phys. Rev. **79**, 651 (1950).
[28] See E. U. Condon and G. H. Shortley, *The Theory of Atomic Spectra* (Cambridge University Press, London, 1935), p. 76.
[29] H. A. Kamers, Z. Physik **53**, 422 (1929).
[30] R. Schlapp, Phys. Rev. **51**, 342 (1937).
[30a] The contribution by this force was estimated by H. Margenau (private communication).

TABLE I. Width of oxygen lines.

K	3	13	21
Species	$K-1\rightarrow K$	$K+1\rightarrow K$	$K-1\rightarrow K$
$\Delta\nu$ (Mc/mm Hg)	2.1	0.87	0.83

to the electric quadrupole moment in the following paragraphs.

The diagonal element of the quadrupole interaction between two linear molecules is known to be[21]

$$\int \Theta_{K,M^2}(1)\Theta_{K',M'^2}(2)V_{12}d\tau$$

$$=(6Q^2/R^5)[\{K(K+1)-3M^2\}/(2K+3)(2K-1)]$$

$$\times[\{K'(K'+1)-3M'^2\}/(2K'+3)(2K'-1)], \quad (54)$$

where Q is the quadrupole moment. Since it is suitably factored, we can calculate it separately for each molecule.

Using the wave functions (53), we can calculate the diagonal element of the quadrupole interaction between two oxygen molecules. The factor which comes from one molecule is

$$K\{(K+1)(K+2)-3M^2\}/\{(2K+1)(K+1)(2K+3)\} \quad \text{for } J=K+1, \quad (55a)$$

$$\{K(K+1)-3\}\{K(K+1)-3M^2\}/\{K(K+1)(2K+3)(2K-1)\} \quad \text{for } J=K, \quad (55b)$$

$$(K+1)\{K(K-1)-3M^2\}/\{K(2K+1)(2K-1)\} \quad \text{for } J=K-1. \quad (55c)$$

This interaction being proportional to R^{-5}, we use Eq. (27b) to calculate the width parameter, and thus the average of the square root of the potential difference is required. In calculating the mean value for the colliding molecules, all of Eqs. (55) may be replaced by a single expression

$$(K^2-3M^2)/4K^2, \quad (56)$$

since the mean K is very large at room temperature. The mean root of Eq. (56) is

$$(1/2K)^2\left\{\int_0^{K/\sqrt{3}}(K^2-3M^2)^{\frac{1}{2}}dM + \int_{K/\sqrt{3}}^{K}(3M^2-K^2)^{\frac{1}{2}}dM\right\}=0.254\cdots, \quad (57)$$

which does not depend on K. Thus,

$$\Delta\nu=(0.254)2^{\frac{1}{2}}\Gamma(7/4)(kT/M)^{\frac{1}{2}}Q\hbar^{-1}\langle|A|\rangle N, \quad (58)$$

where

$$A=(55a)-(55b) \quad \text{for } K+1\rightarrow K,$$
$$A=(55c)-(55b) \quad \text{for } K-1\rightarrow K.$$

[21] H. Margenau, Revs. Modern Phys. **11**, 1 (1939).

For simplicity, we shall limit our consideration here to the case of $M=M'$.

Gordy's experimental results[27] are shown in Table I. We see in this table that the width decreases as K increases and that the $K+1\rightarrow K$ line is a little broader than the $K-1\rightarrow K$ line.

For $K=3$, the calculation may be performed numerically, the results being

$$\Delta\nu=8.6\times10^{24}Q \text{ Mc/mm Hg} \quad \text{for } K+1\rightarrow K, \quad (59a)$$

$$\Delta\nu=8.4\times10^{24}Q \text{ Mc/mm Hg} \quad \text{for } K-1\rightarrow K, \quad (59b)$$

at room temperature.

In order to explain the experimental result of Gordy, Q must be 2.5×10^{-26}. Although there is no direct measurement of Q, we know that the experimental curve of Lassettre and Dean[32] for molecules with single bonds predicts for a fictitious molecule with a single bond of the same internuclear distance as oxygen, $Q=3.4\times10^{-26}$; and for the pressure absorption of this molecule, a somewhat lower value is required.[33] Thus our value of Q may be said to be of a plausible order.

For large K, expanding A in powers of $1/K$, we obtain

$$\Delta\nu=(1.84\times10^{25}Q/K^{\frac{1}{2}})[1-(3/8K)+\cdots] \quad \text{for } K+1\rightarrow K, \quad (60a)$$

$$\Delta\nu=(1.84\times10^{25}Q/K^{\frac{1}{2}})[1+(3/8K)+\cdots] \quad \text{for } K-1\rightarrow K. \quad (60b)$$

Thus we can see that the width parameter decrease as K increases, in agreement with the experimental result. In these formulas the coefficients of the second terms in parentheses are not certain, but they make the $K+1\rightarrow K$ line narrower than the $K-1\rightarrow K$ line. The calculated width parameters for the other two lines in the table are 1.24 and 1.00 Mc/mm Hg for the $13+1\rightarrow13$ and $21-1\rightarrow21$ lines, respectively, if $Q=2.5\times10^{-26}$. They are near to the experimental values, but too large.*

Recently, Beringer and Castle[34] have observed the magnetic resonance spectrum of oxygen, and measured the widths of some lines. Since in their case the transition is different from the kind discussed above, our theory cannot be applied directly.[34a] However, if their width is due to the electric quadrupole moment as is assumed in this paper, its temperature dependence may be predicted by Eq. (27b), that is,

$$\Delta\nu\propto T^{-\frac{1}{2}} \text{ at constant pressure.}$$

It is interesting that Beringer and Castle's experi-

[32] E. N. Lassettre and L. B. Dean, Jr., J. Chem. Phys. **17**, 317 (1949).

[33] M. Mizushima, Phys. Rev. **76**, 1268 (1949); **77**, 149 (1950).

* *Note added in proof:* Recently, R. S. Anderson, W. V. Smith, and W. Gordy have measured the width of fourteen lines from $K=1$ to 23 of oxygen. Their results for lines of K larger than 11 agree very well with our $K^{-\frac{1}{2}}$ formula (60). Their new data yield $Q=3.6\times10^{-26}$ (Anderson, Smith, and Gordy, private communication.)

[34] R. Beringer and J. G. Castle, Jr., Phys. Rev. **81**, 82 (1951).

[34a] H. Margenau has made some theoretical calculations on this case (private communication).

mental data at 300°K and 85°K lie midway between the T^{-1} and $T^{-\frac{1}{2}}$ dependences.

VII. THE ROTATIONAL ABSORPTION LINES OF LINEAR MOLECULES

There are many data on this kind of absorption line.[35] In this case, the London force need not be considered, since its contribution may be smaller than that of the dipole interaction. The matrix element of the dipole interaction (31) for a linear molecule is[31]

$$(JMJ'M'|V|jmj'm')$$
$$=(\mu^2/2R^3)\{A(-M)A(M')\delta_{m,M-1}\delta_{m',M'+1}$$
$$+A(M)A(-M')\delta_{m,M+1}\delta_{m',M'-1}$$
$$-2B(M)B(M')\delta_{m,M}\delta_{m',M'}\}.$$

where

$$A(\pm M)=\left[\frac{(J\pm M+2)(J\pm M+1)}{(2J+3)(2J+1)}\right]^{\frac{1}{2}}\delta_{j,J+1}$$
$$-\left[\frac{(J\mp M+1)(J\mp M)}{(2J+1)(2J-1)}\right]^{\frac{1}{2}}\delta_{j,J-1},$$
$$B(M)=\left[\frac{(J+M+1)(J-M+1)}{(2J+3)(2J+1)}\right]^{\frac{1}{2}}\delta_{j,J+1}$$
$$+\left[\frac{(J+M)(J-M)}{(2J+1)(2J-1)}\right]^{\frac{1}{2}}\delta_{j,J-1}. \quad (61)$$

London calculated the intermolecular potential by the second-order perturbation method.[31] If it were valid, we could easily calculate the width; but unfortunately this is not the case. At room temperature, the molecules with J values satisfying $\hbar^2J(J+1)/2I=kT\simeq3\times10^{-14}$ erg are most common; that is, $J_{max}\simeq30$ for $I=10^{-38}$, while the intermolecular potential μ^2/R^3 is about 10^{-14} at 5A. Thus, the latter potential is usually larger than the energy difference of successive rotational states $\hbar^2J/I$. For this reason, we cannot use the second-order perturbation theory; and, on the contrary, an approximation neglecting the diagonal elements may be better.

In the latter approximation, the eigenvalue is proportional to R^{-3}; thus, by Eq. (27a) the mean potential difference is required in calculating the width. By anticipating this, we take the root mean square of the matrix element over M and M' at the beginning, for simplicity. Then our matrix is

$$(JJ'|V|jj')=(2/3)^{\frac{1}{2}}(\mu^2/R^3)\{(2J+1)(2J'+1)\}^{-\frac{1}{2}}$$
$$\times\{(J+1)^{\frac{1}{2}}\delta_{j,J+1}+J^{\frac{1}{2}}\delta_{j,J-1}\}$$
$$\times\{(J'+1)^{\frac{1}{2}}\delta_{j',J'+1}+J'^{\frac{1}{2}}\delta_{j',J'-1}\}. \quad (62)$$

Since the rotational quantum number of the colliding molecule is usually very large, Eq. (62) may be approximated by

$$(JJ'|V|jj')=3^{-\frac{1}{2}}(\mu^2/R^3)(2J+1)^{-\frac{1}{2}}$$
$$\times\{(J+1)^{\frac{1}{2}}\delta_{j,J+1}+J^{\frac{1}{2}}\delta_{j,J-1}\}\{\delta_{j',J'+1}+\delta_{j',J'-1}\}. \quad (63)$$

It is convenient to take the basis of our matrix in the following order:

$$J=\quad 0 \qquad\qquad 1 \qquad\qquad 2$$
$$J'=\underbrace{\cdots l-1,\, l,\, l+1,\, \cdots}_{n}\ \underbrace{\cdots l-1,\, l,\, l+1,\, \cdots}_{n}\ \underbrace{\cdots l-1,\, l,\, l+1,\, \cdots}_{n}.$$

Then, it can easily be shown that a matrix

$$\mathbf{S}=\mathbf{s}+\mathbf{s}+\mathbf{s}+\cdots, \quad (64)$$

where $\mathbf{s}$ is a transformation matrix which diagonalizes the energy matrix of periodic potential problem, can transform our matrix (63) into the following form

$$\mathbf{V}=\mathbf{v}_1+\mathbf{v}_2+\cdots+\mathbf{v}_n, \quad (65)$$

where

$$\mathbf{v}_l=\frac{\mu^2}{R^3}\cos\frac{2l\pi}{n}\begin{pmatrix} 0 & 2(1/3)^{\frac{1}{2}} & 0 & 0 & \cdots & & \\ & 0 & 2(2/9)^{\frac{1}{2}} & 0 & \cdots & & \\ & & 0 & \cdots & \cdots & & \\ & & & \cdots & \cdots & & \\ & & & \cdots & \cdots & & \\ \text{symmetric} & & & & 0 & 2\{(J+1)/(6J+3)\}^{\frac{1}{2}} & \cdots \\ & & & & & 0 & \cdots \\ & & & & & & \cdots \end{pmatrix}, \quad (66)$$

In Eqs. (64) and (65), + means the direct sum.

[35] W. Gordy, Revs. Modern Phys. **20**, 668 (1948).

TABLE II. Width parameter of rotational lines (linear molecules).

Molecule	μ (Debye)	J	$\Delta\nu_{obs}$(Mc/mm Hg)	$\Delta\nu_{calc}$
ICl	0.65	0→1	3.2[a]	2.9
		3→4	5.5[b]	0.8
HCN	2.88	0→1	25[c]	50
ClCN	2.5	1→2	25[d]	21.5
BrCN	2.94	2→3	21[d]	20
ICN	3.71	3→4	20[d]	24
OCS	0.72	1→2	6[d]	2

[a] R. T. Weidner, Phys. Rev. **72**, 1268 (1947).
[b] Townes, Merritt, and Wright, Phys. Rev. **73**, 1334 (1948).
[c] Smith, Gordy, Simmons, and Smith, Phys. Rev. **75**, 260 (1949).
[d] Townes, Holden, and Merritt, Phys. Rev. **74**, 1113 (1948).

The eigenvalues of Eq. (66) may be approximated as follows. The eigenvector which corresponds to the lowest eigenvalue is

$$\left[1, 1, \left(\frac{3}{2}\right)^{\frac{1}{2}}, \left(\frac{2\cdot5}{3\cdot3}\right)^{\frac{1}{2}}, \cdots \left(\frac{1\cdot3\cdot5\cdots3\cdot7\cdot11\cdots}{2\cdot4\cdot6\cdots1\cdot5\cdot9\cdots}\right)^{\frac{1}{2}}, \times\left(\frac{2\cdot4\cdot6\cdots5\cdot9\cdot13\cdots}{3\cdot5\cdot7\cdots3\cdot7\cdot11\cdots}\right)^{\frac{1}{2}}, \cdots\right]. \quad (67)$$

Thus the lowest eigenvalue is

$$-\frac{4}{\sqrt{3}}\left(1+1+\frac{3}{2}+\frac{10}{9}+\cdots+\frac{1\cdot3\cdots3\cdot7\cdots}{2\cdot4\cdots1\cdot5\cdots}+\frac{2\cdot4\cdots5\cdot9\cdots}{3\cdot5\cdots3\cdot7\cdots}+\cdots\right)^{-1}\frac{\mu^2}{\nu R^3}\cos\frac{2l\pi}{n}, \quad (68)$$

where ν is the order of the matrix (66). Since

$$\lim_{\nu\to\infty}\frac{1\cdot3\cdots3\cdot7\cdots}{2\cdot4\cdots1\cdot5\cdots}=\prod^{\infty}\frac{(n-1/2)(n-1/4)}{n(n-3/4)}=\frac{\Gamma(1)\Gamma(7/4)}{\Gamma(3/2)\Gamma(5/4)}=1\cdot144\ldots,$$

$$\lim_{\nu\to\infty}\frac{2\cdot4\cdots5\cdot9\cdots}{3\cdot5\cdots3\cdot7\cdots}=\prod^{\infty}\frac{n(n+1/4)}{(n+1/2)(n-1/4)}=\frac{\Gamma(1/2)\Gamma(5/4)}{\Gamma(1)\Gamma(3/4)}=1.311\ldots,$$

Eq. (68) is

$$-1.88(\mu^2/R^3)\cos(2l\pi/n) \quad (69)$$

at the limit $\nu\to\infty$.

The next eigenvalue can be approximately obtained if we neglect the first row and column of Eq. (66) and follow the same procedure as above. Successively taking the same procedure, we obtain the following series as an approximation to the eigenvalues

$$-1.88a, -1.79a, -1.77a, -1.76a, \cdots \qquad a=(\mu^2/R^3)\cos(2l\pi/n). \quad (70)$$

In this approximation, the difference of the $(J-1)$th and Jth values is nearly $0.09/J^2$. In Eq. (70), the values are certainly too low except for the first,[36] so the first difference is too small. Moreover, we treated Eq. (66) as an infinite matrix, while actually it is of order about J^* if the rotational energy is of the same order of magnitude as the intermolecular perturbation at the rotational quantum number J^*. In the infinite matrix, the eigenvalue converges to $4a/6^{\frac{1}{2}}$, while in the finite matrix it tends to zero. From these two reasons, we may suppose that the difference of the $(J-1)$th and Jth eigenvalues is expressed by $0.2/J$.

The difference of the eigenvalues is small compared with the eigenvalue itself. If we can assume that all the eigenvalues are equal, the transformation by $\mathbf{T}$ in Eq. (13) can be omitted. In this case, our equation which determines the transition probability is

$$da_J/dt=\mu_{J,J-1}F\exp\left\{i\omega t-i\int^t(0.2\mu^2/(\hbar R^3 J))\times\cos(2l\pi/n)dt\right\}a_{J-1}. \quad (71)$$

Since the perturbation is proportional to R^{-3},

$$\Delta\nu=(\pi/2)\langle\{0.2\mu^2/(\hbar J)\}\cos(2l\pi/n)\rangle N=\{0.2\mu^2/(\hbar J)\}N \quad (72)$$

by Eq. (27a). This formula is compared with experiment in Table II. Although general agreement is seen, a serious discrepancy occurs in the 3→4 line of ICl, the reason for which is not clear. It is possible that our theory, which neglects the energy difference between rotational states in comparison with the intermolecular interaction, may not be suitable to treat such molecules as HCN which have very small moments of inertia.

VIII. ROTATIONAL ABSORPTION LINE OF SYMMETRIC TOP MOLECULES

The matrix of the dipole interaction for this case is the one already given by Eq. (33). Since the eigenvalue of this matrix is very difficult to obtain, we shall approximate it by the diagonal element.

From the selection rule $\Delta M=0, \pm1$, we see that the orientation of the molecule scarcely changes in the optical transition. Thus, the difference of the intermolecular potential, which is required in the calculation of the width of absorption line $J-1$, $K\to J, K$, is

$$\Delta p=2(\mu^2/R^3)\{KK'MM'/[J'(J'+1)]\}\times\{[J(J-1)]^{-1}-[J(J+1)]^{-1}\}\equiv\hbar\Delta\mu/R^3 \quad (73)$$

in our approximation. Since it is proportional to R^{-3}, the formula which gives the width is again Eq. (27a).

[36] R. Courant and D. Hilbert, *Methoden der mathematischen Physik I* (Verlag. Julius Springer, Berlin, 1931), p. 28.

TABLE III. Width parameter of rotational lines (symmetric top molecules).

Molecule	μ (Debye)	I_a/I_b	J	$\Delta\nu_{obs}$ (Mc/mm Hg)	$\lvert K\rvert$	$\Delta\nu_{calc}$
CHF_3	1.59	0.55	1→2	18[a]	1→1	23
					0→0	9
CH_3F	1.83	4.5	0→1	20[a]	0→0	23

[a] Gilliam, Edward, and Gordy, Phys. Rev. 75, 1015 (1949).

The rotational energy of a symmetric top molecule is

$$E=aJ(J+1)+bK^2,$$
$$a=\hbar^2/(2I_a),\quad b=\hbar^2\{(2I_c)^{-1}-(2I_a)^{-1}\},\tag{74}$$

where I_a and I_c are the principal moments of inertia of this molecule ($I_a=I_b$). In almost all molecules at room temperature, a and b are much smaller than kT. For this reason we can calculate the average of $|\Delta\mu|$ classically as

$$\langle|\Delta\mu|\rangle=(\mu^2/\hbar)|K/(J^2-1)|\,|a/b|\,|(1+b/a)^{\frac{1}{2}}-1|$$
$$=(\mu^2/\hbar)|K/(J^2-1)|$$
$$\times\{I_c/|I_a-I_c|\}\,|(I_a/I_c)^{\frac{1}{2}}-1|.\tag{75}$$

Thus the width parameter is

$$\Delta\nu=(\pi/2)(\mu^2/\hbar)|K/(J^2-1)|$$
$$\times\{I_c/|I_a-I_c|\}\,|(I_a/I_c)^{\frac{1}{2}}-1|N$$
$$\text{for } J-1,\ K\to J,\ K.\tag{76}$$

Another method is to use the root mean square of the eigenvalues. The corresponding eigenvalues of lower and upper states may not be so different for the usual collisions where J' is very large. In this case, the mean of the energy difference can be replaced by the difference of the mean. Using the root mean square and assuming the gaussian distribution, we have

$$\langle|\Delta\mu|\rangle=(8/3\pi)^{\frac{1}{2}}(\mu^2/\hbar)|K|$$
$$\times\{[J(J-1)]^{-\frac{1}{2}}-[J(J+1)]^{-\frac{1}{2}}\}$$
$$\times\{I_c/|I_a-I_c|\}\,|(I_a/I_c)^{\frac{1}{2}}-1|$$
$$\text{for } J-1,\ K\to J,\ K.\tag{77}$$

TABLE IV. Width parameter of rotational lines (symmetric top molecules).

Molecule	I_a/I_b	J	$\Delta\nu_{obs}$ (Mc/mm Hg)	μ_{calc} (Debye)	μ_{calc}
PF_3	0.56	1→2	16[a]	1.6	1.5
		2→3			
CF_3Cl	1.7	2→3	50[b]	3.0	0.5
		3→4			
$CHBr_3$	0.15	0→1	0.8[c]	0.34	0.7

[a] Gilliam, Edward, and Gordy, Phys. Rev. 75, 1015 (1949).
[b] D. K. Coles and R. H. Hughes, Phys. Rev. 76, 858 (1949).
[c] Kojima, Tsukada, and Hagiwara, private communication.

Although this result is formally different from Eq. (75), we can see that their numerical values are near.

Since the matrix **A** vanishes identically for $K=0$, we cannot use the above formula in this case. However we can use the preceding formula (72) because a symmetric top molecule with $K=0$ behaves like a linear molecule.

There are only a few experimental results with which we can compare our formula (76). In Table III, the line $J=1\to2$ of CHF_3 is composed of three lines corresponding to $K=1, 0, -1$, whose widths are separately shown in the table. If the splitting of these lines is much smaller than $\Delta\nu$, the width of the total line is about 15 Mc/mm Hg, which agrees with the experimental result.

There are some other results where the data are not so complete. In Table IV, the dipole moment is not known for all molecules, and J is not clearly cited in the original papers for two molecules. In the fifth column μ is estimated from the width by our formulas, and in the last column the same quantity is estimated from the other methods such as bond dipole moment or electronegativity scale. The very large value of $\Delta\nu$ for CF_3Cl may be due to the unresolved splitting of the components. Since Coles and Hughes observed the width at 0.1 mm Hg, the K splitting of about 2 Mc may be able to account for this large $\Delta\nu$.

The author wishes to extend his thanks to Professor M. Kotani and the members of his laboratory for their advice and criticism. It is also his great pleasure to express his gratitude to Professor H. Margenau for his interest and kind advice, and to Professor W. Gordy for his kind communications.

The Third Spectrum of Copper (CuIII)

A. G. SHENSTONE AND L. WILETS*
Princeton University, Princeton, New Jersey
(Received October 27, 1950)

An analysis of the second spark spectrum of copper is given. The identified levels include all those due to $3d^9$, $3d^84s$, $3d^84p$ except the ^2S and ^2P based on $3d^8\,{}^1S$. The six levels $3d^9(^2F)5s\ {}^4F$, ^2F have been found and allow the calculation of an I. P. of 37.08 volts. A number of levels of $3d^84d$ are present also, but $3d^74s^2$, which should be lower, has not been found.

A PARTIAL analysis of the second spark spectrum of copper (CuIII) was made by Gibbs and Vieweg in 1929. It was published in abstract only,[1] but the details were communicated to one of us in 1932. Nothing more was done until the fall of 1949, when it seemed to us that the analysis should be completed before the *Atomic Energy States*, which is being published by the Bureau of Standards, had reached that point in the periodic table.

Two other partial analyses of CuIII have been published. With the first of these, made by Rao,[2] the present analysis is in complete disagreement. The second analysis, put forward tentatively by L. and E. Bloch,[3] classified a number of lines correctly and identified several significant differences. An unfortunate error in the difference between the leading levels of the low ^4F led the authors astray, so that the analysis is, on the whole, incorrect.

TABLE I. Even levels of CuIII.

$3d^9$	$a^2D_{5/2}$	0.0
$3d^9$	$a^2D_{3/2}$	2071.8
$3d^9(^2F_{7/2})4s$	$a^4F_{9/2}$	60804.9
$(^2F_{7/2})4s$	$a^4F_{7/2}$	62065.0
$(^2F_{7/2})4s$	$a^4F_{5/2}$	63143.6
$(^2F_{5/2})4s$	$a^4F_{3/2}$	63886.3
$(^2F_{5/2})4s$	$a^2F_{5/2}$	67016.6
$(^2F_{5/2})4s$	$a^2F_{7/2}$	68963.6
$(^1D)4s$	$b^2D_{3/2}$	77967.6
$(^1D)4s$	$b^2D_{5/2}$	78779.4
$(^2P)4s$	$a^4P_{1/2}$	80305.2
$(^2P)4s$	$a^4P_{5/2}$	80422.8
$(^2P)4s$	$a^4P_{3/2}$	80551.5
$(^2P)4s$	$a^2P_{1/2}$	85446.4
$(^2P)4s$	$a^2P_{3/2}$	86133.0
$(^1G)4s$	$a^2G_{7/2}$	89017.7
$(^1G)4s$	$a^2G_{9/2}$	89045.9
$(^2F_{7/2})5s$	$e^4F_{9/2}$	193369.0
$(^2F)4d$	1	193519.2
$(^2F)4d$	3	194031.6
$(^2F_{7/2})5s$	$e^4F_{7/2}$	194115.6
$(^2F)4d$	$e^4G_{5/2}$	194330.8
$(^2F)4d$	4	195060.4
$(^2F)4d$	5	195342.2
$(^2F)4d$	6	195516.9
$(^2F_{5/2})5s$	$e^4F_{5/2}$	195553.2
$(^2F_{5/2})5s$	$e^2F_{5/2}$	195787.1
$(^2F_{5/2})5s$	$e^4F_{3/2}$	196444.9
$(^2F)4d$	7	196740.2?
$(^2F)4d$	8	197053.9
$(^2F)4d$	$f^2F_{5/2}$	197373.9
$(^2F_{5/2})5s$	$e^2F_{7/2}$	197398.4
$(^2F)4d$	9	197898.7
$(^2F)4d$	10	198299.4
$3d^8\,{}^3F_4$	(Limit)	299145

Our nearly complete analysis is based on new observations throughout the spectrum, and all of the lines of any appreciable intensity are now accounted for. The great majority of the lines fall between λ2000 and λ1500, although there is a very strong and important group extending from λ829 to λ672, comprising all the combinations of the lowest term $3d^9\ {}^2D$. The spectrum photographs in the vacuum region were taken with our 2-meter 30,000-line per inch grating. The source was a condensed spark between copper electrodes about 5 mm apart in an atmosphere of pure helium at about 60-cm pressure. The gas was allowed to stream through the slit into the spectrograph where the pressure was about 4 mm. The grating is permanently adjusted with its normal at λ1500 and the source was placed so as to give a stigmatic image at about λ1000. The lines then showed, over the whole plate, sufficient stigmatism to allow a definite differentiation of the various stages of ionization. Arc lines hardly appeared at all; first spark lines were strong in the middle and tapered towards the ends; second spark lines were slightly polar and third spark lines were very polar. The times of exposure varied from 30 seconds to 45 minutes, making possible accurate measurement of all but the weakest lines. The standards of wavelength included the lines of copper,[4] nitrogen, oxygen, and carbon in various stages of ionization.[5] Although the spectrum CuII provides excellent standards when excited in the hollow cathode discharge, this is by no means true when the lines emanate from a spark. Only those lines which are due to transitions from intermediate levels to low levels maintain their positions, the others being displaced by several wave numbers towards longer wavelengths. In addition to the grating observations, a few lines of longer wavelength were measured on plates taken with a Hilger *E*-1 quartz instrument. The list of lines, Table IV, includes all identified and unidentified lines of reasonable intensity.

A discussion of the analysis of CuIII necessitates a

* AEC Predoctoral Fellow.
[1] R. C. Gibbs and A. M. Vieweg, Phys. Rev. **33**, 1092(A) (1929).
[2] B. V. R. Rao, Z. Physik **88**, 135 (1934).
[3] L. and E. Bloch, Compt. rend. **200**, 2017 (1935).
[4] A. G. Shenstone, Trans. Roy. Soc. (London) **235**, 195 (1936).
[5] J. C. Boyce and H. A. Robinson, J. Opt. Soc. Am. **26**, 653 (1936).

comparison with the iso-electronic spectra CoI[6] and NiII.[7] In this comparison, the following relation was used extensively. If the positions of the levels of a given configuration are plotted as ordinates, the successive ions being displaced by equal intervals on the axis of abscissas, then the points for a given level lie very nearly on a straight line. In the analysis of CuIII this relation was of very great assistance. It failed only in those cases where the additional configurations present in CoI complicate and perturb that spectrum. In such cases, the relation was indeed used to rectify a few of the assignments of configuration in CoI itself.

TABLE II. Odd levels of CuIII.

$3d^8(^3F)4p$	$z^4D_{3\frac{1}{2}}$	118864.3
$3d^8(^3F)4p$	$z^4D_{2\frac{1}{2}}$	120577.5
$3d^8(^3F)4p$	$z^4G_{4\frac{1}{2}}$	121337.2
$3d^8(^3F)4p$	$z^4G_{3\frac{1}{2}}$	121698.5
$3d^8(^3F)4p$	$z^4D_{1\frac{1}{2}}$	121863.7
$3d^8(^3F)4p$	$z^4G_{2\frac{1}{2}}$	122503.6
$3d^8(^3F)4p$	$z^4D_{\frac{1}{2}}$	122637.2
$3d^8(^3F)4p$	$z^4G_{2\frac{1}{2}}$	123440.2
$3d^8(^3F)4p$	$z^4F_{4\frac{1}{2}}$	123549.9
$3d^8(^3F)4p$	$z^2G_{4\frac{1}{2}}$	124442.5
$3d^8(^3F)4p$	$z^4F_{3\frac{1}{2}}$	124557.5
$3d^8(^3F)4p$	$z^4F_{2\frac{1}{2}}$	125381.8
$3d^8(^3F)4p$	$z^4F_{1\frac{1}{2}}$	125744.6
$3d^8(^1F)4p$	$z^2G_{3\frac{1}{2}}$	126093.8
$3d^8(^3F)4p$	$z^2F_{3\frac{1}{2}}$	126829.4
$3d^8(^3F)4p$	$z^2D_{2\frac{1}{2}}$	126891.9
$3d^8(^3F)4p$	$z^2D_{1\frac{1}{2}}$	128435.3
$3d^8(^3F)4p$	$z^2F_{2\frac{1}{2}}$	128679.4
$(^3P)4p$	$z^4P_{1\frac{1}{2}}$	136482.9
$(^3P)4p$	$z^4P_{2\frac{1}{2}}$	136607.3
$(^3P)4p$	$z^4P_{\frac{1}{2}}$	137041.0
$(^1D)4p$	$y^2F_{2\frac{1}{2}}$	138084.0
$(^1D)4p$	$y^2F_{3\frac{1}{2}}$	138982.0
$(^1D)4p$	$y^2D_{1\frac{1}{2}}$	138988.1
$(^1D)4p$	$z^2P_{\frac{1}{2}}$	139260.7
$(^1D)4p$	$y^2D_{2\frac{1}{2}}$	139756.6
$(^1D)4p$	$z^2P_{1\frac{1}{2}}$	140200.9
$(^3P)4p$	$y^4D_{2\frac{1}{2}}$	142426.3
$(^3P)4p$	$y^4D_{1\frac{1}{2}}$	142512.3
$(^3P)4p$	$y^4D_{\frac{1}{2}}$	142550.1
$(^3P)4p$	$y^4D_{3\frac{1}{2}}$	142819.7
$(^3P)4p$	$z^2D_{2\frac{1}{2}}$	144194.2
$(^3P)4p$	$z^2D_{1\frac{1}{2}}$	144875.2
$(^3P)4p$	$y^2P_{1\frac{1}{2}}$	145353.0
$(^1G)4p$	$z^2H_{4\frac{1}{2}}$	146533.6
$(^3P)4p$	$y^2P_{\frac{1}{2}}$	146675.9
$(^1G)4p$	$z^2H_{5\frac{1}{2}}$	147647.0
$(^3P)4p$	$z^2S_{\frac{1}{2}}$	147652.5
$(^1G)4p$	$x^2F_{3\frac{1}{2}}$	147805.9
$(^3P)4p$	$z^4S_{1\frac{1}{2}}$	147816.4
$(^1G)4p$	$x^2F_{2\frac{1}{2}}$	148662.9
$(^1G)4p$	$y^2G_{3\frac{1}{2}}$	153609.2
$(^1G)4p$	$y^2G_{4\frac{1}{2}}$	153808.4

The levels of CuIII are given in Tables I and II. The configurations represented in whole or part are $3d^9$, $3d^84s$, $3d^84p$, $3d^85s$, $3d^84d$, the last two being fragmentary. Those structures account for every strong line observed in the spectrum.

The multiplets due to the transition $3d^8(^3F)4s - 3d^8(^3F)4p$ were found by Vieweg, and the levels appear in our analysis with small numerical corrections. The only alteration in identification is the interchange

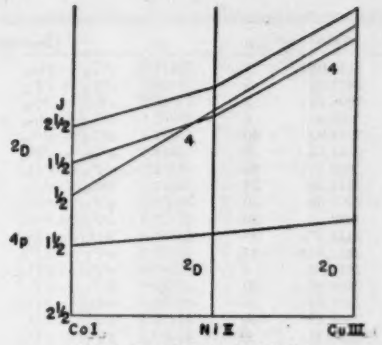

FIG. 1. ^4P and ^2D levels of $3d^84p$.

of $^2D_{1\frac{1}{2}}$ and $^2F_{2\frac{1}{2}}$ in the odd structure. The low levels a^4F and a^2F are excellent examples of the rule given above. They plot as very nearly straight lines in the iso-electronic sequence. The terms z^4D, z^4F, z^4G also show the same behavior. In the z^4G, even a crossing of the straight lines occurs.

The even structure $3d^84s$ is complete except for the usual failure to find $3d^8(^1S)4s^2S$. A plot of this configuration in CoI, NiII, CuIII gives excellent correlation when one uses the assignment of terms in CoI given by G. Racah.[8] He shows conclusively that b^4P and not a^4P belongs to this configuration. The plot shows that a^2P in CoI is probably displaced towards lower values by its proximity to b^2P.

A difficulty arises when one tries to give names to the individual levels which comprise the group ^4P and ^2D. These five levels are shown in Fig. 1, in which the lowest has been taken as zero of ordinates in each case. In CoI there is little doubt that the lowest three levels are mainly of character ^4P and the upper two of character ^2D. In NiII which was analyzed previously to CoI, the upper three were chosen as ^4P. In point of fact, these levels share their characteristics to such an extent in both NiII and CuIII that there is very little evidence on which to make a choice. Such evidence as there is in CuIII, however, makes it more reasonable to select the higher levels as ^4P and the lower as ^2D as in NiII. Racah has done a rough calculation for us of the percentages of ^2D and ^4P character in the individual levels. His results indicate quite definitely that the

TABLE III. Reassignment of terms in CoI.

Term	Assignment Russell	Assignment Proposed
y^2H	$d^7s(^3H)4p$	$d^8(^1G)4p$
x^2H	$d^8(^1G)4p$	$d^7s(^3H)4p$
$y^2S_{\frac{1}{2}}$	$d^8(^1P)4p$	?
$w^2S_{\frac{1}{2}}$	?	$d^8(^3P)4p$
$y^4S_{1\frac{1}{2}}$	$d^8(^3P)4p$	$d^8(^3P)4p^2P_{1\frac{1}{2}}$
$x^4S_{1\frac{1}{2}}$	$d^7s(^3P)4p$	$d^8(^3P)4p$
y^4P	$d^8(^3P)4p$	$d^7s(^3P)4p$
x^4P	$d^7s(^3P)4p$	$d^8(^3P)4p$

[6] Russell, King, and Moore, Phys. Rev. **58**, 407 (1940).
[7] A. G. Shenstone, Trans. Roy. Soc. (London) **30**, 255 (1927).
[8] G. Racah, Phys. Rev. **61**, 537 (1942).

TABLE IV. Lines of CuIII.

λ(Air)	Int.	ν	Classification
2822.05	1	35424.8	$a^3G_{4\frac{1}{2}} - z^3G_{4\frac{1}{2}}$
2812.96	5	35539.3	$a^3G_{4\frac{1}{2}} - z^1F_{3\frac{1}{2}}$
2698.46	3	37047.2	$a^3G_{3\frac{1}{2}} - z^3G_{3\frac{1}{2}}$
2696.39	6	37075.7	$a^3G_{4\frac{1}{2}} - z^3G_{3\frac{1}{2}}$
2643.92	40	37811.4	$a^3G_{4\frac{1}{2}} - z^3F_{3\frac{1}{2}}$
2641.54	8	37845.4	$a^3G_{3\frac{1}{2}} - z^3D_{2\frac{1}{2}}$
2609.31	50	38312.9	$a^1P_{2\frac{1}{2}} - z^1D_{2\frac{1}{2}}$
2522.36	25	39633.4	$a^3G_{3\frac{1}{2}} - z^3F_{2\frac{1}{2}}$
2497.58	20	40026.0	$a^1P_{2\frac{1}{2}} - z^1D_{2\frac{1}{2}}$
2482.34	30	40272.3	$a^1P_{1\frac{1}{2}} - z^1D_{2\frac{1}{2}}$
2438.47	25	40896.9	$b^3D_{2\frac{1}{2}} - z^3D_{2\frac{1}{2}}$
2412.32	15	41441.2	$a^1P_{\frac{1}{2}} - z^1D_{1\frac{1}{2}}$
2412.08	4	41445.4	$a^3P_{1\frac{1}{2}} - z^3D_{2\frac{1}{2}}$
2405.49	20	41558.9	$a^1P_{1\frac{1}{2}} - z^1D_{1\frac{1}{2}}$
2391.73	10	41798.0	$b^3D_{1\frac{1}{2}} - z^1D_{2\frac{1}{2}}$
2368.15	20	42214.1	$a^1P_{\frac{1}{2}} - z^1D_{\frac{1}{2}}$
2363.21	8	42302.3	$a^3P_{\frac{1}{2}} - z^3D_{1\frac{1}{2}}$
2361.56	10	42331.9	$a^1P_{1\frac{1}{2}} - z^1D_{\frac{1}{2}}$
2346.17	40	42609.5	$b^3D_{2\frac{1}{2}} - z^1D_{2\frac{1}{2}}$
2325.48	0	42988.6	$a^3P_{1\frac{1}{2}} - z^3D_{1\frac{1}{2}}$
2320.28	8	43084.9	$b^3D_{1\frac{1}{2}} - z^1D_{1\frac{1}{2}}$
2315.10	4	43181.3	
2312.31	5	43233.5	$a^3P_{1\frac{1}{2}} - z^3F_{2\frac{1}{2}}$
2279.45	2	43856.6	$b^3D_{1\frac{1}{2}} - z^1D_{\frac{1}{2}}$
2279.13	1	43862.8	
2277.43	4	43895.5	$b^3D_{2\frac{1}{2}} - z^1D_{1\frac{1}{2}}$
2271.69	5	44006.4	$a^1P_{2\frac{1}{2}} - z^1F_{3\frac{1}{2}}$
2128.59	0	46964.5	$b^3D_{1\frac{1}{2}} - z^1F_{1\frac{1}{2}}$
2077.81	2	48112.1	$b^3D_{1\frac{1}{2}} - z^3D_{2\frac{1}{2}}$
2077.07	0	48129.4	$a^1P_{1\frac{1}{2}} - z^3D_{1\frac{1}{2}}$
2043.37	5	48923.7	$b^3D_{2\frac{1}{2}} - z^3D_{2\frac{1}{2}}$
2000.78	3	49964.1	$a^3G_{4\frac{1}{2}} - y^3F_{3\frac{1}{2}}$

λ(Vac.)	Int.	ν	Classification
1928.715	2	51848.0	$a^3F_{3\frac{1}{2}} - z^1D_{2\frac{1}{2}}$
1920.653	1	52065.6	
1882.250	2	53127.9	$a^3P_{\frac{1}{2}} - z^3P_{\frac{1}{2}}$
1867.747	50	53540.4	$a^3F_{2\frac{1}{2}} - z^1G_{3\frac{1}{2}}$
1858.685	1	53801.5	$a^3G_{4\frac{1}{2}} - y^1D_{3\frac{1}{2}}$
1840.917	200	54320.8	$a^3F_{3\frac{1}{2}} - z^1G_{4\frac{1}{2}}$
1826.339	10	54754.3	$a^3P_{1\frac{1}{2}} - z^3P_{1\frac{1}{2}}$
1820.339	5	54934.8	
1798.761	5	55593.8	$a^3F_{2\frac{1}{2}} - z^1F_{3\frac{1}{2}}$
1787.902	1	55931.5	$a^1P_{2\frac{1}{2}} - z^1P_{1\frac{1}{2}}$
1783.935	5	56055.9	$a^1P_{2\frac{1}{2}} - z^1P_{2\frac{1}{2}}$
1783.799	20	56060.1	$a^1P_{\frac{1}{2}} - z^1P_{1\frac{1}{2}}$
1780.062	5	56177.8	$a^1P_{1\frac{1}{2}} - z^1P_{1\frac{1}{2}}$
1776.136	20	56302.0	$a^1P_{1\frac{1}{2}} - z^1P_{2\frac{1}{2}}$
1773.697	1	56379.4	$a^3P_{\frac{1}{2}} - y^1D_{1\frac{1}{2}}$
1772.478	2	56418.2	$a^3F_{2\frac{1}{2}} - z^1F_{2\frac{1}{2}}$ and $a^3P_{\frac{1}{2}} - y^1D_{\frac{1}{2}}$
1768.869	200	56533.3	$a^3F_{3\frac{1}{2}} - z^1F_{4\frac{1}{2}}$
1766.219	2	56618.1	$a^1P_{\frac{1}{2}} - z^1P_{\frac{1}{2}}$
1763.935	0	56691.4	$a^1F_{1\frac{1}{2}} - z^1D_{2\frac{1}{2}}$
1762.557	30	56735.8	$a^1P_{1\frac{1}{2}} - z^1P_{\frac{1}{2}}$
1761.155	20	56781.9	$a^3F_{2\frac{1}{2}} - z^1F_{1\frac{1}{2}}$
1760.586	10	56799.3	$a^1F_{2\frac{1}{2}} - z^1D_{2\frac{1}{2}}$
1755.012	20	56979.7	$a^3P_{1\frac{1}{2}} - y^1D_{2\frac{1}{2}}$
1750.391	500	57130.1	$a^3F_{2\frac{1}{2}} - z^3G_{3\frac{1}{2}}$
1741.378	500*d*?	57425.8	$a^3F_{3\frac{1}{2}} - z^3G_{4\frac{1}{2}}$
1741.135	30	57433.8	$a^1F_{3\frac{1}{2}} - z^1D_{2\frac{1}{2}}$
1739.508	300	57487.5	$a^3G_{3\frac{1}{2}} - z^3H_{4\frac{1}{2}}$
1738.648	10	57516.0	$a^3G_{4\frac{1}{2}} - z^3H_{4\frac{1}{2}}$
1738.145	30	57532.6	$a^1P_{2\frac{1}{2}} - y^3F_{2\frac{1}{2}}$
1737.893	30	57540.9	$a^3F_{3\frac{1}{2}} - z^1F_{3\frac{1}{2}}$
1732.998	5	57703.5	$b^3D_{1\frac{1}{2}} - z^1P_{1\frac{1}{2}}$
1728.139	200	57865.7	$a^3F_{2\frac{1}{2}} - z^3F_{2\frac{1}{2}}$
1726.275	5	57928.2	$a^3F_{2\frac{1}{2}} - z^3D_{2\frac{1}{2}}$
1724.810	10	57977.4	$a^1F_{1\frac{1}{2}} - z^1D_{1\frac{1}{2}}$
1722.379	1000	58059.2	$a^1F_{4\frac{1}{2}} - z^1D_{3\frac{1}{2}}$
1717.134	5	58236.6	
1716.400	10	58261.5	$b^3D_{1\frac{1}{2}} - z^1P_{\frac{1}{2}}$
1716.189	1	58268.6	
1713.346	5	58365.3	$a^3F_{3\frac{1}{2}} - z^1F_{2\frac{1}{2}}$
1711.437	30	58430.4	$a^1P_{2\frac{1}{2}} - y^3F_{3\frac{1}{2}}$
1711.257	30	58436.6	$a^1P_{2\frac{1}{2}} - y^3D_{1\frac{1}{2}}$
1709.036	700	58512.5	$a^1F_{3\frac{1}{2}} - z^1D_{2\frac{1}{2}}$
1708.958	200	58515.2	$b^3D_{2\frac{1}{2}} - z^1P_{1\frac{1}{2}}$
1707.500	5	58565.2	$a^1P_{\frac{1}{2}} - y^3D_{1\frac{1}{2}}$
1705.633	400	58629.3	$a^3G_{4\frac{1}{2}} - z^3H_{5\frac{1}{2}}$
1705.333	300	58639.6	$b^3D_{2\frac{1}{2}} - z^1P_{2\frac{1}{2}}$
1704.072	10	58683.0	$a^1P_{1\frac{1}{2}} - y^3D_{1\frac{1}{2}}$
1702.994	500	58720.1	$a^1F_{2\frac{1}{2}} - z^1D_{1\frac{1}{2}}$
1702.349	30	58742.4	$a^3P_{\frac{1}{2}} - z^3D_{1\frac{1}{2}}$
1702.190	300	58747.8	$a^3P_{1\frac{1}{2}} - z^3D_{2\frac{1}{2}}$
1702.102	400	58750.9	$a^1F_{1\frac{1}{2}} - z^1D_{\frac{1}{2}}$
1701.023	400	58788.2	$a^3G_{4\frac{1}{2}} - z^3F_{3\frac{1}{2}}$
1699.581	0	58838.0	$a^1P_{\frac{1}{2}} - z^3P_{\frac{1}{2}}$
1696.202	15	58955.2	$a^1P_{1\frac{1}{2}} - z^3P_{\frac{1}{2}}$
1692.706	300	59077.0	$a^3F_{3\frac{1}{2}} - z^3G_{3\frac{1}{2}}$
1689.051	200	59204.8	$a^1P_{2\frac{1}{2}} - y^3D_{2\frac{1}{2}}$
1688.618	100	59220.0	$a^3P_{\frac{1}{2}} - y^3P_{1\frac{1}{2}}$
1687.134	600	59272.1	$a^1F_{3\frac{1}{2}} - z^1G_{4\frac{1}{2}}$
1686.214	300	59304.5	$b^3D_{1\frac{1}{2}} - y^3F_{2\frac{1}{2}}$
1684.642	500	59359.8	$a^1F_{2\frac{1}{2}} - z^1G_{3\frac{1}{2}}$
1682.695	30	59428.5	$a^3P_{1\frac{1}{2}} - z^3D_{1\frac{1}{2}}$
1682.044	10	59451.5	$a^1P_{1\frac{1}{2}} - y^3D_{2\frac{1}{2}}$
1681.481	300	59471.4	$a^3F_{3\frac{1}{2}} - z^3D_{1\frac{1}{2}}$
1679.151	400	59553.9	$a^1F_{4\frac{1}{2}} - z^1G_{5\frac{1}{2}}$
1677.373	200	59617.0	$a^3G_{3\frac{1}{2}} - z^3F_{2\frac{1}{2}}$
1676.469	15	59649.2	$a^1P_{2\frac{1}{2}} - z^3P_{1\frac{1}{2}}$
1674.602	500	59715.7	$a^3F_{2\frac{1}{2}} - z^3F_{2\frac{1}{2}}$
1671.886	500	59812.7	$a^3F_{3\frac{1}{2}} - z^3F_{3\frac{1}{2}}$
1670.140	500	59875.2	$a^3F_{3\frac{1}{2}} - z^3D_{2\frac{1}{2}}$
1669.273	10	59906.3	$a^3P_{1\frac{1}{2}} - y^3P_{1\frac{1}{2}}$
1660.887	30	60208.8	$b^3D_{1\frac{1}{2}} - y^3D_{1\frac{1}{2}}$
1658.472	200	60296.5	$a^1F_{3\frac{1}{2}} - z^1G_{3\frac{1}{2}}$
1654.574	300	60438.5	$a^1F_{3\frac{1}{2}} - z^1G_{3\frac{1}{2}}$
1653.399	10	60481.5	$b^3D_{1\frac{1}{2}} - z^3P_{\frac{1}{2}}$
1652.010	300	60532.3	$a^1F_{4\frac{1}{2}} - z^1G_{4\frac{1}{2}}$
1651.758	15	60541.6	$a^3P_{\frac{1}{2}} - y^3P_{\frac{1}{2}}$
1642.208	2000	60893.6	$a^1F_{4\frac{1}{2}} - z^1G_{4\frac{1}{2}}$
1639.960	10	60977.1	$b^3D_{1\frac{1}{2}} - y^3D_{2\frac{1}{2}}$
1638.956	300	61014.5	$b^3D_{2\frac{1}{2}} - y^3F_{3\frac{1}{2}}$
1633.192	1	61229.8	$a^3P_{1\frac{1}{2}} - y^3P_{1\frac{1}{2}}$
1629.301	1	61376.0	$a^1F_{3\frac{1}{2}} - z^1G_{2\frac{1}{2}}$
1628.295	300	61413.9	$a^1F_{2\frac{1}{2}} - z^1F_{3\frac{1}{2}}$
1628.088	50	61421.7	$b^3D_{1\frac{1}{2}} - z^3P_{1\frac{1}{2}}$
1626.411	200	61485.1	$a^1F_{3\frac{1}{2}} - z^1F_{4\frac{1}{2}}$
1626.139	200	61495.4	$a^1F_{1\frac{1}{2}} - z^1F_{2\frac{1}{2}}$
1625.500	1	61519.5	$a^3P_{\frac{1}{2}} - z^3S_{\frac{1}{2}}$
1621.723	3	61662.8	$a^3F_{3\frac{1}{2}} - z^3F_{2\frac{1}{2}}$
1620.776	1	61698.8	$a^1F_{4\frac{1}{2}} - z^1G_{3\frac{1}{2}}$
1618.408	5	61789.1	$b^3D_{2\frac{1}{2}} - y^3D_{3\frac{1}{2}}$
1616.607	300	61858.0	$a^1F_{1\frac{1}{2}} - z^1F_{1\frac{1}{2}}$
1616.160	15	61875.1	$a^1P_{2\frac{1}{2}} - y^1D_{2\frac{1}{2}}$
1610.571	75	62089.8	$a^1P_{\frac{1}{2}} - y^1D_{1\frac{1}{2}}$
1609.757	100	62121.2	$a^1P_{1\frac{1}{2}} - y^1D_{2\frac{1}{2}}$
1609.599	50	62127.3	$a^1P_{\frac{1}{2}} - y^1D_{\frac{1}{2}}$
1607.542	100	62206.8	$a^1P_{1\frac{1}{2}} - y^1D_{1\frac{1}{2}}$ and $a^3P_{1\frac{1}{2}} - z^3S_{1\frac{1}{2}}$
1606.837	10	62234.1	$b^3D_{2\frac{1}{2}} - z^3P_{1\frac{1}{2}}$
1606.730	300	62238.2	$a^1F_{3\frac{1}{2}} - z^1F_{2\frac{1}{2}}$
1605.969	300	62267.7	$a^1P_{2\frac{1}{2}} - y^1D_{2\frac{1}{2}}$
1603.146	400	62377.4	$a^1F_{3\frac{1}{2}} - z^3G_{4\frac{1}{2}}$
1600.194	500	62492.4	$a^1F_{3\frac{1}{2}} - z^1F_{3\frac{1}{2}}$
1597.418	10	62601.0	$a^1F_{2\frac{1}{2}} - 2^1F_{1\frac{1}{2}}$
1593.758	1000	62744.8	$a^1F_{4\frac{1}{2}} - z^1F_{4\frac{1}{2}}$
1588.551	3	62950.4	$a^1F_{2\frac{1}{2}} - z^3G_{3\frac{1}{2}}$
1579.353	15	63317.1	$a^1F_{3\frac{1}{2}} - z^1F_{2\frac{1}{2}}$
1571.390	1	63637.9	$a^1F_{4\frac{1}{2}} - z^3G_{4\frac{1}{2}}$
1571.154	3	63647.5	$b^3D_{1\frac{1}{2}} - y^1D_{2\frac{1}{2}}$
1570.202	30	63686.1	$a^1F_{3\frac{1}{2}} - z^3F_{3\frac{1}{2}}$
1569.027	0	63733.8	$b^3D_{1\frac{1}{2}} - y^1D_{1\frac{1}{2}}$
1568.655	2	63748.9	$a^1F_{3\frac{1}{2}} - z^3D_{2\frac{1}{2}}$
1568.564	2	63752.6	$a^1F_{4\frac{1}{2}} - z^1F_{3\frac{1}{2}}$
1565.194	5	63889.8	$a^1P_{1\frac{1}{2}} - z^3D_{2\frac{1}{2}}$
1561.790	3	64029.1	$a^1F_{3\frac{1}{2}} - z^3G_{3\frac{1}{2}}$
1551.932	2	64435.8	

TABLE IV.—(*Continued*).

λ(Vac.)	Int.	ν	Classification
1549.203	10	64549.3	$a^4F_{1\frac{1}{2}} - z^4D_{1\frac{1}{2}}$
1548.867	300	64563.3	$a^2G_{3\frac{1}{2}} - y^2G_{3\frac{1}{2}}$
1544.110	2	64762.2	$a^2G_{3\frac{1}{2}} - y^2G_{4\frac{1}{2}}$
1544.062	2	64764.2	$a^4F_{3\frac{1}{2}} - z^4F_{3\frac{1}{2}}$
1543.438	500	64790.4	$a^2G_{4\frac{1}{2}} - y^2G_{4\frac{1}{2}}$
1543.180	2	64801.3	$a^4P_{2\frac{1}{2}} - y^4P_{1\frac{1}{2}}$
1542.562	2	64827.2	$a^4F_{3\frac{1}{2}} - z^4D_{2\frac{1}{2}}$
1541.970	40	64852.1	$b^2D_{2\frac{1}{2}} - y^4D_{2\frac{1}{2}}$
1531.588	1	65291.7	$a^4F_{2\frac{1}{2}} - z^4D_{1\frac{1}{2}}$
1502.107	1	66573.2	$b^2D_{1\frac{1}{2}} - y^4P_{1\frac{1}{2}}$
1501.173	0	66614.6	$a^4F_{2\frac{1}{2}} - z^4F_{2\frac{1}{2}}$
1487.566	0	67223.9	$z^4D_{2\frac{1}{2}} - e^4F_{3\frac{1}{2}}$
1486.904	10	67253.8	$a^4P_{2\frac{1}{2}} - z^4F_{3\frac{1}{2}}$
1486.659	25	67264.9	$a^4P_{2\frac{1}{2}} - z^4S_{1\frac{1}{2}}$
1484.010	5	67385.0	$b^2D_{2\frac{1}{2}} - y^4P_{1\frac{1}{2}}$
1483.831	15	67393.1	$a^4P_{\frac{1}{2}} - z^4S_{1\frac{1}{2}}$
1481.243	20	67511.9	$a^4P_{1\frac{1}{2}} - z^4S_{1\frac{1}{2}}$
1469.460	2	68052.2	
1469.259	0	68061.5	$z^2F_{3\frac{1}{2}} - 7$
1460.915	10	68450.3	$z^2D_{2\frac{1}{2}} - 5$
1459.568	0	68513.4	$z^2F_{3\frac{1}{2}} - 5$
1458.021	6	68586.1	
1455.200	3	68719.1	$z^2F_{2\frac{1}{2}} - e^2F_{3\frac{1}{2}}$
1451.478	1	68895.3	$z^2D_{2\frac{1}{2}} - e^2F_{3\frac{1}{2}}$
1450.165	3	68957.7	$z^2F_{3\frac{1}{2}} - e^2F_{3\frac{1}{2}}$
1448.512	2	69033.4	
1444.692	1	69218.9	$z^2F_{3\frac{1}{2}} - 9$
1441.635	3	69365.7	
1441.102	2	69391.3	
1440.446	3	69422.9	$z^2G_{3\frac{1}{2}} - 6$
1439.275	2	69479.4	
1438.983	2	69493.5	
1437.645	3	69558.2	$z^4F_{3\frac{1}{2}} - e^4F_{3\frac{1}{2}}$
1437.554	2	69562.6	
1436.994	15	69589.7	$z^2G_{4\frac{1}{2}} - 3$
1436.846	2	69596.9	
1436.376	1	69619.7	$z^2F_{2\frac{1}{2}} - 10$
1432.275	3	69819.0	$z^4F_{4\frac{1}{2}} - e^4F_{4\frac{1}{2}}$
1431.901	3	69837.2	$b^2D_{2\frac{1}{2}} - z^2F_{3\frac{1}{2}}$
1431.671	10	69848.4	$b^2D_{2\frac{1}{2}} - z^4S_{1\frac{1}{2}}$
1430.969	3	69882.7	$b^2D_{1\frac{1}{2}} - z^2F_{2\frac{1}{2}}$
1430.373	3	69911.8	$z^2F_{3\frac{1}{2}} - 7$
1429.201	5	69969.2	$z^4F_{4\frac{1}{2}} - 1$
1428.081	5*l*?	70024.0	$a^2F_{2\frac{1}{2}} - y^2D_{1\frac{1}{2}}$
1425.282	1*l*?	70161.6	$z^2D_{2\frac{1}{2}} - 8$
1425.079	2	70171.5	$z^4F_{2\frac{1}{2}} - e^4F_{2\frac{1}{2}}$
1424.020	5	70223.7	$z^2F_{3\frac{1}{2}} - 8$?
1423.504	10	70249.2	
1418.811	5	70481.6	$z^2D_{2\frac{1}{2}} - f^2F_{3\frac{1}{2}}$ and $z^4F_{4\frac{1}{2}} - 3$
1417.538	10	70544.8	$z^2F_{3\frac{1}{2}} - f^2F_{3\frac{1}{2}}$
1417.124	2	70565.5	$z^4F_{4\frac{1}{2}} - e^4F_{3\frac{1}{2}}$
1417.060	2	70568.6	$z^2F_{3\frac{1}{2}} - e^2F_{2\frac{1}{2}}$
1415.478	1	70647.5	$z^2G_{3\frac{1}{2}} - 7$
1414.431	3	70699.8	$z^4F_{1\frac{1}{2}} - e^4F_{1\frac{1}{2}}$
1414.086	2	70717.1	
1412.794	5	70781.1	$z^4F_{4\frac{1}{2}} - e^4G_{4\frac{1}{2}}$
1412.724	5	70785.2	$z^4F_{2\frac{1}{2}} - 5$
1409.248	1	70959.8	$z^4F_{3\frac{1}{2}} - 6$ and $z^2G_{3\frac{1}{2}} - 8$
1408.536	1	70995.7	$z^4F_{3\frac{1}{2}} - e^4F_{2\frac{1}{2}}$
1408.310	1	71007.1	$z^2D_{2\frac{1}{2}} - 9$
1407.196	3	71063.3	$z^4F_{2\frac{1}{2}} - e^4F_{1\frac{1}{2}}$
1407.139	5	71066.2	$a^2F_{3\frac{1}{2}} - y^2F_{3\frac{1}{2}}$?
1405.115	2	71168.6	
1403.763	1	71237.1	$a^2F_{2\frac{1}{2}} - z^2P_{1\frac{1}{2}}$
1403.181	10	71266.6	
1402.917	1	71280.1	$z^2G_{3\frac{1}{2}} - f^2F_{3\frac{1}{2}}$
1402.435	3	71304.6	$z^2G_{3\frac{1}{2}} - e^2F_{3\frac{1}{2}}$
1402.250	5	71313.9	
1401.655	5	71344.2	$z^2G_{4\frac{1}{2}} - e^2F_{3\frac{1}{2}}$
1401.602	5	71346.9	
1401.376	2	71358.4	$z^4F_{2\frac{1}{2}} - 7$
1400.539	3	71401.1	
1399.190	5	71469.9	$z^2F_{3\frac{1}{2}} - 10$
1398.397	5	71510.5	$z^4F_{4\frac{1}{2}} - 4$
1396.417	1	71611.8	$z^4G_{3\frac{1}{2}} - e^4F_{3\frac{1}{2}}$
1395.274	10	71670.5	$z^4G_{4\frac{1}{2}} - e^4F_{4\frac{1}{2}}$
1393.139	3	71780.3	
1391.667	2	71856.3	
1390.306	10	71926.6	
1389.528	5	71966.9	$a^2F_{3\frac{1}{2}} - y^2F_{3\frac{1}{2}}$ and $z^4F_{4\frac{1}{2}} - 6$
1388.276	1	72031.8	$z^4G_{4\frac{1}{2}} - e^4F_{4\frac{1}{2}}$
1386.714	1	72112.9	$z^4G_{3\frac{1}{2}} - e^4F_{3\frac{1}{2}}$
1385.921	3	72154.2	$z^4F_{1\frac{1}{2}} - 9$
1385.380	1	72182.4	$z^4G_{4\frac{1}{2}} - 1$ and $z^4F_{3\frac{1}{2}} - 7$
1384.929	3	72205.9	$z^2G_{3\frac{1}{2}} - 10$
1384.840	5	72210.5	
1384.324	5	72237.4	$z^4F_{4\frac{1}{2}} - e^2F_{3\frac{1}{2}}$
1384.276	2	72239.9	
1382.838	2	72315.1	
1382.561	5	72329.5	
1379.775	2	72475.6	
1379.379	1	72496.4	$z^4F_{2\frac{1}{2}} - 8$
1378.665	2	72533.9	
1378.238	1	72556.4	$z^4G_{3\frac{1}{2}} - 4$
1377.559	2	72592.2	
1377.504	30	72595.1	
1376.807	30	72631.8	$z^4G_{4\frac{1}{2}} - e^4G_{3\frac{1}{2}}$
1375.621	5	72694.4	$z^4G_{4\frac{1}{2}} - 3$
1374.758	3	72740.1	$a^2F_{3\frac{1}{2}} - y^2D_{2\frac{1}{2}}$
1374.298	3	72764.4	
1374.033	3	72778.2	$z^4G_{4\frac{1}{2}} - e^4F_{4\frac{1}{2}}$
1373.305	3	72817.0	
1372.965	3	72835.1	
1372.899	5	72838.6	$z^4G_{3\frac{1}{2}} - 5$
1371.144	10	72931.8	$z^2G_{4\frac{1}{2}} - f^2F_{3\frac{1}{2}}$
1369.988	1	72993.3	$z^4G_{4\frac{1}{2}} - e^4G_{4\frac{1}{2}}$
1369.612	5	73013.4	$z^4G_{3\frac{1}{2}} - 6$
1368.923	2	73050.1	$z^4G_{3\frac{1}{2}} - e^4F_{2\frac{1}{2}}$
1367.646	5	73118.3	
1366.400	3	73185.0	
1365.862	2	73213.8	
1360.922	3	73479.6	
1359.833	0	73538.4	$z^4D_{2\frac{1}{2}} - e^4F_{2\frac{1}{2}}$
1358.440	2	73613.9	$z^4G_{2\frac{1}{2}} - 8$
1358.130	2	73630.7	
1356.424	5	73723.3	$z^4G_{4\frac{1}{2}} - 4$
1353.964	2	73857.2	$z^2G_{4\frac{1}{2}} - 10$
1351.271	3	74004.4	$z^4G_{4\frac{1}{2}} - 5$
1349.441	5	74104.8	
1348.584	3	74151.9	
1348.077	1	74179.7	$z^4G_{4\frac{1}{2}} - 6$
1347.048	3*h*	74236.4	$z^4G_{3\frac{1}{2}} - 7$
1346.062	5	74290.8	
1345.506	2	74321.5	
1344.363	2	74384.7	
1343.730	5	74419.7	
1343.032	2	74458.4	$z^4G_{2\frac{1}{2}} - 9$
1342.193	3*h*	74504.9	$z^4D_{2\frac{1}{2}} - e^4F_{4\frac{1}{2}}$
1341.497	2	74543.6	
1341.178	2*h*	74561.3	
1339.497	5	74654.9	$z^4D_{2\frac{1}{2}} - 1$
1338.858	2	74690.5	
1338.386	2	74716.9	
1337.572	5*h*	74762.3	
1332.985	15	75019.6	
1330.365	2	75167.3	$z^4D_{2\frac{1}{2}} - 3$
1327.178	5	75347.8	
1326.379	3	75393.2	
1324.033	5	75526.8	
1318.582	2	75839.0	$a^4F_{3\frac{1}{2}} - y^2F_{3\frac{1}{2}}$
1316.143	5	75979.6	
1313.313	2	76143.3	
1312.400	10	76196.3	$z^4D_{2\frac{1}{2}} - 4$
1311.863	2	76227.5	
1307.595	3	76476.3	$z^4D_{2\frac{1}{2}} - 8$
1295.700	0	77178.4	$a^2F_{3\frac{1}{2}} - z^2D_{2\frac{1}{2}}$
1271.839	2	78626.3	$a^4F_{1\frac{1}{2}} - y^4D_{1\frac{1}{2}}$
1271.234	5	78663.7	$a^4F_{1\frac{1}{2}} - y^4D_{\frac{1}{2}}$
1259.937	10	79369.0	$a^4F_{2\frac{1}{2}} - y^4D_{1\frac{1}{2}}$
1254.717	3	79699.2	$a^2F_{2\frac{1}{2}} - z^2F_{2\frac{1}{2}}$

TABLE IV.—(*Continued*).

λ(Vac.)	Int.	ν	Classification
1244.377	10	80361.5	$a^4F_{3\frac{1}{2}} - y^4D_{3\frac{1}{2}}$
1238.325	1	80754.2	$a^4F_{2\frac{1}{2}} - y^4D_{2\frac{1}{2}}$
1237.776	3	80790.1	$a^3F_{3\frac{1}{2}} - x^3F_{3\frac{1}{2}}$
1219.290	5	82014.9	$a^4F_{4\frac{1}{2}} - y^4D_{3\frac{1}{2}}$
829.343	5	120577.3	$a^3D_{2\frac{1}{2}} - z^4D_{2\frac{1}{2}}$
816.313	0	122502.0	$a^3D_{2\frac{1}{2}} - z^4G_{3\frac{1}{2}}$
810.124	0	123437.9	$a^3D_{2\frac{1}{2}} - z^4G_{2\frac{1}{2}}$
808.583	20	123673.1	$a^3D_{1\frac{1}{2}} - z^4F_{1\frac{1}{2}}$
802.841	150	124557.7	$a^3D_{2\frac{1}{2}} - z^4F_{2\frac{1}{2}}$
801.154	200	124819.9	$a^3D_{1\frac{1}{2}} - z^2D_{2\frac{1}{2}}$
797.566	100	125381.5	$a^3D_{2\frac{1}{2}} - z^4F_{2\frac{1}{2}}$
795.258	2	125745.4	$a^3D_{3\frac{1}{2}} - z^4F_{4\frac{1}{2}}$
793.065	100	126093.1	$a^3D_{2\frac{1}{2}} - z^4G_{3\frac{1}{2}}$
791.371	300	126363.0	$a^3D_{1\frac{1}{2}} - z^2D_{1\frac{1}{2}}$
789.840	200	126607.9	$a^3D_{1\frac{1}{2}} - z^4F_{2\frac{1}{2}}$
788.462	300	126829.2	$a^3D_{2\frac{1}{2}} - z^2F_{3\frac{1}{2}}$
788.073	400	126891.8	$a^3D_{2\frac{1}{2}} - z^2D_{2\frac{1}{2}}$
778.603	50	128435.2	$a^3D_{3\frac{1}{2}} - z^2D_{3\frac{1}{2}}$
777.125	200	128679.4	$a^3D_{2\frac{1}{2}} - z^2F_{2\frac{1}{2}}$
743.970	30	134414.0	$a^3D_{1\frac{1}{2}} - z^4P_{1\frac{1}{2}}$
743.303	20	134534.6	$a^3D_{1\frac{1}{2}} - z^4P_{2\frac{1}{2}}$
735.224	100	136013.0	$a^3D_{1\frac{1}{2}} - y^2F_{2\frac{1}{2}}$
732.688	5	136483.7	$a^3D_{2\frac{1}{2}} - z^4P_{1\frac{1}{2}}$
732.026	100	136607.2	$a^3D_{2\frac{1}{2}} - z^4P_{2\frac{1}{2}}$
730.365	150	136917.8	$a^3D_{1\frac{1}{2}} - y^2D_{1\frac{1}{2}}$
728.906	2	137191.9	$a^3D_{1\frac{1}{2}} - z^2P_{\frac{1}{2}}$
726.295	10	137685.1	$a^3D_{1\frac{1}{2}} - y^2D_{2\frac{1}{2}}$
723.958	20	138129.6	$a^3D_{1\frac{1}{2}} - z^2P_{1\frac{1}{2}}$
719.506	150	138984.2	$a^3D_{2\frac{1}{2}} - y^2F_{3\frac{1}{2}}$
715.530	200	139756.5	$a^3D_{2\frac{1}{2}} - y^2D_{2\frac{1}{2}}$
713.262	10	140200.9	$a^3D_{2\frac{1}{2}} - z^2P_{1\frac{1}{2}}$
712.473	15	140356.2	$a^3D_{1\frac{1}{2}} - y^4D_{2\frac{1}{2}}$
712.040	5	140441.5	$a^3D_{1\frac{1}{2}} - y^4D_{1\frac{1}{2}}$
711.834	3	140482.2	$a^3D_{1\frac{1}{2}} - y^4D_{\frac{1}{2}}$
703.622	15	142121.8	$a^3D_{1\frac{1}{2}} - x^2D_{2\frac{1}{2}}$
702.112	20	142427.4	$a^3D_{2\frac{1}{2}} - y^4D_{2\frac{1}{2}}$
701.692	15	142512.7	$a^3D_{2\frac{1}{2}} - y^4D_{1\frac{1}{2}}$
700.271	150	142801.9	$a^2D_{1\frac{1}{2}} - x^2D_{1\frac{1}{2}}$
700.182	20	142820.0	$a^3D_{2\frac{1}{2}} - y^4D_{3\frac{1}{2}}$
697.930	20	143280.8	$a^3D_{1\frac{1}{2}} - y^2P_{1\frac{1}{2}}$
693.510	50	144194.0	$a^2D_{2\frac{1}{2}} - x^2D_{2\frac{1}{2}}$
691.557	100	144601.2	$a^3D_{1\frac{1}{2}} - y^2P_{\frac{1}{2}}$
690.250	75	144875.0	$a^3D_{2\frac{1}{2}} - x^4D_{1\frac{1}{2}}$
687.987	100	145351.6	$a^3D_{2\frac{1}{2}} - y^2P_{1\frac{1}{2}}$
686.903	15	145581.0	$a^3D_{1\frac{1}{2}} - z^4S_{1\frac{1}{2}}$
682.171	200	146590.8	$a^2D_{1\frac{1}{2}} - x^2F_{2\frac{1}{2}}$
676.564	300	147805.6	$a^3D_{2\frac{1}{2}} - x^2F_{3\frac{1}{2}}$
672.659	50	148663.7	$a^3D_{2\frac{1}{2}} - x^2F_{2\frac{1}{2}}$

choice of names for the two levels of $J=1\frac{1}{2}$ is correct, but that the names of the two levels with $J=2\frac{1}{2}$ perhaps should be interchanged. The same result is indicated by the g-values in NiII, but the arrangement of the components of the terms would then be very odd, indeed.

The levels of $d^8(^1D)4p$, $d^8(^3P)4p$ and $d^8(^1G)4p$ have all been found, and they show a remarkable similarity of arrangement to their counterparts in NiII. In both spectra, the levels based on ^1D and ^3P are certainly of mixed character, and the assignment of names is consequently of doubtful validity. The one-to-one correspondence of the levels of these two groups of NiII and CuIII is so complete that it might be expected that an extrapolation back to CoI would give an unambiguous selection of the equivalent levels in that spectrum. This is not the case. In the appropriate energy range in CoI there are over 50 observed levels, of which not more than 19 can belong to this part of the d^84p configuration, the others having their origin in d^7sp. The observed levels are so mixed in character that it is perhaps meaningless even to group them into terms. There is a balance of evidence, however, which indicates that a few changes in assignment should be made. The ones we propose are given in Table III.

The lowest term of the CuIII spectrum, $3d^9\ ^2D$, was correctly identified by Vieweg. Its combinations are all below λ830 and are very intense. The ^2D difference 2071.8 is to be compared with the 2042.9 of $d^9s^2\ ^2D$, 2069.0, 2069.3, 2069.2 of $d^9s\cdot s(^1D_{2\frac{1}{2}}-{}^1D_{1\frac{1}{2}})$, and 2069.7, 2069.8, 2070.4, 2071.4 of $d^9s(^3D_3-{}^3D_1)$.

Measurements of a plate which was very much overexposed in the region of the strong multiplets yielded a number of lines of reasonable intensity in the region λ1350 to λ1450. Those lines made it possible to identify a number of high even levels; and, amongst them, were found the six levels comprising $3d^8(^3F)5s\ ^4F$ and ^2F. Since these are in series with the low levels a^4F and a^2F, it is possible to calculate an I. P. in six ways provided one knows the type of convergence and the intervals of the limit in CuIV. The latter are not known, but from a comparison with similar cases in other spectra, they cannot differ materially from the intervals of $3d^84s^2\ ^3F$ of CuII. The convergence is obviously the one which results from the non-crossing rule, i.e., $^4F_{4\frac{1}{2}}$ and $^4F_{3\frac{1}{2}}$ converge to $^3F_4$; $^4F_{2\frac{1}{2}}$ and $^2F_{3\frac{1}{2}}$ to $^3F_3$, and $^4F_{1\frac{1}{2}}$ and $^2F_{2\frac{1}{2}}$ to $^3F_2$. Using this information and assuming from a comparison with other spectra that the Ritz correction is about 1.7×10^{-7}, the length of the series from $a^4F_{4\frac{1}{2}}$ to $^3F_4$ of CuIV is 238340 cm^{-1}. Adding the $^2D_{2\frac{1}{2}}-{}^4F_{4\frac{1}{2}}$ difference of 60805 we obtain an ionization limit of 299145 corresponding to an I. P. of 3708 volts for the removal of a d-electron. In this calculation only the quartet levels were used, the doublets having very different values of the Ritz correction.

A few other high even levels have been found. They originate in the structure $3d^84d$, but the number of combinations is too small for many positive identifications to be made. Many more levels should exist in this neighborhood and an exhaustive but unsuccessful search has been made for them. It is therefore probable that the remaining levels are represented by single or double combinations only. A thorough analysis of this structure in NiII should, with the aid of the CoI analysis, lead to a more complete knowledge of the terms of CuIII.

As usual in spectra in which configurations including d^8 occur, no trace has been found of the levels based on ^1S. A more important lacuna, however, is the absence of the structure $3d^74s^2$. From all the available evidence, it appears that this structure should exist about 15,000 to 30,000ν above $3d^84p$ and should therefore produce multiplets in the easily observed part of the spectrum. No such lines have been observed, and it therefore remains an unsolved problem that the much higher levels of $3d^84d$ are observably excited but the lower ones of $3d^74s^2$ are not.

All identified and unidentified lines of CuIII, of reasonable intensity, are listed in Table IV.

A Self-Consistent Treatment of the Oxygen Dissociation Region in the Upper Atmosphere*

H. E. Moses†
Department of Physics, Columbia University, New York, New York
AND
Ta-You Wu
National Research Council of Canada, Ottawa, Canada
(Received July 5, 1950)

A self-consistent theory is suggested for the determination of the distribution of atomic and molecular oxygen and the temperature in the region 100–140 km of the atmosphere. It is assumed that solar radiation is responsible for the photodissociation of the oxygen molecules, and that the recombination of the atoms by two-body radiative processes is more important than that by three-body collisions (as justified from theoretical considerations). From the postulated conditions for the steady state, namely, for any given volume, (a) the average time rate of dissociations equals that of recombinations, and (b) the average time rate at which radiation energy is absorbed in dissociation processes equals that at which radiation energy is emitted in recombination processes, together with an appropriate form of the barometric equation, it is possible to obtain the concentrations of the molecular and the atomic oxygen and the temperature, all as functions of height, provided the temperature and its gradient are given at one height. Calculations have been carried out for three sets of these boundary values at 100 km, namely, (i) $T=300°K$, $dT/dx=10°/km$, (ii) $T=300°K$, $dT/dx=5°/km$, and (iii) $T=270°K$, $dT/dx=5°/km$. In all these cases, dissociation begins between the heights 90 and 100 km and is not complete until around 150 km. The total gas pressure for various heights above 100 km calculated for case (iii) above agrees quite well with the data obtained from V-2 rocket flights.

In the appendices, three-body recombinations are discussed. The cross section for a three-body recombination process is defined, and its relation with the cross section of its inverse two-body excitation process is obtained on statistical mechanical arguments. Also, the relation between the absorption coefficient for a photodissociation process and the cross section of its inverse radiative recombination process is obtained.

I. INTRODUCTION

IN the upper atmosphere, the atoms and molecules are ionized or dissociated on the absorption of solar radiation of the proper frequencies, and the resulting ions or atoms recombine either in their respective inverse processes, namely, a two-body radiative recombination, or in three-body collisions. The degree of ionization or dissociation of a given atomic or molecular species at any given height depends on the following factors: the intensity of the radiation involved, the density of the gas, the temperature of the gas at that height, and such atomic or molecular quantities as the radiation absorption coefficient and the cross sections for the recombination collisions. The problem of investigating the region in which oxygen is dissociated into atoms has been studied by Wulf and Deming,[1] Majumdar,[2] Rakshit,[3] and Penndorf,[4] after the orginal suggestion of Chapman.[5] While these authors differ in details in the assumptions in their theories, their results depend essentially on an assumption made concerning the total number of oxygen molecules in a column of unit cross section above any given height, which is just the quantity to be calculated from their theories. Thus their results are arbitrary in the sense that they have already been assumed in their calculations. This question of self-consistency and other assumptions in their theories are discussed in Appendix 7. The purpose of the present work is to show that in principle a self-consistent theory can be formulated, in which the temperature and the concentrations of the atoms and molecules of oxygen can all be obtained as functions of the height from a knowledge of the temperature and its gradient at a certain height. The theory is illustrated by an actual calculation in which the most reasonable assumptions are made concerning the processes involved in the region of the atmosphere under consideration. The result obtained differs considerably from those of the previous authors.

To avoid discontinuity in the discussion and the presentation of the theory and the result, we have relegated to the appendices the derivations of equations and some of the arguments and calculations in the theory.

II. GENERAL FORMULATION OF THE PROBLEM

In studying the variation of the temperature and the degree of dissociation of the oxygen molecules as functions of height in the upper atmosphere, it must be assumed that the time τ_{di_2} required to reach dissociative equilibrium is small compared with the time τ_{dif} required to establish diffusive equilibrium and also with the average time interval between winds. That $\tau_{di_2} \ll \tau_{dif}$ is necessary for the existence of a transition region in which oxygen passes from the molecular into the dissociated state is obvious, for otherwise the atoms and molecules will be separated by diffusion in the gravitational field. Calculations (Appendix 3) show that for oxygen, τ_{di_2} is of the order of days, while, on the other hand, τ_{dif} is of the order of years for the pressure

* Publication assisted by the Ernest Kempton Adams Fund.
† Present address: Institute of Mathematics and Mechanics, New York University, New York, New York.
[1] O. R. Wulf and L. S. Deming, Terr. Mag. **41**, 299 (1936); **43**, 283 (1938).
[2] R. C. Majumdar, Indian J. Phys. **12**, 75 (1938).
[3] H. Rakshit, Indian J. Phys. **21**, 57 (1947).
[4] R. Penndorf, J. Geo. Res. **54**, 7 (1949); Phys. Rev. **77**, 561 (1950).
[5] S. Chapman. Phil. Mag. **10**, 367 (1930).

existing at the height 100 km. The situation as to the existence and the frequency of winds at these heights is a more obscure one. As there is still a lack of direct evidence either for or against the existence of winds at such heights, we shall ignore them in the present work, since the assumption of winds of sufficient frequency and strength to churn up this region of the atmosphere would render meaningless the very problem of finding the degree of dissociation and temperature as a function of the height.

We shall then consider the following idealized model of the atmosphere. In certain regions, the most important physical processes taking place are assumed to be the dissociation of the oxygen molecules by solar radiation, and the recombination of the oxygen atoms into molecules. Other constituents, such as nitrogen, will not be considered except in so far as they contribute to the total pressure of the atmosphere. For the dissociation process, it seems quite certain that the most important absorption process leading to dissociation is the absorption in the Schumann-Runge continuum beyond 1750A. We write this process as

$$O_2(X\,^3\Sigma_g^-)+h\nu\rightarrow O(^3P)+O(^1D). \tag{1}$$

We shall denote by σ_ν the absorption cross section (in cm^2) for this process. The cross section σ_ν is defined below. Let $\rho_\nu(\infty)$ be the solar radiation energy density per unit frequency range at the "top" of the atmosphere. On account of the absorption by the molecules lying above x, the density at the height x is given by

$$\rho_\nu(x)=\rho_\nu(\infty)\exp[-\sigma_\nu N_2(x)], \tag{2}$$

where

$$N_2(x)=\int_x^\infty n_2(x)dx, \tag{3}$$

$n_2(x)$ being the number density of oxygen molecules and $N_2(x)$ the number of oxygen molecules in a column of unit cross section above the height x. The number of oxygen molecules dissociated per unit volume per second at the height x is

$$n_2(x)\int_{\nu_0}^\infty[\sigma_\nu c\rho_\nu(x)/h\nu]d\nu$$

where ν_0 is the threshold frequency of the process (1). This statement defines σ_ν. It will be shown later that most of the oxygen atoms are in the ^3P state. Let us denote the coefficient of recombination by B so that the number of recombinations per unit volume per second is $n_P{}^3B$, where n_P is the number density of atoms in the ^3P state. B is in general a function of temperature and hence of height. The condition for a steady state is

$$n_2\int_{\nu_0}^\infty[\sigma_\nu c\rho_\nu(\infty)\exp(-\sigma_\nu N_2)/h\nu]d\nu=Bn_P{}^3(x). \tag{4}$$

Let P be the total pressure, and n the number density of nitrogen molecules. One has

$$dP=-[(2n_2+n_P)M+nM_N]gdx, \tag{5}$$

and

$$P=(n_2+n_P+n)kT, \tag{6}$$

where M, M_N are the atomic weight of oxygen and the molecular weight of nitrogen, respectively. Thus there are four unknown functions n_2, n_P, n, and T which are related by Eqs. (4) and (5) plus (6).

To get rid of the nitrogen in the theory, Rakshit[3] and Penndorf[4] assume that the proportion of nitrogen to oxygen (atomic plus molecular) remains the same at 4:1 at all heights concerned in the problem. This assumption presupposes the constant mixing of the atmosphere by winds. If this is so, the time intervals between winds must be short compared with the time τ_{diff} required to establish diffusive separation and long compared with the time τ_{diss} required to establish dissociative equilibrium. Furthermore, their assumption that at any height

$$nM_N:(n_2+\tfrac{1}{2}n_P)2M=4:1 \tag{7}$$

also implies that the atomic and molecular oxygen do not redistribute themselves. This is equivalent to assuming an atmosphere separated by transparent partitions into parallel layers. Instead of assuming (7) we shall assume that above $\sim$100 km the nitrogen is in diffusive equilibrium with the oxygen (but we shall *not* assume that molecular and atomic oxygen are in diffusive equilibrium with each other). Then one can work with the partial pressure p of oxygen alone so that (5) and (6) become

$$dp=-(2n_2+n_P)Mgdx, \tag{8}$$

$$p=(n_2+n_P)kT, \tag{9}$$

which give the differential equation

$$\frac{d}{dx}[(n_2+n_P)T]=-\frac{Mg}{k}(2n_2+n_P). \tag{10}$$

As there are still three unknown functions $n_2(x)$, $n_P(x)$, $T(x)$ given by Eqs. (4) and (10),[5a] a certain temperature distribution $T(x)$ is assumed in all the above-mentioned investigations. On doing this, and eliminating n_P in (10) by means of (4), one obtains a nonlinear differential equation of the second order for N_2

$$F\left(\frac{d^2N_2}{dx^2},\frac{dN_2}{dx},N_2,T,\frac{dT}{dx},x\right)=0, \tag{11}$$

where F is a known function of the various arguments, and depends on N_2 through integrals of the form of that on the left-hand side of (4). This equation is to be solved subject to the boundary conditions that at a sufficiently low altitude x_0 where the degree of dissociation is probably extremely small, $-N_2'(x_0)$ may be

[5a] Or a similar equation obtained by assuming (7) in (5) and (6).

given a value estimated from another source of information, and at a sufficiently great height, N_2 is small, i.e.,

$$-N_2'(x_0)=n_2(x_0) \text{ given}, \quad N_2(\infty)=0. \tag{11a}$$

In principle, on the assumption of a certain $T(x)$, a definite recombination mechanism and the proportion (7) or an alternative as mentioned above, the problem is reduced to the solution of Eq. (11) subject to the above boundary conditions. The important point is that the n_2, N_2 are thereby completely determined, and any further assumption about any one of these quantities is not only unnecessary but is in fact inconsistent with the problem.

An actual calculation, however, in this manner will entail extremely laborious computations, on account of the complicated form of Eq. (11) and of the nature of the boundary conditions. On integrating the equation numerically upward from x_0 one knows the initial slope $N_2'(x_0)$ but not the function $N_2(x_0)$, so that it is necessary to perform the integration for various values of $N_2(x_0)$ until the solution vanishes monotonically as $x\to\infty$.

In the present paper the authors suggest an alternative self-consistent treatment of the problem in which no assumption above $T(x)$ is made, but instead another physical assumption is made for the steady state. The advantages of this theory are the following: (1) the temperature $T(x)$ determined by the steady state is given by the theory itself without its being assumed on empirical grounds; (2) the form of the differential equation for T and of the boundary conditions on T and dT/dx enables the problem to be solved with much less numerical work than is the case in the treatment discussed above.

III. PROPOSED SELF-CONSISTENT THEORY

We shall show that all the functions $n_P(x)$, $n_2(x)$, $T(x)$ can be obtained as functions of the height x, if, in addition to Eqs. (4) and (10), we postulate that in the region of the atmosphere under consideration, the amount of energy absorbed from solar radiation in the process (1) per unit volume per second be equal to the energy radiated by the recombination processes. The heat loss due to conduction has been neglected as a simplifying assumption, which may be justified, since the rate of loss of heat in any layer by conduction depends on the pressure and on d^2T/dx^2, both of which are small. In the following, we shall illustrate our theory by carrying out some numerical calculations on the basis of some assumed recombination processes. It is to be emphasized that while the exact numerical result depends on these assumptions, the principle of the method is more general and may be applied to future calculations when further empirical information becomes available.

Consider now the processes that lead to the recombination of the oxygen atoms. Wulf and Deming,[1] and recently Penndorf[4] work with the assumption that two oxygen atoms recombine in a three-body collision,

$$O+O+X\to O_2+X^*. \tag{12}$$

In Appendix 5, arguments will be given to show that for the pressures prevalent at and above the height of 100 km, three-body collisions of the type (12) are much less important than two-body radiative recombinations. As no direct experimental data on this point are available and as quantitative theoretical calculations are difficult, we shall base our assumption of two-body recombination on our discussions in Appendix 5. The calculations of Majumdar[2] and Rakshit[3] are also based on the assumption of two-body recombinations.

Of the two-body radiative recombinations, there is first the inverse process of (1), namely,

$$O(^1D)+O(^3P)\to O_2(X\,^3\Sigma_g^-)+h\nu, \tag{1a}$$

whose cross section β_ν is defined in Eq. (16) below. The ^1D state of O has a transition probability $A_D\cong 10^{-2}$ sec^{-1} for the magnetic dipole transition to the ^3P state, emitting the red auroral lines

$$O(^1D)\to O(^3P)+h\nu_{\text{red}}. \tag{13}$$

In view of the short lifetime of $O(^1D)$, we have to consider collisions between two ^3P atoms. In Appendix 6, we give some arguments that make it plausible to assume that the most important recombination process probably involves a dipole transition, such as

$$O(^3P)+O(^3P)(^1\Pi_u)\to O_2(b\,^1\Sigma_g^+)+h\nu_1. \tag{14}$$

We shall denote by β_ν' the cross section of such a process. The $O_2(b\,^1\Sigma_g^+)$ will make a subsequent transition to the normal state of the molecule on emitting the "atmospheric bands"

$$O_2(b\,^1\Sigma_g^+)\to O_2(X\,^3\Sigma_g^-)+h\nu_2. \tag{15}$$

Although this detailed assumption is by no means certain, it seems to have some support in the identification by Meinel[6] and Kaplan[7] of the atmospheric band (0,1) of oxygen in the infrared region of the spectrum of the night sky.[7a]

Let the number density of oxygen atoms in the ^1D state be denoted by n_D. The time rates of change of the concentrations are given by[7b]

---

[6] A. B. Meinel, Trans. Am. Geophys. Union **31**, 21 (1950).

[7] J. Kaplan, Phys. Rev. **78**, 82 (1950).

[7a] The recent discovery of the OH vibration-rotational bands in the night sky spectrum by A. B. Meinel, Astrophys. J. **111**, 555; **112**, 121 (1950) suggests the reactions $O+OH\to O_2+H$, $O+O_2+X\to O_3+X^*$, $H+O_3\to OH+O_2$ as the effective processes for the recombination of the atomic oxygen into molecules. In the present work, we have not considered these processes, since it is not certain that the OH bands come from the same regions of the atmosphere (above 100 km) considered in our problem. Our theory may be applied to these processes when more information becomes available.

[7b] We have neglected the removal of the ^1D state of the oxygen atoms by collisions of the second kind on the following consideration. The cross section of a collision in which the energy of $O(^1D)$ is transferred to the electronic energy of another atom or

$$dn_2/dt=-n_2\int_{\nu_0}^{\infty}(\sigma_\nu c\rho_\nu(x)/h\nu)d\nu+n_F^2\int_0^{\infty}\beta_v'vF(v)dv$$

$$+n_Fn_D\int_0^{\infty}\beta_vvF(v)dv, \quad (16)$$

$$dn_D/dt=n_2\int_{\nu_0}^{\infty}(\sigma_\nu c\rho_\nu(x)/h\nu)d\nu-n_DA_D$$

$$-n_Fn_D\int_0^{\infty}\beta_vvF(v)dv, \quad (17)$$

$$dn_F/dt=n_2\int_{\nu_0}^{\infty}(\sigma_\nu c\rho_\nu(x)/h\nu)d\nu+n_DA_D$$

$$-n_Fn_D\int_0^{\infty}\beta_vvF(v)dv-2n_F^2\int_0^{\infty}\beta_v'vF(v)dv, \quad (18)$$

where $F(v)$ is the velocity distribution function of the atoms with respect to the relative velocity v, and β_v the cross section of (1a). It is seen that unless one ignores the frequent process (13), it is necessary to include such a process as (14) in order to have any steady state expressed by the vanishing of the time rates of change of the concentrations in (16), (17), and (18).

Consider Eq. (17). The transition probability A_D is 10^{-2} per sec. From the calculations later on in this work (Appendix 4), one finds, for $n_F=10^{12}/\text{cm}^3$

$$n_F\int_0^{\infty}\beta_vvF(v)dv\cong10^{-7}/\text{sec}. \quad (19)$$

Hence $O(^1D)$ disappears mostly through the transition (13), and for the steady state, Eq. (17) gives

$$n_2\int_{\nu_0}^{\infty}(\sigma_\nu c\rho_\nu(x)/h\nu)d\nu\cong n_DA_D.$$

Equation (18) then gives, for the steady state,

$$n_DA_D\cong n_F^2\int_0^{\infty}\beta_v'vF(v)dv. \quad (20)$$

Finally consider Eq. (16). The relative importance of the last two terms depends on n_F, n_D, β_v, and β_v'. β_v can be calculated from the observed σ_ν by means of the principle of detailed balancing (Appendix 1). β_v' for such a process as (14) is not known either experimentally or theoretically, but as (14) is assumed to be an allowed dipole transition, β_v' will be of the same general order of magnitude as β_v. As $n_D/n_F\ll1$, we may write Eq. (16) for the steady state in the form

$$n_2\int_{\nu_0}^{\infty}(\sigma_\nu c\rho_\nu(x)/h\nu)d\nu=n_F^2\int_0^{\infty}\beta_v'vF(v)dv. \quad (21)$$

This is recognized as being Eq. (4).

We shall assume another condition for the steady state, namely, that in any given volume of the atmosphere, the energy absorbed from the solar radiation be equal to the radiations emitted by the radiative processes. The energy absorbed in the process (1) is $h\nu$. The energy emitted in the processes (13), (14), (15) is $h(\nu_{\text{red}}+\nu_1^0+\nu_2^0)+\frac{1}{2}mv^2$, where ν_1^0, ν_2^0 are the threshold frequencies in (14) and (15), and $\frac{1}{2}mv^2$ is the kinetic energy of the $O(^3P)$ atoms in the center-of-mass coordinate system. Let χ be the dissociation energy of $O_2(X\,^3\Sigma_g^-)$ into $O(^1D)+O(^3P)$ so that $\chi=h(\nu_{\text{red}}+\nu_1^0+\nu_2^0)=h\nu_0$. Furthermore, let $\chi_1=h\nu_1^0$. The condition for energy balance is then

$$n_2\int_{\nu_0}^{\infty}\sigma_\nu c\rho_\nu(x)d\nu=n_F^2\Big[\int_0^{\infty}(\chi_1+\tfrac{1}{2}mv^2)\beta_v'vF(v)dv$$

$$+(\chi-\chi_1)\int_0^{\infty}\beta_v'vF(v)dv\Big]. \quad (22)$$

To obtain the barometric equation, we shall assume that the nitrogen exists in the molecular state in the region of the atmosphere under consideration, and that its distribution is independent of the oxygen except that at any height x all the component gases have the same gas kinetic temperature. We then have Eq. (10). Equations (21), (22), and (10) are the three basic equations in the theory.

IV. DETAILED CALCULATIONS

We shall now seek the explicit forms of the three basic equations (21), (22), and (10). For this purpose, it is necessary to know the absorption coefficient σ_ν and the recombination cross section β_v' in (21) and (22). The coefficient σ_ν is known both experimentally and theoretically from the work of Ladenburg *et al.*,[8] and of Stueckelberg.[9] The cross section β_v' is not known, but its relation with the corresponding absorption coefficient σ_ν' of the inverse process of (14) can be found by means of the principle of detailed balancing. To avoid the discontinuity of our presentation here, we have given this calculation in Appendix 1. It is shown in Appendix

molecule is small except when there is very close resonance. The cross sections of processes in which the electronic excitation is transferred to the translational vibrational and rotational energy of the colliding atom or molecule are very small. If these are $\sim10^{-4}$ times the gas kinetic cross section then the probability of ^1D being de-excited by particles of concentration $10^{12}/\text{cm}^3$ is only 10^{-3}/sec.

[8] Ladenburg, Van Voorhis, and Boyce, Phys. Rev. **40**, 1018 (1932); R. Ladenburg and C. C. Van Voorhis, Phys. Rev. **43**, 315 (1933).

[9] E. C. G. Stueckelberg, Phys. Rev. **42**, 518 (1932); **44**, 234 (1933). There is a misprint in the second article. The expression $N_j=N\exp[j(j+1)B_0/kT]$ should read

$$N_jf_2(T)=N\exp[-j(j+1)B_0/kT],$$

where $f_2(T)$ is given by Eq. (38).

2 that on writing $\sigma_\nu' = K'\nu f_1(\nu)$, $\sigma_\nu = K\nu f(\nu)$, Eqs. (21) and (22) become

$$n_2\int_{\nu_0}^{\infty} f(\nu)\rho_\nu(x)d\nu = An_P{}^2\int_{\nu_0}^{\infty}\nu^3 f_1(\nu)\exp(-h\nu/kT)d\nu, \quad (23)$$

$$n_2\int_{\nu_0}^{\infty}\nu f(\nu)\rho_\nu(x)d\nu = An_P{}^2\left[\int_{\nu_0}^{\infty}\nu^4 f_1(\nu)\exp(-h\nu/kT)d\nu + (\chi-\chi_1)h^{-1}\int_{\nu_0}^{\infty}\nu^3 f_1(\nu)\exp(-h\nu/kT)d\nu\right], \quad (24)$$

where

$$A = \frac{16r_0{}^2h^2K'G_2\pi^{\frac{1}{2}}}{c^2KG_1'(MkT)^{\frac{1}{2}}}\exp\frac{\chi_1}{kT}, \quad (25)$$

the various quantities being defined in Appendix 2.

The radiation energy density ρ_ν is given by (2) in which $\rho_\nu(\infty)$ at the top of the atmosphere will be assumed to be that of a blackbody of temperature $\theta(\cong 6000°\text{K})$ diluted by the factor W representing the solid angle subtended by the sun divided by 4π, namely, $W = 5.4\times10^{-6}$. The calculations as carried out in this manner will be valid for the case in which the sun is at the zenith all the time. Since the dissociation and recombination processes are slow processes, the average radiation available over day and night may perhaps be better represented by $W/4$.

For the ultraviolet region beyond 1750A, the spectral distribution may be replaced by Wien's law so that

$$\rho_\nu(x) = \tfrac{1}{4}W8\pi h\nu^3c^{-3}\exp(-h\nu/k\theta)\exp[-\sigma_\nu N_2(x)]. \quad (26)$$

From Eqs. (23) and (24), one obtains

$$\frac{\int_{\nu_0}^{\infty}\nu^3 f(\nu)\exp[-\sigma_2N_2-h\nu/k\theta]d\nu}{\int_{\nu_0}^{\infty}\nu^4 f(\nu)\exp[-\sigma_2N_2-h\nu/k\theta]d\nu} = \frac{\int_{\nu_0}^{\infty}\nu^3 f_1(\nu)\exp(-h\nu/kT)d\nu}{\int_{\nu_0}^{\infty}\nu^4 f_1(\nu)\exp(-h\nu/kT)d\nu + (\chi-\chi_1)h^{-1}\int_{\nu_0}^{\infty}\nu^3 f_1(\nu)\exp(-h\nu/kT)d\nu}. \quad (27)$$

It is seen that the solution of Eq. (27) is of the form

$$N_2 = N_2(T). \quad (28)$$

To obtain this solution, we evaluate the integrals on the left-hand side of (27) by using the empirical absorption coefficient $\sigma_\nu = K\nu f(\nu)$. On account of the very rapid decrease of both factors $\exp(-\sigma_\nu N_2)$ and $\exp(-h\nu/k\theta)$ with increase in frequency beyond the threshold ν_0, the most important contribution to the integrals comes from the immediate neighborhood of ν_0. The measurements of Ladenburg *et al.* do not cover this region (from $\nu = 1.71\times10^{15}$ to 1.81×10^{15} per sec). For this region, a theoretical curve for σ_ν has been calculated on the basis of the work of Stuekelberg with constants so chosen that the theoretical curve fits the observed data beyond $\nu = 1.8\times10^{15}$ sec^{-1}. In the absence of any direct experimental data, this procedure seems to be the most reasonable one. We find

$$\sigma_{\nu_0} = 0.68\times10^{-18}\ \text{cm}^2, \quad (d\sigma_\nu/d\nu)_{\nu_0} = 1.12\times10^{-32}\ \text{cm}^2\ \text{sec}.$$

For very large values of $N_2(>2\times10^{19}/\text{cm}^2)$, practically all the contributions to the integrals come from a narrow frequency range $\Delta\nu$ near ν_0, and in this case the expansion

$$\sigma_\nu = \sigma_{\nu_0} + (d\sigma_\nu/d\nu)_{\nu_0}(\nu-\nu_0) \quad (29)$$

will be sufficient. For smaller $N_2(\sim10^{19}/\text{cm}^2)$, the contributions will come from a larger frequency region $\Delta\nu$. In this case, instead of adding another term to the expansion (29), we approximate the σ_ν by (29) with a greater slope. For still smaller values of $N_2(\sim10^{18}/\text{cm}^2)$, we represent the σ_ν curve by a triangle so that the integrations can be carried out analytically.

To evaluate the integrals on the right-hand side of (27), one needs the absorption coefficient $\sigma_\nu' = K'\nu f_1(\nu)$ which is not known. It is seen, however, that on account of the very rapid decrease of the factor $\exp(-h\nu/kT)$ with increase of frequency beyond the threshold $\nu_1{}^0$, all the contribution to the integrals comes only from a small range of frequency beyond $\nu_1{}^0$. Hence we may

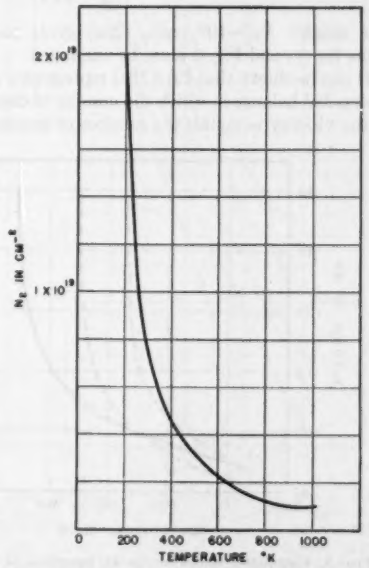

FIG. 1. Theoretical values from Eq. (27) of the total number $N_2[x(T)]$ of oxygen molecules in a column of unit cross section above the height $x(T)$, as a function of T.

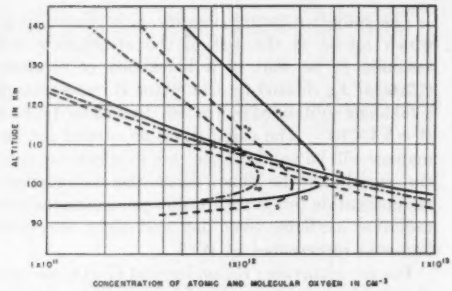

FIG. 2. Calculated number densities n_P and n_2 of atomic and molecular oxygen, respectively, as functions of height. (i) $T=300°K$, $dT/dx=10°/km$: solid curves. (ii) $T=300°K$, $dT/dx=5°/km$: dashes. (iii) $T=270°K$, $dT/dx=5°/km$: dots and dashes.

expand

$$\sigma_\nu'=\sigma_\nu'(\nu_1^0)+C(\nu-\nu_1^0) \tag{29a}$$

and it is necessary only to assume that C has a value of the same order as the corresponding coefficient in (29). On carrying out these calculations, we obtain the solution (28) which is shown in Fig. 1. For large $N_2(>2\times10^{19}/cm^2)$, (28) approaches the form

$$N\cong\frac{1}{(d\sigma_\nu/d\nu)_{\nu_0}}\left[\frac{h}{kT}-\frac{h}{k\theta}+\frac{2}{\nu_1^0}-\frac{2}{\nu_0}\right]$$

$$\cong3.98\times10^{21}\left(\frac{1}{T}-\frac{1}{\theta}\right)\Big/cm^2. \tag{28a}$$

For smaller $N_2(\sim10^{18}/cm^2)$, (28a) gives too high a value for N_2 and Fig. 1 must be employed.

It can be shown that Eq. (28a) represents a condition of detailed balance in which the number of dissociations in the vicinity ν_0 equals the number of recombinations

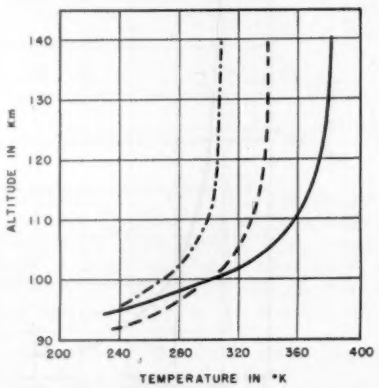

FIG. 3. Calculated temperatures as functions of height. (i) $T=300°K$, $dT/dx=10°/km$: solid curve. (ii) $T=300°K$, $dT/dx=5°/km$: dashes. (iii) $T=270°K$, $dT/dx=5°/km$: dots and dashes.

in the vicinity of ν_0^0. Thus for large values of N_2 (or equivalently for low values of T) there almost prevails detailed balance. However, for small values of N_2 (or large values of T) the mechanism assumed does *not* require detailed balance.

From the numerical solution of (27) as shown in Fig. 1, one obtains, in view of (3), an expression for the concentration of oxygen molecules

$$n_2=-(dN_2/dT)(dT/dx)\equiv P(T)dT/dx. \tag{30}$$

Thus n_2 depends on the height x through $T(x)$ and $dT(x)/dx$.

To obtain the concentration of oxygen atoms n_P, we insert (28) and (30) in (23). Now, to evaluate the integral on the right-hand side of (23), it is necessary to make a stronger assumption concerning σ_ν' than before, namely, that σ_ν' is about the same as σ_ν in the immediate neighborhood of their respective thresholds. On this assumption, one obtains for n_P

$$n_P=Q(T)(dT/dx)^{\frac{1}{2}}, \tag{31}$$

where $Q(T)$ is a somewhat complicated but known function of T. n_P depends on the height x through $T(x)$ and $dT(x)/dx$.

On putting (30) and (31) into Eq. (10), which can be written in the form

$$\frac{d^2T}{dx^2}=-\frac{2}{T}\frac{dT}{dx}\left\{\frac{Mg}{k}+\frac{1}{n_P+2n_2}\frac{dT}{dx}\left[n_2+n_P+T\frac{\partial}{\partial T}(n_P+n_2)\right]\right\}, \tag{32}$$

one obtains a differential equation of the second order for T. Equation (32) can be solved if two boundary values, such as T and dT/dx, are known at a certain height in the region for which the condition of the atmosphere is mainly governed by the processes of dissociation and recombination assumed in the theory. Equations (30) and (31) then give the concentrations n_2 and n_P as functions of the height. Thus it is seen that on the assumptions of the two conditions for the steady state, the temperature is automatically determined by the reaction processes themselves, together with the distributions of the atomic and molecular oxygen. It is in this sense that the present work is free from the additional assumptions that have been found necessary by the other investigators.[1–4]

V. NUMERICAL RESULTS AND DISCUSSION

To solve Eq. (32), we need the temperature and its gradient at a certain height. The empirical results available at present give quite different values for the temperature and its gradient. Thus the data from the V-2 rocket flights give an approximate value of 270°K for the temperature at 100 km,[10] whereas the data from

[10] Best, Havens, and LaGow, Phys. Rev. 71, 915 (1947); R. E. Newall, Jr., Trans. Am. Geophys. Union 31, 25 (1950).

radio wave reflection measurements indicate a value 300°K.[11] It does not seem possible to say which of these values is more reliable, since the former temperature is derived from a pressure curve whose individual readings can be in error by as much as a factor 2, while the latter temperature is derived with the use of cross sections for the collisions between electrons and molecules which may not be accurate. In any case one must also allow for differences arising from difference in latitude and in season in the different measurements. Hence we have solved Eq. (32) by numerical integration for a few values for the temperature and its gradient at 100 km. In the figures the results are plotted for three cases, namely, at 100 km, (i) the temperature T is 300°K and its gradient $dT/dx=10°/\text{km}$, (ii) $T=300°\text{K}$, $dT/dx=5°/\text{km}$, (iii) $T=270°\text{K}$, $dT/dx=5°/\text{km}$. Figure 2 gives the number densities n_2 and n_P, Fig. 3 gives the temperature, and Fig. 4 gives the percentage of dissociation, all as functions of the height, for these three cases.

From Fig. 3 it is seen that the temperature increases with the height, approaching asymptotically a constant value depending on the values of T and dT/dx at 100 km. But in these very high regions, the result of the present calculation is no longer valid, as processes other than the photodissociation and recombination of oxygen become effective. Thus one may understand any deviation in the observed temperature variation with height from the behavior shown in Fig. 3.

From Fig. 2 it is seen that in each case the distribution of atomic oxygen with height shows a maximum as expected. In case (i), the maximum n_P is 2.7×10^{12}/cc and lies at 102 km. In case (ii), the maximum n_P is 1.86×10^{12}/cc and lies at 99 km. In case (iii), the maximum n_P is 1.22×10^{12}/cc and lies at 102 km.

Figure 4 shows that, in all three cases, the degree of dissociation increases rather slowly with height and dissociation is not complete until a height of about 150 km is reached. This result is to be compared with those of Rakshit[3] and Penndorf,[4] who find that the dissociation is practically completed within a layer about 15 km thick.[11a]

All the results represented in Figs. 1, 2, 3, and 4, have been obtained from the two conditions for the steady state, the barometric equation, and the values of T and dT/dx at one given height. As no assumption whatsoever has been made about any of the various number densities, it must be regarded as a satisfactory feature of the theory that the concentration of molecular oxygen at 100 km at least comes out to be quite close to the empirical values, as shown below. To test the results of theory, we shall compare our calculated results with the V-2 roeket data[10] which give the total gas pressure of the atmosphere for all heights up to about 130 km. To make this comparison, the partial

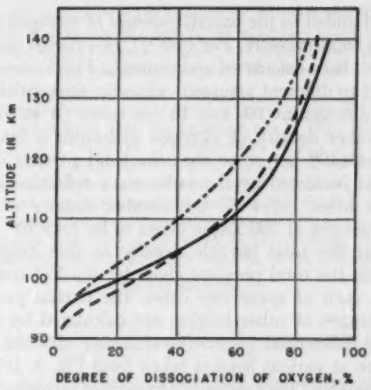

FIG. 4. Calculated degree of dissociation of oxygen as function of height. (i) $T=300°\text{K}$, $dT/dx=10°/\text{km}$: solid curve. (ii) $T=300°\text{K}$, $dT/dx=5°/\text{km}$: dashes. (iii) $T=270°\text{K}$, $dT/dx=5°/\text{km}$: dots and dashes.

pressures of atomic and molecular oxygen are calculated for each of the three sets of boundary conditions above

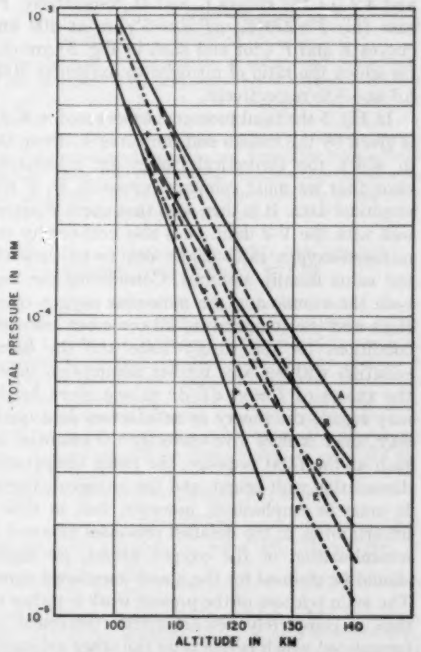

FIG. 5. Total pressure of the atmosphere in mm of Hg as function of height. (i) $T=300°\text{K}$, $dT/dx=10°/\text{km}$: solid curves A, B. (ii) $T=300°\text{K}$, $dT/dx=5°/\text{km}$: dashes C, D. (iii) $T=270°\text{K}$, $dT/dx=5°/\text{km}$: dots and dashes E, F. A, C, E curves: concentration of nitrogen at 100 km so chosen as to give the total pressure at 100 km indicated by the radio wave data. B, D, F curves: concentration of nitrogen at 100 km so chosen as to give the total pressure at 100 km indicated by the V-2 rocket data.

[11] D. F. Martyn and O. O. Pulley, Proc. Roy. Soc. (London) A154, 455 (1936).

[11a] See the discussion of the results of these authors in Appendix 7.

and added to the partial pressure of nitrogen to obtain the total pressure. For case (i), two curves (solid lines) have been calculated and shown in Fig. 5 corresponding to two different assumed values for the partial pressure of nitrogen at 100 km. In one curve (A in Fig. 5) the number density of nitrogen molecules is taken to be 2.54×10^{13} per cc so that the total particle density is that indicated by the radio wave reflection data.[12] In the other curve B, the number density of nitrogen molecules at 100 km is taken to be 1.4×10^{13} per cc so that the total particle density at that height agrees with the total pressure given by the V-2 rocket data. In each of these two cases, the partial pressures of nitrogen at other heights are calculated by means of the differential barometric equation with the temperature at various heights taken from Fig. 3. It is readily found that the concentration ratio of nitrogen to oxygen at 100 km comes out to be 4.2 and 2.2 for curves A and B, respectively.

In an entirely similar manner, two curves C, D (dotted in Fig. 5) are calculated for the case (ii) $T=300°$K and $dT/dx=5°$/km at 100 km. The ratio of nitrogen to oxygen at 100 km then comes out to be 8.1 and 4.9 for the curves C and D, respectively. For the case (iii) $T=270°$K, $dT/dx=5°$/km at 100 km, two curves E and F (dot and dash in Fig. 5) are obtained for which the ratio of nitrogen to oxygen at 100 km is 6.5 and 3.9, respectively.

In Fig. 5 the total pressure as measured in V-2 flights is given by the crosses and the curve V. From the way in which the theoretical curves are calculated, it is clear that we must compare curves B, D, F with the empirical data. It is then seen that curve F agrees very well with the V-2 data. It is also noteworthy that the nitrogen-oxygen ratio comes out to be very close to the value usually assumed. Considering the fact that both the atomic and the molecular oxygen concentrations and the temperature all come out from the two conditions for the steady state and the barometric equation without any further assumption other than the values of T and dT/dx at one given height, one may regard the theory as satisfactory in a qualitative way, since it does give correctly the essential features such as the total pressure, the rising temperature and dissociation with height, and the nitrogen-oxygen ratio. It must be emphasized, however, that in view of the uncertainties in the detailed processes assumed for the recombination of the oxygen atoms, no significance should be claimed for the above-mentioned agreement. The main purpose of the present work is rather to show that a completely self-consistent treatment can be formulated which is free from the other assumptions of the previous investigators, and that this treatment can give reasonable results compared with the empirical data.[12a]

[12] See S. K. Mitra, *The Upper Atmosphere* (The Royal Asiatic Soc. of Bengal, Calcutta, 1948).

[12a] It might be mentioned that if occasional winds occur at intervals larger than the time to establish dissociative equilibrium but short enough to disturb the diffusive equilibrium between the molecular oxygen and nitrogen, the result of the present work will still be largely valid. The effect will be to raise the level of molecular oxygen, or, equivalently, to give molecular oxygen a somewhat lighter mass. The principal result would be that the rate of change with height of the various calculated quantities would decrease somewhat. The authors are indebted to Professor C. H. Townes for pointing this out.

The authors wish to thank Professor H. M. Foley for his interest and discussions on this work, and Miss Lorraine Ourom for carrying out most of the numerical calculations.

APPENDIX 1. RELATION BETWEEN ABSORPTION COEFFICIENT AND RECOMBINATIONS CROSS SECTION

Let $\sigma(P, j, q, \nu; \hat{p}, P')$ be the cross section for the process (1) in which a molecule having the total linear momentum P, the rotational quantum number j, and the vibrational quantum number q, absorbs a photon of frequency ν and dissociates into two atoms having a momentum $\hat{p}$ with respect to each other and a momentum P' for their center of mass. Let $\rho_\nu d\nu$ be the radiation energy density in the frequency range between ν and $\nu+d\nu$, and $n_3(P, j, q)$ be the number of such molecules per unit volume. Then the number of this type of dissociation per unit volume per second is

$$n_3(P, j, q)\sigma(P, j, q, \nu; \hat{p}, P')(c\rho_\nu/h\nu)d\nu. \tag{33}$$

Let $n_D(P_D)dP_D$, $n_P(P_P)dP_P$ be the number of atoms per unit volume in the ^1D and ^3P states having momenta between P_D and P_D+dP_D, and between P_P and P_P+dP_P, respectively. We define the cross section $\beta(\hat{p}, P'; P, j, q, \nu)$ by stating that the following expression

$$n_D(P_D)n_P(P_P)\beta(\hat{p}, P'; P, j, q, \nu)[1+c^3\rho_\nu/8\pi h\nu^3]v \tag{34}$$

represents the number of radiative recombinations per unit volume per second which are the inverse of process (1). In these recombinations two atoms of relative momentum $\hat{p}$ and total momentum P' recombine by a radiative transition to form a molecule whose state is described by P, j, q. For convenience, we shall write σ for $\sigma(P, j, q, \nu; \hat{p}, P')$ and β for $\beta(\hat{p}, P'; P, j, q, \nu)$. We let v represent the relative velocity of the atoms.

β can be determined in terms of σ by means of the principle of detailed balancing. For this purpose, let us assume the system to be in thermodynamical equilibrium so that $n_D(P_D)$, $n_P(P_P)$, $n_3(P, j, q)$ obey the Boltzmann statistics and $\rho_\nu d\nu$ is the energy density for black body radiation, all distributions being characterized by the same temperature T. The principle of detailed balancing states that

$$n_3(P, j, q)\sigma c\rho_\nu d\nu/h\nu = n_P(P_P)n_D(P_D)\beta[1+c^3\rho_\nu/8\pi h\nu^3]v. \tag{35}$$

Now one has

$$n_3(P, j, q) = \frac{4\pi(2j+1)n_3 e^{\chi/kT}}{h^3 f_1(T, 2M)f_2(T)f_3(T)} \exp\left(-\frac{P^2}{4MkT}\right) \times\exp\left(-\frac{j(j+1)h^2}{4\pi^2 r_0^2 MkT}\right)\exp\left(-\frac{qh\omega}{kT}\right)P^2dP, \tag{36}$$

and

$$n_P(P_P)n_D(P_D) = \frac{16\pi^2 n_D n_P}{h^6 f_1\left(T, \frac{M}{2}\right)f_1(T, 2M)} \exp\left(-\frac{P'^2}{4MkT}\right) \times\exp\left(-\frac{P^2}{MkT}\right)P'^2dP'\hat{p}^2d\hat{p}, \tag{37}$$

where χ is the energy of dissociation (including the zero-point energy), r_0 the equilibrium distance between the atoms, ω the vibrational frequency of the molecule, and M the mass of the oxygen atom. $f_1(T)$, $f_2(T)$, $f_3(T)$ are the partition functions respectively of translational, rotational, and vibrational motion

and are given by

$$f_1(T, M) = (2\pi MkT)^{\frac{1}{2}}/h^3,$$
$$f_2(T) = 4\pi^2 Mr_0^2 kT/h^2, \tag{38}$$
$$f_3(T) = e^{\chi/kT}(1-e^{-h\omega/kT}).$$

Also one has

$$\rho_\nu = 8\pi h\nu^3 c^{-3}(e^{h\nu/kT}-1)^{-1}. \tag{39}$$

The conservation of momentum before and after collision gives

$$P = P'. \tag{40}$$

The conservation of energy gives

$$h\nu + \frac{P^2}{4M} + \frac{j(j+1)h^2}{4\pi^2 Mr_0^2} + qh\omega = \frac{P'^2}{4M} + \frac{p^2}{M} + \chi. \tag{41}$$

The relation between the concentrations of atoms and molecules at equilibrium is given by the reaction isochore, namely,

$$\frac{n_P n_D}{n_2} = \frac{2G_1}{G_2}\frac{f_1(T, 2M)f_1(T, M/2)}{f_1(T, 2M)f_2(T)f_3(T)}, \tag{42}$$

where G_2 is the electronic and nuclear degeneracy of the molecule, G_1 is the statistical weight of the atoms, and the "symmetry factor" 2 represents an additional degeneracy arising from the fact that the nuclei of the atoms are identical.

Substitution of (36) through (42) into (35) gives[12b]

$$\beta = 4(2j+1)(G_2/G_1)(h^2\nu^2/M^2c^2v^2)\sigma. \tag{43}$$

The ratio of β to σ is thus independent of temperature, as it should be, since β and σ are atomic properties. The ratio of β to σ could also have been obtained from quantum mechanics using Dirac's transition probabilities. The ratio of β to σ is then simply proportional to the ratio of the density of atomic states to that of molecular states.[12c]

Actually we are more interested in finding β', the recombination coefficient for the process (14), rather than β, since most of the atoms recombine by this process. Defining σ' as the detailed cross section for the inverse process of (14), we have

$$\beta' = 4(2j+1)(G_2'/G_1')(h\nu/Mcv)^2\sigma' \tag{43a}$$

where G_1' is the statistical weight of the two atoms in the ^1P state, which is different from G_2'.

APPENDIX 2. EQUATIONS FOR THE STEADY STATE IN THE DETAILED MODEL

In Eq. (21) and (22), for simplicity, we have neglected to indicate the dependence on the rotational and vibrational states of the molecule. We can rewrite them to include the dependence by using σ and β' defined above. Equations (21) and (22) become

$$\sum_{P,j,q}\int_{\nu_0}^{\infty} n_2(P, j, q)(\sigma c\rho_\nu/h\nu)d\nu = \sum_{P',p} n_P(P_P)n_P(\bar{P}_P)\beta' v(1+c^3\rho_\nu/8\pi h\nu^3), \tag{44}$$

and

$$\sum_{P,j,q}\int_{\nu_0}^{\infty} n_2(P, j, q)\sigma c\rho_\nu d\nu = \sum_{P',p} n_P(P_P)n_P(\bar{P}_P)h\nu\beta' v(1+c^3\rho_\nu/8\pi h\nu^3). \tag{45}$$

Here $n_P(P_P)n_P(\bar{P}_P)$ is to be replaced by a distribution given in terms of the relative momentum p of the recombining atoms and the momentum P' of their center of mass. The frequency ν and the relative velocity v are related by the law of conservation of energy.

The values of j in (44) should be restricted to even integers, since the nuclei of the oxygen atoms are identical and have zero spin. However, in our case where the rotational levels are highly excited so that sums over j are replaced by integrals, the effect of using only even values of j cancels out, excepting in the case of the reaction isochore, where the effect has already been taken into account by the symmetry factor 2. Hence we shall not explicitly use the restriction.

At temperatures which are believed to exist in the 100 km region, we may assume that the molecules are in their lowest vibrational state of the lowest electronic state. Since χ is of the order of 7 volts, whereas the rotational energy is of the order 0.02 volt, we shall regard ν_0 as a constant given by $h\nu_0 = \chi$. This is in agreement with the observation that the Schumann-Runge continuum starts quite sharply at the wavelength 1751A.

We shall now make use of the result of Stueckelberg for σ. The expression Γ_{kW} in Stueckelberg's paper[9] is, in our notation

$$\Gamma_{kW} = (2j+1)\sigma c\rho_\nu d\nu/h\nu,$$

and

$$\sigma_\nu = \sum_j \frac{(2j+1)}{f_3(T)}\sigma \exp\left[\frac{j(j+1)h^2}{4\pi^2 Mr_0^2 kT}\right] = \frac{64\pi^{7/3}}{3c}\cdot\frac{M}{2h^2\gamma a}\mathfrak{M}^2(r_1)\nu f(\nu), \tag{46}$$

where γ, a, and $\mathfrak{M}(r_1)$ are constants which Stueckelberg determines from the empirical results of Ladenburg *et al.* The function $f(\nu)$ can be calculated from the data given by Stueckelberg.[9] It should be noted that σ_ν is independent of the temperature as it should be, since it is a molecular property.

Since we wish to find β', it is seen from (43a) that we must know σ'. The cross section σ' has not been measured or calculated. We shall make the reasonable assumption that σ_ν' has a form similar to that for σ_ν. Thus we write

$$\sigma_\nu' = \sum_j \frac{(2j+1)}{f_3(T)}\sigma' \exp\left[\frac{j(j+1)h^2}{4\pi^2 Mr_0^2 kT}\right] = K'\nu f_1(\nu). \tag{46a}$$

On using the laws of conservation of energy and momentum, Eqs. (43a), (46), and (46a), and neglecting the induced emission in (44) and (45) which is very small, one finally obtains the equations for the steady state in the form (21) and (22) in the paper. It is seen that even though one starts with a different value for the rotational temperature from the translational temperature, only the translational temperature appears in Eqs. (21) and (22). The rotational temperature has dropped out on account of the averaging process in (46).

APPENDIX 3. TIME REQUIRED TO REACH DISSOCIATIVE STEADY STATE

To find the time required to reach the dissociative steady state when an atmosphere initially consisting of molecular oxygen at constant temperature throughout is illuminated by sunlight, it is necessary to integrate Eq. (18) from the time sunlight is turned on to the time at which $dn_P/dt = 0$. However, this time is infinite. Hence we shall find instead the time required to reach 10 percent of the final dissociation, say, and multiply this time by 10. This time will represent a sort of relaxation time giving the order of magnitude for the time required to reach the dissociative steady state.

On neglecting the recombinations Eq. (18) becomes

$$dn_P/dt = An_2, \tag{47}$$

where the coefficient A is given, in view of (18), (26), and (46), by

$$A = \tfrac{1}{2}W(8\pi/c^2)\int_{\nu_0}^{\infty}\nu^2 f(\nu)\exp[-\sigma_\nu N_2 - h\nu/k\theta]d\nu. \tag{48}$$

If the region which is considered is at 100 km, where N_2 is large, only that part of the integrand which is near ν_0 contributes. Hence near ν_0 we write $\sigma_\nu = \sigma_{\nu_0} + (d\sigma_\nu/d\nu)_{\nu_0}(\nu-\nu_0)$ in the integrand and find

$$A = (2\pi/c^2)WK\exp(-K\nu_0 f' N_2 - h\nu_0/k\theta) \times \int_{\nu_0}^{\infty}\nu^2 f(\nu)\exp[-\{K(\nu_0 f' + f)N_2 + h/k\theta\}(\nu-\nu_0)]d\nu, \tag{49}$$

where $f = f(\nu_0)$ and $f' = f'(\nu_0)$. Since the exponential factor in the integrand decreases very rapidly with increasing ν, we may write

[12b] Compare this relation with the corresponding formula for the cross sections of photo-ionization of an atom and the inverse radiative recombination between the ion and the electron, given by E. A. Milne, Phil. Mag. 47, 209 (1924).

[12c] The authors are indebted to Dr. A. Bohr for this observation.

the integral as

$$\nu_0 \beta' [K(\nu_0 f' + f) N_2 + h/k\theta]^{-1}.$$

A is a function of the time and altitude through the variable $N_2(x)$. As only orders of magnitude are being estimated, we shall simplify the calculation by giving $N_2(x)$ a constant value in time, which will represent the average value. According to Fig. 1, the value of $N_2(x)$ at 100 km for the case $T=300°$K at 100 km in the dissociative steady state is $\simeq 7\times 10^{13}$. With this value, one gets for the time for dissociation steady state about 10 days. Even if this estimate is too small by a factor 10, this time is still shorter than the time required for the establishment of diffusive equilibrium, which is of the order of years for this height.[12]

APPENDIX 4. THE RADIATIVE RECOMBINATION COEFFICIENT

Having found β, one can calculate the recombination coefficient for two oxygen atoms, one of which is in the ^1D state and the other in the ^3P state. It is given by

$$B = \int_0^\infty \beta_\nu v F(v) dv = 2.19\times 10^{-32} T \text{ cm}^3/\text{sec}. \tag{50}$$

For $T=300°$K, we have $B=6.56\times 10^{-20}$ cm^3/sec. This can be compared with the result given by Nicolet[13] for two oxygen atoms approaching each other along the level giving the Herzberg bands, namely, $B=7.6\times 10^{-20}$ cm^3/sec.

It can be shown that, under the assumption about σ_ν' made earlier, the recombination coefficient for two oxygen atoms, both in the ^3P state, is

$$B' = \int_0^\infty \beta_\nu' v F(v) dv = (G_1/G_1')(\nu_1^0/\nu_0)^2 B \cong \tfrac{1}{5} B.$$

With these recombination coefficients, since $n_D \ll n_P$, it can be seen that the number of recombinations per sec of type (1a) is much less than that for the process (14), i.e.,

$$n_P n_D B \ll\ll n_P^2 B'.$$

Hence our assumption that (14) is a more important process than (1a) for the formation of molecules is justified.

APPENDIX 5. CROSS SECTIONS FOR THREE-BODY RECOMBINATION COLLISIONS

We wish to investigate the relative importance of three-body recombination collisions of the type (12)

$$O+O+X \rightarrow O_2(X\,{}^3\Sigma_g^-) + X^* \tag{12}$$

and two-body radiative recombination collisions of the type (14). The coefficient of a two-body radiative collision can be calculated from the absorption coefficient of the inverse process, as shown in Appendix 1. We shall obtain below a similar relation between the coefficients of the 3-body process (12) and of its inverse 2-body process. Before doing that, we shall make an estimate of a three-body collision coefficient on the basis of the classical kinetic theory.

Consider the process (12), in which the particles are represented by spheres of radius a moving with an average velocity v. Simple considerations show that the number of three-body collisions (a particle X collides with a system of two O atoms when they are within a distance $2a$ of each other) per unit volume per second is $2\pi v a^5 [O]^2 [X]$, where the brackets indicate number densities. If one takes $a=1.5\times 10^{-8}$ cm, then, at temperatures of a few hundred degrees absolute, the coefficient $C=2\pi v a^5$ of three-body collisions in this sense is 1.5×10^{-32} cm^6/sec. This must now be multiplied by the ratio of statistical weights of the molecular state $^3\Sigma_g^-$ of O_2 and the atomic state $(^3P+{}^3P)$, namely, 3/81. Thus if every 3-body collision, according to this classical model, leads to the formation of O_2, the coefficient C is 5×10^{-33} cm^6/sec. This rather optimistic estimate is about 10^3 times smaller than the values deduced from experiments on gases other than oxygen.[14]

We shall now make a more detailed study of three-body collisions. Consider the inverse process of (12), namely,

$$O_2 + X^* \rightarrow O + O + X \tag{51}$$

which is a two-body collision. The cross section for the three-body collision (12) can then be obtained in terms of the two-body collision cross section of (51) by means of the principle of detailed balancing. We shall examine all the possible two-body processes (51). Since the three-body collision cross section will be proportional to the two-body collision cross section, only that two-body process which is the most probable need be considered.

The particles which exist in the region of the upper atmosphere in which we are interested are electrons, oxygen atoms, oxygen molecules, and nitrogen molecules. It is possible to disregard the electrons as an important third body, since the maximum electron density is of the order of 10^6/cm^3 and is very much smaller than the densities of oxygen atoms, molecules, and nitrogen molecules, namely, 10^{11}/cm^3, 10^{12}/cm^3, and 10^{13}/cm^3, respectively. We shall hence only consider two-body collisions (51) in which the third body X is an atom or a molecule.

Consider now the dissociation of a diatomic molecule in (51). There are two cases possible: (a) the molecule may jump from a vibrational state of the normal electronic state to a vibrational state in the continuum of the same electronic state, or (b) it may jump from a vibrational state of the normal electronic state to an excited repulsive electronic state. In the case (a), the third body may supply this energy of vibrational excitation from its kinetic energy of translational motion, or from its electronic energy, and if the third body is a molecule, from its vibrational energy. Now the probabilities of such processes are very small,[15] and we may consider only the case (b). This process of the transfer of the electronic energy of one particle to the electronic energy of a molecular is similar to the one in which two atoms exchange excitation energy upon collision. The calculation of Stueckelberg indicates that the probability of such a transfer can be quite large in certain cases.[16] Hence we shall assume that the most important process (51) is a collision in which X transfers its energy of electronic excitation to an oxygen molecule.

We shall now define a "cross section" for the three-body collision (12). Let the electronic states of the two atoms arising from (51) be denoted by a and b, their number densities by n_a and n_b, respectively. Let the number density of oxygen molecules having momentum P, rotational quantum number j, and vibrational quantum number q be denoted by $n_2(P, j, q)$. Let $\sigma_2(P, j, q, P_z^*; P', p, P_z)$ be the cross section for a collision in which an oxygen molecule in the state P, j, q is dissociated by an electronically excited third body of momentum P_z^* and the number density $n_z^*(P_z^*)$. The number of collisions (51) per unit volume per second is then

$$\sigma_2 u^* n_2(P, j, q) n_z^*(P_z^*), \tag{52}$$

where u^* is the relative velocity of the oxygen molecule and the excited X^*.

Let the number density of atoms in the state a and having a momentum between P_a and $P_a + dP_a$ be denoted by $n_a(P_a)dP_a$. The number density of atoms in state b will be denoted similarly. Let $n_x(P_X)$ be the number density of unexcited X having a momentum P_x. The number of three-body recombinations (12) per unit volume per second is given by the following expression, which defines the "cross section" σ_3 for the three-body process (12):

$$n_a(P_a) n_b(P_b) v \sigma_3(P', p, P_z; P, j, q, P_z^*) n_z(P_z), \tag{53}$$

where v is the relative velocity of the oxygen atoms with respect to each other. Thus, the cross section σ_3 is of the dimension area $\times$volume, so that it can be interpreted as the cross section per unit concentration of the third body X.

[12] M. Nicolet, Mem. inst. roy. meteorologique de Belgique, No. 19 (1943).

[14] E. Rabinowitch, Trans. Faraday Soc. 33, 283 (1937).

[15] N. F. Mott and H. S. W. Massey, *The Theory of Atomic Collisions* (Oxford University Press, London, 1949), Chapter XII.

[16] Reference 15, Chapter VIII.

The statement of detailed balance is

$$\sigma_2 u^* n_2(P, j, q) n_x^*(P_x^*) = n_a(P_a) n_b(P_b) \sigma_2 v n_x(P_x), \quad (54)$$

where the number densities are given by the Boltzmann theorem, all quantities being characterized by the same temperature. The $n_2(P, j, q)$ and $n_a(P_a)n_b(P_b)$ are given by expressions similar to (36) and (37). Also, we have

$$n_x(P_x) = \frac{4\pi G_x n_{x1}}{h^3 f_1(T, M_x) f_t} \exp\left(-\frac{\epsilon + P_x^2/2M_x}{kT}\right) P_x^2 dP_x, \quad (55)$$

$$n_x^*(P_x^*) = \frac{4\pi G_x^* n_{x1}}{h^3 f_1(T, M_x) f_t} \exp\left(-\frac{\epsilon^* + P_x^{*2}/2M_x}{kT}\right) P_x^{*2} dP_x^*, \quad (55a)$$

where n_{x1} is the total number of the third body X per unit volume, M_x the atomic or molecular weight of X, ϵ and ϵ^* are the electronic energies of the normal and the excited states, respectively, G_x and G_x^* their statistical weights, and f_t is the partition function of the electronic states, of X. We shall replace the momenta P and P_x^* and P' and P_x by the relative momentum of the third body with respect to the molecule P_r, P_r^* and the total momentum P_t, P_t^* of the whole system, the unstarred and starred referring to values before and after collision, respectively. The conservation of momentum and energy gives

$$P_t = P_t^*$$

and

$$\frac{P_t^{*2}}{2(2M+M_x)} + \frac{P_r^{*2}}{2\mu} + \frac{j(j+1)h^2}{4\pi^2 M r_0^2} + qh\omega = \frac{P_t^2}{M} + \frac{P_r^2}{2\mu} + \frac{P_x^2}{2(2M+M_x)} + (\epsilon - \epsilon^*) + \chi,$$

where

$$\mu = 2MM_x/(2M+M_x).$$

Substitution of all of these into (54) and the use of the reaction isochore similar to (42) lead to the relation

$$G_x^* G_2 (2j+1) u^{*2} \sigma_2 du^* = \pi G_x G_1 (M/h)^3 \sigma_3 u^2 du v^2 dv, \quad (56)$$

where u is the relative velocity of the third body with respect to the center of mass of the pair of atoms after collision, and G_1 and G_2 are the statistical weights of the oxygen atoms and molecules, respectively. It is seen that the ratio of σ_3 to σ_2 is independent of the temperature, as it should be, since the cross sections are atomic and molecular properties.

The relation (56) is quite general. We shall now assume that only exchange of electronic energy plays a part, so that no translational energy is transferred, i.e., $u = u^*$. Furthermore, since σ_2 is greatest at resonance, we may set $\chi = \epsilon^* - \epsilon$. We shall assume that the molecule is in its normal vibrational state, and that the kinetic energy of the dissociated atoms comes from the rotational energy of the molecule. On replacing the discrete rotational states by a continuum, and using the relation between the velocities u, u^*, v given above, the relation (56) simplifies to

$$\sigma_3 = 2\pi h r_0^3 (u G_2 G_x^* / M v^2 G_1 G_x) \sigma_2. \quad (57)$$

It is easy to see that σ_3 is of dimension length to the fifth power.

The total number Q_3 of three-body recombination collisions per unit volume per second is obtained by integrating (53) over all velocities v and u. As σ_3 has been assumed to depend only on the exchange of electronic energy, it will be an insensitive function of the velocities. Hence, we have

$$Q_3 = 2\pi h r_0^3 (G_2 G_x^* / M G_1 G_x) \langle u \rangle_{av} \langle 1/v \rangle_{av} n_2 n_a n_b \sigma_2. \quad (58)$$

The average value of $1/v$ is obtained from the Boltzmann distribution in velocity for the reduced mass of the oxygen molecule, and $\langle u \rangle_{av}$ is obtained for the reduced mass μ defined previously. The factor G_x^*/G_x is of the order unity. Hence the total number of three-body recombinations per unit volume per second is given by

$$Q_3 = 10^{-30} \sigma_2 n_a n_b n_x = C n_a n_b n_x, \quad (59)$$

where C is the three-body recombination coefficient. To estimate the value of C, one needs the two-body collision cross section σ_2. Now σ_2 is in general smaller than, or of the order of, the gas kinetic cross section, but for some cases may be considerably larger at resonance. For lack of both theoretical and experimental information for the system $O_2 + X^*$ in (51), we shall take for σ_2 the gas kinetic value 10^{-15} cm^2 and obtain

$$C = 10^{-30} \text{ cm}^6/\text{sec}.$$

To estimate the relative importance of two-body and three-body collisions at the height of about 100 km, we shall take for n_x the value 10^{13}/cm^3 which is of the order of the total number density of gas molecules at that height. For the two-body radiative recombination, we have, from Appendix 4, the value $B' = 10^{-20}$. Hence the ratio of two- to three-body recombinations at this height is given by

$$Q_2/Q_3 = (B' n_a n_b)/(C n_a n_b n_x) = 10^3. \quad (60)$$

For greater heights and hence smaller n_x, three-body recombinations will be still less important.

This and the simple estimate made at the beginning of this appendix lead us to assume two-body recombinations in our calculations.

It might be mentioned that Fowler uses a similar three-body treatment in his discussion of electron capture by an ion.[17]

APPENDIX 6. RADIATIVE RECOMBINATIONS BETWEEN TWO OXYGEN ATOMS

To investigate the relative importance of the possible radiative recombinations between two O(^3P) atoms, we first note that the following types of states can arise from two such atoms: $^1\Sigma_g^+$, $^1\Sigma_u^-$, $^1\Pi_g$, $^1\Pi_u$, $^1\Delta_g$, $^3\Sigma_u^+$, $^3\Sigma_g^-$, $^3\Pi_u$, $^3\Pi_g$, $^3\Delta_u$, $^5\Sigma_g^+$, $^5\Sigma_u^-$, $^5\Pi_g$, $^5\Pi_u$, $^5\Delta_g$. Of these, $X\,^3\Sigma_g^-$ is the normal state. Three other states have been identified from the analysis of the spectrum, namely, $b\,^1\Sigma_g^+$, $a\,^1\Delta_g$, $A\,^3\Sigma_u^+$. The other states have not yet been located.

We shall investigate the nature of the process or processes that contributes most to the recombination of the atoms on the basis of the following arguments. It is generally believed that the source of energy of radiation emitted in the night sky is the recombination of oxygen atoms into molecules, although the exact mechanisms whereby the various lines and bands in the spectrum are excited are not known with definiteness. Since the intensity of the night sky radiation is found to change only inappreciably during the whole night, it follows that not more than a small fraction, say perhaps 1/100, of the oxygen atoms present at sunset can have disappeared during the night, i.e.,

$$10 \cdot 60^2 n_P^2 \int_0^\infty \beta_v' v F(v) dv \leqq \frac{1}{100} n_P.$$

For the height where n_P is $\sim 10^{13}$/cm^3, this gives for the recombination coefficient the order of magnitude $\leqq 3 \times 10^{-19}$ cm^3/sec. This value can be compared with the value calculated in Appendix 4 for the recombination process (1a) which involves an allowed dipole transition. Thus it seems most probable that the process or processes contributing most to the recombination of the oxygen atoms involve allowed dipole transition.

There are two possibilities for such recombinations: (1) two O(^3P) atoms approaching each other in a state which combines by dipole transition to form the normal state $X\,^3\Sigma_g^-$, and (2) two O(^3P) atoms approaching each other in a state which combines to form a stable excited state by dipole transitions. Reference to the list of possible states formed from two O(^3P) atoms given above shows that the only state that combines with $X\,^3\Sigma_g^-$ by dipole transitions is the $^3\Pi_u$-state. This state has not been found, but either it must be strongly repulsive, or the potential energy curve has a weak minimum at large nuclear separation, for otherwise absorption bands from the ground state would have been found. In either case, the transition probabilities to the lower vibrational states of $X\,^3\Sigma_g^-$ will be small on account of the Franck-Condon principle. Transition probabilities to highly

[17] R. H. Fowler, *Statistical Mechanics* (Cambridge University Press, London, 1936), Sec. 17.6.

excited vibrational states of $X\,^3\Sigma_g^-$ will also be small, since at large nuclear separations the matrix element of the dipole moment of the system will be small.

Passing on to the case (2), it is seen that two $O(^3P)$ atoms approaching each other in the state $^1\Pi_u$ will be in a position to make a dipole transition to the state $b\,^1\Sigma_g^+$. The potential curve of $^1\Pi_u$ is not known, but it is not impossible that it has a weak minimum or is weakly repulsive in such a way that the turning point (where the horizontal line representing the kinetic energy of the approaching atoms intersects the potential curve) lies vertically above the neighborhood of the minimum of the $b\,^1\Sigma_g^+$ curve. In these cases, the transition probabilities will be of the order estimated above.

The resulting molecule in the state $b\,^1\Sigma_g^+$ can go down to the normal state $X\,^3\Sigma_g^-$ either on emitting the so-called atmospheric bands with transition probabilities of the order 0.1 per second, or in a collision of the second kind with another atom or molecule. The cross section for the transfer of energy of electronic excitation of one particle to the kinetic energy of a heavy particle (atom or molecule) is very small. As the collision frequency in a gas of number density 10^{13}/cm^3 is of the order 20 per second, the radiative transition mentioned above may be more important than the de-excitation by collisions of the second kind with atoms or molecules. The identification of the atmospheric bands in the infrared spectrum of the night sky[6,7] seems to lend some weight to this suggested mechanism.

APPENDIX 7. DISCUSSIONS OF THE WORK OF PENNDORF AND OF RAKSHIT

A. We shall first examine Penndorf's work.[4] Penndorf starts with an atmosphere having an assumed temperature distribution $T(h)$ and total pressure distribution $P(h)$ before dissociation by solar radiation takes place. On assuming the proportion given by (7), the total oxygen concentration $[O_2]_t$ before dissociation is calculated by means of the relation,

$$P(h)=([N_2]_t+[O_2]_t)kT. \tag{61}$$

Let A^* be the number of quanta of solar radiation absorbed in a thickness s per unit cross section per second at the height h, and $J_{\lambda\lambda}$ be the number of quanta in the solar radiation per $10A$ interval crossing unit area per second at the height h. Let k_λ'' be the absorption coefficient ($k_\lambda''=\sigma_\nu$ of the present paper) and let the subscript G denote the steady state. Then†

$$A^*=\int J_{\lambda\lambda}[1-\exp(-sk_\lambda''[O_2]_G)]d\lambda, \tag{P-21}$$

and for the upper regions where $sk_\lambda''[O_2]_G\ll 1$,

$$A^*=s[O_2]_G\int J_{\lambda\lambda}k_\lambda''d\lambda. \tag{P-22}$$

For either (P-21) or (P-22), one has

$$A^*=f_1[O_2]_Gs, \tag{P-23, 24}$$

which defines f_1 as the probability per second of a molecule at the height h absorbing a dissociating photon from the solar radiation. The steady state is given by

$$f_1[O_2]_G=k[M]_G[O]_G^2, \tag{P-18}$$

where k is the recombination coefficient for three-body processes. For the upper regions where the dissociation is almost complete, Eq. (P-18) is replaced by (P-19), which is obtained from (P-18) by setting $[O]_G$ equal to $2[O_2]_t$.

(1) It is seen from Table IV of Penndorf's paper‡ that the assumption

$$[O_2]_G+\tfrac{1}{2}[O]_G=[O_2]_t \tag{P-9}$$

has been made. This implies that the oxygen atoms and molecules do not readjust themselves after dissociation has taken place. This is equivalent to assuming an atmosphere which is separated into parallel layers by transparent partitions before the solar radiation is "turned on." As a consequence of assumption (P-9), there results an inconsistency. The total pressure $P(h)$ with which the calculation is started is that given by (61). After dissociation has taken place, the total pressure is given by

$$P(h)=([N_2]_t+[O_2]_G+[O]_G)kT,$$

which in view of (P-9) becomes

$$P(h)=([N_2]_t+[O_2]_t+\tfrac{1}{2}[O]_G)kT, \tag{62}$$

which is obviously different from that given by (61) except where there is no dissociation. To illustrate this, let us consider the height 130 km. From the assumed $T=330°$K and $P=0.00011$ mb and the relations (7) and (61), Penndorf obtains $[O_2]_t=3.92\times10^{11}$/cc, and $[N_2]_t=1.78\times10^{12}$/cc, as shown in Table II. Now, according to Table IV, which has been calculated on the basis of Table II, the oxygen is almost completely dissociated so that $[O]_G=7.84\times10^{11}$/cc; but this would have led to a total pressure of 1.17×0.00011 mb, contradicting the original assumed value. The difficulty emphasized here is not so much with the factor 1.17 as with the intrinsic impossibility of obtaining $[O_2]_t$ or $[O]_G$ from (62) on any assumed $T(h)$ and $P(h)$ without the use of Eq. (11).

(2) Consider now the central part of the calculation in Penndorf's paper. The procedure of the calculation is described as follows: "The calculations started at 130 km, where the amount of $[O_2]_G$ is found to be small, and formula (22) was used. . . . Having computed A^* by numerical integration, f_1 was obtained by (23). Thereupon, the amount of oxygen atoms or molecules in the equilibrium state was computed by either (18) or (19). Since $[O_2]_G$ resulting from formula (19) enters the basic equation for the absorption (20), the correct value had to be found by testing until the value used in the exponent equaled the result of (19)."

Now Eq. (P-18) or (P-19), together with the assumption (P-9), gives only one equation containing two unknowns $[O_2]_G$ and f_1. The quoted paragraph above seems to have stated that f_1 is obtained from (P-21) and (P-23) (or P-22 and P-24); but Eq. (21) or (P-22) is not an additional equation for f_1 and $[O_2]_G$ in the sense that it can be combined with (P-18) or (P-19) to give f_1 and $[O_2]_G$, since A^* is not known from any other relation than Eq. (P-21) or (P-22) itself. Thus, it is not clear how $[O_2]_G$ and f_1 could have been obtained from essentially a single equation—namely, (P-18) or (P-19). In fact it is not clear how A^* could have been obtained by "numerical integration" at all, since $J_{\lambda\lambda}$ at the height h depends on $f_\lambda^\infty[O_2]_Gdh$ according to Eq. (2), and to find $[O_2]_G$ at all heights is exactly the central part of the problem.

On trying to reconstruct Penndorf's procedure, it seems that the only reasonable way the calculation could have been started is as follows. At 130 km, $J_{\lambda\lambda}$ was assumed to have the value of the solar radiation unattenuated by absorption by the overlying layers. With this $J_{\lambda\lambda}$ at 130 km, f_1 was calculated for this height from (P-23), and with this f_1, $[O_2]_G$ was calculated from (P-19). This $[O_2]_G$ was then inserted into (P-22) to give A^* for a layer of 1 km thick, and the reduction in $J_{\lambda\lambda}$ therein, so that $J_{\lambda\lambda}$ for the next layer below could be calculated.

If this is the actual procedure adopted by Penndorf, then the following objection may be raised. On the technical side, since $J_{\lambda\lambda}$ depends exponentially on the total number $N_2=f_\lambda^\infty[O_2]_Gdh$ of the existing molecules above h, the calculated result will depend very strongly on the assumption made about N_2. The assumption that $J_{\lambda\lambda}$ at 130 km has the full, or any other, value of the solar radiation implies that $k_\lambda''N_2\ll1$, and this in turn implies that the oxygen is highly dissociated at and above 130 km; but this is exactly what is to be calculated from the theory and must not be assumed in the calculation. In principle, the objection is that the problem is already completely determined by Eq. (11) and the boundary conditions (11a) and will be inconsistent with any further assumption about N_2. It is the failure to recognize this that has led to this and the other difficulty with the total pressure discussed above.

† For convenience we follow Penndorf's notations in this Appendix and denote by (P-18) Eq. (18) in his paper, etc.

‡ There are many misprints in the exponents under $[O_2]_G$ in Table IV.

(3) Another debatable point in Penndorf's work is the assumption that the oxygen atoms recombine in three-body processes. The relative importance of two-body and three-body processes has been discussed in Appendix 5 above. It may perhaps be mentioned here that since no provision is made for the emission of radiation in Penndorf's theory, the oxygen will keep on transforming solar radiation into the kinetic energy of the atoms and molecules, with a consequent continual rise in the temperature of the atmosphere; for at the low pressure and low values of the d^2T/dh^2 in this part of the atmosphere, the loss of heat by conduction is very slow.

(4) The result given in Table VII for the time of "half-recombination" in the absence of solar radiations does not seem right. One certainly expects the time taken for "half-recombination" to be shorter the greater the value of the coefficient of recombination k_1. The reverse, however, is shown in Table VII.

B. Consider now Rakshit's work.[3] As Rakshit's work is a refinement of, and supersedes, the earlier work of Majumdar,[2] it will be sufficient to confine our discussions to Rakshit's paper.

(1) Rakshit also assumes a given temperature distribution $T(h)$ and the proportion (7). From $T(h)$ and the total pressure P at 80 km, the total pressure and the partial pressure p of oxygen before dissociation are calculated for other heights. Here, as in Penndorf's work, the assumption (P-9) is also made, with the same consequent difficulty with the pressure. Thus at 115 km, the assumed $T=300°K$ and $P=1.50\times10^{-4}$ mm of mercury lead to the partial pressure p of oxygen $p=3.00\times10^{-6}$ mm as given in Table II. On the other hand, from Table III, one finds for the partial pressure p_d after dissociation the value 5.4×10^{-6} mm, contradicting the original total pressure assumed.

(2) Rakshit calculates the total number N_2 of oxygen molecules in a column of unit cross section above the height h by means of the relation $N_2=pNH$, where p is the partial pressure of oxygen before dissociation, H the height of the homogeneous atmosphere for O_2, and N the number of molecules of a gas per cc at standard temperature and pressure. It is not clear how H has been obtained, but the use of the partial pressure of oxygen molecules before dissociation instead of that of the existing molecules is obviously unjustified. Thus, Rakshit's calculation is open to the same objections discussed in A, (1) and (2), above.

(3) Rakshit assumes that the recombination process is simply the reverse of the dissociation process—namely, (1a). The distribution of oxygen atoms in the ^3P and ^1D states is assumed to be given by the Boltzmann theorem. Now for $T=300°K$, the Boltzmann factor is $\exp(-77)$ so that the concentration of ^1D atoms will be extremely small and the dissociation process becomes practically unidirectional. For this reason, recombinations involving two ^3P atoms, even though very improbable, have to be considered. Failure to consider these would lead to too high an estimate for the degree of dissociation.

That the calculated values for the degree of dissociation x are not too high is due to an error in the calculation. The ratio $n_A'n_B/n_{AB}$ should have been $4Nx^2\exp(-E/kT)/(1-x)$ instead of the expression $Nx^2/(1-x)$ given by Rakshit, since $n_A'=n_B\exp(-E/kT)$ and hence $n_A'\ll n_B$. E is the energy difference between the ^1D and the ^3P states of oxygen. When this correction is made, Eqs. (12), (14), and (15) in Rakshit's paper should all be multiplied by the factor $\frac{1}{2}\exp(E/kT)\cong\frac{1}{2}\exp(77)$ on the right-hand side. It is seen that Rakshit's theory, when correctly calculated, would have led to too high values for x for all heights.

(4) The relation between the absorption coefficient ψ_ν ($\psi_\nu=\sigma_\nu$ in the present paper) and the recombination cross section β_ν of the reverse process as obtained by Rakshit depends on the temperature of the gas. This cannot be correct, the correct relation being (43) given in Appendix 1 above.

PHYSICAL REVIEW VOLUME 83, NUMBER 1 JULY 1, 1951

On the Dispersion of Resistivity and Dielectric Constant of Some Semiconductors at Audiofrequencies

C. G. Koops*
Philips Research Laboratories, N. V. Philips Gloeilampenfabrieken, Eindhoven, Netherlands
(Received March 20, 1951)

Semiconducting $Ni_{0.4}Zn_{0.4}Fe_2O_4$, prepared in different ways, has been investigated. It appeared that the ac resistivity and the apparent dielectric constant of the material show a dispersion which can be explained satisfactorily with the help of a simple model of the solid: there should be well-conducting grains separated by layers of lower conductivity. Dispersion formulas are given. There is good agreement between experiment and theory.

I. INTRODUCTION

MEASUREMENTS by Blechstein[1] in 1938 showed that certain manganese ferrites have an astonishingly high apparent dielectric constant. Brockman, Dowling, and Steneck[2] also found such high dielectric constants in ferromagnetic cores made of ferrites which had been developed in this laboratory.[3] This property was, in fact, essential in the theory for the dimensional resonance effects in these cores investigated by these authors.

In order to obtain more quantitative information about the behavior of the ferrites, precise impedance measurements were carried out with disks and rods of several compositions. In the present paper the measurements at room temperature and a phenomenological theory of the impedance of NiZn ferrite and its dispersion are given.

II. EXPERIMENTAL DETAILS

A new alternating current bridge constructed and already described by Köhler and Koops[4] was used. The

* This paper has been written by Dr. J. Volger of this laboratory from observations and calculations left by the late Ir. Koops (deceased October 22, 1950).

[1] E. Blechstein, Physik. Z. **39**, 212 (1938).

[2] Brockman, Dowling, and Steneck, Phys. Rev. **77**, 85 (1950).

[3] J. L. Snoek, *New Developments in Ferromagnetic Materials* (Elsevier Company, New York, 1947).

[4] J. W. L. Köhler and C. G. Koops, Philips Research Repts. **1**, 419 (1946).

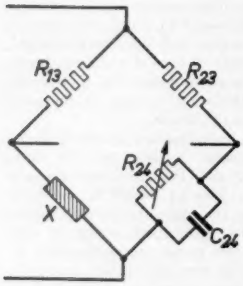

FIG. 1. Principle of bridge.

principle of the measurement is shown in Fig. 1. The sample X was compared with a resistance R_{24} shunted by a capacitance C_{24}. R_{24} had a sufficiently low self-inductance, C_{24} a sufficiently small loss angle. R_{23} and R_{13} were standard resistances of 1000Ω and 10000Ω, respectively, with very small time constants. The way in which certain errors, possibly introduced by the geometry of the bridge network, were almost completely reduced is discussed by Köhler and Koops.

After the bridge and the Wagner earth connections have been balanced, the impedance X of the sample can be calculated in the usual way. In fact, the parallel resistance R_p and the parallel capacitance C_p of the sample are determined:

$$X^{-1}=R_p^{-1}+j\omega C_p. \tag{1}$$

From R_p and C_p the apparent resistivity ρ_p and the apparent relative dielectric constant ϵ_p of the material were calculated with the help of

$$R_p=\rho_p d/O, \tag{2}$$

$$C_p=\epsilon_0\epsilon_p O/d, \tag{3}$$

O and d being the cross section and height of the cylindrical sample. (Giorgi units are used.) Also the loss angle δ can be calculated:

$$\tan\delta=(R_p\omega C_p)^{-1}=(\rho_p\omega\epsilon_0\epsilon_p)^{-1}. \tag{4}$$

III. RESULTS AND DISCUSSION

The results given below were obtained on a ceramic disk of $Ni_{0.4}Zn_{0.6}Fe_2O_4$. This spinel had been prepared by milling together the constituent oxides, prefiring at 1000°C, milling again, molding the disk, and firing it at 1280°C, after which the sample was slowly cooled in air. No second phase was detected by x-ray analysis. Mr. Gorter of this laboratory was entrusted with the preparing of the materials.

TABLE I. Room temperature data of $Ni_{0.4}Zn_{0.6}Fe_2O_4$ fired in air at 1280°C and cooled slowly in air.

ν(c/s)	$10^{-2}\rho_p$(Ωm)	ϵ_p	tanδ
0	202	—	—
160	187	1980	3.05
250	175	1870	2.20
500	143	1520	1.66
1000	104	1090	1.59
2000	74	610	2.00
4000	58	256	3.03
8000	52	93	4.7
16000	50	37	6.1
32000	49	22	5.2
64000	48	17	3.4
100000	47	16	2.4

The disk had a diameter of 36 mm. First, a series of measurements were made with the disk at a thickness of 6 mm. Afterwards the thickness was reduced to 1.1 mm by grinding. It appeared, however, that the calculated ρ_p and ϵ_p of the ferrite were not at all affected by this change of thickness.

Electrodes were deposited on both sides of the disk by evaporating silver in vacuum. The sample was then clamped between two suitable copper plates, which formed sufficiently short leads to the bridge itself.

Table I gives the results obtained. See also Figs. 2 and 3.

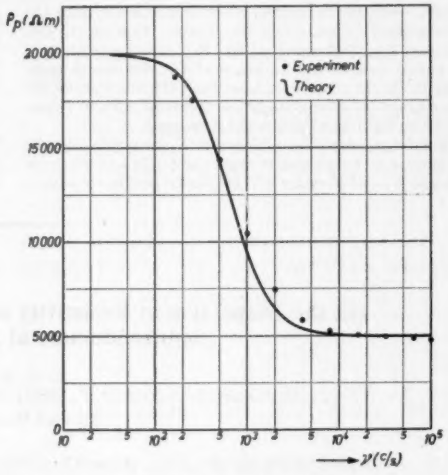

FIG. 2. Dispersion of resistivity.

What can be the quantitative explanation of this remarkable dispersion of both ρ_p and ϵ_p? It is clear that neither dimensional effects as found by Brockman *et al.*[2] nor skin effect play a part here. The material being an electronic semiconductor, it is also very unlikely that an intrinsic dispersion of the conduction mechanism itself would exist at such very low frequencies, as is the case here.

A good phenomenological theory of the dispersion can be based, however, upon the assumption that R_p and C_p result from an equivalent circuit as shown in Fig. 4, in which R_1, R_2, C_1, and C_2 are constants. It is well known from ac theory that R_p and C_p then obey dispersion formulas. From a purely circuit-theoretical point of view it can be proved that two capacitors and two resistors are needed in order to build up a two-pole having a finite value of dc resistance and showing the

typical tanδ *vs* ω curve with one hump which have been found with the material. Self-inductance has been omitted. In any real model obviously only resistors with parallel capacitors may be assumed, and therefore the circuit shown in Fig. 4 is chosen.

The model indicated might be justified by taking into account the barrier layers which may be present between the material and the electrodes (caused by impurities). With the sample under investigation, however, the electrodes proved to have no influence upon the measurements of ρ_p and ϵ_p, since ρ_p and ϵ_p were quite the same with a thick disk and a thin one.

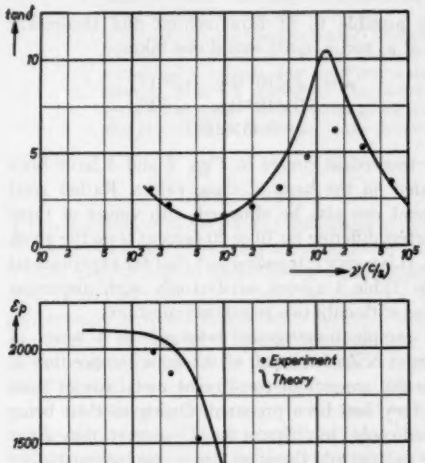

FIG. 3. Dispersion of dielectric constant and tanδ.

It is very probable, therefore, that layers of lower conductivity must be assumed to be present in the solid itself.

It must be noted here that an inhomogeneity model has already been proposed as a means of explaining certain characteristics of the tanδ *vs* ω curves of dielectrics.[5,6] See also the paper by Blechstein,[1] who, by mixing graphite or metal powder and paraffin wax, prepared artificial samples which showed the same high apparent dielectric constant as found in his ferrites.

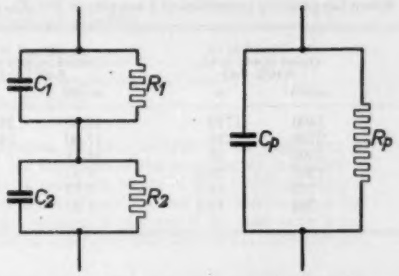

FIG. 4. If the right-hand circuit is equivalent to the left-hand one, with C_1, C_2, R_1, and R_2 constants, then C_p and R_p are not constants with respect to the frequency but obey dispersion formulas.

One thus arrives at the model shown in Fig. 5. The solid is imagined to consist of well-conducting grains separated by poorly conducting layers, while the current is assumed to flow along parallel alignments of grains, as has been drawn.

Let x be the ratio of the thickness of the layers to the thickness of the grains, and let ρ_1, ρ_2, ϵ_1, and ϵ_2 denote the resistivity and the relative dielectric constant of the layers (1) and grains (2), respectively. Suppose $x \ll 1$. If, moreover, sideway admittances between the grains are omitted, one easily computes with the help of common ac calculus

$$\rho_p = \rho_p^{\infty} + \frac{\rho_p^{0} - \rho_p^{\infty}}{1+\tau_\rho^2\omega^2} \tag{5}$$

with

$$\left.\begin{aligned} \rho_p^{\infty} &= \frac{\rho_1\rho_2(\epsilon_1+x\epsilon_2)^2}{\rho_1\epsilon_1^2+x\rho_2\epsilon_2^2}, \\ \rho_p^{0} &= x\rho_1+\rho_2, \\ \tau_\rho &= \epsilon_0\left(\frac{\rho_1\rho_2(\rho_1\epsilon_1^2+x\rho_2\epsilon_2^2)}{x\rho_1+\rho_2}\right)^{\frac{1}{2}}. \end{aligned}\right\} \tag{6}$$

Likewise,

$$\epsilon_p = \epsilon_p^{\infty} + \frac{\epsilon_p^{0} - \epsilon_p^{\infty}}{1+\tau_\epsilon^2\omega^2} \tag{7}$$

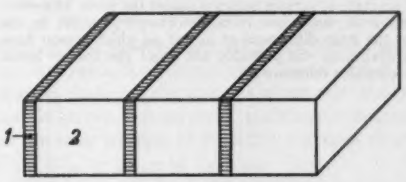

FIG. 5. Model of a grain-structured conductor. Layers of poorly conducting material separate the grains.

[5] J. C. Maxwell, *Electricity and Magnetism* (Oxford University Press, London, 1873), Vol. I, Sec. 328.

[6] K. W. Wagner, Ann. Physik 40, 817 (1913); Arch. Electrotech. 2, 371 (1914).

TABLE II. Room temperature properties of 4 samples of $Ni_{0.4}Zn_{0.6}Fe_2O_4$, fired at 1300°C in oxygen or air and cooled slowly or rapidly.

	1a sintered in O_2, cooled slowly in O_2, 0.10% FeO		1b sintered in O_2, cooled rapidly in air, 0.38% FeO		2a Sintered in air, cooled slowly in air, 0.07% FeO		2b sintered in air, cooled rapidly in air, 0.42% FeO	
$\nu(c/s)$	$\rho_p(\Omega m)$	ϵ_p	$\rho_p(\Omega m)$	ϵ_p	$\rho_p(\Omega m)$	ϵ_p	$\rho_p(\Omega m)$	ϵ_p
1×10^3	5400	1710	12.80	28200	1360	4300	10.8	39000
8×10^3	2700	218	12.00	14000	702	1280	10.3	21500
1×10^5	2300	32	11.11	716	495	66	8.9	1320
1×10^6	1295	18.1	8.65	97	463	30.7	6.78	147.5
6×10^6	790	15.9	8.15	51.6	403	26.0	5.66	82.1
35×10^6	704	13.8	5.95	42.1	290	22.4	4.43	68.5

with

$$\left.\begin{aligned} \epsilon_p^{\infty} &= \frac{\epsilon_1\epsilon_2}{\epsilon_1+x\epsilon_2}, \\ \epsilon_p^{0} &= \frac{x\rho_1^2\epsilon_1+\rho_2^2\epsilon_2}{(x\rho_1+\rho_2)^2}, \\ \tau_\epsilon &= \epsilon_0\frac{\rho_1\rho_2(\epsilon_1+x\epsilon_2)}{x\rho_1+\rho_2}. \end{aligned}\right\} \quad (8)$$

Thus,

$$\tau_\epsilon = (\rho_p^{\infty}/\rho_p^{0})^{\frac{1}{2}}\tau_\rho. \quad (9)$$

If the measured ρ_p and ϵ_p are to fit the dispersion equations (5) and (6), it is impossible to obtain more than 4 independent quantities from experiment. In the phenomenological theory, presented here, however, there are 5 quantities, and in order to calculate these from the data it is necessary to make one more assumption. Let this assumption be

$$\epsilon_1 = \epsilon_2, \quad (10)$$

which is quite reasonable.[7] Since $x \ll 1$ and $\rho_1 \gg \rho_2$, formulas (6) and (8) are reduced to

$$\left.\begin{aligned} \rho_p^{\infty} &= \rho_2, \\ \rho_p^{0} &= x\rho_1+\rho_2, \\ \tau_\rho &= \epsilon_0\epsilon_2[\rho_1^2\rho_2/(x\rho_1+\rho_2)]^{\frac{1}{2}}, \end{aligned}\right\} \quad (11)$$

$$\left.\begin{aligned} \epsilon_p^{\infty} &= \epsilon_2, \\ \epsilon_p^{0} &= \epsilon_2\cdot\frac{x\rho_1^2+\rho_2^2}{(x\rho_1+\rho_2)^2}, \\ \tau_\epsilon &= \epsilon_0\epsilon_2\frac{\rho_1\rho_2}{x\rho_1+\rho_2}. \end{aligned}\right\} \quad (12)$$

[7] This assumption is based upon the knowledge that the true dielectric constant of various oxides is almost the same. Moreover, only small local deviations from stoichiometry might be the reason for the large differences of ρ_1 and ρ_2 which appear here, and such deviations will probably not affect the true dielectric constant. (See also reference 8.)

It is possible to fit experimental and theoretical values of ρ_p and ϵ_p quite well if one takes:

$$\rho_1 = 3.3\times10^6\ \Omega m, \quad \epsilon_1 = 17,$$
$$\rho_2 = 5.0\times10^3\ \Omega m, \quad \epsilon_2 = 17,$$
$$x = 0.45\times10^{-2}.$$

The theoretical curves in Figs. 2 and 3 have been calculated on the basis of these values. Rather good agreement can also be obtained with values of these parameters differing by 10 or 20 percent from the given values. It is a very interesting fact that the experimental data in Table I agrees satisfactorily with dispersion formulas with only two relaxation constants.

The sample investigated belonged to a series of samples of NiZn ferrite all of the same composition as regards the amount of constituent metal oxides from which they had been prepared. Owing to their being fired and cooled in different ways, however, they differ in Fe^{2+} content and therefore also in specific resistance.[8] All samples showed the same sort of dependency of ρ and ϵ on frequency. Table II gives a survey of some room temperature measurements.

The measurements at 1, 6, and 35 Mc/sec have been carried out by Dr. Gevers of this laboratory. Dr. Gevers determined ρ_p and ϵ_p of the sample by tuning an *LC*-circuit, the capacitor of which was shunted by the sample. The dispersion interval of these samples does not lie in the audiofrequency range. The phenomenological theory given above does not apply in every respect to the data in Table II; e.g., ϵ_p happens to fall off at lower frequencies than does ρ_p, which is not in accordance with (9). Possibly the existence of more than two relaxation constants τ, or even quite a range of them, plays a part here.

A number of measurements on other semiconducting materials will be published in the near future.

[8] Verwey, Haayman, Romeyn, and v. Oosterhout, Philips Research Repts. 5, 173 (1950).

Quantum Statistics of Fields

A. E. Scheidegger and C. D. McKay
Department of Physics, Queen's University, Kingston, Ontario, Canada
(Received January 22, 1951)

Gibbs' theory of ensembles of classical mechanical systems has been modified for the application to quantum-mechanical systems by Klein. In this paper, the formalism of the latter author is applied to hamiltonians of different types of field theories and thus a consistent theory of field thermodynamics is obtained without explicitly referring to the statistical behavior of particles that are "contained" in the fields. Speaking in terms of particles, the thermodynamics obtained in this way is the same as for a mechanical system where only the temperature is known, but no other conditions such as the number of particles, the total charge, etc.

Specifically, the thermodynamic functions of the nonrelativistic and relativistic Schrödinger fields, Dirac's electron field, and the electromagnetic field are deduced. The statistics of the nonrelativistic fields correspond to ordinary Bose and Fermi statistics of an ensemble of identical particles; the relativistic cases, however, yield new expressions. The thermal equilibrium at low temperatures of the Dirac electron field turns out to be the "vacuum" state as described in the hole theory. Finally, it is also shown that the application of the present formalism to the electromagnetic field leads back to Planck's radiation theory.

I. INTRODUCTION

In connection with the present difficulties in quantum theory of fields it occurred to us that one source of trouble may be that no distinction is made between the positive and negative directions of the time axis. To any nonphysicist it would hardly seem justified to assume equivalence of past and future. Somehow the arrow of the time axis should be inferred into our physical laws. In ordinary mechanics this inference of the time-arrow is obtained by the passage to thermodynamics by means of statistics. Thus it seems to us that statistical methods might shed some light onto the significance of some of the difficulties encountered in present field theories.

The application of statistical mechanics to field theories has been tried before. Thus it is known that Planck applied statistics to the electromagnetic field which led him to the discovery of quantum mechanics in 1900. It is also known that Debye[1] found another deduction of Planck's radiation theory which does not use the equilibrium of the field with other systems.

However, it appears to us that all these previous investigations are somehow inconsistent in their methods. Planck used "resonators" which are supposed to be in thermal equilibrium with the radiation field, and then applied statistical mechanics to an ensemble of such resonators. Debye[1] applied a phenomenological method of counting nodes of waves in a given volume. Similarly, in all more modern treatments of the quantum statistics of "fields," one first quantizes the field and then applies statistics to the particles, the prescriptions for the statistical "weight" of the configurations of the particles being deduced from the degeneracy of the state of the corresponding field. In such a way it is possible to explain the behavior of certain types of particles at certain temperatures (see e.g., Schrödinger's[2] monograph). The thermodynamics of the particles, then, is thought to be identical with the thermodynamics of the corresponding field. This is, however, somewhat questionable, since the interpretation of a field theory as a particle theory can be obtained only by renormalizing infinite terms in the expressions for the energy, etc., and it is by no means evident *a priori* that these renormalizations are the same in a quantum statistics of fields.

On the other hand, it is well known that one has definite prescriptions for dealing with the statistics of ensembles of systems. In classical mechanics one can define a canonical ensemble of systems; then the thermodynamic functions are found by a method devised by Gibbs (see reference 2). The modifications of Gibbs' scheme which are necessary in quantum mechanics have been found by Klein.[3] These remarks show that one actually has all the means for a straightforward application of statistics to any field theory; but, as far as we know, the problem has never been treated in this direct way. An attempt has been made recently by Kaempffer,[4] who tried to deduce the behavior of an ensemble of identical particles from a wave theory. However, his results were not obtained by a consistent application of quantum statistics to the wave field, but rather by phenomenological methods of counting nodes of waves or the like, analogous to the procedures of Debye.[1]

Thus it seems desirable to attempt a consistent quantum statistical treatment of various wave fields,[5] such as the nonrelativistic and relativistic Schrödinger fields, Dirac's electron field, and the electromagnetic field. In the present paper we shall confine ourselves to vacuum fields. Speaking in terms of particles, this means that we shall consider systems where only the temperature is known, but no other additional conditions such as the total number of particles, the total charge, etc.

[1] See, for instance, *Handbuch d. Physik* (Geiger-Scheel), vol. 24, 1, p. 9.
[2] E. Schrödinger, *Statistical Thermodynamics* (Cambridge University Press, London, 1946).
[3] O. Klein, Z. Physik 72, 767 (1931).
[4] F. Kaempffer, Z. Physik 125, 487 (1949).
[5] G. Wentzel, *Einführung in die Quantentheorie der Wellenfelder* (Deuticke, Wien, 1943).

The question to which physical situations these premises and thus the results are applicable is here of minor importance. Our principal aim is to follow all the statistical consequences of those theories which are commonly used to describe some of the elementary fields; up to the bitter contradiction with physical possibilities, if necessary.

The structure of the present field theories is such that there is a hamiltonian for each of the vacuum fields known. Then, different vacuum fields are linked together in a rather arbitrary and tentative way by assuming interaction terms. Thus it seems to us that the first obvious thing to do is to consider the vacuum fields alone, especially since the general theory permits the existence of such vacuum fields. The extension of the present formalism to the interaction of different fields is the object of further investigations which we hope to present in a future publication.

II. GENERAL THEORY

We summarize first the principles of Gibbs' statistical mechanics as applied to an ensemble of arbitrary mechanical systems. If $H(p_k, q_k)$ denotes the hamiltonian of the systems concerned, then one can define a canonical ensemble as follows:

$$P=(1/Z)\exp(-\vartheta H). \tag{2.1}$$

Here Pd^fpd^fq is the probability of finding the system with coordinates between q_i and q_i+dq_i and momenta between p_i and p_i+dp_i. The partition function is given by

$$Z=\int \exp(-\vartheta H)d^fqd^fp. \tag{2.2}$$

With the knowledge of Z, one can find all the thermodynamic functions of the ensemble, namely, the Helmholtz free energy F

$$F=-\vartheta^{-1}\log Z=-\vartheta^{-1}\log\int \exp(-\vartheta H)d^fpd^fq \tag{2.3}$$

the temperature T

$$T=1/k\vartheta \tag{2.4}$$

and the entropy

$$S=-\partial F/\partial T=-kT\int P\log P d^fpd^fq. \tag{2.5}$$

The modifications which have to be made in these formulas if one is dealing with quantum-mechanical systems, have been set up by Klein.[3] It is seen that one has to replace P by Neumann's density matrix $\mathbf{P}$, which is defined as follows:

$$(P)_{nm}=c_nc_m^*, \tag{2.6a}$$

if a certain state of the system in an ensemble is given by ψ (ψ is normalized)

$$\psi=\sum c_i v_i, \tag{2.6b}$$

where the v's are the eigenfunctions of the hamiltonian. The formulas (2.1) to (2.5) all remain valid if the integrations are replaced by the traces of the matrices which occur as integrands. Thus we have for a canonical ensemble

$$\mathbf{P}=(1/Z)\exp(-\vartheta\mathbf{H});\quad \bar{A}=\text{trace}\mathbf{PA}, \tag{2.7}$$

where A denotes an arbitrary observable and $\bar{A}$ its expectation value in the ensemble (matrices are denoted by faced types). Furthermore, we have

$$Z=\text{trace}\exp(-\vartheta\mathbf{H}), \tag{2.8}$$

$$F=-\vartheta^{-1}\log Z=-(1/\vartheta)\log\text{trace}\exp(-\vartheta\mathbf{H}), \tag{2.9}$$

$$T=1/k\vartheta, \tag{2.10}$$

$$S=-\partial F/\partial T=-kT\,\text{trace}\mathbf{P}\log\mathbf{P}. \tag{2.11}$$

The next step is to apply our scheme to a field theory. It is known that in all cases of interest one can find a diagonal representation for the hamiltonian, and thus it will be particularly easy to set up the quantum statistics of fields by means of Eqs. (2.8)–(2.11).

III. THE NONRELATIVISTIC SCHRÖDINGER FIELD

As a first example, we treat the nonrelativistic Schrödinger field. The field equation is

$$i\hbar\dot{\psi}=-\frac{\hbar^2}{2m}\Delta\psi. \tag{3.1}$$

It may be represented in the hamiltonian form as follows (see Schiff,[4] Sec. 46):

$$\mathfrak{L}=i\hbar\psi^*\dot{\psi}-\frac{\hbar^2}{2m}\,\text{grad}\psi^*\,\text{grad}\psi, \tag{3.2}$$

$$\mathfrak{IC}=-\frac{i\hbar}{2m}\,\text{grad}\pi\,\text{grad}\psi. \tag{3.3}$$

The total hamiltonian may be written as the following symbolic sum in a diagonal matrix representation:

$$\mathbf{H}=\sum_K \mathbf{N}_K E_K, \tag{3.4}$$

E_K being the eigenvalues of the one-particle Schrödinger equation. $\mathbf{N}_K$ has diagonal elements N_K ranging from 0 to infinity in integer steps. For particles in a box (a "periodicity cube" of volume V) one has

$$E_K=p^2/2m=\hbar^2K^2/2m. \tag{3.5}$$

Having the eigenvalues of the hamiltonian, we may now consider an ensemble of such fields and define the Neumann density matrix as

$$\mathbf{P}=(1/Z)\exp(-\vartheta\mathbf{H}). \tag{3.6}$$

The important quantity Z, the partition function, is

[4] L. I. Schiff, *Quantum Mechanics* (McGraw-Hill Book Company, Inc., New York, 1949).

then

$$Z=\text{trace}\exp(-\vartheta\mathbf{H})=\sum_{NK}\exp(-\vartheta\sum N_K E_K) \quad (3.7)$$

or

$$\log Z=\sum_K \log\sum_0^\infty \exp(-N_K E_K/kT)$$
$$=-\sum_K \log\{1-\exp(-E_K/kT)\}. \quad (3.8)$$

We wish to replace the sum in the above expression by an integral. In the periodicity cube, K is restricted to the values given by

$$K^2=(2\pi)^2L^{-2}\{n_x^2+n_y^2+n_z^2\}, \quad (3.9)$$

where n_x, n_y, n_z are all integers or zero, and L^3 the volume of the cube. Thus, except for surface terms which may be neglected with respect to the volume terms as K-space becomes continuous, each K has associated with it a volume of K-space

$$d^3K=(2\pi)^3/L^3=(2\pi)^3/V. \quad (3.10)$$

Hence we obtain

$$(1/V)\log Z=$$
$$-(2\pi)^{-3}\int \log\{1-\exp(-E_K/kT)\}d^3K \quad (3.11)$$

or else, since E_K depends only on K^2,

$$F/V=(2\pi)^{-3}kT\int_0^\infty \log\{1-\exp(-\hbar^2K^2/2mkT)\}4\pi K^2dK, \quad (3.12)$$

$$S/V=-(2\pi)^{-3}k\int_0^\infty \log\{-1\exp(-\hbar^2K^2/2mkT)\}4\pi K^2dK$$
$$+\frac{1}{(2\pi)^3}\frac{1}{T}\int_0^\infty \frac{\hbar^2K^2}{2m\{\exp(\hbar^2K^2/2mkT)-1\}}4\pi K^2dK, \quad (3.13)$$

$$\frac{E}{V}=\frac{1}{(2\pi)^3}\int_0^\infty \frac{1}{2m}\frac{\hbar^2K^2}{\exp(\hbar^2K^2/2mkT)-1}4\pi K^2dK. \quad (3.14)$$

These integrals can be computed. Actually, they are similar to the expressions which one obtains for the statistics of Einstein-Bose particles. The reason for this is, of course, that the nonrelativistic Schrödinger field is fully equivalent to a system of oscillators with symmetric states. Thus it is seen that a straightforward application of quantum statistics to the field is equivalent in the present case to an application of Bose statistics to the particles "contained" in the field. This is not quite the same thing as concluding that the particles "contained" in such a field must obey Bose statistics. Heretofore, statistics have been applied only to the particles, never to the field (except for the paper of Kaempffer[4]); only the symmetry properties for the eigenfunctions of the particles have been inferred from the quantum theory of fields.

Incidentally, the values of the above integrals are[7]

$$\frac{F}{V}=-\frac{(2\pi m)^{3/2}}{\hbar^3}(kT)^{5/2}\sum_{n=1}^\infty \frac{1}{n^{5/2}}, \quad (3.15)$$

$$\frac{S}{V}=\frac{5}{2}\frac{(2\pi m)^{3/2}}{\hbar^3}k^{5/2}T^{3/2}\sum_{n=1}^\infty \frac{1}{n^{5/2}}, \quad (3.16)$$

$$\frac{E}{V}=\frac{3}{2}\frac{(2\pi m)^{3/2}}{\hbar^3}(kT)^{5/2}\sum_{n=1}^\infty \frac{1}{n^{5/2}}. \quad (3.17)$$

These expressions check with those obtained earlier by Kaempffer[4] by his more phenomenological methods.

The formulas (3.15) to (3.17) hold for all temperatures. This corresponds, thus, to an Einstein-Bose gas where there are an infinite number of particles available in a reservoir without kinetic energy.[8] Obviously, one may interprete Eq. (3.14) as (Stieltjes' integral)

$$E=\int E_K dN(K), \quad (3.18)$$

in which

$$dN(k)/V=\tfrac{1}{2}\pi^{-2}K^2dK/\{\exp(\hbar^2K^2/2mkT)-1\} \quad (3.19)$$

is the number of "particles" per unit volume between K and $K+dK$. Thus, the number of particles which are energized and thus "contained" in the field is

$$\frac{N}{V}=\frac{(2\pi m)^{\frac{3}{2}}}{\hbar^3}(KT)^{\frac{3}{2}}\sum_{n=1}^\infty \frac{1}{n^{\frac{3}{2}}} \quad (3.20)$$

which again corresponds to the formula for an Einstein-Bose gas.

IV. THE SCHRÖDINGER-GORDON FIELD

The relativistic generalization of the case treated in the last section is the Schrödinger-Gordon field. Each field variable satisfies the equation (Wentzel,[5] p. 29)

$$(\Box-\mu^2)\psi=0. \quad (4.1)$$

The lagrangian and the hamiltonian turn out as follows (Wentzel,[5] p. 29):

$$L=\tfrac{1}{2}\int(\dot\psi^2-c^2|\text{grad}\psi|^2-c^2\mu^2\psi^2)d^3x, \quad (4.2)$$

$$H=\tfrac{1}{2}\int\{\pi^2+c^2|\text{grad}\psi|^2+c^2\mu^2\psi^2\}d^3x, \quad (4.3)$$

π and ψ being regarded as canonical variables. In momentum space representation, one finds the hamiltonian

$$H=\tfrac{1}{2}\sum\{p_K^*p_K+\omega_K^2q_K^*q_K\}, \quad (4.4)$$

[7] C. D. McKay, "Thermodynamics of fields," thesis, Queen's University Library, Kingston, 1951.

[8] The total number of particles is thus *not* an independent variable.

with

$$\omega_K^2 = c^2(\mu^2 + K^2). \tag{4.5}$$

For p_K, q_K, H a matrix representation can be found (Wentzel,[5] p. 34); the eigenvalues of H turn out to be

$$(H)_{N_K N_{K'} \ldots} = \sum_K \hbar(N_K + 1)\omega_K. \tag{4.6}$$

Thus, in the representation where **H** is a diagonal matrix, we can again define the Neumann density matrix by (3.6) and the partition function Z now becomes

$$Z = \sum_{N_K} \exp(-\vartheta H_{N_K}) = \sum_{N_K} \exp\{-\sum_K \vartheta\hbar\omega_K(N_K + \tfrac{1}{2})\}$$
$$= \prod_K \exp(-\tfrac{1}{2}\vartheta\hbar\omega_K)/\{1 - \exp(-\vartheta\hbar\omega_K)\}. \tag{4.7}$$

Thus $\log Z$, which alone enters into the thermodynamic functions, becomes

$$\log Z = -\sum_K \log\{1 - \exp(-\vartheta\hbar\omega_K)\} - \tfrac{1}{2}\vartheta \sum_K \hbar\omega_K. \tag{4.8}$$

As in the last section, the sum is replaced by an integral by means of (3.10), whence we obtain

$$(1/V)\log Z = -(2\pi)^{-3} \int \{\log[1 - \exp(-\vartheta\hbar\omega_K)] + \tfrac{1}{2}\vartheta\hbar\omega_K\} d^3K \tag{4.9}$$

or else, since ω_K depends only on K^2,

$$F/V = (2\pi)^{-3} kT \int \log\{1 - \exp(-\hbar\omega_K/kT)\} 4\pi K^2 dK, \tag{4.10}$$

$$S/V = -(2\pi)^{-3} k \int \log\{1 - \exp(-\hbar\omega_K/kT)\} 4\pi K^2 dK + \frac{k}{(2\pi)^3} \int \frac{\hbar\omega_K}{kT} \frac{1}{\exp(\hbar\omega_K/kT) - 1} 4\pi K^2 dK, \tag{4.11}$$

$$\frac{E}{V} = \frac{1}{(2\pi)^3} \int \frac{\hbar\omega_K}{\exp(\hbar\omega_K/kT) - 1} 4\pi K^2 dK. \tag{4.12}$$

Herein, the last term of (4.9) has been dropped, since, although it is infinite, it is independent of the temperature (if multiplied by kT) and just gives rise to an infinite zero-point energy. Thus we need indeed the *same* renormalization as in the interpretation of a *single* field as an ensemble of particles.

The integrals can be computed; they lead to series of hankel functions of the argument (nmc^2/kT) which is usually very large. Hence the hankel functions may be replaced by their asymptotic expansions, and one obtains finally[7]

$$\frac{F}{V} = -\frac{(2\pi m)^{3/2}}{h^3} (kT)^{5/2} \sum_{n=1}^{\infty} \left\{ \frac{1}{n^{5/2}} \exp\left(-n\frac{mc^2}{kT}\right) \times \left[1 + \frac{15}{8n}\frac{kT}{mc^2} + \cdots\right]\right\}, \tag{4.13}$$

$$\frac{S}{V} = \frac{(2\pi m)^{3/2}}{h^3} k^{3/2} T^{1/2} \sum_{n=1}^{\infty} \left\{ \frac{1}{n^{3/2}} \exp\left(-n\frac{mc^2}{kT}\right) \times \left[1 + \frac{35}{8n}\frac{kT}{mc^2} + \cdots\right]\right\}, \tag{4.14}$$

$$\frac{E}{V} = \frac{(2\pi m)^{3/2}}{h^3} (kT)^{3/2} mc^2 \sum_{n=1}^{\infty} \left\{ \frac{1}{n^{3/2}} \exp\left(-n\frac{mc^2}{kT}\right) \times \left[1 + \frac{27}{8n}\frac{kT}{mc^2} + \cdots\right]\right\}. \tag{4.15}$$

The total number of particles "contained" in the field at a given temperature is, similarly to (3.19),

$$\frac{N}{V} = \frac{(2\pi m)^{3/2}}{h^3} (kT)^{3/2} \sum_{n=1}^{\infty} \left\{ \frac{1}{n^{3/2}} \exp\left(-n\frac{mc^2}{kT}\right) \times \left[1 + \frac{15}{8n}\frac{kT}{mc^2} + \cdots\right]\right\}. \tag{4.16}$$

It is an interesting observation that, in the present case, one cannot obtain the formulas of Sec. III by letting c approach infinity. Thus, the statistics of the Schrödinger-Gordon field is quite different from that one of the nonrelativistic field. In the particle-picture, one can interpret Eqs. (4.13)–(4.16) as an expression of the fact that the number of *existing* particles is in thermal equilibrium with the surroundings. If the temperature is raised, then the kinetic energy of the particles already present in the field is raised, in addition to more particles being created. Thus, part of the thermal energy is contained in the rest mass of the particles. It is only natural that the nonrelativistic equations cannot describe such a case. There, in the particle-picture the particles are assumed to be already created and to be only raised from an "unobservable" state without any kinetic energy into a state which is observable.

Since the Schrödinger-Gordon equation is supposed to hold for mesons, one should expect that Eqs. (4.13) to (4.16) are valid for the meson field. The number of mesons present per unit volume should be in thermal equilibrium with the surroundings according to (4.16); if the temperature is lowered, the mesons must disintegrate and not merely disappear into an "unobservable" state. At room temperature (68°F) the meson density is very small (for μ-mesons):

$$N = 10^{-1.89 \times 10^9} \text{ cm}^{-3}. \tag{4.17}$$

One may object that one cannot speak of the disintegration of the mesons without considering their decay products. However, it should be kept in mind that the mesons, in the present formalism, are annihilated and do not decay into other particles. This is a consequence of the Schrödinger-Gordon equation. Therefore, if certain particles in nature do not disintegrate but only disappear into an unobservable state when the tempera-

ture is lowered, one should note that the Schrödinger-Gordon equation cannot be the right equation for them; or else one has to invent some explanation why more mesons are present than are given by Eq. (4.17). We are grateful to Professor Schrödinger for suggesting that one might get such an explanation by saying that the mesons do not disintegrate, but are absorbed by the nucleons. The nucleons themselves are certainly not in thermal equilibrium. There are much too many of them left. Unless one considers the transformation of nucleons into electromagnetic radiation impossible, one must be astonished that there is so much matter with rest mass $\neq 0$ left in the universe, and one must regard it as a relic of 2 or 3 billion years ago that has not yet reached equilibrium.

Finally, we could perhaps remark that in this section, too, the counting prescriptions of Einstein and Bose hold, for the N_K's run from 0 to ∞ and each combination is enumerated just once. Nevertheless, the thermodynamic functions are quite different from those in ordinary Bose statistics.

V. SPINOR FIELDS

In this section we shall treat fields "containing" particles which obey the exclusion principle.

The *nonrelativistic* case for such fields is obtained by taking the ordinary Schrödinger equation (3.1), but assuming anticommutation, rather than commutation, rules for ψ and its conjugate. This leaves the matrix representation (3.4) for H unchanged, but the matrix $\mathbf{N}_K$ has now the form

$$\mathbf{N}_K=\begin{pmatrix}0 & 0\\ 0 & 1\end{pmatrix}. \tag{5.1}$$

Hence, the partition function Z becomes

$$Z=\text{trace}\exp(-\vartheta\mathbf{H})=\sum_{N_K=0,1}\exp(-\vartheta\textstyle\sum_K N_K E_K) \tag{5.2}$$

and

$$\log Z=\textstyle\sum_K \log\sum_{N_K}\exp(-N_K E_K/kT)$$
$$=\textstyle\sum_K \log\{1+\exp(-E_K/kT)\}, \tag{5.3}$$

which differs from (3.8) only in some signs. The eigenvalues E_K are given by (3.5), as before. In a similar way to Sec. III one can proceed to calculate the thermodynamic functions and obtains the following expressions as for a Fermi-Dirac gas:

$$F/V=-(2\pi m)^{3/2}h^{-3}(kT)^{5/2}\textstyle\sum\{(-1)^{n+1}/n^{5/2}\}, \tag{5.4}$$

$$S/V=(5/2)(2\pi m)^{3/2}h^{-3}k^{5/2}T^{3/2}\textstyle\sum\{(-1)^{n+1}/n^{5/2}\}, \tag{5.5}$$

$$E/V=(3/2)(2\pi m)^{3/2}h^{-3}(kT)^{5/2}\textstyle\sum\{(-1)^{n+1}/n^{5/2}\}. \tag{5.6}$$

Thus the particle-picture of such a field corresponds to that one of the nonrelativistic Schrödinger field; except that for the particles, Fermi instead of Bose statistics is applied. Again, by raising the temperature, some particles are lifted out of an infinite reservoir with no kinetic energy.[8]

More interesting is the *relativistic* case. The hamiltonian of the quantized Dirac equation is in a suitable matrix representation (Wentzel,[5] p. 162; Schiff,[6] p. 352)

$$\mathbf{H}=\sum_{K,s}\mathbf{N}_{Ks}E_{Ks} \tag{5.7}$$

with $\mathbf{N}_{Ks}$ as given by (5.1). The eigenvalues E_{Ks} of the Dirac equation are (Schiff,[6] p. 351)

$$E_{Ks}=+(h^2c^2K^2+m^2c^4)^{\frac{1}{2}} \quad \text{for } s=1,2, \tag{5.8a}$$

$$E_{Ks}=-(h^2c^2K^2+m^2c^4)^{\frac{1}{2}} \quad \text{for } s=3,4 \tag{5.8b}$$

and thus may be positive or negative.

Thus we can find the partition function Z:

$$Z=\textstyle\sum_{N_{Ks}}\exp(-\vartheta\sum_{Ks}N_{Ks}E_{Ks})$$
$$=\textstyle\prod_{Ks}\{1+(\exp-\vartheta E_{Ks})\} \tag{5.9}$$

and

$$\log Z=\textstyle\sum_{Ks}\log\{1+(\exp-\vartheta E_{Ks})\} \tag{5.10}$$

and the thermodynamic functions

$$F=-kT\log Z$$
$$=-kT\textstyle\sum_{Ks}\log\{1+\exp(-E_{Ks}/kT)\}, \tag{5.11}$$

$$S=k\textstyle\sum_{Ks}\{(E_{Ks}/kT)/[\exp(E_{Ks}/kT)+1]$$
$$+\log[1+\exp(-E_{Ks}/kT)]\}, \tag{5.12}$$

$$E=\textstyle\sum_{Ks}E_{Ks}/\{\exp(E_{Ks}/kT)+1\}. \tag{5.13}$$

If we set

$$E=\textstyle\sum N(K,s)E_{Ks}, \tag{5.14}$$

it follows that

$$N(K,s)=1/\{\exp(E_{Ks}/kT)+1\}. \tag{5.15}$$

Thus, so far, the thermodynamic functions are the same as in the nonrelativistic case for electrons, except for the summation over s which arises from the spin of the particles.

However, we observed that now half of the eigenvalues E_{Ks} are negative, whereas heretofore the energy eigenvalues have always been positive. For low temperatures such that

$$|E_{Ks}|\gg kT \tag{5.16}$$

we obtain in the particle-picture that

$$N(K,s)\cong 1 \tag{5.17}$$

for all negative energy eigenvalues. This means that in thermal equilibrium at low temperatures all the negative energy states are occupied. Thus we obtain that the "normal" state of the field at low temperatures is exactly the vacuum state as postulated by Dirac in his hole theory, which serves to substantiate the present formalism.

The summation over the negative states makes the sums in (5.10) to (5.15) divergent; naturally, there is an infinite number of particles present in the negative states. Only the deviation from the vacuum state is physically interesting.

Thus one has to renormalize everything so that it is zero for $T=0$. It is seen that all one has to do is to take the sums only for the positive eigenvalues of the energy and to double their value. Furthermore, the summation over the spins gives an additional factor 2. Thus we have

$$F=-4kT\sum_K \log\{1+\exp(-E_K/kT)\}, \tag{5.18}$$

$$S=4k\sum_K\{\log(1+\exp(-E_K/kT)+(E_K/kT)[\exp(E_K/kT)+1]^{-1}\}, \tag{5.19}$$

$$E=4\sum_K E_K/\{\exp(E_K/kT)+1\}, \tag{5.20}$$

$$N=4\sum_K 1/\{\exp(E_K/kT)+1\}. \tag{5.21}$$

The sums can be approximated by integrals and the latter expanded into asymptotic expressions. One then obtains[7] the following formulas which are analogous to the expressions (4.13) to (4.16):

$$\frac{F}{V}=-4\frac{(2\pi m)^{3/2}}{h^3}(kT)^{5/2}\sum_1^\infty\frac{1}{n^{5/2}}\exp\left(-n\frac{mc^2}{kT}\right)\times(-1)^{n+1}\left\{1+\frac{15}{8n}\frac{kT}{mc^2}+\cdots\right\}, \tag{5.22}$$

$$\frac{S}{V}=\frac{4}{T}\frac{(2\pi m)^{3/2}}{h^3}(kT)^{3/2}mc^2\sum_1^\infty\frac{1}{n^{3/2}}\exp\left(-n\frac{mc^2}{kT}\right)\times(-1)^{n+1}\left\{1+\frac{35}{8n}\frac{kT}{mc^2}+\cdots\right\}, \tag{5.23}$$

$$\frac{E}{V}=4\frac{(2\pi m)^{3/2}}{h^3}(kT)^{3/2}mc^2\sum_1^\infty\frac{1}{n^{3/2}}\exp\left(-n\frac{mc^2}{kT}\right)\times(-1)^{n+1}\left\{1+\frac{27}{8n}\frac{kT}{mc^2}+\cdots\right\}, \tag{5.24}$$

$$\frac{N}{V}=4\frac{(2\pi m)^{3/2}}{h^3}(kT)^{3/2}\sum_1^\infty\frac{1}{n^{3/2}}\exp\left(-n\frac{mc^2}{kT}\right)\times(-1)^{n+1}\left\{1+\frac{15}{8n}\frac{kT}{mc^2}+\cdots\right\}. \tag{5.25}$$

These relativistic formulas correspond to the nonrelativistic ones in a similar way to the one outlined when we were dealing with the Schrödinger-Gordon equation. Again, it is not possible to obtain the nonrelativistic expressions by letting c approach infinity. In the particle-picture, one would say that (5.22) to (5.25) describe the thermal equilibrium of electron-positron gas mixture which contains an equal number of particles of either kind. Thus, the energy of creation for each pair of electrons and positrons is contained in the thermal energy of the field.

At room temperature (68°F), the equilibrium state is almost Dirac's vacuum state. The number of particles per unit volume deviating from the vacuum state is

$$N/V=10^{-8.63\times10^{4}}\ \text{cm}^{-3}. \tag{5.26}$$

VI. THE ELECTROMAGNETIC FIELD

As the last application of the formalism outlined in this paper we take the electromagnetic field. One expects to obtain the Stefan-Boltzmann expressions for which, thus, a new derivation is supplied.

The hamiltonian of the electromagnetic field may be represented in the following symbolic form (Wentzel,[6] p. 117)

$$\mathbf{H}=\sum_K \hbar c|K|(\mathbf{N}_K^{(1)}+\mathbf{N}_K^{(2)}+\mathbf{1}). \tag{6.1}$$

Hence the partition function Z becomes

$$Z=\sum_{N_K^{(1)},\,N_K^{(2)}}\exp\{-\vartheta\sum_K(N_K^{(1)}+N_K^{(2)}+1)\hbar c|K|\} \tag{6.2}$$

or

$$\log Z=-2\sum_K\log\{1-\exp(-\vartheta\hbar c|K|)\}-\vartheta\sum_K\hbar c|K|. \tag{6.3}$$

Equation (6.3) is the same expression as for the Schrödinger-Gordon field, except for the factor 2 and

$$\omega_K=\hbar c|K|. \tag{6.4}$$

Hence we obtain the same expressions as in (4.10) to (4.12) except for that factor 2 and $m=0$. The integrals can be calculated,[7] and yield

$$\frac{F}{V}=\frac{kT}{\pi^2}\int_0^\infty\log\left\{1-\exp\left(-\frac{\hbar cK}{kT}\right)\right\}K^2dK=-\frac{8}{45}\frac{\pi^5k^4T^4}{h^3c^3}, \tag{6.5}$$

$$\frac{S}{V}=\frac{k}{\pi^2}\int_0^\infty\left\{\frac{\hbar cK}{kT}\Big/\left[\exp\left(\frac{\hbar cK}{kT}\right)-1\right]-\log\left[1-\exp\left(-\frac{\hbar cK}{kT}\right)\right]\right\}K^2dK=\frac{32}{45}\frac{\pi^5k^4}{h^3c^3}T^3, \tag{6.6}$$

$$E/V=(1/\pi^2)\int_0^\infty K^3\hbar c dK/\{\exp(\hbar cK/kT)-1\}=\frac{8}{15}\frac{\pi^5k^4}{h^3c^3}T^4, \tag{6.7}$$

which is indeed what was expected.

VII. CONCLUSION

In spite of many applications of quantum statistics to field theories, a consistent treatment of this subject had not yet been given before. In the foregoing sections we have shown that Klein's[3] formalism of quantum statistics can be applied to field theories without the need of much alteration. In some instances the thermodynamic functions were very similar to those for an ensemble of like particles; in others modifications had to be made.

The statistics of the nonrelativistic fields correspond to ordinary Bose and Fermi statistics of an ensemble of identical particles and thus agree with the results obtained by Kaempffer.[4] The relativistic cases, however, are different and yield new expressions where the number of existent particles is in equilibrium with the surrounding thermal conditions. It is considered as a considerable support for the present formalism that the thermal equilibrium at low temperatures of the Dirac electron field is automatically the "vacuum" state as described in the hole theory. Finally, the fact that the application of our formalism to the electromagnetic field leads back to Planck's radiation theory had to be expected.

It seems to us that the treatment given here is much more straightforward and direct than the approach of Debye[1] and Kaempffer[4] to the statistics of waves. We should like to emphasize once more that here we are not primarily concerned with the particles that are "contained" in the field, but with the statistics of the field only. The notion of "particles" is used only for convenience because it turned out that the calculation of the traces of the matrices representing the distribution functions is most easily performed in the N-representation which permits one to talk about "particles."

In conclusion, we should like to acknowledge our indebtedness to colleagues and students who have shown much interest in the progress of this work. We are especially grateful to Professor Bergmann in Syracuse and Professor Preston in Toronto for valuable discussions and helpful advice. Professors Green and Schrödinger in Dublin have read and criticized the manuscript and made pertinent suggestions; we wish to thank them. We are also indebted to the Reuben Wells Leonard Foundation for awarding a fellowship to one of us (C.D.M.) which made this research possible.

PHYSICAL REVIEW VOLUME 83, NUMBER 1 JULY 1, 1951

A Calculation of the Electron Affinity of Sodium*

R. M. THALER†
Brown University, Providence, Rhode Island
(Received March 13, 1951)

A wave function of the form $\Phi=\varphi(r_1,r_2)(1+cr_{12})$ is assumed for the $(3s)$ electrons of Na^-, to take into account the polarization effect of the added electron, an effect neglected by the Hartree method. On this basis the electron affinity of sodium is calculated to be $+1.2$ ev and therefore the negative ion is stable. The decrease in energy relative to the Hartree result is mainly due to the increased separation and consequent lowered interaction potential energy of the $(3s)$ electrons. Since the $(4s)$ electrons of K^- should be strongly polarized, the electron affinity of potassium can be estimated to be about $+0.7$ ev.

I. INTRODUCTION AND THEORY

ALTHOUGH the negative sodium ion Na^- probably can exist as a stable structure, calculation of its energy by the method of the self-consistent field[1] leads to a negative electron affinity, indicating an unstable ion (to the accuracy of the approximation). The reason is that the Hartree-Fock method cannot take into account the polarization effect of the added electron, an effect which contributes very largely to the stability of a negative ion.[2]

To take account of the polarization of the two outer shell electrons, it is necessary to adopt a wave function which depends on the interelectronic distance r_{12} between the outer electrons, as well as on their distances r_1, r_2 from the nucleus. The simplest wave function of this kind is

$$\Psi=U(r_3,\cdots,r_N)\Phi(r_1,r_2,r_{12}), \tag{1}$$

where the inner ten electrons are represented by the numbers $3,\cdots,N(N=12$ for $Na^-)$, and the outer two electrons are labeled 1 and 2. If the wave function U of the Na^+ core is chosen as a product of one-electron functions, it follows from the variation principle that U is essentially the self-consistent field function.[3] Similarly, if exchange is included U becomes the Hartree-Fock function, a determinant of one-electron functions. We are led in either case to an equation for Φ, which

* Presented at the February, 1951 meeting of the American Physical Society in New York. Part of a dissertation submitted in partial fulfillment of the requirements for the degree of Doctor of Philosophy at Brown University.

† Now at Yale University, New Haven, Connecticut.

[1] D. R. Hartree and W. Hartree, Proc. Cambridge Phil. Soc. **34**, 550 (1938).

[2] This question is discussed by D. R. Hartree, Rep. on Prog. in Phys. **11**, 113 (1948) and E. Conwell, Phys. Rev. **74**, 268 (1948).

[3] There is a slight difference between U and the s.c.f. function because Φ is not the Hartree function. However, the distinction is only a theoretical one, since the wave function U is negligibly influenced by the outer wave functions.

when expressed in atomic units runs as follows:

$$\epsilon\Phi=-\tfrac{1}{2}\nabla_1^2\Phi-\tfrac{1}{2}\nabla_2^2\Phi$$
$$-\left[\frac{11}{r_1}+\frac{11}{r_2}-\sum_{i=3}^{N}\frac{\int U^*U(1/r_{1i}+1/r_{2i})d\tau_3\cdots d\tau_N}{\int U^*Ud\tau_3\cdots d\tau_N}-\frac{1}{r_{12}}\right]\Phi$$
$$=-\tfrac{1}{2}\nabla_1^2\Phi-\tfrac{1}{2}\nabla_2^2\Phi+V(r_1)\Phi+V(r_2)\Phi+\frac{1}{r_{12}}\Phi. \quad (2)$$

Here ϵ is the energy of the outer two electrons [see Eq. (5)].

Equation (2) corresponds to the variation equation

$$0=\delta\int\Phi^*\left(\tfrac{1}{2}\nabla_1^2+\tfrac{1}{2}\nabla_2^2+\epsilon-V(r_1)-V(r_2)-\frac{1}{r_{12}}\right)\Phi d\tau_1 d\tau_2. \quad (3)$$

We choose Φ as

$$\Phi=\varphi(r_1,r_2)(1+cr_{12})=v(r_1)v(r_2)(1+cr_{12}) \quad (4)$$

where $v(r)$ is the Hartree-Fock radial wave function[1] for the Na^- outer shell ($3s$) electrons and c is an adjustable parameter.

The energy integral for the outer two electrons can then be written as

$$\epsilon=\int\Phi^*H_{3s}\Phi d\tau=\frac{E_H+c\int[r_{12}\varphi^*H_{3s}\varphi+\varphi^*H_{3s}(r_{12}\varphi)]d\tau+c^2\int r_{12}\varphi^*H_{3s}(r_{12}\varphi)d\tau}{1+2c\int\varphi^*\varphi r_{12}d\tau+c^2\int\varphi^*\varphi r_{12}^2d\tau}$$
$$=(E_H+a_1c+a_2c^2)/(1+b_1c+b_2c^2). \quad (5)$$

Here $H_{3s}\Phi$ is the right-hand side of Eq. (2); $E_H=-0.178_5$ a.u.[1] is the energy calculated by Hartree for the ($3s$) shell; $\varphi(r_1,r_2)$ is considered to be normalized; $d\tau$ is $d\tau_1 d\tau_2$.

II. NUMERICAL CALCULATIONS AND RESULTS

To make the calculation of the coefficients a_1, a_2, b_1 and b_2 practicable, analytic expressions for the itbular functions $\varphi(r)$ and $V(r)$ were found by a method samilar to that of Slater.[4] These expressions were found to be

$$v(r)=1.80e^{-9.65r}-3.00re^{-9.54r}+r^2(0.174e^{-0.903r}+0.00813e^{-0.421r}+0.000794e^{-0.276r}), \quad (6)$$

and

$$V(r)=1/r(1+17.14e^{-3.592r}-12.91e^{-6.588r}+5.848e^{-11.485r}). \quad (7)$$

However, in the actual calculation of a_1, a_2, b_1, and b_2, it proved sufficient to approximate $v(r)$ by

$$v(r)\doteq r^2(0.174e^{-0.903r}+0.00813e^{-0.412r}+0.000794e^{-0.276r}) \quad (8)$$

and $V(r)$ by

$$V(r)\doteq(1/r). \quad (9)$$

These approximations simplify the calculation greatly, without causing very great loss in accuracy. Investigation of the neglected terms reveals that they are small in comparison with the major terms and, moreover, they cancel to first order.

The coordinate system most convenient for evaluating the integrals in Eq. (5) is that employed by Hylleraas[5] in his work on the helium atom, viz.,

$$s=(r_1+r_2),\quad t=(r_1-r_2),\quad u=r_{12}. \quad (10)$$

In this coordinate system the volume element becomes:

$$d\tau=d\tau_1 d\tau_2=\pi^2(s^2-t^2)uds dt du. \quad (11)$$

Under the approximation of Eqs. (8) and (9), the coefficients a_1, a_2, b_1 and b_2 become:

$$a_1\doteq-\frac{1}{4}\int_0^\infty ds\int_0^s du\int_0^u dt\Big\{u^2(s^2-t^2)[(\partial\varphi/\partial s)^2+(\partial\varphi/\partial t)^2]+u(s^2-t^2)\varphi^2+s(u^2-t^2)\varphi\partial\varphi/\partial s+t(s^2-u^2)\varphi\partial\varphi/\partial t-4su^2\varphi^2\Big\}\doteq-4.288; \quad (12)$$

$$a_2\doteq-\frac{1}{8}\int_0^\infty ds\int_0^s du\int_0^u dt\Big\{u^2(s^2-t^2)[(\partial\varphi/\partial s)^2+(\partial\varphi/\partial t)^2]+u(s^2-t^2)\varphi^2+2us(u^2-t^2)\varphi(\partial\varphi/\partial s)+2ut(s^2-u^2)\varphi(\partial\varphi/\partial t)+u^2(s^2-t^2)\varphi^2-4su^2\varphi^2\Big\}\doteq-15.30; \quad (13)$$

$$b_1\doteq-\frac{1}{4}\int_0^\infty ds\int_0^s du\int_0^u dt\{u^2(s^2-t^2)\varphi^2\}\doteq13.93; \quad (14)$$

and

$$b_2\doteq-\frac{1}{8}\int_0^\infty ds\int_0^s du\int_0^u dt\{u^3(s^2-t^2)\varphi^2\}\doteq85.77. \quad (15)$$

[4] J. C. Slater, Phys. Rev. **42**, 33 (1932).

[5] E. A. Hylleraas, Z. Physik **54**, 347 (1929).

In Eqs. (12)–(15), φ is given by the following expression, in consequence of Eqs. (4), (8), and (10):

$$\varphi \doteq (s^4-2s^2t^2+t^4)[1.89(10^{-3})e^{-0.903s} +4.13(10^{-6})e^{-0.421s}+1.77(10^{-4})e^{-0.662s} \times\cosh(0.241t)+1.73(10^{-5})e^{-0.5895s}\cosh(0.313st) +8.07(10^{-7})e^{-0.2455s}\cosh(0.0725t)]. \quad (16)$$

Under the preceding approximations, minimization of Eq. (5) with respect to c leads to the values

$$c=0.108 \quad (17)$$

and

$$\epsilon=-0.234 \text{ a.u.}=-6.33 \text{ ev}. \quad (18)$$

Since the experimental value for the ionization energy of neutral sodium is 5.11 ev, the electron affinity for sodium is thus found to be +1.2 ev, which indicates a stable negative ion.

It follows from the variation principle that an exact solution of Eq. (5) would yield an energy which is an upper bound to the true energy. Therefore, any approximations in the solution of Eq. (5) which tend to increase ϵ strengthen our confidence in the calculated value of ϵ (−6.33 ev) as an upper bound to the true energy. Approximation of the potential energy from Eq. (7) to Eq. (9) leads to an overestimation of ϵ and thus need not concern us. On the other hand, the consequences of approximating the Hartree radial function $v(r)$ [Eq. (6)] by Eq. (8) may be more serious. Although examination of the neglected terms shows that their effect on the energy is small, it is difficult to estimate the error quantitatively. In fact, it is not even certain whether the inclusion of these neglected terms would raise or lower the calculated value of the energy value given in Eq. (18). To circumscribe this error, the largest of those neglected terms which tend to *increase* ϵ (algebraically) were computed. Inclusion of these terms leads to a new value of the energy, ϵ_1, which is algebraically larger than the exact solution of Eq. (5). Carrying out this calculation leads to the values

$$c_1=0.103 \quad (19)$$

and

$$\epsilon_1=-0.227 \text{ a.u.}=-6.14 \text{ ev}. \quad (20)$$

This corresponds to a value of +1.0 ev as a lower bound for the electron affinity of sodium. We thus see that the calculated value of +1.2 ev for the electron affinity of sodium is probably a good approximation to what would result from an exact solution of Eq. (5). In fact, an exact solution might even yield a result somewhat greater than 1.2 ev.

III. ESTIMATE OF POLARIZATION ENERGY

With the new wave function we have here calculated, it is possible to compute the average angular separation of the two outermost electrons. The average value of $\cos\theta$ is given by

$$\langle\cos\theta\rangle_{Av}=\left(\int\Phi^2\cos\theta d\tau\Big/\int\Phi^2 d\tau\right) =\frac{1}{2}\left\langle\frac{r_1^2+r_2^2-r_{12}^2}{r_1r_2}\right\rangle_{Av}=\left\langle\frac{s^2+t^2-2u^2}{(s^2-t^2)}\right\rangle_{Av}\doteq-0.92. \quad (21)$$

Therefore $\langle\theta\rangle\doteq157°$, indicating strong polarization. The Hartree wave functions, on the other hand, lead to an average angular separation of 90°, which corresponds to a completely unpolarized structure.

The average value of the potential energy arising from the mutual electrostatic interaction of the two outer electrons is given approximately by

$$\langle V\rangle\doteq1/\langle r_{12}\rangle\doteq\langle(r_1^2+r_2^2-2r_1r_2\cos\theta)^{-\frac{1}{2}}\rangle. \quad (22)$$

Since the average radius of the outer orbit of Na^- is given by $\langle r_1\rangle=\langle r_2\rangle\doteq4.0$ a.u.,[1] the average of the electrostatic interaction potential is

$$\langle V_H\rangle\doteq0.177 \text{ a.u.} \quad (23)$$

in the Hartree case, whereas we obtain

$$\langle V\rangle\doteq0.129. \quad (24)$$

The difference between these two values of the potential energy of interaction should be roughly that between the energies obtained by the method of the self-consistent field and by the present method. The Hartree outer shell energy for Na^- and the present result [Eq. (18)] differ by 0.055 a.u., and in comparison $\langle V_H\rangle-\langle V\rangle=0.048$ a.u.

The negative ion of potassium is a structure similar to Na^-, having two (4s) electrons in the outermost shell. We may thus expect strong polarization in the outer shell in analogy with our result for Na^-. The assumption of complete polarization [$\langle\cos\theta\rangle=-1$] leads to the result

$$\langle V_H\rangle-\langle V\rangle\doteq1/7.07-1/10=0.0414 \text{ a.u.}, \quad (25)$$

since $\langle r_1\rangle$ and $\langle r_2\rangle\doteq5.0$ a.u.[1] The Hartree value for the outer shell energy of K^- is −0.1425 a.u.,[1] so that an improvement of 0.0414 a.u. results in an outer shell energy of −0.184 a.u. or −5.0 ev. Since the ionization energy of neutral potassium is 4.3 ev, the electron affinity thus estimated is +0.7 ev.

The assumption of an average angular separation of only 150° leads by similar reasoning to an electron affinity of +0.4 ev for K^-. However, it is unlikely that the polarization of K^- is less than that of Na^-, since the polarization of two-electron systems increases with atomic number. We may thus surmise that K^- is stable, although it does not have so great an electron affinity as sodium.

The author wishes to thank Professor A. O. Williams, Jr., under whose direction this work was done, and Professor D. R. Hartree who supplied some unpublished tables of $V(r)$ for sodium.

Color Centers in Additively Colored Alkali Halide Crystals Containing Alkaline Earth Ions

FREDERICK SEITZ
University of Illinois, Urbana, Illinois
(Received March 21, 1951)

The measurements of Pick on the absorption bands produced in additively colored crystals of KCl and NaCl containing additions of divalent ions are reviewed and an interpretation of the origin of these bands is presented. Specific models are given for the Z_1, Z_2, and Z_3 centers responsible for the absorption bands observed by Pick. These resemble models proposed by Pick, but differ in several essential points. It is concluded that the divalent ions remain atomically dispersed in KCl when the crystal is quenched to room temperature from elevated temperatures, whereas some of the divalent ions and their associated positive-ion vacancies migrate to *F*-centers during the quenching process in NaCl. The observations also suggest that the divalent ions are not very mobile in KCl until a temperature near 200°C is attained, although the pair consisting of a positive and a negative ion vacancy becomes significantly mobile in the vicinity of 100°C. A number of experiments are proposed which may provide a more stringent test of the models suggested.

I. INTRODUCTION

PICK,[1] Heiland and Kelting[2] have examined several novel absorption bands which are obtained in additively colored specimens of KCl and NaCl to which divalent ions, calcium, strontium, and barium have been introduced. The results appear to be capable of sufficiently straightforward interpretation to merit discussion at this time.

II. EXPERIMENTS ON KCl

The experimental facts for KCl, on which attention will be focused first because of the greater wealth of experimental material, are as follows:

(1) The crystals were prepared by adding between 2 and 60 times 10^{-4} mole fraction of alkaline earth chloride to the melt from which the specimens were grown. Pick, who made the most careful measurements on the absorption bands of the crystals, did not determine the amount of divalent salt in the crystals; however the measurements of Kelting and Witt[3] on the equilibrium distribution of the divalent salts between liquid and solid indicate that only about one-tenth of the divalent salt in the melt appears in the solid when growth takes place at a rate of the order of 0.04 mm per minute or less, so that the mole fraction in the solid probably ranges between 10^{-5} and 3×10^{-4} in the various specimens investigated. The crystals were additively colored by heating them in potassium vapor, a density of color centers in the range from 0.3 to 1.0×10^{17} per cc being employed in the work. It may be observed that the density of alkaline earth ions should exceed this range in all cases if the divalent salt did not evaporate preferentially from the melt.

(2) If the additively colored KCl crystals are held well above 250°C and are then quenched, the normal *F*-band appears (Fig. 1), exactly as in a crystal which does not contain divalent salt. Pick states that the *F'*-band can be produced in the normal way[4] by irradiating the crystal in the *F*-band at temperatures near −90°C, where the *F'*-centers are stable.

(3) If the crystals are irradiated with wavelengths lying in the *F*-band when the crystal is at room temperature, some of the *F*-centers are converted into new centers, termed Z_1. The Z_1 centers, which are not found in pure alkali halides, possess an absorption band which lies somewhat on the long wavelength side of the *F*-band (Fig. 1b, c). The two bands can be separated unambiguously only by cooling the crystal to low temperatures (−215°C) where both become relatively narrow. The entire *F*-band cannot be converted into the Z_1 band; a substantial portion of the former always persists. Irradiation of the crystal in the Z_1-band at temperatures near room temperature or below does not alter this band; the Z_1-centers appear to be stable and are not reconverted into *F*-centers. The quantum efficiency for conversion from the *F*-band to the Z_1-band has apparently not been measured in additively colored crystals.

(4) If the crystal containing a mixture of *F*- and Z_1-centers is heated to temperatures near 110°C, or somewhat above, the Z_1-band vanishes and is replaced by a new band, Z_2. In addition the intensity of the *F*-band increases, implying that some of the Z_1-centers are reconverted into *F*-centers and others are converted into new centers, termed Z_2.

(5) The process of generating Z_1-centers can be repeated by irradiating in the *F*-band at room temperature after the Z_1-centers have been converted into *F*- and Z_2-centers by heating. A portion of these new Z_1-centers may then be converted into Z_2-centers by heating near 110°C. Thus the density of Z_2-centers may be built up in stages by reiteration of this procedure.

(6) The Z_2-centers may be destroyed by heating the crystal above 200°C, in which case the *F*-band reemerges when the specimen is quenched.

[1] H. Pick, Ann. Physik **35**, 73 (1939); Z. Physik **114**, 127 (1939).
[2] G. Heiland and H. Kelting, Z. Physik **126**, 689 (1949).
[3] H. Kelting and H. Witt, Z. Physik **126**, 697 (1949).
[4] See, for example, H. Pick, Ann. Physik **31**, 365 (1938); R. W. Pohl, Physik Z. **39**, 36 (1938); N. F. Mott and R. W. Gurney, *Electronic Processes in Ionic Crystals* (Oxford University Press, London, 1940), Chapter IV.

(7) When the crystal containing a mixture of F- and Z_2-centers is irradiated near $-90°C$ with light lying in either of these bands, both bands diminish in intensity. F'-centers and a new type of center, termed Z_3, are generated. The absorption band associated with the Z_3-center resembles the F'-band in the sense that it is very broad, even at low temperatures. However its peak lies on the short wavelength side of the F-band. Pick concludes from the general behavior of the Z_3-band that the Z_3-center bears the same relation to Z_2-center that the F'-center does to the F-center.

(8) Heiland and Kelting[5] have found that an additively colored crystal of KCl crystal containing calcium yields a broad "colloidal" band when annealed at 250 degrees for 90 minutes. Apparently the stoichiometric excess alkali metal and the calcium chloride will for a "colloidal" precipitate during this process.

(9) Harten[6] has measured the photocurrents produced by x-rays in "pure" KCl, which contains of the order of 10^{-3} percent Ca and Ba, and in specimens containing of the order of 10^{18} Ca, Sr, or Ba atoms per cc. In all four cases the range of carriers, which are presumably principally electrons, seems to be dependent upon the density of foreign atoms below $-180°C$, as if the impurity had a cross section of about 10^{-18} cm^2 for capturing the electrons. The photocurrents rise above $-180°C$, the temperature at which the rise occurs being dependent upon the nature of the divalent addition. In the case of the "pure" specimens and those containing Ca and Sr, the photocurrent near and above $-100°C$ seems to be independent of the impurity content, as if the electrons were captured by a trapping center other than the divalent impurity. The capture cross section of the impurities is then less than 10^{-16} cm^2. The photocurrents do not rise to the same extent in the crystals containing Ba; however, Harten concludes that the Ba forms aggregates in this case, in spite of rapid quenching from elevated temperatures.

(10) Hummel[6] has found that crystals of KCl containing Ca darken more deeply under gamma-ray irradiation at room temperature than pure crystals do. The density of color centers increases with increasing concentration of the divalent impurity. Presumably the darkening is associated primarily with F-centers, since experiments described in the next section show that this is the case in NaCl containing divalent impurities.

III. AN INTERPRETATION OF THE EXPERIMENTS ON KCl

Pick[1] has given an interpretation[7] of the centers responsible for the various bands described above. However a somewhat different interpretation will be given here.

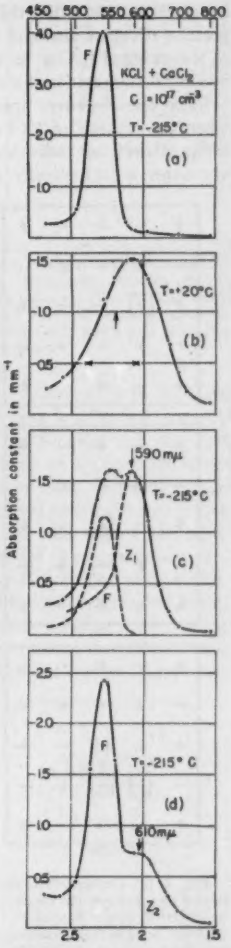

FIG. 1. Absorption bands in additively colored KCl containing $CaCl_2$ (after Pick). (a) The F-band, obtained by quenching to room temperature. The absorption spectrum was measured at $-214°C$ to obtain resolution. These F-centers may be converted to normal F'-centers at $-100°C$ by irradiating in the F-band. (b) The broad absorption band obtained by irradiating in the F-band near room temperature. This broad band contains both the F-band and the Z_1-band, unresolved. (c) The specimen possessing the broad band shown in (b) at room temperature is cooled to liquid air temperature and the F-band and Z_1-bands are resolved as shown. (d) The Z_2-band is developed from the Z_1-band by heating the specimen shown in (b) and (c) to the neighborhood of 110°C. The F-band is also enhanced relative to the value shown in (c). (d) was obtained from absorption measurements carried out at $-125°C$ after heating to 110°C, in order to obtain better resolution of the Z_2-band.

Following well-accepted arguments,[8,9] we shall assume that the F-centers are to be associated with single electrons trapped in halogen-ion vacancies (Fig. 2(a)), whereas F'-centers are associated with pairs of electrons trapped in halogen-ion vacancies (Fig. 2(b)). Similarly we shall assume that the divalent ions enter the crystal substitutionally and are accompanied by positive-ion vacancies (Fig. 2(c)). The work of Etzel and

[5] H. U. Harten, Gött. Nach., p. 15 (1950).
[6] H. Hummel, thesis, Göttingen University (1950).
[7] Pick has interpreted the Z_1-center as the result of trapping an electron at a divalent ion with which a positive-ion vacancy is permanently associated; the Z_2-center is interpreted as the result of combining an electron with an isolated divalent ion to which no vacancy is attached; the Z_3-center is regarded as a Z_2-center which has captured a second electron. At the time Pick's interpretation was offered, little direct information was available concerning the mobility and energy of association of the various aggregates. The wartime research on skiatrons and the post-war studies of diffusion and ionic conductivity have made it possible to re-evaluate these models and offer the alternatives proposed in the text.
[8] N. F. Mott and R. W. Gurney, reference 4.
[9] F. Seitz, Revs. Modern Phys. 18, 384 (1946).

Maurer[10] indicates that the energy of association of the positive divalent ions and the positive-ion vacancies is of the order of 0.3 ev, so that such association should be almost complete in the vicinity of room temperature.

Since the F-centers appear in relatively pure form when the crystals of KCl are quenched from elevated temperatures, we may assume that the halogen-ion vacancies are atomically dispersed and are occupied

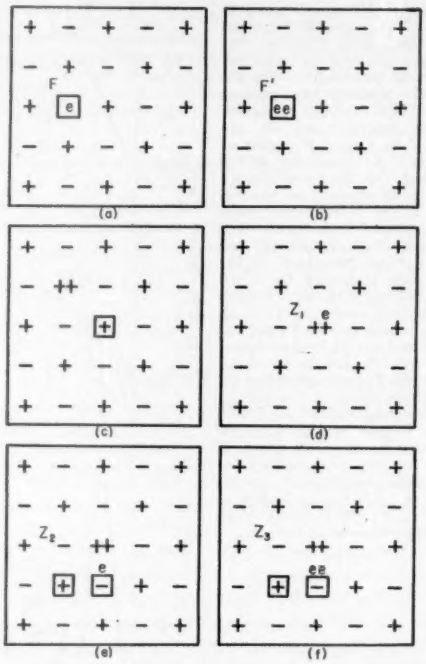

FIG. 2. (a) The conventional F-center consisting of an electron bound to a halogen-ion vacancy. (b) A representation of the conventional F'-center having two electrons bound to a halogen-ion vacancy. (c) The pair consisting of a divalent ion and an associated positive-ion vacancy. (d) The Z_1-center described in the text, consisting of an electron bound to a divalent ion in an otherwise perfect crystal. (e) The Z_2-center described in the text, obtained by combining a Z_1-center and a pair consisting of a positive- and a negative-ion vacancy. The electron is presumably shared by the divalent ion and the halogen-ion vacancy. (f) The Z_3-center, obtained at low temperatures when the Z_2-center captures a second electron, as in the formation of an F'-center from an F-center. If the Z_2-center retained its electrons at temperatures nearer room temperature, one might expect the positive-ion vacancy to migrate away, forming a new, neutral center. Presumably the electron evaporates first.

by electrons in exactly the same way as in an additively colored crystal which does not contain a significant quantity of alkaline earth metal.

It is simplest to assume that the divalent ions, with their associated vacancies, are also dispersed almost at random in the specimens of KCl. However, this assumption cannot be made without discussion. Mapother, Crooks, and Maurer[11] have given evidence to show that cadmium diffuses very rapidly in sodium chloride, as if the attached positive-ion vacancy imparted an unusually high mobility to it in the manner proposed for alloying agents in metals by Johnson and Wagner.[12] Although the measurements of Mapother, Crooks, and Maurer are only semi-quantitative, they are not inconsistent with the view that the time required for the divalent ion to jump from one lattice position to another, in such a way as to contribute to its diffusion, is nearly the same as the jump time for a free positive-ion vacancy, that is about 10^{-2} sec at room temperature.[13] Should the jump-time for the divalent ions be this small in KCl, any one divalent ion should be able to meet another, and in fact meet an F-center, in a time of the order of several hours. It is possible that Pick's experiments on KCl were carried out sufficiently rapidly that the divalent ions did not have time to combine with one another or with F-centers before the various stages of irradiation were set into effect. We shall see in Sec. IV that direct combination of the divalent ions and F-centers, through diffusion of the former and without the intervention of radiation, has probably been observed in NaCl. Apparently we must conclude that the divalent ions are more mobile in NaCl than in KCl. The same conclusion has been drawn independently by Burstein, Oberly, Henvis, and Davisson[14] from a study of the temperature dependence of the change in absorption bands arising from additions of lead to NaCl and KCl. It is found that the bands change much more noticeably with time near room temperature in NaCl than in KCl, as if the lead may cluster in the course of several days in the former material, but not in the latter.

In this connection, it is interesting to note that the divalent ions may become at least partly immobilized at room temperature through relatively weak association. When two divalent ions, which have positive-ion vacancies attached, approach one another within the crystal, they will be subject to an electrostatic interaction which results from the dipole moment of the pair consisting of divalent ion and vacancy and to a repulsion which arises from the elastic distortion the pairs engender in the lattice. The electrostatic attraction reaches its maximum when the dipoles are antiparallel and the divalent ions are separated by the distance of the cubic unit cell, as in Fig. 3(a). It may be seen that a halogen ion lies between the divalent ions

[10] H. Etzel and R. J. Maurer, J. Chem. Phys. **18**, 1003 (1950).

[11] Mapother, Crooks, and Maurer, J. Chem. Phys. **18**, 1231 (1950).

[12] R. P. Johnson, Phys. Rev. **56**, 814 (1939); C. Wagner, Z. physik. Chem. **38B**, 325 (1937).

[13] This value of the jump-time is deduced from the experiments on the mobility of positive ion-vacancies in the alkali halides. See, for example, Etzel and Maurer (reference 8); C. Wagner and P. Hantelmann, J. Chem. Phys. **18**, 72 (1950); H. Kelting and H. Witt (reference 3).

[14] Burstein, Oberly, Henvis, and Davisson, Phys. Rev. **81**, 459 (1951).

and between the positive ion vacancies which neighbor them. Presumably this configuration has a stability of the order of 0.3 ev for separation into divalent ion-vacancy pairs. Actually, if such clusters have sufficient time to form, some of the divalent ions should have had sufficient time to migrate to the vicinity of F-centers, where we should expect the formation of a relatively stable unit consisting of an electron, a divalent ion, a negative-ion and a positive-ion vacancy—a unit which will presently be identified with the Z_2-center. Since the F-band appears in unmolested form after the crystal is quenched to room temperature, we shall assume that the divalent ions in KCl do not diffuse rapidly and remain dispersed.

When the crystal containing F-centers is irradiated with light lying in the F-band at any temperature above 100°K, electrons are freed[15] and wander about the lattice. They can be trapped by other centers, to form stable F'-centers[4] if the temperature is not above 180°K. Apparently this process is strongly favored over any other in the low temperature region, so that F'-centers are formed in preference to centers involving electrons and divalent ions, perhaps because the dipole electrostatic field of the divalent ion and its associated positive-ion vacancy, which is relatively immobily bound to it at temperatures below 180°K, does not offer a stable state for the electron. On the other hand, the F'-center is thermally unstable at room temperature in KCl, so that the electron must wander until it meets a stable trap. The two possible traps are: (1) halogen-ion vacancies from which electrons have been ionized and (2) divalent ions which are either temporarily dissociated from their positive-ion vacancy or from which the positive-ion vacancy is ejected during the period of time which the electron spends in the vicinity of the divalent ion. An F-center will be reformed in the first case; we shall assume that the Z_1-center is an isolated divalent ion which has captured an electron (Fig. 2(d)). It is evident that the Z_1-center described here will not have a strong attraction for a positive-ion vacancy because it is electrically neutral.

The experiments show that the Z_1-band of KCl cannot be bleached by irradiation in the Z_1-band. We apparently must conclude that the thermal fluctuations available even at room temperature are not sufficient to free the electron from the first excited level before a transition occurs to the ground state. In other words, we must conclude that the thermal energy required for liberation of the electron in the first excited state of the Z_1-center is at least three times as large as the value[16] for the F-center (~0.075 ev), which exhibits similar behavior below 100°K. Although both centers are neutral, this difference in behavior is perhaps not difficult to understand: since the oscillator strength[17]

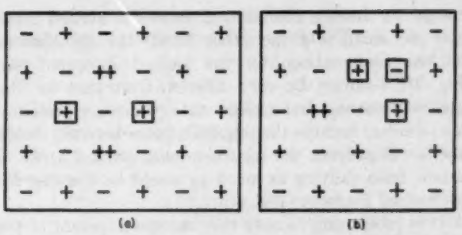

FIG. 3. (a) The weak aggregation of two pairs consisting of divalent-ions to which positive-ion vacancies are attached. It will be noted that the halogen ion lies midway between the two divalent ions and the two positive-ion vacancies. (b) The stable arrangement of the complex formed by combining a divalent ion to which a positive-ion vacancy is attached and a pair consisting of a positive- and a negative-ion vacancy.

for the transition from the ground state to the first excited state of the F-center is as large as 0.8, we may conclude that the charge distribution for the first excited state is not spread over an appreciably larger volume than that of the ground state. Hence the equilibrium nuclear configuration will be similar to the two states. On the other hand, we may expect the equilibrium nuclear configuration for the negative-ion vacancy from which the electron has escaped to be appreciably different from that for the first excited state, for the excess positive charge is no longer neutralized and the presence of the vacancy allows freedom for motion. It follows (Fig. 4(a)) that the thermal activation

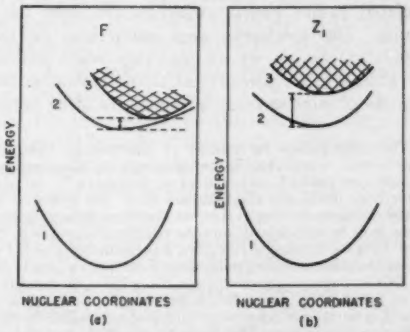

FIG. 4. Schematic Franck-Condon diagram for the energy levels in an F-center and a Z_1-center. The vertical axis represents energy and the horizontal the configurational coordinates of the nuclei near the centers. In both cases curve 1 represents the ground state, curve 2 represents the first excited state and 3 represents the ionization levels. The excited discrete levels between curves 2 and 3 are not shown. It is assumed that the coordinates for energy are nearly the same in states 1 and 2 for both centers because the charge distributions are not widely dissimilar. Moreover, it is assumed that the configurational coordinates are substantially different for the bound and ionized states (free halogen-ion vacancy) of the F-center because of the freedom of motion permitted by the presence of the vacancy. On the other hand, it is assumed that the configurational coordinates are not changed greatly near the Z_1-center by freeing the electron because the ions are closely packed. The vertical arrows represent the thermal activation energies for the transition from the first excited state to the ionization levels in the two cases.

[15] See, for example, G. Glaser and W. Lehfeldt, Gött. Nach. FGII, 91 (1936); H. Rögener, Gött. Nach. FGIII, 219 (1941).
[16] See N. F. Mott and R. W. Gurney, reference 4, p. 136.
[17] F. G. Kleinschrod, Ann. Physik 27, 97 (1936).

energy for freeing the electron from the excited state may be small. On the other hand, the equilibrium nuclear configuration for the ionized Z_1-center (see Fig. 2(d)) cannot be very different from that for the ground state and first excited state (which are probably also similar) because the repulsive forces between closed shells will prevent the relatively close-packed array of atoms from shifting as much as would be the case for an ionized F-center (Fig. 4(b)).

It is interesting to note that the development of the Z_1-band at the expense of the F-band becomes increasingly difficult as the former grows. This fact is possibly a consequence of the increase in concentration of halogen-ion vacancies, which have a large cross section[18] for capture of electrons.

The positive-ion vacancies, which are released from the divalent ions when they capture electrons to form Z_1-centers, and the halogen-ion vacancies, which are produced by ionization of the F-centers, should combine to form the mobile pairs which the writer[19] has presumed play a very important role in the bleaching and coagulation of F-centers and in their generation by x-rays. If these were sufficiently mobile at room temperature to diffuse 10^5 or 10^6 atomic spacings in the times of interest in these experiments, we would expect both the F-band and the Z_1-band to be modified by combination with negative-ion vacancies. In fact Scott and Bupp,[20] studying additively colored crystals of KCl containing 5×10^{17} F-centers per cc, observed the formation of R- and M-centers when the crystals were irradiated rather heavily with an arc light for 85 minutes. The specimens were maintained at room temperature by air jet cooling. This result indicates that, at least in the pure crystal, the pairs should diffuse distances of interest to us in the course of 85 minutes at room temperature. It is possible that a small number of R- and M-centers were formed in Pick's experiments during the conversion from the F-band to the Z_1-band, but were not investigated because they lie toward the red end of the spectrum. It is also possible that the vacancy pairs, produced by combination of the positive- and negative-ion vacancies, are captured by pairs formed of the divalent ions and their associated positive-ion vacancies. The concentration of the latter should exceed that of the F-centers and of the Z_1-centers. The center formed in this way is shown in Fig. 3(b). Simple calculations indicate that it should not have an energy of association larger than 0.5 ev. On the other hand, even this moderate inhibition may be sufficient to prevent the formation of R-centers and M-centers at room temperature in the time of observation.

The Z_1-centers are transformed into Z_2-centers when the crystal is heated above 110°C. The increase in temperature stimulates the mobility of the vacancies and hence the diffusion of ions. If the conversion $Z_1\rightarrow Z_2$ were primarily the result of migration of the divalent ions, we would expect the F-band to be modified as a result of combination of F-centers and the divalent ions. Instead the F-band actually is enhanced, presumably because some of the Z_1-centers lose electrons through thermal ionization, probably when positive ion vacancies are nearby, and these electrons are captured by the halogen-ion vacancies which were produced earlier, when the Z_1-centers were formed by ionization of the F-centers.

It seems reasonable to assume that the increase in temperature permits a fraction of the negative-ion vacancies which have combined with positive ion vacancies and formed pairs, to diffuse to these Z_1-centers that have not decomposed and produce the center shown in Fig. 2(e). This is a neutral unit consisting of the pair of vacancies of opposite sign, the electron and the divalent ion. We shall identify this configuration with the Z_2-center.

It is also possible that the electrons freed thermally from the Z_1-centers generate Z_2-centers by combining with the units shown in Fig. 3(b), which were produced during the transformation from the F-band to the Z_1-band by aggregation of the positive-negative-ion vacancy pairs and the divalent ions. A positive-ion vacancy would be ejected from the unit shown in Fig. 3(b) once it has captured an electron. The halogen-ion vacancy would then move nearer the divalent ion.

As mentioned previously, the Z_2-center could be formed directly from the F-center by combination of this with a divalent ion which has migrated to an adjacent site with the aid of an associated positive-ion vacancy. If our identification of Z_1 and Z_2 are correct, we may conclude from the absence of Z_2-centers in the freshly quenched specimen that the divalent ions are not very mobile in KCl, as was emphasized earlier.

Since the Z_2-center possesses two vacancies, we

[18] The cross section for capture of electrons by halogen-ion vacancies may be estimated in the following way. The experiments of Glaser and Lehfeldt and of Rögener (reference 12) on photoconductivity in colored alkali halides show that F-centers may capture electrons to form F'-centers. The cross section σ_f for this process may be determined from the relation $N_f\sigma_f=\beta/v(w/E)$ in which N_f is the density of F-centers, β is the mobility of the conduction electrons (assumed to be about 5 cm² per volt-sec in NaCl and KCl at room temperature), v is the velocity of thermal motion of the electron (about 10^7 cm per sec at room temperature) and w/E is the ratio of Schubweg w to field strength E in the photoconductive experiments. This leads to values of σ_f of the order of 3×10^{-15} cm² in the range of temperature in which F'-centers are stable. The study of photoconductivity in the transition from F' to F-centers in a specimen having nearly equal densities of F- and F'-centers (see F. Domanic, reference 18) shows that near -120°C w/E is nearly equal to the value of this ratio for the photocurrent observed at the same temperature in the transition from F to F' in a specimen having an equal number of F-centers. This result implies that the cross section σ_v for capture of an electron by a halogen-ion vacancy is also of the order of 3×10^{-15} cm² near -120°C. The work of Domanic indicates that this cross section rises very rapidly in going to lower temperatures, becoming 20 times larger near liquid hydrogen temperatures. Presumably the highly excited states of the F-center become stable toward thermal dissociation at very low temperatures, so that the capture cross section attains a value near 6×10^{-14} cm².

[19] See reference 9. Also G. J. Dienes, J. Chem. Phys. **16**, 959 (1948).

[20] A. B. Scott and L. P. Bupp, Phys. Rev. **79**, 341 (1950).

might expect it to have a low thermal activation energy for the freeing of an electron from the first excited state, as is the case for F-centers. The experiments indicate that the Z_2-center, like the F-center and unlike the Z_1-center, does bleach, at least in part, when irradiated with light absorbed in the Z_2-band.

The isolated negative-ion vacancies become transformed into F- or Z_2-centers during the thermal treatment near 110°C, so that they are not available to impede the formation of new Z_1-centers when the crystal is irradiated in the F-band (or the Z_2-band (?)) at room temperature, in agreement with observations.

We might expect the Z_2-center to be able to hold a second electron if the F-center can. The close symmetry between the Z_3-band and the F'-band suggests at once that the Z_3-center is formed in this way (Fig. 2(f)). We shall return in the next section to the question of the tightness with which a Z_3-center holds the positive-ion vacancy.

The interesting fact that the long wavelength limit of Z_3-band lies on the high energy side of the Z_2-band implies that the second electron in the Z_3-center is about as tightly bound as the first, unlike the situation in the case of the F- and F'-center. This receives a fairly natural explanation in terms of the models proposed here. The negatively charged F'-center resembles the negative hydrogen ion, H^-, very closely in the sense that the two electrons are bound to a more or less central field. On the other hand, the two electrons in the Z_3-center make use of the attractive field of both the halogen-ion vacancy and the divalent-ion. One may regard the extra negative charge as arising from the positive-ion vacancy. The latter will attempt to shift away from the electron distribution—a possibility that has no analogue in the F'-center. As a result, the equilibrium configuration of the atoms in the Z_3-center may correspond to an arrangement of the Z_2-center of high energy. Hence the ionization energy of the Z_3-center may be relatively large.

Harten's experiments on the photocurrents produced by x-rays in crystals which contain divalent impurities, but are not additively colored, seem to show that the center consisting of a divalent impurity and its associated positive-ion vacancy has a capture cross section less than 10^{-16} cm^2 near room temperature, although the value is near 10^{-15} cm^2 below -180°C. In fact, the results suggest that the electrons are captured preferentially by centers other than the divalent impurities when the latter are present to concentrations of 10^{18} per cc or less, and do not form aggregates.

Hummel's observation that crystals containing divalent impurities darken more easily and more deeply than pure crystals implies that the divalent impurities may play an important role in the formation of F-centers by irradiation. The precise nature of this role is obscure. However it is possible that the divalent ions with associated vacancies are excellent traps for the holes produced during irradiation, that the holes are immobilized by being captured at these units, and that the electrons are then captured preferentially at dislocations where they form F-centers by an as yet undisclosed process.[21] This aspect of the present problem merits extended investigation.

The foregoing models suggest a number of critical experiments:

(1) One would expect the Z_2-centers to be formed directly during a relatively slow cooling of the crystal to room temperature. The experiments of Heiland and Kelting referred to in Sec. II (paragraph 8) are not sufficiently refined to test this point, for they annealed the specimens so long that large aggregates were formed. This process has been observed in NaCl (see next section).

(2) It is possible that at least small components of the R- and M-bands are produced during conversion of the F-band into the Z_1-band. It is also possible that Z_2-centers will be formed in a second irradiation in the F-band, after a primary irradiation in which a "saturated" value of Z_1-centers have been formed, provided sufficient time (an hour or a day) is allowed between the two irradiations to permit the positive- and negative-ion vacancies to combine and diffuse to divalent ions, where they form the units shown in Fig. 3(b).

(3) The Z_2-centers should be a source of photoelectrons which, like the F-centers, become inefficient at temperatures near or below 100°K.

(4) In contrast, the Z_3-centers should yield photoelectrons even near the absolute zero of temperature[22] since the Z_3-band, like the F'-band, should correspond to transitions from a discrete bound state to the ionization continuum.

(5) Electrons should be liberated when the Z_1-band is converted into the F-band and Z_2-band by warming the specimen to the vicinity of 110°C.

(6) For reasons which will become clear in the next section, we should expect to form Z_1-centers by irradiation in the Z_2-band at temperatures not so low that F'- and Z_3-centers are formed. This process appears to be observed in specimens of NaCl analogous to those considered here.

(7) Evidently experiments on the diffusion of divalent ions, extending the work of Etzel and Maurer, would be highly informative.

(8) It would be highly desirable to investigate the V-centers which are formed when crystals containing divalent additions are irradiated with x-rays, for Hummel's observations suggest that divalent impurities may play an important role in the process of darkening with x-rays or other ionizing radiations.

---

[21] F. Seitz, Phys. Rev. **79**, 890 (1950).

[22] The ability of F'-centers to produce photoelectrons even near 0°K has been demonstrated by F. Domanic, Ann. Physik **43**, 187 (1943).

IV. FURTHER EXPERIMENTAL RESULTS ON NaCl

Pick[1] has also described, in much less complete fashion, experimental results for additively colored NaCl containing strontium. The principal results are:

(1) The F-band does not appear alone when the crystal is quenched from elevated temperatures. Instead it is accompanied by a band, A, which can be bleached to yield both an increase in F-centers and additional centers which absorb in a region B between the F-band and the A-band. Pick identifies the A-band with the Z_2-band in KCl and identifies the B-band with the Z_1-band of KCl. This identification is in excellent agreement with the views put forth in the previous section if we assume that the divalent ions are appreciably more mobile in NaCl than in KCl, so that some of the F-centers combine with divalent ions, to which positive-ion vacancies are associated, during the quenching step. We saw previously that one might expect to form Z_2-centers directly from F-centers by migration of the divalent ions if this migration is sufficiently rapid.

We might expect to form F-centers and Z_1-centers at room temperature by freeing electrons from Z_2-centers as a result of irradiation in the Z_2-band. Once electrons have been freed from the Z_2-centers, we should expect the positive-ion vacancy to carry the negative-ion vacancy away from the divalent ion since the energy of association of the pair of vacancies with the divalent ion must be very small compared with the energy of association of a pair of oppositely charged vacancies.[23,24] Some of the isolated divalent ions may then capture photoelectrons and form Z_1-centers. Similarly, the remaining free electrons may combine with the negative-ion vacancies of a fraction of the neutral pairs of vacancies to form F-centers and free positive-ion vacancies, which may eventually combine with the remaining isolated divalent ions. Since the vacancies should diffuse away from the Z_2-center very soon after it is ionized, the Z_2-center would not be regenerated as rapidly as the F-centers are regenerated by combination of free electrons and negative-ion vacancies, when Z_1-centers are produced by irradiating in the F-band.

(2) As in KCl, the Z_1-band cannot be bleached by irradiating the crystal with light in this band. It can be converted into the F-band and the Z_2-band by warming the crystal.

(3) The F-band and Z_1-band appear when clear NaCl which contains strontium, but does not contain excess sodium, is irradiated with x-rays. The F-centers are presumably formed by the same process as in pure alkali halides, that is by the freeing of vacancies from clusters, cracks, or dislocations and the trapping of electrons and holes in these vacancies. The crystals possessing strontium should exhibit the Z_1-band, as observed, if the assignment of the previous section is correct, for some of the electrons will be trapped by isolated divalent ions which are dispersed in the crystal. We would not expect to find the Z_2-band if the irradiation is not carried on at elevated temperatures, at least immediately after the irradiation, for the rapid alternation of charge on a Z_2-center as it alternately captures electrons and holes would cause it to disintegrate by the same process that operates when Z_2-centers are converted into F- and Z_1-centers by irradiation in the Z_2-band.

It is interesting to note that F-centers are formed preferentially, relative to Z_1-centers, during x-ray irradiation at room temperatures. This observation suggests that the divalent impurities with attached positive-ion vacancies do not have a large cross section for capturing electrons, in good agreement with Harten's observations. Thus the electrons prefer to wander until they find centers with a larger cross section. The latter presumably are the traps from which F-centers may be formed.

There is another interesting point to note: During irradiation of the crystal with light lying in the Z_2-band at room temperature, some of the electrons freed by the light must approach Z_2-centers. Presumably the Z_3-centers, which would be formed if the electrons were captured, are unstable at room temperature and the electron either is not captured or is released after capture. On the other hand, if the electron persisted sufficiently long for a positive-ion vacancy to be ejected, an entirely new center consisting of two electrons, a halogen-ion vacancy and a divalent ion would be produced (see caption to Fig. 2(f)). This would have certain similarities to the R-centers obtained[9] during coagulation of F-centers and might be very stable. It would be interesting to see if it can be produced at temperatures somewhat below room temperatures where the positive-ion vacancies have not lost their mobility and where the F'-centers of NaCl are stable. It is not improbable that the activation energy[24] required to free a positive-ion vacancy from the Z_3-center is sufficiently larger than the activation energy required to free the electron that the latter will occur preferentially at any temperature where the Z_3-center is unstable; however, the alternative possibility exists.

The writer is indebted to Dr. Pick for extensive discussions of this topic, even though the latter has maintained a reserved attitude toward the views presented in this paper.

[23] The negative-ion vacancy should hold the positive-ion vacancy more tightly than the divalent ion. The energy of association of the latter with the positive-ion vacancy is about 0.3 ev (see Etzel and Maurer, reference 8). The energy of association of a positive- and negative-ion vacancy is probably nearer 1 ev (see Seitz, reference 7, and the calculations mentioned in reference 20).

[24] I am indebted to Dr. John Reitz of Los Alamos for a description of calculations of the binding energies of various clusters in NaCl and KCl, carried out by him and Dr. Gammel. These investigators have found that the binding energy of a pair of vacancies of opposite sign is 0.9 ev and the binding energy of a cadmium ion and a positive-ion vacancy in NaCl is 0.3 ev. On the other hand, this work shows that the activation energies required to dissociate these units may be appreciably larger than the energies of association. This suggests that the Z_3-center will probably always dissociate by ejecting an electron.

On the Interpretation of Resonance Levels and Their Widths in Terms of the Scattering Length and the Effective Range

T. TEICHMANN
Palmer Physical Laboratory, Princeton University, Princeton, New Jersey
(Received January 17, 1951)

The so-called effective range formula for nuclear scattering is deduced from the nuclear dispersion formalism for a fairly general class of potentials. It is shown that only in the case of zero angular momentum scattering is the angular momentum uniquely determined from the low energy variation of the cross section. The relation between the scattering length and effective range on the one hand and the parameters of nuclear dispersion theory (resonance levels and reduced widths) is briefly discussed.

I. INTRODUCTION

LOW energy nuclear collisions may be described by two types of parameters. In the case of n–p scattering at zero angular momentum, for instance, it is usual to consider $\tan\delta = Q$ (δ = phase shift), and to express $k\cot\delta = k/Q$ in the form

$$k\cot\delta = -1/a + \tfrac{1}{2}r_0k^2 + pr_0^3k^4 + \cdots, \qquad (1.1)$$

where a is the scattering length, r_0 the effective range, etc.[1] The cross section is then given by

$$\sigma = (4\pi/k^2)[Q^2/(1+Q^2)]. \qquad (1.2)$$

Similar formulas may also be obtained for p–p scattering (see Bethe, reference 1) and for scattering at higher angular momenta. In each case the quantity $k\cot\delta$ (or something closely related) is expanded in a Taylor series in k^2 (i.e., substantially in the energy), and the cross section is characterized by various *length* parameters, a, r_0, p, $\cdots$etc., which are in some way characteristic of the scattering potential.

On the other hand, when rather larger energy ranges are considered, or when the compound nucleus (formed by the two colliding nuclei) is rather complicated, it is also common to use certain *energy* parameters characteristic of the compound system, *viz.*, the resonance levels E_λ, and the reduced widths γ_λ^2. To this end one introduces the so-called derivative matrix[2] R (which is, of course, a scalar in the case of pure scattering), given by

$$R = \sum_\lambda [\gamma_\lambda^2/(E_\lambda - E)] \qquad (1.3)$$

in terms of which[3]

$$Q = -(F - RF')/(G - RG'). \qquad (1.4)$$

Here F/r_c, G/r_c are the regular and irregular solutions[4] of the two-particle colliding system, evaluated at $r = r_c$, r being the relative separation of the two particles. r_c is the "radius" of the compound system. For $r > r_c$, the system may be treated as a two-particle collision with the well-known centrifugal and coulomb interaction between the particles, for which the corresponding functions F, G have been calculated by Yost, Wheeler, and Breit.[4] (However, the following treatment does not depend on the particular forms of F and G, and can be presumed to include a wide class of external potentials, for which F, G have the forms given in (2.5) and (2.7). See also (2.8).) For $r < r_c$, the system is supposed merged into a compound nucleus characterized by R.[5]

From (1.1) and (1.4) it is clear that it must be possible to derive the right-hand side of (1.1) from the known properties of R, F, and G. This should render it possible to derive at once the generalization of (1.1) for all angular momenta, for a coulomb potential, and generally for a large class of external potentials (see the remark above). The result should be expected to illuminate the nature both of the energy parameters E_λ, γ_λ^2 and of the length parameters a, r_0, $\cdots$ etc. (Such a connection is also mentioned on related grounds by Blatt and Jackson.[1])

Such a relation is to be expected, not only for the reason given above, but also from the nature of the derivations of the two quantities $k\cot\delta$ and R, as given by Bethe[1] and Wigner,[6] respectively. Both these quantities are simple fractional linear forms in the logarithmic derivations of incoming and outgoing waves of unit amplitude (with energy dependent coefficients), and in both cases a functional equation of the type

$$f(E_2) - f(E_1) = (E_2 - E_1)g(E_2, E_1) \qquad (1.5)$$

is obtained. In the derivation of (1.1) given by Bethe, $f = k\cot\delta$, and a solution for f is obtained as a power series in E (i.e., in k^2). In the dispersion-theoretic treatment of Wigner, $f = R$, and solution of the functional equation (1.5) (taking into account the particular form of $g(E_2, E_1)$) yields the expression (1.3) for R. It is thus natural to expect a fairly intimate connection

[1] See H. A. Bethe, Phys. Rev. **76**, 38 (1949), for a full and neat derivation of this result, which was originally surmised by Landau and Smorodinsky, J. Phys. Acad. Sci. U.S.S.R. **8**, 154 (1944), and first proved by variational methods by J. Schwinger [see J. Blatt and J. D. Jackson, Phys. Rev. **76**, 18 (1949)].

[2] E. P. Wigner and L. Eisenbud, Phys. Rev. **72**, 29 (1947), R is simply the inverse logarithmic derivative of $r\times$ the internal wave function ($r < r_c$) evaluated at $r = r_c$.

[3] See E. P. Wigner, "On the statistical distribution of the widths and spacings of nuclear resonance levels" (unpublished).

[4] Yost, Wheeler, and Breit, Phys. Rev. **49**, 174 (1937).

[5] The validity of such a model, and the changes implied by a more rigid adherence to reality have been discussed elsewhere. See reference 4 and also E. P. Wigner, Phys. Rev. **73**, 1002 (1948); T. Teichmann, Ph.D. thesis, Princeton (1949).

[6] E. P. Wigner, Phys. Rev. **70**, 15 (1946).

between $k\cot\delta$ and R, apart from the purely formal one mentioned earlier.

II. DERIVATION: GENERAL METHOD

The method of deriving the "effective range" formula (1.1), or its analogs, from the expression for Q is very simple, though some of the details may be a bit messy in the general case (arbitrary external potential) if the functions F and G are rather complicated.

To begin with, one writes

$$\cot\delta=1/Q=-(G-RG')/(F-RF')$$
$$=-\frac{G}{F}+\frac{k}{FF'}-\frac{k/F'^2}{(F/F')-R}. \quad (2.1)$$

This follows from the usual normalization adopted for F and G

$$F'G-FG'=k, \quad (2.2)$$

the dash denoting differentiation with respect to r, not with respect to kr. The form (2.1) is used in order to avoid mixing the irregular function G (with its often displeasing properties for small values of the argument), and expressions involving R. One also has

$$R=\sum_\lambda \frac{\gamma_\lambda^2}{E_\lambda-E}=\sum_{j=0}^{\infty} R_j k^{2j}, \quad (2.3)$$

where

$$\left.\begin{aligned} R_0&=\textstyle\sum_\lambda(\gamma_\lambda^2/E_\lambda),\\ R_j&=(\hbar^2/2m)^j(\textstyle\sum_\lambda \gamma_\lambda^2/E_\lambda^{j+1}).\end{aligned}\right\} \quad (2.4)$$

Since F and G are solutions of a second-order differential equation of the type

$$u''(r)+[k^2-W(r)]u(r)=0 \quad (2.5)$$

and satisfy the linear independence (wronskian) relation (2.2), they are expressible respectively in the forms

$$F=C(kr)^\mu\Phi, \quad \mu>0, \quad (2.6)$$

$$G=[(2\mu+1)C]^{-1}(kr)^{-\mu+1}\Psi+A(\log r+\bar{g})F. \quad (2.7)$$

Here $C=C_\mu(k)$, $A=A_\mu(k)$, and $\bar{g}=\bar{g}_\mu(k)$ depends at most on μ and k, but not on r, while Φ, Ψ are power series in kr, beginning with the term 1, whose coefficients may also involve k. A particular example is given by the coulomb wave functions (see reference 4).

It should be noted that the assumption of the forms (2.6) and (2.7) for F and G, respectively, implies a certain restriction on the potential $W(r)$. Roughly speaking, this means that $W(r)$ must satisfy the condition[7]

$$r^2W(r)\to\text{constant}<\infty, \text{ as } r\to 0. \quad (2.8)$$

Of course, all the usual potentials, such as centrifugal, coulomb, exponential, Yukawa, and gaussian satisfy this requirement.

Φ and Ψ may both be expressed in the form[8]

$$\Phi(r)=\phi_0(r)+k^2\phi_1(r)+k^4\phi_2(r)+\cdots, \quad (2.9)$$

where the $\phi_n(r)$, $n=0, 1, 2, \cdots$ are independent of k, and satisfy

$$\phi_n(0)=\delta_{n0}.$$

Clearly $(r/\mu)\Phi'(r)+\Phi(r)=\Phi(r)$ has a similar form, and hence so have the functions $M=\Psi/\Phi$, $N=1/\Phi\bar{\Phi}$, $\Lambda=1/\bar{\Phi}^2$, and $\Upsilon=\Phi/\bar{\Phi}$. Thus

$$\frac{G'}{F'}=\frac{G}{F}-\frac{k}{FF'}=A(\log r+\bar{g})+C^{-2}(kr)^{-2\mu+1}\left[\frac{M}{2\mu+1}-\frac{N}{\mu}\right]$$

and hence

$$\cot\delta=-A(\log r_c+\bar{g})$$
$$-C^{-2}(kr)^{-2\mu+1}\left[\frac{M}{2\mu+1}-\frac{N}{\mu}+\frac{r_c\Lambda/\mu^2}{(r_c\Upsilon/\mu)-R}\right].$$

Writing

$$\bar{g}=\tfrac{1}{2}g+\tfrac{1}{2}g',$$

where $\frac{1}{2}g'$ is the k-independent part of $\bar{g}$, one readily finds that

$$\frac{1}{A}\cot\delta+\tfrac{1}{2}g+\frac{(kr)^{-2\mu+1}}{AC^2}\left\{\frac{M}{2\mu+1}-\frac{N}{\mu}+\frac{r_c\Lambda/\mu^2}{(r_c\Upsilon/\mu)-R}\right\}$$
$$=-(\log r_c+\tfrac{1}{2}g') \quad (2.10)$$

is independent of k, and hence of energy. If $A=0$, i.e., if both solutions of the differential equation (2.5) are expressible as a power series (about $kr=0$) times some power of kr, one finds instead

$$\cot\delta=-\frac{(kr_c)^{-2\mu+1}}{C^2}\left\{\frac{M}{2\mu+1}-\frac{N}{\mu}+\frac{(r_c\Lambda/\mu^2)}{(r_c\Upsilon/\mu)-R}\right\}. \quad (2.11)$$

Equations (2.3), (2.9) and the subsequent remarks ensure that the expression in the brackets in both (2.10) and (2.11) may be expanded in a power series in k^2, which will in general be of the form

$$-\alpha+\tfrac{1}{2}r_0k^2+pr_0^3k^4+\cdots, \quad (2.12)$$

where the coefficients α, r_0, $p\cdots$ depend on r_c and the various R_j, but not on k. (2.10) and (2.11) thus yield respectively, the formulas

$$k^{2\mu-1}C^2[\cot\delta+\tfrac{1}{2}Ag-A\beta]$$
$$=-r_c^{1-2\mu}[-\alpha+\tfrac{1}{2}r_0k^2+pr_0^3k^4\cdots] \quad (2.13)$$

and

$$k^{2\mu-1}C^2\cot\delta=-r_c^{1-2\mu}[-\alpha+\tfrac{1}{2}r_0k^2+pr_0^3k^4\cdots]. \quad (2.14)$$

[7] See P. M. Morse and M. Feshbach, *Methods of Theoretical Physics* (Technology Press, Cambridge, Massachusetts, 1946), for full mathematical details.

[8] Such an expansion has been given explicitly (for Φ) in the case of a coulomb and centrifugal potential by J. G. Beckerley, Phys. Rev. **67**, 11 (1945).

The coefficients C, A, g, β, α, r_0, p, $\cdots$, etc., may be evaluated as described above, but it is not of very great interest to do this in general. The particular cases usually treated are discussed below. Before leaving the general discussion it is perhaps not unimportant to note that for certain particular internal potentials ($r<r_c$), R_0 may have a value such that the term independent of k in $(r_c\Upsilon/\mu)-R$ vanishes, and in this case the expression (2.12) must be augmented by a term in $1/k^2$. (See Eq. (3.8).)

III. NO EXTERNAL INTERACTION

Consider first the case where there is no external interaction between the two colliding particles, so that the potential $W(r)$ has the form

$$W(r)=l(l+1)/r^2 \tag{3.1}$$

if the system has l units of angular momentum. The case $l=0$ contains nearly all the essential details, and is treated at some length here, and the corresponding results and changes for $l>0$ will merely be stated at the end of this section.

For $l=0$

$$F(r_c)=\sin kr_c, \quad G(r_c)=\cos kr_c \tag{3.2}$$

and thus

$$\begin{aligned} k\cot\delta &= k\tan kr_c-(1+\tan^2 kr_c)/(k^{-1}\tan kr_c-R) \\ &= -a^{-1}+\tfrac{1}{2}r_0k^2+pr_0^3k^4+\cdots. \end{aligned} \tag{3.3}$$

One then finds directly that

$$a=r_c-R_0, \tag{3.4}$$

$$\tfrac{1}{2}r_0=r_c-r_c^2/a+(\tfrac{1}{3}r_c^3-R_1)/a^2, \text{ etc.} \tag{3.5}$$

Equation (3.4) shows that if the scattering length a is greater than the radius r_c of the compound system, then the latter must have at least one strongly bound state E_1, such that

$$\Big|\sum_{E_\lambda<0}(\gamma_\lambda^2/E_\lambda)\Big|>\sum_{E_\lambda>0}(\gamma_\lambda^2/E_\lambda).$$

Since δ (or the collision matrix U) is invariant to any changes made in the assumed radius r_c of the compound system, provided only that the total potential is not changed, Eqs. (3.4), (3.5), etc., are to be regarded as expressing necessary relations which must hold between the parameter r_c (which may be varied) and the various R_n. It has been pointed out elsewhere (Teichmann, reference 5) that the behavior of the "external" functions F and G, and that of the derivative function R just so compensate as to render δ (or U) independent of the choice of r_c (or even of the boundary conditions on the internal system). The present treatment is interesting in that it shows much more plainly (though only in the case of pure scattering) the effect on R of specific choices of r_c. (For instance if $r_c=a$ (provided $a>0$), then $R_0=0$.)

Equation (3.5) shows that r_0 is not necessarily positive, and that $r_0\geqslant 0$ only if

$$R_1\leq\frac{(r_c-R_0)^3}{3}+\frac{R_0^3}{3}. \tag{3.6}$$

This of course implies a certain restriction on the potentials. Examples of potentials for which $r_0<0$ have been given previously;[9] but even in the case of the square well r_0 may be less than zero for certain choices of $V_0r_c^2$ (V_0=depth of well).

Since in this case

$$R_1=(k^2+\kappa^2)^{-\frac{1}{2}}\tan[(k^2+\kappa^2)^{\frac{1}{2}}r_c], \quad \kappa^2=2mV_0/\hbar^2,$$

one can readily calculate that $r_0<0$ if

$$\begin{aligned} (\lambda+\tfrac{3}{2})\pi-\frac{1}{(\lambda+\tfrac{3}{2})\pi(1-1/\sqrt{3})}\lesssim\kappa r_c\lesssim(\lambda+\tfrac{3}{2})\pi \\ -\frac{1}{(\lambda+\tfrac{3}{2})\pi(1+1/\sqrt{3})}, \end{aligned} \tag{3.7}$$

$\lambda=0, 1, 2, \cdots$. Qualitatively this means that r_0 will be less than zero[10] if there is at least one bound state and the first virtual state is just a little above zero energy. A little consideration shows that this result is also to be expected from the forms (2.4) of R_0 and R_1 combined with Eq. (3.6).

If R_0 should be fortuitously be equal to r_0, then the right-hand side of (3.3) must be replaced instead by the expression

$$-1/(\beta k^2)-\alpha_0+\alpha_1k^2, \tag{3.8}$$

where

$$\beta=\tfrac{1}{3}r_c^3-R_1. \tag{3.9}$$

Since the cross section is given by

$$\sigma=(4\pi/k^2)\sin^2\delta=4\pi/(k^2+k^2\cot^2\delta), \tag{3.10}$$

this means that while in the usual case (3.3) the cross section tends to the constant value

$$\sigma\to 4\pi a^2 \tag{3.11}$$

for zero energy, it may, under suitable conditions (*viz.*, for potentials for which $R_0=r_c$) go to zero as k^4 at low energies; i.e.,

$$\sigma\simeq 4\pi\beta^2k^4 \tag{3.12}$$

even though the scattering is at zero angular momentum (see the remarks below on scattering at $l>0$). In the case of the square well such a condition obtains

[9] See V. Bargmann, Revs. Modern Phys. **21**, 488 (1949). The author is indebted to Dr. Bargmann for this remark.

[10] Functions of the forms of R, whose imaginary part is positive in the upper half-plane and negative in the lower half-plane, and whose only singularities are poles, are known as R functions, and have been considered in some detail by E. P. Wigner, Ann. Math. **53**, 36 (1951). He showed, for example, that a fractional linear transformation $(aR+b)/(cR+d)$, with positive determinant $ad-bc>0$ is also an R-function. The above simple example shows that Q is *not* in general an R-function, though it may be approximated by one in any energy range in which the variation of F and G may be neglected.

when

$$\tan\kappa r_c = \kappa r_c, \tag{3.13}$$

i.e., for

$$\kappa r_c \simeq (\lambda+\tfrac{3}{2})\pi - [(\lambda+\tfrac{3}{2})\pi]^{-1}$$

which lies between the limits given in (3.7) above.

Equations (3.8) and (3.12) give the correct energy dependence of the scattering when the scattering length vanishes. Under more extreme conditions ($R_0=r_c$, $R_1=\frac{1}{3}r_c^3$) one can easily see that $k\cot\delta \sim k^{-4}$, so that the cross section tends to zero as k^8 (i.e., E^4), and so on. Finally, if there is no internal interaction at all, $R=F/F^1$ at all energies, and the cross section vanishes identically at all energies.

In the general case, $l>0$,

$$\begin{aligned} F_l(r) &= (\pi kr/2)^{\frac{1}{2}} J_{l+\frac{1}{2}}(kr), \\ G_l(r) &= (-1)^l (\pi kr/2)^{\frac{1}{2}} J_{-l-\frac{1}{2}}(kr). \end{aligned} \tag{3.14}$$

Referring to (2.6) and (2.7) one has $A=0$, $\mu=1$, and

$$C=C_l=1/(2l+1)!!=1/(2l+1)(2l-1)\cdots 5\cdot 3\cdot 1. \tag{3.15}$$

Thus

$$k^{2l}(k\cot\delta_l) = -\alpha_l + \tfrac{1}{2}r_{0l}k^2 + \cdots, \tag{3.16}$$

where

$$\alpha_l = 1/a_l = \frac{1}{2l+1}\left(\frac{r_c+lR_0^{(l)}}{r_c-(l+1)R_0^{(l)}}\right)\frac{r_c^{-2l-1}}{C_l^2}, \tag{3.17}$$

etc. The superscript l on R_0, denotes that the R function must be calculated for the compound system with angular momentum l; in general the $R^{(l)}$ will be different for different l's. Hence, when there is no external interaction to affect the centrifugal field $l(l+1)/r^2$, the cross section will generally vary as k^{4l} (i.e., as E^{2l}) for small values of energy, though in special cases (see remarks above in the case $l=0$) it may vary as[11] k^{4l+4}. For instance, in the case of a square well of radius r_0 and depth $V_0=\hbar^2\kappa^2/2m$ the condition for this exceptional case is

$$J_{l+\frac{1}{2}}(\kappa r_c)/J_{l-\frac{1}{2}}(\kappa r_c) = \kappa r_c/(1-l). \tag{3.18}$$

(See also (3.13) above.)

Consideration of the significance of the various quantities involved in (2.10), say, shows that the above phenomenon may generally be expected to occur when the logarithmic derivative of the zero energy internal wave function (i.e., the wave function of the finite isolated compound system) taken for $r=r_c$, is equal to the logarithmic derivative of the zero energy regular external wave function evaluated at the same radius, i.e., when

$$R\Big|_{\substack{k=0\\ r=r_c}} = \frac{F}{F'}\Big|_{\substack{k=0\\ r=r_c}}. \tag{3.19}$$

[11] See also N. F. Mott and H. S. W. Massey, *The Theory of Atomic Collisions* (Oxford University Press, London, 1950).

It is thus clear that the energy variation of the cross section at low energies does *not* uniquely determine the angular momentum l except in the case $l=0$. For instance, a low energy variation $\sigma \sim E^2$ may be due *either* to P scattering, or to a peculiarity of the potential leading to condition (3.19), etc.

IV. EXTERNAL COULOMB FIELD

With the preparation of Sec. II, and the formulas of Yost, Wheeler, and Breit, it is no great hardship to compute the expression for $k\cot\delta$ in the case of a coulomb force between the two colliding particles.

Using the notation of II and III, and the results of YWB, one has

$$C=C_l'=C_l\left[(1+\eta^2)\left(1+\frac{\eta^2}{4}\right)\cdots\left(1+\frac{\eta^2}{l^2}\right)\right]^{\frac{1}{2}} \times\left(\frac{2\pi\eta}{(\exp 2\pi\eta)-1}\right)^{\frac{1}{2}}, \tag{4.1}$$

C_l being given as $1/(2l+1)!!$ by (3.15) and

$$A=(e^{2\pi\eta}-1)/\pi, \tag{4.2}$$

$$g_l(k) = 2\log k + 2\sum_1^l \frac{s}{s^2+\eta^2} + 2\eta^2\sum_1^\infty \frac{1}{s(s^2+\eta^2)}, \tag{4.3}$$

$$g_l' = 2\left(\gamma - \sum_1^{2l+1}\frac{1}{s}\right) + 2\log 2,$$

$$\gamma = 0.57\cdots \text{ (Euler's constant)}, \tag{4.4}$$

where

$$\eta = 1/r_b k \tag{4.5}$$

with

$$r_b = \hbar^2/mZ_1Z_2e^2 \tag{4.6}$$

(the Bohr radius of the colliding system). Then one obtains

$$\prod_{s=1}^{l}\left(k^2+\frac{1}{s^2r_b^2}\right)\left[\frac{2\pi\cot\delta_l}{e^{2\pi\eta}-1}+g_l(k)\right] = r_b(-\alpha_l'+\tfrac{1}{2}r_{0l}'k^2+\cdots). \tag{4.7}$$

The quantity $[2\pi\ \cot\delta_l/(e^{2\pi\eta}-1)+g_l(k)]$ will be denoted by $f_l(k)$ in accordance with the notation of Breit, Condon, and Present.[12]

The coefficient

$$\prod_1^l\left(k^2+\frac{1}{s^2r_b^2}\right)\frac{2\pi}{e^{2\pi\eta}-1}$$

of $\cot\delta_l$ tends to $k^{2l}\cdot k$ for large k, but for small k it tends to zero as $\exp(-2\pi/r_bk)$, so that $\cot\delta_l$ tends to infinity much more rapidly than k^{-2l-1} (which occurs for uncharged particle (n-p) scattering), and the form

[12] Breit, Condon, and Present, Phys. Rev. **50**, 825 (1936).

of the cross section as a function of k (or energy) is substantially independent of l for small energies. As had already been pointed out by Bethe[1] for the case $l=0$, this shows that the coulomb effects swamp both the specifically nuclear, and the centrifugal effects at low energies.

The quantities α', r_0', $\cdots$, etc., are functions of the various R_s and the functions $\phi_0(r_c)$, etc., described in Sec. II. Since r_c/r_b is small ($\sim 1/20$), reference to YWB or Beckerley shows that it is a good approximation to use the expression (3.4) (3.5) (3.17) (*mutatis mutandis*) to determine α_l', γ_{0l}', $\cdots$, etc. Thus one finds

$$\alpha_l' \simeq \alpha_l + \frac{1}{r_b}(r_b^l/l!)^2[2\log r_c + g_l'], \tag{4.8}$$

etc., α_l being given in form by (3.17). It should be noted that R will not in general be the same as in the case of uncharged particle scattering. Only in the case of identical compound systems may the same R be used in (3.17) and (4.8).

V. RELATION TO THE THEORY OF NUCLEAR REACTIONS

If the collision is one in which the compound system can disintegrate in several ways, then considerations of the above type become much more complicated and less perspicuous, both for "proper" reactions (in which the outgoing components are different from the incoming ones), and for scattering. Consequently, only some general comments are made here about the analogy.

In general, the cross section for a reaction[13] "st" is given by

$$\sigma_{st} = (\pi/k_s^2)\,|\,i(1-U)_{st}\,|^2, \tag{5.1}$$

where U is the n-dimensional unitory symmetric collision matrix. (The subscripts s and t, ranging from 1 to n, denote the n possible initial or final states of the system.) U itself is given by

$$U = \omega\frac{1-iC+iBRB}{1+iC-iBRB}\omega, \tag{5.2}$$

where ω, C, and B are diagonal matrices, given in terms of the regular and irregular functions F, G of the outgoing or incoming pairs of components (F is a diagonal matrix with elements F_s, $s=1, \cdots n$) by

$$\begin{aligned} \omega &= F'/(F'^2+G'^2)^{\frac{1}{2}} + iG'/(F'^2+G'^2)^{\frac{1}{2}}, \\ C &= (FF'+GG')/k, \\ B &= (F'^2+G'^2)^{\frac{1}{2}}/\sqrt{k}. \end{aligned} \tag{5.3}$$

(All these quantities are supposed evaluated at the boundary of the compound systems, i.e., for $r_s=r_{sc}$, etc.) R is the symmetric derivative matrix with elements

$$R_{st} = \sum_\lambda [\gamma_{\lambda s}\gamma_{\lambda t}/(E_\lambda - E)]. \tag{5.4}$$

In the case of pure scattering considered in the earlier part of this paper U is simply a scalar, and it is most convenient to express $\sin^2\delta = \frac{1}{4}\,|\,i(1-U)\,|^2$ in terms of $\cot\delta = (1+U)/i(1-U)$, *viz.*, $\sin^2\delta = 1/(1+\cot^2\delta)$. This simple relation is no longer true in general if U is a matrix and it is necessary to consider $|\,i(1-U)\,|^2$ directly.

In order to see the significance of the quantities one need merely note that, in the case of pure scattering, formulas of the type

$$f(k)\cot\delta = -1/a + \tfrac{1}{2}r_0k^2 + \cdots \tag{5.5}$$

are obtained in most cases, and that the corresponding cross sections are

$$\sigma = 4\pi(f(k)/k)^2a^2[1+k^2a^2[r_0/a - f^2(k)/k^2]\cdots]. \tag{5.6}$$

The factor $(f(k)/k)^2$ gives the energy dependence of the cross section at small energies (e.g., ~ 1 in the case of no external interaction, $\sim k^{4l}$ for scattering at angular momentum l, etc.).

This energy dependence has already been investigated very fully in the general case (many reactions) by Wigner,[14] and, in fact, the value of the first coefficient a^2 is given implicitly in this treatment. Because U is a rather complicated matrix quotient and

$$(1-U) = 1+\omega^2 - 2\omega(1+iC-iBRB)^{-1}\omega, \tag{5.7}$$

it is rather difficult to see what the coefficients really look like in the general analog of (5.5), even in the case of proper reactions, ($s\neq t$) when one need only consider $[(1+iC-iBRB)^{-1}]_{st}$. Reference to (2.6), (2.7), and (5.3) shows that the matrices in this last expression do not always have the simple form of Taylor series in k^2, beginning with 1 (they may, for instance, have an extra factor k), and it is only after taking the absolute value of the matrix element squared that the desired form is obtained.

It is not proposed to carry this general discussion any further here. Even with simple examples (such as are treated in a different connection in reference 13) it is rather difficult to obtain perspicuous results beyond those given by Wigner. It is hoped to give a fuller discussion at some later opportunity.

ACKNOWLEDGMENTS

The author is indebted to Professor V. Bargmann for some helpful discussions and to Professor E. P. Wigner for prepublication copies of his papers (references 3 and 10). This work was assisted in part by the AEC and by the Higgins Fund.

[13] See E. P. Wigner and L. Eisenbud (reference 2) and T. Teichmann, Phys. Rev. **77**, 506 (1950) for further details of this formalism.

[14] E. P. Wigner, Phys. Rev. **73**, 1002 (1948).

The Photodisintegration of He^4 Nuclei by X-Rays from a 100-Mev Betatron*

E. R. Gaerttner and M. L. Yeater
General Electric Research Laboratory, Schenectady, New York

(Received February 8, 1951)

The photodisintegration of He^4 nuclei has been studied in a cloud chamber, with a 100-Mev betatron as a source of x-rays. The predominant reactions observed are $He^4(\gamma,p)H^3$ and $He^4(\gamma,n)He^3$. The angles, θ, at which the protons from the (γ,p) reaction are emitted with respect to the x-ray beam are consistent with a $\sin^2\theta$ distribution. The measured average energy of the x-ray photons producing the γ–p disintegration is approximately 27 Mev. The total integrated photodisintegration cross section is 0.1 ± 0.05 Mev-barn; this value is based on an earlier determination of the absolute nitrogen cross section, obtained by a direct comparison of the number of nuclear disintegrations with the number of positron-electron pairs produced in the gas in the cloud chamber.

INTRODUCTION

An evaluation of photonuclear effects must take into account all modes of disintegration. We have previously used a cloud chamber to survey the photodisintegration phenomena in oxygen,[1,2] nitrogen,[1–3] and carbon[4] (methane). The quantitative results of these experiments have indicated the relative importance of various modes of disintegration and the approximate values of the absolute cross sections.

In the investigation here reported we have used the same cloud-chamber technique to obtain the relative yields of the different modes of disintegration of helium. In addition, we have studied the angular distribution of protons from the (γ,p) reaction in helium, and have obtained an approximate x-ray energy distribution for this process.

The inverse reaction $H^3(p,\gamma)He^4$ has been studied by a group at Los Alamos.[5] They observe a large yield of gamma-rays with an angular distribution which is approximately $\sin^2\theta$. They attribute these gamma-rays to an electric dipole transition in He^4. The range in proton energy from their electrostatic generator was not sufficient to cover the high energy side of what they believe to be a resonance at 2.5-Mev proton energy. The energy of the emitted gamma-ray for this proton energy is 21.6 Mev. This is lower than the mean value which we obtain for the (γ,p) process.

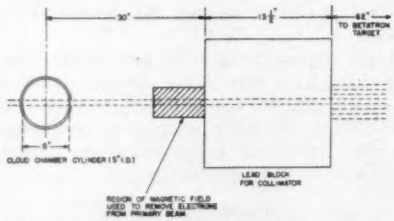

FIG. 1. Arrangement of collimator and cloud chamber in the x-ray beam.

THE EXPERIMENTAL METHOD

The experimental arrangement is shown schematically in Fig. 1. The x-rays from the 100-Mev betatron are collimated by a system of lead slits; the beam measures $\frac{1}{8}$ inch vertically and $\frac{3}{4}$ inch horizontally at the center of the cloud chamber. The beam is cleared of electrons by a magnet and enters the cloud chamber through a window which is a 0.020-inch thick section of the Lucite wall of the chamber. The cloud chamber is filled with helium and saturated vapor from a 50–50 water-alcohol liquid mixture, at a total pressure of one atmosphere.

A single high intensity pulse of x-rays passes through the center of the cloud chamber at each expansion. The use of the cloud chamber for photodisintegration studies depends upon achieving good contrast between heavy particle tracks and the background of positrons and negative electrons, produced in the Lucite window and the gas of the chamber; the ratio of light to heavy particles is about 10^4. This has been accomplished for a number of light gases through the use of a short droplet growth time. The results obtained for two different growth times are illustrated in Fig. 2. Figure 2(a) shows the electron tracks with a growth time of about 200 milliseconds; Fig. 2(b) shows the contrast achieved for the heavy tracks against the electron background with a growth time of about 50 milliseconds.

An important feature of our technique is the use of overcompression of the cloud chamber following the initial expansion, to aid in the evaporation of the droplets.[6] This is particularly important where large pulse intensities are used and at the same time a rapid recycling of the cloud chamber is desired. With the aid of overcompression, tracks of good quality are obtained at intervals of five seconds. The photographs in this report were taken at this rate.

* This work has been supported in part by the ONR.

[1] E. R. Gaerttner and M. L. Yeater, Phys. Rev. **77**, 714 (1950).
[2] E. R. Gaerttner and M. L. Yeater, Phys. Rev. **79**, 401 (1950).
[3] E. R. Gaerttner and M. L. Yeater, Phys. Rev. **77**, 570 (1950).
[4] E. R. Gaerttner and M. L. Yeater, Phys. Rev. **82**, 461 (1951); see also reference 2.
[5] Argo, Gittings, Hemmendinger, Jarvis, and Taschek, Phys. Rev. **78**, 691 (1950).
[6] E. R. Gaerttner and M. L. Yeater, Rev. Sci. Instr. **20**, 588 (1949).

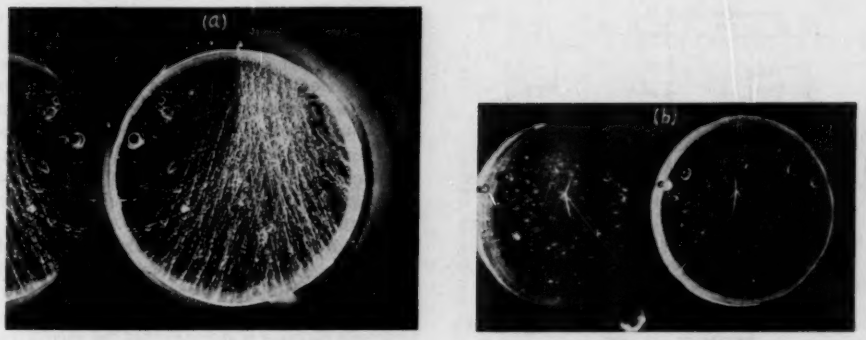

FIG. 2. Effect of growth time on track brilliance. (a) Electron tracks with 200 millisecond growth time. (b) A four-prong star, photographed with 50-millisecond growth time, against a strong electron background.

THE IDENTIFICATION OF THE HELIUM DISINTEGRATIONS

Since the gas in the chamber contains the vapor phase of water and ethyl alcohol in addition to helium, some of the observed disintegrations in the gas are to be attributed to carbon and oxygen. The separation of the flags, consisting of two charged particles, into the helium and carbon or oxygen components is possible because the maximum range of the carbon and oxygen recoils is smaller than the measured recoil track length of many of the observed flags. This conclusion is based on measurements made on carbon and oxygen flags with the cloud chamber filled with methane and oxygen respectively. The observed maximum ranges reduced to one atmosphere pressure for these cases are respectively 0.45 cm and 0.25 cm. From the relative stopping power[7] of methane and oxygen with respect to the helium-vapor mixture, the expected maximum ranges in the latter are respectively 2.0 cm and 1.4 cm. It is found that nearly all flags, in the helium-vapor mixture, for which the recoil is observed to stop have ranges less than 2 cm.

Flags with recoils longer than 2 cm are attributed to helium. Some of the helium flags are not individually identified in this way because of their orientation, which causes the visible recoil length to be less than 2 cm owing to the small depth of the illuminated region. Statistically, however, the total number can be inferred from the identifiable cases by means of a geometrical correction.

A striking characteristic of nearly all the helium flags is the difference in the track density of the two charged particles. An example is shown in Fig. 3. This characteristic is sufficient to establish the reaction as $He^4(\gamma,p)$-H^3 instead of $He^4(\gamma,2d)$. It is also noteworthy that in every case of this type, the resultant momentum of the flag members is in the direction of the x-ray beam.

The identification of a portion of the single tracks (one charged particle) as He^3 from the reaction He^4-$(\gamma,n)He^3$ is made in a similar way. An example is shown in Fig. 4. In this case also track lengths greater than about 2 cm cannot be attributed to carbon or oxygen. Observations in a hydrogen-filled chamber indicate that long singles are not due to stray neutrons. The identification of He^3 recoils is based on track lengths greater than 4 cm.

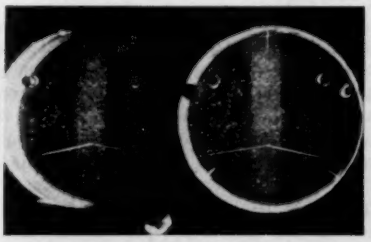

FIG. 3. A $He^4(\gamma,p)H^3$ disintegration. The band across the chamber consists of secondary electrons showing the path of the x-ray beam. Its direction is toward the bottom of the page. There is no magnetic field.

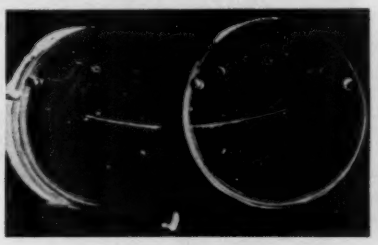

FIG. 4. A $He^4(\gamma,n)He^3$ disintegration. The magnetic field strength is about 9000 gauss.

[7] M. S. Livingston and H. A. Bethe, Revs. Modern Phys. **9**, 245 (1937). The stopping powers given are for alpha-particles of about 6 Mev. These stopping powers are valid also for heavy recoils (e.g., C^{12}) of air range less than 0.3 cm as shown by G. A. Wrenshall, Phys. Rev. **57**, 1095 (1940).

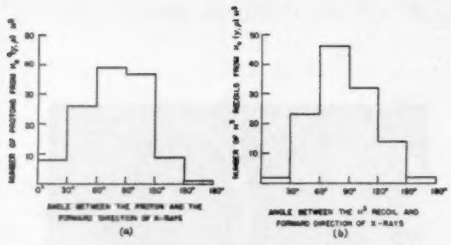

FIG. 5. Angular distribution for $He^4(\gamma,\phi)H^3$ in the laboratory system of coordinates. (a) Proton. (b) Triton.

THE ANGULAR DISTRIBUTION OF THE PROTONS FROM $He^4(\gamma,\phi)H^3$

It is observed that the protons from the $He^4(\gamma,\phi)H^3$ reaction are not emitted with equal probability in all directions; at right angles to the x-ray beam, the probability is much greater than forward or backward. In Fig. 5 are plotted the angular distributions of protons and tritons in the laboratory system. The angles are measured between the x-ray beam and the projection of the flag members in the horizontal plane of the chamber. The number per unit solid angle is approximately the same as the distribution in these histograms because the illuminated region of the cloud chamber is shallow ($\frac{1}{2}$ inch) and the tracks considered all have lengths greater than 2 cm. In Fig. 6 is plotted the angular distribution of tritons in the center-of-mass coordinate system. This is consistent with a $\sin^2\theta$ distribution.

X-RAY ENERGY DISTRIBUTION FOR THE REACTION $He^4(\gamma,\phi)H^3$

The energy of the photon which caused the (γ,ϕ) disintegration can be computed in each case from the forward momentum which the photon imparts to the triton and proton.[8] If only the direction vectors of the momenta are known from angle measurements, as is the case here, then only the ratio of the magnitude of the photon momentum to that of the proton or the triton is determined; this ratio is not sufficient to determine the photon energy uniquely in general, but leads to two theoretical values. All cases which have one value of energy less than 25 Mev are, however, uniquely determined because the alternate value is greater than our maximum x-ray energy of 100 Mev.

Forty percent of the identified helium flags fall in this category and, therefore, have energies definitely between 19.8 Mev (the energy threshold) and 25 Mev. For the remainder of the flags with energy in the indeterminate range, it is assumed that the smaller value of the energy is the correct one in each case. The x-ray energies for the identified helium (γ,ϕ) flags are given in Fig. 7. In Fig. 8 are given the energy, and the angle between proton and triton, for cases with θ between 70° and 110°, for which the energy is more accurately known.

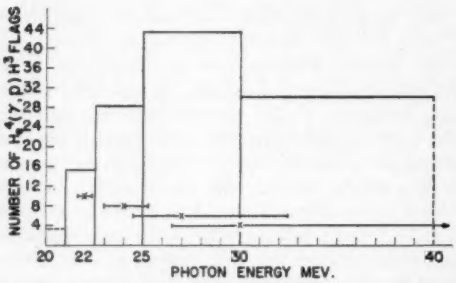

FIG. 7. Energy distribution of the photons inducing the $He^4(\gamma,\phi)$-H^3 reaction. The photon energy is calculated from the forward momentum imparted to the proton and triton (angle measurements only). The horizontal lines give the probable error in the energy measurement at the designated points.

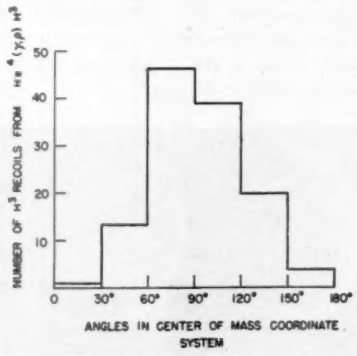

FIG. 6. Triton angular distribution, in center-of-mass system of coordinates, for the reaction $He^4(\gamma,\phi)H^3$. The proton distribution is the mirror image of this.

One flag recoil with a range of 4.4 cm was observed to stop in the illuminated portion of the cloud chamber. This case is reproduced in Fig. 3. The photon energy calculated from the angles is 22.4±0.4 Mev. From this information, the approximate photon energy for a helium flag with the minimum identifiable triton range of 2 cm can be determined.[9] The result is 21 Mev.

The number of helium (γ,ϕ) disintegrations with recoil range less than 2 cm, that is, for photon energy between 19.8 and 21 Mev, is probably less than the number in the corresponding energy interval above 21

[8] We assume that the residual H^3 nucleus from the (γ,ϕ) reaction is unexcited. An excited state in He^3 (analogous to H^3 except for coulomb energy) has been observed by Fowler, Lauritsen, and Tollestrup [Phys. Rev. **76**, 1767 (1949)] at 6.3 Mev; however, the radiative cross section is less than one percent of the radiative cross section for the state in He^4, observed at Los Alamos (reference 5), which is probably involved in the (γ,ϕ) interaction.

[9] See M. S. Livingston and H. A. Bethe, Revs. Modern Phys. **9**, 245 (1937) and H. A. Bethe, Revs. Modern Phys. **22**, 213 (1950).

Mev. The number between 21 and 22.5 Mev is estimated as follows.

There are 52 (γ,p) disintegrations identified which have triton track length greater than 5 cm, from a total of 119 cases with triton track length greater than 2 cm. For these 52 cases, the primary photon energy must have been greater than 22.5 Mev. The fraction of the cases with recoil range greater than 5 cm is actually larger than 52/119, because only 7 to 10 percent of all the 5 cm tracks present will be so oriented in our shallow chamber that the full 5 cm is visible (for a $\sin^2\theta$ distribution of the emitted tritons with respect to the x-rays), whereas approximately 20 percent of all the 2 cm tracks will be measurable. The "geometrical efficiencies" quoted cannot be calculated precisely owing to the uncertainty in the measurement of the track length caused by non-uniformity of illumination near the edges of the light beam. The limiting values indicate that not more than 12 percent of the cases have recoil range between 2 and 5 cm. This is confirmed by the energy distribution, based on angle measurements, given in Fig. 7.

The average photon energy is calculated from the data in Fig. 8. The result is 27 Mev. The inaccuracy of the measured energy for the higher energy cases probably results in an average value which is somewhat too large. This error probably does not exceed 2 Mev, however, as shown by the fact that an average energy of 25 Mev is obtained by neglecting altogether these less accurate high energy cases (above 30 Mev).

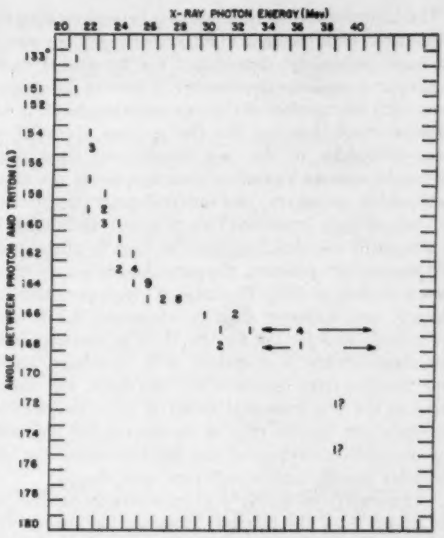

FIG. 8. Helium (γ,p) flags for which the angle between the proton and the x-ray beam is between 70° and 110°. A is the angle between the triton and the proton in the laboratory system of coordinates.

THE YIELD OF THE PHOTONUCLEAR REACTIONS IN HELIUM

(a) (γ,p)

The yield of the (γ,p) reaction in helium has been compared with that of carbon and oxygen by counting the relative numbers of helium and carbon or oxygen disintegrations produced in the mixture of helium and water-alcohol vapor in the cloud chamber. The stars, in which at least three charged particles are observed to emanate from a common point, must have originated with carbon or oxygen nuclei. An example is shown in Fig. 9. In one group of data, 67 stars and 49 identifiable $He(\gamma,p)$ flags with recoil length equal to or greater than 2 cm were observed. The ratio of the yield per atom of $He(\gamma,p)$ and the flags in carbon and oxygen is

$$\frac{49/\eta}{67Kb},$$

where K is the average ratio of flags to stars in carbon and oxygen, η is the detection efficiency for the helium flags, and b is the atomic ratio of helium to carbon and oxygen in the cloud chamber. The quantity K is known from our study of carbon and oxygen, and has the value $K=4$. The value of b is 6.1 at the operating temperature of 25°C. The efficiency η accounts for the cases having such an orientation in the chamber that the tracks pass out of the lighted region or out the side of the chamber with only a short section visible. For the 2 cm visible recoil length, $\eta=0.22$, calculated for a $\sin^2\theta$ distribution. The ratio of $He(\gamma,p)$ to the average flag yield for the carbon and oxygen mixture in the vapor is, therefore, 0.136. From this ratio and the flag cross section for the carbon[4] and oxygen,[1] averaged according to their proportions in the vapor, the absolute cross section for the helium is obtained.[10] The integrated carbon-oxygen value, from our previous experiments, is 0.25 Mev-barn. The integrated $He(\gamma,p)$ cross section obtained from this measurement is, therefore, 0.034 Mev-barn.

FIG. 9. A "star" in helium-vapor mixture in the cloud chamber.

[10] This assumes that the disintegrations in carbon and oxygen are produced by x-rays in approximately the same energy range as in helium.

The helium cross section has also been evaluated by comparison with the yield of flags in nitrogen, for which we have previously[1] determined the integrated cross section by comparing the number of nuclear disintegrations with the number of electron pairs produced in an air-filled cloud chamber. For this purpose, the relative x-ray intensities in the two experiments have been compared with an ionization chamber, using the same instruments, geometry, and betatron peak energy. For 195 helium flags (corrected for efficiency), an ionization of 108 units was obtained; for 430 flags in nitrogen at one atmosphere pressure, the same ionization chamber gave a reading of 15.6. The ratio of yields per atom for $He(\gamma,p)$ and nitrogen flags is, therefore, 0.131. The integrated cross section for the $He(\gamma,p)$ reaction from this measurement is, therefore, 0.04 Mev-barn, based on a nitrogen cross section of 0.3 Mev-barn. The agreement in the two measured values of this cross section is satisfactory for this type of experiment and indicates the internal consistency of the flag data involving the elements helium, carbon, nitrogen, and oxygen.

The accuracy of the $He(\gamma,p)$ cross section depends on the accuracy of the nitrogen cross section and on the uncertainties in the yield ratio. The former is estimated to be accurate within about 20 percent. The accuracy of the yield ratio is determined mostly by statistics and the accuracy of the geometrical efficiency; the estimated error is 35 percent over all.

(b) $(\gamma,2d)$

This reaction should be observed as a "flag" having tracks of equal ionization and with resultant momentum in the forward direction. This yield is no more than one percent of the (γ,p) yield.

(c) (γ,n)

The (γ,n) yield can be evaluated in the same way as the (γ,p) yield. In a portion of the data in which 45 flags with recoil lengths greater than 4 cm were counted, there were observed 59 singles of length greater than 4 cm. Our helium (γ,n) to (γ,p) ratio is, therefore, about 1.3.

(d) $(\gamma,pn$ or $\gamma,2p,2n)$

The yield of the reactions $He^4(\gamma,pn)H^3$ or $He^4(\gamma,2p,2n)$ can, in principle, be estimated from those disintegrations for which the resultant momentum is not in the forward direction of the x-rays. Such flags have been observed in oxygen and methane and account for about 15 percent of the total. When the helium data are corrected for the expected contribution from oxygen and carbon in the vapor, a few cases remain which might be attributed to helium; but within the statistical accuracy of the data, these might still be attributed to carbon and oxygen. On the assumption that these cases are due to helium, the upper limit for their yield is about 20 percent of $He^4(\gamma,p)H^3$.

DISCUSSION OF RESULTS†

The theory of Levinger and Bethe[11] gives the total integrated photonuclear cross section for helium as

$$\int \sigma dW = 0.06(1+0.8x) \text{ Mev barn},$$

where x is the fraction of the nuclear force which is of the exchange type. Our experimental result is 0.1 ± 0.05 Mev-barn. This value, although not sufficiently accurate to indicate the amount of exchange force, gives strong support for the dipole type interaction discussed by them. This conclusion is supported by the observed angular distribution of the protons from the (γ,p) reaction.

The energy of the x-ray photons producing the $He^4(\gamma,p)H^3$ disintegrations has been determined approximately from the momentum imparted to the disintegration products. The resulting energy distribution has a mean value not less than 25 Mev. For a detailed analysis of the excitation function more accurate data are needed—possibly from triton range measurements in a cloud chamber filled with helium at high pressure.

It is a pleasure to acknowledge the support of Dr. E. E. Charlton and the betatron group. We are indebted to Professor H. A. Bethe and Professor P. Scherrer for helpful discussions.

† *Note added in proof.*—Since this work was submitted for publication, it has been brought to the authors' attention that the photodisintegration of helium is being studied by E. G. Fuller and M. Wiener at the National Bureau of Standards (private communication) and by Prof. J. R. Atkinson at the University of Glasgow (private communication from E. W. Titterton). Fuller and Wiener, using photographic emulsions for a detector, find an energy distribution and integrated cross section for the (γ,p) process in approximate agreement with ours. However, their angular distribution for 550 photoprotons is not compatible with a pure $\sin^2\theta$ distribution; they observe about one-half as many forward as at 90° to the x-ray beam.

A theoretical treatment of the photodisintegration of helium has also appeared since our work was submitted for publication: B. H. Flowers and F. Mandl, Proc. Roy. Soc. (London) **206A**, 131 (1951).

[11] J. S. Levinger and H. A. Bethe, Phys. Rev. **78**, 115 (1950).

p-n Junction Transistors

W. SHOCKLEY, M. SPARKS, AND G. K. TEAL
Bell Telephone Laboratories, Inc., Murray Hill, New Jersey
(Received May 24, 1951)

The effects of diffusion of electrons through a thin *p*-type layer of germanium have been studied in specimens consisting of two *n*-type regions with the *p*-type region interposed. It is found that potentials applied to one *n*-type region are transmitted by diffusing electrons through the *p*-type layer although the latter is grounded through an ohmic contact. When one of the *p-n* junctions is biased to saturation, power gain can be obtained through the device. Used as "*n-p-n* transistors" these units will operate on currents as low as 10 microamperes and voltages as low as 0.1 volt, have power gains of 50 db, and noise figures of about 10 db at 1000 cps. Their current-voltage characteristics are in good agreement with the diffusion theory.

I. INTRODUCTION

IN this article we shall consider the phenomena which occur when voltages are applied to a semiconductor consisting of several regions of different conductivity types. Structures of this sort, consisting in particular of two regions of one conductivity type separated by another region of the opposite type, are of great practical interest in transistor electronics. Such structures can also be used to exhibit the behavior of hole and electron diffusion in rather impressive ways. In particular, the phenomenon of "internal contact potentials" can be strikingly demonstrated with such structures.

Transistors in which the nonlinear effects originate within the germanium as a result of the relationships of *p*-type and *n*-type regions are called "*p-n* junction transistors" to distinguish them from point-contact types, in which the metal semiconductor contact often plays an essential role. There are a number of possible *p-n* junction transistor structures: The *p-n-p* transistor has been discussed previously from a theoretical viewpoint.[1,2] In this article we shall consider chiefly the *n-p-n* transistor,[3] the *n*-type phototransistor with a *p-n* hook collector and a *p-n-p-n* transistor with *p*-type emitter and *p-n* hook collector.

In the following sections we shall describe first in simple terms the basic phenomena and effects with which we are concerned. We shall next describe the actual physical structure of several of the *n-p-n* transistors and their electrical characteristics. The theoretical principles will then be put in quantitative form and the current-voltage relationships derived for certain particular models. Finally a direct comparison between theory and experiment will be presented.

II. THE *n-p-n* STRUCTURE AS A TRANSISTOR AND AS A "HOOK MULTIPLIER"

In Fig. 1 we represent an *n-p-n* structure and indicate how it may be used as a transistor. Like the type-A transistor, the current paths between emitter terminal and base and between collector terminal and base have rectifying junctions. Unlike the type-A transistor, however, the rectification arises in the interior of the germanium and not at the contacts between metal leads and the germanium; which are substantially ohmic. There are other important differences between the *n-p-n* and the type-A: In the *n-p-n* the flow of injected carriers takes place chiefly by diffusion rather than by drift in an electric field; the current multiplication at the collector, which makes possible the positive feedback instability of the type-A transistor, is lacking in the *n-p-n* transistor.

In this section we shall give a brief resumé of the theory of the operation of the transistor. Additional details will be found in the cited references. In Secs. V, *et seq.*, some aspects of the theory will be treated analytically. The analysis is simplified by the use of the following assumptions:[4]

(1) The donors and acceptors are fully ionized (this is a good assumption for germanium at room temperature).

(2) The density of minority carriers is much smaller than the density of majority carriers in each region.

(3) The net rate of recombination in any region is linear in the deviation of the minority carrier density from its thermal equilibrium value. (Assumptions (2) and (3) permit us to use linear equations in dealing with the currents arising from carrier injection.)

(4) Space charge is negligible except at the space-charge regions in the *p-n* junctions themselves.

In Fig. 1 we show the energy band diagram for the structure under consideration for zero bias and for biases applied in such a way that the unit becomes an amplifying transistor. Under the latter condition the junction J_c on the right of the figure is biased in the reverse direction. This direction is such that electrons in the *n*-type collector region have low potential energy and cannot climb the potential energy hill to the base region; similarly holes are held in the base region. Electrons in the emitter region, however, may climb the small potential hill into the base region and once in this region may diffuse so that some of them will arrive at the right-hand junction. The flow over the hill depends on the height of the hill and this height may

[1] W. Shockley, Bell System Tech. J. 28, 435–489 (1949).
[2] W. Shockley, *Electrons and Holes in Semiconductors* (D. van Nostrand Company, Inc., New York, 1950).
[3] R. L. Wallace and W. J. Pietenpol, Bell System Tech. J. July, 1951. (This article, to which we shall refer a number of times, deals with a number of practical features which we do not consider here.) It is also scheduled for the Proc. Inst. Radio Engrs. July, 1951.
[4] These assumptions are discussed further in references 1 and 2.

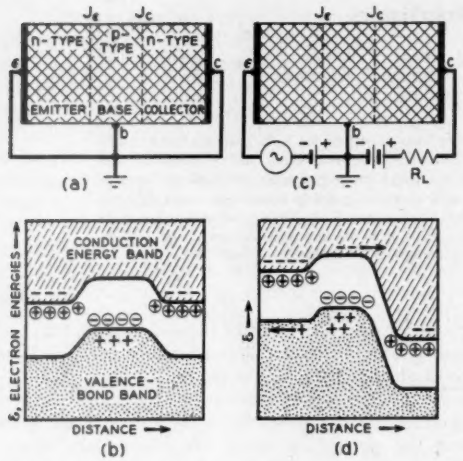

FIG. 1. The *n-p-n* structure and the energy level scheme. (a) and (b) Thermal equilibrium. (c) and (d) Biased as an amplifier.

be varied by applying a variable potential to the emitter while maintaining the base at constant potential. If the base region is very thin, few of the electrons will recombine with holes in it and, as a result, efficient transmission of electron current through the layer will occur. Furthermore, if the emitter region is more highly conducting than the base region, there will be many more electrons available to climb the hill than there are holes to climb the corresponding hill in the opposite direction. As a result, most of the current across the left junction will consist of electrons. Under these conditions the behavior of this device is closely analogous to that of a vacuum tube: the emitter region corresponds to the cathode, the base to the region around the grid wires, and the collector region corresponds to the plate. In favorably designed units the controlled electron current flowing through the base region may be very much larger than the current furnished the base region for control purposes so that the transistor has a current amplification factor that is very high. It may, therefore, be operated like a grounded cathode triode with the emitter region grounded and the signal applied to the base. In Sec. IV some current-voltage characteristics for transistors are shown and for them it may be seen that the current transmission is nearly perfect.

It is interesting to note that both for the vacuum tube and for the transistor, control is accomplished by the interaction of two forms of electron flow. In the vacuum tube, metallic flow in the grid wire controls the flow of thermionic electrons in the space between grid wires. In the transistor, hole flow in the base changes the base-emitter voltage and controls electron flow through the base layer.

The structure shown in Fig. 1 with the same operating biases may be used as a collector with high multiplication in a transistor.[5] It may also be used as a phototransistor.[6] We shall consider the application as a collector in a transistor later and shall describe here how multiplication of photocurrents can occur. For this purpose there need be no electrode connected to the base layer. If light shines on the germanium near the junctions, then the hole electron pairs generated will be separated by the field of the junctions and consequently a current of holes will flow into the base layer. These holes will accumulate in the layer and will charge it positively and thus reduce its potential energy for electrons. As a result more electrons will be able to climb the hill and flow to the collector. The effect of the added holes will die away after the light is removed due to the diffusion of holes into the left region where they combine with electrons and also due to recombination with electrons which diffuse into the base layer. If the layer is very thin, however, and the density of electrons in the left region is very high, then a very large number of electrons will be able to climb over the hill for each hole that is able to enter the emitter region and recombine. In Sec. VII we shall show that the current amplification obtained in this way is proportional to the ratio of the conductivities of the two layers and is inversely proportional to the thickness of the base layer.

An interesting consequence of the diffusion of electrons through the base layer is the occurrence of "internal contact potentials."[7] In order to illustrate these we shall suppose that the base layer is grounded and that a potential is applied to the emitter. If an additional ohmic contact is also made to the base region, it will of course show ground potential. If the contact is rectifying, however, and in particular if it carries most of its current in the form of electrons, its potential will be determined by the electron density in the base layer rather than by the potential established by the grounding contact. The *n*-region on the right represents such a contact. It is found both theoretically and experimentally that if the base layer is grounded, then potentials applied to the region on the left are transmitted through the base layer, although its electrostatic potential is practically unaltered, and exhibit themselves in the region to the right, which tends to "float" (when no current is drawn from it) at a potential approximately equal to that of the left region—at least over a certain range of voltages. Theory and experiment related to this phenomenon are given in Secs. VII and VIII.

III. DESCRIPTION OF EXPERIMENTAL UNITS

The experimental units were made of a piece of single crystal germanium in which a thin *p*-type layer is

[5] W. Shockley, Phys. Rev. **78**, 294 (1950).

[6] J. N. Shive who has developed the phototransistor [Phys. Rev. **76**, 575 (1949)] has proposed this use of the *p-n* hook.

[7] These were first discussed in reference 1. Internal contact potentials for point contacts have been measured by G. L. Pearson and analyzed by J. Bardeen [Bell System Tech. J. **29**, 469–495 (1950)].

interposed between two n-type sections. Units of a variety of conductivity values have been prepared. Typical values for an n-p-n structure as shown in Fig. 1 are: emitter, 100 (ohm-cm)$^{-1}$; base, 1 (ohm-cm)$^{-1}$; and collector, 0.1 (ohm-cm)$^{-1}$. Typical values of lifetime of the minority carrier in the collector section are 300–400 microseconds. The experimental evidence is that lifetimes in the other sections, in which direct measurement of lifetimes is more difficult, do not differ greatly from this. The leads to the three sections are mechanically strong and ohmic in character. The structure thus operates through conditions arising within the interior of the single crystal and not because of phenomena arising at the contacts between the leads and the germanium.

IV. PERFORMANCE CHARACTERISTICS

The performance characteristics of n-p-n transistors will be considered briefly.[8] Since these devices operate uniformly over the surfaces of p-n junctions they may be greatly altered as to the size of the active area, in contrast to point-contact devices. Thus it is possible to increase power output without corresponding increases in current density. One of the larger n-p-n transistors[9] studied as an amplifier had a junction area of 0.3 sq cm, a base layer thickness of about 0.07 cm, and delivered 2.0 watts of undistorted output in class A operation. Its frequency cutoff was about 10,000 cps, this limit being in general agreement with the effect of diffusion through the p-layer as discussed in Sec. IX.

The low power potentialities of these structures have been more thoroughly investigated. A junction area of about 0.01 sq cm and a base layer thickness of about 1.5×10^{-3} cm are typical dimensions for these units. They have operated with gains of 50 db and noise figures of about 10 db to 15 db at 1000 cycles per second. Each of these quantities is an improvement of several orders of magnitude over point-contact transistors. For low signal levels they give essentially full gain with collector voltages higher than 0.1 volt and are, therefore, exceptionally good very low power amplifiers. At some sacrifice in gain they may be operated at efficiencies of 48 to 49 percent out of a theoretical maximum of 50 percent for class A. An oscillator has been constructed by R. L. Wallace, Jr., and D. E. Thomas of this laboratory which operates on 0.6-microwatt input. The same small transistors will also operate as amplifiers with maximum output powers of several hundred milliwatts. A set of operating curves is given in Fig. 2. The frequency cutoff of these units in high gain circuits is determined chiefly by the capacitance of the collector junction and is much lower than the limit set by diffusion through the base layer. A discussion of the capacitative effect will be found in the article by Wallace and Pietenpol.

[8] An extensive presentation of circuit properties is given in reference 3.

[9] The performance of this transistor was discussed at the June, 1950, Inst. Radio Engrs. Conference on Electron Devices at the University of Michigan and also at the July, 1950, Conference on Semiconductors at Reading.

V. THEORETICAL PRINCIPLES AND BOUNDARY CONDITIONS

In this and following sections we shall give analytic form to the ideas discussed in Sec. II. The principal symbols used in dealing with the theory are shown in the accompanying table of notation. In this section and the next we shall deal with the n-p-n structure in general terms and for this reason shall use subscripts "l" and "r" standing for "left" and "right" for the two n-type regions. This permits us to consider impartially cases in which either region may be biased as a collector or as an emitter.

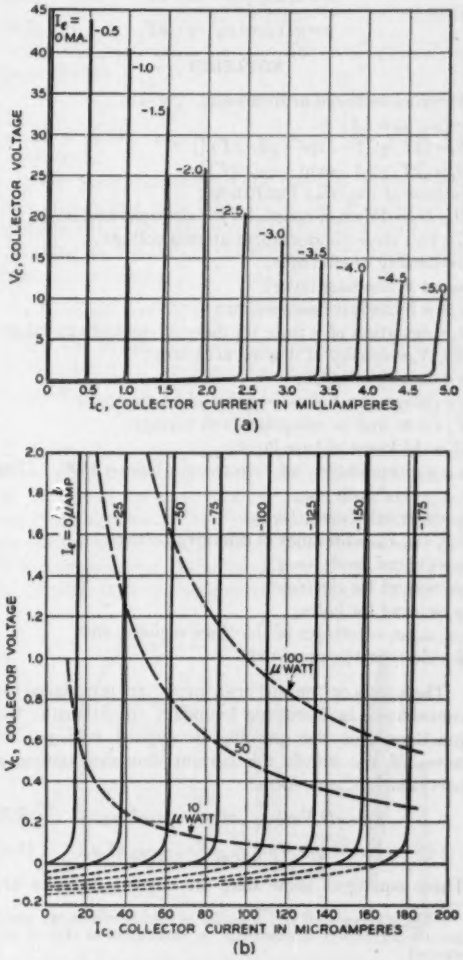

FIG. 2. Current-voltage relationships for an n-p-n transistor.

We shall first discuss the boundary conditions at the junctions when potentials are applied across them.[10] The electrostatic potential ψ in the interior of the semiconductor may have its zero chosen arbitrarily. For our purpose the zero is so chosen that $-q\psi$ is approximately the energy of an electron at a level of energy midway in the energy gap. The exact value of ψ is such that

$$n=n_i \exp q(\psi-\varphi)/kT \tag{5.1}$$

$$p=n_i \exp q(\varphi-\psi)/kT \tag{5.2}$$

under equilibrium conditions. Under nonequilibrium conditions, similar equations determine the "imrefs"[11] φ_n and φ_p in terms of ψ, n, and p as follows:

$$n=n_i \exp q(\psi-\varphi_n)/kT \tag{5.3}$$

$$p=n_i \exp q(\varphi_p-\psi)/kT. \tag{5.4}$$

NOTATION

A = cross-sectional area of unit;
$b=\mu_n/\mu_p=2.1$;
$B_l=(kT/q)[1-\exp(-q\varphi_l/kT)]$;
$B_r=(kT/q)[1-\exp(-q\varphi_r/kT)]$;
e = base of naperian logarithms;
D_n, D_p = diffusion constants for electrons and holes;
G_{ll}, G_{lr}, etc. = conductances at zero voltage;
n = density of electrons;
$n_b=n$ in the base layer;
$n_i=n$ in an intrinsic specimen;
n_1 = deviation of n from its thermal equilibrium value;
N_d, N_a = density of donors, acceptors;
p = density of holes;
q = charge of a hole = $-$charge of an electron;
V, v = dc and ac components of voltage;
W = thickness of base layer;
μ_n, μ_p = mobilities of electrons, holes = 3600, 1700 cm^2/volt sec;
σ_i = intrinsic conductivity;
τ_{pl}, τ_{pr}, τ_{nb} = lifetimes of minority carriers;
φ = (Fermi level)/$(-q)$;
φ_n = imref for electrons;
φ_p = imref for holes;
φ_l, φ_b, φ_r = voltages of the three regions; and
ψ = electrostatic potential.

The imrefs or "quasi-Fermi levels" are introduced for convenience in discussing boundary conditions at the junctions and the meaning of applied voltages. In terms of the imrefs the current densities assume a particularly simple form:

$$I_n=qD_n\nabla n+q\mu_n nE=-q\mu_n n\nabla\varphi_n \tag{5.5}$$

$$I_p=-qD_p\nabla p+q\mu_p pE=-q\mu_p p\nabla\varphi_p. \tag{5.6}$$

These equations show that the current densities are those corresponding to materials with the conductivity appropriate for the electron and hole densities, respectively, and to electric fields derived from the imrefs as potentials. From these relationships it is evident that a given electron current will produce much bigger changes of the imrefs when it flows in a p-type region, where the electron density is small, than it will in an n-type region. In fact the ratio of conductivity by electrons is so great between the two regions that the imref for electrons can be regarded as substantially constant in the n-type region. In accordance with the assumption that the minority carrier density is small compared to the majority density and the assumption that the space charge is negligible, it follows that the potential ψ is substantially uniform in the interior of each region also. If the contacts on regions l and r are so far from the junctions that no injected carriers reach them and are substantially ohmic, then it also follows that the imrefs for electrons in these regions are simply the voltage applied to the two contacts. In accordance with the assumption that current to the base contact is carried by holes, it also follows that the imref for holes in this region is equal to φ_b.

We shall now apply the aforementioned conclusions to the boundary condition at J_l. For simplicity we shall assume that the base is grounded so that we shall consider in general cases in which

$$\varphi_l\neq 0, \quad \varphi_b=0, \quad \varphi_r\neq 0. \tag{5.7}$$

By the reasoning of the preceding paragraph, the imref for electrons is continuous across the junction J_l and in fact has its largest gradient only after the interior of the base region is reached. Consequently we may take φ_n in the base region near J_l as substantially equal to φ_l. The electron density in the base region near J_l is thus given by

$$n(\text{in } b \text{ near } J_l)=n_b \exp(-q\varphi_l/kT), \tag{5.8}$$

where n_b is the thermal equilibrium concentration of electrons at the corresponding point. (This equation follows directly from (5.3) together with the conclusion previously reached that ψ and φ_p in the base layer are unaffected by the applied potentials of (5.7).)

We shall be chiefly concerned with deviations of the densities from their equilibrium values and shall use the subscript 1 to indicate such densities. The deviation corresponding to (5.8) is

$$n_1=n_b[\exp(-q\varphi_l/kT)-1]\equiv -n_{lq}B_l/kT. \tag{5.9}$$

In this expression we have introduced the quantity B_l defined as

$$B_l\equiv(kT/q)[1-\exp(-q\varphi_l/kT)]. \tag{5.10}$$

This symbol is introduced since all the currents with which we shall be concerned depend functionally upon the voltages in the form (5.10). The coefficient kT/q is introduced so that B_l has the dimensions of a voltage and for small values of φ_l, B_l is in fact approximately equal to φ_l.

[10] The notation used here is similar to that of references 1 and 2 and the analysis is substantially an abreviation of that of reference 1.

[11] We are indebted to the most appropriate authority for suggesting this modified name for the quasi-Fermi levels.

Entirely similar reasoning leads to corresponding relationships for the hole density in the l region:

$$p(\text{in } l \text{ near } J_l) = p_l \exp(-q\varphi_l/kT) \tag{5.11}$$

$$p_l = p_l[\exp(-q\varphi_l/kT)-1] \equiv -p_l q B_l/kT. \tag{5.12}$$

VI. THE CURRENT-VOLTAGE RELATIONSHIPS

The analysis of the last section indicates that near J_l the deviations of both hole and electron densities are proportional to B_l. These deviations lead to diffusion currents, which would vanish for the case of thermal equilibrium with $B_l=0$. As a result of the linear approximations discussed in Sec. II, these currents will be proportional to B_l. In Fig. 3 the conventions selected for signs of current are shown. We shall accordingly denote the current into region b due to hole flow across J_l as follows:

$$I_{lp} = G_{llp} B_l. \tag{6.1}$$

For the case of a uniform cross section of area A and material of uniform conductivity and uniform lifetime τ_{pl}, the value of the coefficient may be easily derived:[12]

$$G_{llp} = q\mu_p p_{nl} A/L_{pl} = \sigma_i^2 bA/(1+b)^2 \sigma_l L_{pl} \tag{6.2}$$

in which the diffusion length is given by the equation,

$$L_{pl} = (D_p \tau_{pl})^{\frac{1}{2}}. \tag{6.3}$$

The last form of (6.2) expresses the conductance G_{llp} in terms of the conductivity σ_i of an intrinsic sample and the actual conductivity of the n-type region. The quantity b occurring in the equation is the ratio of mobilities:

$$b = \mu_n/\mu_p. \tag{6.4}$$

The electron current flowing across J_l can also be directly evaluated for the case of $B_r=0$. Even if no potential is applied across J_r, some of the electrons injected across J_l will arrive in the r-region. This is a consequence of the fact that the deviation n_1 is required to be zero at J_r when φ_r is zero. The electron currents across the two junctions are found to be[13]

$$I_{ln} = [(q\mu_n n_b A/L_n) \coth(W/L_n)] B_l \equiv G_{lln} B_l \tag{6.5}$$

$$I_{rn} = -[(q\mu_n n_b A/L_n) \operatorname{csch}(W/L_n)] B_l \equiv G_{rln} B_l. \tag{6.6}$$

The conductance G_{lln} may be expressed in terms of the properties of the base layer as follows:

$$G_{lln} = [\sigma_i^2 bA/(1+b^2)\sigma_b L_n] \coth(W/L_n). \tag{6.7}$$

A similar treatment for J_r leads to a corresponding set of equations. In terms of the G's and the B's the current-voltage relationship may be written as follows:

$$I_l = G_{ll} B_l + G_{lr} B_r \tag{6.8}$$

$$I_r = G_{rl} B_l + G_{rr} B_r \tag{6.9}$$

$$G_{ll} = G_{lln} + G_{llp}, \quad G_{lr} = G_{lrn} \tag{6.10}$$

$$G_{rl} = G_{rln}, \quad G_{rr} = G_{rrn} + G_{rrp}. \tag{6.11}$$

For low voltages we have the approximate relationship,

$$B_l \doteq \varphi_l, \quad B_r \doteq \varphi_r \quad \text{for} \quad |\varphi_{l,r}| \ll kT/q, \tag{6.12}$$

so that the coefficients in Eqs. (6.8) and (6.9) are simply the low voltage conductance components. If the potentials consist of a bias plus a small ac component so that we may write

$$\varphi_l = V_l + v_l, \quad \varphi_r = V_r + v_r, \tag{6.13}$$

then the small signal equations become

$$i_l = g_{ll} v_l + g_{lr} v_r \tag{6.14}$$

$$i_r = g_{rl} v_l + g_{rr} v_r, \tag{6.15}$$

where the relationship between the small g's and the large G's is

$$g_{ll}/G_{ll} = g_{rl}/G_{rl} = \exp(-qV_l/kT) \tag{6.16}$$

while a similar equation applies for the other two coefficients.

From these relationships one can also derive the result that each g is proportional to the deviation of its corresponding GB term from its saturation value corresponding to $B=(kT/q)$. This may be expressed symbolically as follows:

$$g = (\text{deviation of } GB \text{ from saturation}) \cdot (q/kT). \tag{6.17}$$

For the model discussed in connection with Eqs. (6.5) and (6.6), it is evident that symmetry leads to the equation,

$$G_{lr} = G_{rl}. \tag{6.18}$$

If the conductivity varies in an unsymmetrical way, however, in the middle layer or if the lifetime is greater at one side of the layer than the other, then we cannot reach the conclusion that the two G's are equal from symmetry arguments. It can be shown, however, that it is a consequence of the linear assumptions described in Sec. II that the symmetry relationship holds no

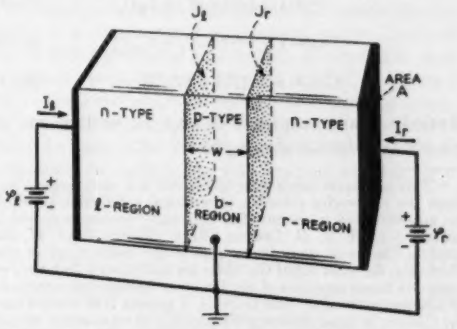

FIG. 3. Dimensions and conventions for voltage and current for an n-p-n structure.

[12] Reference 1, Eqs. (4.20) and (4.21) or reference 2, p. 316. In a specimen of finite cross section, the recombination must be described in terms of a set of normal modes. For the cross sections of the small transistors, the lowest mode dominates and its lifetime may be used in the formulas derived for the one-dimensional case. See reference 1, Appendix V.

[13] Reference 1, Eq. (5.6), modified for electron diffusion.

matter what the geometry of the middle layer. The proof of this result is given in an appendix.[14] This leads us to the conclusion that for the idealized sort of model in which all of the currents are linear in the injected carrier density, the behavior of the transistor is described by three parameters, at least so far as low frequencies are concerned. These parameters are the four coefficients in Eqs. (6.8) and (6.9) with the relationship (6.18) between two of them.

In terms of these coefficients we may define the "alpha" of the unit using either junction as an emitter. The two α's need not be equal and the α for the left junction is given by the relationship,

$$\alpha_l \equiv -(\partial I_r/\partial I_l) \quad [\text{for} \quad \varphi_r \text{ const}] = -G_{rl}/G_{ll}$$
$$= -G_{rln}/(G_{lln}+G_{llp})$$
$$= (-G_{rln}/G_{lln})[G_{lln}/(G_{lln}+G_{llp})] = \gamma_l\beta_l. \quad (6.19)$$

The definition of γ in transistor terminology is the fraction of the current at the emitter junction produced by emitter voltage that is carried by minority carriers in the base; evidently

$$\gamma_l = G_{lln}/(G_{lln}+G_{llp}). \quad (6.20)$$

The fraction of these injected carriers that reaches the collector is defined as β:

$$\beta_l = -G_{rln}/G_{lln} = \operatorname{sech}(W/L_n). \quad (6.21)$$

The "intrinsic α" or α^* of the collector junction is defined as the ratio of change in total current per unit minority carrier current arriving at it. For a simple p-n junction collector, α^* is unity. For a "hook collector," which we treat in the next section, the arrival of injected current provokes a flow of carriers and α^* may be 100 or more.

If the middle layer is thin so that the hyberbolic functions of (6.5) and (6.6) may be approximated by their first terms, we may write

$$\beta_l \doteq 1-\tfrac{1}{2}(W/L_n)^2 \doteq 1 \quad (6.22)$$

$$\gamma_l \doteq 1/[1+(\sigma_b W/\sigma_l L_{pl})] \quad (6.23)$$

$$\alpha_l \doteq 1/[1+(\sigma_b W/\sigma_l L_{pl})] \quad (6.24)$$

$$G_{lln} \doteq \sigma_1^2 bA/(1+b)^2\sigma_b W. \quad (6.25)$$

Entirely similar expressions may be written for J_r simply by interchanging r and l.

[14] This symmetry result may be derived in a more general way from the reciprocity principle of electrical conduction provided no magnetic field is present. The necessary theorem is proved in section 5 of H. B. G. Casimir [Revs. Modern Phys. **17**, 343 1945)]. The proof there shows that in the linear range of conductivity, G_{lr} must equal G_{rl}. Since we have shown that the currents are linear functions of the B's by an independent argument, it follows that we may take $G_{lr}=G_{rl}$ in general. The method used by Casimir is based on Onsager's principle of microscopic reversibility and has an unnecessarily abstract flavor so far as the needs of this article are concerned. The desired theorem can be proved by straightforward analytical methods as is shown in the Appendix.

VII. SPECIAL OPERATING CONDITIONS

We shall next consider the consequences of the equations derived in the previous section for several limiting cases of voltages and currents.

A. Operating as an Amplifier

In order to get into the range of linear behavior it is necessary to apply a sufficiently large reverse bias to the collector so that its current saturates. This condition corresponds to the straight parts of the characteristics shown in Fig. 2. The voltage required to get into this range must exceed about $4kT/q$. After this point is reached the emitter current and collector current may be approximated by

$$I_l = G_{ll}B_l - \alpha_l G_{ll} kT/q \quad (7.1a)$$

$$I_r = -\alpha_l G_{ll} B_l + G_{rr} kT/q$$
$$= -\alpha_l I_l + (G_{rr}+\alpha_l^2 G_{ll})(kT/q). \quad (7.1b)$$

Equation (7.1b) accounts for the parallel lines with currents increasing linearly in I_l shown in Fig. 2 for high collector voltages.

For applications in circuit theory, it is important to know the emitter admittance g_{ll}. To the approximation emphasized in this paper in which series ohmic resistances are neglected, this admittance is $1/r_e$ of the equivalent circuit.[3] The range of interest is usually such that $-\varphi_l > 4kT/q$ so that the application of the reasoning of (6.17) leads to

$$1/r_e = g_{ll} = \partial I_l/\partial\varphi_l = G_{ll}\exp(-q\varphi_l/kT)$$
$$\doteq I_l q/kT \doteq 40 I_l \text{mho}. \quad (7.2)$$

If the unit is operated with grounded emitter and with the collector current saturated, then the input admittance is

$$dI_b/d\varphi_b = d(-I_l-I_r)/d(-\varphi_b)$$
$$= (1-\alpha_l)G_{ll}\exp(-q\varphi_l/kT) \quad (7.3)$$

while the transconductance is $1/(1-\alpha_l)$ larger. Thus if $\alpha_l = 0.99$, there will be a current gain of 100-fold, if the collector current is saturated. The theoretical power gain would be infinite if the collector impedance were infinite corresponding to the ideal saturation of (7.1b). Actually collector resistances of 10^7 to 10^8 ohms are observed. For currents large compared to saturation currents, (7.3) leads to an admittance of $(1-\alpha_l)I_r q/kT = 10^{-2}\times 10^{-4}\times 40 = 4\times 10^{-6}$ mhos for $I_r = 10^{-4}$ amp, a typical value for high gain performance. The power gain will be roughly the ratio of output to input impedances times the square of the current gain and will thus be about $10^7\times 4\times 10^{-6}\times 10^4 \doteq 66$ db for a matched load. As discussed in Sec. IV, gains as high as 50 db have been obtained in practical circuits.

B. Hook Collector in p-n-p-n Transistor

Point contact transistors are frequently observed to have current multiplication in the sense that at a

fixed collector bias, changes in emitter current produce changes in collector current several fold larger. One explanation is that a "p-n hook" is formed at the collector junction so that the "intrinsic α" or α^* of the collector is high. We shall illustrate this theory for the case of an n-type transistor in which holes are injected by a p-n junction emitter and the collector consists of n and p layers.

This structure is represented in Fig. 4 and is shown for bias conditions similar to those discussed for Fig. 1 except for the added emitter region and the absence of a contact to the b layer. Regarded as a transistor, the emitter, base, and collector are e', b', and c'. The operating biases put reverse voltage across J_r and forward across J_l. The base layer b will float at a potential such that the net current to it is zero:

$$I_r+I_l=G_{ll}(1-\alpha_l)B_l+G_{rr}(1-\alpha_r)B_r=0. \quad (7.4)$$

For large reverse biases B_r will be positive and B_l negative and

$$\varphi_l-\varphi_r=V_{c'}, \quad (7.5)$$

where $V_{c'}$ is the voltage on the collector. For large $V_{c'}$, B_r will saturate and φ_l will be determined by

$$B_l=-G_{rr}(1-\alpha_r)(kT/q)/G_{ll}(1-\alpha_l) \quad (7.6)$$

so that the saturation current is

$$I_r(\text{sat.})=(1-\alpha_r\alpha_l)G_{rr}kT/q(1-\alpha_l). \quad (7.7)$$

If holes are injected by e' so that a hole current I_p^* arrives at J_r, then the condition,

$$I_r+I_l+I_p^*=0 \quad (7.8)$$

leads to a change

$$\Delta B_l=-I_p^*/G_{ll}(1-\alpha_l) \quad (7.9)$$

and this produces an increased electron current across J_r which leads to

$$\Delta I_{nr}=G_{rl}\Delta B_l=\alpha_l I_p^*/(1-\alpha_l). \quad (7.10)$$

The "intrinsic α" or α^* of the composite structure is

$$\alpha^*=(\Delta I_{nr}+I_p^*)/I_p^*=1/(1-\alpha_l). \quad (7.11)$$

For the thin layer approximation we see that

$$\alpha^*\doteq 1+(\sigma_l L_{pl}/\sigma_b W). \quad (7.12)$$

Thus for thin layers and for highly conducting l regions, α^* may be made very large.

The reason for calling the structure a "p-n hook" is illustrated in Fig. 4b. The high energy potential for electrons in layer b is low potential for holes. Holes injected by e' become caught in this hook and bias J_l forward so as to provoke the enhanced electron flow.

C. Phototransistor

The structure in Fig. 4 can act as a phototransistor if the hole injection by the emitter junction is simply replaced by hole electron pair generation by light. For this application, the structure has only two terminals, b' and c' of Fig. 4, the region e' being absent. If the hole electron pairs are generated in the neighborhood of J_r, then they will be separated by the field in the junction with a current equivalent to the passage of one hole across J_r for each pair so separated. The hole current across the junction will under these conditions be multiplied just as for the case of the p-n-p-n transistor so that the apparent quantum efficiency for hole electron pairs generated at J_r is

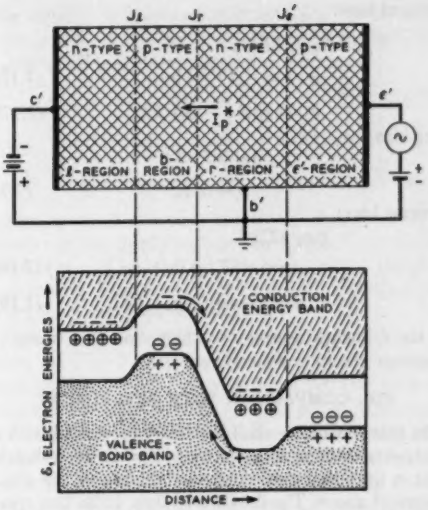

FIG. 4. A p-n-p-n transistor with a p-n hook collector.

apparent quantum efficiency

$$=\alpha^*\doteq 1+(\sigma_l L_{pl}/\sigma_b W) \quad (7.13)$$

by the reasoning that leads to Eq. (7.12). In the following section we shall discuss some values of α^* determined by measurements of photocurrents.

D. Internal Contact Potentials

In order to discuss internal contact potentials we return to a consideration of the three region device of Fig. 3. If b is grounded and region r is allowed to seek its own potential, then potentials applied to region l will produce potentials on region r although the potential measured with an ohmic contact to b would everywhere be zero. The floating potential of region r is determined by setting the total current equal to zero so that we have

$$0=I_r=G_{rl}B_l+G_{rr}B_r \quad (7.14)$$

$$B_r=(-G_{rl}/G_{rr})B_l=(-G_{lr}/G_{rr})B_l=\alpha_r B_l \quad (7.15)$$

$$\exp(-q\varphi_r/kT)=1-\alpha_r+\alpha_r\exp(-q\varphi_l/kT). \quad (7.16)$$

Equation (7.16) expresses φ_r as a function of φ_l and α_r. It takes simple limiting form for extreme bias conditions:

Forward bias:

$$-q\varphi_l/kT \gg 1$$

$$\varphi_r = \varphi_l - (kT/q)\ln\alpha_r \tag{7.17a}$$

$$\alpha_r = \exp q(\varphi_l - \varphi_r)/kT. \tag{7.17b}$$

Zero bias:

$$|q\varphi_l/kT| \ll 1$$

$$\varphi_r = \alpha_r\varphi_l. \tag{7.18}$$

Reverse bias:

$$q\varphi_l/kT \gg 1$$

$$\varphi_r = -(kT/q)\ln(1-\alpha_r) \tag{7.19a}$$

$$\alpha_r = 1-\exp(-q\varphi_r/kT). \tag{7.19b}$$

In the following section, we shall show that these expressions are approximately satisfied.

VIII. COMPARISON WITH EXPERIMENT

In this section we shall be chiefly concerned with an analysis of data on an *n-p-n* transistor and with showing that it may be interpreted on the basis of the theory discussed above. The data were taken under two sets of conditions: In the first the voltages were small compared to (kT/q) and from these the G's were determined using the approximation (6.12). In the second set, a wide range of voltages were used; for all conditions, however, one of the two B's was taken as independent and the other B was either constant or else proportional to the independent B. Consequently, each current is of the form

$$I = c + mB = I_S + m[B-(kT/q)]$$

$$= I_S - I_V\exp(-qV/kT), \tag{8.1}$$

where V is the voltage upon which B depends and

$$I_S = c + (mkT/q) \tag{8.2}$$

is the "saturation" value of the current for large positive values of V and

$$I_V = mkT/q. \tag{8.3}$$

Both I_S and I_V are readily calculated in terms of the G's. In the analysis of the data the measured I_S and I_V values are compared with values computed from the G's, and the dependence of I upon V is investigated.

It should be pointed out that the values of the G's are strongly dependent on temperature. Consider, for example,

$$G_{rl} = b\sigma_i^2 A/(1+b)^2\sigma_p W. \tag{8.4}$$

TABLE 8.1. Zero bias conductances for an *n-p-n* transistor (conductances in micromhos at $T=22°C$).

	Measured	Calculated
G_{11}	8.8 ±0.5	8.8
G_{22}	33.3 ±0.5	33.3
$G_{11}(1-\alpha_1\alpha_2)$	6.9 ±0.5	6.9
$G_{22}(1-\alpha_1\alpha_2)$	26.5 ±0.5	26.4
$\alpha_2=(V_c/V_e)$ for $I_c=0$	0.86±0.02	0.89
$\alpha_1=(V_e/V_c)$ for $I_e=0$	0.22±0.02	0.23
$G_{11}+G_{12}-2G_{21}$	26.2 ±0.5	26.5

In this expression[15]

$$\sigma_i^2 \propto \exp(-\epsilon_G/kT) \tag{8.5}$$

where ϵ_G is the energy gap and

$$\sigma_p \propto T^{-1}. \tag{8.6}$$

Consequently the value of G_{rl} at $T_0+\Delta T = 300°K+\Delta T$ is approximately

$$G_{rl}(T_0+\Delta T) \doteq G_{rl}(T_0)\exp[(\epsilon_G/kT_0^2)+(3/2T_0)]\Delta T$$

$$= G_{rl}(T_0)\exp(0.095+0.005)\Delta T \tag{8.7}$$

so that G_{rl} increases approximately 10 percent per degree C. This increase arises chiefly from σ_i^2 and will be approximately the same for all the G's.

The fact that the G's have large temperature coefficients implies that at fixed voltages the currents will be very sensitive to temperature. This does not mean, however, that in a properly designed circuit, the behavior of the unit will be highly sensitive to temperature. The value of α_1, for example, as shown in (6.24) involves only $\sigma_b W/\sigma_e L_{pe}$ and this has only a small temperature coefficient. At a fixed emitter current, the emitter resistance is proportional to T in °K. Thus the most important quantities from a circuit point of view have small temperature coefficients.

Since in this section we are dealing with a transistor designed to have one terminal as emitter and one as collector, we shall abandon the "left" and "right" terminology and use subscript "1" for the emitter and "2" for the collector as is customary for transistors. The large signal equations are then

$$I_e = G_{11}B_1 + G_{12}B_2 \tag{8.8}$$

$$I_c = G_{21}B_1 + G_{22}B_2 \tag{8.9}$$

and the small signal equations are

$$i_e = g_{11}v_e + g_{12}v_c \tag{8.10}$$

$$i_c = g_{21}v_e + g_{22}v_c \tag{8.11}$$

where each g gepends on its corresponding voltage in the form,

$$g_{ij} = G_{ij}\exp(-qV_j/kT). \tag{8.12}$$

The low voltage conductances were measured at 2 millivolts. For this small voltage

$$B(+2\text{ mv}) = \quad 1.95\text{ mv} \tag{8.13a}$$

$$B(-2\text{ mv}) = -2.05\text{ mv} \tag{8.13b}$$

so that the currents are nearly linear in this range, and the nonlinearity is practically eliminated by averaging the two polarities. With the collector grounded, I_e was measured and G_{11} computed from I_e/V_e. With the collector open circuited, I_e and V_c were measured; for this case $I_e/V_e = G_{11}(1-\alpha_1\alpha_2)$ and $V_c/V_e = -G_{21}/G_{22} = \alpha_2$. Similar data were taken with voltage applied to the

[15] n_i^2 varies as $T^3\exp(-\epsilon_G/kT)$, see reference 2, page 475, and $\mu_n\mu_p$ as T^{-3}, see page 287.

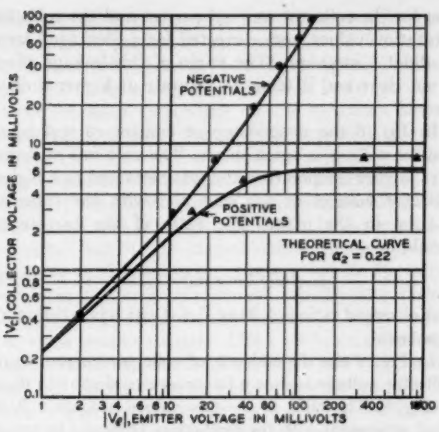
NEGATIVE POTENTIALS
POSITIVE POTENTIALS
THEORETICAL CURVE FOR $\alpha_2 = 0.22$
$|V_c|$, COLLECTOR VOLTAGE IN MILLIVOLTS
$|V_e|$, EMITTER VOLTAGE IN MILLIVOLTS

FIG. 5. Internal contact potential developed on the open circuited collector.

collector. Finally collector and emitter were connected together and the combined currents measured; this gives

$$(I_e+I_c)/V_e=G_{11}+G_{22}-G_{12}-G_{21}. \quad (8.14)$$

The values selected for the G's were: Conductances in micromhos at 22°C

$$G_{11}=8.8, \quad G_{22}=33.3, \quad G_{12}=G_{21}=-7.8. \quad (8.15)$$

These three values fit the seven measurements within the limits of experimental accuracy as shown in Table 8.1. The fact that the fit can be achieved with three constants is not a real test of the theory of Sec. VI, however, since any passive three terminal device in the absence of magnetic fields should satisfy the reciprocity condition and be described by three constants. What the table shows essentially is the consistency of the measurements.

Accurate values for the constants for the base layer were not available for the unit studied. However, the orders of magnitude of the G's are in reasonable agreement with values expected for a structure with constants lying in the ranges expected from the method of fabrication. We shall not attempt to obtain a perfect fit[16] but will choose as an example a structure with $A=0.003$ cm^2, $W=2.5\times10^{-3}$ cm, $\sigma_e=20$, $\sigma_b=10$, $\sigma_c=0.1$, $\sigma_i=(1/60)$ ohm^{-1} cm^{-1}, and lifetimes $\tau_{pe}=40$ and $\tau_{pc}=10$ microseconds. The resulting values for the G's based on Eqs. (6.2), (6.22), and (6.25) are

$$G_{11n}=7.3 \text{ micromhos} \quad (8.16a)$$

$$G_{11p}=0.5 \text{ micromhos} \quad (8.16b)$$

$$G_{22p}=45 \text{ micromhos}. \quad (8.16c)$$

[16] For the simpler case of a p-n junction, the electrical properties have been predicted with an accuracy of about 20 percent from the independently measured constants describing the junction.

The value of β is greater than 0.99 for $\tau_n=40$ microseconds and may be taken as unity so far as the G's are concerned. These values lead to

$$G_{11}=G_{11n}+G_{11p}=7.8 \quad (8.17a)$$

$$-G_{12}=-G_{12n}=\beta_1 G_{11n}=\beta_2 G_{22n}=7.3 \quad (8.17b)$$

$$G_{22}=G_{22n}+G_{22p}=7.3+45=52. \quad (8.17c)$$

According to this interpretation the failure of α_1 to be unity is due chiefly to hole flow across J_e and a similar condition is true of α_2. The base current arises almost entirely from these hole flows with recombination in the base being nearly negligible.

Figures 5 and 6 show the internal contact potential effect. In Fig. 5 the potential V_e is applied and V_c measured while zero current flows to the collector terminal. The data are seen to be in general agreement with the theory and with the value of α_2, corresponding to the collector junction, obtained at low voltage for Table 8.1. Figure 6 shows similar data with the voltage applied to the collector. The data are seen to differ slightly from the theoretical curves for reverse biases. The values of α obtained by applying (7.19b) to these data are

$$\alpha_2=0.226 \quad \text{and} \quad \alpha_2=0.894, \quad (8.18)$$

which shows that the fit is very sensitive to small variations in value of α. The test of Eq. (7.17b), which applies to forward bias, cannot be carried out as satisfactorily because under these conditions the currents are relatively large and the voltage drops across the series resistances of the specimen are not negligible compared to the effects studied. The values obtained are, however, approximately the same as those of Table 8.1.

In Fig. 7, the collector is biased to saturation and I_c and I_e are plotted as functions of V_e. For this case the

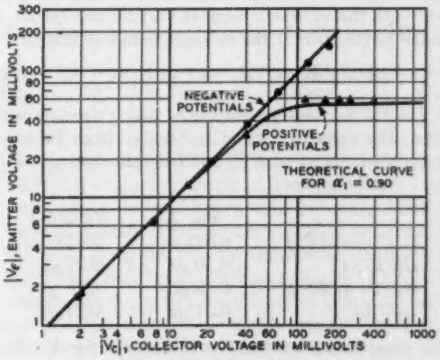
NEGATIVE POTENTIALS
POSITIVE POTENTIALS
THEORETICAL CURVE FOR $\alpha_1 = 0.90$
$|V_e|$, EMITTER VOLTAGE IN MILLIVOLTS
$|V_c|$, COLLECTOR VOLTAGE IN MILLIVOLTS

FIG. 6. Internal contact potential developed on the open circuited emitter.

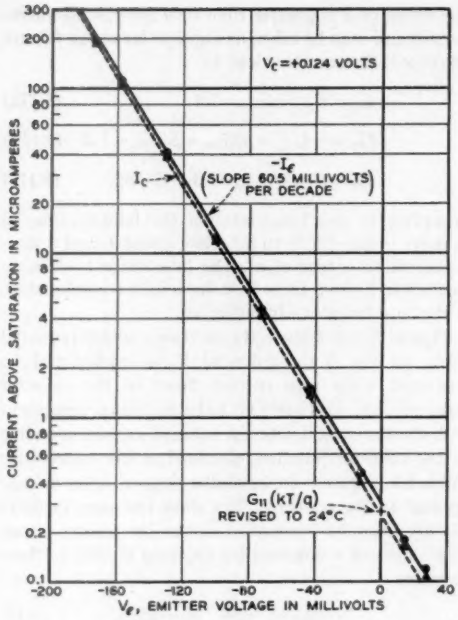

FIG. 7. Emitter and collector currents for the collector biased to saturation.

formulas should be

$$I_e = G_{11}B_1 + G_{12}(kT/q)$$
$$= G_{11}(1-\alpha_1)kT/q - (G_{11}kT/q)\exp(-qV_e/kT) \quad (8.19a)$$
$$I_c = G_{12}B_1 + G_{22}(kT/q)$$
$$= G_{22}(1-\alpha_2)(kT/q)$$
$$+ (\alpha_1 G_{11}kT/q)\exp(-qV_e/kT). \quad (8.19b)$$

It is seen that the lines agree well with the exponential forms and, furthermore, that the slope is in good agreement with theory which requires that for one decade of change in the current the voltage change should be

$$\Delta V = 2.30 \times kT/q = 2.30/39.4 = 59.0 \text{ mv} \quad (8.20)$$

for $T = 297°\text{K}$, the temperature at which the data were taken. The values of I_S and I_V deduced from Table 8.1 (corrected for a ΔT of 2°C) and from the data on which Fig. 7 was based are:

	Fig. 7	Table 8.1
$G_{11}(1-\alpha_1)kT/q$	0.021 μa	0.025 μa
$G_{11}(kT/q)$	0.30 μa	0.27 μa
$G_{22}(1-\alpha_2)kT/q$	0.88 μa	0.78 μa
$\alpha_1 G_{11}kT/q$	0.27 μa	0.24 μa.

The slope terms are simply the values for $V_e = 0$ in Fig. 7. The saturation values were deduced directly from the data. In the voltage range used, the saturation for the collector was not perfect and the collector saturation values were corrected for a "leakage" term of about 1 megohm. (The origin of this leakage effect is not clear and it tends to saturate at higher reverse biases.)

In Fig. 8 the dependence of emitter current upon emitter voltage is again shown. The unit was at somewhat higher temperature and was measured at a higher collector voltage in one case and with the collector floating in the other. The ratio of the two terms should be

$$G_{11}/G_{11}(1-\alpha_1\alpha_2) = 1.25. \quad (8.21)$$

The observed ratio is 1.30 at $V_e = 0$ which is satisfactory agreement.

In Fig. 9 the dependence of collector current upon collector voltage is shown for two cases similar to those of Fig. 8. The ratio of the two values is again 1.30 in good agreement with the prediction. It should be noted, however, that the slope requires 74 millivolts per decade, a value appropriate to an unreasonably high temperature of 103°C. This slope is established for such low currents that it seems difficult to explain it by spurious effects of series resistances.

There is an important difference in the nature of the currents of Fig. 7, which fit the theoretical slope, and those of Fig. 9, which do not. The currents of Fig. 7 consists chiefly of electrons which diffuse through the base layer and arrive at the collector; the evidence for

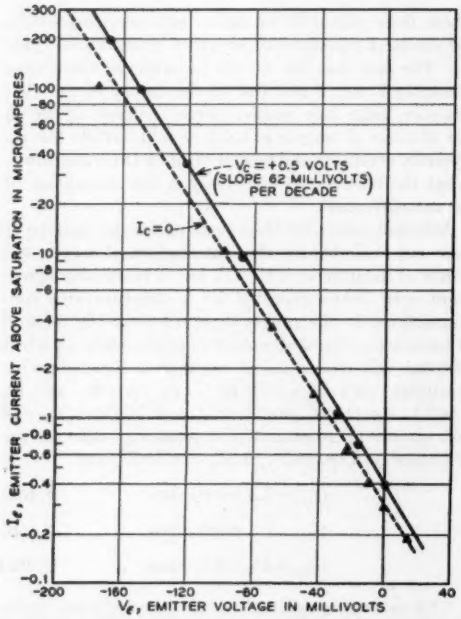
V_c = +0.5 VOLTS
(SLOPE 62 MILLIVOLTS) PER DECADE
$I_c = 0$
I_e, EMITTER CURRENT ABOVE SATURATION IN MICROAMPERES
V_e, EMITTER VOLTAGE IN MILLIVOLTS

FIG. 8. Emitter current for two conditions of collectors.

this conclusion is the value 0.89 for α_1, which implies that only 11 percent of the current is carried by electrons recombining in the base layer or holes diffusing into and recombining in the emitter body (or the reverse processes, depending on the polarity). On the other hand, most of the collector current is probably carried by holes which recombine in the collector body. (This reasoning is in agreement with the attempt to interpret the G's in terms of the structure discussed in connection with (8.17a, b, c).) It is to be expected theoretically that if the recombination process involves trapping on recombination centers,[17] then the rate of recombination will increase less rapidly than linearly with injected carrier density because at high densities the traps tend to saturate. This view has received some experimental support from the work of F. S. Goucher and J. R. Haynes who find an apparent increase in lifetime with increasing carrier density. It may be that this mechanism accounts for failure of the currents to increase as rapidly as they should with increasing voltage in Fig. 9.

Further evidence for nonlinearity in the recombination of holes in the emitter is furnished by the dependence of α_1 upon emitter current. This can be seen in Fig. 7. As the emitter current increases, the ratio of collector to emitter current (above saturation) increases from 0.9 to about 0.95. This is interpreted as being due to the failure of hole current to increase as rapidly with voltage as does emitter current.

The tendency of α to increase with emitter current appears to be a general feature of n-p-n transistors. Wallace and Pietenpol[3] report values as high as 0.995 for α.

Phototransistors made of n-p-n structures are extremely responsive to light and exhibit apparent quantum efficiencies of at least several hundreds. In accordance with the interpretation of Sec. VII C, these efficiencies would lead to α_1 values deduced from $1-(1/\alpha^*)$ comparable to or larger than the highest observed in n-p-n transistors.

IX. SOME DESIGN CONSIDERATIONS

It has been the principal purpose of the preceding sections to examine the consequences of the diffusion theory and compare them with experiment. For this purpose the experimental conditions considered were the simplest: small currents and zero frequency. For practical applications high frequency and larger currents are also of interest. In this section we shall discuss briefly some of the factors of importance in design considerations.

Of great interest is the frequency cutoff. This may be determined by the external circuit or by one or another of several internal features of the transistor. The most fundamental of these latter is that set by the diffusion time through the base layer. This time is

$$\tau_D = W^2/D_n. \tag{9.1}$$

At a circular frequency ω, solutions for n_1 in the base layer are of the form,

$$\exp(i\omega t \pm x(1+i\omega\tau_n)^{\frac{1}{2}}/L_n) \tag{9.2}$$

and this leads to a β value of

$$\beta = \operatorname{sech}(1+i\omega\tau_n)^{\frac{1}{2}} W/L_n. \tag{9.3}$$

For frequencies such that $\omega\tau_n \gg 1$, this reduces to

$$B = 2/[\exp(1+i)(\omega\tau_D/2)^{\frac{1}{2}} + \exp(-1-i)(\omega\tau_D/2)^{\frac{1}{2}}]. \tag{9.4}$$

From this it is evident that for $\omega\tau_D \gg 2$ there is a phase lag of $(\omega\tau_D/2)^{\frac{1}{2}}$ radians and an equal attenuation in nepers. The power gain, which is proportional to β^2 in many cases, drops about 3 db when $\omega\tau_D = 2$ or $f = D_n/\pi W^2 \doteq 30/W^2$. For $W = 10^{-3}$ inch or 2.5×10^{-3} cm this is about 5×10^6 cps.

In addition to this fundamental limitation, there may be limitations due to capacitance and ohmic resistances. We shall illustrate this by considering the grounded emitter form of circuit, which is analogous to a grounded cathode vacuum tube circuit. For this case ac signals are applied to the base and ac voltages are developed on the collector. These voltages charge the capacitance of the base collector junction and this charging current must be furnished by hole flow in the base layer. For a layer

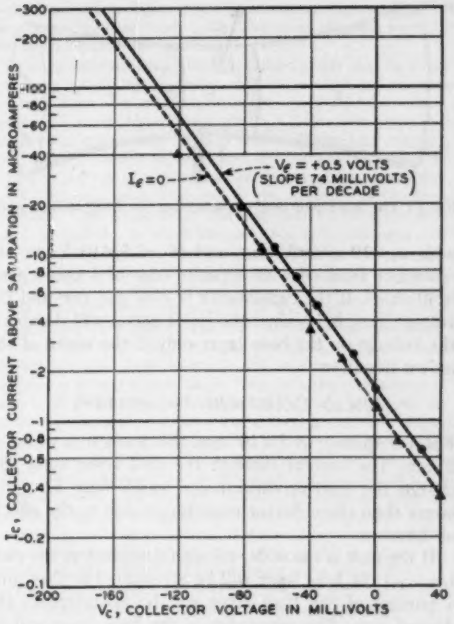

FIG. 9. Collector current for two conditions of emitter.

[17] See reference 2, page 342.

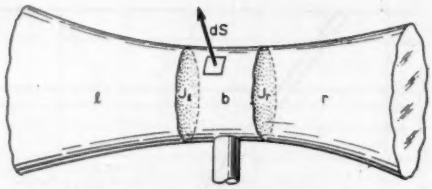

FIG. 10. The base region over whose surface the integration is made.

with $\sigma_b = 10$ ohm^{-1} cm^{-1} and $W = 2.5\times10^{-3}$ cm, the resistance from edge to opposite edge of a unit square is 40 ohms. If the capacitance is 2000 $\mu\mu$f/cm^2 and the voltage gain is 10, then the input signal will dominate the voltage on the base layer only if the width of the unit is less than

$$(10\times\omega\times2\times10^{-9}\times40)^{-\frac{1}{2}}=(\omega8\times10^{-7})^{-\frac{1}{2}}.$$

For a frequency of 5×10^6 cps, this leads to a width of 2 mm. The current through the base layer must also charge the emitter capacitance which may be much larger than the collector capacitance due to the effects of diffusion.

If the unit is too wide, the signal applied at the electrode on the base layer will be attenuated so that only a portion of the base layer will be operative in the desired way. The remainder of the base layer will be dominated by the capacitative voltages and these will induce currents which will lead to large "active" capacitances appearing between emitter and collector.

It is evident that the effects involved will lead to rather detailed calculations for any particular case but that the physical principles required to design *n-p-n* transistors are simply extensions of those well established for *p-n* junctions and *n-p-n* transistors for the low bias, low frequency conditions.

The low noise figures of these transistors cannot be said to be explained in the absence of an established theory of noise generation. They are, however, in rough agreement with a theory based on noise modulation of the recombination mechanism.[17] This theory predicts that each element of volume is a source of (noise current)^2 proportional to the square of the deviation of minority carrier density from its normal value. Applying this criterion to the *n-p-n* structure and comparing it to the type A indicates that the observed difference of 40 db or more between noise figures can be accounted for in terms of the change in current densities and geometries.

X. ACKNOWLEDGMENTS

We are indebted to a number of our colleagues for encouragement and assistance. In particular, we recognize the contribution of J. A. Morton of the transistor development group, whose encouragement resulted in the techniques that made good *p-n* transistors possible. We are grateful to E. Buehler and R. M. Mikulyak who processed the germanium, to W. J. Pietenpol who prepared the particular unit studied, to R. L. Wallace for help with the measurements and the manuscript, and to W. van Roosbroeck for a critical reading of the manuscript.

APPENDIX

Proof of the Equality $G_{lr}=G_{rl}$

We shall prove this equality subject to the assumption that the electron density in the base layer is small compared to the thermal equilibrium hole density. Under these conditions, the effect of injected electrons on the potential distribution may be neglected so that the variation of the electron density from its equilibrium value may be treated by linear equations. In Fig. 10 we represent the situation considered. We shall denote by $I_{nl}(B_l, B_r)$ the current across J_l into the base carried by electrons. The symmetry relation $G_{lr}=G_{rl}$ is then established by proving that

$$I_{nl}(0, B)=I_{nr}(B, 0). \tag{A1}$$

In the base layer we shall suppose that the electrostatic potential ψ and the lifetime τ are arbitrary functions of position. The boundary condition on the external surfaces and at the metal contact will be taken as

$$I_n\cdot dS=-qn_1s|dS|, \tag{A2}$$

where dS is the outward normal, s the surface recombination velocity and

$$n_1=n-n_p \tag{A3}$$

is the deviation of n from the thermal equilibrium value.

We shall denote the solutions corresponding to potentials applied to the two junctions as follows:

$$B_l=B,\quad B_r=0 \qquad n_1,\quad I_n \tag{A4}$$

$$B_l=0,\quad B_r=B \qquad n_1',\quad I_n'. \tag{A5}$$

The currents in question are then

$$I_{nl}(0, B)=-\int_{J_l} I_n'\cdot dS \tag{A6}$$

$$I_{nr}(B, 0)=-\int_{J_r} I_n\cdot dS. \tag{A7}$$

The desired theorem is proved by considering the vector A:

$$A=(n_1/n_b)I_n'-(n_1'/n_b)I_n. \tag{A8}$$

Since $I_n\cdot dS$ is proportional to n_1 on the external surfaces, $A\cdot dS=0$ on these surfaces. Hence, the integral of $A\cdot dS$ over the surface of the base region is

$$\int A\cdot dS=(qB/kT)[-I_{nl}(0, B)+I_{nr}(B, 0)] \tag{A9}$$

since on J_l and J_r we have

$$\begin{aligned} n_1/n_b&=(qB/kT) \text{ on } J_l\\ &=0 \text{ on } J_r \end{aligned} \tag{A10}$$

$$\begin{aligned} n_1'/n_b&=0 \text{ on } J_l\\ &=(qB/kT) \text{ on } J_r. \end{aligned} \tag{A11}$$

Furthermore, it can be shown that $\nabla\cdot A=0$ in the base region and hence that (A9) is zero by Gauss's theorem so that (A1) is proved. The proof that $\nabla\cdot A=0$ is accomplished by showing that $\nabla\cdot(n_1/n_b)I_n'$ is symmetrical in n_1 and n_1' so that the two terms in (A8) have cancelling divergences:

$$\begin{aligned} &\nabla\cdot(n_1/n_b)I_n'\\ &\quad=(1/n_b)(\nabla n_1-n_i\nabla\ln n_b)\cdot I_n'+(n_1/n_b)\nabla\cdot I_n'\\ &\quad=(1/n_b)[(\nabla n_1+n_1qE/kT)\cdot(q\mu_n n_1'E+qD_n\nabla n_1')\\ &\qquad\qquad -q(n_1n_1'/\tau)], \end{aligned} \tag{A12}$$

which is seen to be symmetrical.

Letters to the Editor

PUBLICATION of brief reports of important discoveries in physics may be secured by addressing them to this department. The closing date for this department is five weeks prior to the date of issue. No proof will be sent to the authors. The Board of Editors does not hold itself responsible for the opinions expressed by the correspondents. Communications should not exceed 600 words in length.

Anisotropy of Diffusion in Grain Boundaries*

M. R. ACHTER† AND R. SMOLUCHOWSKI
Metals Research Laboratory, Carnegie Institute of Technology, Pittsburgh, Pennsylvania

(Received March 12, 1951)

THE structure and behavior of grain boundaries are subjects of much recent interest. One of the aspects which draws attention is the question to what extent the structure and property of a grain boundary depends upon the relative orientation of the two grains and upon the orientation of the grain boundary itself. The latter effect is rather small and will not be considered here. There is little doubt that the soap bubble analogy, where only the surface tension plays a role, is a rather rough approximation although it is very convenient for a description of the general aspects of grain boundaries, their topology, etc. In connection with a general study of diffusion along grain boundaries new evidence was obtained which indicates strongly that grain boundary tension or energy alone is not sufficient to describe its state and that crystallographic aspects play a vital role.

The experiment consisted in measuring diffusion of silver along grain boundaries of columnar copper (all grains having one cubic axis parallel to a common direction), the amount of penetration being observed by means of differential etching of silver-rich copper. As previously reported,[1] the preferential diffusion along grain boundaries in the columnar direction turned out to be negligible for angles (θ) between the two grains smaller than about 20 degrees, but increased rapidly for greater angles, reaching a maximum at 45°. Since columnar grains are often not ideally parallel and the deviation may reach values as high as 20–30°, in the above-mentioned study only those pairs of grains were considered which were columnar within 7–8°.

In many instances, at a junction of three grains, a grain boundary along which the columnar diffusion is high joins a grain boundary with low columnar diffusion. Such junctions were of particular interest, since it appeared that often silver supplied by the silver-rich boundary diffused into the silver-free boundary. Such diffusion, which occurred naturally in a direction perpendicular to the columnar direction, afforded a comparison of diffusion in the same grain boundary in two mutually perpendicular directions. The situation is best explained with reference to Fig. 1 (a) and (b), in which the plane represents the perspective view of a boundary between two grains. Each of the two grains has one cubic direction almost in the columnar direction (upward), with an angle α enclosed between them. The plane of that angle makes an angle β with the plane of the boundary (in the drawing it is assumed for simplicity that the two planes intersect along a columnar direction). Angle θ is the previously mentioned angle between two other cubic directions. The experiment indicates that whenever β is near a right angle, then for θ and α less than 20° there is no measurable grain boundary diffusion under the particular experimental conditions. For α small and $\theta > 20°$ there is, as previously indicated, appreciable diffusion in the columnar direction but none perpendicular to it. Finally, for θ small and $\alpha > 20°$ there is appreciable diffusion in the direction perpendicular to the columnar direction but none in the columnar direction. If α is large but β is small, i.e., in the case when the grain boundary has to be represented as an array of screw dislocations rather than edge dislocations,[2] the diffusion is very small. It follows that diffusion along a grain boundary is large along edge dislocations whenever the corresponding angle is large enough and is small perpendicular to these dislocations. The ideal directions of such edge dislocations are indicated by dashed lines in the lower portion of Fig. 1 (a) and (b).

It should be noted here that the large angle required to obtain appreciable grain boundary diffusion casts doubt whether there is any appreciable excess mobility of atoms along individual dislocations. At these large angles the distance between the dislocations is so small that the individuality of the dislocation is lost and one should rather imagine the dislocations being bunched up,

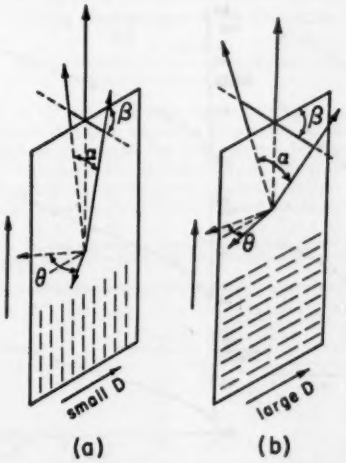

FIG. 1. Dislocations and diffusion in a grain boundary.

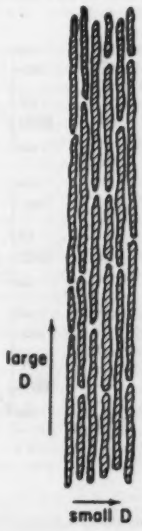

FIG. 2. "Islands of fit" and diffusion in a grain boundary.

forming atomic "channels." The experimental results can be explained perhaps even better by applying Mott's model of a grain boundary.[3] In this picture, which is particularly suitable for angles of the order of 20° and up, the grain boundary is made up of islands of fit surrounded by areas of misfit. The angle between the grains determines the distribution and shape of these islands, as is very schematically illustrated in Fig. 2. The diffusion would occur along the areas of misfit and would always be preferred in a direction parallel to the long axis of the generally elliptical areas of fit. This is, of course, also the direction of the edge dislocations in the other model and agrees with experiment.

* This work was sponsored by an AEC contract; the first author had an AEC Predoctoral Fellowship.

† Now with the Atomic Power Division, Westinghouse Electric Corporation, Pittsburgh, Pennsylvania.

[1] M. R. Achter and R. Smoluchowski, Phys. Rev. **76**, 470 (1949); Proc. Natl. Research Council Conference on "Lattice Imperfections," Pocono Manor, October, 1950.

[2] J. M. Burgers, Proc. Phys. Soc. (London) **52**, 23 (1940); W. T. Shockley, Phys. Rev. **78**, 275 (1950); T. H. van der Merwe, Proc. Phys. Soc. (London) **63**, 616 (1950).

[3] N. F. Mott, Proc. Phys. Soc. (London) **60**, 391 (1948).

Angular Distribution of Protons from $Li^6(d,p)Li^{7*}$, Li^7

D. N. F. Dunbar and F. Hirst
Physics Department, University of Melbourne, Melbourne, Australia
(Received April 12, 1951)

RECENT determinations[1,2] below 1-Mev deuteron energy of the angular distributions of the two groups of protons emitted in this reaction do not agree with one another. Since the forms of the distributions help in the allocation of spin to the excited state of Li^7 near 480 kev, it is important if possible to resolve this difference.

Ilford Type C2 photographic plates have been used in a camera previously described[2] to record the two groups of protons at all angles simultaneously. The total emission of protons at each of 10 angles between 13° and 167° is determined by counting the tracks with a $\frac{1}{4}$" objective and ×6 eyepieces in a binocular microscope. At least two plates are exposed and some 20,000 tracks counted at each energy. The total emission is then divided into the long and short range groups by constructing representative histograms of 600 tracks at five of the ten angles of observation at each deuteron energy. The ratio of long to short range protons varies both with angle and energy. Typical angular distribution curves are shown in Fig. 1.

The angular distributions of the total emission and the long and short range groups are expressed in the form

$$N(\theta)=a_0P_0+a_1P_1+a_2P_2+\cdots+a_sP_s,$$

where $N(\theta)$ is the intensity at an angle θ, P_n is the Legendre polynomial of order n, and a_n is the coefficient of the polynomial of nth order. The coefficients, a_n, are evaluated from

$$a_n=\tfrac{1}{2}(2n+1)\int_{-1}^{+1}N(\theta)P_n d(\cos\theta),$$

by numerical integration using Simpson's rule. When expressions of this form are fitted to the results, it is found that terms as far as a_4P_4 are required to fit the long-range proton curves, while terms as far as a_2P_2 are sufficient for the short-range protons. The simpler expression for the short-range distribution may be partly due to the relatively poor statistics of these results. There is no evidence for the approximate spherical symmetry in the long-range proton distribution at low energies observed by Krone *et al.*[2] The results are of the same form as those of Whaling and Bonner[1] although the asymmetry of the short-range group is more marked in the present results.

The variations of the ratios a_1/a_0, a_2/a_0, a_3/a_0, $\cdots$, with energy for the total emission and the separate groups have been compared with other published results. The agreement between Whaling and Bonner[1] and the present results is in general satisfactory. The greatest discrepancies arise, as may be expected, in the short-range group. Except for a low value at 400 kev, the values of a_1/a_0 for the short-range protons obtained by Whaling and Bonner agree well with the present results, while only the 780-kev point of Krone *et al.* agrees with the other experiments. The values of a_2/a_0 for the short-range protons obtained by both Whaling and Bonner and Krone *et al.* are scattered between 0.2 and −0.2. The present values form a consistent set at about −0.06, however, and appear to be more probable. The decrease in a_1/a_0 observed in all three experiments suggests that the term a_4P_4 is, in fact, significant in the short-range distribution, although this is not substantiated on statistical grounds. The observed distributions indicate that the

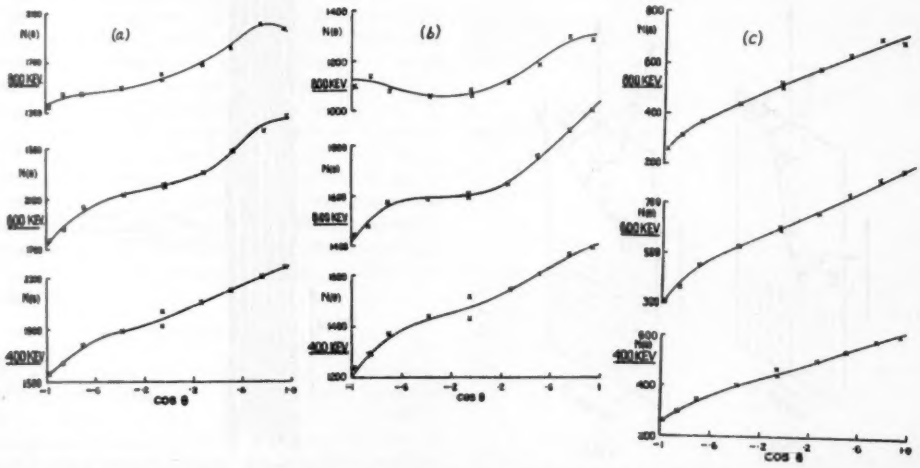

FIG. 1. Relative yield curves (a) for the total proton emission, (b) for the long-range proton group, and (c) for the short-range proton group.

angular momentum of the excited level in Li^7 is $\frac{1}{2}$, rather than 5/2 as suggested by Hanna and Inglis.[5]

The angular distribution of the alpha-particles from the reaction $Li^6(d,\alpha)He^4$ has also been determined for deuteron energies between 200 kev and 1 Mev. The distribution is of the form

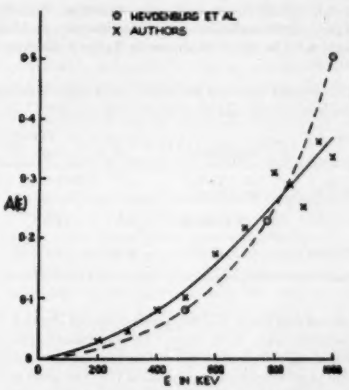

FIG. 2. Variation with energy of the asymmetry in the angular distribution of alpha-particles from the $Li^6(d,\alpha)He^4$ reaction.

$1+A(E)\cos^2\theta$, and the variation of $A(E)$ with energy shown in Fig. 2 confirms the earlier results of Heydenburg *et al.*[4]

A full description of the investigation will appear in the *Australian Journal of Scientific Research*.

[1] W. Whaling and T. W. Bonner, Phys. Rev. **79**, 258 (1950).
[2] Krone, Hanna, and Inglis, Phys. Rev. **80**, 603 (1950).
[3] Martin, Bower, Dunbar, and Hirst, Australian J. Sci. Research **A2**, 25 (1949).
[4] Heydenburg, Hudson, Inglis, and Whitehead, Phys. Rev. **74**, 405 (1948).
[5] S. S. Hanna and D. R. Inglis, Phys. Rev. **75**, 1767 (1949).

Electric Forming in *n*-Germanium Transistors Using Phosphorus-Alloy Contacts

J. P. STELMAK
Radio Corporation of America, Harrison, New Jersey
(Received May 4, 1951)

THE use of temporary large currents through the collector contact of *n*-type transistors to produce permanent improvements in performance has been reported by Bardeen and Brattain.[1] During this forming operation, the role of the contact material, which was stated to be phosphor bronze, was not particularly indicated. Very recently, Pfann[2] has submitted data on the effect of the presence of antimony in the contact material when the contact is electrically formed. With increasing concentration of antimony, a donor impurity, an increase in γ, the current gain, was noted.

Some time ago it was suggested by Mr. L. E. Barton, of RCA Laboratories that the phosphorus content of the collector contact point played an important role in improving transistor gain, when pulse forming was used. Barton's experimental data were of a preliminary kind; the present letter presents more convincing evidence of this hypothesis by tests with specially prepared alloys.

Table I summarizes results obtained with electrical forming of collector contacts containing varying amounts of phosphorus. Average results and range values are given for five transistors in each group in which the collector contact consisted of the copper alloy shown, with emitters of phosphor bronze being the same in all cases.

TABLE I. Pulsing response in transistors to equal pulses applied to collector using phosphorus-alloy collector contacts. Average gain before pulsing = 10 db.

Alloy	Weight % phosphorus	Average power gain after pulsing (db)	Power gain range after pulsing (db)
OFHC Cu (Pure)	0.00	10.5	9–12
No. 3	0.03	17	15–24
No. 5	0.9	24	23–26
No. 7	1.1	25	22–28
Commercial phosphor bronze	0.1	21	20–24

The response to equal forming pulses is presented as the improvement in power gain from an average of 10 db as measured at 5 kilocycles in class *A* amplifier operation. An increase in power gain in all cases was accompanied by an increase in the current gain γ, and in collector current. For comparison, the results obtained with relatively pure OFHC copper and a commercially available phosphor bronze are included. Pulsing response increases rapidly with phosphorus content up to a concentration of about 0.1 percent, beyond which there follows a more gradual rise to what may be a limit.

In another series of experiments, in which phosphor bronze was used for both emitter and collector contacts, the effect of direction of voltage pulse was investigated. In Table II are shown the results

TABLE II. Transistor pulsing response under various conditions of pulsing. Average gain before pulsing = 10 db.

Collector pulsing voltage	Emitter bias voltage during pulsing	Average power gain after pulsing (db)	Power gain range after pulsing (db)
−180 (reverse direction)	0	23	19–24
+22 (forward direction)	0	24	21–25
−90 (reverse direction)	+0.4	22	20–25

of pulsing under the various conditions; the values for each line are the average for five transistors.

As the data show, it has been possible to obtain equivalent effects with voltage pulse in the forward and in the reverse direction; the voltage required in the forward direction is considerably lower since the resistance is also lower in this direction. In both of these cases, the improvement in power gain was accompanied by an increase in reverse current of the pulsed contact, apparently in disagreement with the conclusions of Bardeen and Pfann[3] as to the effect of direction of forming. It has also been observed that the pulsing voltage required to obtain a forming effect is smaller if a positive emitter bias is maintained during forming. This observation is plausible when the effect of positive emitter bias on collector impedance is considered.

In view of these results, pulsing response appears to increase with phosphorus concentration in the contact material and with pulse power input, and, as such, is a function of the heat generated at the point contact. Some fusion at the metal-germanium junction is observable under a microscope after successful forming. A superficial diffusion of phosphorus, or other donor, into the germanium surface under the contact point may account for the change in the height of the potential barrier observed to give increased power and current gain.

[1] J. H. Bardeen and W. H. Brattain, Phys. Rev. **75**, 1209 (1949).
[2] W. G. Pfann, Phys. Rev. **81**, 882 (1951).
[3] J. H. Bardeen and W. H. Brattain, Phys. Rev. **77**, 401 (1950).

Dual Decay of the 50-Day In^{114} Isomer and Angular Momenta of the Excited States of Cd^{114}

ROLF M. STEFFEN
*Department of Physics, Purdue University, Lafayette, Indiana**
(Received May 11, 1951)

ACCORDING to recent measurements[1,2] the 72-sec ground state of In^{114} decays not only by β^- emission into Sn^{114} but also by K-capture and β^+ emission into an excited state of Cd^{114}, from which two successively emitted gamma-rays of 0.548- and 0.715-Mev energy lead to the ground state. A very weak gamma-ray of 1.26-Mev quantum energy has been interpreted as caused by a cross-over transition. Using the measured energy difference between the ground states of In^{114} and Cd^{114} of 2.07 ± 0.2 Mev,[3] the ft value of the K-decay from the In^{114} ground state into the 1.26-Mev level of Cd^{114} comes out to be $\sim$1200. This small value would indicate a superallowed transition, which seems to be improbable in this case. Thus, the question arises as to whether this K-decay originates from the 50-day isomeric state of In^{114}. Since this decay process would require an angular momentum of 4 or 5 for the 1.26-Mev level of Cd^{114}, whereas the K-capture from the In^{114} ground state is only compatible with $I=1$ or $I=2$, a determination of the angular momentum of this Cd level would give decisive information.

By measurement of the angular correlation of the two successively emitted gamma-rays the angular momenta of the two excited levels of Cd^{114} have been investigated.[4] The result of the correlation measurements, obtained with the previously described apparatus,[5] are shown in Fig. 1. The measured points follow, within experimental error, the angular correlation function $f(\theta)=1+0.125\cos^2\theta+0.042\cos^4\theta$, which is characteristic for two quadrupole transitions between states of angular momenta of 4, 2, and 0. The angular momentum 4 of the 1.26-Mev level supports strongly the assumption that this level is reached directly from the 50-day isomer. The ft value, 3×10^8 sec, of this K-decay suggests a first-forbidden transition.

The ft value, 3×10^4 sec, of the β^- decay gives evidence of an allowed transition to the ground state of the even-even nucleus Sn^{114} of zero angular momentum and presumably even parity. Hence, $I=1$ and even parity must be assigned to the ground state of In^{114}. The observed positrons must be due to the beta-transition from the ground state of In^{114} to the ground state of Cd^{114}. The ft value ($\sim10^8$ sec) suggests an allowed transition, indicating again even parity and $I=1$ for the In^{114} ground state. In order to determine the angular momentum and the parity of the 50-day isomeric state, the multipole character of the isomeric transition must be known. Since the previously measured conversion data are not conclusive, the conversion of the 0.192-Mev isomeric transition has been measured in two ways: (a) by comparison of the conversion lines and the β^--spectrum in a spectrometer and (b) by comparison of the absolute number of β-transitions determined in a calibrated spectrometer with the absolute intensity of the 0.192-Mev gamma-radiation using calibrated scintillation and GM-counters.[6] The result is shown in Table I. Besides the theoretical conversion data[7] the table also contains the half-life values of the isomeric state with respect to gamma-emission calculated from Weisskopf's formula.[8] Since the relativistic calculations for α_K are the most reliable, it is concluded that the isomeric transition is an electric 2^4-pole, indicating an angular momentum of 5 and even parity of the isomeric state. The Weisskopf theory gives about 1000 times too large a transition probability for the electric 2^4-pole. The presumably first-forbidden transition to the 1.26-Mev level of Cd^{114} makes it necessary to assign an odd parity to this level.

TABLE I. Conversion data and half-life of the isomeric transition in In^{114}.

	Experiment	Theory el. 2^4	Theory magn. 2^4	Theory el. 2^5
$\alpha_K=N_{eK}/N_\gamma$	(a) 2.4 ± 0.4 (b) 2.2 ± 0.2	2.5	11	57
α_K/α_L	1.10 ± 0.05	2.4	5.5	1.0
$T_{1/2}$gamma, sec	2.1×10^7	3.3×10^4	3.2×10^7	8.7×10^{10}

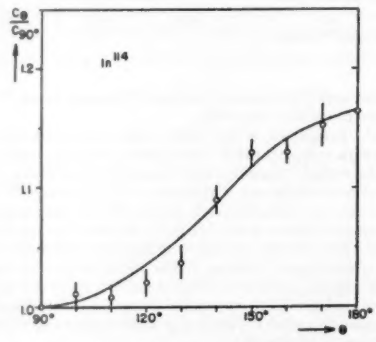

FIG. 1. Angular correlation of the gamma-rays emitted from the Cd^{114} nucleus. The points at $\theta=170°$ and $\theta=180°$ are corrected for the small number of positrons present in the In^{114} decay.

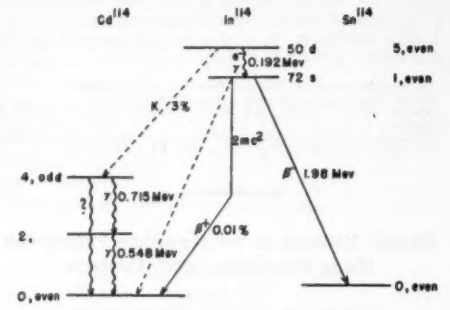

FIG. 2. Disintegration scheme of In^{114}.

Our assignments (Fig. 2) would give for the cross-over transition to the ground state of Cd^{114} a relative intensity $<10^{-7}$, whereas a relative abundance of a few percent has been reported.[9] This makes the interpretation of the 1.26-Mev γ-ray as a cross-over transition doubtful. The final parity assignments to the Cd^{114} levels involved will be made by polarization-correlation experiments which are in progress at this laboratory.

* Supported in part by the AEC.
[1] F. Boehm and P. Preiswerk, Helv. Phys. Acta **22**, 331 (1949).
[2] Mei, Mitchell, and Zaffarano, Phys. Rev. **76**, 1883 (1949).
[3] C. L. McGinnis, Phys. Rev. **81**, 734 (1951).
[4] The In^{114} source has been obtained by the Isotopes Division of the U. S. AEC, Oak Ridge.
[5] Rolf M. Steffen, Phys. Rev. **80**, 115 (1950).
[6] Hart, Russell, and Steffen, Phys. Rev. **81**, 460 (1951).
[7] Rose *et al.*, *Tables of K-Shell Internal Conversion Coefficients* (privately distributed); N. Tralli and I. S. Lowen, Phys. Rev. **76**, 1541 (1941).
[8] V. F. Weisskopf and J. M. Blatt, privately circulated notes, to appear as part of a book on nuclear physics.

Cross Section for Production of Charged π-Mesons in C and H at 90° to a 381-Mev Proton Beam*

M. M. Block, S. Passman, and W. W. Havens, Jr.
Columbia University, New York, New York
(Received May 14, 1951)

A METHOD for measuring the absolute differential production cross section for charged π-mesons has been devised, utilizing the internal 381-Mev proton beam of the Nevis cyclotron. Ilford C2 nuclear emulsions, imbedded in tapered copper and aluminum absorbers, are placed inside the vacuum chamber, 2½" below the target. The geometric arrangement limits the acceptance angles of mesons to 90°±10° to the proton beam direction. The energy interval from 0 to 125 Mev is included in a single 1"×3"×200-micron emulsion. The energy of the mesons is determined from their range in absorber.

The positron annihilation radiation from C^{11}, produced in the reaction $C^{12}(\dot{p}, \dot{p}n)C^{11}$, was used to monitor the exposure. The exposed targets were placed in a standard geometry in a lead shield, with an aluminum converter inserted between the target and a thin end-windowed Geiger tube. The geometry and counter efficiency were determined by calibrating the beta-activity of a solution of Cu^{64} relative to a known RaD+E source of the Bureau of Standards. An absolute calibration was made by coating a known volume of Cu^{64} on the surface of a polyethylene target and measuring its annihilation radiation. The number of protons traversing the target was calculated from the cross section for the C^{11} reaction at 381 Mev, obtained by extrapolating the known data at lower energies.[1]

The plates were scanned under high resolution oil immersion objectives. Only mesons ending in the emulsion and undergoing $\pi-\mu$ decay or star-formation are included in the results. The number of π^+ mesons is directly obtainable from the number undergoing $\pi-\mu$ decay in the emulsion, whereas the number of π^- mesons must be corrected for zero-prong stars and is given by 1.37 times the number of stars found in the emulsion.[2]

The number of mesons detected was corrected for loss due to nuclear interaction in the absorber block. The cross section used for the loss is the geometric area of the nucleus of the absorbing material.[3,4] In addition to the statistical error, the absolute cross sections are subject to a further error of about 15 percent because of uncertainties in calibration of the activity produced in the target, thickness of emulsion before development, and C^{11} production cross section.

A 0.3-g/cm² carbon target was exposed for 2.5 minutes in an average beam current $\sim 5\times10^{-10}$ amp. Figures 1 and 2 show the 90° differential cross section $d^2\sigma/d\omega dE$ for production of π-mesons by 381-Mev protons on carbon. The spectra are based on 550 $\pi-\mu$ decays and 29 observed meson-produced stars.

The π^+ cross section, integrated over meson energy, $d\sigma^+/d\omega$, is $(5.2\pm1.3)\times10^{-28}$ cm² steradian^{-1} carbon nucleus^{-1}, and the integrated π^- cross section is given by $d\sigma^-/d\omega=(4.6\pm1.9)\times10^{-28}$

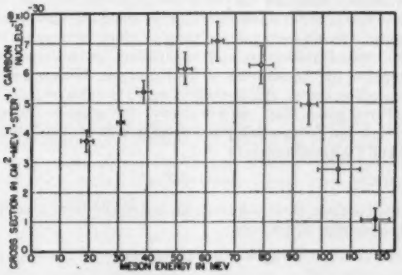

FIG. 1. Differential cross section for π^+ mesons produced in carbon at (90°±10°) from a 381-Mev proton beam (corrected for nuclear absorption).

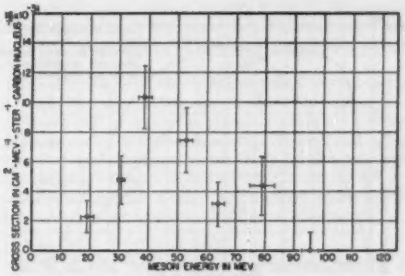

FIG. 2. Differential cross section for π^- mesons produced in carbon at (90°±10°) from a 381-Mev proton beam (corrected for nuclear absorption).

cm²-steradian^{-1} carbon nucleus^{-1}. The ratio of the two integrals $(d\sigma^+/d\omega)/(d\sigma^-/d\omega)=11\pm3$. A preliminary cross section at 90° for the production of positive mesons by protons in hydrogen was found to be $d\sigma(90°)/d\omega=(5.0\pm1.2)\times10^{-28}$ cm² steradian^{-1} by using a polyethylene target and subtracting off the carbon contribution. While spectral resolution is limited by the energy spread in the beam, estimated to have an upper limit of 8 Mev, and the spread due to the low energy mesons losing a considerable fraction of their energy in the target, the total cross section should not be affected appreciably.

We wish to thank Dr. C. S. Wu for her aid in the absolute beta-calibration of our monitoring apparatus.

* This work was assisted by the joint program of the ONR and AEC.
[1] Aamodt, Peterson, and Phillips, UCRL 326 (1949) (unpublished).
[2] F. L. Adelman and S. B. Jones, Phys. Rev. **75**, 1468 A (1949).
[3] Bernardini, Booth, Lederman, and Tinlot, Phys. Rev. **80**, 924 (1950).
[4] Isaacs, Steinberger, and Sachs (private communication).

Analysis of Charged Meson Production by Protons*

S. Passman, M. M. Block, and W. W. Havens, Jr.
Columbia University, New York, New York
(Received May 14, 1951)

THE differential production cross section for π^+ mesons in hydrogen by 343-Mev protons, as measured in Berkeley,[1] exhibits a $\cos^2\theta$ angular dependence in the center-of-mass system, with the meson receiving approximately the maximum available kinetic energy. Using these assumptions and the absolute cross section at 0°,[2] we calculate the total π^+ production cross section at 343 Mev to be $(2.9\pm0.4)\times10^{-28}$ cm². Using our preliminary result for the π^+ production cross section in hydrogen at 90° to a beam of 381-Mev protons,[3] with the same assumptions as above, we obtain the total cross section as $(7.3\pm2.3)\times10^{-28}$ cm². The ratio (σ_{π^+}) at 381 Mev/(σ_{π^+}) at 343 Mev $=2.5\pm0.8$, is consistent with the theory of meson production for matrix elements that depend linearly on the meson momentum.[4]

The π^+ meson differential production cross section from a heavy nucleus was calculated using the following assumptions:

(a) Meson production occurs in a heavy nucleus through nucleon-nucleon interactions.

(b) The momentum distribution of target nucleons before collision is based upon a Fermi degenerate gas model, with a maximum energy of 22 Mev.

(c) The final state nucleon-nucleon interaction requires the meson to receive all the available kinetic energy, T_{max}, in the center-of-mass system. This implies a density of final states proportional to $(T_{max})^{\frac{1}{2}}$.

Figures 1 and 2 show the calculated 90° meson energy distributions obtained by using nucleon-nucleon cross sections containing matrix elements that are either constant (type A), or

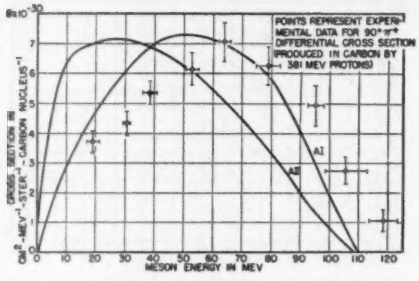
POINTS REPRESENT EXPERIMENTAL DATA FOR 90°π⁺ DIFFERENTIAL CROSS SECTION PRODUCED IN CARBON BY 381 MEV PROTONS
AI
AII
MESON ENERGY IN MEV

FIG. 1. Curve AI is theoretical π^+ differential cross section with constant matrix elements and isotropic production in center-of-mass system. Curve AII is theoretical π^+ differential cross section with same matrix elements and $\cos^2\theta$ angular dependence in center-of-mass system.

proportional to $(T_{\max})^{\frac{1}{2}}$ (type B), and summing over the Fermi momentum distribution. The calculations of type B are in good agreement with our experimental results[3] for carbon at 381 Mev with regard to general shape and location of the peak of the spectrum.

The theoretical curves of type B at 343 Mev are also in good agreement with experiment when the spectral shapes of the 343-Mev 90° π^+ meson energy distributions from carbon and lead[5] are altered by correction for a geometrical nuclear absorption cross section. Although the theoretical curves are arbitrarily normalized to give the experimental total 90° cross section for each bombarding energy, the type BI calculation predicts an increase in this cross section of 1.6 from 343 Mev to 381 Mev, consistent within the statistical error with the experimentally determined ratio of 2.1 ± 0.7. It is interesting to note that, while the positive meson cross section increases by the factor just given, the total 90° negative meson cross section does not increase significantly in changing the incident proton energy from 343 Mev to 381 Mev. This increase in the π^+/π^- ratio with increasing proton energy is in the opposite direction to the behavior predicted from exclusion principle arguments.[6]

The assumption of no interaction in the final nucleon states, with a resulting density of states proportional to $[T(T_{\max}-T)]^{\frac{1}{2}}$, and either constant or energy dependent matrix elements,[7] results in a much poorer fit to the 343-Mev and 381-Mev experimental data, when corrected for nuclear absorption.

If one uses an experimentally determined carbon momentum distribution from the pick-up effect,[8] instead of a Fermi distribution, the theoretical π^+ meson energy spectrum of type BI fits well, and explains the experimentally observed high energy tail.

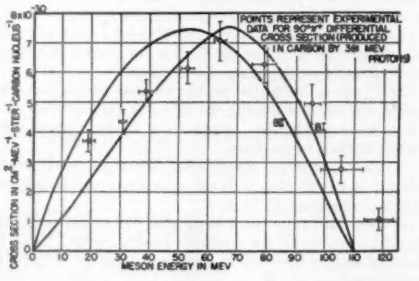
POINTS REPRESENT EXPERIMENTAL DATA FOR 90°π⁺ DIFFERENTIAL CROSS SECTION (PRODUCED IN CARBON BY 381 MEV PROTONS)
BI
BII
MESON ENERGY IN MEV

FIG. 2. Curve BI is theoretical π^+ differential cross section using Fermi distribution for nucleons with matrix elements proportional to $(T_{\max})^{\frac{1}{2}}$ for isotropic production in center-of-mass system. Curve BII is theoretical π^+ differential cross section with same matrix elements and a $\cos^2\theta$ angular dependence in the center-of-mass system.

In conclusion, analysis of π^+ meson production by protons in hydrogen and in carbon suggests that the matrix elements for this process are linearly proportional to the meson momentum and that the meson receives approximately the maximum available kinetic energy in the center-of-mass system.

* This work was assisted by the joint program of the ONR and AEC.
[1] Results of Cartwright, Richman, Whitehead, Wilcox, Peterson, Iloff, and Sherman, as quoted by Watson and Brueckner in UCRL-856 Rev. (1950), and by private communication from C. Richman.
[2] Data of Cartwright, Richman, Whitehead, and Wilcox (private communication), corrected for a geometrical nuclear absorption cross section.
[3] Block, Passman, and Havens, Phys. Rev. **83**, 167 (1951).
[4] K. M. Watson and K. A. Brueckner, UCRL-856 rev. (1950).
[5] C. Richman and H. A. Wilcox (carbon), Phys. Rev. **78**, 496 (1950); M. Weissbluth (lead), Ph.D. thesis UCRL 568.
[6] G. F. Chew and J. L. Steinberger, Phys. Rev. **78**, 497 (1950).
[7] Analogous to the calculation of T. B. Taylor and G. F. Chew, Phys. Rev. **78**, 86A (1950).
[8] G. F. Chew and M. L. Goldberger, Phys. Rev. **77**, 470 (1950).

The Interaction of Lattice Vibrations with Electrons in a Metal

GREGOR WENTZEL
Institute for Nuclear Studies, University of Chicago, Chicago, Illinois
(Received December 4, 1950)

BARDEEN[1] and Fröhlich[2] have advocated the view that the phenomenon of superconductivity is basically dependent on a strong interaction between the electrons and the vibrations of the crystal lattice. The observation that the critical temperature varies with the isotopic weight lends support to such a view. As a first step in the theoretical investigation, the question has been studied how the ground state of an electron gas is affected by the interaction with the lattice vibrations or sound waves. Energetically, the pertinent quantity is the self-energy of the electron gas due to a virtual emission and re-absorption of phonons. Fröhlich,[3] calculating this self-energy by second-order perturbation theory, finds that certain modifications of the unperturbed ground state, which may suggest the existence of superconductive states, are energetically favored provided the coupling strength exceeds a certain minimum value. Using Fröhlich's notation, let ν be the number of free electrons per atom in the lattice and F a dimensionless quantity, proportional to the square of the coupling strength and involving, besides the atomic mass, the velocity of (longitudinal) sound and electronic quantities [see Eq. (2.9) in reference 2]. Then the stated condition for superconductivity reads

$$\begin{aligned} 4\nu^{\frac{1}{2}}F>1 \quad &\text{if} \quad \nu>\tfrac{1}{4}, \\ 4\nu F>1 \quad &\text{if} \quad \nu<\tfrac{1}{4} \end{aligned} \tag{1}$$

[see Eq. (3.19) in reference 2].

One may doubt whether the perturbation method provides a good enough approximation if the interaction is so strong. As a criterion, it may be asked how strongly the velocity of a longitudinal sound wave is affected by the interaction with the electrons. This means calculating the correction $\delta\omega$ to the frequency ω of a sound wave of given wave number k or, using the quantized field language, the self-energy of a phonon of given momentum $\hbar k$ due to its virtual absorption and re-emission, or emission and re-absorption, by the electrons of the Fermi gas. With second-order perturbation theory, this is easily done for the ground state of the gas (Fermi sphere filled, outside empty); but actually, the result is true even for Fermi equilibrium distributions at "low" temperatures ($KT\ll$Fermi energy):

$$\delta\omega=-2\nu F\omega. \tag{2}$$

(Actually, there is, in addition, an imaginary term describing a true absorption of phonons:

$$\delta\omega=-2\nu F(1+is\pi/2v)\omega, \tag{2'}$$

where s = sound velocity, v = Fermi boundary velocity. It has been assumed that $s\ll v$, and also $\hbar k\ll mv$.)

Equation (2) means that the longitudinal sound velocity

$s=(\omega+\delta\omega)/k$, as compared with its unperturbed value $s_0=\omega/k$, is given by

$$s=s_0(1-2\nu F+\cdots). \tag{3}$$

Clearly, a rapid convergence of the perturbation expansion requires

$$2\nu F\ll 1$$

which excludes Fröhlich's cases (1). Taking the second-order approximation literally, one would conclude from (1) and (3): $s<s_0/2$ for all values of ν, and even $s<0$ for $\nu>2^3$, which is absurd.

What actually happens with the lattice vibrations if $2\nu F\gtrsim 1$ becomes clearer by studying a one-dimensional model of a metal, *viz.*, a linear lattice allowing phonons and electrons to propagate in two opposite directions only. Supposing the electron gas to be close to the ground state, in the sense that the interactions affect only electrons with velocities near the Fermi boundary velocities ($\pm v$), it is then possible, according to Tomonaga,[2] to describe the electrons in terms of an equivalent boson gas[4] whose hamiltonian is of the familiar form

$$H_e=\tfrac{1}{2}\Sigma_k\,(P_k^*P_k+\Omega_k^2Q_k^*Q_k). \tag{4}$$

Here, Q_k is the amplitude of a density wave:

$$\int dx\exp(-ikx)\sum_{p=1,2}\psi_p^*\psi_p,$$

except for a normalization factor, and P_k is the canonically conjugate quantity as defined by Tomonaga [see Eqs. (3.4) and (3.5) in reference 3]. For the phonons (lattice vibrations) we have similarly

$$H_s=\tfrac{1}{2}\Sigma_k\,(p_k^*p_k+\omega_k^2q_k^*q_k). \tag{5}$$

The wave number-frequency relations in the two cases are

$$\Omega_k=vk,\quad \omega_k=sk. \tag{6}$$

Now, the electron-lattice coupling can be simply described by adding the interaction term

$$H_i=\tfrac{1}{2}\Sigma_k\,c_k(Q_k^*q_k+Q_kq_k^*). \tag{7}$$

Indeed, the operator $Q_k^*q_k$ corresponds to a process in which any electron acquires a momentum $\hbar k$ by absorption or emission of a phonon of momentum $\pm\hbar k$. Disregarding other interactions for the time being, we have for the total hamiltonian

$$H=H_e+H_s+H_i. \tag{8}$$

Because H is bilinear in the canonical variables, rigorous solutions are readily obtained by transforming to normal coordinates. The freqdencies of the normal vibrations are

$$2^{-\frac{1}{2}}[\Omega_k^2+\omega_k^2\pm\{(\Omega_k^2-\omega_k^2)^2+4c_k^2\}^{\frac{1}{2}}]^{\frac{1}{2}}. \tag{9}$$

In the limit of weak coupling, $c_k\to 0$, this means that the sound frequencies ω_k are reduced by a factor

$$1-c_k^2(2\omega_k^2|\Omega_k^2-\omega_k^2|)^{-1}+\cdots, \tag{10}$$

corresponding to the factor $(1-2\nu F+\cdots)$ in (3). (The expression (10) is independent of k because $c_k\sim k^2$.) As the coupling strength increases and the factor (10) approaches the value $\frac{1}{2}$, the rigorous expression (9) indicates that the proper frequencies become imaginary for

$$|c_k|>\Omega_k\omega_k. \tag{11}$$

The proper vibrations are then unstable, in the sense that the potential energy of the coupled oscillators no longer has a true minimum value at the equilibrium position ($Q_k=q_k=0$); the corresponding surface becomes saddle-shaped. As a consequence, the lattice would break down.[5]

From this result it is obvious that the hamiltonian (8) is entirely inadequate for the study of the strong coupling case. Other energy terms restoring the stability must be taken into account. One such stabilizing term is the coulomb interaction of the electrons which in our variables is simply[6]

$$H_c=\text{const}\;\Sigma_k\,Q_k^*Q_k\quad(>0)$$

except for an additive constant. Adding H_c to H_s (4), amounts to replacing Ω_k^2 in (4) by $(v^2k^2+\text{const})$ (or attributing a rest-mass to the Bloch-Tomonaga bosons). This insures the stability at least for the low k-values.

A fuller discussion of the one-dimensional model is hardly worth while. For the electron gas in three dimensions no such simple description in terms of bosons is available, but similar complications are to be expected, as even the perturbation theory indicates that the velocity of sound tends toward zero with increasing coupling strength. This makes it imperative to improve the hamiltonian as well as the mathematical technique if the strong coupling assumption is to be taken at all seriously.

[1] J. Bardeen, Phys. Rev. **79**, 167 (1950).
[2] H. Fröhlich, Phys. Rev. **79**, 845 (1950).
[3] S. Tomonaga, Prog. Theor. Phys. **5**, 544 (1950). See also F. Bloch, Helv. Phys. Acta **7**, 385 (1934). Sec. 4.
[4] The specific heat of the one-dimensional boson gas is proportional to T, and it is actually equal to that of the electron gas because

$$\int_0^\infty dx\times(e^x-1)^{-1}=2\int_0^\infty dx\times(e^x+1)^{-1}.$$

[5] As Mrs. M. G. Mayer tells me, this fact was known to her and E. Teller some years ago, and it was for this reason that they gave up an attempt to explain superconductivity on the basis of strong electron-lattice interactions.
[6] See S. Tomonaga, reference 3, Eq. (3.10). Our Q_k is identical with Tomonaga's $\rho_n(L/2\pi n)(n/2n_{max})^{\frac{1}{2}}(k=2\pi n/L)$. Note that for the coulomb potential $J_n\sim n^{-1}$.

Erratum: Determination of the Photo-Nuclear Cross Sections $S^{32}(\gamma,d)P^{30}$, $S^{32}(\gamma,n\dot{p})P^{30}$, and $P^{31}(\gamma,n)P^{30}$

[Phys. Rev. **81**, 815 (1951)]

L. Katz and A. S. Penfold
Department of Physics, University of Saskatchewan, Saskatoon, Saskatchewan, Canada

An error was discovered in the computation of the $S^{32}(\gamma,\frac{n}{d}P)P^{30}$ cross section in the paper of the above title. The activation curve as published in Fig. 2 is correct, but the cross section, as well as the integrated cross section calculated from it, should be larger by a factor of 4. (The ordinate of Fig. 5 should be multiplied by 4.)

The larger contribution to the total photoneutron flux from the $(\gamma,n\dot{p})$ reaction is now in better agreement with that predicted by Cameron[1] for this region of the periodic table.

[1] A. G. W. Cameron, Phys. Rev. **82**, 272 (1951).

Response of Some Scintillation Crystals to Heavy Particles*

C. J. Taylor,† M. E. Remley, W. K. Jentschke, and P. G. Kruger
Department of Physics, University of Illinois, Urbana, Illinois
(Received May 18, 1951)

A relatively small amount of information has been reported concerning the response of scintillation crystals to heavy particles,[1-4] but knowledge of this kind is essential to the successful employment of the scintillation counter technique for quantitative energy measurements of heavy particles.

Protons of 1 to 5 Mev, deuterons and molecular hydrogen ions of 1 to 11 Mev, alpha-particles of 4 to 21 Mev from the University of Illinois cyclotron, and polonium alpha-particles were used in the measurements to be described. The response of anthracene, stilbene, and thallium activated sodium iodide to these particles has been investigated.

The collimated beam from the cyclotron was brought out into air through a thin Nylon window and allowed to strike the scintillating crystal which was mounted in optical contact with an RCA 5819 photomultiplier tube and covered with a 0.16 mg/cm² aluminum foil for a reflector. Aluminum absorbing foils were interposed in the beam to obtain the various particle energies incident on the crystals. Pulses from the photomultiplier were

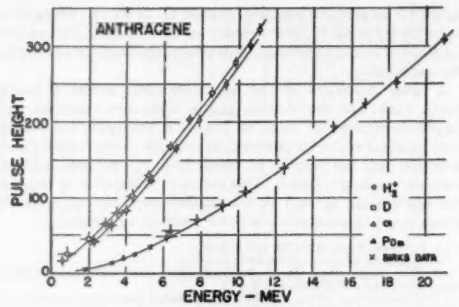

FIG. 1. Response of anthracene to molecular hydrogen ions, deuterons, and alpha-particles. Note that the molecular hydrogen ions are detected as two protons entering the crystal simultaneously.

amplified by a Los Alamos model 100 linear pulse amplifier and analyzed with a twelve-channel pulse amplitude analyzer. Essentially gaussian distributions were obtained with full widths at half-maxima of six to eight percent for the higher energy particles. The determination of the maximum energy of the incident particles accurate to one percent was obtained by measurement of the ranges in air.

The variation of the peak pulse height with energy for the different particles and crystals used is shown in Figs. 1 to 3. The vertical lines indicate estimates of the errors in the pulse heights. As the energy of the particles is reduced by the introduction of absorbers, the initial one percent uncertainty in the maximum energy produces progressively larger uncertainties in the calculated energies of the lower energy particles. The horizontal lines attached to the points show the total variation in energy at a given energy corresponding to a variation of one percent in the initial energy. These are not to be interpreted as errors in the determination of the energies, but rather as the amount by which the entire curve would be translated in energy for a one percent change in the initial energy.

The figures show a distinct difference in the behavior of the organic crystals and sodium iodide. The organic crystals have a nonlinear response of pulse height to energy in the entire region investigated. In sodium iodide protons and deuterons give linear response, while alpha-particles show a nonlinear relation over a low energy region with a linear response above an energy of about 10 Mev. This nonlinear response of the sodium iodide is certainly not due to deterioration of the crystal surface as has

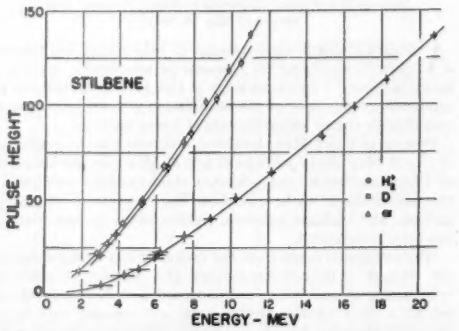

FIG. 2. Response of stilbene to molecular hydrogen ions, deuterons, and alpha-particles. The arbitrary pulse-height scale is the same as in Fig. 1.

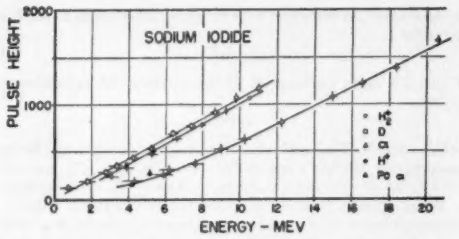

FIG. 3. Response of thallium activated sodium iodide to molecular hydrogen ions, deuterons, and alpha-particles. The arbitrary pulse-height scale is the same as in Figs. 1 and 2.

been proved by experiments with crystals freshly cleaved in a vacuum.

A detailed analysis shows the nonlinearity to be dependent on the ionization density produced by the incident particle. For high specific energy losses, as for example for alpha-particles below 9 Mev, the specific fluorescence (the number of light quanta emitted per centimeter of air equivalent) attains a constant value and is then independent of the specific energy loss.[5]

While this letter was being written, the work of Frey, *et al.*,[6] was reported, which agrees with the results described here.

The authors wish to thank A. L. Atkins, R. O. Kerman, and W. E. Kreger, who determined the cyclotron beam energy.

A more detailed analysis of the data presented here will be published later.

* Assisted by the joint program of the ONR and AEC.
† Now at North American Aviation, Inc.
[1] Harding, Flowers, and Eppstein, Nature **163**, 990 (1949).
[2] E. G. Michaelis, Helv. Phys. Acta **23**, Sup. 3, 155 (1950).
[3] J. B. Birks, Proc. Phys. Soc. (London) **63**, 1294 (1950).
[4] Franzen, Peele, and Sherr, Phys. Rev. **79**, 742 (1950).
[5] W. Cross of Chalk River Laboratory, in a private communication, has reported results in essential agreement with those reported here.
[6] Frey, Grim, Preston, and Gray, Phys. Rev. **82**, 372 (1951).

The Fluorescence Efficiencies of Some Crystals for Electrons and Heavy Particles*

W. K. JENTSCHKE, F. S. EBY, C. J. TAYLOR,†
M. E. REMLEY, AND P. G. KRUGER
Department of Physics, University of Illinois, Urbana, Illinois

(Received May 18, 1951)

THE investigation described in the preceding paper was extended to a study of the fluorescence of anthracene, stilbene, and thallium activated sodium iodide crystals with incident monoenergetic electrons. This extension was particularly directed toward an investigation of the fluorescence efficiency of crystals to electrons as compared to heavy particles with the same specific energy loss. For this reason, electrons with energies of 500 to 5000 ev were used. A pulsed monoenergetic electron beam was provided by a specially constructed cathode-ray gun for examination of this region. The electron beam was focused on the crystal which was mounted on the end of a charge collector. This collector was connected to a vibrating reed electrometer.[1]

The electron beam was pulsed at a rate of ten thousand per second with pulse durations of 0.5 and 2.0 microseconds. Identical results were obtained with both types of pulses, indicating that no long-lived fluorescence of appreciable intensity could have been present. The maximum electron beam current was less than 5×10^{-13} ampere, so that no more than 300 electrons were incident on the crystal during any single pulse. Since the electron beam was defocused over an area of 4 mm² on the crystal, the mechanism for producing fluorescence was the same as for single electrons. The secondary emission coefficients of the crystals used are greater than one for the electron energies investigated, so that no sig-

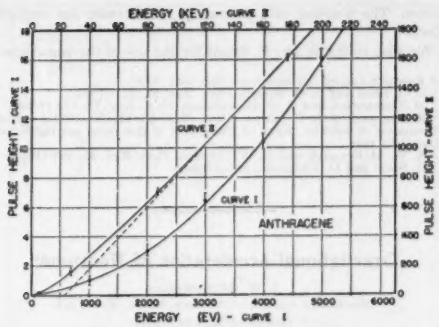

FIG. 1. Response of anthracene to electrons.

nificant charge collection should occur on these insulating crystals. The number of elastically scattered electrons which do not contribute to the pulse height was less than ten percent. The measured pulses were normalized using the conversion electrons of a Cs^{137} source which could be located with the same geometry as the electron beam.

Amplified pulses from the RCA 5819 photomultiplier tube were photographed on a Tektronix high speed oscilloscope. To extend the data of these low energy electrons, internal conversion electrons with energies from 27 kev to 624 kev were obtained from radioactive sources of Te^{137}, Nb^{91}, Hg^{203}, In^{114}, and Cs^{137}. The pulses from these electrons were analyzed with a twelve-channel pulse amplitude analyzer.

The pulse height *vs* energy curves are given in Figs. 1 and 2. The linear portions of the curves for anthracene and stilbene extrapolate to an intercept of about 22 kev on the energy axis, this agreeing with Hopkins' investigation of anthracene.[2] Sodium iodide shows a linear response throughout the energy region from 1000 ev to 624 kev, in agreement with the Stanford group,[3] while below 1000 ev there are indications of a small deviation from linearity.

The response of the anthracene crystal, whose behavior is probably typical of the organic crystals, to different ionizing radiation has been compared in Fig. 3 by considering the variation of the specific fluorescence dL/dx (expressed in arbitrary units per cm air equivalent) with the specific energy loss.

Both the heavy particles and electrons seem to give a region of linear response (the specific fluorescence increasing linearly with energy) but starting at quite different values of dE/dx. At some larger dE/dx, the response becomes nonlinear for both types of particles, and at even larger values of dE/dx the specific

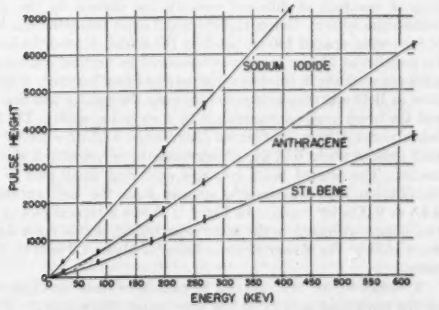

FIG. 2. Response of anthracene, stilbene, and sodium iodide to electrons.

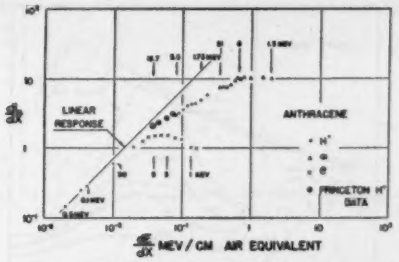

FIG. 3. Dependence of the fluorescence efficiency upon the specific energy loss for heavy particles and electrons in anthracene.

fluorescence saturates. The data for electrons of less than 1000 ev indicate a decrease in dL/dx, but these effects might be due to surface influences of the crystal since the range of a 1000-ev electron in anthracene is only 2.5×10^{-6} cm. However, we do not believe that the different results for the electrons and heavy particles could be due to surface effects, since x-rays of 27 kev which produce electrons inside the crystal gave agreement with the above results.

The valuable assistance of Mr. Chester Lob and the use of the facilities of the Tube Laboratory of the Electrical Engineering Department are deeply appreciated. A complete account of this work will appear at a later date.

* Assisted by the joint program of the ONR and AEC.
† Now at North American Aviation, Inc.
[1] Palevsky, Swank, and Grenchik, Rev. Sci. Instr. **18**, 298 (1947).
[2] J. I. Hopkins, Rev. Sci. Instr. **22**, 29 (1951).
[3] West, Meyerhof, and Hofstadter, Phys. Rev. **81**, 141 (1951).

Coherent Neutron Scattering Cross Section of V^{51}*

A. W. McREYNOLDS
Brookhaven National Laboratory, Upton, New York
AND
R. J. WEISS
Watertown Arsenal, Watertown, Massachusetts
(Received May 11, 1951)

ALTHOUGH the total thermal neutron scattering cross section for vanadium is 5.0 barns, comparable to other nuclei, the coherent part, σ_{coh}, is an order of magnitude less than any other nucleus studied. Shull and Wollan[1] give $\sigma_{coh}<0.1$ barn, since it was too low to be measured by diffraction methods. As V is monoisotopic (spin 7/2), this almost complete incoherence can be accounted for by assuming the two spin scattering amplitudes ($J=3$, $J=4$) times their weight factors ($\frac{7}{16}$, $\frac{9}{16}$) to be equal in magnitude and opposite in sign. Hamermesh and Muehlhause[2] have computed $\sigma_{coh}=0.03b$ (negative phase) using data on the 2700-ev scattering resonance.[3]

The coherent cross section has been determined by the total reflection of a thermal neutron beam from a mirror surface of vanadium. Using a technique previously described by one of us[4] σ_{coh} was compared to σ_{coh} of N_2 (=9.1 barns)[1] by observing the decrease in reflectivity as the pressure of nitrogen gas surrounding the mirror was increased until its index of refraction equaled the index of refraction of vanadium, giving no reflection. The difference from unity, δ, of the index of refraction of solids is given by

$$\delta=n\sigma_{coh}\lambda^2/4\pi^2,$$

where n=number of nuclei/cc. This formula has been verified for gases.[5]

Figure 1 shows the reflection from a 1-min wide beam, incident at ~2.5 min on a 2.5-in. diameter mirror at different gas pressures. In Fig. 2 is shown the reflected intensity of the entire beam,

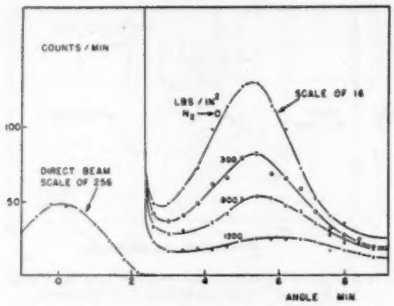

FIG. 1. Thermal neutron beam incident at about 2.5-min angle on vanadium-nitrogen interface and reflected beam at various pressures of N_2.

corrected for background and for scattering in the gas, as a function of pressure. The reflected beam contains all neutrons of wavelength

$$\lambda > \lambda_c = \theta/(2\pi^{\frac{1}{2}})(n_0\sigma_0^{\frac{1}{2}} - n\sigma^{\frac{1}{2}})^{\frac{1}{2}}$$

in the long wavelength portion of the pile flux, $N(\lambda)d\lambda \approx d\lambda/\lambda^5 \times$constant; n and n_0 are nuclei/cc in the gas and mirror, respectively; θ is the incident angle, and λ_c is the critical wavelength. It follows that the reflected intensity, I, varies as $(I/I_0)^{\frac{1}{2}} = 1 - P/P_0$, where P = pressure and P_0 = pressure at which the indexes of refraction are equal. Then we obtain

$$\sigma_0 \text{ (mirror)} = [n(P_0)/n_0]\sigma \text{ (gas)}.$$

From the intercept P_0 in Fig. 2, we have

$$\sigma_{\text{coh}} \text{ (vanadium)} = 0.028b \pm 0.005 \text{ (positive phase)}.$$

On the basis of the above result for σ_{coh} Hamermesh's calculations[8] need be modified only to the extent of adjusting the potential scattering radius, R, from $0.508b^{\frac{1}{2}}(b = 10^{-24}\text{ cm}^2)$ to $R = 0.602b^{\frac{1}{2}}$. We may further add that if the resonance at 2700 ev accounts for the entire thermal absorption cross section ($\sigma_{\text{abs}} = 4.8b$ at 0.025 ev), then from

$$\sigma_{\text{abs}}^{\text{th}} = \pi g \lambda_0^2 \Gamma_n \Gamma_\gamma [40E_0 \text{ (ev)}]^{\frac{1}{2}}/E_0^2 = 4.8b,$$

$\sigma_0^{\text{abs}} = 4\pi\lambda_0^2 g \Gamma_\gamma/\Gamma_\lambda$ = absorption cross section at resonance,

we obtain $\Gamma_\gamma = 1.3$ ev and $\sigma_0^{\text{abs}} = 0.7b$.

Spectrographic analysis of the vanadium gives V = 99.7 percent, Fe = 0.22 percent, Mn = 0.006 percent, Ti = 0.001 percent, C = 0.09 percent. The iron contributes ~0.001 barn to the coherent cross section. The presence of $\frac{1}{4}$ percent of V^{50} likewise has negligible effect.

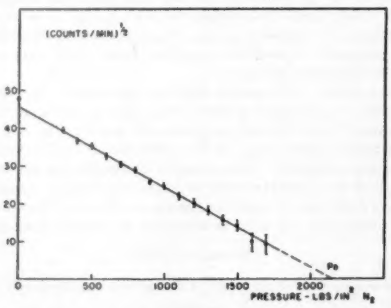

FIG. 2. Total intensity of a thermal neutron beam reflected from a vanadium-nitrogen interface as a function of nitrogen pressure. The intercept ($P_0 = 2130$ lb/in.^{2}) is the pressure at which the index of refraction of nitrogen equals the index of refraction of vanadium.

We wish to thank Dr. P. Bendt for the use of the vanadium.

* Research carried out under contract with AEC.
[1] C. G. Shull and E. O. Wollan, Phys. Rev. **81**, 527 (1951).
[2] M. Hamermesh and C. O. Muehlhause, Phys. Rev. **78**, 175 (1950).
[3] Recent work of S. P. Harris [Phys. Rev. **83**, 235(A) (1951)] indicates a resonance at 3100 ev. None of the results of this paper are significantly affected by this.
[4] A. W. McReynolds and G. W. Johnson, Phys. Rev. **82**, 344 (1951).
[5] G. Snow and D. Kleinman, unpublished.

Gravitational Acceleration of Neutrons*

A. W. McREYNOLDS
Brookhaven National Laboratory, Upton, New York
(Received May 11, 1951)

SINCE the acceleration of gravity is observed to be a universal constant for all matter, including nuclei which are aggregates of nucleons, it is reasonable to assume that a neutron, free of nuclear forces but in a gravitational field, is subject to the same acceleration. The high neutron flux from a reactor makes possible a direct check of this otherwise unsupported assumption.

Acceleration was determined by measurement of the drop of a highly collimated beam of thermal neutrons from the Brookhaven reactor in 12 meters of path, or more specifically the difference in drop of neutrons of different velocity but defined by the same collimating system. Boron carbide and Lucite slits 0.075-cm high $\times$5 cm wide, spaced 150-cm apart in the shield, defined the beam. Its position at 11.6-m range was measured by vertical scanning of a 0.9-cm wide slit in front of a BF_3 proportional counter. A 25-cm filter of BeO was then interposed between the reactor and first slit and the beam position determined by a second scanning. The first beam contains the entire thermal distribution $N(E)dE = Ee^{-E/kT}dE$ with peak at about 0.07 ev, 1A wavelength, or velocity 3.95×10^5 cm/sec. The filtered beam contains only that small part of the distribution with wavelengths greater than the BeO cut-off of 4.4A or 9.00×10^4 cm/sec. In Fig. 1 is shown a typical plot of the two beams, adjusted to the same peak height, indicating a downward shift of the slower neutron beam of about 1.2 mm in 12-m path.

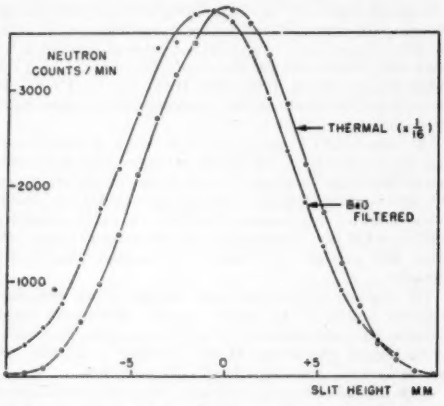

FIG. 1. Positions of thermal and very slow neutron beams at 11.6 meters range showing separation by free fall.

A value of g for neutrons can be calculated from the separation of the centers of gravity of the two beams, the geometry of the collimator and scanning slits, and velocity distributions in the two

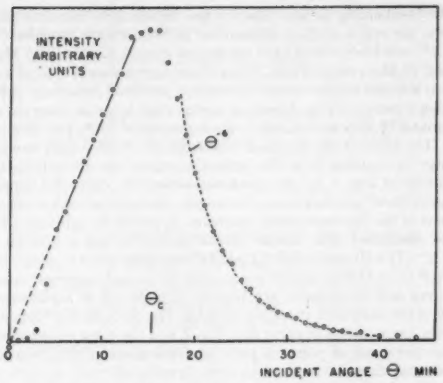

FIG. 2. Intensity of entire reflected beam from glass mirror; incident beam filtered through 25 cm BeO.

beams. The drop d of a neutron of velocity v passing through slits at 0, l_1, and l_2 is given by

$$d=(g/2v^2)(l_2^2-l_1l_2).$$

Therefore, the separation of two beams of velocity distributions v_1, v_2 is

$$\Delta=d_2-d_1=\tfrac{1}{2}g(l_2^2-l_1l_2)[\langle v_1^{-2}\rangle_{Av}-\langle v_2^{-2}\rangle_{Av}].$$

For the thermal beam the average over the maxwellian distribution is $\langle v_1^{-2}\rangle_{Av}=v_{max}^{-2}$. The velocity distribution of the filtered beam was not truly maxwellian, because inelastic scattering in the filter is greater for longer wavelengths. It was therefore measured by reflected intensity from a glass mirror *vs* incidence angle, as shown in Fig. 2. If the flux

$$N(v)dv\propto v^n dv$$

(where $n=3$ for a maxwellian distribution), then reflected intensity beyond the critical angle for 4.4A neutrons should vary as $1/\theta^n$. It was determined from plots of $n=5$ and $n=6$, as seen in Fig. 2, that $n=5.5\pm0.5$. An average over the velocity range 0 to 9.00×10^4 cm/sec (∞ to 4.4A) then gives

$$\langle v_2^{-2}\rangle_{Av}=n+1/n-1(9.00\times10^4)^2=6.5/4.5(9.00\times10^4)^2.$$

These velocity values, together with the average $\Delta=1.22\pm0.06$ mm, from a number of measurements, give

$$g=935\pm70 \text{ cm/sec}^2$$

in agreement, within the experimental error, with the usual value 980.

* Research carried out under contract with AEC.

High Altitude Measurements of the Penetrating Component Intensity of Cosmic Radiation Near the Geomagnetic Equator

A. S. RAO, V. K. BALASUBRAHMANYAM, G. S. GOKHALE, AND A. W. PEREIRA
Tata Institute of Fundamental Research, Bombay, India
(Received May 11, 1951)

THE vertical intensity of cosmic radiation penetrating 10 cm of lead absorber at high altitudes was measured by the authors near the geomagnetic equator (Bangalore 3°N mag.) using free balloon ascents during 1950–1951. The measurements were made with quadruple coincidence GM counter telescopes whose vertical half angles were 13.5° and 24.5°. The most inclined ray

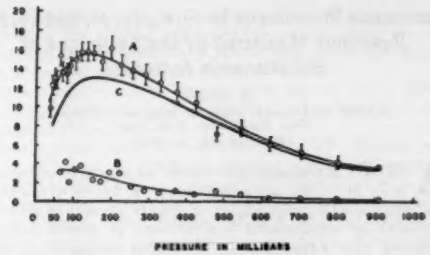

FIG. 1. Vertical intensity of cosmic radiation penetrating 10 cm Pb at Bangalore 3°N mag. A: Composite curve of flights made on 11/21/50, 11/24/50, 2/1/51, 2/8/51, 2/26/51, and 3/8/51. B: Shower intensity curve. C: Difference curve between A and B.

recorded by the telescope had a path length only 10 percent greater than that of a vertical ray. The temperature inside the gondola which contained the apparatus was maintained above 10°C throughout the flight using the "greenhouse effect." Quadruple coincidences, together with atmospheric pressure and temperature inside the gondola were transmitted continuously over a single ultra-high frequency radio carrier to the ground receiving apparatus which recorded the information automatically on a moving paper tape.

The telescopes were tested on the ground for many hours before they were sent up. Their performance was also checked at the highest altitudes reached to insure that they were working satisfactorily during the flight in the following manner. The apparatus always floats for several hours at or near the minimum pressure reached, and a χ^2 test could therefore be applied to the statistical fluctuation of counts recorded in small equal intervals of time during the floating period. It is interesting to note that for the curves in which the scatter of the points was rather large during ascent, the χ^2 fit for the floating region was also poor. This was taken to indicate a possibly defective performance of the equipment, and the entire data of such flights was therefore rejected.

A composite curve of six good flights made at Bangalore is given in Fig. 1, with the rcot mean square deviation marked for each point. From the composite curve given in the figure and the individual curves, which are not shown here, it is seen that the vertical intensity of cosmic radiation penetrating 10 cm of lead absorber at Bangalore 3°N (mag.) rises continuously down to a pressure of about 120 millibars, and then falls gradually down to the lowest pressures reached by the apparatus. This is contrary to the observations of most of the previous workers,[1–4] who made their measurements at higher magnetic latitudes and observed a montonic rise of penetrating intensity up to the greatest heights reached. The hard component intensity curve was corrected for side showers and accidentals by making separate flights with identical telescopes, but with the second counter tray of the quadruple coincidence telescope displaced sideways so that at least two particles are necessary to make a coincidence. The shower and accidental intensity curve and the difference curve, which represents the penetrating component intensity, are also given in the same figure. Although the correction due to side showers and accidentals is rather appreciable at pressures below 200 millibars, it is nevertheless obvious that this does not affect the shape of the penetrating component intensity curve which reaches a maximum at about 120 millibars and then falls with decreasing pressure.

A detailed paper on the results and the experimental technique will be published soon elsewhere.

We are greatly indebted to Professor H. J. Bhabha for his valuable guidance of this work.

[1] E. G. Dymond, Nature **144**, 782 (1939).
[2] Schein, Wollan, and Groetzinger, Phys. Rev. **58**, 1027 (1940).
[3] Schein, Jesse, and Wollan, Phys. Rev. **59**, 615 (1941).
[4] M. A. Pomerantz, Phys. Rev. **73**, 69 (1949).

Resonance Phenomena in (γ, n), $(\gamma, \dot{p})$, and $(\gamma, 2n)$ Reactions Measured by the Technique of Simultaneous Activation

R. SAGANE*
Institute for Atomic Research and Department of Physics, Iowa State College, Ames, Iowa
(Received May 11, 1951)

A STUDY of resonance phenomena, not only in (γ, n) but also in $(\gamma, \dot{p})$, $(\gamma, 2n)$, and perhaps in $(\gamma, \dot{p}n)$ and (γ, γ) reactions, has been made by comparing the saturation intensity of activities produced by simultaneous bombardment of several different elements with x-rays. X-rays of various maximum energies, ranging between 10 Mev and 61 Mev, were made available through the use of the Iowa State College synchrotron.

Tests were made on samples of thin plates of C (polystyrene), Mg, Cu, Mo, and Pb, bombarding most of them simultaneously for

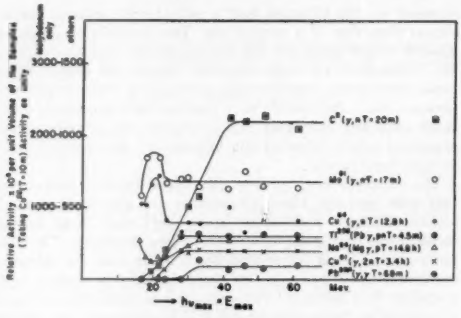

FIG. 1.

suitable periods of time with x-rays of different E_{max}. Sufficient attention was paid to insure constancy of the x-ray intensity during each run. The decay of the radioactivity produced in each of the samples was measured, and saturation intensities were calculated from these data for each of the periods.

The ratios between these saturation intensities and that simultaneously produced in a tentative standard, Cu^{62} [produced by (γ, n), with $T_{\frac{1}{2}} = 10$ min], are plotted in Fig. 1 against E_{max} of

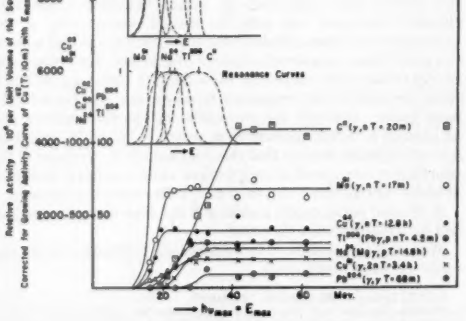

FIG. 2.

the bombarding x-rays. Most of the curves show fair constancy over the region of E_{max} higher than 24 Mev, except those for C^{11}, Cu^{61}, and Pb^{204}, which have resonances around 30 Mev, 24.5 Mev, and 29 Mev, respectively. These three curves show a typical sudden increase at the region of resonance and then constancy at the higher energy region. Irregular sudden rises found in three curves around 18 Mev are caused by the resonance of Cu^{62} ($T_{\frac{1}{2}} = 10$ min).

The effect of the resonance characteristic of the copper monitor may be removed from the activation curves by multiplying the curves of Fig. 1 by the presumed activation curve for copper, normalized for convenience to constant intensity in the low-energy part of the bremsstrahlung spectrum. It should be noted that if it be demanded that *similar simple curves* for the activation of Cu^{62} ($T_{\frac{1}{2}} = 10$ min), Cu^{64} ($T_{\frac{1}{2}} = 12.8$ hr), Mo^{91} ($T_{\frac{1}{2}} = 17$ min), and Na^{24} ($T_{\frac{1}{2}} = 14.8$ hr) should result, then the initially assumed copper curve may be adjusted accordingly with the aid of experimental data obtained with the other nuclides. The curve for Cu^{62} found in this way is shown in curve A of Fig. 2, and the other curves shown are the result of point by point multiplication by this improved monitor curve.

If a simplified,[1] rectangular x-ray spectrum for $E_\gamma \cdot n(E_\gamma)$ *versus* E_γ is assumed, the activity induced in a foil may be represented by

$$N(E_{max}) = A(E_{max}) \int_0^{E_{max}} [\sigma(E_\gamma)/E_\gamma] dE_\gamma.$$

With the assumptions made, simple differentiation of the corrected activation curves shown in Fig. 2 gives $\sigma(E_\gamma)/E_\gamma$. Hence the curves drawn in broken lines in Fig. 2, which are the results with normalization to unity at the maxima, give roughly the resonance curves.

The results obtained in this way are summarized in Table I. The data given here are of rather preliminary nature, but are good enough to say the following:

(A) Resonance phenomena have been found not only in (γ, n) but also in $(\gamma, \dot{p})$ and $(\gamma, 2n)$ reactions. If reactions for Pb samples

TABLE I. Summary of results.

Target	Isotope	Half-life	Reaction	Reson. peak E_n, Mev	Half-width Mev	Measured rel. activity per unit volume	Approx. rel. integr. cross section
Cu	Cu^{62}	10 min	(γ, n)	18 ± 1	6 ± 2	10,000	1
Cu	Cu^{64}	12.8 hr	(γ, n)	17.5 ± 1.5 -0.5	4 ± 1.5	400	2
Cu	Cu^{61}	3.4 hr	$(\gamma, 2n)$	24.5 ± 2	4 ± 1.5	200	0.05
Mo	Mo^{91}	17 min	(γ, n)	17.5 ± 1.5	4 ± 1.5	2800	2
Mg	Na^{24}	14.8 hr	$(\gamma, \dot{p})$	22 ± 3	12 ± 3	300	1
C	C	20 min	(γ, n)	30 ± 4	14 ± 3	1100	—
Pb	Pb^{204}	68 min	(γ, γ) · or $(\gamma, 2n)$	29 ± 4	4 ± 1.5	10	—
Pb	Tl^{204}	4.7 min	$(\gamma, \dot{p}n)$ or $(\gamma, \dot{p})$	23.5 ± 2	5.5 ± 1.5	30	—

are assumed as (γ, γ) and $(\gamma, \dot{p}n)$, resonances are also found in these reactions.

(B) By comparing relative saturation intensities of different activities obtained by simultaneous bombardment, one can get fair accuracy for resonance energies. This is quite free from troublesome systematic errors in absolute calibration of ion chambers.

(C) The width of the resonance differs from one reaction to another, although the sharpest group appears to have a width of the order of 4 Mev.

(D) The resonance curve for Cu^{62} (curve A, Fig. 2), obtained here by a new method, is in good accord with the curves obtained recently,[2] but differs appreciably from that obtained earlier.[3]

The author wishes to express his heartiest gratitude to Dr. L. J. Laslett and Dr. D. J. Zaffarano for their continued interest and help given during the course of the experiment. Thanks are also due

Dr. G. W. Fox for the privilege of working at the synchrotron laboratory of the Iowa State College.

* On leave from Tokyo University, Tokyo, Japan.
[1] Compare with distribution curves given by Heitler, The Quantum Theory of Radiation (Oxford University Press, London, 1944), Fig. 14, p. 170.
[2] McElhinney *et al.*, Phys. Rev. **75**, 542 (1949); Johns *et al.*, Phys. Rev. **80**, 1062 (1950); B. C. Diven and D. M. Almy, Phys. Rev. **80**, 407 (1950).
[3] G. C. Baldwin and G. S. Klaiber, Phys. Rev. **73**, 1156 (1948).

Cloud-Chamber Observations of the Neutral *V*-Particle Disintegration*†

R. W. Thompson, Hans O. Cohn, and R. S. Flum
Indiana University, Bloomington, Indiana
(Received May 10, 1951)

In a sea level magnet cloud-chamber experiment on penetrating showers, now in progress, nine examples of the V^0-particle disintegration process[1] have been observed. The cloud chamber, of 11-inch inside diameter and 3-inch illuminated depth, is mounted between the poles of an iron electromagnet producing a uniform magnetic field of 3100 gauss. Track distortions produced by the chamber are empirically determined for long tracks to correspond to radii of curvature of about 100 meters, so that the maximum detectable momentum is about 10 Bev/c. The chamber is actuated by a Geiger counter arrangement which favors the detection of penetrating showers produced in a lead layer immediately above the chamber.

In two of the V^0-particle photographs, the positive particle is identified to be a proton. In the first of these (film No. 92), shown in Fig. 1, the positive particle has a momentum of 0.38 ± 0.06 Bev/c, and the track is heavily ionizing by an estimated factor of 3 to 6, to be compared with a factor of 5 for a proton of this momentum. The negative particle is ejected toward the back of the chamber and the track is too short to permit an accurate measurement of the momentum.

In the second case (film No. 55), the momentum of the positive particle is 0.75 ± 0.1 Bev/c, and the track is 2 to 4 times minimum ionization. A proton of this momentum would be heavily ionizing by a factor 2. The negative particle has a momentum of 0.24 ± 0.02 Bev/c, and the track is of minimum ionization, so the negative particle cannot be much heavier than a π-meson. Under the assumption that the event represents the disintegration of a V^0-particle into a proton and a negative π-meson ($\theta=23.8°$), the Q-value of the disintegration is 28 ± 10 Mev, which corresponds to a V^0-mass of $2165\pm20m_e$.

An apparently similar example (film No. 51; $p_+=1.2\pm0.2$ Bev/c, $p_-=0.22\pm0.01$ Bev/c, $\theta=28.6°$) gives $Q=31\pm5$ Mev, or a V^0-mass of $2170\pm10m_e$.

On the other hand, we have observed a V^0 disintegration, shown in Fig. 2, in which the positive particle, although of minimum ionization, has a momentum of only 0.27 ± 0.03 Bev/c, and thus cannot be much heavier than a π-meson. A proton of this momentum would be heavily ionizing by a factor 10. The negative particle, of momentum $1.3_{-0.6}^{+1.0}$ Bev/c, is very near minimum ionization and so cannot be identified. The fact that the momentum of the negative particle is much greater than that of the positive particle suggests, although it does not prove, that the negative particle is much heavier than the positive particle. It is interesting to consider the possibility that a negative proton is involved. Under this assumption, the V^0-mass is about $2220m_e$, a value which is similar to those given above. Thus, if the event represents the decay of a V^0-particle with mass corresponding to the values given above, the particle here observed is likely to be a negatively charged nucleon. These arguments are quantitatively but not qualitatively changed if a light neutral particle is produced in the disintegration (3-particle disintegration).

However, the event may be equally well explained by the assumption of a different type of V^0-particle, of about $1020m_e$, which decays into two π-mesons. The asymmetry in the momenta would then be understood if the negative π-meson had been emitted in the forward direction in the center-of-mass system.

Very recently, the Manchester group has published an account[2] of very beautiful and extensive work from which closely similar conclusions have been drawn concerning the V^0-particles and their disintegration fragments.

Fig. 1. V^0-disintegration resulting in a heavily ionizing proton.

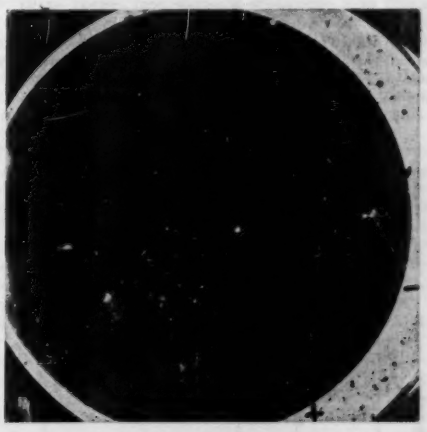

Fig. 2. V^0-disintegration in which the positive particle is probably a π-meson.

* This work has been assisted by a grant from the Frederick Gardner Cottrell Fund of the Research Corporation.
† Reported at the Washington meeting of the American Physical Society, Phys. Rev. **83**, 194 (1951).
[1] G. D. Rochester and C. C. Butler, Nature **160**, 855 (1947); Seriff, Leighton, Hsiao, Cowan, and Anderson, Phys. Rev. **78**, 290 (1950); V. D. Hopper and S. Biswas, Phys. Rev. **80**, 1099 (1950); Bridge, Harris, and Rossi, Phys. Rev. **82**, 294 (1951); W. B. Fretter, Phys. Rev. **82**, 294 (1951).
[2] Armenteros, Barker, Butler, Cachon, and Chapman, Nature **167**, 501 (1951).

Scintillating Liquids as Neutron Detectors*

C. E. Falk, H. L. Poss, and Luke C. L. Yuan
Brookhaven National Laboratory, Upton, New York
(Received May 16, 1951)

RECENT investigations[1,2] have shown that various solutions scintillate when excited by ionizing particles. As liquid scintillators are organic solutions[2] with a large number of hydrogen nuclei per cm³, it seemed worthwhile to investigate the behavior of these liquids under neutron bombardment.

The liquids were tested in cylindrical glass cells placed on magnetically shielded 5819 photomultipliers operated at 1000 volts. The resulting pulses went through a cathode-follower, fast amplifier, and scaler. Only integral bias curves were taken with the controlling bias being applied at the scaler input.

The first experiments were performed by irradiating a 0.5 percent terphenyl-xylene (both commercial grade) solution with 14-Mev neutrons. The neutrons were obtained by bombarding a thick (H^3-Zr) target with 700-kev deuterons accelerated by the Brookhaven electrostatic generator (later experiments at the Department of Terrestrial Magnetism, Carnegie Institution, Washington, D. C., were performed with 400-kev deuterons). The counting solution was placed in a cylindrical glass cell of 1¼-in. diameter and 1-in. length which was surrounded by aluminum foil. The cell was placed with its axis pointing toward the target at an angle of 110° with respect to the deuteron beam and at a distance of 40 in. from the target. The resulting integral bias curve is shown as curve *A* in Fig. 1. The efficiency of the counter could be calculated as the recoil He^4 nuclei of the $H^3(d,n)He^4$ reaction were counted by a proportional counter at 90° with respect to the deuteron beam. The efficiency of this cell was between 5 to 10 percent depending on that point on the bias curve plateau which was used for the calculation. As this arrangement looked very promising, various factors affecting pulse-height distribution and efficiency were investigated.

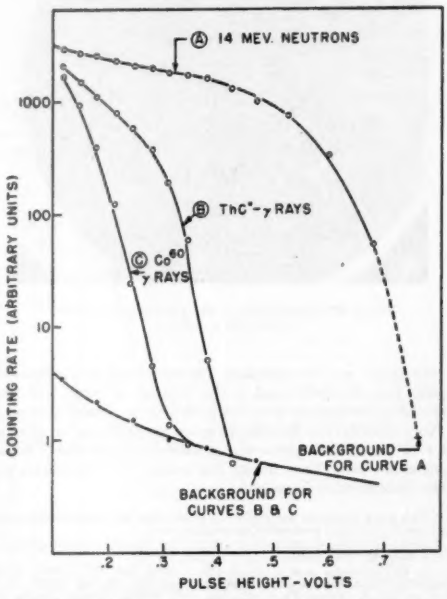

FIG. 1. Integral bias curves for neutrons and γ-rays using a 1-in. cell (terphenyl-xylene) with glass bottom. The relative counting rates of the three curves are not significant.

Since the spectrum of the xylene-terphenyl mixture[3] extends into the ultraviolet region and as light is lost at every reflecting surface, one would expect a better pulse-height distribution as well as larger pulses if the liquid were placed in direct contact with the photomultiplier surface and if the reflecting surfaces were inside the glass cell. For this reason the bottom of the glass cell was removed, the inside surfaces aluminized, and the cell cemented

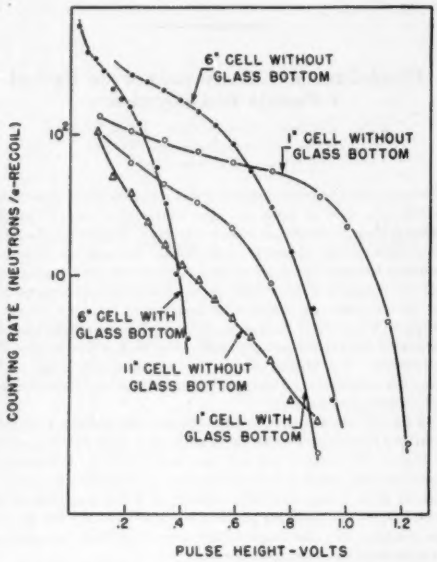

FIG. 2. Integral bias curves produced by 14-Mev neutrons in aluminized glass cells of various lengths filled with terphenyl-xylene solution.

to the photomultiplier. The resulting improvement can be seen in Fig. 2.

Cells of different length were bombarded with 14-Mev neutrons to determine the variation of efficiency with length. As can be seen from Fig. 2, a 6-in. cell still produces a plateau even though the maximum pulse height has been reduced. The efficiency is about three times as high as that of a 1-in. cell. The 11-in. cell shows no plateau at all. Consequently it seems inadvisable to use cells much larger than 6 in., as the efficiency does not increase proportionally to the length and the pulse-height distribution deteriorates rapidly beyond 6 in. of liquid.

A solution of 0.5 percent terphenyl (reagent grade) and purified *m*-xylene as well as a solution of 0.3 percent terphenyl in phenyl ether with 0.005 percent of diphenylhexatriene[4] showed no appreciable difference from the commercial grade 0.5 percent terphenyl-xylene solution when bombarded with 14-Mev neutrons.

The response of the terphenyl-xylene solution to neutrons and γ-rays of various energies has been investigated and the results are shown in Figs. 1 and 3. The 4.4 and 2.6-Mev deuterons were obtained by bombarding a deuterium gas target with 2-Mev deuterons in the electrostatic generator of the Department of Terrestrial Magnetism of the Carnegie Institution and placing the counter at different angles (backgrounds were determined using hydrogen gas in the target chamber). In both the γ-ray and neutron case the pulse height (cutoff for γ-rays, and height at plateau knee for neutrons) seemed to increase more slowly than the respective energies. Nevertheless it is quite evident that in the case of neutrons good energy biasing can be performed.

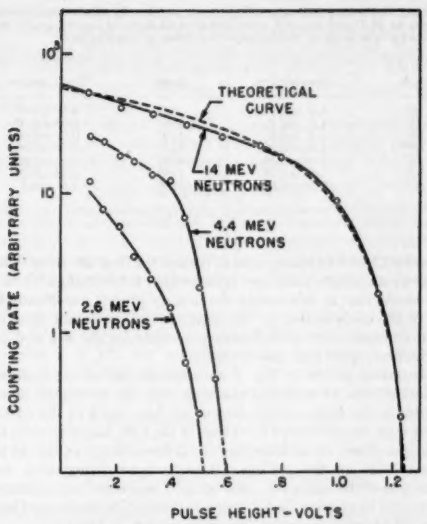

FIG. 3. Relative pulse-height distributions produced by various energy neutrons in an 1-in. terphenyl-xylene cell, the scintillating solution being in direct contact with the 5819. The relative counting rates of the three curves are not significant. The dashed curve is the expected pulse distribution for 14-Mev neutrons assuming only one isotropically distributed collision of the neutron in the liquid.

The above facts show essentially that liquid scintillators have the following advantages as fast neutron detectors: (a) very high efficiencies, (b) fairly good energy response so that energy-biasing is possible, and (c) great simplicity in preparation and construction. Their main disadvantage is their disproportional response to γ-radiation. Consequently these counters are most useful in experimental arrangements where the γ-ray background is either very weak or consists of γ-rays of low energy as compared to the neutron energy. Experiments involving $d-d$ and $d-t$ neutrons meet these conditions exceptionally well. Counters of this type have been used to measure total cross sections for 14-Mev neutrons with good results.[5]

We should like to express our thanks to: Dr. E. O. Salant for his over-all aid, Dr. G. Friedlander for his valuable advice concerning the chemistry of the solutions, Dr. R. C. Anderson for the preparation of the *m*-xylene, Drs. M. Tuve and N. Heydenburg of the Carnegie Institution for the use of their accelerator, and the crews of the Brookhaven and Carnegie Institution Van de Graaffs for their able cooperation.

* Research carried out under the auspices of the AEC.
[1] G. T. Reynolds *et al.*, Phys. Rev. **78**, 488 (1950).
[2] H. Kallmann and M. Furst, Phys. Rev. **79**, 857 (1950).
[3] F. B. Harrison and G. T. Reynolds, Phys. Rev. **79**, 732 (1950).
[4] H. Kallmann, Nucleonics **8**, 32 (1951).
[5] H. L. Poss and Luke C. L. Yuan, Phys. Rev. (to be published).

Magnetization Processes in a Ferrite

G. T. RADO AND A. TERRIS
Naval Research Laboratory, Washington, D. C.
(Received May 14, 1951)

IN a recent Letter to the Editor entitled "The magnetization process in ferrites," Went and Wijn[1] (WW) advance certain generalizations which require comment. On the basis of experiments performed on some ferrites possessing high permeability, WW state categorically that in their opinion the initial permeability, as well as the field-independent part of the high frequency permeability, is related to a pure rotational process. They assert, moreover, that "These results are contradictory to the conclusions reached by Rado *et al.*[2] (RWE), that the initial permeability of ferrites is determined by reversible Bloch-wall displacements." However, RWE did not arrive at such a generalization, but discussed one particular ferrite (ferramic *A*) only. Furthermore, the mechanism of wall displacement (including its inertia) was invoked for the explanation of only one of the two resonances observed in the magnetic spectrum. It should also be noted that this particular ferrite possesses a rather low initial permeability, and that its properties were not studied by WW. In view of these facts it is clear that there is no basis for contradictions regarding reversible magnetization processes. Irreversible processes, on the other hand, were not investigated by RWE.

Although there is no disagreement between the actual conclusions of WW and RWE, there are important differences between the methods used in the two papers for identifying the nature of the reversible processes which determine the static initial permeability (μ_{stat}) in a given substance. It may well be that μ_{stat} is indeed determined by rotations in the ferrites studied by WW. However, their conclusion is based solely on the approximate applicability of Snoek's relation between μ_{stat} and the rotational resonance frequency. As pointed out by RWE, that relation does not provide a valid method for distinguishing between rotations and wall displacements, because under certain conditions (which may or may not exist in WW's samples) the formula for the wall resonance frequency may give practically the same result as Snoek's formula. It is because of these uncertainties that RWE have proved the existence of wall displacements by preparing very small particles (which are probably single domains) of ferramic *A* and then showing that in such particles the wall displacement resonance disappears, whereas the rotational resonance frequency is substantially unchanged from that in ordinary samples of ferramic *A*.

Recent experiments provide strong confirmation for the conclusion that μ_{stat} in ferramic *A* is primarily due to wall displacements. We measured the "work of magnetization,"[3] *E*, in polycrystalline samples of the same material (Company batch No. 165)[4] as used by RWE for the magnetic spectrum and, as shown below, found that *E* is definitely too large to permit attributing the measured μ_{stat} to rotations. If magnetic interactions are neglected (their effect cannot alter the final conclusions), reversible rotations in cubic polycrystals are described[3,5,6] by $(\mu_{stat}-1)=aM_s^2/|K|$, and $E=|K|/b$, so that we may put $(\mu_{stat}-1)=aM_s^2/bE$. Here $a=1.88$ or 2.28, and $b=5.00$ or 7.50, depending on whether the anisotropy constant, *K*, is >0 or <0; M_s is the saturation magnetization. Using $M_s=99$, the measured $E\approx 6.0\times 10^3$ ergs/cm^3 leads to a calculated $\mu_{stat}\leq 1.6$, a value much smaller than the observed $\mu_{stat}=19.6$. The conclusion that the latter value is primarily due to wall displacements is not affected by the possibility of irreversible processes contributing to the measured *E*, because at least $\frac{3}{4}$ of *E* arises from the high field region where hysteresis effects were found to be definitely absent. Finally, it is gratifying that the values $|K|\approx 3.0\times 10^4$ or 4.5×10^4 (depending on whether $K>0$ or <0) measured by this approximate method agree as well as may be expected with the values $|K|\approx 4.4\times 10^4$ or 6.7×10^4 estimated from RWE's observed frequency of natural microwave resonance. The temperature dependence of these effects will be reported later.

[1] J. J. Went and H. P. J. Wijn, Phys. Rev. **82**, 269 (1951).
[2] Rado, Wright, and Emerson, Phys. Rev. **80**, 273 (1950).
[3] For a definition of *E*, and an outline of the calculation of *b*, see L. Néel, J. phys. radium **9**, 193 (1948).
[4] Samples of ferramic *A* purchased more recently were found to have a different chemical composition and different magnetic properties. The two resonances reported on by RWE were also observed in fired mixtures of pure MgO and Fe_2O_3 prepared at this laboratory.
[5] For a calculation of *a*, see R. Gans, Ann. Physik (Leipzig) [V] **15**, 28 (1932).
[6] It is assumed that $|K|$ greatly exceeds the energy density due to internal strains. See reference 2.

Elastic d-p Scattering at 190 Mev

MARTIN O. STERN AND ARNOLD L. BLOOM
Radiation Laboratory, Department of Physics, University of California, Berkeley, California
(Received May 14, 1951)

AS a result of recent theoretical interest, a comprehensive program has come into being, the purpose of which is to deduce some properties of the neutron-neutron interaction at high energies.

So far, p-p experiments have been carried out by Birge[1] at 100 Mev, and by Chamberlain, Segrè, and Wiegand[2] at (among other energies) 120 Mev. Professor Wilson M. Powell[3] is engaged in the study of n-d scattering using 90-Mev neutrons. We are measuring the scattering on protons, both elastic and inelastic, of the 190-Mev deuterons of the Berkeley 184-in. cyclotron. In all these experiments the relative velocities are comparable.

In this letter, we present our results to date on the elastic d-p scattering, first reported by one of us (A.L.B) at a recent meeting[4] of the American Physical Society. A more complete report, giving the details of the experiment, and possibly extending the data to larger and smaller angles, will be published in the near future.

The experimental arrangement was akin to that used by Chamberlain and Wiegand.[5] Deuterons scattered out of the cyclotron were collimated and made to impinge on a target. Coincidences between protons and deuterons were observed by means of stilbene crystals. Either one crystal, or two in coincidence, detected the scattered protons; another crystal, in coincidence with the former, the deuterons. Suitable tests were performed to convince us that only the desired events were being observed.

Carbon and polyethylene targets were used alternately to obtain the scattering cross section by subtraction. The data accumulated so far are shown in Fig. 1. The differential scattering cross section, in 10^{-27} cm^2 sterad^{-1} in the center-of-mass system, is shown as a function of the angle of deflection of either particle in that system. Table I gives the weighted averages of the cross sections for a given angle. The slight relativistic correction has been taken into account.

The solid curve of Fig. 1 shows the theoretical cross section as given by Chew.[6] Evidently, the fit is excellent from 60° to 110°, but at larger angles the measured cross section is lower than Chew's; this means that at this energy the pick-up process which causes a rise in the cross section in this region is less important than the Born approximation with Serber potentials for the n-p and p-p interaction would lead one to expect.

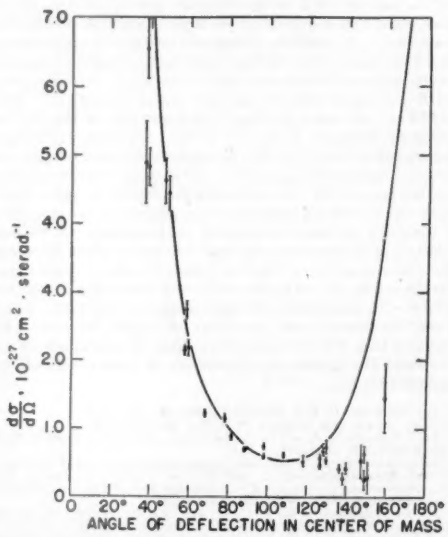

FIG. 1.

TABLE I. Differential scattering cross sections in the center-of-mass system, in 10^{-27} cm^2 sterad^{-1}, averaged over all data for a given angle, as a function of the angle of deflection in the center-of-mass system.

Angle	Cross section	Angle	Cross section
38°	5.4 ±0.4	98°	0.65 ±0.05
48°	4.5 ±0.4	108°	0.61 ±0.05
58°	2.3 ±0.2	118°	0.52 ±0.09
68°	1.22 ±0.09	128°	0.55 ±0.05
78°	1.16 ±0.10	138°	0.40 ±0.05
82°	0.89 ±0.08	149°	0.44 ±0.09
88°	0.70 ±0.06	159°	1.5 ±0.5

The errors shown in Fig. 1 are compounded of the standard deviations due to counting statistics and the estimated uncertainties in the factor which determines how much of the carbon count must be subtracted from that of the CH_2 target to yield the hydrogen effect. In addition, certain systematic errors, due to the uncertainties in the voltage plateaus, beam integration, and steadiness of the beam, etc., may occur. These have been estimated to amount to no more than 7 percent standard deviation, and have been taken into account in the errors quoted in Table I.

We wish to thank Dr. O. Chamberlain and Dr. E. Segrè for their constant assistance and interest in this work. This work was performed under the auspices of the Atomic Energy Commission.

[1] R. W. Birge, Phys. Rev. **80**, 490 (1950).
[2] Chamberlain, Segrè, and Wiegand, Phys. Rev. **81**, 284 (1951).
[3] W. M. Powell (to be published).
[4] A. L. Bloom and M. O. Stern, Phys. Rev. **81**, 660 (A) (1951).
[5] O. Chamberlain and C. Wiegand, Phys. Rev. **79**, 81 (1950).
[6] G. F. Chew, Phys. Rev. **74**, 809 (1948).

Nuclear Compressibility and Fission

W. J. SWIATECKI
Institute for Theoretical Physics, Copenhagen, Denmark
(Received May 16, 1951)

AS is well known, many features of the fission phenomenon find a simple explanation in the theory of the compound nucleus; and, in particular, it has been possible to arrive at an approximate estimate of the critical fission energy for heavy nuclei. So far, however, no simple explanation has been found for the pronounced asymmetry of the nuclear division in fission.[1] In a search for an explanation of this phenomenon we have examined the effects of nuclear compressibility and of the polarizability of nuclear matter (separability of neutrons and protons), and it seems that these effects may play an important part in fission.

The reason is that the deformation energy of a nucleus is a small difference between large changes in electrostatic and surface energies, and that consequently even relatively small corrections to the estimate of these energies may have a decisive influence.

As a model of the nucleus we used a drop of a classical, compressible, polarizable neutron-proton fluid whose density distribution is constantly changing as the fission proceeds. Only the "adiabatic" approximation was considered, in which the density distribution at any instant is given by the equilibrium distribution corresponding to the instantaneous deformation. The total energy of the nucleus was taken to be the sum of volume, coulomb, and surface energies in the absence of compressibility plus a (negative) correction ΔE due to compressibility. That there is in general a factor in ΔE which favors asymmetric fission can be seen as follows: if the volume of the nucleus which is undergoing fission is divided conceptually into two regions corresponding to the nascent

fission fragments, the density redistribution due to compressibility can be thought as due to (a) a transfer of matter from one region to the other and (b) the remaining density adjustment. Now (a) will contribute only if the fragments are unequal; and therefore, the associated energy decrease will be greatest for some asymmetric configuration.

We can separate ΔE into ΔE_{scale} and ΔE_{red}, associated with a uniform change of scale and a redistribution of density inside the nucleus, respectively. The former is easily shown to be:

$$\Delta E_{\text{scale}} = -(1/2E_v'')[(2-3\dot{\gamma})E_s - E_c]^2, \tag{1}$$

where E_c, E_s are the coulomb and surface energies calculated in the absence of compressibility, E_v'' is the nuclear compressibility coefficient,[2] and $\dot{\gamma} = (n/\gamma)d\gamma/dn$ is a dimensionless parameter giving the dependence of the specific surface energy γ on the bulk density n.

A general method of calculating the density redistribution and ΔE_{red} for a nucleus of *any shape* was developed along the lines of reference 2. If $f(\mathbf{r})$ and $g(\mathbf{r})$ denote the deviations of the local proton and neutron densities from their average values, it is found that (using the notation and assumptions of reference 2)

$$g(\mathbf{r})/f(\mathbf{r}) = \text{constant} = (S-Q)/(S+Q), \tag{2}$$

$$f(\mathbf{r}) = e(S^{-1}+Q^{-1})[\bar{v}-v(\mathbf{r})], \tag{3}$$

$$\Delta E_{\text{red}} = -\tfrac{1}{2}e^2(S^{-1}+Q^{-1})\int[\bar{v}-v(\mathbf{r})]^2, \tag{4}$$

where $v(\mathbf{r})$ is the electrostatic potential of a *uniform* proton distribution, $\bar{v}$ is the average of $v(\mathbf{r})$ over the nucleus, e is the proton charge, S and Q are coefficients related to separability and compressibility[2] [e.g., $Q=(4/9n)(E_v''/A)$], and the integration in Eq. (4) extends over the nucleus.

To find the correction to the threshold energy and the "barrier" against asymmetric fission[3, 4] one should repeat the calculations of reference (3) with ΔE included in the deformation energy. As an estimate of these effects we have calculated $\Delta E(\lambda)$ for the configuration of tangent spheres as a function of λ, the ratio of the radii. Figure 1 gives ΔE_{scale} and ΔE_{red} for $A=235$, $E_s^0=587$ Mev, $E_c^0=827$ Mev (undistorted surface and coulomb energies), $E_v''=60.62A$ Mev (see reference 2; an upper limit $E_v'' \lesssim 96A$ Mev has since been obtained under certain assumptions). In Eq. (4) S^{-1} can then be neglected in comparison with Q^{-1}, so that ΔE is just proportional to $(E_v'')^{-1}$.

With $\dot{\gamma}=0.3$ (estimated by using results of reference 5) $\Delta E(\lambda)$ falls away rapidly from $\lambda=1$, thus decreasing the energies of asymmetric with respect to symmetric configurations. In fact it can be shown[3] that the increase in energy of an incompressible nucleus, when a small asymmetric $\alpha_1 P_1(\cos\theta)$ term is added to the expansion of the saddle-point shape in Legendre polynomials, is $+0.113\alpha_1^2$ (in units of E_s^0), whereas the addition of our ΔE changes this to $-0.043\alpha_1^2$, so that *the asymmetric configuration now has lower energy*. [Note that for tangent spheres $\lambda=(1-\frac{1}{2}\alpha_1)/(1+\frac{1}{2}\alpha_1)$.]

The effect of compressibility affords, therefore, a possible explanation of the asymmetry of fission. The present estimates are crude, but they have brought to light a large effect which does not appear to be sensitive to the approximations made.

We are not in a position to deduce the size of the asymmetry. The minimum in ΔE occurs at a fragment mass ratio of 8:1, but this neglects the dependence on λ of the energy of the incompressible configurations. A tentative estimate of this dependence gives a mass ratio $\sim$2:1.

The calculations also indicate that the compressibility may have a considerable effect on the threshold energy. Actually, the order of magnitude, as given by $\Delta E(1)-\Delta E(0)=5.7$ Mev, is comparable with the empirical threshold energy. This problem and the allied question of the effect of compressibility on nuclear stability are being studied further.

The effect on ΔE of changes in γ due to changes in the curvature of the nuclear surface (like ΔE_{scale} of order $A^{1/3}$) was found to be small.

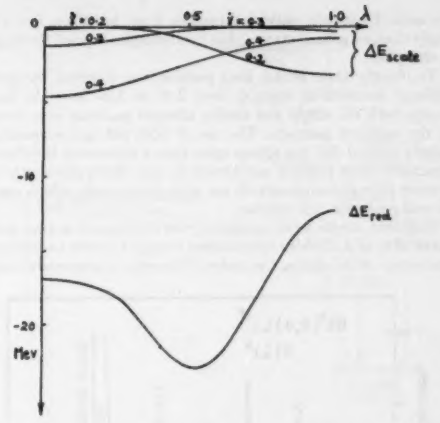

FIG. 1. Corrections ΔE_{scale}, ΔE_{red} due to compressibility for the configuration of tangent spheres as functions of λ, the ratio of the radii.

Quantitative results may be obtained in the future by repeating the calculations of reference 3 with ΔE included in the energy. The asymmetry of the saddle-point shape may provide a possible method of estimating E_s'' empirically.

A fuller account of these investigations will be published in the *Communications* of the Copenhagen Academy of Science.

I wish to thank Professor N. Bohr for his interest in this work, my colleagues at the Institute for many valuable discussions, and the Department of Scientific and Industrial Research (London) for an award.

[1] Plutonium Project, Revs. Modern Phys. **18**, 513 (1946).
[2] W. J. Swiatecki, Proc. Phys. Soc. (London) **63A**, 1208 (1950).
[3] S. Frankel and N. Metropolis, Phys. Rev. **72**, 914 (1947).
[4] J. Jungerman, Phys. Rev. **80**, 285 (1950).
[5] W. J. Swiatecki, Proc. Phys. Soc. (London) **64A**, 226 (1951).

Low Excited States in Li^6 and Be^9

C. P. BROWNE,* R. M. WILLIAMSON,† D. S. CRAIG, AND D. J. DONAHUE
University of Wisconsin, Madison, Wisconsin‡
(Received May 7, 1951)

VARIOUS investigators[1] have reported an energy level in Li^6 at about 2.5 Mev. Pollard and Margenau[1] find a resonance in the yield of alpha-particles scattered by deuterons indicating a level at 2.4 Mev, and Hushley[1] has observed 3-Mev gamma-radiation when beryllium is bombarded with protons. There is also some indication of a resonance in the yield of deuterons scattered from helium in the early data of Heydenberg and Roberts.[1] Unpublished work of Boyer[1] on the $Li^7(d,t)Li^6$ reaction indicates a level at approximately 2.3 Mev in Li^6.

In the present experiment alpha-particles from the reaction $Be^9(p,\alpha)Li^{6*}$ have been observed with a spherical electrostatic analyzer.[2] Protons of well-defined energy from the Wisconsin cylindrical analyzer were allowed to strike targets of thin beryllium foils or thin layers of beryllium evaporated onto nickel foils of 1×10^{-5} cm thickness. The energy of particles emitted at 135° from the incoming beam are measured with the spherical analyzer. A scintillation counter is used for detection. Figure 1 is a plot of number of emitted particles *vs* energy for an incident beam energy of 2.35 Mev. Peaks corresponding to singly, doubly, and triply charged Li^6 particles and doubly charged alpha-particles from the ground-state reaction are found. In addition, peaks attributed to singly and doubly charged alpha-particles from the excited state

are seen. Elastically scattered protons from beryllium and the singly charged ground state alphas have energies beyond the range of this plot.

To identify these peaks, their position was observed for three different bombarding energies from 2.35 to 3.29 Mev. At each energy both the singly and doubly charged particles were found at the expected positions. The use of both foil and evaporated targets verified that the alphas came from a reaction in beryllium. Reactions with possible contaminants and elastically scattered protons from contaminants do not give rise to peaks which could be confused with this reaction.

Sufficient counts to fix accurately the alpha-particle edge were taken only at 2.555 Mev bombarding energy. In order to calculate the energy of the alphas, the center of this edge was compared with

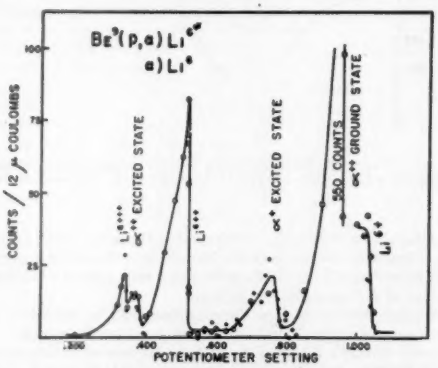

FIG. 1. Alpha and Li^6 counts vs potentiometer setting from 10-microinch beryllium bombarded with 2.35-Mev protons. Potentiometer setting is approximately energy/charge in Mev. Closed and open circles represent data taken with different amplifier gain settings normalized to equalize background counts. Other data at 2.55-Mev bombarding energy from an evaporated beryllium target were used to determine the position of the alpha-edge.

the center of an edge of protons of known energy scattered from thick platinum. Incident proton energies were obtained by calibrating the cylindrical analyzer against the $Li^7(p, n)Be^7$ threshold.[2]

Relativistic corrections were applied to both analyzers and the relativistic expression used to calculate Q values. The targets were heated during bombardment, and after the data were taken scattered protons from carbon contamination on the target were observed. The amount of carbon present had a negligible effect on the measured Q values. The result obtained is -0.064 ± 0.005 Mev. The 0.1 percent uncertainty in the lithium (p, n) threshold[3] adds an additional uncertainty of 0.06 kev to Q. Table I lists the major errors and their effect on the Q value.

Using our value of 2.123 ± 0.004 Mev[4] for the Q of the ground state reaction, the energy level of Li^6 is 2.187 ± 0.009 Mev. The error of our measurement is 0.007 Mev, while the added error of 0.002 Mev is due to the uncertainty in the $Li(p, n)$ threshold.

The slope of the high energy edge of thick target data is such that an upper limit of 8 kev may be given to the width at half-maximum of the excited level. At 2.34-Mev bombarding energy, the ratio of doubly charged ground-state alphas to the sum of singly and doubly charged excited-state alphas was about 8. The differential cross section at 135° in the laboratory system for the excited state reaction was estimated to be $2.2\pm1\times10^{-27}$ cm²/steradian based on a knowledge of the solid angle and resolution of the spherical analyzer.[2]

TABLE I. Summary of errors.

Quantity	$Be^9(p, \alpha)Li^{6g}$ Error	Effect on Q	$Be^9(p, p')Be^{9g}$ Error	Effect on Q
Bombarding energy	0.7 kev	0.5 kev	1.7 kev	1.5 kev
Emitted energy	2.0 kev	4.0 kev	0.60 kev	0.8 kev
Uncertainty in angle	3 min	0.6 kev	3 min	0.2 kev
Total error of our measurement		5 kev		2.5 kev
Lithium (p, n) threshold uncertainty	0.1%	0.06 kev		2.4 kev

Inelastically scattered protons from an energy level in Be^9 (previously reported at 2.422 ± 0.005 Mev from data on $B^{11}(d, \alpha)Be^{9*}$) were observed at a bombarding energy of 3.46 Mev. Our measurement gives the level at 2.433 ± 0.005 Mev. The differential cross section for inelastic scattering at 135° is $1.4\pm0.4\times10^{-27}$ cm²/steradian at 3.46-Mev incident energy. From this data, an upper limit of 3 kev may be given to the level width. Table I lists the estimated errors of both measurements.

* Now at M.I.T., Cambridge, Massachusetts.
† Now at Duke University, Durham, North Carolina.
‡ Work supported by the Wisconsin Alumni Research Foundation and the AEC.
[1] For bibliography see Hornyak, Lauritsen, Morrison, and Fowler, Revs. Modern Phys. 22, 291 (1950).
[2] Browne, Craig, and Williamson, Rev. Sci. Instr., to be published.
[3] Herb, Snowdon, and Sala, Phys. Rev. 75, 246 (1949).
[4] Unpublished.

The Mass-Differences $C^{12}(H^1)_4-O^{16}$, $C^{12}(H^1)_2-N^{14}$, and $C^{12}(H^1)_3-N^{15}$

K. OGATA AND H. MATSUDA
Department of Physics, Faculty of Science, Osaka University, Osaka, Japan
(Received May 18, 1951)

THE Bainbridge-Jordan type mass spectrograph which had been installed in the Osaka University was disassembled in the middle of 1943, and its reconstruction and improvement were commenced in 1947 and completed near the end of 1950. Features of its improvement were in the collimating system and in the evacuating system. The collimating system consists of a hole with a diameter of 0.5 mm, and a slit whose width is 0.005–0.008 mm and whose length is 0.2 mm; the distance between them is 45 cm. The energy-selecting slit, which is placed immediately after the energy selector, is 0.08 mm wide. The photographic plate is located nearly along the direction focusing plane through the double-focusing point, because the depth of velocity focusing is deeper than the direction focusing. The evacuating system consists of one 6-in. fractionating oil diffusion pump, two 4.5-in. oil diffusion pumps, and one mercury diffusion pump with liquid air trap, the vacuum being about $7-8\times10^{-6}$ mm Hg at the operating condition. The ions are created by the ordinary gas discharge in a cylindrical glass discharge-tube with a diameter of about 50 mm and a length of about 50 cm; while a stable electric discharge is maintained using a 20-kv transformer with a rectifier and a 2-μf smoothing condenser. The photographic plates used in this experiment are of the Schumann-type prepared in our laboratory.

Under the above-mentioned conditions, the total breadth of a line of medium intensity near the double-focusing point is about 0.01 mm and the dispersion for a one percent mass difference is about 5.82 mm, resulting in an experimental resolving power of about 58,000. The mass-scale calibration is made by using the separation of $Br^{79}-Br^{79}H^1$ and $Br^{81}-Br^{81}H^1$ for each plate, where the masses of Br^{79}, Br^{81}, and H^1 are assumed to be 78.943, 80.941, and 1.0081, respectively; the masses of Br being the mean values of Aston's[1] and ours,[2] while the mass of H^1 is taken from the Mattauch-Flammersfeld table.[3]

With this apparatus, the mass differences of $C^{12}(H^1)_4-O^{16}$, $C^{12}(H^1)_2-N^{14}$, and $C^{12}(H^1)_3-N^{15}$ have been determined. The results are listed in Table I. The table also contains the $(C^{12})_2(H^1)_4-C^{12}O^{16}$ and $(C^{12})_2(H^1)_4-(N^{14})_2$ mass differences, which were measured in order to check whether any discrepancy exists between atomic-molecular doublets and molecular-molecular

TABLE I. Observed mass differences.

Doublet	No. of doublets measured	ΔM 10^{-4} MU
$C^{12}(H^1)_4-O^{16}$	75	364.43 ± 0.05
$(C^{12})_2(H^1)_4-C^{12}O^{16}$	35	364.51 ± 0.06
weighted mean		364.47 ± 0.04
$C^{12}(H^1)_2-N^{14}$	36	125.94 ± 0.02
$(C^{13})_2(H^1)_4-(N^{14})_2$	18	251.99 ± 0.05
weighted mean		125.97 ± 0.03
$C^{12}(H^1)_3-N^{15}$	45	233.95 ± 0.05

doublets, such as Ewald found.[4] The errors given are estimated from the probable errors based on the internal consistency of the data and also from the error that may occur in the mass scale calibration.

These results indicate that the mass differences of molecular-molecular doublets are in good agreement with those of atomic-molecular doublets within the probable error, for both $C^{12}(H^1)_4-O^{16}$ and $C^{12}(H^1)_2-N^{14}$. Consequently, the weighted mean of $C^{12}(H^1)_4-O^{16}$ and $(C^{13})_2(H^1)_4-C^{12}O^{16}$, and that of $C^{12}(H^1)_2-N^{14}$ and $(C^{13})_2(H^1)_4-(N^{14})_2$, are taken to be the mass differences of $C^{12}(H^1)_4-O^{16}$ and $C^{12}(H^1)_3-N^{14}$, respectively. The mass differences obtained in this way are in fair agreement with Nier's recent values[5] of 364.43 ± 0.22 for $(C^{12})_2(H^1)_4-C^{12}O^{16}$, and 125.97 ± 0.21 for $C^{12}(H^1)_2-N^{14}$. However, our values for $C^{12}(H^1)_3-N^{14}$ and $C^{12}(H^1)_3-N^{15}$ are both slightly larger than those of Ewald,[6] 125.23 ± 0.12 and 233.08 ± 0.20, respectively. Also, there is a great discrepancy between our value for $C^{12}(H^1)_4-O^{16}$ and the recent value, 363.67 ± 0.19, calculated from transmutation data.[7]

From values for the $C^{12}(H^1)_2-N^{14}$ and $C^{12}(H^1)_3-N^{15}$ mass differences and $H^1=1.0081297\pm0.032\times10^{-4}$, listed in the Mattauch-Flammersfeld table,[3] the $N^{15}-N^{14}$ mass difference is $0.997332\pm0.06\times10^{-4}$. On the other hand, this mass difference can be obtained from the Q-value of the $N^{14}(d,p)N^{15}$ reaction and the $d-p$ mass difference. Thus, assuming the Q-value to be 8.615 Mev from Malm and Buechner's recent data,[8] and the $d-p$ mass difference to be 1.006582 as calculated by Tollestrup *et al.*,[9] the $N^{15}-N^{14}$ mass difference turns out to be 0.997330. The agreement between the two values is excellent. However, if we use Nier's recent value[10] of 1.008165±4 for H^1, together with our results, the $N^{15}-N^{14}$ mass difference becomes $0.997367\pm0.06\times10^{-4}$, which is slightly larger than that calculated from the transmutation data.

The authors wish to thank Dr. A. Sugimoto for kindly supplying the concentrated sample of N^{15}.

[1] F. W. Aston, Nature **141**, 1096 (1938).
[2] K. Ogata, Phys. Rev. **75**, 200 (1949).
[3] J. Mattauch and A. Flammersfeld, Isotopic Report (Verlag. d. Zeits. f. Natur., Tübingen, Germany, 1949).
[4] H. Ewald, Z. Naturforsch. **3a**, 114 (1948).
[5] A. O. Nier and T. R. Roberts, Phys. Rev. **81**, 507 (1951).
[6] H. Ewald, Z. Naturforsch. **1**, 131 (1946).
[7] H. E. Duckworth, private communication.
[8] R. Malm and W. W. Buechner, Phys. Rev. **80**, 771 (1950).
[9] Tollestrup, Fowler, and Lauritsen, Phys. Rev. **78**, 372 (1950).
[10] A. O. Nier, Phys. Rev. **81**, 624 (1951).

Angular Correlation of Successive Gamma-Ray Quanta in Cu^{65}

T. WIEDLING AND ALLAN CARLSSON
Laboratory of Physics, University of Stockholm, Stockholm, Sweden
(Received May 8, 1951)

SIEGBAHN *et al.*[1] have given the disintegration scheme of Ni^{65} (Fig. 1). From their measurements they concluded that the excited levels of 1.12 Mev and 1.49 Mev for Cu^{65} have the angular momenta 7/2 and 5/2, or 9/2 and 5/2. The spin of Cu^{65} in the ground state[2] is known to be 3/2.

An investigation of the angular correlation between the two γ-rays in cascade would give more precise information about the

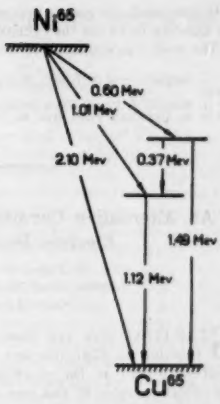

FIG. 1. Disintegration scheme of Ni^{65} (Siegbahn *et al.*).

levels. The angular correlation spectrometer used here consisted of two scintillation counters with 1P21 multipliers and anthracene crystals. The coincidence circuit had a resolving time of about 0.19 μsec.

The Ni^{65} source used was produced by deuteron bombardment of nickel. The deuteron energy was about 7 Mev.

It should be noted that the cascaded energies of 0.37 Mev and 1.12 Mev have rather weak intensities, about 10 and 20 percent, respectively.

The preliminary results of the measurements are given in Fig. 2. If Cu^{65} has a spin of 3/2 in its ground state and it is supposed that the spin of the 1.12-Mev state is 5/2 and that of the 1.49-Mev state is 9/2, one gets, according to Hamilton,[3] for the ratio $f(\pi)/f(\frac{1}{2}\pi)$ between the 180° and 90° directions, a value of 0.90 for a quadrupole-dipole radiation and 1.91 for quadrupole-quadrupole radiation. The first case is in the opposite direction to our experimental value, and the second case is ruled out since this theoretical value is too great and falls far outside the experimental error. Thus we can immediately eliminate a spin of 9/2 for the highest energy state.

If we take a spin of 7/2 for the highest state and if we suppose that we have a quadrupole-quadrupole radiation, we expect

FIG. 2. Angular correlation between the 0.37-Mev and 1.12-Mev gamma-rays. The dashed line represents the calculated angular correlation for dipole-dipole radiation; the solid line represents that for dipole-quadrupole radiation. The circles represent the experimental points.

$f(\pi)/f(\frac{1}{2}\pi)=0.32$, i.e., in the opposite direction to the experimental value.

Finally we may have a dipole-dipole or a dipole-quadrupole radiation. Figure 2 shows, in addition to our experimental points, the angular correlation functions $f(\theta)=1+0.077\cos^2\theta$ (the dashed line) for dipole-dipole radiation and $f(\theta)=1+0.194\cos^2\theta$ (the solid line) for dipole-quadrupole radiation. Our experimental points fit the latter function very well.

A detailed description of the experiment and a discussion of the results will be given in *Arkiv für fysik*.

In conclusion we wish to express our thanks to Dr. K. Siegbahn for allowing us to use the cyclotron of the Nobel Institute.

The work was supported by the Swedish Atomic Committee.

[1] K. Siegbahn and A. Ghosh, Arkiv. f. Mat. Astron. Fysik **36A**, No. 36 (1949).
[2] R. Ritschl, Z. Physik **79**, 1 (1932).
[3] D. R. Hamilton, Phys. Rev. **58**, 122 (1940).

An Alternative Covariant Formulation of the Electron-Positron Theory

O. Costa de Beauregard
Institut Henri Poincaré, Paris, France
(Received April 17, 1951)

STARTING with von Neumann's[1] well-known distribution function $(\psi, E_r\psi)$, one sees easily[2] through Stone's[3] theorem that $(\psi, e^{ivR}\psi)$ is the so-called characteristic function of a hermitian operator R; this may also be written (ψ, f), where f is that solution of

$$-idf/dy = Rf \tag{1}$$

which, for $y=0$, reduces to ψ. When the hamiltonian is time-independent, comparison of (1) with the wave equation shows that $(\psi(t), \psi(t+y))$ is the characteristic function of the total energy,[4] which may then be equivalently represented by the operator $\partial^4 = \partial^t/i$ ($\hbar$ and c are taken as 1, $x_4 = it$).

If ψ_1 and ψ_2 are two solutions of Dirac's equation for an electron moving in an external (nonquantized) 4-potential, and $\delta u^i = [dx_j dx_k dx_l]$ is the volume element on a spacelike surface σ, we let

$$(\psi_1, \psi_2) = \int\int\int_\sigma \bar{\psi}_1 \gamma^i \psi_2 \delta u_i, \tag{2}$$

where $\bar{\psi} = \psi^+\gamma^0$; $\gamma^0 = \gamma^4$; $i, j, k, l = 1, 2, 3, 4$. When integrated at constant time, this expression is the ordinary hermitian scalar product, whose fundamental properties are retained in the general case.

According to the property $(\psi, \psi) \geq 0$, the expression

$$F_\sigma(y_1{}^i, y_2{}^i) = (\psi(x^i + y_1{}^i), \psi(x^i + y_2{}^i))_\sigma \tag{3}$$

is such that, c_p and $y_p{}^i$ being N complex constants and Minkowskian vectors,

$$\Sigma_{p,q}\, c_p{}^* c_q F(y_p{}^i, y_q{}^i) \geq 0. \tag{4}$$

Transforming the difference $F_{b,a} \equiv F_{\sigma b} - F_{\sigma a}$ into a 4-fold integral, and taking Dirac's equation into account, one finds (with $\delta\omega = dx_1 dx_2 dx_3 dx_4/i$)

$$F_{b,a}(y_1{}^i, y_2{}^i) = e\int\int\int\int \{A^k(x^i + y_2{}^i) - A^k(x^i + y_1{}^i)\} \times \bar{\psi}(x^i + y_1{}^i)\gamma_{ik}\psi(x^i + y_2{}^i)\delta\omega. \tag{5}$$

In two important cases F is a function of $y_2{}^i - y_1{}^i$ only, and thus, according to (4) and to Bochner's[5] criterion, is a characteristic function

1—when A^k remains constant along all axes parallel to some 4-vector Y^i and when $y_1{}^i$ and $y_2{}^i$ are parallel to Y^i; this is seen by (5) where one takes σ_b as σ_a is translated parallel to Y^i. For a free electron, the above property holds for any direction in space-time.

2—when σ is a hyperplane $\mathcal{P}$ and when $y_1{}^i$ and $y_2{}^i$ are parallel to $\mathcal{P}$; this is the well-known convolution property.

If the above Y^i is timelike, we take as σ a $\mathcal{P}$ normal to it, and the time axis parallel to it; for a free electron, we take as σ any spacelike surface. According to (1) with ∂^u/i ($u = 1, 2, 3$) or H as R, to the commutativity of translations, and to the exponential's multiplicative property, one sees that $(\psi(x^i), \psi(x^i + y^i))_\sigma$ is the characteristic function of the total 4-momentum $(p^u, p^4 = iW)$. Thus, by combining two very different, though well-known, conditions, relativistic symmetry will be formally preserved in the following calculations.

Now we take an electron which, initially in a Lorentzian frame $\mathcal{L}_1$ and finally in another Lorentzian frame $\mathcal{L}_2$, moves in a time-independent 4-potential; alternatively, we take an electron which is initially or finally free. The transition occurs through an arbitrarily varying 4-potential acting during a finite time. If we take the above $\mathcal{P}_1$ (or σ_1) and $\mathcal{P}_2$ (or σ_2) as infinitely remote, respectively, in past and future, (5) gives the variation of the characteristic function of the total energy-momentum. Its 4-dimensional fourier transform, i.e., the variation of the corresponding density distribution function, is

$$g_{+\infty,-\infty}(p^i) = \bar{\varphi}(p^i)\gamma_{ik}\left\{\int a^k(q^i)\varphi(p^i - q^i)\delta\tau_q\right\} - \left\{\int \bar{\varphi}(p^i + q^i)a^k(q^i)\delta\tau_q\right\}\varphi(p^i) \tag{6}$$

$$= \bar{\varphi}(p^i)\gamma_{ik}\left\{\int a^k(q^i)\varphi(p^i - q^i)\delta\tau_q\right\} + \text{conjugate}, \tag{7}$$

where φ and a^k are the 4-dimensional fourier transforms of ψ and A^k (with $\bar{\varphi} = \varphi^+\gamma^0$, $\delta\tau = dp_1 dp_2 dp_3 dp_4/i$, and the factor $1/4\pi^3$ dropped). Thus g is real and, when integrated over all 4-momentum space, is zero, as it had to be; one goes from (6) to (7) by noticing that $a^k(-q^i) = \pm a^{*k}(q^i)$ and $\gamma^k\gamma^k = \mp\gamma^k\gamma^0$, according as $k = 1, 2, 3$ or $k = 4$.

The closed formulas (6) or (7) are not directly applicable to physical questions, since they yield, in the evolution of a given ψ, the difference between the final and initial weights of the same dynamical state, rather than the transition weights between some state p_1, ψ_1 to some state p_2, ψ_2 as do Feynman's[6] formulas.

Four recent notes[7] of ours are here summarized, and some wrong assertions in them corrected.

[1] J. von Neumann, *Mathematische Grundlagen der Quantenmechanik* (Verlag. Julius Springer, Berlin, 1932).
[2] E. Arnous, J. phys. radium **8**, 87 (1947).
[3] M. H. Stone, Proc. Nat. Acad. Sci. **16**, 172 (1930); and Ann. Math. **33**, 643 (1932).
[4] This is closely related to a theorem by Fock and Krylov, J. Phys. (U.S.S.R.) **11**, 116 (1947).
[5] S. Bochner, *Vorlesungen über Fouriersche Integrale* (Akademische Verlagsgesellschaft, Leipzig, 1932).
[6] R. P. Feynman, Phys. Rev. **76**, 749 (1949).
[7] O. Costa de Beauregard, Compt. rend. **232**, 214, 308, 804, 927 (1951).

Paramagnetic Resonance in Alkali Metal Solutions at Low Fields*

E. C. Levinthal and E. H. Rogers
Varian Associates, San Carlos, California
and
R. A. Ogg, Jr.
Department of Chemistry, Stanford University, Stanford, California
(Received April 23, 1951)

WE have made an investigation of paramagnetic resonance in some alkali metal solutions at low magnetic fields. Measurements involving one of these solutions have been reported by Hutchison and Pastor,[1] and Garstens and Ryan.[2] The principal experiments were performed at a frequency of 49.0 Mc in a precession field of approximately 17.5 gauss. The apparatus consisted of a pair of Helmholtz coils and a conventional nuclear induction system, the latter having a tuned probe into which the various samples could be inserted. A brief summary describing a few of the media investigated follows:

1. Solutions of sodium in liquid ammonia.—A sealed faraday tube capable of withstanding a pressure in excess of 10 atmospheres was fabricated containing a fixed quantity of liquid ammonia and metallic sodium. The concentration of the solution could be varied at will by simple distillation techniques, and temperature effects could be observed by placing the tube in several calibrated baths

ranging between dry ice-acetone temperature (−78 deg C) and room temperature. Equipment limitations made it necessary to estimate concentrations from visual color observations, and therefore the behavior of these solutions with respect to concentration variations must be considered somewhat qualitative.

The signal amplitude was found to be dependent upon concentration, being barely visible at approximately $0.0001M$, growing until a maximum amplitude was reached at $0.1M$, and decreasing in amplitude with further increase in concentration. The ratio of signal amplitude to concentration decreased as the concentration changed from $0.0001M$ to $0.1M$. It is entirely possible that the optimum concentration effect may not have been due completely to a decrease in the susceptibility for high concentrations, but may have been due partially to the increase in electrical conductivity of metal-ammonia solutions at high concentrations. Such large conductivities would lower the sensitivity of the system by reducing the Q of the resonant circuit and simultaneously preventing the penetration of the sample by the radiofrequency field.

An experiment was performed with 0.3 cc, $0.1M$, sealed sodium-ammonia sample to determine the effect of temperature on signal width and amplitude. The results appear in Table I.

The table demonstrates that the signal amplitude from sodium-ammonia exhibits a temperature-amplitude effect opposite to that of the nuclear induction proton signal, the latter behaving in accordance with the temperature dependence of the Curie susceptibility law.

At concentrations above the $0.1M$ optimum amplitude concentration, signal widths up to 0.7 gauss were observed, but at smaller concentrations than $0.1M$ no narrowing to less than 0.08 gauss was observed. The ratio of signal amplitude at room temperature to that at dry ice-acetone temperature was dependent upon concentration, being greater for high concentrations ($\sim 0.1M$) than for low ($\sim 0.001M$).

TABLE I. Temperature dependence of signal width and amplitude.

Temperature degC	Full-width at half-max. amplitude gauss	Signal amplitude (percent of amplitude at room temp.)
−78	0.13	8
0	0.08	79
+21	0.08	100

A sealed sample of sodium in liquid ammonia, kept at −78 deg C during the intervals of non-use, has not deteriorated in the eight weeks since its fabrication. The signal amplitude from this sample has not changed measurably in that period.

2. Solutions of lithium in methylamine.—Faraday tube observations of signals from lithium in methylamine (CH_3NH_2) indicated that the functional dependence of width and amplitude on temperature and concentration was generally similar to that of the metal-ammonia solutions. Compared with these metal-ammonia solutions, an increase of width and an approximately proportional increase in amplitude were observed. The amplitude reached an optimum value at approximately $1M$. Lithium-methylamine showed a less pronounced temperature effect on amplitude than was shown by the metal-ammonia solutions. The ratio of amplitude at room temperature to amplitude at dry ice-acetone temperature was 1.3. The narrowest observed full width was 0.4 gauss. A 0.3-cc, $1.2M$, sealed sample deteriorated rather suddenly after being at room temperature continuously for five hours.

3. Solutions of lithium in ethylenediamine.—Paramagnetic resonance was observed in an open test tube solution and a sealed faraday tube solution of lithium in ethylenediamine ($NH_2CH_2CH_2NH_2$). Signal widths of approximately 0.6 gauss (full width) were seen. Chemical deterioration proved to be so rapid as to render impractical further studies of these solutions.

* This document is based on work performed under AEC Contract for the Radiation Laboratory of the University of California.

[1] C. A. Hutchison, Jr., and R. C. Pastor, Phys. Rev. **81**, 282 (1951).

[2] M. A. Garstens and A. H. Ryan, Phys. Rev. **81**, 883 (1951).

On the Addition Energy for Neutrons in the $h_{11/2}$ Shell*

ALLAN C. G. MITCHELL
Indiana University, Bloomington, Indiana
(Received April 27, 1951)

ACCORDING to the nuclear shell model,[1,2] the region of isomerism extending from neutron-number 63 to 81 is explained by the competitive filling in of the $s_{1/2}$, $d_{3/2}$, and $h_{11/2}$ shells. Good spectroscopic measurements exist on some 11 nuclides in the region $N=69$ to $N=81$ and the energy relations between the $s_{1/2}$, $d_{3/2}$, and $h_{11/2}$ states have been ascertained. This note is written to point out an interesting relationship between the energy necessary to add neutrons to the $h_{11/2}$ shell and the mass number.

Information about the isomers under consideration is given in Table I. Of the six Te isomers two, Te^{129} and Te^{131}, are in the product nucleus; and for these the spin of the ground state is known to be $\frac{3}{2}$. Te^{121}, Te^{123}, and Te^{125} show two lines and hence three states. The internal conversion coefficients, the N_K/N_L ratio, and the half-life show that the states lie in the order $s_{1/2}$, $d_{3/2}$, $h_{11/2}$ with the energy difference between the $h_{11/2}$ and $d_{3/2}$ states as shown in Table I. The remaining Te isotopes have only one line, which has the characteristics of magnetic 2^4-pole radiation and hence $h_{11/2}-d_{3/2}$. Of the other nuclei, the only one showing multiple states is Xe^{133}. In this case the 163-kev line is the only one arising from a metastable state of long life. The half-life indicates magnetic 2^4-pole radiation.

If the $h_{11/2}-d_{3/2}$ energy difference is plotted as a function of the mass number, the curve shown in Fig. 1 is obtained. It will be seen that the energy associated with the addition of neutrons to the $h_{11/2}$ state increases only slowly from $N=69$ to $N=77$. From $N=77$ to $N=81$ this energy increases rapidly as the shell becomes nearly filled. All points fall on a smooth curve with the exception of Xe^{133}, which falls a little high. If one plots instead the $h_{11/2}-d_{3/2}$ difference as a function of neutron number N at $Z=$const (52, 54, 56), one obtains a series of smooth, gradually ascending curves.[3] The fact that the energy difference lies on a smooth curve when plotted against the mass number A apparently shows that the addition energy depends on the size of the nucleus and not just on the neutron number.

It is further interesting to note that the $h_{11/2}-d_{3/2}$ difference in Cd^{111} ($Z=48$, $N=63$) is 51 kev and would also lie on a smooth extension of the curve to lower A. However, the decay scheme of

TABLE I. Summary of information about the isomers of Te, Xe, and Ba.

Isomer	Te^{121}	Te^{123}	Te^{125}	Te^{127}	Te^{129}	Te^{131}
Half-life	140 d	90 d	58 d	90 d	30 d	1.2 d
$\gamma(h_{11/2}-d_{3/2})$ energy (kev)	82[a]	88.5	109.7	88.5	106	177
N_K/N_L	0.77	0.92	1.5	0.75	1	2
Δ	4 mag	4 mag	4 mag	4 mag	4 mag	4 mag
$\gamma(d_{3/2}-s_{1/2})$ energy (kev)	213	159	35.5			
Δ	?	1 mag	?			

Isomer	Xe^{131}	Xe^{133}	Xe^{135}	Ba^{133}	Ba^{137}
Half-life	12 d[b]	5.3 d[d]	10–15 min[e]	38 hr[f]	156 sec[g]
$\gamma(h_{11/2}-d_{3/2})$ energy (kev)	163[c]	232[d]	520[e]	276[f]	661[g]
N_K/N_L	?	2.2	?	3.2	4.8
Δ	4 mag	4 mag	?	4 mag	4 mag

[a] All Te isomers measured by R. D. Hill, Phys. Rev. **76**, 333 (1949).
[b] Brosi, DeWitt, and Zeldes, Phys. Rev. **75**, 1615 (1949).
[c] Kern, Mitchell, and Zaffarano, Phys. Rev. **76**, 279 (1949).
[d] I. Bergström and S. Thulin, Phys. Rev. **79**, 538 (1950).
[e] Peacock, Brosi, and Bogard, Plutonium Project Report Mon N-432, p. 58 (1947); ORNL-176, p. 25 (1948); and ORNL-65, p. 64 (1948). *Nuclear Data* (U. S. Government Printing Office, Washington, D. C., 1950), Natl. Bur. Standards (U. S.) Circ. 499.
[f] J. M. Cork and G. P. Smith, Phys. Rev. **60**, 480 (1941).
[g] A. C. G. Mitchell and C. L. Peacock, Phys. Rev. **75**, 197 (1949).

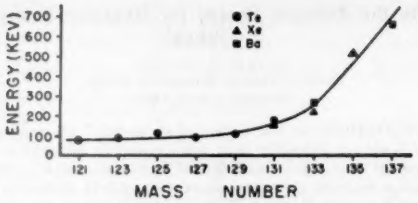

FIG. 1. Energy difference ($h_{11/2}-d_{3/2}$) as function of mass number.

Cd^{111} is rather complicated,[4] and no line corresponding to the $h_{11/2}-d_{3/2}$ transition has as yet been observed. Hence it is not included on the graph or in Table I.

Finally, it will be seen[2] that the $d_{3/2}-s_{1/2}$ difference is decreasing rapidly in the Te isotopes until it disappears at Te^{127}. In the Xe isotopes $s_{1/2}$ lies above $d_{3/2}$ for Xe^{131} but is not seen again at higher mass number.

The author wishes to thank Dr. M. Goeppert-Mayer and Dr. D. R. Inglis for helpful discussions.

* This work was assisted by the joint program of the ONR and AEC.
[1] M. Goeppert-Mayer, Phys. Rev. **78**, 16 (1950).
[2] E. Feenberg and K. C. Hammack, Phys. Rev. **75**, 1877 (1949).
[3] This has been pointed out by R. D. Hill, Phys. Rev. **79**, 1021 (1950).
[4] S. Johansson, Phys. Rev. **79**, 896 (1950).

Gamma-Ray Transitions in B^{10}

DAVID E. ALBURGER
Brookhaven National Laboratory, Upton, Long Island, New York*
(Received May 18, 1951)

IN a recent paper[1] Ajzenberg has proposed a level scheme for B^{10} based on observation of neutron groups from the $Be^9(d, n)B^{10}$ reaction by means of the photographic emulsion technique. The groups correspond to levels in B^{10} at 0.77, 1.79, 2.22, 3.59 Mev and a number of higher excited states. In previous studies[2] by Rasmussen, Hornyak, and Lauritsen the gamma-ray spectrum from the same reaction had been investigated, and quantum transitions

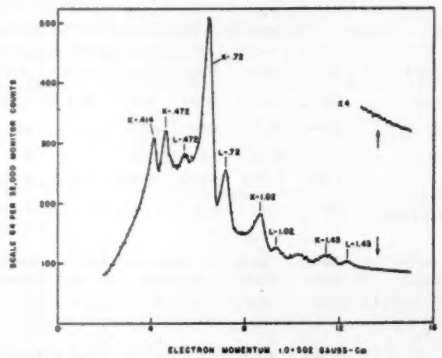

FIG. 1. Spectrum of photoelectric conversion lines below 2 Mev due to gamma-radiation from Be bombarded by 1.2-Mev deuterons. Measurements were made using a lens spectrometer and the deuteron beam was provided by the Brookhaven electrostatic accelerator.

of 0.412, 0.713, 1.017, 1.424, 2.140, 2.856, etc. Mev were found. The relatively high intensity of the 0.713-Mev line and the apparent energy relationships of the various gamma-rays seemed to suggest a scheme of equally spaced levels located at integral multiples of 0.713 Mev above the ground state. However, Ajzenberg pointed out that all of the gamma-rays observed by Rasmussen *et al.* are consistent with the level scheme based on the neutron groups.

Assuming that the level scheme from the neutron work is correct (but using the more accurate energy values of Rasmussen *et al.*) it may be noted that a gamma-ray transition from the 1.73-Mev second excited state of B^{10} to the ground state was not observed by Rasmussen *et al.*, although nearly all other possible transitions between levels occur. Lacking previous knowledge from the neutron groups of the location of the second excited state, a weak gamma-ray of this energy might have been missed.

The gamma-ray spectrum from the $Be^9(d, n)B^{10}$ reaction has been reinvestigated using a deuteron beam from the Brookhaven electrostatic accelerator and a magnetic lens spectrometer to measure the resulting spectrum of prompt gamma-radiation. The target was Be metal 0.005 inch thick located at the standard source position of the spectrometer. Photoelectric conversion electrons due to the emitted gamma-radiation were produced in a 0.001-inch uranium foil attached to the target. In order to normalize the spectrometer count to a fixed number of disintegrations a gamma-ray monitor counter was placed near the target and used to integrate the yield.

Figure 1 shows the spectrum of photoelectrons up to 2 Mev at a bombarding beam energy of 1.2 Mev. The assignments of the lines to the various gamma-rays present are in agreement in respect to energy and relative intensity with the results of Rasmussen *et al.* Their energy values are considered more accurate and have been used to label the peaks in Fig. 1. They have shown that all of these gamma-rays result from the $Be^9(d, n)B^{10}$ reaction except the one at 0.472 Mev which is caused by the $Be^9(d, \alpha)Li^7$ reaction. The region of the spectrum above 2 Mev was not examined here since it is not pertinent to the present investigation.

A search was made in an attempt to detect the possible 1.73-Mev gamma-ray mentioned above. The expected location of the K-shell conversion line of this gamma-ray is shown in Fig. 1 by the arrows; within the statistics of the experiment no such line is found. A gamma-ray intensity for the 1.73-Mev transition of approximately 10 percent of the intensity of the 1.02-Mev gamma-ray could have been detected. It may be concluded that if the level scheme of Ajzenberg is correct then direct transitions from the second excited state to the ground state of B^{10} are unfavored with respect to cascade transitions, presumably because of the relative spins and parities of the three states involved.

* Under contract with the AEC.
[1] F. Ajzenberg, Phys. Rev. **82**, 43 (1951).
[2] Rasmussen, Hornyak, and Lauritsen, Phys. Rev. **76**, 581 (1949).

Nuclear Electron Pairs from $F^{19}(p, \alpha)^*O^{16}$

G. C. PHILLIPS AND N. P. HEYDENBURG
Carnegie Institution of Washington, Department of Terrestrial Magnetism, Washington, D. C.
(Received April 26, 1951)

USING the pressurized electrostatic generator to accelerate protons, the reaction $F^{19}(p, \alpha)^*O^{16}$ yielding pairs of electrons[1] from the excited state at 6.05 Mev in O^{16} has been studied. Detection of the electrons was accomplished by means of two anthracene scintillation counters in coincidence. The resolving time of 10^{-9} second was sufficiently short to discriminate well against the larger gamma-ray background due to the excited states of O^{16} at 6.1, 6.9, and 7.1 Mev that are also formed by the bombardment.[1]

For targets, thin evaporated deposits of CaF_2 on metallic backings were used. Care was taken to reduce to a minimum the amounts of matter in the region of the target and detectors, so as to minimize electron scattering and the production of secondary electrons.

Since previous experiments[1-3] had not been performed with techniques ideal for the determination of the width of states in

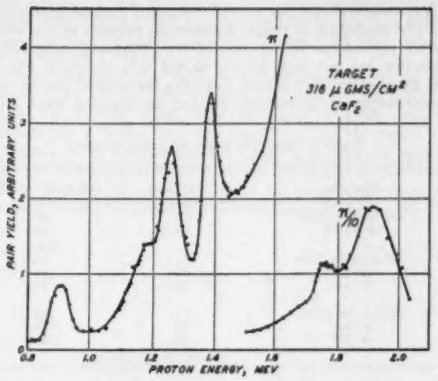

FIG. 1. Excitation curve of the $F^{19}(p; \alpha, \pi)O^{16}$ reaction taken with a CaF_2 target of thickness 316 $\mu g/cm^2$.

Ne^{20} that form the pair emitting states in O^{16}, this has been reinvestigated. The general shape of the excitation curve for pair production is shown in Fig. 1 for the energy interval 0.8 to 2.0 Mev. Five pair resonances occurring at bombarding energies below 1.4 Mev were studied in detail, using very thin targets. These data are shown in Figs. 2 and 3, where for energy calibration the gamma-ray yield as measured by a shielded Geiger counter is also shown. Small gamma-ray effects in the coincidence yield are noted in Fig. 2 for the very strong 873.5- and 935-kev gamma-ray resonances. These effects were difficult to eliminate completely and can be attributed, in this case, to the scattering of secondary electrons between detectors. The observed pair resonances occur at the following bombarding proton energies (their widths are given in parentheses): 710 kev (35 kev), 842 kev (24 kev), 1130 kev (43 kev), 1236 kev (58 kev), and 1367 kev (26 kev). An unsuccessful search was made in the energy region of 730 kev where a resonance for pair emission has been reported.[4]

To provide energy calibration, and to test the energy homogeneity of the beam the 873.5-kev gamma-ray resonance was excited using a very thin target. The observed width was 5.6 kev. Thus the states in Ne^{20} yielding the pair emitting state in O^{16} must have the widths given above and so are considerably wider than the corresponding states in Ne^{20} that excite the gamma-ray emitting states in O^{16}.

The angular correlation of the pairs was determined in the plane normal to the proton beam direction for a bombarding energy of

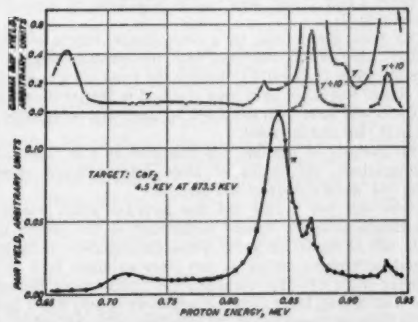

FIG. 2. Excitation curves of the $F^{19}(p; \alpha, \gamma)O^{16}$ and $F^{19}(p; \alpha, \pi)O^{16}$ reactions taken simultaneously using a thin CaF_2 target.

1.23 Mev. These data, uncorrected for the finite solid angle of the counters, can be fitted with the function $1+0.6\cos\theta$ and agree reasonably well with the only other reported observation.[5]

Since the (0 even) to (0 even) transition that is assumed to occur for the pair emission also allows a two-photon decay, a search has been made for pairs of gamma-ray quanta. A thin target was bombarded with a proton energy of 1.23 Mev. Counting rates were

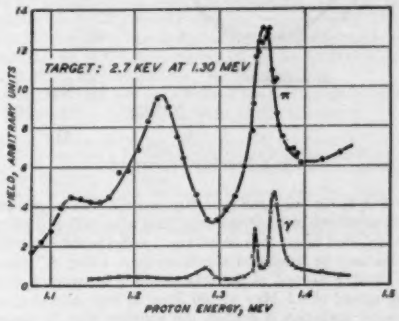

FIG. 3. Excitation curves of the $F^{19}(p; \alpha, \gamma)O^{16}$ and $F^{19}(p; \alpha, \pi)O^{16}$ reactions taken simultaneously using a thin CaF_2 target.

taken with and without sufficient aluminum absorber in front of each crystal to stop all pair electrons originating in the target. The absorber decreased the counting rate by a factor $>10^4$. If one assumes a gamma-ray counting efficiency of about 2 percent for the possible continuous spectrum of gamma-rays, it appears that there are not more than 50 percent as many gamma-ray pairs as there are electron pairs.

[1] Chao, Tollestrup, Fowler, and Lauritsen, Phys. Rev. **79**, 108 (1950).
[2] Bennett, Bonner, Mandeville, and Watt, Phys. Rev. **70**, 882 (1946).
[3] Streib, Fowler, and Lauritsen, Phys. Rev. **59**, 253 (1941).
[4] Devons, Hine, and Lindsey, Harwell Conference (1950).
[5] Devons, Hereward, and Lindsey, Nature **164**, 586 (1949).

Excitation Functions with an Internal Cyclotron Beam*

NORTON M. HINTZ†
Nuclear Laboratory, Harvard University, Cambridge, Massachusetts
(Received May 11, 1951)

THE stacked foil method for obtaining nuclear excitation functions may be used with the internal cyclotron beam if the beam is deflected by multiple coulomb scattering in a thin foil placed in the median plane. Since the "source" of particles is then well defined by the edge of the scatterer, 180° focusing may be utilized to obtain a secondary beam which is very homogeneous in energy.

In a stacked foil experiment, the energy resolution is usually limited by the spread in energy of the incident beam rather than by range straggling in the absorbers. An initial width, ΔE_0, will increase as E^{-1} as the particles penetrate the foils and absorbers. Measurements made on the proton beam of the Harvard cyclotron[1] show a width at half-maximum of 12 Mev at 110 Mev. Consequently, some method must be found to improve the energy definition for stacked foil experiments without an undue sacrifice of intensity.

The arrangement being used at Harvard is shown in Fig. 1. The scattering probe consists of 5 mils of tantalum on a polystyrene rod which passes through a hole in the cyclotron dee. The targets are placed one inch above or below the median plane, and as near the correct azimuthal angle for energy focusing,

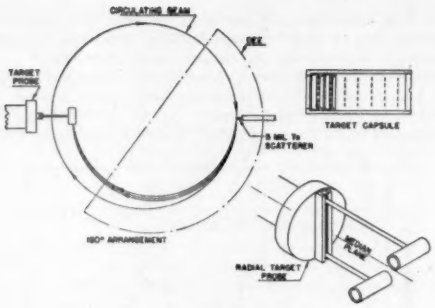

FIG. 1. Experimental geometry.

$\pi(1-n)^{-\frac{1}{2}}$, as the cyclotron geometry permits. The targets consist of foils or pellets, interspersed with brass absorbers and placed in a semi-shielded target capsule held on a radial probe. Several such capsules may be irradiated simultaneously. Using $\frac{1}{16}''$ diameter foils, about $\frac{1}{2}$ percent of the total beam is intercepted with an energy spread of 0.5 Mev at 100 Mev. If high intensity, rather than good resolution is desired, the scatterer may be placed, in the median plane, directly above or below the targets. Particles of all energy are then refocused at the target radius, after one revolution, giving an efficiency of 7.5 percent. No collimation is used in front of the targets, as this was found to spoil the energy resolution and increase the neutron background. Instead, the absorbers were made slightly larger than the foil area.

Three excitation functions for protons on aluminum are shown in Fig. 2. The activities from irradiating Al^{27} have been assigned to F^{18} (112 min), Na^{24} (15 hr), and Na^{22} (2.6 yr). A considerable amount of ~20-min activity was present, presumably owing to C^{11}; but this could not be accurately resolved from the decay curves. Identification of these nuclei rests on half-life, absorption curves, and chemical separations.

Polystyrene foils (C_nH_n) were included in the target assembly to monitor the proton current with the $C^{13}(p, pn)C^{11}$ reaction.[2] In calculating the absolute cross sections shown in Fig. 2, corrections were applied for absorption and scattering of the β-rays counted, a neutron background of a few percent, and loss of protons by nuclear absorption in the absorber stack.

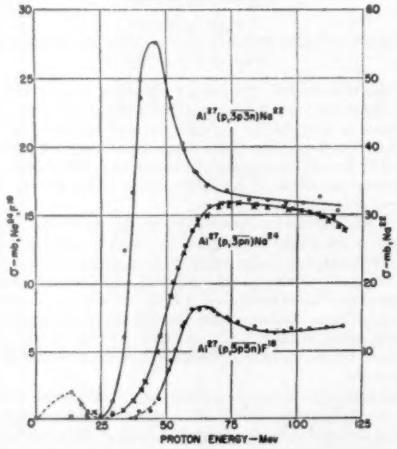

FIG. 2. Excitation functions for protons on aluminum.

A correction should also be made for loss of protons by multiple coulomb scattering. A rough experimental estimate of this effect gives 5 percent loss for protons just traversing their range. This correction has not been applied to the data shown in Fig. 2. The thresholds to be expected, including the sums of the coulomb barrier heights for all particles emitted, are shown in Table I for several modes of emission. It is evident that α-particles or heavier fragments are emitted with high probability in the formation of Na^{22} below 64 Mev and F^{18} below 110 Mev.

TABLE I. Thresholds in the laboratory system.

Reaction	$-Q$, Mev	$-Q$+barrier, Mev
$Al^{27}(p, 3pn)Na^{24}$	32	44
(p, pHe^3)	24	36
$Al^{27}(p, 3p3n)Na^{22}$	52	64
$(p, \alpha d)$	20	32
(p, Li^6)	18.5	30
$Al^{27}(p, 5p5n)F^{18}$	91	110
$(p, 2\alpha d)$	30	49
(p, B^{10})	24	41

I wish to thank Professor Norman F. Ramsey for suggesting this problem and for helpful discussions.

* Assisted by the joint program of the ONR and AEC.
† Assisted by a Shell Development Company fellowship.
[1] N. Bloemberger and P. J. van Heerden, Phys. Rev. **83** (to be published).
[2] Aamodt, Peterson, and Phillips, UCRL-526 (1949).

A High Energy γ-Ray Line in the Spectrum of Mg^{24}

L. E. BEGHIAN, G. R. BISHOP, AND H. HALBAN
Clarendon Laboratory, Oxford, England
(Received May 7, 1951)

IN a previous communication[1] an upper limit (5×10^{-5} photon/disintegration) was stated for the intensity of the 4.14-Mev γ-ray cross-over transition in Na^{24}. Recently, Cavanagh and Turner of AERE Harwell[2] pointed out that measurements with a β-ray spectrometer and kicksorter indicated an intensity of 1 in 2000 disintegrations for a γ-ray line with an energy of about 4.1 Mev. However, the authors state that the possibility remains that the γ-ray is some 4 to 7 percent lower in energy than the cross-over. In view of the apparent contradiction between these two results, a further investigation seemed useful.

As before, an ionization chamber[3] containing deuterium gas (5 atmos) was used with a linear amplifier, but this time the output was examined with a 25-channel kicksorter. It was found possible to resolve a high energy photoproton peak from the γ-ray background (Fig. 1).

This peak corresponds to a photoproton energy of (0.695 ± 0.025) Mev, which, combined with the binding energy of the deuteron, gives (3.62 ± 0.05) Mev for the γ-ray energy. A line of this energy would not have been observed in the previous search since it would have been swamped by the γ-ray background accepted in that measurement.

The intensity of the line was measured as 1 in (2500 ± 250) disintegrations, the results of three determinations agreeing within the statistical errors of 3 percent.

Above this line a long tail was recorded which was indistinguishable from the natural background of the counter (0.25 count/min at 30,000 ion pairs). From the statistical deviation of several background counts we can place an upper limit on the intensity of the 4.14-Mev γ-line as 2×10^{-6} photons per disintegration. This is even lower than the previously quoted upper limit.

The over-all linearity of the amplifier plus kicksorter was checked with a calibrated pulse generator throughout the runs.

The relation between proton pulse height and channel number was found to be correct within 2 percent by ascertaining the positions of the photoproton peaks produced by the 2.618-Mev γ-line of RdTh and the 2.758-Mev γ-line of Na^{24}.

Three measurements were made in consecutive weeks with sources of Na_2CO_3 and NaF irradiated to about 100 mC in the pile at AERE Harwell. First, with the source far away from the counter the 2.76-Mev line was recorded; then the source was brought close to measure the high energy γ-line. Known attenuation was introduced to bring the pulse height into the kicksorter range. Bringing the source close to the counter increases the average ionization current due to γ-rays, and it was necessary to

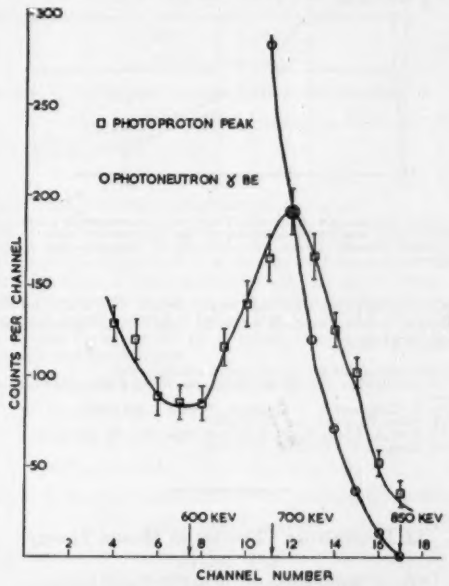

FIG. 1. Photoproton distribution from Na^{24} γ-rays disintegrating deuterium in ion chamber; and deuterium recoils from RdTh-γ-Be neutrons.

check the validity of extrapolating the energy calibration from the low energy region to the expected photoproton energy. This was done by examination of the deuteron recoil spectrum produced by a RdTh-γ-Be source with successive increases of the γ-ray background. No significant shift with γ-ray intensity was observed, and the position of the end point of the recoil spectrum agreed with the expected maximum energy (848 kev) to within 3 percent.

It is difficult to reconcile the correct position of the recoil spectrum end point with an instrumental shift of the photoproton peak. The possibility of positive ion effects in the chamber has been considered carefully, and calculation showed that the worst possible case of reduction of pulse height would produce a loss of 10 percent. Taking the extreme case of 10 percent and adding the calibration errors, etc., the photoproton energy might be as high as 790 kev and the energy of the γ-ray accordingly 3.81 Mev.

It is unlikely that the line is due to impurities in the irradiated material, since the same results were obtained with Na_2CO_3 and NaF, and the counting at the peak decreased with the period of Na^{24}.

It is interesting to compare the upper limit for the 4.14-Mev cross-over line (2×10^{-6}) with the theoretical predictions by Blatt and Weisskopf.[4] Assuming the well-known 4^+, 2^+, 0^+ assignment for the 4.14-Mev, 1.37-Mev, and ground-state level of Mg^{24}, the probability of the 4.14-Mev $(2)^4$-pole relative to the 2.76-Mev $(2)^2$-pole becomes 10^{-6}.

As to the new line (the energy of which as stated, lies between 3.6 and 3.8 Mev) it has to be decided whether it is due to a transition from the 4.14 Mev level to a new level at (400 ± 100) kev or to a transition from a new (3.7 ± 0.1)-Mev level to the ground state. The first alternative can be excluded by considering the various transition probabilities concerned in such a scheme (again using the calculations of Blatt and Weisskopf). The only possible transition probability would need an assignment of 7^+ to the (400 ± 100)-kev level. Similarly, for the second alternative we can exclude all spin and parity assignments for the 3.7-Mev level other than 2^+ or 2^-, or values above 7 for the spin.

We are indebted to Lord Cherwell for his interest in this work and for extending to us the facilities of this laboratory.

[1] Bishop, Halban, and Wilson, Phys. Rev. **77**, 416 (1950).
[2] P. Cavanagh and J. F. Turner, Cambridge Phil. Soc., to be published. We are indebted to the authors for communicating their manuscript to us and for a stimulating discussion.
[3] Wilson, Beghian, Collie, Halban, and Bishop, Rev. Sci. Instr. **21**, 699 (1950).
[4] J. M. Blatt and V. F. Weisskopf, privately circulated notes to appear as part of a book on nuclear physics. The authors believe the formula to be correct to a factor of $10^{\pm1}$.

Continuous γ-Radiation of β-Emitters*

L. MADANSKY AND F. RASETTI
The Johns Hopkins University, Baltimore, Maryland
(Received May 5, 1951)

IT has long been known that a weak continuous γ-radiation is emitted in the β-decay of nuclei.[1] The theory of the effect was first given by Knipp and Uhlenbeck[2] and Bloch,[3] and later extended to include forbidden β-transitions and different kinds of β-interactions by Chang and Falkoff.[4]

The increased efficiency of detection of γ-radiation allowed by the use of scintillation counters suggested a new and more quantitative investigation of the phenomenon. Sources of P^{32} and RaE of the order of 0.1 millicurie were used. The γ-radiation was measured by means of NaI(Tl) crystals (about $1\times1\times0.5$ cm), a 5819 phototube, a linear amplifier, and a one-channel discriminator. The γ-continuum to be investigated and γ-ray lines for energy calibration were also observed and photographed on an oscilloscope screen. Both the total intensity and the spectral distribution of the continuum were studied.

To avoid admixture of ordinary bremsstrahlung produced in the stopping of the β-rays, the following arrangement was used. The sources were deposited on relatively thin supports (3 mg/cm² Cellophane for P^{32} and 3 mg/cm² Ni for RaE) and placed at about 15 cm from the lead-shielded detector. A beam from the source was allowed through a $\frac{1}{2}$-inch hole placed at half the distance between source and detector. This diaphragm was covered with a $\frac{1}{2}$-inch Lucite plate to absorb the β-rays completely. Various tests have satisfied us that with this geometry ordinary bremsstrahlung produced in the support and other materials near the source did not exceed a few percent of the total measured γ-intensity.

Energy calibration of the pulse size was obtained by measuring the position of the peaks due to the 87-kev line of Cd^{109}, the 47-kev line of RaD, and the annihilation radiation. In the low energy region investigated (30–300 kev) it was assumed that the pulse represented the energy dissipated in the crystal by photoelectric absorption, as the photoelectric cross section in NaI at these energies is much larger than the scattering cross section. Corrections were applied to the measured pulse-size distribution to allow for the following factors: (1) absorption in the Lucite plate, (2) efficiency of the crystal (this was calculated by means of the known absorption coefficients in I and Na); and (3) lack of resolution of the detecting system. For the last purpose, the shape of the peaks due to monochromatic lines was measured and found to be approximately represented by gaussian curves with a width at half-

maximum $2w(\ln 2)^{\frac{1}{2}}=38$ kev. For the purpose of comparing the experimental spectra with the theory, the theoretical spectral distribution $S(k)$, ($k=h\nu/mc^2$), corrected for absorption and crystal efficiency, was transformed by numerical integration into the distribution

$$F(k)=\int_0^{w_0-1} S(k')\exp[-(k-k')^2/w^2]dk',$$

which should directly correspond to the measured one.

Figure 1 shows the theoretical curves of $F(k)$ and the experimental points for both P^{32} and RaE. In the latter case, the use of the function $S(k)$ for allowed transitions is questionable, since RaE is a heavy nucleus and exhibits a forbidden β-spectrum. The agreement of the low energy continuum with the theory seems to indicate lack of sensitivity of the γ-spectrum to the forbiddenness of the β-transition in this energy region.

Within the measured energy range, the theoretical and experimental spectra agree closely (Fig. 1), and we shall assume that they also agree in the higher and lower energy regions. The theoretical curve of $S(k)$ and a curve corrected for absorption and crystal efficiency are shown in Fig. 2. To determine the absolute intensity of the continuum of P^{32}, all pulses above 90 kev ($0.175\ mc^2$) were counted, and referred to the number of β-decays from the same source. The number of β-rays was measured with a Geiger counter and corrected for absorption in air and counter window. We found 2.4×10^{-3} γ-quanta above 90 kev per β. The ordinates of the $S(k)$ curves in Fig. 2 are normalized according to this figure. From the normalized curve of $S(k)$ we plotted a curve of $kS(k)$ and by graphical integration from zero to the upper energy limit, we found that the energy emitted by P^{32} in the form of γ-radiation is 3.2×10^{-3} mc^2 per β. For RaE, the number of γ-quanta above 90 kev was 1.6×10^{-3} per β.

The theoretical value for the total intensity in P^{32} can be found by integrating the exact expression for $kS(k)$ neglecting Z-dependence and assuming an allowed β-transition. This number is 2.4×10^{-3} mc^2 per β.

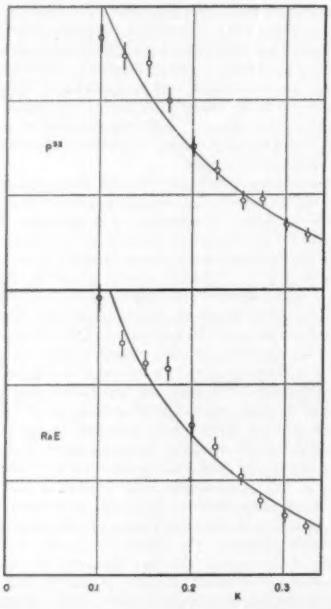

FIG. 1. Continuous γ-ray spectra. Curves represent the theoretical function $F(k)$, circles experimental points. Ordinate scale is arbitrary.

We conclude that both the total intensity and the spectral distribution show no significant discrepancy with the theory. The total intensity in P^{32} had been measured by Wu[1] with essentially the same result. No evidence was obtained for the emission of characteristic x-radiation from RaE reported by Bramson.[5]

Preliminary experiments on $\beta-\gamma$ angular correlation by discriminating the energies of both radiations, show a strong forward-

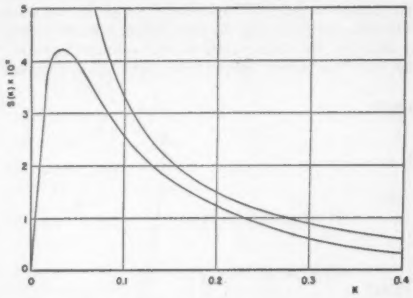

FIG. 2. Continuous γ-ray spectra. Upper curve represents the theoretical function $S(k)$ normalized according to the experimental value of the integrated intensity. Lower curve corrected for absorption and crystal efficiency.

backward asymmetry for high energy β-rays. This effect and the shape of continua emitted in highly forbidden β-transitions are being investigated.

* Research carried out under contract with the AEC.

[1] C. S. Wu, Phys. Rev. **59**, 481 (1941), also includes references to earlier work.
[2] J. K. Knipp and G. E. Uhlenbeck, Physica **3**, 425 (1936).
[3] F. Bloch, Phys. Rev. **50**, 272 (1936).
[4] C. S. Wang Chang and D. L. Falkoff, Phys. Rev. **76**, 365 (1949).
[5] S. Bramson, Z. Physik **66**, 721 (1930).

An Equivalence Theorem in Meson Theory

K. V. ROBERTS
King's College, Cambridge, and H. H. Wills Physical Laboratory, University of Bristol, England

(Received May 7, 1951)

THE following equivalence theorem may be of interest; it arose during a discussion with Dr. N. Kemmer.

It is well known that the lagrangian for the charged scalar meson field, for example, interacting with the electromagnetic field, may be written in either of the two equivalent forms

$$\mathcal{L}_a=\chi(\chi^2U^\dagger U-U_i^\dagger U^i) -ie\chi(A_iU^\dagger U^i-A^iU_i^\dagger U)-e^2\chi A_iA^iU^\dagger U, \quad (1)$$

$$\mathcal{L}_b=\tfrac{1}{2}i(\psi^*\beta^i\partial_i-(\partial_i\psi^*)\beta^i\psi)+\chi\psi^*\psi+e\psi^*\beta^iA_i\psi, \quad (2)$$

where

$$U^i=\partial^iU, \quad U_i^\dagger=\partial_iU^\dagger, \quad (3)$$

and

$$\begin{aligned}\Gamma_k^*\beta_i\psi&=i\chi g_{ki}U, & \psi^*\beta_i\Gamma_k&=-i\chi g_{ki}U^\dagger,\\ \Gamma_k^*\psi&=U_k-ieA_kU, & \psi^*\Gamma_k&=U_k^\dagger+ieA_kU^\dagger.\end{aligned} \quad (4)$$

(The notation of Harish-Chandra[1] is used throughout.)

The different types of vertex which can occur in a Feynman-Dyson graph are known[2] to correspond to the different terms in the interaction lagrangian $\mathcal{L}^i$. It is therefore remarkable that the two interaction lagrangians, $\mathcal{L}_a{}^i$ and $\mathcal{L}_b{}^i$, are not the same, so that while only 3-vertices occur in case (b), both 3-vertices and 4-vertices occur in case (a). The purpose of this note is to show that this

difference is compensated by a difference in the propagation factors associated with some of the lines, so that both formulations lead to the same S-matrix.

To obtain the correct propagation factors,[2,3] it is convenient to write the lagrangian equations in the general form

$$-\left\{\frac{\partial \mathfrak{L}^f}{\partial \phi^\alpha}-\partial_i\left(\frac{\partial \mathfrak{L}^f}{\partial \phi_i{}^\alpha}\right)\right\}=\frac{\partial \mathfrak{L}^i}{\partial \phi^\alpha}-\partial_i\left(\frac{\mathfrak{L}^i\partial}{\partial \phi_i{}^\alpha}\right), \tag{5}$$

where $\mathfrak{L}^f$ is the free lagrangian, $\mathfrak{L}^i$ is the interaction lagrangian, ϕ^α is an arbitrary field function, and $\phi_i{}^\alpha=\partial_i\phi^\alpha$. Thus in case (a)

$$\begin{aligned}-\chi^2U^\dagger-\chi\partial^iU_i{}^\dagger&=ie\chi A^iU_i{}^\dagger+ie\chi\partial^i(A_iU^\dagger)-e^2\chi A_iA^iU^\dagger,\\ -\chi^2U-\chi\partial_iU^i&=-ie\chi A_iU^i-ie\chi\partial_i(A^iU)-e^2\chi A_iA^iU,\end{aligned} \tag{6}$$

while in case (b)

$$\begin{aligned}i\partial_i\psi^*\beta^i-\chi\psi^*&=e\psi^*\beta^iA_i,\\ -i\beta^i\partial_i\psi-\chi\psi&=e\beta^iA_i\psi.\end{aligned} \tag{7}$$

In case (a) the Feynman function $\Omega_F(x)$ satisfies the equation

$$-(\chi^2+\chi\Box)\Omega_F(x)=i\delta(x), \tag{8}$$

with $\Box=\partial^i\partial_i$, so that

$$\Omega_F(x)=-(1/\chi)\Delta_F(x), \tag{9}$$

where $\Delta_F(x)$ is the Feynman solution of the equation

$$(\Box+\chi^2)\Delta_F(x)=i\delta(x). \tag{10}$$

(The operator on the left of (8) is the same as the operator on the left of the second Eq. (6); similarly for Eqs. (12) and (7), respectively. Equation (9) is not the most general definition for the Feynman function, but it is correct here because the conditions for Lemma III of part III are satisfied). The factors associated with the lines are therefore:

$$\left.\begin{aligned}\{U(x),U^\dagger(y)\}&\quad -(1/\chi)\Delta_F(x-y),\\ \{U(x),U_k{}^\dagger(y)\}&\quad -(1/\chi)\partial\Delta_F(x-y)/\partial y^k,\\ \{U^i(x),U^\dagger(y)\}&\quad -(1/\chi)\partial\Delta_F(x-y)/\partial x_i,\\ \{U^i(x),U_k{}^\dagger(y)\}&\quad -(1/\chi)\partial^2\Delta_F(x-y)/\partial x_i\partial y^k.\end{aligned}\right\} \tag{11}$$

In case (b) the function $\mathbf{\Omega}_F(x)$ is a matrix, satisfying the equation

$$-(i\beta^i\partial_i+\chi)\mathbf{\Omega}_F(x)=i\mathbf{I}\delta(x), \tag{12}$$

where $\mathbf{I}$ is the unit matrix. Multiplying (12) by

$$-[(\Box+\chi^2)/\chi+i\beta^k\partial_k-(1/\chi)\beta^j\beta^k\partial_j\partial_k], \tag{13}$$

and using the relations

$$\beta^i\beta^j\beta^k+\beta^k\beta^j\beta^i=\beta^ig^{jk}+\beta^kg^{ij}, \tag{14}$$

one obtains the equation

$$\begin{aligned}(\Box+\chi^2)\mathbf{\Omega}_F(x)=-i[(\Box+\chi^2)/\chi+i\beta^k\partial_k\\ -(1/\chi)\beta^j\beta^k\partial_j\partial_k]\mathbf{I}\delta(x),\end{aligned} \tag{15}$$

so that[4,5]

$$\mathbf{\Omega}_F(x)=-[(\Box+\chi^2)/\chi+i\beta^k\partial_k-(1/\chi)\beta^j\beta^k\partial_j\partial_k]\mathbf{I}\Delta_F. \tag{16}$$

The variables ψ, ψ^* of the interaction representation (b) may be divided into two sets $\hat{0}$, $\hat{0}^\dagger$ and $\hat{0}^i$, $\hat{0}_i{}^\dagger$ say, according to

$$\begin{aligned}\Gamma_k{}^*\beta_l\psi&=i\chi g_{kl}\hat{0}, & \psi^*\beta_l\Gamma_k&=-i\chi g_{kl}\hat{0}^\dagger,\\ \Gamma_k{}^*\psi&=\hat{0}_k, & \psi^*\Gamma_k&=\hat{0}_k{}^\dagger.\end{aligned} \tag{17}$$

To get the correct propagation factors for these new variables, one transforms the matrix $\mathbf{\Omega}_F(x)$ by the appropriate pairs of matrices occurring in (17), so that the factor for the pair $\{\hat{0}^i(x),\hat{0}_k{}^\dagger(y)\}$, for example, is

$$\Gamma^{i*}\mathbf{\Omega}_F(x-y)\Gamma_k. \tag{18}$$

Equation (18), and the three similar expressions, may be evaluated with the help of the relations

$$\begin{aligned}\beta_k\beta^l\Gamma_m&=\Gamma_kg^l{}_m, & \Gamma_k{}^*\beta_l\beta_m&=g_{kl}\Gamma_m{}^*,\\ \Gamma_k{}^*\beta^l\Gamma_m&=0, & \Gamma_k{}^*\Gamma_l&=g_{kl}.\end{aligned} \tag{19}$$

The factors obtained in this way are:

$$\left.\begin{aligned}\{\hat{0}(x),\hat{0}^\dagger(y)\}&\quad -(1/\chi)\Delta_F(x-y),\\ \{U(x),U_k{}^\dagger(y)\}&\quad -(1/\chi)\partial\Delta_F(x-y)/\partial y^k,\\ \{U^i(x),U^\dagger(y)\}&\quad -(1/\chi)\partial\Delta_F(x-y)/\partial x_i,\\ \{U^i(x),U_k{}^\dagger(y)\}&\quad -(i/\chi)g_k{}^i\delta(x-y)-(1/\chi)\partial^2\Delta_F(x-y)/\partial x_i\partial y^k.\end{aligned}\right\} \tag{20}$$

Only the last of these differs from the corresponding factor (11). The extra term $-(i/\chi)g_k{}^i\delta(x-y)$ evidently links two 3-vertices together, thus producing an effective 4-vertex which is just equivalent to the extra 4-vertex which appears in (a). This ensures that the two S-matrices are always the same.

The interaction representations (a) and (b) are actually identical: they have the same field variables, hamiltonian operators, invariant commutation rules, and equations of motion. But because the interaction lagrangians $\mathfrak{L}_a{}^i$ and $\mathfrak{L}_b{}^i$ are not the same, that part of the interaction hamiltonian function $\mathfrak{IC}^i$ which must be counted as a 'higher-order term', and therefore dropped,[3] is defined differently in the two cases. Our discussion illustrates the fact that this term need not always be surface-dependent. It also shows that the propagation factors for the lines of a Feynman-Dyson graph are not adequately defined by the invariant commutation rules, nor by the free equations of motion, but only by the inhomogeneous lagrangian equations,[3] written in the form (5).

Similar equivalence theorems hold in vector meson theory, etc.

[1] Harish-Chandra, Proc. Roy. Soc. (London) A**186**, 502 (1946).
[2] The lagrangian methods here are justified by a general scheme of dynamics developed by the author, contained in a series of papers under the general title "On the Quantum Theory of the Elementary Particles." Part I has already been published [see reference (5)], parts II and III are in press, and parts IV and V are in preparation. See also the important papers by Z. Koba, Prog. Theor. Phys. **5**, 139, 696 (1950); and K. Nishijima, Prog. Theor. Phys. **5**, 331, 813 (1950).
[3] D. C. Peaslee, Phys. Rev. **81**, 94 (1951).
[4] T. Kinoshita, Prog. Theor. Phys. **5**, 473 (1950).
[5] K. V. Roberts, Proc. Roy. Soc. (London) A**204**, 123 (1950).

The Angular Correlation Theorem and the Elimination of Interference Terms

H. A. Tolhoek and S. R. de Groot
Institute for Theoretical Physics, University of Utrecht, Netherlands
(Received May 18, 1951)

In theoretical considerations on angular correlation use is made of a theorem that enables one to avoid certain interference terms.[1] On this subject of elimination of interference terms we have proved a theorem that contains the mentioned theorem as a special case.

We consider a transition probability from an initial state i, which may be a "mixture," via certain intermediate states e to one or more final states f. It is assumed that its value is determined by second-order perturbation theory in such a way that we can take other factors than the matrix elements together in one factor A

$$P_{if}=A\,\Sigma_f\,S_1S_2\,|\,\Sigma_e\,(i|H_1|e)(e|H_2|f)\,|^2. \tag{1}$$

(S_1 and S_2 denote summations that have to be carried out for certain variables in $(i|H_1|e)$ and $(e|H_2|f)$ respectively.) Under certain conditions mentioned below, interference terms in (1) can be eliminated, so that we can reduce (1) to the simplified form

$$P_{if}=A\,\Sigma_f\,\Sigma_e\,[S_1|(i|H_1|e)|^2][S_2|(e|H_2|f)|^2]. \tag{2}$$

In order to indicate the conditions under which (1) and (2) are equivalent we define a density matrix ρ by

$$(e_1|\rho|e_2)=NS_1(i|H_1|e_1)^*(i|H_2|e_2). \tag{3}$$

N is a normalization factor by which ρ is normalized. e_1 and e_2 denote two of the fundamental states that have been taken as intermediate states in (2).

We now state that (1) and (2) are equivalent if ρ, defined by (3), is in diagonal form for the fundamental states ψ_e, used in (2).

To prove this theorem we write

$$\left.\begin{aligned}|\Sigma_\epsilon (i|H_1|\epsilon)(\epsilon|H_2|f)|^2 &= \Sigma_\epsilon |(i|H_1|\epsilon)|^2 |(\epsilon|H_2|f)|^2 \\ &+ \sum_{(\epsilon_1\neq\epsilon_2)} \Sigma_{\epsilon_1,\epsilon_2} (i|H_1|\epsilon_1)^*(i|H_1|\epsilon_2)(\epsilon_1|H_2|f)^*(\epsilon_2|H_2|f).\end{aligned}\right\} \quad (4)$$

Now, if ρ is in diagonal form, we have according to (3)

$$S_1(i|H_1|\epsilon_1)^*(i|H_2|\epsilon_2)=0 \quad (\epsilon_1\neq\epsilon_2). \quad (5)$$

According to (4) and (5) we see that (1) reduces to (2) if ρ is in diagonal form for the states ψ_ϵ, and the theorem is proved.

We now give an alternative expression for ρ by which the meaning of ρ can more easily be understood than from the definition (3) of ρ. Consider the wave function of an arbitrary intermediate state ψ_{med}, which can be expressed as

$$\psi_{\text{med}}=\Sigma_\epsilon c_\epsilon \psi_\epsilon \quad (6)$$

by means of the fundamental states ψ_ϵ chosen in (1) and (2). From (6) it follows that

$$\int \psi_{\text{med}}^* \rho \psi_{\text{med}} = \Sigma_{\epsilon_1,\epsilon_2} c_{\epsilon_1}^* c_{\epsilon_2} (\epsilon_1|\rho|\epsilon_2). \quad (7)$$

If we define the partial transition probabilities $P_{i,\text{med}}{}^p$ by

$$P_{i,\text{med}}{}^p = N' S_1 |(i|H_1|\text{med})|^2, \quad (8)$$

where N' is a constant factor, we obtain

$$\int \psi_{\text{med}}^* \rho \psi_{\text{med}} = N'' P_{i,\text{med}}{}^p, \quad (9)$$

where N'' is a normalization constant. It is easily seen that (9) can be used as a definition of ρ alternative to (3).

We want to stress that the values of $P_{i,\text{med}}{}^p$, when known only for the fundamental states ψ_ϵ but not for their linear combinations, do not yet supply complete information on the transition probabilities $i\to\epsilon$. For this we must either calculate (3), or $P_{i,\text{med}}{}^p$ for every ψ_{med}.

To obtain the angular correlation theorem stated by Falkoff and Uhlenbeck[1] (and proved later by Lloyd[2] and Lippmann[3]) as a special case of our theorem, we remark that the z axis is an axis of rotational symmetry of ρ, if the first of two successive particles is emitted along this axis. This leads to a diagonal form for ρ if the ψ_ϵ are eigenfunctions of the z component of the total angular momentum, so that (1) and (2) are equivalent for these ψ_ϵ.

The proof of our theorem has features in common with the considerations of Lippmann,[3] but the use of the density matrix enables us to go further. Our theorem could, namely, also be applied if no axis of rotational symmetry for ρ exists, as in the case of $\gamma-\gamma$ angular correlation of aligned nuclei. We must then try to find states ψ_ϵ, for which ρ is in diagonal form.

We have used the representation of the state of a system after a transition by a density matrix [as in (9)] in an earlier paper,[4] where a partially polarized electron beam was represented by a density matrix.[5] Before that, we used the density matrix to prove another theorem on transition probabilities.[6]

[1] D. L. Falkoff and G. E. Uhlenbeck, Phys. Rev. **79**, 323 (1950).
[2] S. P. Lloyd, Phys. Rev. **80**, 118 (1950).
[3] B. A. Lippmann, Phys. Rev. **81**, 162 (1951).
[4] H. A. Tolhoek and S. R. de Groot, Physica **17**, 81 (1951).
[5] H. A. Tolhoek and S. R. de Groot, Physica **17**, 1 (1951).
[6] H. A. Tolhoek and S. R. de Groot, Physica **15**, 833 (1949).

Intensity of Ultraviolet Radiation from Solar Flares

R. N. SEDRA
Faculty of Science, Fouad I University, Cairo, Egypt
(Received May 2, 1951)

SOLAR flares are classified[1-3] according to their intensities in the increasing order of magnitudes (1, 2, 3, and 3+), where 3+ represents the most intense flare. It is well established that most solar flares are accompanied by synchronous magnetic disturbances usually called "crochets."[4] It is natural to assume that the change in the earth's magnetic field accompanying the flare is dependent on the intensity of the ultraviolet radiation emitted. The following calculation is based on the assumption that these crochets are intensifications of diurnal magnetic variations.

The diurnal magnetic variations have been successfully explained by the diamagnetic theory.[5] For a magnetized long free path ion gas, the intensity of magnetization I is given by

$$I=-3nkT/2H,$$

where T is the absolute temperature, k is Boltzmann's constant, n is the ion density, and H is the magnetic field. Assuming that the solar ultraviolet flash produces an ion cloud, we may calculate its magnetic effect by replacing it by a bar magnet. The magnetic pole strength per unit area, σ, is equal to $I/4\pi$. Therefore,

$$\sigma=-3nkT/8\pi H.$$

Following the Maris and Hulburt[6] assumption in taking the end, S, of the magnet to be 300 km thick and 1000 km wide, the magnetic strength ρ of S is given by

$$\rho=-(9nkT/8\pi H)\times 10^{15}.$$

Taking the distance of the ionized layer from the earth to be 200 km and neglecting the effect of the north pole N, the field F due to S is given by:

$$F=-(nkT/\pi H)\times 2.81.$$

Substituting $T=1000°$, $k=1.372\times10^{-16}$ erg per degree Kelvin, and $H=0.5$ gauss, one gets

$$n=-F\cdot 4\times 10^{13}. \quad (1)$$

The relation between the rate of ion production and the intensity of incident radiation is given by[7]

$$q=\beta n' i/w,$$

where q is the number of ion pairs produced per cm³ per sec at height h, w is the energy absorbed in ionizing one molecule, β is the atomic absorption coefficient, n' is the number of molecules per cc at height h, and i is the intensity of the incident radiation at height h. Substituting $w=14$ ev $=14\times1.6\times10^{-12}$ erg, $\beta=3.2\times10^{-17}$ cm², and n' at height 200 km$^3=2.5\times10^{25}$, one obtains

$$i=q\times 2.8\times 10^{-4}. \quad (2)$$

To test the above calculations, we shall take one of the results observed by Newton. He observed, on the 3rd of July, 1941, a solar flare accompanied by a crochet which gives a change in H of -13γ. Calculating the ionic density n from Eq. (1), we find that its value is 5.2×10^8. Also, calculating the intensity of incident radiation from Eq. (2), we find its value to be 8.09×10^2 erg cm^{-2} sec^{-1}. Gledhill and Syendrei[7] obtained an estimate of the normal solar radiation above the earth's atmosphere from ionospheric data. Their value amounts to 0.313 erg cm^{-2} sec^{-1}. Comparing the result obtained from this calculation with that of Gledhill and Syendrei, we notice that our result is greater by a factor of about 2500, which is reasonable with the intense radiation emitted during the solar flare.

[1] H. W. Newton, Mon. Not. R. Astr. Soc. **103**, 244 (1943).
[2] H. W. Newton, Mon. Not. R. Astr. Soc. **104**, 4 (1944).
[3] M. A. Ellison, Nature **163**, 749 (1949).
[4] H. W. Newton, Mon. Not. R. Astr. Soc., Geophys. Suppl. **5**, 200 (1948).
[5] Ross Gunn, Phys. Rev. **32**, 133 (1928).
[6] H. B. Maris and E. O. Hulburt, Phys. Rev. **33**, 412 (1929).
[7] Gledhill and Syendrei, Proc. Phys. Soc. (London) **63**, 429 (1950).
[8] E. O. Hulburt, Revs. Modern Phys. **9**, 45 (1937).

The Effect of Finite Nuclear Size in Beta-Decay*

M. E. ROSE AND D. K. HOLMES
Oak Ridge National Laboratory, Oak Ridge, Tennessee
(Received May 9, 1951)

IN the analysis of the β-spectrum of heavy radioactive nuclei it is necessary to examine the effect of the finite nuclear radius insofar as this effect appreciably influences the behavior of certain of the electronic wave functions at the nuclear radius.[1] In fact, for

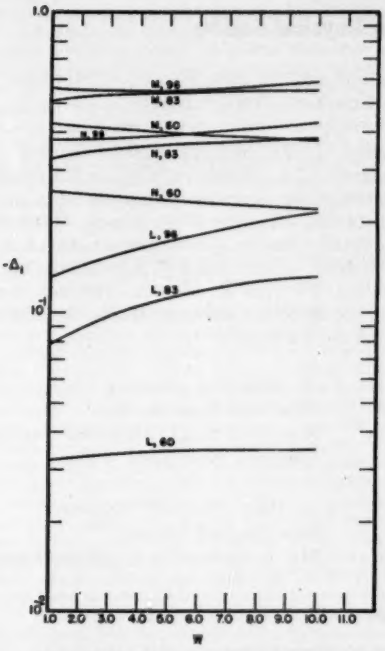

FIG. 1. The correction factor $\Delta_1(j=\frac{1}{2})$ as a function of electron energy W (total energy) in units mc^2. The curves marked L, M, N correspond to $\Delta_1(L)$, $\Delta_1(M)$, $\Delta_1(N)$, respectively, and the numbers affixed to the curves give the value of Z.

given angular momentum j, the "small" component f for $\kappa=-j-\frac{1}{2}$ and the "large" component g for $\kappa=j+\frac{1}{2}$ are sensitive to deviations from the coulomb field.[1] Thus, in the correction factors C_{nx} of Greuling[2] which are linearly dependent on the three wave function combinations L, M, N, one would expect the greatest influence on M and the least for L. This is, in fact, exhibited by the results given below.

The calculation of the finite size correction is straightforward and is based on methods described elsewhere.[1] The smeared out charge distribution inside the nucleus is represented by a scalar potential

$$V=V_0[1+a_2(r/r_0)^2+a_4(r/r_0)^4], \quad r\leqslant r_0, \tag{1}$$

where the constants are fixed by continuity of V, dV/dr and by charge distortion,[3] although the results are insensitive to the latter. The internal wave functions are joined to the usual regular plus irregular coulomb field solutions[4] at $r=r_0$. Then the effect of finite nuclear size is represented by $\Delta_k(M)$, etc., where

$$M_k=M_k(0)[1+\Delta_k(M)] \tag{2}$$

and similar expressions for L_k and N_k. Here $M_k(0)\cdots$ represents the point nucleus value[5] and $k=|\kappa|=j+\frac{1}{2}$.

The results for electrons[6] are shown in Figs. 1 and 2 for $k=1$ and 2, respectively. For $k\geqslant 3$ the Δ-factors are rather small. As expected the influence of the finite size of the nucleus (a) decreases rapidly with increasing j, (b) is important only for $Z>\sim 60$ and (c) is greatest for M, least for L. The latter fact implies an appreciable effect on the β-decay only for nth forbidden transitions ($n\geqslant 1$) and for spin change equal to n (unfavorable parity change in the case of $G-T$ interactions). The negative sign of Δ_k is due to the depression of $\langle V^2\rangle$, averaged over the nucleus.[1]

Since M_k is the dominant term for heavy nuclei and since the coefficients of M_{n+1} (and N_{n+1}) vanish, the energy insensitivity of $\Delta_k(M)$ and $\Delta_k(N)$ imply an essentially allowed spectrum shape for first-forbidden transitions. However, some change in ft value is to be expected when the finite nuclear size effects are included. On the other hand, for second and higher forbidden transitions, the spectrum shape is changed, because of the rapid k-variation of the Δ-factors. Thus a relatively greater depression of the spectrum is to be expected at the low energy end as compared to the high energy region. The spectrum modification is, of course, greater for the larger maximum energies W_0.

It is clear that the effect of the finite size of the nucleus is unimportant for the allowed transitions and the favorable parity change

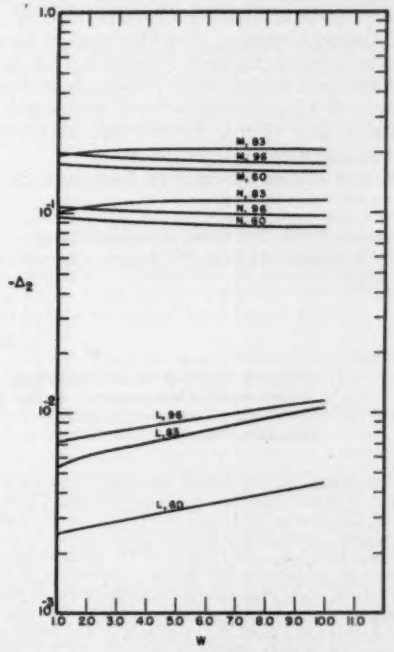

FIG. 2. Same as Fig. 1 but for $k=2$, $j=3/2$. Note change of ordinate scale.

transitions with $G-T$ selection rules. The only well-investigated case for which the finite size corrections should be important is the RaE spectrum. An attempt to fit the observed spectrum with finite size corrections, using pure invariant β-interactions, was unsuccessful. However, recent evidence (made available since the completion of this work) points to a complex spectrum in this case.[6]

The authors wish to express their appreciation to Mrs. N. Dismuke for numerical work.

* This paper is based on work performed for the AEC at the Oak Ridge National Laboratory.

[1] M. E. Rose, Phys. Rev. **82**, 389 (1951). The "small" and "large" radial functions are there denoted by u_1 and u_2, respectively.

[2] E. Greuling, Phys. Rev. **61**, 568 (1942).

[3] E. Feenberg, Phys. Rev. **59**, 593 (1941).

[4] M. E. Rose, Phys. Rev. **51**, 484 (1937). The irregular solutions are obtained by changing the sign of γ in the regular solutions given in this reference.

[5] A more detailed discussion as well as further numerical results (including values of Δ_k for positron emission) will appear in a forthcoming ORNL report.

[6] S. Moszkowski (private communication).

Proceedings of the American Physical Society

Minutes of the Joint Meeting of the New England Section and the New York State Section at Rensselaer Polytechnic Institute, Troy, New York, April 6–7, 1951

A JOINT meeting of the New England Section and the New York State Section of the American Physical Society was held at Rensselaer Polytechnic Institute, Troy, New York, April 6 and 7, 1951. Two hundred twenty physicists registered for the meetings. Provisions were made for tours of Behr Manning Company and W. and L. E. Gurley Company. Saul Dushman of General Electric Research Laboratory gave the dinner address *Random Thoughts on the Philosophy of Science.*

Titles of invited papers of a symposium on Radiation and Health Physics and abstracts of fourteen contributed papers follow.

The new officers for the New York State Section are:

Chairman—GAIL P. SMITH, Corning Glass;
Vice Chairman—LLOYD P. SMITH, Cornell University;
Secretary—L. W. PHILLIPS, Buffalo University;
Treasurer—C. L. HENSHAW, Colgate University;
Members of the Executive Committee—ROLLAND J. GLADIENX, Kenmore High School; HERMAN W. HOERLIN, Ansco; *Continuing on the Executive Committee*—MADELEINE F. CONTANT, Hartwick College; DONALD R. MOREY, Eastman Kodak; and the *Retiring Chairman*, W. R. FREDRICKSON, Syracuse University.

C. L. ANDREWS, *Secretary*
New York State Section
New York State College for Teachers
Albany 3, New York

A. G. HILL, *Secretary Treasurer*
New England Section
M.I.T. Cambridge 39, Massachusetts

Invited Papers

Biological Effects of Nuclear Radiations. H. M. ROZENDAAL, *General Electric Research Laboratories.*
Detection and Measurement of Nuclear Radiations. GORDON L. BROWNELL, *Massachusetts General Hospital and Massachusetts Institute of Technology.*
Protection from Radiation. G. FAILLA, *Columbia University.*

1. Luminosity of the Aurora Borealis.* DONALD KEITH BERKEY, *Colgate University.*—An auroral arc photographed by Carl W. Gartlein[1] at 10:11 p.m., EST, October 15, 1949, has been studied. It extended in an East-West direction in latitude 47°N, and from longitude 75°W to 81°W. These locations are based on the probability that the lower edge of the arc is at a height of 100 km.[2,3] Photometric measurements show that the maximum luminance is seven km above the lower border. The vertical distances l from the maximum to the points where the upper border had a relative luminance of 2/3, 1/2, and 1/3, are shown in Table I. Also shown are the corresponding distances l to the lower border. The shape of the curve agrees with that predicted by Harang,[4] having points of inflection both in the upper and lower portions, and having a sharp lower cutoff. The lower l-values are in good agreement with experimental results obtained by Harang on 15 auroras, but the upper figures are somewhat larger than his averages. Results such as this can be used to estimate the "scale height," $H=kT/mg$ of the atmosphere.

TABLE I.

Distance in km	$l_{2/3}$	$l_{1/2}$	$l_{1/3}$
Upper	15	23	32
Lower	6	7	9

* This work was done under ONR contract.
[1] Project of The National Geographic Society.
[2] Carl Stormer, Terr. Mag. and Elect. **53**, 251 (1948).
[3] L. Vegard and O. Krogness, Geofys. Pub. **1**, No. 1, 149 (1920).
[4] Leiv Harang, Terr. Mag. and Elect. **51**, 381 (1946).

2. A Heat Laboratory to Develop a Mature Philosophy of Experimentation. KENT D. LAWSON, *Rensselaer Polytechnic Institute.*—Pressure of time, especially in larger schools, tends to discourage undergraduates' curiosity, initiative, and ideals. The Heat Laboratory required of physics majors in their last term at RPI attempts to revive and supplement the students' interest. Basic ingredients in this program include: (1) time to think in laboratory—elimination of formal requirements, allowance for an individual's ability, interest, and state of mind; (2) stimulus to think for one's self—individual experimentation, challenging situations, provision for actual experimentation, and opportunity to enjoy physics. The students face seven to twelve experimental situations. The planning phase of experimentation (mostly comparison of methods in terms of possible secondary effects) and the phase of preliminary experimentation are emphasized. During half the course, students determine the necessity for attention to what is actually taking place; in the last half, they determine the necessity for various attitudes and traits of character in making maximum use of the scientific method. Students come to realize they must develop their own philosophy of experimentation if they are ever to become physicists. Even simple situations afford opportunity for developing ideas. One experimental situation will be described to show the special suitability of a heat laboratory for conveying ideas.

3. Effects of Aging and Cooling on the Ultraviolet Spectra of Alcohols.* GLADYS A. ANSLOW AND HELEN H. FIFE, *Smith College.*—To test the origin of weak absorption in the 25,000–42,000 cm^{-1} region of the ultraviolet spectra of alcohols, whether it be impurities or association effects, the spectra of

the isomeric forms of propyl, butyl, and amyl alcohols in isooctane solutions were taken immediately after distillation, after aging for several weeks, and in some cases after several hours of cooling near 0°C. Specific absorption resulted even though precautions were taken against impurities. In the interpretation the possibilities of CH···O intra- and interassociation were considered, since onsets occur which correlate with CH excitation. Increased absorption occurs in aged and cooled solutions, indicating the effects of Tyndall scattering from the larger polymers. OH···O onsets previously[1] identified as originating in long chain polymers or in linear dimers were accentuated by aging.

* Supported by the ONR and the Research Corporation.
[1] Paper to appear in *Transactions of the Faraday Society*, presented at September meeting in Cambridge, England.

4. Further Measurements of Molar Refraction of Carbon Dioxide as a Function of Density.* CLARENCE E. BENNETT AND VICTOR H. COFFIN, *University of Maine.*—Measurements of molar refraction for CO_2 have been continued after the manner described in earlier papers,[1] using the displacement interferometer. Previous measurements indicated a negative variation of molar refraction with density from 0.00 to 0.06 g/cc which was not in accord with molar polarization measurements reported by Keyes and Oncley[2] at M.I.T. Recent work, however, involving several hundred individual readings with fresh samples of bone-dry CO_2 from different cylinders, and using improved equipment, appears to alter the earlier conclusions. A plot of molar refraction against density shows less spread of the points, and is more nearly linear than before. Moreover, the slope of the new curve seems indistinguishable from zero, which is more nearly in accord with the current view that CO_2 does not have a permanent dipole. The results are still inconsistent, however, with the molar polarization measurements which show a positive slope when plotted against density.[2] The work is being continued in an attempt further to reduce the spread of the plotted points.

* Assisted by the ONR.
[1] C. E. Bennett, Phys. Rev. **45**, 200 (1934). F. B. Oleson and C. E. Bennett, Phys. Rev. **60**, 171 (1941). J. H. Coffin and C. E. Bennett, Phys. Rev. **75**, 215 (1949).
[2] F. G. Keyes and J. L. Oncley, Chem. Revs. **19.3**, 195 (1936).

5. Centripetal Force and Automobiles. MARVIN J. PRYOR, *New York State College for Teachers.*—A table-top model makes possible an experimental demonstration of the application of centripetal force to the automobile. Level circular tracks are marked out on a ninety-centimeter disk bordered by a guard rail. Above the disk is a platform representing a small section of banked highway. This platform is hung by a rigid suspension from the cross of a "T" that stands at the center of the disk. The connection is made by using a hinge. A special protractor is mounted on the "T" for determining the degree the "highway" is banked. The disk rests on a forty-centimeter wheel so that it may be belt driven by a Cenco motor-driven rotator provided with a two-centimeter pulley. In use, a car is placed on the platform and the revolutions counted for various inclinations assumed by the platform. Numerical calculations check the experimental. Friction may be made almost negligible by turning the rubber car across the highway. For the horizontal tracks, where friction alone provides the centripetal force, the disk's speed is increased until the car slips from its track and against the guard rail.

6 and 7. Electron Diffraction Problems. GEORGE R. HOLZMAN* AND KENNETH H. MOORE, *Rensselaer Polytechnic Institute.*

I. Performance of the Redesigned R.P.I. Electron Diffraction Unit.—The R.P.I. electron diffraction apparatus has been redesigned and rebuilt to obtain higher resolution and more convenient and flexible operation. Several electron optical problems have been successfully solved and a half-intensity beam width of less than 50 microns is readily obtained using a space charge limited cross-over as source and a single magnetic lens. A simple method for plotting the axial field of the magnetic lens was developed. The addition of improved magnetic shielding plus proper sample charge neutralization together with the new projection system has improved the resolution more than fivefold. Alignment problems are virtually nonexistent. Improvements in the vacuum system enable use of the apparatus in less than ten minutes after the insertion of new undried plates, while pump-out from (dry) atmospheric pressure requires about 1½ minutes, even though no complicated air locks are used. Some typical plates will be shown.

* Now with Behr-Manning Corporation, Watervliet, New York.

II. Studies of the Epitaxy (Oriented Overgrowth) of Certain Halides Deposited on Mica and on Mica Surfaces Covered by Organic Films.—Optical experiments have shown that a number of the iodides (KI, RbI, NH_4I, etc.) not only re-orient to match mica when deposited on a freshly cleaved surface, but will also do so when an amorphous organic film (Formvar, chlorinated rubber, cellulose acetate, etc.) of considerable thickness is laid down first. Electron diffraction studies show that this orientation, for organic films hundreds or even thousands of angstroms thick, may be so complete as to yield a complete pseudo-single-crystal pattern. Reflection patterns of the rear face of organic films show that vacuum-evaporated materials penetrate the film, but air-sublimed iodides which also orient completely do not. Several interpretations of the apparent long-range surface forces are possible.

8. An Upper Limit for Sound Pressure in a Spherically Diverging Field.* CLAYTON H. ALLEN,† *The Pennsylvania State College.*—Experimental measurements of sound pressure in a spherically diverging sound field in air show the development of harmonics due to finite amplitude distortion in an initially sinusoidal wave during propagation. A continuation of these measurements to higher intensities and greater distances from the source show that the wave acquires a maximum amount of distortion and attains a "stable" form in which it is essentially sawtoothed in shape. These observations substantiate existing theory;[1–3] however, the experimental observations appear to go beyond the theory by indicating further that in the steady state, as the wave attains its stable form, the acoustic pressure approaches an upper limit which is independent of the power output from the source. The absolute value of this limit may be a function of source configuration and the properties of state of the medium, but in the experimental, spherically diverging field the limiting pressure was found to vary explicitly with distance x from the source as $1/x^{3/2}$.

* Part of this work was supported by Signal Corps Contract.
† Now with Corning Glass Works, Corning, New York.
[1] Thuras, Jenkins, and O'Neil, J. Acoust. Soc. Am. **6**, 173 (1933).
[2] E. Fubini-Ghiron, Alta Frequenza **4**, 530 (1935).
[3] R. D. Fay, J. Acoust. Soc. Am. **3**, 222–241 (1931).

9. Dimensional Changes in Nickel-Zinc Ferrite in the Neighborhood of the Curie Temperature. R. C. DESHPANDE AND A. A. BURR, *Rensselaer Polytechnic Institute.*—In this investigation the dimensional behavior of nickel-zinc ferrite in the neighborhood of the Curie temperature was followed by means of precision x-ray techniques. A backreflection-type powder camera in which a special low temperature furnace was incorporated was used. The ferrite was made of NiO, ZnO, and Fe_2O_3 in percentage ratios of 15, 35, and 50; and Curie temperatures were found to be 78°C and 95°C from graphs of initial permeability *vs* temperature. X-ray patterns showed the structure to be a single-phase spinel. Lattice parameters

were measured using FeKα and CrKα radiation, and variations with temperature were plotted in the neighborhood of the Curie temperatures. Some measurements were made using silver powder as an internal standard. An expansion in lattice dimensions similar to other magnetic materials was noted up to the Curie temperature, but beyond this, a contraction of 0.12 percent was observed. The expansion behavior is related to magnetostriction effects, but contraction is believed to be a type of dipole effect which is related to the atom positions in the spinel structure.

10. Counting Michelson Interferometer Fringes with a Multiplier Phototube. MYRON A. JEPPESEN, *Bowdoin College.*—A multiplier phototube is used to register the successive fringes formed by a Michelson interferometer. The output from the cell is applied to a cathode-ray oscilloscope for measurement of wavelength differences by the "visibility" method of Michelson. One advantage of this arrangement is the ease with which the minima in fringe visibility may be observed and counted. An electronic scaler may be used in place of the oscilloscope to count individual fringes.

11. A New Cold Electric Arc. CHARLES G. SMITH, *Raytheon Manufacturing Company.**—Arcs were realized in mercury vapor between clean massive polished terminals of both Ta and Mo. The cathode, although not a wick for drawing up liquid, extends down into a pool of mercury which serves as a coolant. A transverse magnetic field drives the arc at abnormally high maximum retrograde speed. A field parallel to arc stream between plane parallel terminals raises the cathode voltage and causes gross changes of the spectrum. At a field of 10,000 oersteds the HgII spectrum is brilliant, like HgI, and even HgIII is prominent. The maximum voltage between anode and cathode was about 16.5. Random fluctuations of voltage were observed not to exceed 0.75 volt, and hence cannot serve to explain the spark spectrum. Cathode current density was apparently below 100 amperes per sq cm for all cases studied. The high retrograde mobility, low current density, peculiar spark spectrum, variation of cathode voltage in a longitudinal field, are all characteristic of the new arc. Studies of these phenomena are being continued in the hope of realizing a satisfactory theory of cold arcs.

* This work was done in part at Harvard University.

12. Grain Density in Nuclear Emulsions as a Function of Temperature.* MARTIN CAULTON AND W. A. MCKINLEY, *Rensselaer Polytechnic Institute.*—The variation of the grain density of tracks caused by alpha-particles and protons in nuclear emulsions in the temperature range from −190°C to 20°C is studied. Alpha-particles from polonium produced tracks in Kodak NTB 50-micron emulsions which were examined for visibility and grain density as a function of temperature. Tracks of knock-on protons produced in the emulsion by neutrons from a polonium-beryllium source are also studied. The decrease in grain density at lower temperatures of these tracks is compared with the results of other observers,[1,2] who used less sensitive emulsions. The grain density of alpha-tracks at −190°C is approximately 35 percent of that density at 20°C. Tentative measurements on proton tracks show a reduction of about 50 percent in grain density at −190°C. Results from the grain density measurements at various temperatures over the complete range will be given.

[1] C. C. Dilworth, *Cosmic Radiation* (Interscience Publishers, Inc., New York, 1949).
[2] E. M. Dollman, Rev. Sci. Instr. 21, 118 (1950).
* Supported by the Rensselaer Polytechnic Institute Research Fund.

13. Regularities in Nuclear Quadrupole Moments. B. M. BROWN, *Cornell University.*—A plot of nuclear quadrupole moments as a function of N and Z shows certain regularities which correspond to the completion of nuclear shells, the most striking feature being the change of sign of the qudrupole moment at the proton or neutron numbers 2, 8, 20, 50, 82, 126. These curves indicate the nuclei which are likely to have large quadrupole moments. On the basis of this plot, large quadrupole moments are expected in the case of certain rare earth nuclei and the least abundant isotope of osmium, Os^{187}. To date, these expectations are not confirmed by experiment.

14. The Charging of Aerosols in a Corona Discharge. EUGENE W. PIKE, *Raytheon Manufacturing Company.*—Quantitative calculation of the rates at which aerosol particles would be expected to gain charge, in passing through a corona discharge in air, as a result of the various expected processes, indicates that the present conventional explanations cannot account for the observed facts. Specifically, neither ion diffusion nor the induced dipole in the aerosol mote can account for the observed charges on motes smaller than 10 microns. It seems probable, from present knowledge, that photoelectric effect is responsible for the charging of particles in the positive corona, and that electron diffusion may dominate in the negative corona. Some evidence is found for an expected limitation, by cold emission, on the negative charge a mote can carry.

MINUTES OF THE MEETING HELD AT WASHINGTON, D. C., ON APRIL 26–28, 1951

THE 305th meeting of the American Physical Society, being the 1951 Spring Meeting at Washington, D. C., was held on Thursday, Friday, and Saturday, April 26, 27, and 28, 1951. Washington meetings have normally been pleasant, but this one will be long remembered as that of an innovation which evoked the enthusiastic praise of all who spoke of it (and they were many). All of our sessions were held either in the Shoreham Hotel, or in the Wardman Park Hotel, or in the National Bureau of Standards; and the sofas and halls of the Shoreham displaced the lawns of the Bureau from their ancient role as the scene of the informal colloquies which many of our members seem to treasure even more highly than the sessions. Without wishing in the least to minimize the contribution of the two hotels, I must point out that the lanterns, the screens, the blackboards, and the registration personnel were generously provided by the Bureau. Our gratitude is richly deserved by the Local Committee, and in particular by its Chairman, Hugh Odishaw, by Mrs. Claire Marton, and by Messrs. Ralph O'Dette, F. D. Moncure, and H. H. Rosen. With Mrs. Marton originated the idea of transferring our sessions to hotels; the Secretary admits to an initial skepticism which the event proved groundless. This innovation will be continued unless something happens to frustrate it.

The Meeting was probably the largest of our history with respect to attendance (there were 2150 registants!) and with its 283 contributed papers fell only a little short of the 1951 New York record. There were two half-day Symposia devoted to work of the National Bureau of Standards, one on the achievements of computing machines in the field of physics, one on stable isotopes and their uses; there were five invited papers in addition to those comprised in the symposia. Our Division of High-Polymer Physics had three sessions consisting partly of invited and partly of contributed papers. The entire scientific programme is republished on following pages.

The banquet of the Society was held on Friday evening in the Terrace Room of the Shoreham Hotel, with an attendance of 272. E. U. Condon spoke of the National Bureau of Standards and A. T. Waterman of the National Science Foundation.

The Council met on Thursday morning. Two candidates were elected to Fellowship and one hundred and twenty-nine to Membership; their names are appended.

The Council considered the problem of financing *Science Abstracts*, of which journal the Institution of Electrical Engineers (London) has increased the subscription rates: this is neither a cause for surprise nor a cause for blame, since both the unit printing costs and the size of the journal have risen considerably. Though final action is reserved until the June meeting, our members who want either *Physics Abstracts* or *Electrical Engineering Abstracts* may expect to pay an extra *$2.00* and those who want both, an extra *$7.50*. These subscription rates will fall very far short of meeting our share of the costs of *Science Abstracts;* the Society will make an additional contribution to the fixed charges of that pair of journals. Further details will be given in the next issue of these *Proceedings*.

Passing to a more cheerful subject: our Washington meeting occurred in the semicentennial year of the National Bureau of Standards, an institution which over and above its scientific eminence has the distinction of having entertained more of our members at meetings of the Society than any other. Mindful both of this special contribution to the Society and of the value of the Bureau to the science of physics, the Council authorized the presentation of a scroll to the National Bureau of Standards. The text of this scroll (which is subjoined) was read aloud at the banquet of the Society by President Lauritsen, and the scroll itself will be delivered to the Bureau in due time. It is but a small return for the many services of the Bureau to the American Physical Society.

The Nominating Committee assembled on the Friday afternoon, and nominated to office in the Society, for terms commencing in 1952, the following Fellows: J. H. Van Vleck for *President;* Enrico Fermi for *Vice-President;* K. K. Darrow for *Secretary;* G. B. Pegram for *Treasurer;* R. B. Brode and W. V. Houston for posts on the *Council* (four-year terms); W. P. Allis, F. G. Brickwedde, W. B. Fretter, Conyers Herring, H. W. Leverenz, and Arnold Nordsieck for posts on the *Board of Editors* with allocation to *Physical Review* (three-year terms); S. K. Allison and N. F. Ramsey for posts on the *Board of Editors* with allocation to *Reviews of Modern Physics* (three-year terms). Messrs. Van Vleck, Pegram, and Darrow were nominated also by the membership-at-large.

According to reports reaching the office of the Society, we have lost through death one of our Honorary Members (V. Bjerknes) and also F. R. Bichowsky, R. A. Gardner, W. D. Harkins, J. W. Hornbeck, E. Ossofsky, H. F. Reid, C. E. Skinner, J. C. Southard, L. B. Spinney, and W. B. White.

Elected to Fellowship at the 1951 Washington Meeting: R. Becker and K. I. Roulston.

Elected to Membership at the 1951 Washington Meeting: Richard B. Allen, Carroll O. Alley, Jr., Donald E. Andersen, Elliot R. Babcock, Alfred E. Bakanowski, José A. Balseiro, Richard G. Barnes, Eugene H. Beach, Harold J. Bernstein, Hugo W. Bertini, Howard Boyet, Francisco D. A. Q. A. Brandão, Hezzie R. Brannon, Jr., Wallace R. Brode, David F. Brower, Douglas E. Brown, Mary Patricia Burgan, Daniel K. Butler, James W. Butler, Joseph J. Caldwell, Jr., Robert J. Campana, James G. Campbell, John P. Carcelli, Byron M Carmichael, Warren P. Chernock, Emerson V. Clarke, Jr., Clarence S. Clay, Henderson Cole, Lawrence P. Dale, G. Conrad Dalman, Richard G. Davis, Harold R. Day, Ajay S. Divatia, Kenneth W. Downes, William E. Drummond, Walter P. Dyke, John J. Earshen, Howard W. Etzel, Donald J. Farmer, Harry E. Felthauser, Billy B. Fisher, Carl C. Frankenfield, Alan D. Franklin, Arthur A. Frost, John Gaffney, Alper Garren, Myer Geller, Raymond A. Gilbert, Harold Glaser, David Green, Graham D. Gutsche, Frank S. Ham, Joe S. Ham, Franklin A. Hamm, Philip N. Hambleton, Edward F. Hammel, Wesley H. Harker, Alfred B. Harris, John P. Heller, Donald A. Hicks, Robert M. Hill, Frank A. Horak, Chao-Sheng Hung, Syoji Ichimura, Frederick R. Innes, Kenneth K. Innes, Robert A. Isaacs, Arthur C. Johnson, Jerome Joseph, Sylvan Katz, James M. Kennedy, John G. King, William C. King, Kenneth E. Kissell, Milton M. Klein, Myron W. Knapp, Elton E. Kohnke, Jerome M. Lavine, Samuel H. Levine, R. van Lieshout, Raphael M. Littauer, Olin S. Lutes, Donald H. Lyons, Leonard A. Mann, Robert S. Margulies, Samson A. Marshall, Frederick H. Martens, Carl G. Matland, Laurence R. McAneny, Laurence H. Mead, Richard K. Neumann, Gerard K. O'Neill, Gordon N. Patterson, William Pavluk, Milton O. Peach, William O. Pederson, Julius Perel, Paul J. Persiani, Jacques C. Poirier, Robert M. Powell, Ernest Rabinowicz, Harlan K. Reynolds, Jasper E. Richardson, Benjamin W. Roberts, Jr., Robert Rosenberg, Richard J. Runge, John B. Rutherford, Thomas

F. Schatzki, Delmar O. Seevers, Faison T. Sessoms, Joseph Shapiro, Hari D. Sharma, Sidney Singer, Karl Sittel, Morgan Sparks, Arthur J. Steele, Richard T. Swim, Avon L. Thompson, Ernest W. Titterton, Louis Toller, Arthur G. Tweet, John Vislocky, Alan T. Waterman, Jr., James B. Weddell, Robert E. Whitfield, Raphael H. Widman, Alan M. Winkelstein, Gaurang B. Yodh, Charles J. Zablocki, and Robert W. Zwanzig.

KARL K. DARROW, *Secretary*,
American Physical Society
Columbia University
New York 27, New York

Text of the Scroll Presented to the National Bureau of Standards

TO THE

NATIONAL BUREAU OF STANDARDS

GREETINGS

The Council of the American Physical Society extends to the National Bureau of Standards its felicitations on the completion of fifty years of outstanding service to the science of physics in all of its aspects, in all of its departments, and in all of its applications. Since its foundation the National Bureau of Standards has been one of the most notable institutions in the promotion of physics, and this not merely in the United States but in the entire world. The Council also remembers with gratitude and affection the nearly fifty occasions on which the National Bureau of Standards has been host to the American Physical Society, affording it as many opportunities of meeting under the most pleasant of conditions and with the most admirable collaboration from the staff of the Bureau. These occasions have also given to the members of the Society wonderful opportunities for becoming acquainted with the staff of the Bureau and with its excellent work. The Council hopes and expects that the National Bureau of Standards will continue to flourish perpetually, and steadily to increase the debt which is already owed to it by all physicists of the United States and of the world. In these congratulations and in these expectations, the Council is confident that it expresses the feelings of the entire membership of the American Physical Society.

Given at the meeting held by the Council of the American Physical Society at the National Bureau of Standards on the 26th of April, 1951.

C. C. LAURITSEN, *President*
K. K. DARROW, *Secretary*

J. H. VAN VLECK, *Vice-President*
G. B. PEGRAM, *Treasurer*

Errata Pertaining to Papers C6, C7, D8, E2, J8, J10, K7, K8, Q8, QA7, QA10, RA6, SA5, SA7, WA7, and Y6

C6, by J. W. T. Dabbs and L. D. Roberts. In line 5, the display formula should read: $S/R=S_0/R-b/2T^2+234T^3/\theta^4-CH^3/2T^2$. In line 10, $\theta=146°$K should read $\theta=101°$K.

C7, by L. D. Roberts and J. W. T. Dabbs. The title should read **A New Method for the Measurement of Absolute Temperature and Entropy at and below 1°K.**

D8, by R. M. Williamson, D. P. Browne, D. J. Donahue, D. S. Craig, and K. W. Jones. The last two Q values listed should be 7.159 and 15.578 Mev instead of 7.175 and 15.75 Mev, respectively.

E2, by S. Krimm and A. V. Tobolsky. Princeton University in the by-line should read Textile Research Institute and Princeton University.

J8, by H. A. Enge. In the fourth line from the end, 0.595, 0.366, 0.392, 0.405, etc., should read: 0.595, 0.366, 0.338, 0.325, etc.

J10, by D. M. Van Patter, A. Sperduto, and H. Enge. In line 10, 5.99, 5.13, 4.97, 3.87, and 3.27 Mev should read: 5.99, 5.16, 4.99, and 3.27 Mev.

K7, by F. I. Boley and L. J. Laslett. In line 9, $Ft=\pm5.4\times10^4$ sec, should read: $Ft\cong7\times10^4$ sec. In line 13, following the next to last sentence, add: Because the energy of the Fe^{55} spectrum probed somewhat higher than employed in the comparison spectra, a careful examination of the amplifier linearity was undertaken; linearization of the gain removes the apparent forbidden shape of the Fe^{55} spectrum, as might be expected from the low Ft product.

K8, by G. E. Boyd and B. H. Ketelle. In line 9, omit "followed by a 2.20-Mev gamma-ray."

Q8, by D. J. Zaffarano and F. I. Boley. In line 12, a preliminary value of 4.2 Mev should read: a preliminary value of 5.2 Mev.

QA7, by R. K. Osborn. A footnote should be added, reading: Supported by the AEC.

QA10, by Louis Goldstein. In line 6, quantities of which should read: quantities which. In line 7, models should read model.

RA6, by John S. Ross and Kiyoshi Murakawa. The title should read: **Hyperfine Structure of Te^{123} and Te^{125}.**

SA5, by Bernard L. Cohen. In line 10, $r/\dot{\theta}r$ should read: $\dot{r}/\dot{\theta}r$.

In line 10, $\left[\dot{\theta}-\left(\frac{eH}{mc}\right)\dot{\theta}\right]$ should read: $\left[\frac{\dot{\theta}-\frac{eH}{mc}}{\dot{\theta}}\right]$.

SA7, by E. C. Gregg, Jr. A footnote should be added, reading: Supported by the AEC.

WA7, by L. L. Foldy. A footnote should be added, reading: Supported by the AEC.

Y6, by Preston B. Carwile. In line 9, A comparison of the results show that, should read: A comparison of the results shows that. . . .

PROGRAMME

THURSDAY MORNING AT 10:00

Shoreham, Main Ballroom

(R. B. LEIGHTON presiding)

Cosmic Rays, Mainly Showers and Stars

A1. Low Energy Spectrum of Heavy Primary Cosmic Rays. H. L. REYNOLDS,* D. M. RITSON, AND E. P. WOODRUFF, *University of Rochester.*—A series of measurements have been made on two stacks of plates flown at geomagnetic latitude 55° to determine the energy spectrum of the heavy primary radiation down to energies corresponding to the geomagnetic cutoff. The stacks consisted of photographic plates interspersed with absorber, one stack reaching an altitude of 110,000 feet. Energies and charge were determined from simultaneous range and δ-ray or grain counts in insensitive plates. The range covered is from 10 to 80 grams per cm^2. Detailed flux data resulting from this work will be presented. This work was performed under the joint program of the AEC and ONR.

* AEC Predoctoral Fellow.

A2. Nature of the Soft and Hard Component of the Cosmic Radiation Close to the Top of the Atmosphere.* M. VIDALE AND MARCEL SCHEIN, *University of Chicago.*—Data will be presented in which the vertical intensity of the cosmic radiation traversing 0, 4, 7.5, and 12 cm of lead was determined as a function of latitude and altitude. The data were obtained through the courtesy of ONR, with the aid of General Mills balloons which were flown at 28°N, 41°N, and 55°N geomagnetic latitude. The rate of ascent was very slow in most of the flights (down to 150 ft/min), so that accurate measurements of the intensity of the various cosmic-ray components could be obtained in the stratosphere up to altitudes of 94,000 ft. The soft component shows a very small latitude effect between 41°N and 55°N in the neighborhood of its maximum, whereas the hard component shows a large effect at these altitudes. This fact strongly indicates that the soft component at these altitudes originates predominantly from neutral mesons[1] which are produced abundantly in the cosmic radiation only at energies greater than 4 Bev (cut-off energy at 41°N).

* Assisted by the joint program of the ONR and AEC.
[1] B. Rossi, Revs. Modern Phys. 20, 537 (1948).

A3. Structure of the Soft Component at Low Altitudes. E. D. PALMATIER,* *Cornell University.*—Telescopes constructed from thin-walled aluminum Geiger counters were used to determine the absolute intensity of the total radiation as a function of zenith angle, altitude, and minimum energy of the particles. Studies were conducted of the various errors associated with such measurements, particularly those arising from counter wall phenomena and extensive showers. The soft component intensity for various energy bands was obtained in the usual manner from the corrected total intensities by subtraction of the hard component.[1] It is apparent that the electronic radiation at low altitudes does not possess a simple structure but can be divided into two components as follows: (a) E_m component—comprising about 70 percent of the electronic component at Ithaca and 40 percent at Echo Lake and agreeing in altitude variation and in intensity with that predicted on the basis of meson knock-ons and of decay electrons arising from a three particle mu meson decay. (b) E_s component—very energetic and possessing very steep altitude and zenith angle dependences similar to the N component.

* Now at the University of North Carolina, Chapel Hill, North Carolina.
[1] W. Kraushaar, Phys. Rev. 76, 1045 (1949).

A4. A Dual Cloud Chamber Study of Extensive Air Showers.* G. M. BRANCH, *Cornell University.*—The nature of penetrating particles in extensive air showers was investigated with a dual cloud chamber assembly during the summer and fall of 1949 at Echo Lake, Colorado. Two rectangular cloud chambers of dimensions 24″×12″×12″, each containing five ¼″ Pb plates, were placed one above the other and separated by a 6″ layer of lead. The chambers were expanded simultaneously for incident air showers containing one or more penetrating particles as detected by extension counter trays near the apparatus and shielded trays between the chambers. The photographs obtained demonstrate the existence of nuclear cascades contributing to the successive development of the electronic component in air showers. About 40 percent of the charged penetrating component in air showers is found to be strongly interacting, in qualitative verification of the interpretation of recent shielded counter experiments. Also, 80 percent of the nonlocally produced associated penetrating particles in the lower chamber are observed to have angular deviations of less than 3° from their respective air shower axes, corresponding to momenta greater than 2 Bev/c. Representative photographs showing the complex nature of air showers will be presented.

* Supported in part by a grant from the Research Corporation.

A5. Cloud-Chamber Observations of Forked Tracks in Penetrating Showers.* R. W. THOMPSON, HANS O. COHN, AND R. S. FLUM, *Indiana University.*—Examples of the forked tracks previously reported[1,2] have been obtained in a sea-level experiment designed to study penetrating showers. A 12-inch diameter magnet cloud chamber below 4 inches of lead is triggered by an array of counters which responds preferentially to events in which two or more penetrating particles are produced in the lead above the chamber. Stereoscopic photographs of forked tracks of the inverted V-type have been obtained under conditions which permit determination of the charge and momentum of the visible particles and the angle between the tracks. The experiment is in progress and the results of these measurements will be reported.

* Assisted by a grant from the Frederick Gardener Cottrell Fund of the Research Corporation.
[1] G. D. Rochester and C. C. Butler, Nature 160, 855 (1947).
[2] Seriff, Leighton, Hsiao, Cowan, and Anderson, Phys. Rev. 78, 290 (1950).

A6. Electron Showers and Sprays at High Altitude. SOPHIE OLEKSA, E. P. NEY, AND C. L. CRITCHFIELD,* *University of Minnesota.*—A Wilson cloud chamber with four vertical ¼″ Pb plates was flown at 90,000 feet in Minnesota, 55°N magnetic latitude. The pictures were examined for electron showers having ten or more particles at shower maximum ($\geq$1-Bev showers) and for "spray" events of more than six prongs. The criteria were the same as those employed in the investigation of these phenomena in horizontal plates flown under the same

conditions.[1] The flux of cascade generating radiation is about three times greater for the vertical plates than for the horizontal plates. Presumably this arises from multiplication of the soft component in the longer average path near the horizon. If spray-producing radiation is effective in the same solid angle as that for showers, its flux appears to be greater also for horizontal directions. The possibility that sprays are cascades[2] implies a rather complicated geometrical factor, however, and the results are being analyzed.

* Work assisted by joint program of the ONR and AEC and by a grant from the Graduate School of the University of Minnesota.
[1] Critchfield, Ney, and Oleksa, Phys. Rev. **79**, 402 (1950).
[2] R. R. Rau, Phys. Rev. **80**, 914 (1950).

A7. The Dependence of Star Production Rates on Absorbers and Altitude. HARRIET H. FORSTER, *University of Southern California.*—The photographic technique has been used to investigate the effect of absorbing material on the rate of star production. Photographic plates, mainly Ilford C2 emulsions and Kodak minimum ionization plates 100μ thick and shielded with lead and paraffine have been exposed at sea level and at altitudes of 10,000 and 30,000 ft, respectively. The plates were placed horizontally and surrounded on all sides by sheets of absorbing material so that the absorber thicknesses were 11.3, 17, 22.6, 33.9, and 56.5 g/cm^2 in the case of lead and 1.5, 3.5, 7.2, and 15.3 g/cm^2 in the case of paraffine. With each set of plates surrounded by absorbing material, plates without absorber were exposed simultaneously. A comparison of the rates of star production in the different sets yields a distinct transition effect for lead; for paraffine no such effect has been observed for the thickness of absorber employed. Data concerning the magnitude of the transition effect and its dependance on altitude will be shown and the results discussed with relation to the work by other authors on stars and penetrating showers.

A8. The Stars Initiated by Synchrotron Gamma-Rays.* SEISHI KIKUCHI, *Cornell University.*—The results of an analysis of stars as well as of single tracks recorded in photographic emulsions exposed to a beam of synchrotron gamma-ray beam of maximum energy of 300, 250, 200, and 150 Mev will be reported. Both C2 and G5 emulsions were used. The excitation curve for star production is quite similar to that of meson production. The cross sections in millibarn per equivalent quantum obtained at above-mentioned energy values are 6.04 ± 0.41, 5.62 ± 0.56, 2.55 ± 0.19 and 1.95 ± 0.18, respectively. About five percent of the stars are associated with a meson track of varying energies. These results seem to show that the stars are produced by π-meson created in the interior of the nucleus followed by the collision with or the absorption by the nucleon in the same nucleus as it is produced. The number of single tracks at 300-Mev excitation is about twice the number of stars. The number of protons coming out of stars is about twice that of single proton tracks. The energy distribution and angular distribution of these protons as well as alpha-particles are studied.

* This work was performed under contract with the ONR.

A9. Meson Production in Cosmic-Ray Stars of Very High Energy.* MARCEL SCHEIN AND J. J. LORD, *University of Chicago.*—Very high energy nuclear interactions were observed in Ilford G5 emulsions exposed at elevations greater than 90,000 ft. A study was made of a proton collision with a silver nucleus in which 95 charged particles were emitted. The number of the charged mesons produced was determined from conservation of charge considerations of all emitted tracks. It was found that at least 55 tracks of minimum ionization must be due to mesons and 11 to high energy protons. The star had a very narrow core of minimum ionization particles which were emitted within half-width of 0.01 of a radian. The energy of the incident proton was estimated to be 3×10^{13} ev. The mechanism of this nuclear collision favors multiple meson production from the first nucleon-nucleon collision.[1] It is assumed that these mesons can give rise to the production of additional mesons in subsequent collisions in the same nucleus.[2] Similar events produced by α-particles and heavy nuclei will be discussed. The absolute frequency of occurrence of stars with energies greater than 10^{13} ev strongly indicates that the primary spectrum does not fall off as fast as it has previously been assumed for $E>10^{13}$ ev.

* Assisted by the joint program of the ONR and AEC.
[1] E. Fermi, Prog. Theor. Phys. **5**, 570 (1950).
[2] W. Heitler and L. Janossy, Helv. Phys. Acta **23**, No. 4, 417 (1950). L. S. Osborne, Phys. Rev. **81**, 239 (1951).

A10. Transition Effect in Pb of the Star-Producing Radiation in the Stratosphere. M. M. SHAPIRO, M. BIRNBAUM, F. W. O'DELL, AND B. STILLER, *Naval Research Laboratory.*—Behavior of the *N*-component of the cosmic rays in Pb at a mean atmospheric depth of 2 cm Hg and geomagnetic latitude 55°N was explored by measuring star frequency *versus* depth in an absorber which spent 7 hours above 3 cm Hg in a balloon flight. Vertical orientation of 400μ Ilford G5 emulsions inside a "canyon" in the Pb permitted detailed investigation of the transition curve. Observation of 3000 stars ($\geq$3 prongs) yields these tentative conclusions: the frequency of *large* stars ($\geq$6 "gray" and black tracks) first increases with depth, saturates between 25 and 60 g/cm^2, then drops gradually toward 155 g/cm^2. There are indications of two peaks in the region of saturation, with maxima near 25 and 60 g/cm^2. *Small* stars show similar, but less pronounced, characteristics. They differ, however, in two features: an initial drop to $\approx$15 g/cm^2, and a general upward trend which extends to depths $\approx$70 g/cm^2. Results will be compared with those of other workers.[1]

[1] J. J. Lord and M. Schein, Phys. Rev. **75**, 1956 (1949). Blau, Nafe, and Bramson, Phys. Rev. **78**, 320 (1950).

A11. Study of Nuclear Explosions Using a Cloud Chamber Containing a NaI Crystal.* G. SALVINI AND GEO. T. REYNOLDS, *Princeton University.*—A general difficulty of GM counter and cloud-chamber cosmic-ray experiments measuring high energy nuclear cross sections is that the probability of detecting the nuclear events depends on the number and angular spread of the relativistic particles and on the distribution of the energy between nuclear particles and the electromagnetic component (neutral mesons). To avoid this difficulty a cloud chamber (18″×18″×8″) has been prepared containing a large NaI crystal, viewed by photo-multipliers outside the chamber. The evaporation products of nuclear explosions in the crystal furnish the signal that triggers the chamber. This allows an unbiased study of the relativistic particles and the electromagnetic component arising from the explosions. Plates of carbon and lead were used in the chamber. Preliminary measurements have been made of (1) the mfp in carbon of the relativistic particles emitted in the explosions and (2) the electromagnetic component emitted in order to compare the probabilities of charged and neutral mesons in these high energy interactions. The performance of the cloud chamber and the results at sea level will be discussed.

* Supported by the joint program of the AEC and ONR.

A12. A Cloud-Ionization Chamber for the Study of Cosmic-Ray Nuclear Interactions.* H. W. LEWIS, W. W. BROWN, D. O. SEEVERS, AND E. W. HONES, *Duke University.*—A combination cloud chamber and ionization chamber in which the gas (argon at 51 lb in^{-2} saturated with iso-amyl alcohol) is common to both chambers is described. The ion chamber, a 3¼-in. diameter brass cylinder 8 in. in length open at both ends and having a $\frac{1}{8}$ in. central wire, is mounted coaxially with the cloud chamber, which has a useful rectangular volume 10 in.×10 in.×8 in. A burst occurring in the ion

chamber generates a pulse which is used to trigger the expansion mechanism. Rapid reduction of the cylinder voltage from −1800 volts to ground, after electron collection is over, prohibits any appreciable motion of positive ions and thus permits observation of the tracks of the burst producing particles. In preliminary tests at sea level, cosmic-ray bursts from cascade showers and from stars occurring in the wall (up to 10 prongs) and in the gas (up to 5 prongs) of the ion chamber have been observed.

* This work was supported by the joint program of the ONR and AEC.

A13. Spectrum and Path Length for Nuclear Interaction of Cosmic-Ray Protons.* CHARLES E. MILLER, JOSEPH E. HENDERSON, D. S. POTTER, AND J. TODD, JR., *University of Washington.*—A magnetic cloud chamber was used to photograph those charged particles stopping in 15 and 30 cm of lead placed just below the chamber. Because of nuclear interactions the 30 cm of lead absorber is sufficient to stop almost all protons even at energies above 1 Bev as well as the secondary products of their nuclear collisions. As mesons show ionization energy loss only, all those of sufficient range emerge from the absorber block and actuate one of the anticoincidence counters completely surrounding it. The distribution in momentum of negatively charged particles photographed in this way shows a rapid cut-off above the momentum corresponding to the range of μ-mesons for the absorber thickness used while the corresponding intensity of positive particles is still large at momenta of 2 Bev/c. The pos.-neg. difference at momenta well above the meson cutoff is taken to represent protons. This data along with previous observations is sufficient to determine both the spectrum and nuclear path length (path length for removal) of protons. The nuclear path length in lead for protons of 0.5–1.0 Bev is found to be about 160 g/cm^2.

* Assisted by the joint program of the ONR and AEC.

THURSDAY MORNING AT 10:15

Shoreham, West Ballroom

(H. L. DRYDEN presiding)

Ultrasonics and Fluid Dynamics

B1. Ultrasonic Absorption in Some Halogenated Methylenes, Ethanes, and Ethylenes. DANIELE SETTE, *Istituto Nazionale di Ultracustica, Rome.**—In order to get information about the influence of the structure of liquids on elastic relaxation, measurements of ultrasonic absorption were performed in eight organic halides, in the temperature range 40°C, −20°C. A pulse method was used at 30 Mc/sec. In the methylene series the absorption coefficient has high values and decreases in the order: chloride, bromide, iodide. The temperature coefficient is positive. In a series of dichloroethane, while the absorption coefficient of 1,1 dichloroethane increases with the temperature, the coefficients of 1,2 dichloroethane and of 1,2 dibromoethane decrease when the temperature rises. Moreover, the absorption is larger in the bromothan in the chloro-substitute. For *cis*-dichoroethylene the value of α/ν (α amplitude abs. coeff, ν frequency) at 20°C, is 540 10^{17}, for *trans*-dichloroethylene it is 356 10^{17} sec^2/cm. The absorption increases with temperature, for both liquids. These results indicate that the ultrasonic absorption is largely dependent on the structure of liquids and on the characteristics of the short range forces among neighboring molecules. It seems, besides, that the dipole moment often does not have a direct importance on the phenomena, except in fixing the relative position of molecules.

* Work done with the help of a grant of Italian Research Council, at the Catholic University of America, Washington D. C., aided by ONR contract.

B2. Intensity Dependence of the Coefficient of Absorption of Ultrasonic Waves.* FRANCIS E. FOX, *Catholic University of America.*—It has been observed that the amplitude coefficient of absorption (α) of continuous ultrasonic waves in water increases for intensities above 0.05 watt/cm^2. It has been suggested that this is caused by cavitation, although visible cavitation appears only at much higher intensities. Since cavitation, in general, should lead to an increase in the absorption coefficient; measurements of α as a function of the intensity I should yield data for testing cavitation theories, as well as general theories of the liquid state. α was measured at 10 mc in out-gassed water, water saturated with air, and water saturated with CO_2, and at 5 mc in CCl_4, for intensities as high as 5 watts/cm^2. The values of α_1/α_0 are given for comparison, where α_1 is the absorption coefficient at 1 watt/cm^2 intensity, and α_0 is the low intensity α: air free water −2.7; water saturated with air −2.7; water saturated with CO_2 −2.2; CCl_4 −1.25.

* Work assisted by ONR contract.

B3. Dispersion and Absorption of Ultrasonics in Nitrogen.* ALFRED JOSEPH ZMUDA, *Catholic University of America.*—By means of the interferometer, the velocity and absorption of ultrasonic waves in nitrogen were measured at the frequency of 2.992 mc/sec, in the pressure range of 2.09 to 76 cm of Hg at a temperature of 29°C. A dispersion of velocity was found ranging from 354.3 meters/sec to 364.4 meters/sec. The ratio ($\alpha_{exp}/\alpha_{class}$) dropped from 1.40 to 1.32, and the corresponding value of C_v/R dropped from 2.50 to 2.08. The increase in velocity and the decrease in ($\alpha_{exp}/\alpha_{class}$) is interpreted as owing to the slow exchange of energy between the translational and rotational degree of freedom. The relaxation time for the rotation was found to be 1.2×10^{-9} sec.

* Work supported by the ONR.

B4. A Statistical Mechanical Approach to Turbulence. WILLEM V. R. MALKUS, *University of Chicago.*—The lack of uniqueness in solutions of hydrodynamical equations applicable to open systems necessitates the search for a criterion to determine the most probable solution. The phrase "most probable" can have meaning in the statistical mechanical sense of the *a priori* probability of a quasi-ergodic ensemble. One might hope to obtain a most probable solution by maximizing the *a priori* probability of the velocity distribution function averaged over space and time and constrained both by macroscopic continuity relations and by boundary conditions. A less general method would be to compare several given steady state, or mean, velocity distributions to determine their respective probabilities as a function of such parameters as these distributions may contain. As one aspect of such problems, the flow between parallel plates and in pipes is considered. The probability of the laminar motion is compared with that of an arbitrary mean motion. A variational optimiza-

tion of the arbitrary motion permits the establishment of a criterion for the onset of turbulence and determines the momentum transport to the walls as a function of the mean velocity. The results obtained are compared with the empirically established relations.

B5. The Model Firing Range: A Pressurized Range for Small Caliber Projectiles in Free Flight. V. E. BERGDOLT, A. J. GREENWALD, AND D. B. SLEATOR, *Aberdeen Proving Ground.*—The small pressurized range has been developed to study experimental flows about projectiles in free flight at Mach numbers up to 4 and at air densities attainable at pressures up to 30 atmospheres. Outside the range, at a set of windows, the flow field is observed with a Mach-Zehnder interferometer. Since the effective duration of the source is relatively long, a rotating mirror-camera system is used to stop the projectile on the film. Investigations in the source size theory of the Mach-Zehnder interferometer have shown that the best fringes are formed perpendicular to the plane of centers of the optical elements. To satisfy this criterion, the interferometer has been modified so that the plane of centers is vertical and the fringes horizontal. The recent development of the monochromator light source and the reorientation of the interferometer have resulted in interferograms of consistently good quality. The effect of increased air density is apparent in the comparison of fringe shift patterns for the same projectile at range pressures up to 5 atmospheres.

B6. Monochromatic Light Source for Interferometry of High Speed Gas Flows. D. B. SLEATOR, V. E. BERGDOLT, AND F. D. BENNETT, *Aberdeen Proving Ground.*—Interferometry of air flows about supersonic projectiles requires a high intensity light source with short duration and a high degree of monochromaticity. It is shown that a BH6 mercury flash tube and liquid prism monochromator together produce a satisfactory solution to the problem. Conventional glass filters fail because of excessive breadth of pass band; while interference type filters impose excessive requirements on intensity and collimation of the light. Analysis is given of the problem of maximizing light transmission through the monochromator, and the design of a liquid prism instrument employing CS_2 refractive medium is discussed. Finally, comparison of interferograms shows the improvement achieved over a conventional Wratten filter.

B7. Experimental Verification of Source Size Theory for the Mach-Zehnder Interferometer. G. D. KAHL AND F. D. BENNETT, *Aberdeen Proving Ground.*—The simplified theory of the Mach-Zehnder interferometer developed by the latter author is tested. The reduction in the visibility of fringes formed by the interferometer owing to an extended area light source is shown experimentally. This reduction is shown to be caused by the superposition of two separate effects which are characteristic of the two angular coordinates of the unit vector pointing from the center of the collimating lens toward each point in the plane of the area-type source. The relation of each of the effects to that coordinate characterizing it is demonstrated experimentally to agree with the theory. The result of combining these two effects from all of the points of an area-type source is seen experimentally to cause the "focusing" of the visible fringes, and to limit them to a finite region of the intersecting beams determined by the size and shape of the source.

B8. Effect of Random Errors in Fringe Shift on Interferogram Reductions of Axi-symmetric Flows. F. D. BENNETT, *Aberdeen Proving Ground.*—A description of the adaptation to Eniac computation of the equation for density ratio $(\rho/\rho_0)_i$ in terms of fringe shifts for an interferogram of an axi-symmetric flow has previously been given.[1] On the hypothesis that the disturbance be divided into N zones of equal radial increment w, a simple expression can be derived connecting the rms error Σ_i of the density ratio with the rms error σ_j of fringe shift at each zone. Further simplifications are possible if $\sigma_j = \sigma$ for all j with the result that a bound for Σ_i may be obtained which varies as $[w(2r_i+w)]^{-\frac{1}{2}}$. Data from interferogram reductions are presented and comparison is made between apparent random errors in the $(\rho/\rho_0)_i$ values and those predicted by the bound on Σ_i.

[1] Phys. Rev. 76, 880A (1949).

B9. Electrical Properties of Detonation Shocks. J. SAVITT AND R. H. F. STRESAU.—In detonation velocity measurements, time signals are frequently obtained from probes which are connected electrically by the ionized gases of the shock front. Since the accuracy of time measuring devices is frequently affected by the nature of the electrical signal received from such probes, measurements have been made of the electrical properties of the ionized paths. The apparatus consist of a condenser, the probe, a vacuum thermocouple, and a fluxmeter or peak micro voltmeter. The condenser is discharged through the heater of the vacuum thermocouple, and the energy delivered can be determined either from the peak voltage at the thermocouple terminals or from the voltage-time integral as measured by a fluxmeter. The apparatus is calibrated using a switch of proven negligible loss. When the probe is substituted for the switch, the difference between the reading obtained and the calibration is interpreted as the loss at the probe. By determining this loss as function of voltage, capacitance, and thermocouple heater resistance, the electrical properties of the ionized gases in the gap may be studied. Measurements have been made of these properties as functions of the relative position of the explosive charge and the probes.

THURSDAY MORNING AT 10:15

NBS, Materials Testing

(W. P. ALLIS presiding)

Electrical Phenomena in Gases; Cryogenics

C1. Formation of Metallic Arcs.* G. F. HULL, JR., AND J. W. MEYER, *Dartmouth College.*—When metallic contacts carrying a current are separated, the contact may be bridged by a small globule of metal, following which an arc may be formed. Cathode-ray oscillograms of the voltage across separating contacts have been obtained for twenty different metals ranging from Sn to W. These oscillograms show a rise in voltage first to the melting point of the metal and a second rise to the boiling point before the arc strikes. For the metals investigated, the voltages at the melting and boiling points agree within a few percent with those predicted theoretically. From the oscillograms, minimal length arc characteristics for gold and

platinum have been obtained. Examination of all the oscillograms which contain arcs (several thousand) shows that an arc is always preceded by the formation of a metallic bridge. Further investigation of arcs formed by exploding small wires of the same dimensions as bridges shows that the wire is first melted and then vaporized before the arc strikes. Calculation shows that the energy expended in vaporizing and ionizing the vapor of the small wire corresponds to the energy expended in producing the minimal length arc.

* Assisted by the ONR.

C2. Measurement of Electron Temperatures in a Pulsed, Electrodeless, Toroidal Discharge Tube. W. H. BOSTICK, W. W. STRIKER, AND M. F. GROVER, *Tufts College.*—An electrodeless, gaseous, toroidal discharge tube threaded by an energized pulse transformer core gives a fairly bright pulsed excitation of the gas for pressures from 1000 down to 15 microns. A small probe, connected to ground through a resistance and protruding into this discharge, will attain either positive or negative potentials (up to 1000 volts) depending upon the particular conditions of the discharge. It is inferred that under certain conditions electrons in the plasma become fairly well separated from the positive ions and are then almost totally responsible for the negative potential attained by the probe. A measurement of probe current and voltage then enables one to measure electron temperatures of 10^6 degrees Kelvin for a distribution which appears to be maxwellian.

C3. Recombination between Electrons and Atomic Ions. MANFRED A. BIONDI, *Westinghouse Research Laboratories.*—Values of electron-ion recombination coefficients have been reported[1,2] which are from 10^2 to 10^5 times larger than those predicted by quantum theory for radiative capture of an electron by an ion. The present investigation is directed at determining the capture mechanism responsible for these large recombination coefficients. In low pressure helium (0.5 mm–3 mm Hg), it is found that atomic lines are emitted in the afterglow, in contrast to the observations of Johnson *et al.*[3] for higher pressures (10–30 mm Hg) where molecular bands were observed. Absolute intensity measurements show that for each electron lost by recombination, roughly one quantum of visible radiation is emitted. The observed lines originate from high lying states ($n=4, 5, 6$) which are all less than 1.5 volts below ionization potential. These results are difficult to reconcile with Bates' suggestion[3] of dissociative recombination of electrons with He_2^+ ions, since the dissociation energy of the latter is undoubtedly greater than 1.5 ev.

[1] M. A. Biondi and S. C. Brown, Phys. Rev. **76**, 1697 (1949).
[2] Johnson, McClure, and Holt, Phys. Rev. **80**, 376 (1950).
[3] D. R. Bates, Phys. Rev. **77**, 718 (1950).

C4. Transfer of Excitation in Atomic Collisions. T. HOLSTEIN AND IRA B. BERNSTEIN, *Westinghouse Research Laboratories.*—The cross section for the transfer of excitation in a collision between two atoms is calculated under the assumptions that only two states of the compound system are involved, and that the nuclear motion can be treated classically, i.e., prescribed as a function of time. These assumptions lead to a system of two coupled first-order linear differential equations for the transition amplitudes. The argument here is the time, as opposed to the internuclear separation which appears in the pair of second-order equations of previous quantum-mechanical treatments of the problem.[1,2] The cross section is then determined, either rigorously or approximation-wise, depending on the various assumptions as to the interaction. The results, which yield the expected resonance cross section and demonstrate exponential decrease for increasing deviation from resonance, are compared with those of Stueckelberg.[2]

[1] F. London, Z. Physik **74**, 143 (1932).
[2] E. C. G. Stueckelberg, Helv. Phys. Acta **5**, 369 (1933).

C5. Imprisonment of Resonance Radiation in Sodium Vapor. A. O. MCCOUBREY, D. ALPERT, AND T. HOLSTEIN, *Westinghouse Research Laboratories.*—The imprisonment of resonance radiation ($\lambda=5890$A and 5896A) in sodium vapor has been measured by methods previously described.[1] For vapor densities less than 10^{14} atoms/cc, for which the line shape is determined by Doppler broadening, the imprisonment time is found to rise monotonically with vapor density. This rise, as well as the absolute magnitude of the time constant, is in agreement with theory.[2] For vapor densities higher than 10^{14} atoms/cc, where dispersion-type pressure broadening prevails, the imprisonment time becomes independent of vapor density. This behavior is also in agreement with theoretical predictions.[2]

[1] Alpert, McCoubrey, and Holstein, Phys. Rev. **76**, 1257 (1949).
[2] T. Holstein, Phys. Rev. **72**, 1212 (1947), and subsequent unpublished calculations.

C6. The Entropy of $MnSO_4\cdot(NH_4)_2SO_4\cdot 6H_2O$ from 0.25°K to 4.2°K in a Magnetic Field. J. W. T. DABBS AND L. D. ROBERTS, *Oak Ridge National Laboratory.*—In connection with the nuclear alignment program here it is necessary to know the entropy of $MnSO_4\cdot(NH_4)_2SO_4\cdot 6H_2O$ in a magnetic field. Assuming no saturation, Casimir[1] gives

$$S/R=(S_0/R)(b/2T^2)+(234T^3/\theta^3)-CH^2/2T^2$$

the symbols having their usual meanings. We have extended, somewhat, previous work on this salt, notably by Benzie and Cook,[2] and Gorter,[3] to find the range of H and T over which this function applies. With $T=(T^*-0.03)$°K, $b=0.033$°K^2, and $\theta=146$°K, per mole of Mn^{++}, we find that the above function describes the behavior of the salt within a few percent from 0.25°K to 4.2°K in the region down to $S=S_0-6.2\times10^7$ ergs/°K. The experiment consisted of the ballistic measurement of T^* and also of the dependence of the adiabatic susceptibility on the applied H for various demagnetization conditions.[1–3] The sample was a sphere compressed from powdered salt.

[1] H. B. G. Casimir, *Magnetism and Very Low Temperatures* (Cambridge University Press, 1940).
[2] R. J. Benzie and A. H. Cooke, Proc. Roy. Soc. (London) **A63**, 213 (1950).
[3] C. J. Gorter, *Paramagnetic Relaxation* (Elsevier Publishing Company, 1947).

C7. A New Record for the Measurement of Absolute Temperature and Entropy at and below 1°K. L. D. ROBERTS AND J. W. T. DABBS, *Oak Ridge National Laboratory.*—The experimental method of the above paper covers only a limited entropy-temperature region. To extend this we use integrals proposed by Casimir: $\Delta S=\int(dM/dT)_H dH$ with temperature constant, and $\Delta T=\int(dM/dS)_H dH$ with entropy constant. Our technique may be used to measure either of the above partial derivatives, but we will discuss $(dM/dS)_H$ only. Two identical secondary coils connected in opposition are placed in the highly uniform field of a large solenoid magnet. In each of these coils a sphere of paramagnetic salt is placed, and their positions are so adjusted that the net quantity of charge generated in the secondary circuit, upon switching off a field H from the large solenoid, will be proportional to the difference of magnetic moment of the two spheres, $\Delta M(H)$. With the help of an auxiliary coil, one isothermally magnetizes the two spheres to slightly different fields and thus to slightly different entropies at 1°K. This known entropy difference, ΔS_0, is essentially constant in an adiabatic demagnetization. Then, $\Delta M(H)$ is measured isentropically as a function of H as indicated above, for *this* ΔS_0. The required partial derivative is then $\Delta M(H)/\Delta S_0$ and the temperature interval $\Delta T(H)$ may be obtained by the graphical integration of this quantity. Experiments are in progress.

THURSDAY MORNING AT 10:00

Shoreham, Terrace Room

(KATHERINE WAY presiding)

Reactions of Transmutation, Hydrogen through Beryllium

D1. The Proton-Proton Reaction and Energy Production in the Sun. EDWARD FRIEMAN, *Polytechnic Institute of Brooklyn*, AND LLOYD MOTZ, *Columbia University*.—Recent revisions of the experimental cross sections for the processes in the carbon cycle[1] have indicated that the proton-proton[2] reaction, $H^1+H^1 \rightarrow H^2+e^+$, can be expected to outweigh by a considerable factor the carbon cycle in the production of energy in stars like the sun. The recent estimates of how big this factor is have been based on the theoretical cross section for the proton-proton reaction calculated for nontensor forces.[3] We have recalculated the cross section for this reaction using tensor forces. The deuteron wave functions employed were those calculated by Feshbach, Schwinger, and Harr,[4] who used central and tensor potentials of the meson type with different ranges. It is shown, using this new cross section, that the proton-proton reaction is even more important as a source of solar energy than had previously been indicated.

[1] R. N. Hall and W. A. Fowler, Phys. Rev. **77**, 197 (1950).
[2] I. Epstein, Ap. J. **112**, 207 (1950).
[3] H. A. Bethe and C. Critchfield, Phys. Rev. **54**, 248 (1938).
[4] Unpublished report.

D2. He_4+T Reactions. E. ALMQVIST, K. W. ALLEN, J. T. DEWAN, AND T. P. PEPPER, *Chalk River Laboratory*.—An unresolved ion beam (20 μamp) of helium (10 percent He^3) is accelerated to 200 kv and used to bombard a target of tritium absorbed in titanium. The following reactions have been observed:

$$He^3+T \rightarrow \alpha+d+14.3^\circ \quad (1)$$
$$\rightarrow He^5+p+11.3 \text{ Mev} \quad (2)$$
$$\rightarrow \alpha+n+p+12.1 \text{ Mev.} \quad (3)$$

The range distribution of the charged particles has been obtained in 200-micron Ilford C2 photographic emulsions covered with 3 mg/cm² Al foil. Measurement of 500 tracks reveals three groups with ranges of approximately 12, 350, and 540 microns and in addition a broad continuum up to 560 microns. The first two groups correspond to the α-particles and deuterons from reaction (1), the third group to the protons from reaction (2), and the continuum to the protons from reaction (3). These assignments were confirmed by energy measurements obtained with a thin KI crystal and 5819 photo-multiplier. Observed at 50° to the ion beam, reactions (1) and (3) are about equal in intensity, while reaction (2) occurs in fewer than 10 percent of the disintegrations. A few 14.7-Mev protons from the He^3+d reaction were observed and were used as an energy calibration point for the scintillation counter.

D3. The Angular Distribution of the Products of the T(d, n)He^4 Reaction. J. L. FOWLER,* J. E. BROLLEY, JR., AND E. J. STOVALL, JR., *Los Alamos Scientific Laboratory*.—Gaseous tritium was bombarded with a focused beam of 10.5-Mev deuterons accelerated by the cyclotron. Charged particles emerged from the reaction volume through plane dural windows. Deuteron-proton scattering provided a method for analysis of the hydrogen impurity. The charged particles passed through two slits which, in conjunction with beam defining slits, fixed the reaction volume. They were counted in a proportional counter. The complete system was contained in a cylindrical vacuum chamber. Alpha-particles were counted from 33° to 94° center-of-mass angle of alpha-particle. Window scattering was investigated by doubling the thickness of dural. No significant difference in cross-section determination was observed. The reaction cross section over this range is estimated to have an absolute error of ±3.5 percent. The range 94° to 180° was studied by neutron counting. Considerably higher pressure of tritium in a different gas cell was used. Detection was done with the radioactivity produced by the $Cu^{63}(n, 2n)Cu^{62}$ reaction, and proton recoil proportional counter telescope. The errors of these measurements are considerably higher. A plot of the angular dependence of the cross section will be presented. From the plot one notices a close similarity[1] to the reaction $He^3(d, p)He^4$ both in magnitude and angular variation.

* Now at Oak Ridge National Laboratory, Oak Ridge, Tennessee.
[1] J. C. Allred, Phys. Rev. **77**, 753 (1950).

D4. Photo-Disintegration of He^4. E. G. FULLER AND M. WIENER, *National Bureau of Standards*.—A study is being made of the photo-disintegration of He^4 using nuclear emulsions in a geometry similar to that used in a previous study of the photo-disintegration of deuterium.[1] Several exposures with different peak energies have been made with the University of Illinois 24-Mev betatrons and the Bureau of Standards 50-Mev betatron in an attempt to sort out the effects of the various competing processes. The neutron background effects were negligible in the 50-Mev betatron exposures. A preliminary analysis has been made of about 1000 tracks. For photon energies up to 23 Mev the results are obscured by corrections for heavy particle recoils and background. These corrections and the comparison of these results with a study made of the inverse reaction,[2] will be discussed. Above 23 Mev the (γ, p) cross section rises to a broad maximum centered at about 27 Mev. The peak cross section is about $7(10)^{-28}$ cm². The angular distribution of the high energy protons in the center-of-mass system is of the form $\sigma(\theta) \sim a+b \sin^2(\theta)$, where $a/b \simeq 2 \pm 1$.

[1] E. G. Fuller, Phys. Rev. **79**, 303 (1950).
[2] Argo, Gittings, Hemmendinger, Jarvis, and Taschek, Phys. Rev. **78**, 691 (1950).

D5. On the $Li^6(n, \alpha)$ Reaction. M. PESHKIN AND A. J. F. SIEGERT, *Northwestern University*.—J. H. Roberts *et al.*[1] have measured the cross section for the $Li^6(n, \alpha)$ reaction close to resonance (250 kev) and found that the angular distribution of the tritons is of the form $A \cos^2\theta + B \cos\theta + C$. The resonance is known to be due to P capture,[2] by which odd compound states of angular momentum 1/2, 3/2, or 5/2 could be formed. The above angular distribution excludes the possibility of pure 1/2. Preliminary measurements at 600 kev[3] show a marked decrease in the ratio A/B, in agreement with the assumption that the angular distribution is determined by P and S capture and $P-S$ interference, the S capture occurring without resonance. A possible connection between this picture and the strong resonance in the total neutron cross section[3] of natural Li and the possibility of deciding whether the compound nucleus has angular momentum 3/2 or 5/2, or whether there is an almost degenerate combination of some pair of 1/2, 3/2, 5/2, or even all three, will be discussed.

[1] Roberts, Darlington, and Haugsnes, Bull. Am. Phys. Soc. **26**, No. 1, abstract C7 (1951).
[2] R. K. Adair, Revs. Modern Phys. **22**, 249 (1950).
[3] J. H. Roberts and H. M. Mann (following abstract).

D6. The Angular Distribution of $Li^6(n, \alpha)H^3$ for 600-kev Neutrons.* J. H. ROBERTS AND H. M. MANN, *North...astern University*.—The angular distribution for $Li^6(n, \alpha)H^3$ for

270-kev neutrons has been previously reported.[1] The same method is being used to determine the angular distribution for 600-kev neutrons. Li^6-loaded C2 100μ emulsions wrapped in Cd were exposed by J. Morris Blair to $Li^7(p, n)Be^7$ neutrons from the Argonne electrostatic generator. The angle between the direction of neutron incidence and the triton track is measured for all tracks meeting geometrical selection criteria. About 2000 tracks have been measured and divided into 15° intervals in the center-of-mass system. Corrections are made for the background of epithermal neutrons and neutrons at the 250-kev resonance energy. The distribution is highly asymmetric, even more than at 270 kev. The triton yield is highest in the forward direction, has a minimum around 110°, and rises some in the backward direction. The ratio of the forward triton intensity to the backward appears to be around 3:1. Theoretical calculations are reported in an accompanying abstract.[2]

* Supported by the AEC.
[1] Roberts, Darlington, and Haugsnes, Bull. Am. Phys. Soc. **26**, No. 1, abstract C7 (1951).
[2] M. Peshkin and A. J. F. Siegert (preceding abstract).

D7. Electrostatic Analysis of Lithium Reactions.* D. S. CRAIG, C. P. BROWNE, D. J. DONAHUE, R. M. WILLIAMSON, AND R. E. BENENSON, *University of Wisconsin.*—Kinetic energies of product particles of the following reactions have been measured with a spherical electrostatic analyzer[1] using an energy resolution of 500. Bombarding particle energies were determined by a cylindrical electrostatic analyzer calibrated against the $Li^7(p, n)Be^7$ threshold. The angle of observation (134°32′) of the product particles was determined by direct measurement and by scattering protons from a deuterium target. The following are preliminary Q values. Estimates of uncertainties will be given.

Reaction	Q (Mev)
$Li^6(p, He^3)\alpha$	4.027
$Li^7(d, p)Li^8$	−0.181
$Li^7(p, p')Li^{7*}$	−0.4785
$Li^6(d, d')Li^{6*}$	−0.4773.

* Work supported by the AEC and the Wisconsin Alumni Research Foundation.
[1] Craig, Browne, and Williamson, Phys. Rev. **81**, 304 (1951).

D8. Beryllium and Tritium Reaction Energies.* R. M. WILLIAMSON, C. P. BROWNE, D. J. DONAHUE, D. S. CRAIG, AND K. W. JONES, *University of Wisconsin.*—Using equipment referred to in the preceding abstract, the following preliminary Q values have been obtained:

Reaction	Q (Mev)
$Be^9(p, p')Be^{9*}$	−2.43
$Be^9(p, d)Be^8$	+0.5581
$Be^9(p, \alpha)Li^6$	2.123
$Be^9(p, Li^6)He^4$	2.136
$Be^9(p, \alpha')Li^{6*}$	−0.06
$Be^9(d, Li^7)He^4$	7.175
$T(d, \alpha)n$	17.75.

Final values and estimated errors, along with data on target contamination and magnetic field effects, will be given. The level at 2.18 Mev (corresponding to $Q = -0.06$ Mev) reported in Li^8 was observed at three different bombarding energies and is believed to be the level at ~2.3 Mev previously reported[1] from $Li^7(d, t)Li^{6*}$ reaction. The target of tritium in thick zirconium showed a rapid decrease of tritium density near the surface. It is therefore only possible at present to put a lower limit on this Q.

* Work supported by the AEC and the Wisconsin Alumni Research Foundation.
[1] Hornyak, Lauritsen, Morrison, and Fowler, Revs. Modern Phys. **22**, 304 (1950).

D9. Interpretation of (d, n) Angular Distributions.* W. HECKROTTE AND L. SCHECTER, *University of California, Berkeley.*—Recently, determinations[1] have been made of the spatial distributions of neutrons which result from bombardment of various targets by 20-Mev deuterons from the 60-inch cyclotron at Berkeley. In some cases the distributions show small-angle structure which can be interpreted by the mechanism recently proposed by S. T. Butler. This structure is determined by the spins and parities of the nuclear states involved. The experimental method does not allow an identification of the states of the final nucleus, and the observed distributions result from a superposition of the contributions from the various final states. But in the cases of Be^9, Al^{27}, and Cu^{63}, it is possible to show that probably only one of the final states enters in determining the angular distribution. For the $Be^9(d, n)B^{10}$ reaction, production of the ground state of B^{10} only was assumed, and the theoretical and experimental agreement is good enough to assign parity and possible spin values of Be^9. For the $Al^{27}(d, n)Si^{28}$ reaction, similar considerations show that production of the ground state of Si^{28} is unlikely, and the parity and the possible spin values of the resulting excited state have been determined. Similar information is also possible from the $Cu^{63}(d, n)Zn^{64}$ reaction.

* This work was performed under the auspices of the AEC.
[1] L. Schecter, Phys. Rev. **81**, 652A (1951).

D10. Scintillation Spectrometer Measurements of Gamma-Rays from Proton Bombardment of Be^9 and C^{13}. R. L. WALKER AND R. B. DAY, *California Institute of Technology.*—Preliminary measurements of the energies of gamma-rays emitted in a few nuclear reactions have been made with the scintillation counter technique now in common use. A selected 5819 photomultiplier was used in conjunction with a NaI(Tl) crystal 1½ inches in diameter and 1½ inches long. The equipment was checked by using gamma-rays of known energies between 0.5 and 7.4 Mev. The strong gamma-radiation from the 2.56-Mev proton resonance[1] of Be^9 has an energy 3.55±0.07 Mev. This gamma-ray probably emitted by the residual nucleus Li^{6*} left after alpha-particle emission in the $Be^9(p, \alpha)Li^{6*}$ reaction.[1] Further investigation of the origin of this gamma-ray is planned, since a 3.6-Mev level in Li^6 is of special interest as the analog of the ground state in the isobaric nucleus, He^6. The 554-kev proton resonance in C^{13} produces prominent gamma-radiation near 8 Mev and 2.3 Mev, and much weaker radiation near 4 Mev. At this proton energy, no appreciable radiation between 5 and 6 Mev was observed, in contrast to previous reports.

* Supported by the ONR and AEC.
[1] W. J. Hushley, Phys. Rev. **67**, 34 (1945).

D11. Gamma-Rays from Deuteron Bombardment and Slow Neutron Capture. W. E. MEYERHOF, H. RODERICK, AND L. G. MANN, *Stanford University.*—In order to calibrate a NaI(Tl) scintillation detector for slow neutron capture gamma-ray studies we have bombarded Be and C with 2.7-Mev deuterons. In the case of Be, gamma-rays of 6.7 and 6.0 Mev the latter probably originating from the 6.76-Mev level of B^{10}, have been found in addition to other known gamma-rays. In the case of C, gamma-rays of energy 6.1, 4.3, 3.8, and 3.1 (known) Mev have been observed. The 6.1γ is as yet unassigned. The 4.3γ is perhaps due to excitation of the 4.4-Mev level of C^{13} by inelastically scattered $C^{13}(d, p)$ protons. The 3.8 and 3.1γ originate from known levels of C^{13}. Using the above data for calibration we have started the study of slow neutron capture gamma-rays from Cu, Fe, Pb, and other elements. Cu, Fe, and Pb show the prominent ground-state transitions reported by Kinsey *et al.*[1] Fe shows in addition a prominent gamma-ray of 5.9 Mev, probably due to Fe^{56}. A 1.7-Mev gamma-ray needed to complete the cascade to the ground state of Fe^{57} has not yet been found.

[1] Kinsey, Bartholomew, and Walker, Phys. Rev. **78**, 481 (1950).

D12. Energy Release in the Disintegration of Be^8. R. R. CARLSON, *University of Chicago.*—A beryllium target of less than one-kev thickness was bombarded with protons accel-

erated to 372 kev by a Cockcroft-Walton generator. The scattered protons and the products of the reactions $Be^9(p, d)Be^8$ $Be^9(p, \alpha)Li^6$, which are known to occur, were observed at 90° to the beam with a cylindrical electrostatic analyzer. The thin beryllium targets were prepared by evaporation onto nickel foils of average thickness about 100A. This made possible the observation of particles whose energies were less than that of the scattered protons. Preliminary measurements indicate a continuous distribution of particles exists with its upper edge corresponding to doubly charged particles of energy 223 kev. This is attributed to the alpha-particles from the breakup of Be^8. Since carbon accumulation on the target can give an apparently low value for the edge of this distribution, measurements were made on fresh targets only and the position of the Li^6 peak measured at the beginning and end of every run. These peaks gave a Q value of 2.12 Mev for the reaction $Be^9(p, \alpha)Li^6$ in agreement with the accepted value. Using the known Q value for the reaction $Be^9(p, d)Be^8$, the above result gives the energy release in the Be^8 break-up as 72 ± 5 kev. This is to be compared with the value 89 ± 5 kev previously measured.[1]

[1] Tollestrup, Fowler, and Lauritsen, Phys. Rev. 76, 428 (1949).

THURSDAY MORNING AT 9:30

NBS, East Building

(L. A. WOOD presiding)

Symposium of the Division of High-Polymer Physics
Transitions in Polymers

E1. Factors Influencing Glass Formation and Crystallization in Polymers. T. G. FOX, JR., *Rohm and Haas Company.* (30 min.)

Contributed Papers

E2. X-Ray Scattering from Polystyrene as a Function of Temperature. S. KRIMM AND A. V. TOBOLSKY, *Princeton University.*—The x-ray diffraction pattern of unoriented polystyrene has been investigated as a function of temperature with a Geiger counter spectrometer. It has been found that the relative peak intensities of the two halos in the pattern depends on the temperature. The ratio of the intensity of the outer to that of the inner halo is essentially constant between room temperature and about 90°C, at which temperature it falls linearly to a lower value which is then constant above about 160°C. The Bragg spacings corresponding to the peaks of these halos are practically constant up to 160°C; above this temperature the spacings increase. An interpretation of these changes in the x-ray scattering pattern is aided by a study of the pattern of oriented polystyrene, it having been possible to obtain x-ray evidence of orientation. These data suggest that the main mechanism of expansion of the material differs in the various temperature regions as a result of structural changes taking place with change in temperature. Specific volume-temperature data tend to support this view. Possible bearing of this information on the second-order transition in amorphous polymers is discussed.

E3. Pressure—Volume Relationships of Rubber and Other Polymers. C. E. WEIR, *National Bureau of Standards.*—The effect of pressure on the volume of raw rubbers and other polymers was studied at room temperature in the pressure range 1000–10,000 atmos. Measurements were made by the piston displacement method. The total decrease in volume ($\Delta V/Vo$) of rubber specimens was approximately 15 percent at 10,000 atmos., which is about twice the volume change expected to occur between room temperature and the second-order transition temperature. No transitions were observed in the rubbers studied, all pressure-volume curves being smooth. All volume changes of polymeric materials studied are of the same order of magnitude.

E4. Studies in Plasticization of Polyvinyl Chloride. III. The Plasticized State: A Special Application of Solubility Principles. M. L. DANNIS, *B. F. Goodrich Company Research Center.*—The behavior of plasticized polyvinyl chloride is considered to be that of a two-component, two-phase system. The dielectric loss factor peak at a fixed frequency defines a transition temperature analogous to the freezing temperature in low molecular weight systems. Transition temperature depressions with added plasticizer follow Flory's crystallization point lowering theory for some PVC-plasticizer systems, but deviate for others. From solution theory analogy, the cohesive energy density of PVC is estimated at 93 cal/cc and the behavior segment as 9 polymerized vinyl groups.

E5. Length-Temperature Behavior of Rubbers.* M. J. FORSTER AND R. L. ANTHONY, *University of Notre Dame.*—As a supplement to stress-temperature and volume dilatometric methods of investigating the second-order transition in rubbers, studies of length-temperature behavior were undertaken. Samples of several rubbers were stretched at 40°C to various initial extensions, under constant loads. They were permitted to creep at that temperature until the time rate of change of length became negligibly small. The temperature was then lowered in steps down through the transition region, and the length-temperature behavior was studied. A wide variety of L *vs* T curves was observed, the shape of the curve obtained in each case depending strongly upon the initial extension and whether this extension was above or below the thermoelastic inversion value. For the rubbers studied, the second-order transition temperature (or region) appears to increase rapidly with increasing initial extension for extensions below the thermo-elastic inversion value, and then to decrease with further increase in initial extension.

* Supported in part by the ONR.

E6. The Determination of the Degree of Crystallinity in Natural Rubber by Dilatometric Methods. RICHARD N. WORK, *National Bureau of Standards.*—The expansivity of amorphous and partially crystalline natural rubber has been determined at temperatures below the glass-transition temperature, T_g, by means of an automatic photoelectric recording interferom-

eter, and above T_g, by means of volume dilatometers in addition to the interferometer. The degree of crystallinity was calculated from the change in expansivity on crystallization above the transition and the expansivity below the transition by a method based on a suggestion of Parks.[1] The expansivity below the transition was found to be independent of the extent of crystallization. Results are expressed in terms of the volume fraction of crystallized rubber for each percent volume decrease upon crystallization, where the actual volume change is reduced to a value at 25°C. Preliminary results give about 10 percent crystallinity for each percent volume decrease. This result is in accordance with x-ray measurements of Goppel and Arlman.[2]

[1] G. S. Parks, J. Chem. Phys. 4, 459 (1936).
[2] J. M. Goppel and J. J. Arlman, Appl. Sci. Research A1, 347–52 and 462–74 (1948).

General High-Polymer Physics

E7. Dielectric Constant of Rubber-Carbon Black Mixtures. CLINTON M. DOEDE, *Connecticut Hard Rubber Company.*—A study has been made of the effect of the carbon black concentration, carbon black particle size, and frequency of the applied voltage upon the dielectric constant of vulcanized and unvulcanized rubber-carbon black mixtures. The dielectric constant has been shown to increase with carbon black concentration, decrease with the frequency of the applied voltage, and for a given black concentration and frequency, to increase very rapidly with decrease in particle radius when the particle radius is of the order of one-tenth micron or less. These observations have been explained with the assumption that the interparticle distances must be sufficiently small to allow interaction of the fields of activity surrounding adjacent particles. This interpretation is in agreement with the observations of Freundlich and of Kallman and Wilstätter.

E8. Theory of Reinforcement in Hydrocarbon and Silicone Rubbers. HENRY A. FAIRBANK, CHARLES A. WALKER, AND CLINTON M. DOEDE, *Connecticut Hard Rubber Company.*—Comparison of extensive data on the effect of pigments on the tensile strength of silicone rubber with similar data on natural rubber and GR-S indicates that the mechanism of reinforcement in three types may be considerably different. In particular, it is noted that the increase in tensile strength at break owing to reinforcing pigments is relatively small (less than 25 percent) in the case of natural rubber but several-fold in the case of GR-S and silicone rubber. Current theories of rubber reinforcement do not adequately account for the differences noted for these types of rubber. It is suggested that the tensile strength at break of unreinforced rubbers (high for natural rubbers and low for GR-S and silicone rubbers) is determined not alone by the strength of the rubber-rubber bonds but by the presence of local imperfections or tear centers. Thus a very important function of the pigment in GR-S and silicone rubber may be the localization of tears. A similar theory is current in studies of strength of metals.

THURSDAY AFTERNOON AT 2:15

NBS, East Building

(A. V. TOBOLSKY presiding)

Symposium of the Division of High-Polymer Physics

The Relative Effects of Frequency and Temperature on Dynamic Mechanical Properties

EA1. Introduction to the Symposium. A. V. TOBOLSKY, *Polytechnic Institute of Brooklyn.* (30 min.)

EA2. The Use of Reduced Variables to Describe Temperature and Frequency Dependence of Dynamic Mechanical Properties. J. D. FERRY, *University of Wisconsin.* (30 min.)

EA3. Dynamic Studies on Polysobutylene. T. W. DE WITT, *Mellon Institute of Industrial Research.* (20 min.)

EA4. Temperature and Frequency Effects on Dynamic Properties: Results of the Cooperative Programme. R. S. MARVIN, *National Bureau of Standards.* (20 min.)

EA5. Temperature and Frequency Effects in the Dynamic Behavior of Swollen and Unswollen Rubber. A. W. NOLLE, *University of Texas.* (30 min.)

EA6. Summary and Discussion. H. S. SACK, *Cornell University.* (30 min.)

THURSDAY AFTERNOON AT 2:15

Shoreham, Main Ballroom

(R. E. MARSHAK presiding)

Production and Capture of Mesons and Electron Pairs

F1. Energy Spectra of π-Mesons Produced at 90° from a 385 Mev Proton Beam.* M. M. BLOCK, S. PASSMAN, AND W. W. HAVENS, JR., *Columbia University.*—Charged π-meson energy spectra from thin targets bombarded by the internal 385-Mev proton beam of the Nevis Cyclotron are being measured. Ilford C-2 nuclear emulsions are imbedded in tapered copper and aluminum absorbers, placed inside the cyclotron vacuum chamber, 2½" below the target, and shielded so as to

receive mesons emitted only at $(90\pm10)°$ from the beam direction. The energy interval from 0 to 125 Mev is included in a single plate. Only those mesons ending in the emulsion and undergoing decay or forming stars are included in the spectra. Using a 0.3 g/cm² carbon target, a π^+ energy spectrum based on 425 π-μ-events has been obtained. When corrected for nuclear absorption,[1] the spectrum exhibits a peak at about 60 to 70 Mev, with half-maxima at about 30 and 90 Mev. This spectrum will be discussed relative to theoretical predictions for meson production. Spectra of other materials are being investigated.

* This work was assisted by the joint program of the ONR and AEC.
[1] Bernardini, Booth, Lederman, and Tinlot, Phys. Rev. **80**, 924 (1950).

F2. Production of Neutral Mesons by γ-Rays Incident on Hydrogen.* A. SILVERMAN AND M. STEARNS, *Cornell University.*—The reaction $h\nu+H'\rightarrow\pi^0+H'$ is being investigated by bombarding a thin polyethylene target with γ-rays from the 305-Mev Cornell Synchrotron. The reaction is observed by detecting coincidences between the recoil proton and one of the decay γ-rays from the π^0 meson. By measuring the energy and angle of the recoil proton, the energy of the incident γ-ray and the π^0 energy and angle are determined. The proton energy is measured by its pulse height in a NaI crystal in which it expends all its energy. The carbon background was determined for each energy interval and constituted about 40 percent in the lowest energy interval and about 10 percent in the highest. The protons were observed at $30°\pm3°$ corresponding to mesons at about 90° for incident γ-ray energies between 200–300 Mev. Preliminary results yield a differential cross section $(d\sigma/d\Omega)90°=2\times10^{-30}$ cm² per steradian per Q. The cross section as a function of energy is as follows:

E(Mev)	215	240	265	290
$\frac{(d\sigma/d\Omega)90°}{10^{-30}}$	2.4 ± 0.7	2.7 ± 0.7	4.7 ± 0.7	9.1 ± 0.9

Further work is in progress.

* Supported by ONR.

F3. Production of Photo-Mesons from Deuterium and Other Light Elements.* R. M. LITTAUER AND D. WALKER, *Cornell University.*—Targets of light elements were bombarded by gamma-rays from the 300-Mev electron synchrotron. Charged mesons emitted at 135°, with energies of about 50 Mev, were focused magnetically onto an array of counters. Cloud-chamber[1] and absorption studiess howed negligible contamination of the meson beam by electrons. Relative counting rates for π^- and π^+ mesons were measured for each target. Results are summarized below (errors are statistical; yields normalized to $D=1.00$):

Nucleus	π^-/π^+ Ratio	π^+ Yield/Proton	π^- Yield/Neutron
H		1.20 ± 0.16	0.01 ± 0.12 (per proton)
D	1.39 ± 0.24	1.00 ± 0.14	1.00 ± 0.12
Be	2.25 ± 0.11		
C	1.04 ± 0.05	0.70 ± 0.02	0.50 ± 0.02
O	0.97 ± 0.11	0.58 ± 0.04	0.40 ± 0.03
S	0.78 ± 0.05	0.54 ± 0.02	0.30 ± 0.02

Inequality of the meson life-times would modify the observed π^-/π^+ ratios.

* This work was performed under contract with the ONR.
[1] M. Camac *et al.*, Bull. Am. Phys. Soc. **26**, No. 1, 48 (1951).

F4. Studies on the Production of Neutral Mesons by Protons.* B. J. MOYER, R. MADEY, R. H. HILDEBRAND, N. KNABLE, AND R. HALES, *University of California, Berkeley.*—Experiments are in progress in the deflected 340-Mev proton beam of the 184″ cyclotron. Measurements of the yield of neutral mesons *vs* target Z will be reported. For the special case of $p-p$ collisions the yield is observed to be zero ±2 percent of the yield from p-carbon nucleus collisions. The range of error should be reduced by experiments now in progress. Previous efforts at measuring π^0 production from $p-H^2$ collisions employing internal targets and a pair counter have suggested a yield of the order of 10 percent of that from p-oxygen nucleus collisions, but probable errors were at least 50 percent of the effect. In measurements of π^0 production in H^1 and H^2, the yield is so low as to preclude coincidence detection of decay photons. Single high energy photons are detected by counters recording each electron of a pair produced in a $\frac{1}{8}$″ Pb converter and separated by scattering. Data are being obtained on the correlation angle distribution for the coincident photons from π^0 decay, which will yield the π^0 momentum distribution. Early results show a maximum yield at a correlation angle near 90° when the counters-target plane is normal to the beam.

* This work was performed under the auspices of the AEC.

F5. Production Ratio of Photo-Mesons from Beryllium.* HENRICH A. MEDICUS, *University of California, Berkeley.*—The method which was used for the determination of the ratio of negative to positive π-mesons produced from photons on carbon[1] has been applied to beryllium. The collimated x-ray beam of the synchrotron (electron energy 322 Mev) strikes the beryllium target. The mesons emerge from the target at an angle of 90° to the beam direction and are detected in 200-μ Ilford C2-emulsions after traversing appropriate absorbers. The ratio, π^-/π^+, is determined from the observed numbers of σ-mesons and π-μ-decays. The preliminary ratio is 2.0 ± 0.3 for the energy range 40–70 Mev. This is considerably higher than the value of 1.3 for carbon. This effect can be explained from the higher neutron-proton ratio in the beryllium nucleus and from the fact that the loosely bound neutron participates relatively strongly in the meson production.

* This work was supported by the AEC and the Schweigerische Arbeitsgemeinschaft für Stipendien in Mathematik und Physik.
[1] Peterson, Gilbert, and White, Phys. Rev. (to be published). McMillan, Peterson, and White, Science **110**, 579 (1949).

F6. μ^- Meson Capture Studies Using Large Liquid Scintillators: I. Apparatus.* F. B. HARRISON AND J. WARREN KEUFFEL, *Princeton University.*—Two large-area scintillation counters are now being used to study processes related to the capture of μ^- mesons in heavy elements. Each counter consists of a copper tank $1''\times12''\times12''$, filled with terphenyl in toluene. Four 1P21 photomultipliers are used. The efficiency for minimum ionizing particles and the relative time lags between the two scintillator tanks have been measured using a beam of fast mesons selected by an auxilliary counter telescope. With a discriminator setting such that 300 noise pulses are counted per sec, the efficiency averaged over the entire tank surface is about 80 percent. The relative lag distribution between the two tanks is approximately gaussian, with a mean deviation of 3 mμ sec. Pairs of photomultipliers are connected in parallel, then mixed by means of cathode followers, amplified with a gain of 200 and a rise-time of about 10 mμ sec, clipped, and fed to a chronotron timing circuit. Echo pulses, probably caused by phosphorescence, are observed to follow the main pulse in a given tank, with a continuous distribution of delays whose average value is around one μsec.

* Supported by the joint program of the AEC and ONR.

F7. μ^- Meson Capture Studies Using Large Liquid Scintillators: II. Results.* J. WARREN KEUFFEL AND F. B. HARRISON, *Princeton University.*—Evidence has been obtained for the existence of delayed non-ionizing radiations, presumably low-energy gamma-rays or neutrons, associated with the nuclear capture of μ^- mesons in Cu and Sb. Preliminary values for the mean lifetime of the μ-meson in these elements are: Cu, Cu, 120 ± 50 mμ sec.: Sb, 53 ± 20 mμ sec. The errors quoted are

statistical; the instrumental errors will permit a much better precision. We have employed the following disposition: G-M tray A, 7.5 cm of Pb, scintillator tank S_1, 40 g/cm² of Cu or Sb, anticoincidence G-M counters X, scintillator tank S_2, additional anticoincidence counters X. The relative lag between the pulses in S_1 and S_2 is photographically recorded for events (AS_1S_2-X). The background owing to bremsstrahlung of decay electrons has been taken into account. The results support the Wheeler picture of the meson capture process[1] and should lead to an improved value for the coupling constant between μ-mesons and nuclei.

* Supported by the joint program of the AEC and the ONR.
[1] J. A. Wheeler, Revs. Modern Phys. 21, 133 (1949).

F8. Decay and Capture of Mesons in Photographic Emulsions.* W. F. FRY, *Iowa State College.*—Meson events have been studied in Eastman NTB-3 plates which were exposed to cosmic radiation in the stratosphere. A total of 41 π-μ-decays, 118 negative π-stars, and 500 mesons which stopped in the emulsion without associated particles other than electrons, were studied. It is estimated that 68 ± 7 percent of the μ-mesons decayed in the emulsion. One or more low energy electrons in the interval from 15 to 70 kev were observed from 58 of the mesons which stopped in the emulsion without associated particles other than electrons. In 10 cases, two such electrons were observed from the same meson. In 2 cases, three electrons were observed. The energy distribution of these electrons can be represented by $N(E)\sim\exp(-E/E_0)$. One or more low energy electrons were observed from 22-meson stars. No electrons of energy gretter than 0.2 Mev were observed from the meson stars. The energy distribution and the percentage of low energy electrons from meson stars and from μ-mesons are the same, within statistical limits. These facts indicate that the low energy electrons tre due to the interaction of the negative mesons with the electronic shells of the heavy atoms in the emulsion.

* Supported in part by grants from the Research Corporation and the Iowa State College Research Foundation.

F9. Nuclear Interactions of μ-Mesons Underground. S. HAYAKAWA, *Cornell University.*—The nuclear interactions of μ-mesons detected in two underground experiments, (a) by George and Evans with photographic plates, and (b) by Cocconi and Cocconi-Tongiorgi with neutron counters, are analyzed. Both experiments can be explained by the interaction with matter of the electromagnetic field of the μ-mesons. Most of the nuclear disintegrations underground are produced either directly by the μ-mesons or by the N-component in equilibrium with them. An interpretation is given of the neutron showers of experiment (b) using the following pictures: (1) a μ-meson is scattered by a nucleon in a Pb nucleus, and its recoil nucleon starts a nucleon cascade; (2) a nucleon produced above the apparatus enters the Pb absorber and keeps on developing the nucleon cascade inside it. In both cases each step of the development of the nucleon cascade leads to the production of neutrons of moderate energies (1–10 Mev). The multiplicity spectra of the neutron showers thus generated are calculated. Both the shapes and the average multiplicities are in fair agreement with the experimental data. Other questions concerning the interaction of μ-mesons are discussed.

F10. A Search for Nuclear Disintegrations Associated with the Stopping of μ-Mesons in Argon Gas.* G. W. MCCLURE, *Bartol Research Foundation.***—A high pressure ionization chamber operating in conjunction with an anticoincidence counter controlling arrangement to detect the entrance of slow penetrating particles has been used to set an upper limit on the frequency of star production by μ-mesons captured in argon. To determine the background rate of ion chamber events not associated with meson capture, the chamber was operated part of the time with an equivalent filling of nitrogen—a gas having a low μ^- capture probability. All of the larger ionization pulses which occurred in either gas could be attributed either to slow mesons (85 percent) or protons (15 percent) which stopped in the chamber without producing nuclear events in the gas. Comparison of the argon and nitrogen pulse height distributions indicates that, if any, less than 18 percent of the negative μ-mesons stopped in argon produce stars in which the ejected charged nucleons have a combined energy greater than 5 Mev.

* Assisted in part by the ONR and AEC.
** Experimental work performed at the University of Chicago.

F11. Pair Production by Electrons. MORTON CAMAC, *Cornell University.*—An experiment was started to observe pair production by electrons in the nuclear field by measuring the positrons emitted from a target irradiated directly by the synchrotron electron beam. Positrons produced in the target are bent out of the donut through a thin aluminum port by the magnetic field. These are detected in a counter telescope consisting of a thin-walled proportional counter, two inches of aluminum, and a NaI crystal detector with approximately a 15-Mev bias. For a coincidence in the two counters an ionizing particle must have at least 40-Mev energy. The positrons can be produced either directly by the electrons or through a double process in which bremsstrahlung is first produced and then converted into pairs in the same target. Using the bremsstrahlung beam as a monitor the direct process is independent of the target thickness, while the double process varies linearly. Thus, we get a direct comparison of the two effects. Preliminary data give a ratio of the cross section of the direct to the double effect of from 0 to 0.003 for the case of the positron having about 90 percent of the initial electron energy of about 250 Mev.

F12. Energy Sharing of Electron Pairs at 17 Mev. B. DAYTON, *Cornell University.**—The energy sharing between positrons and electrons near the ends of the relative energy spectrum has been measured in Al, Cu, Sn, and Pb. The pairs were produced by the 17-Mev lithium gamma-rays. The experiment, employing coincidence counting, was designed to disclose any sizable asymmetry between positron and electron energies, such as might be expected for pair production in heavy elements. These measurements, together with an absolute calibration of the gamma-ray yield from the cyclotron,[1] also provide absolute differential cross sections for pair production and Compton scattering. Applying the Bethe-Heitler and Klein-Nishina formulas to the known spectrum[2] of the lithium gamma-rays, differential cross-section curves have been prepared to compare to the experimental distributions. Qualitatively, the experimental cross sections are in good agreement with theory, though they are low by 10–15 percent for Sn and Pb, both for pair production and Compton scattering. The asymmetry found is possibly significant for Pb and Sn, but it is certainly masked by the statistical errors for Cu and Al.

* Now at the Massachusetts Institute of Technology.
[1] McDaniel, Walker, and Stearns, Phys. Rev. 80, 807 (1950).
[2] R. L. Walker and B. D. McDaniel, Phys. Rev. 74, 315 (1948).

F13. Evidence for Formation of Positronium in Gases.* MARTIN DEUTSCH, *Massachusetts Institute of Technology.*—We find that in some gases a considerable fraction of positrons is annihilated much more rapidly than can be explained on the assumption that they are moving freely through the gas. This indicates their attachment to bound structures where the electron density is high. There is strong evidence that in N_2, for example, this structure is a free positronium atom. Many of these atoms survive for about 10^{-7} sec in the ^3S state in which two-quantum annihilation is forbidden. Evidence for the continuous gamma-ray spectrum owing to

the three-quantum annihilation has been found with a scintillation spectrometer. Addition of 5 percent of NO to N_2 reduces the number of delayed annihilations by a factor of 3 and removes the continuous gamma-spectrum. This is interpreted as conversion of the ^3S to the ^1S state, which decays in 10^{-10} sec. This conversion can occur in NO by electron exchange. O_2, in which conversion can occur only for atoms with more than 1.6 ev kinetic energy, behaves intermediate between N_2 and N_2+NO.

* Supported in part by the joint program of the AEC and ONR.

THURSDAY AFTERNOON AT 2:30

Shoreham, West Ballroom

(R. M. BOZORTH presiding)

Ferromagnetic Substances

G1. Motion of a Domain Wall in Fe_3O_4. J. K. GALT. *Bell Telephone Laboratories.*—A diamond-shaped ring of Fe_3O_4, with each leg along a direction of easy magnetization, is cut from a synthetic single crystal[1] of Fe_3O_4 with its face in a 110 plane. This sample is expected to have a simple domain pattern analogous to that observed in silicon iron by Williams and Shockley.[2] The hysteresis loop has the expected square shape, with a coercive force of 0.25 oersted. Pictures of the domain pattern will be shown. Initial permeability *vs* frequency follows a relaxation curve with $\mu=5000$ at $\nu=0$ and a relaxation frequency of approximately 2000 cycles. Wall velocity in cm/sec is about 10^3 times the applied field in oersteds. The relaxation time computed from these measurements will be compared with that deduced from the width of the ferromagnetic resonance line.

[1] The crystal used was made available by Professor A. von Hippel (Laboratory for Insulation Research, M.I.T.). This crystal growth work was sponsored on contract jointly by the ONR, the Army Signal Corps, and the Air Force.
[2] H. J. Williams and W. Shockley, Phys. Rev. **75**, 178 (1949).

G2. Old Data on Hall Effect in Nickel. EMERSON M. PUGH, N. ROSTOKER, AND A. I. SCHINDLER, *Carnegie Institute of Technology.*—Old Hall effect data on ferromagnetics are generally consistent with the relation $E_H=R_0(H+\alpha 4\pi M)ib$. Extensive data by A. W. Smith[1] on pure nickel taken over wide ranges of magnetic field H and temperature θ is shown to be consistent with an R independent of H and θ and an α independent of H but increasing rapidly with θ. For this analysis, data from Weiss and Forrer[2] giving M *vs* H for nickel over the same ranges of H and θ, were needed. The relationship appears to hold above and below the Curie point temperature and above and below the magnetic fields required for saturation.

[1] A. W. Smith, Phys. Rev. **30**, 1 (1910).
[2] P. Weiss and R. Forrer, Ann. Physik **5**, 153 (1926).

G3. Hall Effect in Copper-Nickel Alloys. A. I. SCHINDLER AND EMERSON M. PUGH, *Carnegie Institute of Technology.*—The Hall constant R_0 and the field parameter α defined by $E_H=R_0(H+\alpha 4\pi M)ib$ have been experimentally determined for various alloys of copper and nickel. A brief description of the apparatus and a summary of the results will be given. The Hall constant R_0 increases with copper content until a maximum is reached at about 30–40 percent copper. It then decreases with increasing copper content. The number of conduction electrons as calculated from the Hall constant R_0 is consistent (within a factor of two) with magnetic data and the existing band picture of the alloy system. The field parameter α varies approximately linearly with copper content from 10 for pure nickel to 40 for 30 percent Cu—70 percent Ni at room temperature.

G4. Hall Effect and the Technical Magnetic Force. N. ROSTOKER, *Carnegie Institute of Technology.*—The Bloch-Sommerfeld theory of conductivity has been applied to the calculation of momentum transferred to a crystal lattice by conduction electrons in the presence of a magnetic field for the following cases: (i) pure electronic conduction, (ii) pure hole conduction, (iii) simultaneous electronic and hole conduction. In the first two cases the technical magnetic body force $\mathbf{f}=(\mathbf{J}\times\mathbf{B})/c$ results entirely from the action of the Hall electric field on the crystal lattice. In the third case the body force is partially due to momentum transfer and partially due to the action of the Hall electric field. In the case of nickel, it is entirely due to momentum transfer. The unusual experimental results obtained for the Hall effect in ferromagnetics are discussed in the light of these calculations.

G5. Optical Rotation by Ferromagnetic Substances. CHARLES KITTEL, *Bell Telephone Laboratories.*—The plane of polarization of light experiences a rotation on transmission through ferromagnetic bodies (faraday effect) and also on reflection at the surfaces of ferromagnetic bodies (Kerr effect). The quantum theory of the faraday effect has been discussed by Hulme,[1] employing the formalism of spin-wave theory, and he succeeds in accounting for the order of magnitude of the observed[2] saturation rotation in iron, which is 380,000 degrees per centimeter. We discuss a rather simpler model leading to the faraday rotation and point out the additional substantial changes in the rotation which are caused by the incomplete quenching of the orbital angular momentum of the ground state of the magnetic atoms. The effect of incomplete quenching have recently been discussed by Van Vleck, Polder, and the author in connection with the interpretation of ferromagnetic resonance and gyromagnetic ratio experiments. The effect on the rotation may be as large as the effect considered by Hulme.

[1] H. R. Hulme, Proc. Roy. Soc. (London) **A135**, 237–257 (1932); see also O. Halpern, Ann. Physik [5] **12**, 181 (1932).
[2] H. König, Optik **3**, 101–119 (1948).

G6. Neutron Diffraction Studies of Antiferromagnetism in Manganous and Nickelous Fluoride. R. A. ERICKSON* AND C. G. SHULL, *Oak Ridge National Laboratory.*—Neutron diffraction studies have been made on MnF_2 and NiF_2 between 20 and 300°K. Both compounds were found to be antiferromagnetic with Curie points between 70 and 80°K. In the region of magnetic saturation the data can be accounted for by a model in which the magnetic moments of the paramagnetic ions are directed along the short axis of the tetragonal system, as indicated by the susceptibility measurements of Griffel and Stout[1] on a single crystal of MnF_2, and the magnetic and chemical unit cells are of the same size. The temperature dependence of the integrated intensity in the magnetic reflections was found to be in agreement with that cal-

culated from the spontaneous magnetization predicted by Van Vleck[3] for a simple antiferromagnetic lattice.

* Graduate Fellow of the Oak Ridge Institute of Nuclear Studies.
[1] M. Griffel and J. M. Stout, J. Chem. Phys. 18, 1455–58 (1950).
[3] J. H. Van Vleck, J. Chem. Phys. 9, 85–90 (1941).

G7. Magnetostrictive Vibration of Prolate Spheroids of Nickel and Nickel-Iron Alloys.* J. S. KOUVELITES, L. W. MCKEEHAN, AND F. J. BECK, *Yale University.*—Small centrally-clamped ferromagnetic specimens have been subjected to an alternating, axial magnetic field and allowed to vibrate longitudinally in the frequency region of their fundamental mode. The static magnetic bias, simultaneously impressed on the specimens, was brought up along the static magnetization curve to a point well above the "knee" and then taken around a complete hysteresis loop. The analysis of the vibrational response yielded values for several magnetic and mechanical parameters: magnetostriction constant, incremental permeability, modulus of elasticity, etc. The variation of these parameters with composition and magnetic bias has been examined qualitatively in the light of present domain theory. While all the specimens were similarly annealed before measurement, the nickel was studied in an untreated state, as well.

* Assisted by the ONR.

G8. Recrystallization of Fe-Co Alloys.* B. SAWYER, R. SMOLUCHOWSKI, AND R. W. TURNER, *Carnegie Institute of Technology.*—In connection with the previously reported[1] influence of magnetic field on the recrystallization texture of Fe–Co alloys a systematic study of recrystallization of these alloys is being conducted. The recrystallization texture is a sum of three ideal orientations: (100)·[110], (100)·[110]∼15° and (111)·[110]∼15°, and the experiment shows that the relative proportion of a given texture is a function of temperature of recrystallization. At temperatures below 700° the apparently predominant texture is (100)[110], which is similar to the texture in rolled material before recrystallization. With increasing temperature the other two textures gain in intensity, and in the proximity of 900°C there is no trace of the low temperature texture. This behavior allows to estimate the respective activation energies and correlates with the influence of magnetic field. All measurements in this study are made with help of the continuous pole figure camera.[3] A new positioning of the sample increased by 50 percent the area of the stereographic projection covered in one exposure and the only missing part is that within 45 degrees of the center.

* Research sponsored by a contract with AEC.
[1] R. Smoluchowski and R. W. Turner, J. Appl. Phys. 20, 745 (1949).
[3] R. Smoluchowski and R. W. Turner, Physica 16, 397 (1950).

THURSDAY AFTERNOON AT 2:15

Wardman Park, Continental Room

(WALTER GORDY presiding)

Microwave Spectra and Magnetic Resonance

H1. The Spin of O^{18}. S. L. MILLER,* A. JAVAN, AND C. H. TOWNES, *Columbia University.*†—Observation of the microwave absorption spectrum of $O^{16}O^{18}$ and $O^{18}O^{18}$ in the 5-mm region shows that the spin of O^{18} is zero. In the region between 58,300 mc and 59,900 mc all of the expected $O^{16}O^{18}$ and $O^{18}O^{18}$ lines have been observed and identified. Their positions are predicted closely by Schlapp's formula with appropriate changes in constants for isotopic substitutions. The $K=8$, $J=7\rightarrow 8$ transition which should be at about 58,600 mc, the $K=6$, $J=5\rightarrow 6$ transition at about 59,375 and the $K=4$, $J=5\rightarrow 4$ transition at about 59,400 mc for $O^{16}O^{18}$ are all missing. Other observations on O^{18} had failed to disclose quadrupole hyperfine structure, and the $O^{16}O^{18}$ lines show no evidence of magnetic hyperfine structure, which indicates a zero spin for O^{18}. However, real proof that the spin of O^{18} is zero rests on the method of alternating intensities in the homonuclear molecule $O^{18}O^{18}$. Since alternate rotational levels of $O^{18}O^{18}$ do not exist and it is the same levels which are forbidden in $O^{16}O^{16}$, the spin of O^{18} is zero and the O^{18} nucleus follows Bose-Einstein statistics. Magnetic hyperfine structure found in $O^{16}O^{17}$ indicates an O^{17} spin greater than $\frac{1}{2}$. The authors wish to thank Professor A. O. Nier for a sample of enriched oxygen.

* AEC Predoctoral Fellow.
† Work supported by the AEC.

H2. The Quadrupole Moment of O^{17}. S. GESCHWIND, G. R. GUNTHER-MOHR, AND C. H. TOWNES, *Columbia University.**—Hyperfine structure due to O^{17} in the microwave absorption spectrum of OCS has previously been searched for without success.[1,2] Hyperfine splitting in the $J=1\rightarrow 2$ transition of OCS has now been found in a high resolution spectrometer. The O^{17} spin appears to be 5/2, although this has not yet been unambiguously determined because of incomplete resolution of the spectrum. The quadrupole coupling constant, however, can be definitely given as $eqQ=-1.2\pm 0.2$ Mc/sec. Estimating q in OCS at the oxygen nucleus as $3.4\pm 1.2\times 10^{15}$ esu, the quadrupole moment is $Q=-0.005\pm 0.002\times 10^{-24}$ cm². The sign and very small magnitude of this quadrupole moment are in agreement with expectations from the single-particle model. The small magnitude indicates that the odd neutron in O^{17} produces very little distortion of the closed shell of 8 protons and 8 neutrons. The authors are grateful to Professor A. O. Nier for supplying a sample of oxygen enriched in O^{17}.

* Work supported by the AEC.
[1] W. Low and C. H. Townes, Phys. Rev. 75, 529 (1949).
[2] Bianco and Roberts, Thesis, Iowa State University, 1950.

H3. The Hyperfine Structure of the $^2P_{\frac{1}{2}}$ Metastable State of the Stable Chlorine Isotopes.* V. JACCARINO AND J. KING, *M.I.T.*—The hfs of the metastable $^2P_{\frac{1}{2}}$ state of the Cl^{35} isotope has been observed by the atomic beam resonance method. The $(2, -1\leftrightarrow 2, -2)$ low frequency line has been measured in fields up to 350 gauss, using the $(3, -1\leftrightarrow 3, -2)$ low frequency line of the $^2P_{\frac{1}{2}}$ state of Cl^{35} to calibrate the magnetic field. From this a tentative value of

$$\Delta\nu_{\frac{1}{2}}^{35}=2a_{\frac{1}{2}}^{35}=2135\pm 11 \text{ mc/sec}$$

has been established. The high frequency $\Delta F=\pm 1$ lines are now being investigated in the Zeeman region to observe $\Delta\nu$ directly for both isotopes. The results of these experiments should allow a direct comparison of the magnetic hyperfine interaction of the chlorine isotopes, without the complication of the presence of an electric quadrupole interaction as in the $^2P_{\frac{3}{2}}$ states. This ratio is of interest since the ratio as measured in the $^2P_{\frac{3}{2}}$ states of the chlorine isotopes differs from the ratio

of the magnetic moments as measured by the nuclear resonance method by an amount considerably outside the quoted experimental uncertainties.[1]

* This work has been supported in part by the Signal Corps, the Air Materiel Command, and ONR.
[1] W. G. Proctor and F. C. Yu, Phys. Rev. 81, 20 (1951).

H4. *l*-type Doubling Transitions in DCN. YU TING, THOMAS L. WEATHERLY, AND DUDLEY WILLIAMS, *The Ohio State University*.—Absorption lines due to direct transitions between *l*-type doubling levels within a given rotational energy level of a linear molecule were first reported by Shulman and Townes[1] for the molecules OCS and HCN. The present work has revealed the existence of absorption lines due to similar transitions in the DCN molecule. The observed splittings $\Delta\nu$ and the q-values defined by $q=\Delta\nu/J(J+1)$ are given in Table I. The value of q calculated from Nielsen's expression[2]

TABLE I. *l*-type doubling transitions in DCN.

Rotational level	Observed frequency $\Delta\nu$	Observed q-value
11	24,539.2 ± 0.1 mc/sec	185.903 ±0.001 mc/sec
12	28,993 ±15 mc/sec	185.89 ±0.15 mc/sec

for *l*-type doubling is 183.6 mc/sec. The observed q-value for DCN is 1.2 percent higher than the calculated value, whereas the observed q-value for HCN is 0.9 percent lower than the calculated value.

[1] R. G. Shulman and C. H. Townes, Phys. Rev. 77, 421 (1950).
[2] H. H. Nielsen, Phys. Rev. 75, 1961 (1949).

H5. Microwave Absorption Spectrum of Formic Acid Vapor.* JOHN D. ROGERS AND DUDLEY WILLIAMS, *The Ohio State University*.—A study of the microwave spectrum of formic acid vapor has revealed absorption lines at the following frequencies: 22,326.42±0.11; 22,471.14±0.04; 23,203.41 ±0.04; 24,568.99±0.03; 27,817.12±0.13; and about 31,200 mc/sec. On the basis of infrared data, Stark patterns, and variation of line intensity with variations in temperature, it has been possible to identify some of the observed lines with certain rotational transitions of monomeric HCOOH. From the frequencies associated with the $J_\tau=0_0\rightarrow1_{-1}$ and $J_\tau=5_{-4}\rightarrow5_{-3}$ transitions, it is possible to obtain values of the rotational constants B and C appropriate to these transitions; the values obtained are $B=0.399901\pm0.000002$ cm^{-1} and $C=0.349696\pm0.000002$ cm^{-1}. Assuming that HCOOH is a planar molecule[1] and that the relation $I_C=I_A+I_B$ *is applicable*, one obtains a value $A=2.7855$ cm^{-1}.

* This work was done in connection with Contract AF 19(122)-13 between the Geophysical Research Laboratories and the Ohio State University Research Foundation.
[1] S. H. Bauer and R. M. Badger, J. Chem. Phys. 5, 852 (1937).

H6. The Low Temperature Infrared Spectrum of Solid Neopentane. R. M. HAINER, M. ELAINE HUNGERMAN, AND GILBERT W. KING, *Arthur D. Little, Inc.*—The infrared spectrum of solid neopentane has been observed at 77° and 4°K. Its infrared active vibrations have threefold degeneracy, removed by the crystalline field. The gas-phase band at 1475 cm^{-1} is resolved into components at 1489, 1474, and 1466. The 1376-cm^{-1} band shows two lines at 1364 and 1361 with indication of a third at 1366. The 1249-cm^{-1} band appears at 1261 with possible components at 1264, 1261, and 1258. The 921-cm^{-1} band appears as a singlet, unchanged in position, with width corresponding to an unresolved triplet with separations less than 1.5 cm^{-1}. On the basis of intensity, the magnitude of splitting, and the shift from gas to solid, the first three bands are probably of the same type, the 921 band being the skeletal frequency. At 77°K the widths of components are determined by their natural widths (cm^{-1}) and not by the instrument. Since neopentane is spherical and the most likely molecule to have quantized molecular rotation, a stringent test for this hypothesis was made by observation at 4°K, where at 1370 cm^{-1} neither narrowing nor improved resolution was obtained although experimental conditions were favorable.

H7. New Microwave Data on Trichlorides of Elements of the Fifth Column.* P. KISLIUK AND C. H. TOWNES, *Columbia University*.—From the width and contour of the unresolved $J=5\rightarrow6$ transition[1] of $AsCl_3$, $(eqQ)_{As}$ may be estimated as -173 ± 20 Mc, significantly less than that[2] of AsF_3. The $J=6\rightarrow7$ transition of $SbCl_3$ has been observed at slightly above room temperature (31°–45°). From the $Sb^{121}Cl_3^{35}$ line at 24,554 Mc and the $Sb^{123}Cl_3^{35}$ line at 24,510 Mc, the internuclear distance and bond angle may be given as 2.325 ± 0.005A and 99.5 ± 1.5°. The lines due to $SbCl_3^{35}Cl^{37}$ and $SbCl^{35}Cl_3^{37}$ as well as the $J=7\rightarrow8$ transition of $SbCl_3^{35}$ were also observed. All of the $SbCl_3$ lines were extremely broad due to the unresolved Sb hyperfine structure and higher vibrational states, being roughly 35 Mc wide. The ratio of the Sb quadrupole moments may be estimated from line widths as approximately 1.3, in agreement with recent more precise measurements,[3] but in disagreement with an older value.[4] The quadrupole effects of the chlorine nucleus may be neglected in both of these cases.

* Work supported jointly by the Signal Corps and ONR.
[1] P. Kisliuk and C. H. Townes, J. Chem. Phys. 18, 1109 (1950).
[2] Dailey, Rusinow, Shulman, and Townes, Phys. Rev. 74, 1245 (1948).
[3] C. C. Loomis and M. W. P. Strandberg, M.I.T.R.L.E. Tech. Rpt. No. 167 (1950).
[4] K. Murakawa and S. Suwa, Phys. Rev. 76, 433 (1949).

H8. The Structure and Dipolmoment of Trioxane.* E. AMBLE,† *Columbia University* (Introduced by C. H. TOWNES).—The $J=1\rightarrow2$ transition for trioxane $C_3^{12}H_6O_3^{16}$ and the $J=1\rightarrow2$ transition for $C_2^{13}C^{12}H_6O_3^{16}$ have been observed and measured:

$C_3^{12}H_6O_3^{16}$	$J=1\rightarrow2$		21,094.3 Mc
$C_2^{13}C^{12}H_6O_3^{16}$	$J=1\rightarrow2$	$K=0$	20,900 Mc
	$J=1\rightarrow2$	$K=1$	20,804 Mc.

The molecule is symmetric top, and the structure which gives the best fit to the observed frequencies is a chairform ring with C−O bond distance 1.41A and $\angle C-O-C=\angle O-C-O=109°$. Electron diffraction experiments give $1.40\pm.02$ for the bond distance and $112°\pm3°$ for the angles.[1] Further work on isotopic species of this molecule is in progress. The dipolmoment of the molecule has been measured by the first stark shift as $2.08\pm.01$ Debye units. Measured in benzene solution, the moment has been found to be 2.18 Debye.[2]

* Work supported jointly by the Signal Corps and ONR.
† On leave from Oslo University.
[1] P. W. Allen and Sutton, Acta Cryst. Vol. 3, Part I, 46, 72 (January, 1950).
[2] A. A. Maryott and S. F. Acree, J. Research Natl. Bur. Standards 33, 71 (1944).

H9. Optical Detection of Radiofrequency Resonance. Lifetime of the $^3P_1$ State of Hg.* J. BROSSEL, *M.I.T.*—Changes in the degree of polarization of resonance radiation, induced by radiofrequency resonance between Zeeman sublevels,[1] have been studied for the even and 199 isotopes of Hg. The radiofrequency resonance line shape is accurately accounted for by theory.[2] The extrapolated line width for zero rf amplitude leads to a lifetime of 1.55×10^{-7} sec for the even isotopes at 0°C, which is about 30 percent longer than previous estimates. Preliminary measurements for Hg^{199} indicate a value of the lifetime for the $^3P_1$ level within 5 percent of the above value, in contradiction to some recent measurements.[3]

* This work was supported in part by the Signal Corps, Air Materiel Command, and ONR.
[1] A. Kastler and J. Brossel, Compt. rend. 229, 1213 (1949); Brossel, Sagalyn, and Bitter, Phys. Rev. 79, 196–225 (1950).
[2] F. Bitter and J. Brossel, Technical Report No. 176, Research Laboratory of Electronics, M.I.T. (1950).
[3] R. Lennuier and J. L. Cojan, Compt. rend. 231, 1450 (1950).

H10. A Fine Structure in Nuclear Induction Signals from Ethyl Alcohol. M. E. PACKARD AND J. T. ARNOLD, *Stanford University*.—The construction of a nuclear induction ap-

paratus which will resolve lines separated by about 1 milligauss out of 7600 gauss has enabled us to see structure in signals from protons in organic compounds. This resolution is achieved by the use of a shimmed and stabilized electromagnet which has 12-inch pole pieces; and the use of a cylindrical sample 2 mm by 1 cm. The nuclear induction signal is observed on an oscilloscope. Confusing transient effects are reduced by sweeping the magnetic field at a rate of about 10 milligauss per second. Nuclear induction signals from protons in ethyl alcohol show three well-separated lines which correspond to the OH, CH_2, and CH_3 groups. The CH_2 and CH_3 peaks are split into at least four and three lines, respectively, spaced by 1.5 ± 0.5 milligauss. Neither the OH peak in ethyl alcohol nor the OH and CH_3 peaks in methyl alcohol show such splitting. The separation between the OH and CH_3 lines decreases by about a factor of two for a temperature change from -80°C to $+70$°C, while the spacing between the CH_2 and CH_3 lines is not measurably altered.

[1] Arnold, Dharmatti, and Packard, to be published in the *Journal of Chemical Physics*.

H11. Nuclear Magnetic Resonance Effects in Gases.* FRANK VERBRUGGE AND ROBERT L. HENRY, *Carleton College*.—The saturation method[1] has been used to study nuclear magnetic resonance in gaseous ethane from a pressure of 8 atmospheres through its critical pressure. Within experimental error, the product PH_1 remains constant, where P is the pressure and H_1 is the rf field strength required to reduce the output of the "lock-in" amplifier by a given factor. This result is consistent with the theoretical proportionality[1] to P of T_1 (spin-lattice relaxation time) and T_2 (spin-spin relaxation time), if one assumes that $H_1^2T_1T_2$ determines the degree of saturation. Using the reported values[2,3] of T_1 and T_2 for water and taking $T_1=T_2$ in agreement with theory, the line width for ethane varies from 9×10^{-4} gauss at 8 atmospheres to 4×10^{-3} gauss at 34 atmospheres.

* Work supported by the Research Corporation.
[1] Bloembergen, Purcell, and Pound, Phys. Rev. **73**, 679 (1948).
[2] E. L. Hahn, Phys. Rev. **76**, 145 (1949).
[3] H. A. Thomas, Phys. Rev. **80**, 901 (1950).

THURSDAY AFTERNOON AT 2:30

NBS, Materials Testing

(E. C. CRITTENDEN presiding)

Invited Papers

I1. The Work and Plans of the Physikalisch-Technische Bundesanstalt. A. SCHEIBE, *Physikalisch-Technische Bundesanstalt, Braunschweig*. (40 min.)

I2. Temperature Effects in Electron-Bombardment Conductivity and in Impurity Semiconductors. W. EHRENBERG, *Birkbeck College, London*. (40 min.)

THURSDAY AFTERNOON AT 2:15

Shoreham, Terrace Room

(C. C. LAURITSEN presiding)

Reactions of Transmutation, Boron Onwards; Electron Capture

J1. Cross Section for the $B^{10}(n, \alpha)$ Reaction from 0.35 to 2.6 Mev Neutron Energy.* D. W. MILLER,† BEN PETREE, AND C. H. JOHNSON, *University of Wisconsin*.—The cross section for the $B^{10}(n, \alpha)$ reaction was measured as a function of neutron energy using a cylindrical proportional counter containing BF_3 and argon. Good pulse height resolution was obtained in this counter by the use of guard sleeves around the central wire, which were held at an intermediate voltage to reduce end effects. Disintegration pulses from the counter were recorded photographically. The disintegration cross section was found to lie below the 1/v extrapolation of the thermal cross section except at the peak of a resonance observed at 1.9 Mev, where the cross section coincides with the 1/v extrapolation. This resonance has a width of about 400 kev, a peak value of 0.53 barn, and a total variation of the cross section of 0.35 barn. The ratio of the number of disintegrations leading to the ground state of Li^7 to the number leading to the excited state increases smoothly from 0.2 at 0.35 Mev to a maximum of 2.3 at 1.9 Mev, and decreases again to 0.8 at 2.6 Mev.

* Work supported by the AEC and the Wisconsin Alumni Research Foundation.
† AEC Predoctoral Fellow.

J2. Neutron Yield and Angular Distribution for $B^{11}(d, n)C^{12}$ and $B^{10}(d, n)C^{11}$. W. H. BURKE AND J. R. RISSER, *The Rice Institute*.*—Relative yields of neutrons from thin targets of (1) natural boron and (2) separated B^{10} bombarded by deuterons were measured in the energy range 0.3 to 1.9 Mev. Yield curves were similar when made either with a counter which had approximately equal sensitivity for neutrons of all energies or with a gas recoil counter biased to count only the most energetic groups. Broad low resonances occur in the forward direction at about 0.9 Mev for B^{10} and at about 1.1 and 1.6 Mev for B^{11}. Angular distributions in the range 1.0 to 1.8 Mev show maxima in the forward direction: at 0° for B^{11} and at about 35° for B^{10}.

* Assisted by the ONR and AEC.

J3. Angular Distribution of Gamma-Rays from $B^{11}+H^1 \rightarrow C^{12}+\gamma$. B. D. KERN,* C. D. MOAK, W. M. GOOD, AND G. P. ROBINSON, *Oak Ridge National Laboratory*.—It has been found that the gamma-rays from this reaction consist of a single transition to the ground state[1] accompanied in greater amount by a 12.1-Mev and a 4.6-Mev gamma-ray in cascade. The 12.1 Mev is known to come out first.[2] Besides using these

gamma-rays to study the scintillation spectrometer, the latter is being used to study the angular distribution of these gamma-rays. The angular distribution between the two cascade γ-rays is being studied as well as the angular distributions of the separate γ-rays with the beam. So far it has been found that the 12-Mev radiation has a distribution $w(\vartheta) = \text{const}(1+0.15\cos^2\vartheta)$. The 16.7-Mev radiation is isotropic to within the present error of measurements which, due to the small yield, is still greater than 10 percent.

* Now at University of Kentucky.
[1] R. L. Walker, Phys. Rev. 79, 172 (1950).
[2] R. L. Walker (private communication).

J4. Q Values of the $C^{13}(d,p)C^{13}$, $Be^9(d,p)Be^{10}$, and $O^{16}(d,p)O^{17}$ Reactions. ERNEST D. KLEMA AND G. C. PHILLIPS, *The Rice Institute.*—An annular magnet similar to the one used at M.I.T. by W. W. Buechner[1] and his associates has been constructed at The Rice Institute. The magnet has been used to study the above (d, p) reactions produced by the Rice Institute pressurized electrostatic accelerator. The energy of the incident deuterons was measured in terms of the 0.8735-Mev $F^{19}(p\,\alpha'\gamma)O^{16}$ resonance, using a zinc fluoride target 2 kev thick for the incident protons. The magnetic field of the annular magnet was both measured and held constant to ± 1.5 gauss during runs by means of a proton magnetic moment regulator designed and constructed by Mr. Richard D. Jones. The values obtained for the Q's of the above reactions are 2.732 ± 0.006, 4.591 ± 0.008, and 1.918 ± 0.008 Mev, respectively. The neutron-proton mass difference as calculated from the present data for carbon and the data given by other workers for the Q's of a closed cycle of reactions involving C^{12} and C^{13} is 0.789 ± 0.008 Mev.

[1] Buechner, Van de Graaff, Strait, Stergiopoulos, and Sperduto, Phys. Rev. 74, 1257 (1948).

J5. The Reaction $C^{14}(p,n)N^{14}$.* W. M. PRESTON, J. J. G. MCCUE, W. D. ROSEBOROUGH, JR., AND C. GOODMAN, *M.I.T.*—The reaction $C^{14}(p, n)N^{14}$ has been studied by Shoupp[1] and the inverse reaction, $N^{14}(n, p)C^{14}$, by Johnson and Barschall.[2] Since the same levels in the compound nucleus N^{15} can be excited, one expects that the resonances in the yields of the two reactions will be identical in half-width and will occur at energies differing by the $C^{14}(p, n)N^{14}$ threshold, $E_t = 0.664$ Mev.[1] We have investigated the $C^{14}(p, n)N^{14}$ yield with a resolution of about 3 kev with the following results for the positions of the resonances.

TABLE I.

(This paper) E_{max}	(Shoupp) E_{max}	(Johnson and Barschall) E_{max}	(Johnson and Barschall) $E_{max}+0.664$
1.165	1.14	0.499	1.163
1.308	1.30	0.640	1.304
1.669	1.47?	0.993	1.657
2.081	2.05	1.415	2.079

Our agreement with Johnson and Barschall is seen to be excellent; the (p, n) yield curve looks very similar to the (n, p) yield (Fig. 3 of their article).

* This work was supported by BuShips and the ONR.
[1] Shoupp, Jennings, and Sun, Phys. Rev. 75, 1 (1949).
[2] C. H. Johnson and H. H. Barschall, Phys. Rev. 80, 818 (1950).

J6. Excited States of N^{15} and F^{19} from $C^{13}(\alpha\,p)N^{16}$ and $O^{16}(\alpha\,p)F^{19}$.* M. L. BULLOCK, W. O. MCMINN, V. K. RASMUSSEN, AND M. B. SAMPSON, *Indiana University.*—Protons produced by the bombardment of carbon and oxygen with the external 21-Mev cyclotron α-beam were observed at 90°. Particle energies were obtained from the range in aluminum using a proportional counter biased to count only those protons near the end of their range. The carbon targets were a 0.7 mg/cm² Aquadag film and C_2H_4 gas. If the observed proton groups are attributed to $C^{13}(\alpha\,p)N^{16}$, they give the ground state of N^{15} and excited levels at 5.4 and 6.5 Mev, corresponding to the known[1] levels at 5.3 and 6.3 Mev. The oxygen target was research grade oxygen gas from the Matheson Company. The four proton groups observed, if attributed to $O^{16}(\alpha\,p)F^{19}$, correspond to the ground state of F^{19} and excited levels at 1.4, 2.7, and 3.8 Mev. The first two levels have been previously reported.[1,2]

* This work was assisted by the joint program of the ONR and AEC.
[1] Hornyak, Lauritsen, Morrison, and Fowler, Revs. Modern Phys. 22, 291 (1950).
[2] M.I.T. Progress Report, July 1, 1950, p. 169.

J7. Alpha-Groups from $Al^{27}(d,\alpha)Mg^{25}$.* EDWARD C. TOOPS, FREDERICK E. STEIGERT, AND MILO B. SAMPSON, *Indiana University.*—The $Al^{27}(d, \alpha)Mg^{25}$ reaction has been investigated at 90° and 124° with Eastman NTA nuclear track plates. Magnetically analyzed 10.8-Mev deuterons bombarded a thin (0.17 mg/cm²) aluminum target. Analyses of 3500 alpha-tracks at 90° gives eighteen well-defined groups. At 124°, 1500 tracks give sixteen groups. The Q values of groups one to eleven, in the range 6.58 to 0.63 Mev, check with previous proportional counter work at various angles.[1] Q values of -0.44, -1.16, -1.54, -1.91, -2.37, -3.06, and -3.85 Mev may be assigned to groups twelve through eighteen. A complete energy level diagram will be presented.

* This work was assisted by the joint program of the ONR and AEC.
[1] Schelberg, Sampson, and Cochran, Phys. Rev. 80, 574 (1950).

J8. Magnetic Analysis of $Al^{27}(d,p)Al^{28}$ Reaction.* H. A. ENGE.** *M.I.T.*—The existence of an excited state at 31 kev in Al^{28} has been previously reported.[1] While bombarding thin aluminum targets with 2.0- and 1.8-Mev deuterons, more than thirty other relatively intense proton peaks have been observed that can be assigned to the $Al^{27}(d, p)Al^{28}$ reaction. Most of the peaks form clusters, the average peak separation being about 60 kev, although separations as low as 13 kev have been measured. In addition, considerable low yield structure has been observed, indicating that the energy spectrum of Al^{28} is far more complicated than previously anticipated. The Q-values of the twenty-eight most intense groups are, 5.494, 5.463, 4.479, 4.127, 3.869, 3.357, 3.296, 3.226, 3.010, 2.916, 2.842, 2.514, 2.036, 1.907, 1.621, 1.562, 1.463, 0.809, 0.735, 0.595, 0.366, 0.392, 0.405, 0.059, -0.241, -0.298, -0.361, -0.817, accurate to 10 kev or less. The observed level scheme of Al^{28} is in good agreement with that found by previous workers as far as the positions of the clusters are concerned.

* This work has been assisted by the joint program of the AEC and ONR.
** On leave of absence from the University of Bergen, Bergen, Norway.
[1] Enge, Van Patter, Buechner, and Sperduto, Phys. Rev. 81, 317 (1951).

J9. Neutrons from Deuterons on Si^{29}.* C. P. SWANN AND AND C. E. MANDEVILLE, *Bartol Research Foundation.*—A thick target of $Si^{29}O_2$ (isotopic concentration 69 percent) has been irradiated by deuterons at 1.4 Mev supplied by the Bartol van de Graaff statitron. Recoil protons knocked on in the forward direction by neutrons from $Si^{29}(D, n)P^{30}$ were observed in photographic plates making angles of zero and 90 degrees with the incident deuterons. *Tentative* Q-values are 0.02, 1.70, 2.90, and 3.60 Mev. The data will be correlated with results obtained from $Si^{28}(D, n)P^{29}$ and $Si^{30}(D, n)P^{31}$.

* Assisted by the joint program of the ONR and AEC.

J10. An Investigation of the $Si^{29}(d,\alpha)Al^{27}$ and $Si^{29}(d,p)Si^{30}$ Reactions.* D. M. VAN PATTER, A. SPERDUTO, AND H. ENGE,** *M.I.T.*—Silicon-dioxide targets enriched in the Si^{29} isotope have been bombarded by 1.8-Mev deuterons, and the emitted proton and alpha-particle groups have been analyzed by a high resolution magnetic spectrograph. From a comparison with the groups observed from a natural SiO_2 target, a number of groups have been assigned to the Si^{29} isotope. The measured Q-values for five previously unreported $Si^{29}(d, \alpha)Al^{27}$

alpha-groups are, 5.99, 5.13, 4.97, 3.87, and 3.27 Mev, corresponding to the ground state and four excited states of Al^{27}. Six $Si^{29}(d, p)Si^{30}$ proton groups having Q-values of 8.39, 6.14, 4.87, 4.60, 3.31, and 2.77 Mev, have been tentatively identified, corresponding to the ground state and five excited states of Si^{30}. These Q-values are considered to be reliable to 20 kev. Several less intense groups have not yet been identified. The possibility that some of the observed groups may have additional structure is being investigated. (The silicon isotopes were obtained from the Stable Isotopes Division, AEC, Oak Ridge.)

* This work has been supported by the joint progran of the ONR and AEC.
** Now on leave from the University of Bergen, Bergen, Norway.

J11. The (p, n) Reaction on Separated Isotopes of Chromium.* J. J. G. McCue, J. A. Lovington, and W. M. Preston, *M.I.T.*—We have measured the relative neutron yield from thin chromium targets, enriched, respectively, in Cr^{50} and Cr^{54}, as a function of proton energy in the range 1.5 to 2.5 Mev. The (p, n) threshold is about 2.2 Mev for Cr^{54} and below 1.5 Mev for Cr^{50}. In this region, most of the resonance levels in the compound nuclei Mn^{54} and Mn^{56} seem to be resolved with targets 2 to 3 kev thick. Just above $E_p = 2.2$ Mev, the spacing of virtual levels is about 5 kev for Mn^{54} and 8 kev for Mn^{56}. Using the best estimates available for the neutron binding energies, it appears that the level spacing in Mn^{54} (an odd Z-odd N nucleus) is substantially less than in Mn^{56} (an odd Z-even N nucleus) when measured at equal energies of excitation above the ground state.

* This work was supported by the Bureau of Ships and the ONR.

J12. Excitation Function of $Au^{197}(d, p)Au^{198}$ and $Au^{197}(d, 2n)Hg^{197}$.* K.-H. Sun, F. A. Pecjak and B. Jennings, *Westinghouse Research Laboratories* and A. J. Allen and J. F. Nechaj, *University of Pittsburgh.*—A ten-minute bombardment of the mono-isotopic element gold with 15-Mev deuterons yields activities with 2.7*d* and 1.0*d* half-lives by the reactions $Au^{197}(d, p)Au^{198}$ and $Au^{197}(d, 2n)Hg^{197}$. Hg^{197} is known to have an isomer Hg^{197m}, which also emits soft internal conversion electrons and has a half-life identical with Au^{198}(2.7*d*). By absorption studies and the technique of half-life peeling, it is possible to separate the yields of the Au^{198}, Hg^{197}, and Hg^{197m}. The standard stack foil method, with 0.0007″ Au foils, was used in the excitation study. The yield of the $Au^{197}(d, p)Au^{198}$ reaction started at 8-Mev deuteron energy, increased rapidly at 10 Mev, and reached a maximum at about 14.3 Mev. For the $Au^{197}(d, 2n)Hg^{197}$ reaction, the yield started at 9 Mev, increased rapidly at 10 Mev, and continued, with no sign of leveling off, at 15 Mev. The relative yield of $Au^{197}(d, p)Au^{198}$ and $Al^{27}(d, p\alpha)Na^{24}$ was also measured.

* Assisted by the joint program of the ONR and AEC.

J13. Capture of Electrons by Protons Traversing Hydrogen Gas. H. Kanner and F. L. Ribe, *University of Chicago.*—Using the proton beam from a high voltage accelerator, the electron-capture cross section for protons in hydrogen gas has been measured at energies between 34 and 149 kev. The protons entering a chamber which could be filled with hydrogen were bent by a magnetic field into a detector. As gas was admitted and capture processes occurred, some of the protons were neutralized and did not follow a circular path to the detector. From the attenuation of the proton beam with gas pressure, the capture cross sections σ_c were derived. σ_c has the values 1.52×10^{-16} and 2.30×10^{-16} cm² at the limiting energies given above. The limiting value of the ratio n_+/n_0 (protons to atoms) attained after traversal, at constant velocity, of hydrogen gas is given by σ_l/σ_c, where σ_l is the electron loss cross section for hydrogen atoms.[1] Direct measurement of this ratio agreed with the individual cross sections of these measurements, and those of Montague *et al.*, to 10 percent. n_+/n_0 is unity in hydrogen at a velocity of 1.44 Bohr units $(e^2/\hbar)$, which may be compared with the traversal of metals by protons, for which $n_+/n_0 = 1$ is attained at 0.95 Bohr unit.[2]

[1] Allison, Montague, and Ribe, Phys. Rev. **81**, 294 (1951).
[2] T. A. Hall, Phys. Rev. **79**, 504 (1950).

Friday Morning at 10:00

NBS, Materials Testing

(J. B. Nichols presiding)

Session of the Division of High-Polymer Physics

Invited Paper

JA1. Studies of High Polymers by Nuclear Absorption. R. S. Codrington, F. McCaffrey, B. A. Mrowca, and E. Guth, *University of Notre Dame.* (30 min.)

Contributed Papers

JA2. Nuclear Magnetic Resonance Absorption in Proteins. T. M. Shaw and K. J. Palmer, *Western Regional Research Laboratory.*—Nuclear magnetic absorption has been observed for hydrogen nuclei in wool, horn, silk, egg albumin, collagen, gelatin, glycine, and a number of other solids. For the proteins, the absorption, observed at 25°C and a relative humidity of about 40 percent, consists of a single line of complex shape. The line appears to consist of a narrow peak superimposed symmetrically on a broad band. Step-wise removal of water from the proteins results in corresponding reduction in amplitude and finally the disappearance of the narrow line. A line width of approximately 6 gauss was obtained for thoroughly dried horn keratin. In general, lines observed for temperatures near 100°C are slightly narrower than for 25°C. For callogen, however, heating causes thermal contraction and the line width at 100°C is much narrower than at 25°C. Upon cooling to 25°C the resonance line broadens and is indistinguishable from that observed for unheated collagen. The correlation between line width of the resonance absorption peak and crystallinity as determined by x-ray diffraction has been made for several of the proteins studied.

JA3. The Three-Dimensional Patterson Function of Air-Dried Lysozyme Chloride. Robert B. Corey, Jerry Dono-

HUE, AND KENNETH N. TRUEBLOOD, *California Institute of Technology*, AND KENNETH J. PALMER, *Western Regional Research Laboratory*.—Quantitative x-ray data for all CuK_α reflections from crystals of air-dried lysozyme chloride have been collected at the Western Regional Research Laboratory. About 650 spots corresponding to 200 separate forms of (*hkl*) were indexed and their intensities visually estimated. The minimum spacing observed was about 6A. These data have been used at the California Institute of Technology to calculate the three-dimensional Patterson function. The conspicuous maxima of this function may be divided into two general classes: first, those which occur within about 12A of the origin and are probably associated with intramolecular interactions, and, second, those which occur beyond 20A and are probably associated with intermolecular distances within the crystal. An interpretation of the details of the Patterson function indicates that regions of relatively high density are to be found at the following positions in the unit cell: $x=0.27$, $y=0.44$, $z=0.25$; $x=0.24$, $y=0.36$, $z=0.00$; and equivalent positions.

JA4. Dynamic Shear Properties of Isobutylene Polymers as a Function of Cross-Linking. I. L. HOPKINS, *Bell Telephone Laboratories* (Introduced by W. O. BAKER).—Recent developments in the technique of measuring the dynamic shear properties of rubber-like polymers by means of tuning forks will be described. Results of the application of this technique to non-cross-linked, cross-linked, and loaded polyisobutylene within a frequency range of 0.1 to 13.7 kc will be described. Within this range both G' and G'' increase approximately with the square root of the frequency, with the proportionality factor increasing with cross-linking and loading. The functional relationship between modulus and chain length between cross links is discussed, and compared with that found by Flory[1] for static conditions.

[1] Paul J. Flory, Ind. Eng. Chem. **38**, 417 (1946).

JA5. Energy Dissipation in Vibrating Fibers. W. G. HAMMERLE AND D. J. MONTGOMERY, *Textile Research Institute*.—Experiments on energy dissipation in fibers at small amplitudes of stretching vibration have shown a dependence of dissipation on frequency that has not been explained on the basis of either Newtonian linear or Eyring nonlinear damping. On the other hand, for many rather highly crystalline materials, the classical viscous explanation does appear adequate. In an attempt to explain the observed frequency dependence for both classes of materials, we have investigated the dissipation per cycle of sinusoidal longitudinal vibration. Preliminary calculations indicate that for materials with large intermolecular binding energies, the dissipation per cycle is proportional to frequency, in conformity with the classical theory. We are in process of evaluating the dissipation for materials where the binding energies are relatively small. The dissipation per cycle, in any case, turns out to be proportional to the square of the amplitude. We have not yet completed evaluation of the temperature dependence. In materials where entropy forces are small compared with internal energy forces, such as in crystals and highly cross-linked polymers, our results indicate a correlation of the elastic modulus with dissipation in substances of the same general type. However, experimental data are not yet sufficiently plentiful to make suitable comparison possible.

JA6. The Application of Nutting's Equation to the Viscoelastic Behavior of Certain Polymeric Systems. ROLF BUCHDAHL AND LAWRENCE E. NIELSEN, *Monsanto Chemical Company*.—The Nutting equation $-\epsilon=\psi\times\tau^{\beta}\times t^{n}$, where ϵ = strain, τ = stress, t = time and ψ, β, and n are material constants, is applicable to a large number of polymeric systems, such as plasticized polyvinyl chloride, styrene-butadiene copolymers, polystyrene, etc. It has been shown that the material constant n, which determines essentially the time dependence of the deformation process, is closely related to the damping coefficient as obtained from dynamic mechanical measurements: the temperature dependence of n and δ (damping coefficient) are about the same; and, in some cases, there exists a simple quantitative relationship between the two constants. Furthermore, it has been shown that in the case of styrene-butadiene copolymers n varies with the differences in gel content and gel structure. For semipermanent gel structures, such as exist in polystyrene above the second-order transition point, n becomes a function of time, as would be expected. Over a wide stress range, there also appears to be a dependence of n on stress and the significance of this relationship with respect to the stress dependence of the damping coefficient is discussed briefly.

JA7. Flow Behavior of Highly Concentrated Cetane Solutions of Low Molecular Weight Polyisobutylenes.* A. B. BESTUL AND H. V. BELCHER, *National Bureau of Standards*.—Flow measurements were made with the McKee worker-consistometer on cetane solutions of 10, 30, 50, 70, and 90 weight percent of four polyisobutylenes with viscosity average molecular weights between 50,000 and 100,000 and on the bulk polymers. Measurements were made on all solutions at 100°F and on the bulk polymers at 100°, 200°, and 300°F. The results cover rates of shear ($\dot{\gamma}$) from 20 to 200,000 sec^{-1} and shearing stresses (s) from 2000 to 5,000,000 $dynes/cm^2$. For concentrations up through 50 percent the relation $\dot{\gamma}=(\text{const}_1)s+(\text{const}_2)s^2$ appears reasonably suitable for extrapolating the results to zero shearing stress. For higher concentrations, including the bulk polymers, the relation $\dot{\gamma}=(\text{const}_1)s+(\text{const}_2)s^3$ is preferable. No previously proposed flow relation is valid over the total range of the data. The temperature variation of the ratio $s/\dot{\gamma}$ (viscosity) for the bulk polymers at constant s remains nearly constant as s is increased from zero; however, this variation at constant $\dot{\gamma}$ decreases as $\dot{\gamma}$ is increased from zero.

* The work reported here was supported by the Reconstruction Finance Corporation, Office of Rubber Reserve.

JA8. The Behavior of Macromolecules in Sedimentation and Diffusion. F. R. EIRICH AND H. F. MARK, *Polytechnic Institute of Brooklyn*.—The diffusion and sedimentation of colloidal electrolytes and proteins has received detailed theoretical and experimental attention, although usually conditions were applied under which charge effects are suppressed. In electrically charged chain molecules the ordinary charge effects tend to be overshadowed by the effects of the accompanying shape changes. In ultracentrifugation the situation is complicated by both influences occurring to a comparable extent. We have tried to clarify the situation by suitable variations of polymer and electrolyte concentration. Preliminary results indicate that, if shape changes are assumed as they can be calculated from viscosity behavior, reasonable charges for the polymer molecules follow. The influence of ions of the same sign as the chain molecule has also been investigated.

JA9. Densities and Optical Properties of High Polymers. MAURICE L. HUGGINS, *Eastman Kodak Company*.—Equations and constants deduced from data on simple organic liquids are used to compute densities, refractive indices, and optical dispersions which high polymers would have if they were liquid. Corrections for rigidity, crystallinity, and the presence of plasticizers and solvents are discussed. Comparisons are made with experimental data, where available.

FRIDAY MORNING AT 9:45

Shoreham, West Ballroom

(M. L. POOL presiding)

Radioactive Nuclei, Tritium through Cerium; Neutrinos

K1. Limit on Neutrino Mass from Tritium Beta-Spectrum. DONALD R. HAMILTON, W. P. ALFORD, AND LEONARD GROSS,* *Princeton University.*—A hemispherical electrostatic integral beta-spectrograph[1] (energy resolution 120 volts at 20 kilovolts) has been used to investigate the tritium spectrum[2] near the end point. The strongest source used (tritium in zirconium) has essentially infinite thickness for tritium electrons. The spectrum of this source is distorted at voltages more than 1.5 kilovolts below the end point; to within experimental error the spectrum for the last 1.5 kilovolts agrees with that to be expected for zero neutrino mass; preliminary results give (neutrino mass) $\leqslant$ 250 electron volts = (electron mass)/2000. A thinner and less intense source gives an undistorted spectrum down to 10 kilovolts and (neutrino mass) $\leqslant$ 500 volts. The end point is found to be 19.4$\pm$0.4 kilovolts, the uncertainty arising in the absolute voltage calibration. This work has been supported in part by the joint program of the ONR and AEC and by the Eugene Higgins Scientific Trust Fund. Tritium was obtained from the AEC.

* AEC Predoctoral Fellow, 1948–49.
[1] D. R. Hamilton and L. Gross, Rev. Sci. Instr. 21, 912 (1950).
[2] Curran *et al.*, Phil. Mag. 40, 53 (1949). G. C. Hanna and B. Pontecorvo, Phys. Rev. 75, 983 (1949).

K2. Beta- and Gamma-Radiation of Al^{31} and the Mass of Al^{27}.* H. T. MOTZ, *Brookhaven National Laboratory.*—The spectrum of 2.3-minute Al^{31} has been studied using samples activated in the Brookhaven nuclear reactor and a lens spectrometer with a resolution of 2 percent. A gamma-ray energy of 1.785$\pm$0.015 Mev has been found by external conversion in a uranium foil. The beta-spectrum from a 2-mg/cm^2 source has been fitted to a Kurie plot for an allowed transition from approximately 1 Mev to the end point. The end point has been found to be 2.83$\pm$0.03 Mev. No beta-transition to the ground state of Si^{31} has been observed. Such a transition is less than 2 percent of the observed beta-decay to the excited state. These results are in general agreement with previous studies of Al^{31}. The observed total disintegration energy of 4.615 $\pm$0.035 Mev does not agree with the writer's calculations of the Al^{31} and Si^{31} masses,[1] but is in good agreement with recent reaction data obtained at MIT.[2] A more consistent set of masses from Ne^{20} to S^{32} results from an Al^{27} mass approximately 0.2 mmu higher than the value 26.989 83$\pm$0.000 08 given by Ewald and Mattauch,[3] which was used in reference 1.

* Research carried out under contract with AEC.
[1] H. T. Motz, Phys. Rev. 81, 1060 (1951).
[2] D. M. Van Patter (private communication).
[3] J. Mattauch and H. Ewald, Physik. Z. 44, 181 (1948).

K3. A 25-Day Activity in P^{32} Samples.* ERLING N. JENSEN AND R. T. NICHOLS, *Iowa State College.*—The radiations from P^{32} have been examined with a thin magnetic lens spectrometer. The maximum energy of the 14.3-day beta-activity was determined as 1.704$\pm$0.008 Mev. An additional beta-activity has been observed in three separate $S^{32}(n, p)P^{32}$ shipments from Oak Ridge, though it was masked for the first two or three weeks by the 14.3-day activity. From seven beta-spectra taken of one sample, over a period of 144 days, the half-life was found to be 26$\pm$3 days and the maximum beta-energy 0.26$\pm$0.02 Mev. It is estimated that the 25-day activity formed about one percent of the initial activity of the sample. Using a sample which had decayed for 10 months, at which time the unknown activity was estimated to be more than 90 percent of the total activity, a half-life of 25.2$\pm$0.5 days was measured. A similar activity has been observed in the beta-spectra of a source from a $P^{31}(n, \gamma)P^{32}$ reaction. These data, on the low energy beta-activity, are in disagreement with the results of Agnew[1] and Warshaw, Chen, and Appleton.[2]

* This work was performed at the Ames Laboratory of the AEC.
[1] H. M. Agnew, Phys. Rev. 77, 655 (1950).
[2] Warshaw, Chen, and Appleton, Phys. Rev. 80, 288 (1950).

K4. The Nuclide P^{33}. R. K. SHELINE, R. B. HOLTZMAN, AND C. Y. FAN, *University of Chicago.*—P^{33} has been produced by the bombardment of sulfur, sodium sulfide, and lithium chloride with 48-Mev gamma-rays produced by the University of Chicago betatron. The reactions involved are $S^{34}(\gamma, p)P^{33}$, $Cl^{35}(\gamma, 2p)P^{33}$, and $Cl^{37}(\gamma, \alpha)P^{33}$. The phosphorus was separated as the phosphomolybdate and as the magnesium ammonium phosphate. The P^{33} activity has a 25$\pm$2-day half-life with a 0.25$\pm$0.01-Mev negative beta-ray. There is less than 0.1 (0.5 Mev) gamma per beta. The activity was observed in the presence of P^{32}, and its ratio to the P^{32} activity did not change with chemical purification. The Fermi plot of the beta-ray spectrum was straight with a logft value of 5.1.

K5. Neutrino Recoils Following the Capture of Orbital Electrons in A^{37}. G. W. RODEBACK AND J. S. ALLEN, *University of Illinois.*—An improved apparatus for studying the recoil nuclei following the disintegration of A^{37} through the capture of orbital electrons has been constructed. Two electron multipliers placed at 90° with respect to each other define the effective volume of the gaseous source. The velocity of the recoil ions is studied by measuring their time-of-flight over an average distance of 5 cm between the source volume and the ions counter. Our experimental results give two well-defined peaks of coincidence counting rate *versus* delay time. The first peak extends from zero time to about 1 microsecond with the same magnitude as the second peak. The origin of the first peak is being investigated. Both the position and the width of the second peak correspond closely to the values expected for the 9.7-electron volt recoil ions originating in the source volume and predicted by conservation of momentum and energy in the A^{37} decay process. No additional recoils have been observed out to a delay time 6 times that of the second peak.

K6. Radioactive A^{39} from $A^{40}(\gamma, n)$ Reaction.* MARVIN HOFFMAN, *Iowa State College* (introduced by L. J. LASLETT).—Natural argon gas was irradiated in the x-ray beam of the 70-Mev synchrotron. The bombarded gas was then used as filling gas for a Geiger counter and counted; thus, no low energy radiation might go unobserved. Data taken in this manner compare with that taken by surrounding a thin-wall glass counter with the bombarded gas. Activities attributable to Cl^{39}, Cl^{38}, and a 145$\pm$15-sec activity were observed. Assigning[1] the 145-sec activity to A^{39}, all expected activities are observed and accounted for.

* Work was performed at the Ames Laboratory of the AEC.
[1] A. Zucker and W. W. Watson, Phys. Rev. 80, 966 (1950).

K7. Beta-Spectrum of Fe^{55}. F. I. BOLEY* AND L. J. LASLETT, *Iowa State College.*†—Fe^{55} (8.9 min) has been prepared by irradiation of a 1-mil iron foil in the Iowa State College synchrotron and the positron spectrum examined with a scintillation spectrometer. Pulse heights were recorded photographically and the 0.62-Mev internal-conversion line from Cs^{137} used for calibration. A Kurie plot of the data leads to an end-

point of 2.5±0.1 Mev. The spectrum appears to be of the first-forbidden type ($Ft = \pm 5.4 \times 10^4$ sec), for which the "*a*" correction of Konopinski[1] is appropriate. The forbidden shape is corroborated by comparison spectra obtained with Y^{90} and P^{32} sources, the Y^{90} requiring the "*a*" correction, while the P^{32} data do not. Corrections for the finite resolution of the instrument[2] have been applied to all data.

* Socony-Vacuum Research Fellow.
† This work was performed in the Ames Laboratory of the AEC.
[1] E. J. Konopinski, Revs. Modern Phys. **15**, 209 (1943).
[2] J. P. Palmer and L. J. Laslett, to be published.

K8. Radioactivity of Tc^{93}, Tc^{95}, Tc^{96}, and Tc^{101}. G. E. Boyd and B. H. Ketelle, *Oak Ridge National Laboratory*.—The disintegrations of 2.75-hr Tc^{93}, 60-d Tc^{95}, 4.20-d Tc^{96}, and 13.5-min Tc^{101} were studied using a magnetic lens beta-spectrometer, a gamma-scintillation spectrometer, and coincidence methods. The positron spectrum of Tc^{93} is simple with an end point of 0.800±0.005 Mev followed by a 1.32-Mev gamma-ray. Tc^{93} decays largely (*ca* 90 percent) by orbital electron capture followed by a 2.20-Mev gamma-ray. No 6.7-hr Mo^{93} daughter activity resulted from the 2.75-hr Tc. Good photo-peaks showing gamma-rays of 0.20, 0.58, 0.80, and 1.03 Mev in the 60-d Tc^{95} were observed in agreement with recent spectrometer measurements.[1] Observations on the gamma-spectrum of the 4.20-d Tc^{96} also confirmed Medicus, *et al.* In addition, low intensity lines at 1.65, 1.89, and 2.39 Mev were found which may arise from cross-over transitions. The gamma-ray spectrum of 13.5-min Tc^{101} consists of a strong line at 0.30 together with a weaker line at 0.56 Mev, and one or more lines of very low intensity at slightly higher energy. Coincidence counting showed that over 95 percent of the disintegrations of Tc^{101} proceed through a 1.20±0.05-Mev beta followed by the 0.30-Mev gamma. No short-lived isomer could be found.

[1] Medicus, Preiswerk, and Sherrer, Helv. Phys. Acta **23**, 299 (1950).

K9. Cross-Over Transition in Tc^{99m}. J. W. Mihelich, M. Goldhaber, and Elizabeth Wilson,* *Brookhaven National Laboratory*.—Medicus, Maeder, and Schneider[1] have shown that Tc^{99m} (6 hr) decays in two steps: A (1.8±0.3)-kev transition followed by a (141.2±0.5)-kev transition with the latter identified from its *K*-conversion coefficient as a magnetic dipole transition. We have found the expected cross-over transition by photographing the internal conversion electrons from a thin Tc^{99m} source in a high resolution 180° magnetic beta-spectrograph. Two *K* and *L* lines were observed, corresponding to γ-rays of 140.1±0.5 kev and 142.1±0.5 kev. The difference is 2.0±0.1 kev. From the relative intensity of the electron lines the cross-over transition can be estimated to take place in about 1 percent of the disintegrations and can be assigned to a $p\ 1/2 \rightarrow g\ 9/2$ transition (2^4 magn). The small energy difference between the $g\ 9/2$ ground state and the 7/2+excited state, as well as a still smaller difference (9.3 kev) observed by Bergström[2] for Kr^{83} can be interpreted by assuming that the $(g\ 9/2)^3$ or ^{7} configurations have two low lying states: 7/2+ and $g\ 9/2+$.

* Research carried out under contract with the AEC.
[1] Medicus, Maeder, and Schneider, Helv. Phys. Acta **22**, 603 (1949); Phys. Rev. **81**, 652 (1951).
[2] I. Bergström, Phys. Rev. **81**, 638 (1951).

K10. Classification of Nuclear Isomers.* A. W. Sunyar and M. Goldhaber, *Brookhaven National Laboratory*.—Nuclear isomers have been reclassified and the following conclusions reached. The lifetime-energy relations of Axel and Dancoff[1] and the K/L ratios calculated by Hebb and Nelson[2] yield spin differences which are one unit too high for electric 2^3 and 2^4 transitions. Electric 2^3 transitions are 100 or more times slower than expected from Weisskopf's formula.[3] Electric 2^4 and 2^5 transitions are also slower than given by Weisskopf, but very few examples are known. Magnetic 2^4 transitions agree very well with Weisskopf's formula. For these transitions, K/L ratios are lower than calculated by Tralli and Lowen.[4] This discrepancy cannot be explained by admixture of electric 2^5 transitions. The isomeric transitions in the $g\ 9/2$ shell, previously assigned no parity change, are explained as electric 2^3. This is interpreted by assuming that for the configurations $(g\ 9/2)^{3, 5, \text{ or } 7}$, 7/2+ and $g\ 9/2$ states are comparable in energy. The 7/2+ state is lower in nearly half the cases.

* Research carried out under contract with the AEC.
[1] P. Axel and S. M. Dancoff, Phys. Rev. **76**, 892 (1949).
[2] M. H. Hebb and E. Nelson, Phys. Rev. **58**, 486 (1940).
[3] See R. D. Hill, Phys. Rev. **81**, 470 (1951).
[4] N. Tralli and I. S. Lowen, Phys. Rev. **76**, 1541 (1949).

K11. Gamma-Rays Emitted in the Disintegration of the 36-hr Rhodium (105).* C. E. Mandeville and E. Shapiro, *Bartol Research Foundation*.—Earlier measurements[1, 2] have indicated a gamma-ray at ~0.3 Mev in the decay of Rh^{105} (36 hr). More recent data[3] seem to show the absence of gamma-rays. Consequently purified metallic ruthenium was irradiated for ten hours by slow neutrons in the Oak Ridge pile, and the radiations of Rh^{105}, grown from its 4.5-hr ruthenium parent, were reinvestigated. After irradiation, the rhodium was separated from ruthenium by distillation of RuO_4 from a perchloric-sulfuric acid solution. The gamma-ray activity was followed for three half-periods, and the observed half-life was 35±1 hr. Lead absorption curves at time zero and forty hours later yielded a quantum energy of 0.3 Mev. Comparative measurements with the beta-spectrum of the 5-day Bi^{210} showed that bremsstrahlung effects were negligible.

* Assisted by the joint program of the ONR and AEC.
[1] Sullivan, Sleight, and Gladrow, Plutonium Project Report CC-1493 (1944).
[2] C. E. Mandeville and E. Shapiro, Phys. Rev. **80**, 125 (1950).
[3] R. B. Duffield and L. M. Langer, Phys. Rev. **81**, 203 (1951).

K12. Nuclear Spectra of Ba^{131} and Cs^{131}.* Robert Canada and A. C. G. Mitchell, *Indiana University*.—The nuclear spectra of Ba^{131} and Cs^{131} were measured in a magnetic lens spectrograph. Both elements decay by orbital electron capture. The sources were prepared by the irradiation of barium with neutrons in the Oak Ridge Pile. Barium was separated chemically, and the daughter cesium was separated by ion column techniques. The spectrum of Ba^{131} consisted of gamma-rays at 122, 196, 213, 241, 371, and 497 kev. Cs^{131} exhibits no gamma-rays or positrons. The particle spectrum consists of Auger electrons only. No lines corresponding to the 163-kev level of the 12-d metastable Xe^{131} or the 80-kev state of Xe^{131} were found.

* Supported by the joint program of the ONR and AEC.

K13. Gamma-Rays in the Decay of the Radio-Isotopes of Cerium.* H. B. Keller† and J. M. Cork,‡ *Argonne National Laboratory*.—The enriched isotopes of cerium were obtained from the Isotope Division of the Oak Ridge National Laboratory and bombarded in the Argonne heavy water moderated nuclear reactor. The activities thereby induced were examined for conversion electrons in a permanent magnet-type, photographic beta-spectrometer. The gamma-rays deduced from the experimental data are summarized below:

Radio-isotope	Gamma-rays (kev)	Mode of decay	Half-life
Ce^{137}	253.4	*K* capture	36 hr
Ce^{139}	166.0; 275.2	*K* capture	140 d
Ce^{141}	145.7		28 d
Ce^{143}	57.5; 290.6; 348.4	β	33 hr
Ce^{144}	34.0; 41.3; 46.8; 53.7 80.9; 95.0; 100.5; 134.5	β	300 d
Pr^{144}	61.0	β	17.5 min

Decay schemes will be proposed.

* Supported in part by the joint program of the ONR and AEC.
† Phoenix Project Fellow, University of Michigan.
‡ University of Michigan.

FRIDAY MORNING AT 9:45

Shoreham, Main Ballroom

(C. C. LAURITSEN presiding)

Symposium on Stable Isotopes

L1. A Review of the Production and Uses of Stable Isotopes Enriched Electromagnetically from 1945 to 1951. C. P. KEIM, *Oak Ridge National Laboratory.* (35 min.)

L2. Contributions of Stable Isotopes to Atomic Spectroscopy. J. R. MCNALLY, JR., *Oak Ridge National Laboratory.* (35 min.)

L3. Uses of Stable and Enriched Isotopes in the Study of Artificially-Produced Radioisotopes. M. L. POOL AND D. N. KUNDU, *Ohio State University.* (30 min.)

L4. Recent Developments in Mass Spectroscopy. A. O. C. NIER, *University of Minnesota.* (35 min.)

FRIDAY MORNING AT 9:45

Wardman Park, Continental Room

(J. H. VAN VLECK presiding)

Scattering

M1. Scattering of π^+ Mesons by Carbon.* M. SKINNER AND C. RICHMAN, *University of California, Berkeley.*—A carbon target 2.7 cm thick was placed in the 54-Mev π^+ meson beam[1] of the Berkeley 184-in. synchro-cyclotron. Mesons scattered from the carbon at 90° were detected in nuclear emulsions embedded in copper absorbers. To obtain a reasonable ratio of meson to background tracks in the emulsions it was necessary to sacrifice good angular and energy resolution. Some mesons that scattered at angles as low as 60° or as high as 130° were accepted. The energy spectrum of the scattered mesons, after leaving the carbon target, is continuous from zero Mev to the maximum meson energy. By integrating the spectrum, one obtains a value for the differential scattering cross section. (This value is somewhat lower than the true differential cross section, since at any point in the carbon target there is a minimum energy which a meson must have after scattering in order to leave the carbon.) On the basis of 50 scattered mesons, this differential cross section for the scattering of 47 Mev π^+ mesons at 90° from carbon is $(2.2\pm1.0)\times10^{-26}$ cm^2 sterad^{-1}.

* This work was performed under the auspices of the AEC.
[1] Richman, Skinner, Merritt, and Youtz, Phys. Rev. **80**, 900 (1950).

M2. Scattering of π-Mesons. M. H. JOHNSON, *Naval Research Laboratory.*—The collision between a moderately energetic meson and a nucleus can be described approximately as a collision between a meson and free nucleons whose initial momentum distribution is determined by the nuclear state. Using conservation laws, the differential cross section for collisions in which the meson's vector momentum lies within a prescribed interval may then be written as an integral over a surface in the space of the relative momentum. The integrand contains the product of the differential scattering cross section and the initial momentum distribution. Portions of the surface where the nucleon's final momentum takes on values forbidden by the exclusion principle are omitted from the integration. The nuclear model in which the nucleons are a degenerate Fermi gas has been examined in detail. The exclusion principle eliminates collisions with meson energy gain and greatly reduces the number of collisions with small meson energy loss. However, an extreme variation of the scattering cross section with angle and energy is necessary to obtain a distribution, indicated by experiment,[1] in which almost all inelastic collisions occur with an energy loss greater than 80 percent.

[1] G. Bernardini, Invited Paper H3, Bull. Am. Phys. Soc. **26** (February 1–3, 1951).

M3. Multiple Scattering of Particles in Nuclear Emulsions.[1] DALE R. CORSON, *Cornell University.*—The multiple scattering of 40-, 115-, 195-, and 280-Mev electrons and positrons has been measured in *G*-5 emulsions by the Fowler[2] technique. After the "noise" has been eliminated, the mean scattering angle for a 100μ cell can be represented by $(\alpha(100))_{Av}=K/E$, where α is measured in degrees, E in Mev, and $K=26\pm1$. The determination of K is based on measurement of a combined total track length of 90 cm. The multiple scattering of nonrelativistic protons has been studied by calculating, for each proton track (ending in the emulsion and longer than 500μ), a parameter $P=(R^{0.56}\alpha(x)/x^{\frac{1}{2}})_{Av}$, where α is the scattering angle in degrees for a cell length of x microns at a residual range of R microns. For 75 proton tracks, P is measured to be 5.9 ± 1.0. For mesons, P is about 14.

[1] Assisted by the joint program of the ONR and AEC.
[2] P. H. Fowler, Phil. Mag. **41**, 169 (1950).

M4. Backscattering of Secondary Electrons.* G. J. HINE,** *M.I.T.*—The scattering of secondary electrons produced by γ-rays in materials of various atomic numbers has been studied as a function of the γ-ray energies. A collimated γ-ray beam from different isotopes passes through two square ionization chambers with extremely thin walls (0.00025″ Al). By placing absorbers of various materials between the two chambers, the emission of secondary electrons in the backward and forward direction can be determined. The backscattering of Compton electrons has been found to vary as $\log(Z+1)$, where Z is the atomic number of the absorber. The same type of increase in backscattering with increasing Z of the backscattering material has been observed previously for β-rays by other investigators. In addition to the Compton electrons, the emission of photoelectrons becomes apparent in high Z materials. The emission of secondary electrons in the forward direction appears to be reduced in proportion to the backscattered intensity. Therefore, e.g., a carbon absorber irradiated with the Co^{60} γ-rays, emits more than twice as many secondary elec-

trons in the forward direction as a lead absorber. A number of practical applications which follow from this investigation will be discussed.

* This work has been assisted by the joint program of the ONR and AEC.
** Special Research Fellow of the National Cancer Institute, Bethesda, Maryland.

M5. The Evaluation of Multiple Scattering Losses in Charged Particle Experiments. W. C. DICKINSON AND D. C. DODDER,* *Los Alamos Scientific Laboratory.*—In nucleon-nucleon scattering or reaction experiments, where the nuclear particles must traverse a foil or a thick layer of gas, the net loss of particles owing to multiple scattering may not be negligible. A graphical integration method is given for the easy determination of the fractional loss of particles. The multiple scattering theory of E. J. Williams[1] is used to obtain the mean square spatial angle of multiple scattering in the foil or gas. The results obtained, using Williams' theory and the graphical method, are compared with experimental determinations of multiple scattering losses. Theory and experiment are found to be in satisfactory agreement.

* Now at the University of Minnesota.
[1] E. J. Williams, Proc. Roy. Soc. (London) **169**, 531 (1939); Phys Rev. **58**, 292 (1940).

M6. Elastic Scattering of γ-Rays by a Coulomb Field. R. GLUCKSTERN AND F. ROHRLICH, *Cornell University.*—This effect, also called Delbrück or potential scattering, was calculated for zero angle. A laborious but exact calculation by the Feynman method yields the complex scattering amplitude in terms of known functions (elliptic, etc.). It is verified that the imaginary (absorptive) part, $a_1(\omega, 0)$, is exactly $\omega/4\pi$ times the total pair production cross section.[1] Using this cross section, one can find numerically the real (dispersive) part $a_1(\omega, 0)$ by analytic continuation. The result agrees with the independently obtained exact formula for a_1. For small energies $a_1 \sim \omega^3$; for large energies, $a_1 \sim \omega$; $a_2 \sim \omega \ln\omega$. It is to be noted that a_1 is always positive, since the vacuum is able to provide an arbitrarily large number of pairs if the necessary energy is available. At threshold $a_1 = 0.069$, $a_2 = 0$; near 4 Mev a_1 and a_2 are equal. Typical values are

E	a_1	a_2	$d\sigma(0)/d\Omega$ for Pb
1.33	0.12	0.006	0.15 mb/sterad
7.0	1.9	2.9	0.12 b/sterad
200	75	395	1.6 kb/sterad

The energies are in Mev, the amplitudes in units of $(\alpha Z)^2 r_0$.

[1] Jost, Luttinger, and Slotnick, Phys. Rev. **80**, 189 (1950).

M7. Proton-Proton Scattering at 5.86 Mev.* E. J. ZIMMERMAN** AND P. G. KRUGER, *University of Illinois.*—The differential cross section for proton-proton scattering at 5.86±0.06 Mev has been measured using a scattering chamber filled with hydrogen. Proportional counters in coincidence reduced background to a negligible amount. The cyclotron beam through the scattering chamber charged a high resistance, polystyrene-dielectric condenser to a voltage accurately measured with a vibrating-reed electrometer. Twenty thousand scattered protons were counted at each angle. Errors other than statistical were estimated to be 0.7 percent, giving a total standard deviation of 1 percent for each cross section measured. Analysis of the data gives an S-wave phase shift of 55.6°±0.3° and indicates a possible P-wave phase shift of −0.36°±0.22°. The following cross sections in millibarns per steradian were obtained (center-of-mass system): 26°: 99.4; 30°: 89.3; 40°: 83.9; 50°: 83.8; 60°: 86.5; 70°: 86.9; 80°: 88.2; 90°: 87.3; 100°: 87.2; 110°: 87.7. Scattering of protons by oxygen in the same chamber gave important checks on the performance of the apparatus.

* Assisted by the joint program of the ONR and AEC.
** AEC Predoctoral Fellow, 1948–1950.

M8. Proton-Proton Scattering at 345 Mev. O. CHAMBERLAIN, E. SEGRÈ, AND C. WIEGAND, *University of California, Berkeley.*—Previously reported[1] measurements on the differential scattering cross section in elastic proton-proton collisions have been extended to include scattering at small angles from the beam. A digest of the results is contained in Table I.

TABLE I.

Angle θ C.M. system in degrees	Differential cross section C.M. system in 10^{-27} cm²/sterad	Error (Std. Deviation) in diff. cross section in 10^{-27} cm²/sterad
Using a liquid hydrogen target:		
11.3	5.2	0.5
15	3.5	0.3
21	3.3	0.3
33	3.5	0.2
43	3.4	0.2
53	3.3	0.2
Using a CH_2 target:		
36	4.1	0.3
44	4.0	0.3
46	3.8	0.2
52	3.8	0.2
61	3.8	0.3
64	3.6	0.3
71	3.7	0.2
80	4.0	0.3
88	3.7	0.2

Comparisons will be made to theoretical results of R. S. Christian, R. Jastrow, and others which involve both $n-p$ and $p-p$ scattering at high energies. Through the Radiation Laboratory, this work has been supported by the AEC.

[1] Chamberlain, Segrè, and Wiegand, Phys. Rev. **81**, 284 (1951).

M9. The Scattering of 9.7-Mev Protons by Deuterons. A. H. ARMSTRONG,* J. C. ALLRED, R. O. BONDELID, AND L. ROSEN, *Los Alamos Scientific Laboratory.*—The range and intensity distribution of 9.7±0.15 Mev protons scattered by deuterons have been investigated by means of the Los Alamos multiple nuclear-plate camera. A collimated beam of approximately mono-energetic protons was obtained from the 60-inch cyclotron of the Crocker Laboratory at Berkeley. Values of the differential elastic scattering cross section have been determined for fifty center-of-mass angles between 15° and 176°. The shape of the cross-section curve can be inferred from the following representative cross-section values in millibarns at the corresponding center-of-mass angles in degrees: 148 (30°); 97 (60°); 49 (90°); 25 (110°); 21 (120°); 26 (130°); 84 (150°); 190 (170°). The minimum of the curve lies on a continuous straight line of negative slope formed by the minima of the cross-section curves for lower energy data.

* On leave from Wellesley College, Wellesley, Massachusetts.

M10. Elastic Proton-Deuteron Scattering at 240 Mev.* R. D. SCHAMBERGER, *University of Rochester.*—The internal proton beam of the 130″ Rochester synchro-cyclotron has been used to measure the elastic proton-deuteron cross section. The apparatus includes two scintillation counters to detect the protons and deuterons scattered from a heavy paraffin target, and the associated electronics to record the singles and coincidence rates. The cross section relative to the $C^{12}(p, pn)C^{11}$ cross section is obtained by measuring the C^{11} beta-activity of the target. With the present apparatus, measurements are feasible for a limited range of scattering angles. The laboratory scattering angle for the proton must be greater than 12° to permit detection of the low energy deuteron. The upper limit on the scattering angle will be determined by the magnitude of the cross section. A laboratory cross section of less than 2 mb/sterad at a proton scattering angle of 45° would be very difficult to measure. Data will be presented on the cross section in this angular range.

* Assisted by the joint program of the AEC and ONR.

M11. The Elastic Scattering of Protons by Mg^{24}.*,† F. P. MOORING,** E. GOLDBERG, S. G. KAUFMANN,‡ L. J. KOESTER,‖ AND D. SAXON, *University of Wisconsin.*—Protons from the electrostatic generator were used to bombard thin $Mg^{24}F_2$ targets evaporated onto spectroscopically pure graphite backings, and the elastically scattered protons were observed at a laboratory angle of 164±5°. A 90° magnetic analyzer separated the proton groups, and a proportional counter distinguished between proton pulses and fluorine alpha-pulses. The elastic differential scattering cross-section curve for incident proton energies of 0.396 to 3.936 Mev shows nine levels of the compound nucleus Al^{25}. The level reported by Grotdal, *et al.*,[1] for 0.417 Mev protons was not observed. The elastic scattering yield below 0.8 Mev was assumed to be Rutherford and was used to determine differential scattering cross-section values.

* Work supported by the AEC and the Wisconsin Alumni Research Foundation.
† Mg^{24} was produced by the Y-12 Plant, Carbide and Carbon Chemicals Corporation, on allocation from the Isotopes Division of the AEC.
** Now at Fairchild Engine and Airplane Corporation, Oak Ridge, Tennessee.
‡ Now at Argonne National Laboratory, Chicago, Illinois.
‖ AEC Predoctoral Fellow.
[1] Grotdal, Lönsjö, Tangen, and Bergström, Phys. Rev. **77**, 296 (1950).

M12. Elastic Scattering of Protons by Mg^{24};* Interpretation of Results.† L. J. KOESTER,‡ E. GOLDBERG, S. G. KAUFMANN, F. P. MOORING, AND D. SAXON, *University of Wisconsin.*—Of the nine resonances mentioned in the preceding abstract, seven are narrow and well separated, while the remaining two are broad and overlap some of the others. Momentum analyses taken in the vicinity of several of the higher resonances indicate that the partial width for inelastic scattering is relatively small. A complete analysis of the data is in progress in which the phase shift at a given energy is separated into a resonance term and a potential term. Assuming a value for the interaction radius, one can use coulomb wave functions to compute the phase shift owing to potential scattering for each partial wave. Effects of overlapping levels are considered. A graphical method is used to combine the Rutherford, resonance, and potential contributions to the scattered amplitude.

* Mg^{24} was produced by the Y-12 Plant, Carbide and Carbon Chemicals Corporation, on allocation by the Isotopes Division of the AEC.
† Work supported by the AEC and the Wisconsin Alumni Research Foundation.
‡ AEC Predoctoral Fellow.

M13. Theory of Multiple Scattering, Particularly of Electrons. MING CHEN W. YU AND EUGENE GUTH, *University of Notre Dame.*—For the multiple scattering of light or particles by a finite plane-parallel without energy loss, the "spherical harmonic" (S.H.M.) method as developed generally, for solving the Boltzmann integro-differential equation to nth approximation for any anisotropic single scattering law developable into a series of legendre polynomials. To any approximation, the S.H.M. method is proved to give the same formal solution as the "gauss quadrature method" (G.S.M.) as developed by Wick and Chandrasekhar, the only difference being in the boundary conditions. Both the S.H.M. and the G.S.M. are applied to the multiple scattering of electrons by a finite medium. The Goudsmit-Saunderson and Williams theories are shown to be the small angle and Fokker-Planck approximations to the Boltzmann equations neglecting back scattering. We obtain nth approximations not only for the forward but also for the back scattering. The relation of our work to that by Bothe, Rose, Bethe and Smith, Moliere, Snyder-Scott, and Lewis will be discussed.

FRIDAY MORNING AT 9:45

Shoreham, Terrace Room

(J. E. GOLDMAN presiding)

Metals

N1. Theory of Mobility of Grain Boundaries.* R. SMOLUCHOWSKI, *Carnegie Institute of Technology.*—Motion of a grain boundary during grain growth can be represented as a process of disordering of a group of n atoms on one side of the grain boundary and an ordering of a similar group of atoms on the other side of the grain boundary in continuation of the crystalline lattice of the growing grain. A simple extension of Mott's theory of viscous slip along grain boundaries allows to include the surface energy of the boundary and to estimate V, the rate of motion of a boundary, when the motion is caused by the curvature of the boundary itself. Using experimental data of various authors on aluminum, silver, and brass, the average number of atoms n is obtained and the constant V_0 in the equation $V = V_0 \exp(-nL/kT)$ is theoretically calculated in agreement with experiment for the three metals. (L is the heat of fusion.)

* Research sponsored by an AEC contract.

N2. Diffusion along Individual Grain Boundaries.* R. SMOLUCHOWSKI AND M. R. ACHTER, *Carnegie Institute of Technology.*—The structure of grain boundaries is still the subject of much speculation. There is, however, little doubt that the structure depends upon the relative orientation of the two grains and of the grain boundary itself. In order to get an insight into these phenomena the diffusion of silver along individual grain boundaries of columnar copper (common direction of one cubic axis of all grains) has been studied. The experiments, conducted at a rather low temperature so as to enhance the grain boundary diffusion as compared to volume diffusion, indicate that grain boundary diffusion is greatest when the angle between the two grains is around 45 degrees. The rate of diffusion drops rapidly with decreasing (or increasing) angle and reaches the rate of volume diffusion at an angle of 20 (or 70) degrees. This result suggests that at small angles the grain boundary can be described as an array of individual parallel dislocations, while at higher angles the dislocations bunch up and the grain boundary is better described in terms of Mott's islands of fit and of misfit.

* Research sponsored by an AEC contract.

N3. Anisotropy of Grain Boundary Diffusion.* M. R. ACHTER AND R. SMOLUCHOWSKI, *Carnegie Institute of Technology.*—It has long been assumed that a metallic grain boundary can be described as a layer of highly disordered atoms in which little, if any, correlation with the crystalline lattice of the two grains exist. However, a closer analysis based either on the dislocation model or on the "island" model indicates that this is over simplification and that the structure of a grain boundary in general has a definite directionality. In order to prove this a study was made of diffusion of silver along individual grain boundaries of copper in two mutually perpendicular directions. It appears that diffusion along grain

boundaries is anisotropic and this anisotropy depends upon the relative orientation of the grains. As a rule, whenever the grain boundary can be represented as an array of parallel edge dislocations, then diffusion is faster in the direction of the dislocations. A similar interpretation is obtainable on the "island" model.

* Research supported by an AEC contract.

N4. Absorption by Beryllium in the Neighborhood of the *K* Edge.* D. H. TOMBOULIAN AND R. W. JOHNSTON, *Cornell University.*—Following the experimental procedure described in a previous report,[1] preliminary measurements have been carried out on the absorption by Be in the spectral range 80 to 300A. The absorbers consisted of metallic foils or layers of Be deposited on Zapon backing films by evaporation. The absorption curve reveals a rather sharp *K* edge located at approximately 110A. Though no previous measurements seem to have been reported on the absorption spectrum of Be, the position of the edge is in agreement with that observed previously[2] in the emission spectrum of Be. The available observations indicate the existence of secondary structures on the short wavelength side of the *K* edge. So far, it has not been possible to arrive at reliable values of the absorption coefficient owing to uncertainties in the nature and in the thickness of the absorbers used.

* Supported in part by the ONR.
[1] E. M. Pell and D. H. Tomboulian, Phys. Rev. **76**, 172 (1949).
[2] H. W. B. Skinner, Trans. Roy. Soc. (London) **239**, 95 (1940).

N5. Spectrographic Study of the Electron Energy Bands in Metals.* R. H. KINGSTON AND E. M. GYORGY.—With the equipment described in the previous paper it has been possible to reproduce with excellent agreement O'Bryan and Skinner's curves for Na, Mg, and Al. As a result of the ability to run consecutive curves on the spectrograph at intervals of five minutes or less, it is possible to observe the slow contamination of the surface of the specimen after the initial evaporation of the material on to the target. Skinner, in unpublished correspondence, has found that the metals Ti through Zn do not show sharp emission edges as would be expected from the electron theory of metals. Tentative data which we have taken on manganese indicate that this is also true even at the low bombarding voltages we have been using. Before further studies to determine whether the broad emission edges in the transition metals are a result of satellite and Auger effects rather than a definite anomaly in electronic structure we are investigating potassium and calcium, since they lie midway between the transition metals and aluminum, which shows a very sharp edge.

* This work was supported in part by the Signal Corps, the Air Materiel Command, and ONR.

N6. A High Vacuum Recording Spectrograph for the Study of Solids in the 50–1000A Range*. E. M. GYORGY AND R. H. KINGSTON.—The two-meter grazing-incidence vacuum spectrograph used by O'Bryan and Skinner[1] for the study of the emission bands of solids has been rebuilt to operate with improved sensitivity and speed. The major modification is the replacement of the photographic plate by a Be-Cu photomultiplier which is designed to traverse the Rowland circle, giving a continuous record of photon-counting rate as a function of a wavelength. With the photo-multiplier it is possible to take as many separate curves as desired, subject to x-ray target condition, without opening the spectrograph, which is normally evacuated to better than 10^{-6} mm Hg. In addition, the sensitivity is increased about a thousandfold; i.e., with a photographic plate the target current and voltage needed are 10–100 ma and about 3000 volts for a one- to three-hour exposure. Using the photo-multiplier, however, we require only 2–3 ma at voltages of 300–500 volts, and the complete emission band may be recorded in a matter of about 5 minutes.

* This work was supported in part by the Signal Corps, the Air Materiel Command, and ONR.
[1] H. M. O'Bryan and H. W. B. Skinner, Phys. Rev. **45**, 370 (1934).

N7. Frequency Dependence of Elastic Constants and Losses in Nickel. W. P. MASON, H. J. MCSKIMIN, AND R. M. BOZORTH, *Bell Telephone Laboratories.*—The elastic constants of nickel crystals,[1] and their variation with magnetic field (ΔE effect), have been measured by a 10-megacycle ultrasonic pulsing method.[2] The constants of three crystals agree well with each other when the crystals are magnetically saturated, but vary with domain distribution when demagnetized. The maximum ΔE effect observed is much less (3 percent) than has been observed at lower frequencies (20 percent). By measuring the ΔE effect and the decrement of polycrystalline rods at low frequencies, it is shown that the small effect observed at 10 megacycles is due to shielding in single domains by micro-eddy currents. From the initial slope of the decrement-frequency curve, and also from the frequency of maximum decrement, the size of the average domain is found to be about 0.03 mm. Actual domains in single nickel crystals have been observed optically by Williams, who finds domain widths of 0.02 to 0.2 mm. Our results then indicate that regions swept by domain walls, displaced by stresses, correspond to whole domains of the original structure.

[1] Bozorth, Mason, and McSkimin, Phys. Rev. **75**, 1954 (1949).
[2] H. J. McSkimin, J. Acoust. Soc. Am. **22**, 413 (1950).

N8. The Thermal Conductivity of Titanium between 20 and 273 Degrees Kelvin. CARL J. RIGNEY, *Southern Illinois University*, AND LESTER I. BOCKSTAHLER, *Northwestern University.*—Measurements were made on cylindrical rods approximately 8 mm in diameter and 72 mm long mounted inside an evacuated hollow copper cylinder. The top of the rod supported a heating coil, while the other end firmly fitted into the base of the copper container which was immersed in a refrigerant. Corrections for radiation and spurious conduction were made by a substitution method. Results for a specimen of commercially pure titanium and a titanium alloy containing 2.8 percent chromium and 1 percent iron are tabulated below. The error for any determination does not exceed five percent except at 20°K, where it is less than ten percent.

Temperature	Conductivity in watts cm^{-1} C $degrees^{-1}$	
Deg K	Ti	Alloy
273	0.20	0.13
195	0.21	0.10
90	0.18	
80	0.17	0.06
20	0.12	

N9. Periodic Schottky Deviations for Molybdenum and Tungsten. E. A. COOMES, E. G. BROCK, AND A. L. HOUDE, C.S.B., *University of Notre Dame.*—Periodic deviations in the Schottky effect have been studied for the thermionic emission from molybdenum and tungsten filaments. These studies were made both for the clean state obtained by flashing, and for contaminated states obtained by electropositive and electronegative films deposited on the clean filaments. The range of applied fields was 10^3 to 4×10^5 volts cm^{-1}, and the range of temperatures was 1400°K to 1850°K. The positions of maxima and minima as determined experimentally support the mirror image model. Variations of amplitude with temperature were also consistent with this model. Contamination by an electronegative film caused the phase to shift to higher fields, in contrast to the shift to lower fields resulting by an electropositive contamination.

N10. A Collective Description of Particle Interactions. DAVID PINES, *University of Pennsylvania*, AND DAVID BOHM, *Princeton University.*—A new method of treating a dense assembly of strongly interacting particles, which was applied previously to the case of transverse electromagnetic interactions between electrons,[1] has now been extended to the coulomb interactions in a dense electron gas. Instead of solving the individual particle equations of motion, we introduce collective coordinates which are effectively the normal coordi-

nates of the system as a whole. In a suitable approximation, these coordinates, as a result of the coulomb interaction, oscillate harmonically with a determinable characteristic frequency and describe the major part of the charge density. The remainder of the charge density produces a screened coulomb potential for electron-electron interaction with a screening radius which can be expressed in terms of the average particle kinetic energy and the particle density. This collective method can be applied to a general interparticle potential $V(\mathbf{x}_i-\mathbf{x}_j)=\Sigma_k (V_k/L^3)\exp i\mathbf{k}\cdot(\mathbf{x}_i-\mathbf{x}_j)$. One can show that for a given wave number, $\mathbf{k}$, the criterion that this method provide a better approximation then a description in terms of the individual particles is $nV_k>2T/3$, where n is the particle density, and T is the mean particle kinetic energy. Thus, strong forces and high particle density favor collective behavior, while high random velocities oppose it. The relation of our method to Tomanaga's one-dimensional treatment[2] will be discussed.

[1] D. Bohm and D. Pines Phys. Rev. (to be published).
[2] S. Tomanaga, Progress of Theoretical Physics.

N11. Application of Collective Description to Electron Interactions in a Metal. DAVID BOHM, *Princeton University*, AND DAVID PINES, *University of Pennsylvania*.—Application of our collective description to electron interactions in a metal requires a quantum mechanical treatment. This has been accomplished by means of a suitable canonical transformation which expresses the individual particle coordinates and momenta in terms of collective coordinates and momenta associated with the normal modes of the system. The hamiltonian then reduces to the sum of three groups of terms; harmonic oscillator terms associated with normal modes, effective kinetic energy terms associated with the individual particles, and a residual term describing screened coulomb electron interactions. For a typical metal, the screening radius is approximately one-third the interparticle distance,[1] so that the mean free path for electron-electron collisions is ten times the interparticle distance. Our analysis thus tends to justify the usual Bloch approximation, which neglects electron interactions. We also predict a phenomenon analogous to Čerenkov radiation; *viz.*, a very fast electron will transfer energy to the normal modes of the metal in integral multiples of the basic quantum of collective oscillation. Experiments tending to verify this prediction will be discussed.[2]

[1] D. Bohm and D. Pines, Phys. Rev. **80**, 903 (1950).
[2] C. Herring (private communication).

N12. The Influence of Electric Field on Electric Current in Metallic Conductor. OLEG YADOFF, *Columbia University*.—It is known that the resistance of metallic conductors set in a magnetic field has increased with the increase of the field intensity. We observed a new phenomenon: influence of electric field on electric current. This action is manifested in a decrease in resistance. If we apply electric concentric field to a conductor through which electric current flows, we have a noticeable decrease in resistance. The demonstrated apparatus consists of a receiving charge wire conductor placed concentrically in a metal tube the wall of which has been connected to a pole of electrostatic generator. The current may be ac or dc the electrostatic pole may be positive or negative. The effect begins to show from 10 kv:cm. Through the action of this field we may increase the current—20 percent more than the normal intensity. The pressure in the test apparatus, as well as the nature of the gases used has certain importance. But in all cases the phenomenon exists and can be perfectly observed. The phenomenon is accompanied by some physical changes. For example, during many experiments we observed that if we introduced some gas, smoke, etc., into the apparatus, the action of this phenomenon was to destroy them.

FRIDAY MORNING, 9:45 to Noon

NBS, East Building

(A. V. ASTIN presiding)

Work of the National Bureau of Standards, Part I

P1. The Current Research Programme of the National Bureau of Standards. A. V. ASTIN. (20 min.)
P2. Atomic Systems as Primary Standards. R. D. HUNTOON.
P3. Penetration and Diffusion of X-Rays and Electrons. U. FANO.
P4. The Spectra of Artificial Elements. W. F. MEGGERS.
P5. Recent Results in Supraconductivity and Superfluidity. J. R. PELLAM.
P6. Physical State of Outer Atmosphere. A. G. MCNISH.

FRIDAY AFTERNOON, 2:00 to 4:15

NBS, East Building

(W. R. BRODE presiding)

Work of the National Bureau of Standards, Part II

PA1. Monte Carlo Methods for Calculating Eigenvalues. J. H. CURTISS.
PA2. Application of Electronic Digital Computers to Physical Problems. R. J. SLUTZ.
PA3. Automatic Programmed Computing Machines for Optical Design. I. C. GARDNER.
PA4. Crystal Synthesis. H. F. MCMURDIE.
PA5. The Hot-Wire Technique in Aerodynamic Research. G. B. SCHUBAUER.
PA6. Recent Developments in Acoustics. R. K. COOK.

FRIDAY AFTERNOON AT 2:15

Shoreham, West Ballroom

(J. M. CORK presiding)

Radioactive Nuclei Beyond Cerium

Q1. The Radiations from Hafnium. S. B. BURSON, K. W. BLAIR, H. B. KELLER, AND S. WEXLER, *Argonne National Laboratory.*—Four activities in Hf, induced by neutron bombardment in the Argonne Laboratory reactor, have been investigated by spectrometric and counting techniques. Isotopic assignments were verified by activation experiments on the enriched isotopes obtained from the Oak Ridge National Laboratory. Each decay process was verified by ascertaining which orbital electron work functions yielded the most consistent results when fitted to the internal conversion lines from the gamma-rays associated with an activity. These results are summarized in the table:

Activity	Process	Gamma-ray energies in kev
$_{72}Hf^{181}$ (45 d)	420 kev β^-	611, 481, 344, 136, 133
$_{72}Hf^{180m}$ (5.5 hr)	Isomeric	442, 330, 214, 93.2, 56.8
$_{72}Hf^{179m}$ (19 sec)	Isomeric	161
$_{72}Hf^{175}$ (70 d)	*K*-capture	342, 228, 113, 89.1

The 5.5-hour activity was found to be an isomeric state of $_{72}Hf^{180}$ and thus a violation of the Mattauch Rule for even-even nuclei. Delayed coincidence curves showed that the 420-kev beta-ray of $_{72}Hf^{181}$ leads directly to a 22-microsecond metastable state of $_{73}Ta^{181}$.

Q2. Long-Lived Gamma-Radiation Following Neutron Capture in Iridium. J. M. CORK, J. M. LEBLANC, A. E. STODDARD, W. J. CHILDS, C. E. BRANYAN, AND D. W. MARTIN, *University of Michigan.*—A continued spectrometric study of iridium, irradiated in the high neutron flux of the Argonne pile, shows many electron lines not previously observed. The half-life of Ir^{192} is found to be 78 days and the isotope decays both by beta-emission to Pt^{192} and by *K* capture to Os^{192}. About 45 electron lines are observed including Auger lines for both osmium and platinium. The electron lines having *K-L-M* differences characteristic of platinium yield 9 gamma-rays with energies between 135.9 and 611.2 Kev. These energies fit remarkably well as transitions within a simple nuclear structure of 6 levels. There appear to be 4 gamma-rays in Os^{192} associated with the *K*-capture process. Four single electron lines cannot be uniquely assigned. A single gamma-ray of energy 327.5 Kev is emitted following the beta-decay of Ir^{194} to Pt^{194} with a 19-hour half-life. This project was supported jointly by the ONR and the AEC.

Q3. Angular Correlation of the Gamma-Rays Emitted from the Excited States of Pt^{198}.* R. M. STEFFEN AND D. M. ROBERTS, *Purdue University.*—The nuclide Au^{198} ($T_{\frac{1}{2}} = 5.6$ d) decays by *K*-capture into Pt^{198} leading to two excited states of 0.688-Mev and 0.358-Mev energy and also[1] by β^- emission into Hg^{198}. The angular correlation of the two successively emitted gamma-rays following the *K*-capture has been measured, using the apparatus described before.[2] The experimental data are well represented by the correlation function $f(\theta) = 1 - (15/13)\cdot\cos^2\theta + (16/13)\cdot\cos^4\theta$, which is characteristic for two quadrupole transitions between states of angular momentum 2,2 and 0.[3] The conversion coefficients[1] of the two gamma-rays indicate electric quadrupole transitions suggesting the same parity for all three levels involved. These assignments, however, lead to the difficulty that the cross-over transition should be predominant, whereas the intensity of this transition has been measured to be less than 5 percent. The spin and parity assignments of all the excited levels involved in the dual decay of Au^{198} will be discussed.

* Supported in part by the AEC.
[1] Steffen, Huber, and Humbel, Helv. Phys. Acta **22**, 167 (1949).
[2] R. M. Steffen, Phys. Rev. **80**, 115 (1950).
[3] D. R. Hamilton, Phys. Rev. **58**, 122 (1940).

Q4. The Radiations of Tl^{199} and Tl^{200}.* H. I. ISRAEL, T. L. HARLOR, AND R. G. WILKINSON, *Indiana University.**—The gamma-rays of Tl^{199} and Tl^{200} produced by alpha-particle bombardment of gold have been investigated in a 180°-shaped field spectrometer. The photo-electrons and internal conversion electrons were studied with carrier-free sources prepared by electrodeposition from a solution containing the chemically separated radiothallium. The activities associated with the 7-hour Tl^{199} and the 27-hour Tl^{200} were easily differentiated by following the decay rates. In the case of Tl^{199}, conversion lines at 50, 60, 70, 120, 140, 160, 190, 220, 240, 310, and 450 kev were observed. These can be considered to be associated with gamma-rays from Hg^{199} with energies of 70, 150, 200, 230, 320, and 540 kev. These values are in good agreement with those reported[1] in a study of the decay of Au^{199} to Hg^{199}. In the disintegration of Tl^{200}, photo-electrons and internal conversion electrons were observed which can be ascribed to gamma-rays of Hg^{200} with energies of 0.36, 0.57, 0.83, and 1.2 Mev. Coincidence studies by Cuffey in this laboratory show that at least two of the gamma-rays are in cascade. A decay scheme consistent with the measured energies and the coincidence-absorption data will be proposed. No positrons were found in either case.

* This work was supported by the joint program of the ONR and AEC.
[1] Beach, Peacock, and Wilkinson, Phys. Rev. **76**, 1585 (1949).

Q5. An Alpha-Gamma Angular Correlation in the Decay of Radiothorium.* J. K. BELING, B. T. FELD, AND I. HALPERN, *M.I.T.*—The angular correlation between the short-range alpha-particles and the gamma-rays of ~85 kev emitted in the decay of radiothorium has been measured. Both radiations were detected with scintillation counters. The gamma-phosphor was a NaI(Tl) crystal, $\frac{1}{4}$ inch thick, and the alpha-detector was a flake of anthracene 0.01 inch thick. Data were taken for the first ten hours after chemical separation of RdTh from its decay products, and differential discrimination was employed on both alpha- and gamma-pulses. The observed correlation is roughly $1+\sin^2 2\theta$, in disagreement with an earlier measurement.[1] Recent experiments[2] indicate that the decay involves gamma-rays of energies 83.3 and 86.8 kev which do not occur in cascade and that the 83.3-kev radiation is three times more intense than the 86.8 kev. These energies have not as yet been resolved in this experiment but the average energy has been confirmed. Provided that two gamma-rays of comparable intensity are not emitted successively, the correlation can be ascribed to a principal mode of decay having spins 0-2-0 for the sequence $RdTh \xrightarrow{\alpha} ThX^* \xrightarrow{\gamma} ThX$. The possibility of cascade emission is being investigated.

* Assisted by the joint program of the ONR and AEC.
[1] Kul'chitski, Latyshev, and Bulyginski, Bull. Acad. Sci. URSS, Sér. Phys. **13**, 331 (1949).
[2] M. Riou, J. phys. radium **11**, 185 (1950).

Q6. Disintegration of Np^{239}. R. L. GRAHAM AND R. E. BELL, *Chalk River Laboratory.*—The radiations of Np^{239} have been studied by millimicrosecond coincidence techniques in two thin lens beta-ray spectrometers placed end to end. Np^{239} emits a complex beta-ray spectrum with end points at 705±15

kev (7 percent), 435±15 kev (46 percent), and 310±20 kev (47 percent), and conversion lines due to gamma-transitions of 49, 57, 61, 67, 210, 227, and 276 kev. Delayed-coincidence measurements showed that the 210-, 227-, and 276-kev transitions follow a state of half-life $(1.1\pm0.1)\times10^{-9}$ second. Coincidence studies on focused conversion lines showed that the 227- and 276-kev transitions are not in cascade, and that the 67- and 210-kev transitions are in cascade. Fermi plots of coincidences between nuclear beta-rays and the 210-, 227-, and 276-kev transitions all have end points at 435 kev. No radiations were found coinciding with the 705-kev beta-spectrum, which thus leads to the ground state of Pu^{239}. The 435-kev spectrum goes to a 276-kev level of half-life $(1.1\pm0.1)\times10^{-9}$ second, which is de-excited by the gamma-transitions 276 kev, or (227 and 49) kev or (210 and 67) kev. The 310-kev beta-spectrum goes to a level at about 394 kev. The information found here agrees generally but not in detail with the disintegration scheme of Kohman.[1]

[1] Nuclear Data, Nat. Bur. Standards Circular No. 499 (1950).

Q7. Conversion Lines and Beta-Spectra of Np^{239}. E. P. TOMLINSON, H. W. FULBRIGHT, AND J. J. HOWLAND, JR., *Princeton University and Brookhaven National Laboratory.*—The momentum distribution of electrons emitted by Np^{239} has been studied using a 20-cm radius high resolution double focusing magnetic spectrometer of the Siegbahn-Svartholm type. Eighty-eight electron lines were observed with varying degrees of certainty down to an energy of 3 kev. Most of these lines were obtained with a full width at half-maximum in Np between 0.3 and 0.4 percent. About two-thirds of the lines are accountable as conversion electrons from 11 gamma-rays. A Kurie analysis of the underlying beta-spectra gives clearly at least four beta-groups and possibly other lower energy groups. Preliminary values, in kev, for the gamma-ray energies are 286, 277, 254, 228, 209, 105, 67.5, 61.4, 57.0, 49.0, 44.2. Preliminary values for the beta-ray end points, in Mev, are 0.715, 0.654, 0.44, 0.33. The energy level scheme of Pu^{239} will be discussed on the basis of these data. The work was supported in part by the joint program of the ONR and AEC.

Q8. Radiation Spectra from Short-Lived Nuclides.* D. J. ZAFFARANO AND F. I. BOLEY,† *Iowa State College.*—Spectra have been obtained from nuclides with half-lives larger than 0.1 second made by x-rays from the Iowa State College synchrotron. A short pneumatic tube is used to transfer the sample to a scintillation spectrometer which employs photographic pulse height registration on a moving film to record the data. Calibration is effected with Cl^{34} (4.45 Mev) and Y^{90} (2.24 Mev) sources. Fermi plots of S^{31} (3.2 sec),[1] Cl^{32} (~2.4 sec),[2] and Ca^{39} (1.06 sec) indicate maximum positron energies of 3.74±0.2, 3.70±0.2, and a preliminary value of 4.2 Mev, respectively. These belong to the group of radioactive nuclei having one fewer neutron than proton.[1,2] Their relationship to the other members of the group will be discussed.

* This work was performed in the Ames Laboratory of the AEC.
† Socony-Vacuum Research Fellow.
[1] Schelberg, Sampson, and Mitchell, Rev. Sci. Instr. 19, 458 (1948).
[2] White, Creutz, Delsasso, and Wilson, Phys. Rev. 59, 63 (1941).

Q9. Measurement of γ-Ray Energies with a Scintillation Spectrometer.* E. DER MATEOSIAN, *Brookhaven National Laboratory.*—A scintillation spectrometer especially useful for the study of energies of short-lived γ-ray emitters has been developed. The light output from a NaI-Tl activated crystal is recorded with the help of a DuMont oscilloscope and a Polaroid camera. Some of the results of interest are the following. The β-emitter Ti^{51} (6 min) shows the same γ-rays as the K-capturer Cr^{51} (26 d). In both cases a 320-kev state of V^{51} is excited. Mo^{101} (14.5 min) and its daughter Tc^{101} (15 min), which had both been reported[1] to have a γ-ray of 300 kev, are found instead to possess γ-rays of 150 kev and 260 kev, respectively. Nb^{94m} (6.6 min), for which a weak γ-ray of 1.3 Mev[1] had been reported (probably following a weak β-branch) is found instead to have a γ-ray of 0.9 Mev.

* Research carried out under contract with AEC.
[1] See K. Way, *et al.*, Nuclear Data, Nat. Bur. Standards Circular 499.

Q10. A Type of Correlation of the Half-Lives of β^- Emitters for Odd Isotopic Numbers. D. N. KUNDU AND M. L. POOL, *Ohio State University.*—For nuclei on the neutron excess side of the valley of stability, the logarithm of the half-life t of β^- emitters of odd A is approximately a linear function of Z for a constant value of $I=A-2Z$. Both odd and even Z have been examined for values of I from 1 to 25. In some cases the linearity holds through a range of 1 to 10^{10} in half-lives. From this linear relationship $\log t=\alpha Z+\delta$, it follows that within this range, $|M|^2f=Ae^{-\alpha Z}$, where $|M|$ is the nuclear matrix and f the usual integral Fermi function. The constant α has approximately the same value 0.59 for all values of I. This may be compared with $\alpha=0.35$ obtained previously for β^+ emitters in a similar study. The interpretation is that the slope of instability is steeper on the β^+ side than the β^- side of the valley. The curves help predict the half-lives of probable isotopes for given Z and I. Though, in general, both $|M|^2$ and f may individually be complicated functions of Z, the product $|M|^2f$ has simple exponential charge dependence for about 65 percent of known β^- emitters of Seaborg classification A.

Q11. The Assay of Radioactive Water by a Methane Proportional Counting Method. CHARLES V. ROBINSON, *New England General Hospital.*—In a suitable vacuum system, radioactive water can be combined with methyl Grignard reagent to give radioactive methane which can be collected in a counting chamber by partial trapping with liquid nitrogen. Subsequent operation of the chamber as a proportional counter gives a measure of the specific activity of the water.[1] A method of assay based on these principles is being used for routine measurements in surgical studies employing tritium as a water tracer.[2] The method gives s standard deviation less than 1 percent on repeated measurements, shows no significant "memory effect" from one sample to the next, and is relatively convenient for a gas phase method. Some details of the apparatus and technique will be described.

[1] The preliminary work on this method is to be published: C. V. Robinson, Rev. Sci. Instr.
[2] Under Public Health Service Grant.

FRIDAY AFTERNOON AT 2:00

Wardman Park, Continental Room

(H. A. BETHE presiding)

General Theory

QA1. Representation of Nucleon-Nucleon Singlet Scattering. G. BREIT AND M. C. YOVITS,* *Yale University.***—This paper is concerned with the calculation of the f function which depends on phase shift K and energy E only. It is constant for potentials having zero range, varies linearly with E for short range potentials, and determines $K(E)$ conveniently in a wide

energy range. The calculation of the power series in E representing f for a given potential is shown to be possible by means of the expansion

$$[f-f^{(0)}]/(E/c^2)=\sum_0^\infty \int_0^\infty [(u_p{}^s)^2-u_p{}^2]dr$$

$$+\sum_0^\infty \int_0^\infty [u_p{}^s u_{p+1}{}^s-u_p u_{p+1}]dr,$$

where $f^{(0)}$ is the energy independent term, p is an integer, and u_p is the term containing E^p in the power series expansion of u in E; u is $C_0\mathfrak{F}/\sin K$ in standard notation. The function u^s is the comparison function for zero range force; u^s is varied with E to fit f. The functions u_p were first used by Jackson and Blatt to obtain terms in E^2 and E^4. The series shown contains E^{2p} in the term in $u_p{}^2$ and E^{2p+1} in the term in $u_p u_{p+1}$. An analogous expansion in a linear parameter multiplying a part of the potential energy has a similar structure. Applications will be discussed.

* AEC Predoctoral Fellow.
** Assisted by the joint program of the ONR and AEC.

QA2. Relativistic Symmetry in the Basic Formulation of Quantum Theory. O. COSTA DE BEAUREGARD, *Institut Henri Poincaré, Paris.*—The spinning-particle-in-a-field theory has been given relativistic symmetry. A *state* is identified when one knows ψ on a space-like surface $\mathcal{S}$; the *evolution* of ψ is given by the associated cauchy problem. The definition of hermitian scalar products is generalized, so as to be given on $\mathcal{S}$; nevertheless, conserving its fundamental properties, which allow the construction of a hilbert space. As the operator of the total energy, the hamiltonian is replaced by $h\partial/i\partial t$; the stochastic distribution related to $\mathcal{S}$ of the four operator $h\partial^k/i$ is described by its so-called *characteristic function*, introduced into quantum theory by E. Arnous, through Stone's and Bochner's theorems.[1] Formulas are given for the variation between two $\mathcal{S}$'s of the *characteristic* and *distribution* functions of $h\partial^k/i$, the latter leading to Feynman's rules in his well-known *positron theory*. Our theory proceeds entirely from two Notes of October 1947 in the *Comptes Rendus*, where we suggested the interpretation of the positron subsequently developed by Feynman; it is being presented in a series of Notes in the *Comptes Rendus* (1950–1951).

[1] Stone and Bochner, J. phys. radium **8**, 87–93 (1947).

QA3. Invariance of Two-Body Interactions Under Space and Time Inversion. R. A. FERRELL,* *Princeton University.*—We will indicate the unsuitability of the usual inversion operators and replace them with operators defined differently, giving two examples. These operators for a quantum mechanical system are a matter of convention; but in the classical limit, the expectation values of the velocities, v_i, must differ in sign for corresponding inverted states. The conventional inversion operators are not acceptable, for they reverse the momenta, p_i, instead of v_i. Equivalently expressed, the convention is not gauge invariant. We replace the conventional operator O by O', determined from (*A*) $O'v_iO'^{-1}=-v_i$. This gives $O'=UO$, with U unitary. With hamiltonian $H=\Sigma_i \times p_i{}^2/2m_i+\Sigma_i a_i p_i+\Sigma_i b_i p_i+V$, where a_i, b_i, V independent of p_i, $Oa_iO^{-1}=a_i$, $Ob_iO^{-1}=-b_i$, and (*B*) $\partial a_i/\partial x_j=\partial a_j/\partial x_i$, all i, j, one finds $U=\exp -2i/h\int \Sigma_i m_i a_i dx_i$. If (*B*) *invalid*, no O' satisfies (*A*); and *for a given state, a corresponding inverted state with the required properties does not exist.* When (*B*) valid, O' is gauge invariant, and linear terms of $O'HO'^{-1}$ and H agree. Choosing gauge so $a_i=0$, $O'=O$, and $\Sigma_i a_i p_i$ reduces to static terms. Example I: electron in uniform magnetic field. There is a space O' but no time O'. Example II: many velocity dependent *two-body interactions*, termed non-invariant by Wigner and Eisenbud,[1] are now actually inversion invariant but equivalent to static forces. Therefore, their list of invariant forces remains unaffected.

* AEC Predoctoral Fellow.
[1] Wigner and Eisenbud, Proc. Nat. Acad. Sci. U. S. **27**, 281 (1941).

QA4. A Unified Field Theory with Varying Charge and Mass. H. C. CORBEN, *Carnegie Institute of Technology.**—Field equations and geodesic equations of motion for a point particle are derived from a unified field theory in five dimensions, the extra metric elements being given by $g_{i5}=\alpha A_i$, $g_{55}=1+\alpha^2\Phi$, α being a constant independent of the particle, A_i the electromagnetic potentials, and Φ a scalar field. The charge e and mass m of the particle are introduced as $e=M\alpha(dx^5/d\tau)$, $m=M(ds/d\tau)$, with $d\tau^2=g_{\mu\nu}dx^\mu dx^\nu$, $ds^2=g_{ij}dx^i dx^j$ (μ, $\nu=1\cdots5$, i, $j=1\cdots4$), M being a constant characteristic of the particle. The geodesic equations then yield a modified Lorentz force equation in which e and m are not necessarily constants of the motion, even if $\Phi=0$ and there is no gravitational field ($g_{ij}=0$ $(1\neq j)$, $g_{11}=g_{22}=g_{33}=-1$, $g_{44}=1$). Even a neutral particle in the presence of one that is charged has a charge induced on it, the total charge on the two being constant only if $\Box\Phi=0$ in the linear approximation. The effect is negligible for two particles of equal mass at relative rest if $r\gg m\alpha^2$. The mass of a neutral particle exceeds that of a charged particle characterized by the same M by an amount, which corresponds to the neutron-proton mass difference, if $\alpha=e_0/\mu$, where e_0 is the free proton charge, and $\mu=95$ times the mass of the electron. In the linear approximation, the field equations become, for no gravitational field, $\Box A_i=-j_i$, $\partial_i A_i=\psi$, $\partial_4 A_i=0$, $\partial_4\psi=0$, with $\Phi=(2x^5\psi/\alpha)$ ($c=1$), j_i being proportional to T_{i5}, where $T_{\mu\nu}$ is an energy momentum current tensor describing the fields other than A_i, ψ which may be present.

* Supported by ONR contract.

QA5. Parameters and Constraints in Quantized Field Theories.* PETER G. BERGMANN, *Syracuse University.*—Covariant field theories can be brought into a canonical formulation either with or without the introduction of so-called parameters. In the latter method, the four space-time coordinates become automatically q-numbers, and their canonical conjugates are the energy and linear momentum densities.[1] The algebraic constraints in a parametrized theory are four more than in the other formalism. It will be shown that both in the classical and in the quantized theory, parametrization is a reversible procedure in the sense that the appearance of additional q-numbers is more apparent than real and can be reversed by an appropriate unitary transformation. Work in progress at present intends to examine the effect that singularities of the field may have.

* Supported by ONR.
[1] P. G. Bergmann and J. H. M. Brunings, Revs. Modern Phys. **21**, 480 (1949).

QA6. On the Range of Application of the Lagrange and Hamilton Formalisms. PETER HAVAS, *Lehigh University.*—Lagrange's and Hamilton's formalism are usually regarded as encompassing only forces, Q_i, which are either derivable from a potential or for which a function U can be found such that $Q_i=d/dt(\partial U/\partial\dot{q}_i)-\partial U/\partial q_i$ (e.g., the Lorentz force). The general conditions under which the equations of motion are the euler-lagrange equations of a variational principle have been investigated by several authors,* and a rather stringent set of conditions was established. It was, however, apparently overlooked that there are cases in which these conditions are not fulfilled originally, but can be satisfied by multiplying the equations of motion by a suitable "integrating factor." In particular, the one-dimensional equations of motion under arbitrary velocity-dependent forces are always derivable from a variational principle. The hamiltonian can be obtained from the lagrangian as usual. If the forces do not depend explicitly

on the time, it is still a constant of motion, although it is not the energy. Cases of motion in more than one dimension, which can be brought under this scheme, and the problem of quantization will also be discussed.

* A. Hirsch, Math. Ann. 50, 429 (1898) and references given there.

QA7. On the Second Quantized Dirac Theory of Spin ½ Particles. R. K. OSBORN, *Case Institute of Technology*.—The second-quantized Dirac hamiltonian for free electrons is transformed by a canonical transformation to a representation in which the positive and negative energy wave operators are separately represented by two component operators. The transformation employed is the second-quantized analog of the one derived by Foldy and Wouthuysen[1] in their discussion of the one-particle dirac theory and its non-relativistic limit. This transformation is then applied to the wave operators and the hamiltonian in the second-quantized, charge-conjugate formalism for Dirac particles. The wave operators for positrons and electrons become linearly-independent two-component operators, and the hamiltonian separates into an electron and a positron part, each of which contains only the corresponding two-component wave operators. It is shown that the independent wave operators for electrons and positrons anticommute. Work is in progress to investigate the interactions between spin ½ particles and the electromagnetic and meson fields in this representation.

[1] L. L. Foldy and S. A. Wouthuysen, Phys. Rev. 78, 29 (1950).

QA8. Multiple Quantization. A. E. SCHEIDEGGER, *Queen's University*.—An inspection of the canonical quantization procedure shows that it is essentially an algebraic one. The time-dependent generalized coordinates q_k, which are classically subject to the lagrangian differential equations, are reinterpreted as (time-dependent) hermitian operators in a hilbert space. Thus, it is seen that quantization leads from a time-dependent hilbert vector (the q_k's) to another time-dependent hilbert vector, which suggests that it is a "circular" process, and may be repeated. The ordinary Schrodinger equation, however, is not suitable for further quantization, since reality is essential for a quantizable hilbert vector. Also, the Schrodinger equation contains only first-order time derivatives, the analogous lagrangian equations, however, contain second-order ones. Both facts can be taken care of by constructing differential equations for the real and imaginary parts of the Schrödinger function. These equations are then analogous to the lagrangian equations from which the quantization was started. They form the closing link in the quantization as a "circular" process. This method is applied to obtain the third quantization of the Schrödinger-Gordon equation. Speculations that an infinitely multiple quantization of classical equations may yield the true description of nature, are suggested.

QA9. Gauge-Independent Quantum Electrodynamics. F. J. BELINFANTE AND J. S. LOMONT, *Purdue University*.—Pauli's gauge-independent quantum electrodynamics (*Handbuch der Physik*) not quantizing longitudinal fields, earlier generalized to include positon theory, has been reformulated in interaction representation. The interaction operator W depends on the complete surface σ on which it operates. We defined W for flat surfaces only, as $(\mathbf{E}_{II}^2/8\pi)+(\mathbf{E}_{II}.\mathcal{E}/4\pi)-\mathbf{j}.\mathcal{A}$ in a Lorentz frame in which σ is t=constant. Here, $\{\mathcal{E}, \mathcal{B}\}$ is the quantized field tensor for transverse photons in interaction representation; the current density four-vector $\{\rho, \mathbf{j}\}$ is expressible in terms of spinors ψ and $\bar{\psi}$; $\mathcal{A}(x)=\int d^3x'\ \mathrm{curl}'\mathcal{B}(x')/4\pi r$ and $\mathbf{E}_{II}(x)=-\nabla V(x)=-\nabla\int d^3x'\rho(x')/r$ are given functionals of the gauge-independent field variables on σ. The integrability of the generalized Schrödinger equation for translations and rotations of σ (time dependence and Lorentz transformation of $\Psi[\sigma]$) is proved. In Heisenberg representation, ψ is no longer a spinor, and not $\{\mathcal{E}, \mathcal{B}\}$ but $\{\mathbf{E}, \mathcal{B}\}$ forms a tensor, where $\mathbf{E}=\mathcal{E}+\mathbf{E}_{II}$, thence $\mathcal{E}=\mathbf{E}_{\perp}$. Omission of self-energy from $(\mathbf{E}_{II}^2/8\pi)$ disturbs integrability and Lorentz invariance of the Schrödinger equation, unless one simultaneously postulates, as in integro-causal quantum field theory, the unallowability of self-interaction through virtual photons from $(\mathbf{E}_{II}.\mathcal{E}/4\pi)-\mathbf{j}.\mathcal{A}$.

QA10. On Coherent Scattering Processes in Liquids. LOUIS GOLDSTEIN, *Los Alamos Scientific Laboratory*.—The coherent scattering structure factor of liquids for x-rays and slow neutrons will be shown to determine completely both the correlation function and the direct local interaction function of liquids, quantities of which are the only operating elements of the general static liquid models of Ornstein and Zernike. Of these functions only the former has been derived, so far, from the data accumulated essentially on the coherent scattering of x-rays by liquids. It will be shown that the directly available experimental structure factors completely determine the even moments of these molecular distribution functions. The zeroth moment of the correlation function augmented by unity is essentially the liquid concentration fluctuation which determines its isothermal compressibility. These quantities thus become directly derivable from the structure factor measurements without any arbitrary and uncertain manipulations. In terms of the liquid model, a straightforward method leads to the total incoherent slow neutron scattering cross sections in liquids. These should yield important information on their energy spectrum not available through other types of scattering processes, such as x-rays, for instance.

QA11. Phase Space Description for the Multiple Scattering of Waves. WILLIAM L. LEHMANN AND MELVIN LAX, *Syracuse University*.—The solution of a wave problem leads to a wave function $\psi(r; r_1, r_2, \cdots r_n)$ describing the amplitude of radiation at r due to scatterers at $r_1, r_2, \cdots r_n$. One prefers, however, to obtain the answer in terms of the density and directionality of the radiation *versus* position, i.e., in terms of the density of radiation in phase space. The space density of the radiation is, in fact, described by $\langle|\psi(r; r_1, \cdots r_n)|^2\rangle$, where an average is taken over an ensemble of scatterer positions. A simultaneous description of the density of the radiation in ordinary space and momentum space may not seem to be possible because of the Heisenberg uncertainty principle. There is, in fact, no *unique* phase space description. Following a suggestion of Wigner's,[1] it is possible, however, to introduce a phase space density $F(k, r)$: $F(k, r)=(2\pi)^{-3}\int \exp[i\mathbf{k}\cdot\rho]d\rho\langle\psi^*(r+\frac{1}{2}\rho)\psi(r-\frac{1}{2}\rho)\rangle$. An integral equation, found previously by one of us, for $\langle\psi^*(r')\psi(r)\rangle$ can now be transformed into an integral equation for $F(k, r)$. The significance of the latter integral equation will be discussed.

[1] E. P. Wigner, Phys. Rev. 40, 749 (1932). See also J. E. Moyal, Proc. Cambridge Phil. Soc. 45, 1, 99 (1949).

QA12. Spin-Spin Interaction in the Spectrum of FeIII. R. E. TREES, *University of Pennsylvania*.—The term intervals of one quintet and seven triplets of the d^5 configuration of FeIII[1] have been analyzed in an effort to detect effects of spin-spin interaction. The mean deviation of the experimentally given intervals from the Lande interval rule was 44 cm^{-1}. Correction for non-diagonal spin-orbit elements reduced this to 9 cm^{-1}. The value of the Lande radial parameter was $\zeta_d=429\pm16$. The elements of spin-spin interaction were calculated for d^5 configurations, using methods of G. Racah. The spin-spin interactions are determined by two radial parameters, M_0 and M_2, defined by Marvin.[2] These were found by least squares, using the deviations from the Lande rule not accounted for by non-diagonal spin-orbit interactions as the data to be fitted, to have the values $M_0=0.304$ and $M_2=0.018$. The correction for spin-spin interaction reduced the residual deviation of 9 cm^{-1} to 4 cm^{-1}. It is concluded that spin-spin

interactions have an appreciable, though small, effect on the term intervals in this spectrum.

[1] B. Edlen and P. Swings, Astrophys. J. 95, 532 (1942).
[2] H. H. Marvin, Phys. Rev. 71, 102 (1947).

QA13. An Equivalence of Classical and Quantum Mechanical Treatments of Radiation. M. H. HULL, JR., *Yale University.**—It is well known that the results of quantum-electrodynamics are in close agreement with a classical model employing radiation oscillators. The results of Wigner and Weisskopf have been generalized by Breit, who showed that for dipole radiation and for photons with energies within the natural line breadth the similarity of results can be explained in terms of the possibility of identifying suitable multiples of classical dynamical variables (amplitude of transition oscillator, amplitudes of radiation oscillators) with quantum probability amplitudes (those for the atomic excited state and for the excitation of radiation oscillators). In the present paper, this correspondence is extended to cases including retardation effects and multipole radiation. It is shown that the equivalent classical current systems can always be set up.

* Assisted by the joint program of the ONR and AEC.

QA14. Heat Conduction In Simple Metals.* MARTIN L. STORM,** *New York University.*—The partial differential equation of heat conduction is a non-linear equation when the temperature dependence of the thermal parameters (i.e., the thermal conductivity K, and S, the product of the density and the specific heat at constant pressure) is taken into account. It is shown that a mathematical condition for the transformation to linear form of the one-dimensional, non-linear, partial differential equation of heat conduction is the constancy of $[1/(KS)^{\frac{1}{2}}]d/dT \log(S/K)^{\frac{1}{2}}$. This discovery is the motivation for an investigation of the relations between the thermal parameters of simple metals on the bases of the theory of solids and available experimental data. It is found that KS is essentially constant, its variation with temperature being much less than that of either K or S considered separately. It is also shown as a result that the condition for the above-mentioned transformation is valid for simple metals. Applications of the transformed equation to the solution of problems in heat conduction are considered.

* Work supported by the ONR and the Office of Air Research.
** Now at the Naval Ordnance Laboratory, White Oak, Maryland.

FRIDAY AFTERNOON AT 2:00

Shoreham, Terrace Room

(K. LARK-HOROVITZ presiding)

Crystals and Semiconductors

R1. New Methods of Phase Determination in X-Ray Crystal Analysis.* RAY PEPINSKY AND WILLIAM COCHRAN,† *The Pennsylvania State College.*—Two new methods of phase determination in x-ray analysis have been explored on X-RAC. Both make use of knowledge of the known bounds and expected shape of a density function. Method I involves the use of Cesaro means, temperature-corrected fourier coefficients, or other techniques for reducing the number of coefficients involved in a synthesis. The characteristics of Fejer's and Poisson's kernels, and the kernel $(1+\cos x)^n$, are discussed in this connection. Method II involves a modification of an unpublished method of D. Sayre, already successfully applied by him. Sayre's method utilizes the properties of the squared density-function, and the relations of this to the original function. It can be strengthened, by considering $F(h, k)/f(h, k) = \bar{F}(h, k)$'s as fourier coefficients of a *partial* sharpened-up density function ρ_n, formed from a few of the largest $\bar{F}(h, k)$'s. The condition that ρ_n must have positive regions which go much higher than the negative can be imposed by requiring $\int \rho_n^2 dA$ = maximum positive. When the number of terms is small, this requires $s(h, k) = s(h^1, k^1)s(k+h^1, k+k^1)$, where $s(h, k)$ indicates the sign of $F(h, k)$. The method has been applied successfully to the determination of the previously-unknown structure of glutamine.

* Development supported by ONR.
† Rockefeller Foundation Fellow.

R2. Lithium-Ammonium Tartrate, a New Ferroelectricum. WALTER J. MERZ,* *The Pennsylvania State College.*—We have found that $LiNH_4C_4H_4O_6 \cdot H_2O$ becomes ferroelectric at low temperatures and has a Curie point at about 106°K (−167°C). Although this crystal is strongly related crystallographically and chemically to rochelle salt ($KNaC_4H_4O_6 \cdot 4H_2O$), we observe the following principal differences. The ferroelectric direction is along the b axis, whereas in rochelle salt it is along the a axis. There is just one molecule of water of crystallization instead of the four which were considered as a main feature in rochelle salt. The Curie point is much lower (for rochelle salt θ is at room temperature). We measured the dielectric constants in all 3 directions. They all show a value of only about 9 at room temperature. ϵ_a and ϵ_c stay about constant when the temperature is lowered, whereas ϵ_b has a sharp peak at $\theta = 106$°K. The crystal also shows the typical minimum in the resonance frequency at θ, since it becomes very soft. Hysteresis loops show, quite in analogy to other ferroelectrics, the onset of a spontaneous polarization at θ and an increase in this polarization when the temperature is lowered. We are now also investigating other crystals of the same alkali tartrate group.

* Investigation supported by Office of Air Research.

R3. Neutron Diffraction Studies on Vitreous Silica.* W. O. MILLIGAN, *The Rice Institute*, H. A. LEVY, AND S. W. PETERSON, *Oak Ridge National Laboratory.*—Neutron diffraction patterns of transparent vitreous silica plates have been obtained at wavelengths of 1.21A (sodium chloride monochromator) and 0.764A (single copper crystal monochromator). A neutron crystal spectrometer similar in design to that of Wollan and Shull was employed. Six well-defined diffraction maxima were observed, in contrast to a single broad peak and three ill-defined peaks observed by Warren with x-rays; but, in general, agreement with the several diffraction peaks reported by Melkonian and Ruderman from neutron velocity selector transmission studies. The intensities were corrected for absorption and were converted to absolute intensities, using diffraction peaks from nickel powder. Data from both wavelengths agree closely, except at low angles near the incident beam. The scattering curve is similar to that of Webber for soda-lime glass. A radial distribution curve has been calculated for vitreous silica, using the method of Warren. Integrations were carried out with an IBM calculator. The radial distribution curve shows five well-resolved peaks at

distances of about 1.58, 2.56, 3.02, 4.0, and 5.1A. Less well-defined peaks were observed at 5.9, 6.6, 7.4, 9.0, and 9.7A. The positions and areas of the peaks are in close agreement with the results of Warren and co-workers. The detection of additional peaks and the observed higher resolution suggest that neutron diffraction studies offer advantages over x-ray studies for the examination of amorphous and colloidal materials. The greater usefulness of neutrons is attributed primarily to the angular independence of neutron scattering cross sections.

* Work done in part under the research participation program of the Oak Ridge Institute of Nuclear Studies for the AEC.

R4. Directional Breakdown Effects in Ionic Crystals.* ELMER L. OFFENBACHER AND HERBERT B. CALLEN, *University of Pennsylvania.*—Although the breakdown strength of ionic crystals is independent of crystal orientation, the breakdown paths proceed in definite crystallographic directions which are determined by the temperature. Von Hippel has suggested a breakdown mechanism, involving slow electrons, which is able to predict breakdown strengths fairly satisfactorily. As a resolution of the directional paradox he has also suggested that the breakdown paths depend upon the behavior of fast electrons. We have accordingly attempted to develop a specific mechanism leading to the appropriate directional sensitivity of fast electrons. The directional asymmetry of the Brillouin zone of the phonons and the selection rules for electron-phonon collisions caused the total collision probability to depend on electron direction, and the electron tends to migrate in the direction of smallest scattering probability. We have computed the differences in collision probability for various directions and find that the 111, 110, and 100 directions are each preferred in specific energy ranges. Plausible criteria for the selection of the dominant direction at a given temperature lead to rough agreement with the observations of J. W. Davisson, which, however, are insufficient to provide a decisive test of theory.

* Supported in part by ONR.

R5. The Absorption Spectra of Pure and Colored Alkali Halide Crystals.* D. L. DEXTER,† *University of Wisconsin.*—The absorption cross section per electron is calculated for ultraviolet radiation in NaCl at the first exciton band, at the exciton series limit, at the *F*-band, and at the *F*-center series limit. The *F*-center wave functions used are similar to those determined by Tibbs.[1] The exciton wave function is taken to be that of an electron bound to a stationary positive hole, multiplied by the lattice function of Tibbs.[1] The continuum wave functions used are hydrogenlike continuum wave functions spread out by the dielectric constant of the crystal. The calculated cross sections are in agreement with experiment within a factor of about 2. This agreement tends to verify Mott's suggestion that the small hump or plateau seen at about 0.6 ev above the *F*-band in some absorption data[2] represents the series limit of transitions of the *F*-center electron. Qualitative extension of these results will be made to other crystals.

* Research supported in part by ONR.
† Now at the University of Illinois.
[1] S. R. Tibbs, Trans. Faraday Soc. **35**, 1471 (1939).
[2] F. G. Kleinschrod, Ann. Physik **27**, 97 (1936).

R6. Electromotive Force in Illuminated Alkali Halide Crystals Caused by a Gradient in the Color Center Density. GERHART GROETZINGER AND SAM BARILE, *Lewis Laboratory, NACA.*—Color centers with a density gradient were produced in thirty NaCl and KBr crystals in two ways: (1) Crystals of approximate dimensions of 1×1×0.5 cm were exposed for 15 minutes to x-rays produced by a beryllium window tube operated at 50 kv and 30 ma, the x-rays entering through one of the square faces. (2) Crystals were colored by the pointed cathode method and subsequently cut to the above-mentioned dimensions in a way that [as in (1)] a gradient essentially in the direction of the small dimension was obtained. Emf's in the crystals in the direction of the gradient produced by uniform illumination with white light (tungsten ribbon filament lamp) were determined in the following way: using a vibrating reed electrometer effectively shunted by a 10^8-ohm resistor as a null-indicator, the voltage between two Aquadag electrodes on the square faces was measured by compensation. Potential differences of about one-tenth of a volt were thus observed, the more densely colored part of the crystal being positive. The emf's are indicative of a difference in concentration and/or mobility of conduction electrons and holes.

R7. Study of X-Ray Induced Optical Absorption Bands in CaF_2. SAM BARILE, *Lewis Laboratory, NACA* (Introduced by G. GROETZINGER).—The absorption spectrum of CaF_2 crystals containing color centers was investigated as a function of temperature and time elapsed after having been irradiated with x-rays under various conditions. Crystals, 0.5 cm thick, were exposed to x-rays from a beryllium window tube operated at 50 kv and 30 ma for as much as 20 hr. Under these conditions saturation of the color center density is reached. Absorption measurements were made with a Beckman spectrophotometer in the range between 2100 and 10,000A. A fourth weak absorption band previously unobserved has been found near 2280A. The intensities of the four absorption bands of crystals irradiated at room temperature decreased (within experimental error) to the same extent after being heated at various temperatures for various time intervals. Furthermore, no difference in the relative intensities of the bands was found between crystals irradiated at room temperature and elevated temperatures (200°F).

R8. A Theory of the λ-Point Transition in Ammonium Chloride. N. K. POPE, *Chalk River Laboratory.*—The potential energy of an ammonium ion due to its angular displacement from an equilibrium position is expanded in a series of spherical top wave functions. Those terms in the potential energy which depend on the angular displacements of other ammonium ions are replaced by their average values. The number of terms in the potential energy is greatly reduced by applying symmetry conditions for the ammonium ion and for the lattice. The first angle dependent term in the potential energy has T_d^1 symmetry; the second has O_h^1 symmetry; the third term has higher symmetry and tends to bind the ammonium ion to the equilibrium orientation which is common to the first two terms. It is shown classically that such a potential function gives rise to a transition which corresponds to a sudden increase in the angular motion of the ammonium ions. This result is consistent with the neutron diffraction measurements by G. H. Goldschmidt and D. G. Hurst[1] on ND_4Cl.

[1] G. H. Goldschmidt and D. G. Hurst, Paper HA11, Bull. Am. Phys. Soc. **26**, No. 1, 58 (1951).

R9. Electrical Properties of Titanium Dioxide Semiconductors. R. G. BRECKENRIDGE AND W. R. HOSLER, *National Bureau of Standards.*—Measurements have been made of the Hall effect and resistivity of titanium dioxide that had been made semiconducting by reduction in hydrogen for various times and temperatures. The samples included ceramics and rutile single crystals oriented in both the *a* and *c* directions. The temperature range covered was from −190°C to 500°C. The results of the Hall effect measurements indicate that the charge carriers are electrons. The number of electrons in these strongly reduced materials approaches a constant value of the order of 10^{17} to 10^{18}/cm³ at low temperatures and increases by a factor of *ca* 10^2 as the temperature is raised to 500°C. The resistivity of the samples varies slowly with temperature over the same range, usually passing through a broad maxima. No major differences were noted between the densely

fired ceramics and the single crystal samples in either orientation, although the electron mobility in the crystals is somewhat smaller in the a than in the c direction. The observed mobilities in all cases were low.

R10. Effect of Impurity Content on the Specific Heat of Germanium.* I. ESTERMANN AND J. R. WEERTMAN, *Carnegie Institute of Technology.*—It has been reported[1] that the specific heat of Ge has an anomaly at 80°K. Since Ge forms a monatomic lattice of the diamond type, it was difficult to associate the excess specific heat with any known lattice process. Preliminary measurements of the specific heat curve of Ge carried out by one of us in 1944 on a pure Ge sample failed to show the reported anomaly. New measurements with much higher precision were carried out with a very pure and a less pure sample of 10^{20} impurity centers per cm³. The results show that the excess of specific heat of the impure over the pure sample is no more than the order of one percent. No anomaly of the type reported by Simon and Critescu was found.

* Assisted by the ONR and the Research Corporation.

[1] S. Critescu and F. Simon, Z. physik. Chem. (B)25, 273-282 (1934).

R11. The Photo-Voltaic Effect of Survace $P-N$ Barriers in Germanium. B. J. ROTHLEIN, *Sylvania Electric Products, Inc.*—Surface barriers on germanium can be made having an exceptionally high photo-voltaic response. These barriers can be used as a cell possessing high signal to noise ratio owing to their use at zero current. The shape of the spectral response curve at room temperature is similar to what has previously been reported for germanium;[1] the decay in response with increased chopping frequency, however, appears somewhat greater. The characteristics of this effect will be described.

[1] M. Becker and H. Y. Fan, Phys. Rev. 78, 301 (1950).

R12. Germanium Rectifier Characteristics. R. N. HALL, *General Electric Research Laboratory.*—Rectifiers made from purified germanium wafers whose opposite faces are strongly doped with donor and acceptor impurities have electrical characteristics which follow a simple theoretical formula over a current range extending from the saturation reverse current to several hundred amperes per cm² in the forward direction in the temperature range between 200° and 400°K. Since the region in which holes and electrons recombine is the well-defined volume between the impurity layers, the calculation of the diode current is not difficult and is given by

$$I=(q\ln/\tau)[\exp(qv/2kT)-1].$$

The high purity region has a thickness l, while n and τ are the concentration and lifetime of the carriers in intrinsic germanium. The factor of ½ in the exponential results from the use of a volume recombination rate which is essentially linear in the concentrations of holes and electrons. The rectifier characteristics indicate that the direct recombination of holes and electrons, which varies as the product of their concentrations, becomes appreciable only at very high forward currents. The experiments give a volume recombination time for the linear process of 0.0002 sec at room temperature, while the lifetime for direct recombination is of the order of 0.03 sec.

R13. Motion of Vacancies in a One-Dimensional Homogeneous Lattice. YÜ-CHANG HSIEH* AND I. BLOCH, *Vanderbilt University.*—An atom in a perfect crystal is assumed to be in a stationary one-dimensional potential well. When one of its neighbors is removed, the atom finds itself in a wider well with a "hump" in the middle; its wave function then becomes a wave packet which moves back and forth between the two lattice sites. The motion of this wave packet is related to the coefficient of diffusion of "holes" in the lattice, and hence to the coefficient of self-diffusion of the substance composing the lattice. This crude model indicates that even at low temperatures "holes" diffuse rather rapidly, because of the tunnel effect.

* Now at Purdue University, Lafayette, Indiana.

R14. Photo-Conductivity of Trapped Electrons in the Alkali Halides. J. J. OBERLY, *Naval Research Laboratory.*—The photo-conductivity of the color center bands (F, R, M, N, S) associated with trapped electrons in alkali halide crystals has already been reported.[1] Quantitative measurements have now been made at room temperature on crystals irradiated with soft x-rays to obtain the relative photo-current per absorbed photon for the various types of centers. This relative response is proportional to the quantum yields if the ranges (Schubwege) of the electrons freed from the various centers are the same. In KBr all of the bands are found to be photo-conductive after their formation by x-rays or by optical bleaching of other bands. However, both the F- and M-bands can be made relatively non-photo-conductive by bleaching them with F- and M-light, respectively. The "soft" fractions of the bands which bleach readily are the photo-conductive portions, while the residual "hard" absorption is caused by non-photo-conductive centers. The peak absorption wavelength of the hard F centers is slightly shorter, corresponding to the B-band of Petroff. The hard type of center has not been observed for the other bands which is an indication of the similarity of the F- and M-bands on one hand and of the R- and N-bands on the other.

[1] J. J. Oberly and E. Burstein, Phys. Rev. 79, 217 (1950).

FRIDAY AFTERNOON AT 2:15

Shoreham, Main Ballroom

(A. O. NIER presiding)

Nuclear Masses, Abundances, and Magnetic Moments

RA1. Atomic Masses in the Region About Mass 40. T. L. COLLINS, ALFRED O. NIER, AND WALTER H. JOHNSON, JR., *University of Minnesota.*—The double-focusing mass spectrometer already described[1] has been used to measure masses of isotopes near $M=40$ by the doublet method, comparisons being made with hydrocarbons. H^1 and C^{13} were taken as 1.008165±4 and 12.003842±6, respectively.[2] The isotopes measured and the packing fractions ($\times 10^4$, all negative) computed were as follows: S^{33}, 5.41; S^{34}, 6.24; Cl^{35}, 5.71; Cl^{37}, 6.03; A^{36}, 5.83; A^{38}, 6.59; K^{39}, 6.12; K^{41}, 6.10; Ca^{42}, 6.60; Ca^{43}, 6.36; Ca^{44}, 6.99; Ca^{45}, 6.72; Sc^{45}, 6.62. The probable errors varied between 0.01 and 0.02. Fluctuations from nuclide to nuclide follow approximately those predicted by the Bohr-Wheeler formula except about Ca^{40} and Ca^{48}, where the nuclides are actually somewhat more stable than the formula predicts. The discrepancy is especially marked for Ca^{48}.

[1] A. O. Nier and T. R. Roberts, Phys. Rev. 81, 507 (1951).
[2] A. O. Nier, Phys. Rev. 81, 624 (1951).

RA2. Masses of Th^{232} and U^{235}. GEORGE S. STANFORD AND HENRY E. DUCKWORTH, *Wesleyan University.**—The mass spectrograph has been used to photograph doublets at mass number 58 consisting of singly-charged Fe^{58} and quadruply-charged Th^{232}, at mass number 116 consisting of singly-charged Sn^{116} and doubly-charged Th^{232}, and at mass number 119 consisting of singly-charged Sn^{119} and doubly-charged U^{238}. The following packing fraction differences were measured: Th^{232}—Fe^{58}, $\Delta f = 13.17 \pm 0.06$: Th^{232}—Sn^{116}, $\Delta f = 9.89 \pm 0.03$: and U^{238}—Sn^{119}, $f = 10.24 \pm 0.03$. Using the known packing fractions[1] of Fe^{58}, Sn^{116}, and Sn^{119} of -8.43 ± 0.07, -5.30 ± 0.05, and -4.79 ± 0.05, respectively, the packing fraction of Th^{232} is found to 4.64 ± 0.10 from the Th—Fe comparison, 4.59 ± 0.06 from the Th—Sn comparison, and that of U^{238} is found to be 5.45 ± 0.06. The corresponding masses are $Th^{232} = 232.1070 \pm 0.0012$ and $U^{238} = 238.1297 \pm 0.0015$. Some remarks will be made concerning the agreement between these mass values and that[2] of $Pb^{208} = 208.0422 \pm 0.0015$ on the basis of radioactive decay data.

* Supported by the AEC.
[1] To be published.
[2] H. E. Duckworth and R. S. Preston, Phys. Rev. (to be published).

RA3. Masses of Xe^{129} and Xe^{132}. CORT L. KEGLEY AND HENRY E. DUCKWORTH, *Wesleyan University.**—The mass spectrograph has been used to photograph a triplet at mass number 43 consisting of singly-charged C_3OH_3 and C_4H_7 and triply-charged Xe^{129}, and a second triplet at mass number 44, consisting of singly-charged CO_2 and C_3OH_4 and triply-charged Xe^{132}. The following packing fraction differences were measured: $C_3H_7 - Xe^{129}$, $\Delta f = 20.15 \pm 0.02$; $C_3OH_3 - Xe^{129}$, $\Delta f = 11.68 \pm 0.025$; $C_3OH_4 - Xe^{132}$, $\Delta f = 13.08 \pm 0.025$; $CO_2 - Xe^{132}$, $\Delta f = 4.90 \pm 0.02$. Using the masses[1] $H^1 = 1.008147$ and $C^{12} = 12.003794$, the packing fractions of Xe^{129} and Xe^{132} are computed to be -4.23 ± 0.02 and -3.99 ± 0.05, respectively, corresponding to the masses $Xe^{129} = 128.94543 \pm 0.00026$ and $Xe^{132} = 131.94733 \pm 0.00066$. It is hoped that masses will also be reported for Kr^{82}, Kr^{84}, and Kr^{86}. Typical mass spectra will be shown.

* Supported by the AEC.
[1] K. T. Bainbridge (private communication).

RA4. Nuclear Reaction Energies and Nuclear Masses as Integral Multiplies of a Natural Unit of Mass and Energy. ENOS E. WITMER, *University of Pennsylvania.*—About a year ago the writer pointed out that one-eleventh of the rest mass of the negative electron appeared to be a natural unit of mass and energy for nuclei and elementary particles not subject to β-decay. This unit of mass and energy was designated *the prout*. Furthermore, it was pointed out that the neutron and many other nuclei subject to β-decay appeared to follow the integral rule. Recently, "Energy levels[1] of light nuclei, III" appeared, giving a more accurate and extensive set of values for nuclear reaction energies. These data as well as other recent data support the hypothesis stated above very well. These results are self-consistent, so that it is possible to make a table of nuclear masses in prouts up to about Ne^{20}. Because of the slight uncertainty in M_p/m this has been done both with 20196 prouts and 20197 prouts as the proton mass. In the second case the nuclear masses in prouts are A prouts larger. But the *nuclear masses in mass units* differ only in the sixth or seventh decimal places in the two cases, since O^{16} is standard.

[1] Hornyak, Lauristen, Morrison, and Fowler, Revs. Modern Phys. 22, 291 (1950).

RA5. A New Method for the Measurement of the Isotopic Abundance of Solids. H. SOMMER AND J. A. HIPPLE, *National Bureau of Standards.*—Several measurements of isotopic abundance have been made on a modified Dempster mass spectrometer to demonstrate a method of using electrical detection with a high frequency vacuum spark source. The use of electrical detection is made possible by measuring the ratio of the selected ion current to a representative sample of the total ion current produced by the spark source. Although the emission from the source fluctuates erratically owing to the nature of the spark, the observed ratio remains essentially constant. The successful use of this instrument for quantitative analysis of solids has been previously described.[1] Tentative results of the measurement of the isotopic abundance of nickel, copper, and magnesium yield values with accuracies comparable to other recently published results. For example, the value obtained for the isotopic abundance of copper in atom percent is: $Cu^{63} = 68.94 \pm 0.26$; $Cu^{65} = 31.06$. The results obtained for magnesium agree closely with those of Hibbs and Redmond.[2]

[1] Gorman, Jones, and Hipple, to be published in Anal. Chem.
[2] R. F. Hibbs and J. W. Redmond, Carbon and Carbon Chemicals Corporation Report Y-290, November 24, 1948.

RA6. Hyperfine Structure of Te^{123} and Te^{125}. JOHN S. ROSS AND KIYOSHI MURAKAWA, *University of Wisconsin.**—Hyperfine structure spectrograms obtained with a liquid-air cooled hollow-cathode source using enriched isotopes show that the Te^{125} I line $\lambda 2530.7 (5p^4\ ^3P_1 - 5p^3 6s\ ^5S_2)$ consists of two components 0.113 cm^{-1} apart, the shorter frequency being the stronger. Thus, the magnetic moment of Te^{125} is negative, since Te^{125} and Te^{123} are known to have spin $\frac{1}{2}$. The line $\lambda 2385.7 (5p^4\ ^3P_1 - 5p^3 6s\ ^3S_1)$ was found to be single to an accuracy of 0.03 cm^{-1}. Using these data and appropriate hyperfine structure formulas,[1] the value $\mu(Te^{125}) = -0.74 \pm 0.20$ n.m. was obtained. From the large splitting of the Te II lines $\lambda 5449$ and $\lambda 5311$ the ratio μ^{125}/μ^{123} was found to be $1.188 \pm .010$, which gives the result $\mu(Te^{123}) = -0.62 \pm 0.20$ n.m. This indicates that both nuclei are probably in an $S_{\frac{1}{2}}$ state, which is in agreement with the prediction of Mayer's nuclear shell theory.

* Supported by the ONR.
[1] M. F. Crawford and L. A. Wills, Phys. Rev. 48, 69 (1935).

RA7. Hyperfine Structure of Tungsten.* JOHN A. VREELAND AND KIYOSHI MURAKAWA, *University of Wisconsin.*—The hyperfine structure of the tungsten spectrum was examined with a Fabry-Perot etalon, using two samples enriched in W^{180} and W^{182}, respectively. The structure of W^{183} in more than twenty-five arc lines was measured, and the splittings of more than twenty terms determined. The value of the magnetic moment of W^{183} was found to be $+0.08 \pm 0.02$ n.m. The isotopic displacement effect in the arc lines gave $\Delta(W^{186} - W^{184}) : \Delta(W^{184} - W^{183}) : \Delta(W^{183} - W^{182}) = 1.00 : 1.13$ $(\pm 0.01) : 1.02$ (± 0.02).

* Supported by the ONR.

FRIDAY AFTERNOON AT 2:15

NBS, Materials Testing

(W. J. LYONS presiding)

High-Polymer Physics and Biophysics

S1. Apparatus for Determining the Dielectric Behavior of Liquids, Gels, and Solids at Audiofrequencies. EDWIN R. FITZGERALD* AND ROBERT F. MILLER, *B. F. Goodrich Company Research Center.*—Apparatus has been developed for determining the dielectric behavior of liquids, gels, and solids of the type encountered in plasticized polymer systems over the entire range of plasticizer concentration. A combination dielectric cell with plane, parallel electrodes and a guard ring, suitable for use from 15 to 15,000 cps at temperatures from −100 to +150°C has been constructed and used in measurements on plasticized polyvinyl chloride and other systems. Included also is the variation of dielectric constant and loss factor with frequency and temperature for dimethyl thianthrene, tricresyl phosphate, di-2-ethyl hexyl phthalate, a polyvinyl chloride—dimethyl thianthrene gel (90 percent dimethyl thianthrene by volume), and a butadiene-acrylonitrile copolymer. Activation energies of dipole rotation are found to be 46.0 kcal/mole (−4 to −20°C) for dimethyl thianthrene, 41.8 kcal/mole (−31 to −44°C) for tricresyl phosphate, and 24.2 kcal/mole (−51 to −71°C) for di-2-ethyl hexyl phthalate. These compare with activation energies of viscous flow of 46 kcal/mole (at −3°C) for dimethyl thianthrene and 25 kcal/mole (at −44°C) for di-2-ethyl hexyl phthalate determined from falling ball and rotating cylinder viscosity measurements. The agreement between activation energies of viscous flow and dipole rotation is thus marked; but it must be pointed out that the activation energies for viscous flow decrease with rising temperature, while there was no observed change in activation energies of dipole rotation over the narrow temperature ranges in which they were determined.

* Now Physics Department, University of Wisconsin.

S2. A Rheometer for Measuring Dynamic Viscosities and Rigidities.* H. MARKOVITZ, P. M. YAVORSKY, R. C. HARPER, JR., L. J. ZAPAS, AND T. W. DEWITT, *Mellon Institute.*—The design of this instrument as used for liquids is similar to that of the coaxially cylindrical elastometer of Goldberg and Sandvik,[1] but differs from theirs in that it can also be adapted to solids and in that its use is not limited to resonant frequencies. The rheometer has a mechanical drive which can cause oscillations at the fixed angular amplitude of 1° and at frequencies from 1 to 100 cycles per second. The amplitude and phase difference of the response are obtained from the electrical signals produced by coils attached to the moving elements and oscillating between the poles of permanent magnets. Measurements can be made from −60°C to 100°C. With newtonian liquids the behavior of the instrument is in good agreement with that predicted by theory. Measurements with non-newtonian liquids indicate that amplitude of vibration here is low enough so that the results are independent of rate of shear. Results obtained with solid polymers are similar to those reported for like materials by other techniques.

* Work supported by the Office of Rubber Reserve, Reconstruction Finance Corporation, Washington, D. C.

[1] H. Goldberg and O. Sandvik, Anal. Chem. **19**, 123 (1947).

S3. A Stress-Temperature Study of Polyethylene. S. LEONARD DART, *American Viscose Corporation.*—A series of samples was prepared by relaxing a highly stretched polyethylene monofilament various amounts. This series was then used in a stress-strain-temperature-length study. With increasing relaxation, the linear thermal expansion coefficient changed from a large negative value to a large positive maximum and then decreased to a stable value. A stress-strain breakdown of this series shows a large negative entropy force at low stretches changing to a large positive one at high stretches. The internal energy force generally shows a behavior inverse to this. A comparison is made between the entropy force as measured by the stress-temperature method and that calculated from the linear thermal expansion coefficient and the Young's modulus. A plot of the initial Young's modulus of each member of the series against extension shows good agreement with kinetic theory and yields an "internal pressure" of about 1000 atmospheres.

S4. Combined Thermal and Primary Ionization Effects on a Bacterial Virus.* W. R. ADAMS AND ERNEST POLLARD, *Yale University.*—Since a primary ionization causes a sharp localized rise in temperature, it is possible that at least part of the biological action of primary ionization is of the nature of local thermal action. If this viewpoint is correct, there should exist a definite relationship between temperature effects and radiation effects. To test this, dry *T*-1 bacteriophage was used because of its relative stability at temperatures of 100°C. The results show that when *T*-1 bacterial virus is bombarded by deuterons or x-rays at temperatures well above room temperature, the inactivation proceeds definitely faster. On the other hand, when the virus is bombarded by x-rays at −73°, there is no significant change in the rate of inactivation. It is thus seen that although there is a relationship between the two processes, this relationship is not such as to permit explanation of radiation effects as purely thermal. The interpretation of these results is not obvious, but it may be suggested that the effect of heat is to lower the energy requirement for radiation action and thus increase the radius of action of an ionization under the thermally altered conditions.

* Assisted by the AEC.

S5. Inactivation of Penicillin by Deuteron Bombardment.* MARGUERITE DAVIS AND ERNEST POLLARD, *Yale University.*—The bombardment of large enzyme molecules by deuterons has shown that the presence of a primary ionization anywhere in a large fraction of the molecule causes inactivation. This effect of primary ionization can therefore be used as a test of molecular organization. To check whether some large scale process such as heat is responsible rather than primary ionization, a small molecule, of low temperature stability, namely, penicillin, was bombarded by deuterons in the usual way. The results show that penicillin is very stable to deuteron bombardment and the inactivation curve corresponds to the requirement that one primary ionization be produced in a volume of 700A^3, which is to be compared with the figure 360A^3 expected from the molecular weight. Therefore, the fact that penicillin is organized in small molecules is shown by this technique.

* Assisted by the AEC.

S6. Inactivation of Enzymes by Soft X-Rays. W. R. GUILD,* *Yale University.*—The low voltage x-ray tube described previously[1] has been used to inactivate enzymes in order to determine relative cross sections which can be compared with the results obtained with deuteron bombardment.[2] Since the x-ray

tube delivers to the order of 10^8 roentgens per minute to a thin film of protein, the enzymes can be inactivated in reasonably short time, of the order of 30 minutes for 37 percent survival. So far catalase, urease, and chymotrypsin have been inactivated, with urease having the largest cross section and chymotrypsin the smallest. Further results will be reported.

* AEC Predoctoral Fellow.
[1] Bull. Am. Phys. Soc. 26, No. 1, abstract D7 (1951).
[2] E. C. Pollard, Am. Scientist 39, 99 (1951).

S7. Behavior of Hemoglobin Under Irradiation.* R. K. APPLEYARD, *Yale University.*—The investigation of dog carboxyhemoglobin irradiated by fast charged particles has been continued.[1] The low ion-density part of the cross section *vs* ion density curve has been examined, and preliminary experiments have been carried out on the correlation of antigenic enzymatic and spectroscopic assays of the material. The splitting of the heme-globin linkage by irradiation has been further investigated.

* Assisted by the AEC.
[1] Bull. Am. Phys. Soc. 26, No. 1, 15 (1951).

S8. Electron Bombardment of Enzymes and Viruses.* M. SLATER, *Yale University.*—Equipment has been constructed so that the 0.1-μamp beam of 1.5-Mev electrons, available from the Yale linear electron accelerator under present low power operation, can be used for bombarding the viruses and enzymes previously studied[1] by deuteron, ultraviolet, x-ray, and heat inactivation. Measurements of differential energy loss, using two magnetic spectrometers, are being taken. These are compared to theoretical values and yield, with the inactivation data, target volumes. When combined with the deuteron data, this gives the slope-at-the-origin of the cross section *vs* ionization-density curves, and indication of target shapes.

* Assisted by the ONR and AEC.
[1] Pollard, Setlow, *et al.*, Bull. Am. Phys. Soc. 26, No. 1, 15 (1951).

S9. The Use of Indicator Particles in Ultracentrifugation. H. T. EPSTEIN AND MAX A. LAUFFER, *University of Pittsburgh.*—In many instances, the size and shape of colloidal particles cannot be determined because the particles cannot be obtained sufficiently purified and concentrated to be detected by the usual methods: schlieren, light-scattering, electron microscopy, etc. An ultracentrifuge technique has been developed which allows the determination of the sedimentation constant of the particles to a fair accuracy, provided only that their presence can be detected by some means (physical, chemical, or biological). An indicator particle of known sedimentation constant is added in high enough concentration to be visible as a boundary in the usual schlieren system. The solution is then sedimented in a separation cell until the indicator particle boundary has just reached the barrier. Analysis of the contents of the inner compartment for presence or absence of the colloidal particles then allows the sedimentation constant of the indicator particles to be established as either an upper or a lower limit to the sedimentation constant of the colloidal particles. By using a set of indicator particles with different sedimentation constants, both upper and lower limits can be established for the sedimentation constant of the colloidal particles.

S10. On the Localization of Positron Emitting Isotopes in the Human Body.* MYRON L. GOOD AND FRANK R. WRENN, JR., *Duke University.*—The application of the intrinsic directional properties of the annihilation quanta to the problem of localizing radioactive sources in the human (or animal) body has been explored experimentally. Two NaI—Tl scintillation counters in coincidence detect the arrival of annihilation quantum pairs arising from a positron source; in the absence of scattering, a coincidence counting rate signifies the presence of the source on a straight line joining the two detectors. No collimators are necessary. If scattering is severe, collimators may be employed, their effects being essentially to eliminate the counting of radiation scattered in the body. The method is capable, in principle, of precision limited only by the positron ranges, or the $\approx 1/137$ radian spread of the annihilation quanta. The proposed application of the method to the detection and localization of brain tumors will be discussed. Data taken with a source embedded in a dummy human head will be presented to show the effects of source size, scattering, and diffuse radioactive background. Comparisons with a single collimated scintillation counter will be presented.

* Supported by the AEC.

S11. Relation of the Energy Flux of 22.5-Mev Betatron X-Rays to Ionization Measurements. J. S. LAUGHLIN AND J. W. BEATTIE, *University of Illinois, Chicago.*—The absolute intensity of a carbon filtered 22.5-Mev peak betatron x-ray beam has been calorimetrically determined. A thermistor embedded in a lead cylinder which was exposed to the x-ray beam was employed as a temperature sensitive arm of a wheatstone bridge. Construction of the calorimeter and irradiated cylinders will be described. A heating coil embedded in the cylinder was employed for calibration. The ionization produced in a cavity ionization chamber of known volume immersed in water was measured with the same x-ray beam. The relation obtained was 4580 ± 95 ergs/cm^3—esu/cc, where the esu/cc was measured at equilibrium depth in water. This is equivalent to an absorption of 98 ergs/gram—esu/cc of water. In terms of the reading of the 25-r Victoreen thimble chamber centered in an 8-cm Lucite cube, the flux measured was 4895 ± 100 ergs/cm^2—roentgen (Victoreen). Calibration of other methods of measuring the roentgen will be described.

FRIDAY EVENING AT 7:00

Shoreham Hotel

(C. C. LAURITSEN presiding)

Banquet of the American Physical Society

(Title to be announced): A. T WATERMAN, *Director-Nominate, National Science Foundation*

(Title to be announced): E. U. CONDON, *Director, National Bureau of Standards.*

SATURDAY MORNING AT 9:45

Shoreham, Terrace Room

(R. R. WILSON presiding)

Apparatus of Nuclear Physics; Bremsstrahlung

SA1. 170-Inch Synchrocyclotron at the University of Chicago. H. L. ANDERSON AND JOHN MARSHALL, *University of Chicago.*—A 170-inch synchrocyclotron has been under construction at the University of Chicago for 3½ years. It is designed to accelerate protons to 450 Mev and deuterons and alpha-particles to 260 Mev and 520 Mev, respectively. Initial operation was achieved on February 16 with the acceleration of deuterons to a radius of 77 inches and a magnetic field of 17600 gauss, which corresponds to the design energy. The average energy of the beam striking a target is certainly somewhat less because of radial oscillations whose amplitude is still unknown. At a repetition rate of 50 cycles per second, the beam strikes a target for approximately one millisecond, i.e., a duty cycle of 5 percent. Measurements of neutron intensity in the beam from a copper target indicate a deuteron current of about 0.1 microampere. Any further progress will be reported.

SA2. Design of the Stanford Billion-Volt Linear Electron Accelerator.* M. CHODOROW, A. ELDREDGE, E. L. GINZTON, W. W. HANSEN,† J. H. JASBERG, C. B. JONES, R. L. KYHL, R. B. NEAL, AND P. A. PEARSON, *Stanford University.*—The principles of a traveling-wave linear electron accelerator have been described.[1] A design has been made for a machine which should be capable of reaching a billion volts. Trial models are in operation at 6 Mev and at 30 Mev. The high intensity traveling electromagnetic wave which provides the accelerating field is at a frequency of 3000 Mc/sec. It is generated by high power klystron amplifier tubes developed for this purpose. There is one klystron for each ten feet of accelerator tube. The electrons are to be accelerated in 1.0 microsecond pulses with a repetition rate of 60 pulses per second.

* Assisted by the joint program of the ONR and AEC.
† Posthumously.
[1] Ginzton, Hansen, and Kennedy, Rev. Sci. Instr. 19, 89 (1948).

SA3. Progress in Construction and Operation of the Stanford Billion-Volt Linear Electron Accelerator.* P. A. PEARSON, R. B. NEAL, R. L. KYHL, C. B. JONES, J. H. JASBERG, W. W. HANSEN, E. L. GINZTON, A. ELDREDGE, AND M. CHODOROW, *Stanford University.*—Eighty feet of accelerator tube and associated power sources have been constructed. Fifty feet have been operated, driven by five klystrons, each delivering about 10 megawatts peak power. 135-Mev electrons have been obtained in 0.1-microsecond pulses with an average current of 3×10^{-10} amp or about 3×10^{7} electrons per pulse. A spot focus is obtained despite the lack of orbit stability. There seems to be no difficulty in extending the length of the accelerator; and construction is continuing.

* Assisted by the joint program of the ONR and AEC.

SA4. Multiple Cavity Accelerator of Electrons.* B. L. MILLER AND W. C. PORTER, *Bartol Research Foundation.*—An accelerator comprising 5 resonant cavities operated on the divided output of a 10 cm (nominally 1 megawatt) magnetron has produced electron beams up to 1.4 Mev. The energy spectrum has been measured at different power levels, and it is found that approximately 50 percent of the output is bunched around the peak energy in all cases. Absorption curves in aluminum and other materials confirm the peak energy; the linearity of the aluminum curve is indicative of the energy homogeneous bunch. By detuning one or more of the cavities and using variable total power, the peak on the energy spectrum curves can be moved over the region 0.1 to 1.4 Mev. With the present gun injecting 1.0 microamperes at 13 kilovolts, the total current output is 0.1 microampere, which represents a transmission of 10 percent. An earlier 3-cavity model producing 0.7-Mev electrons had been adjusted to give 54 percent transmission. The first cavity is a buncher cavity which increases the total current by a factor of 2, fast component by 4; for the earlier model, the corresponding figures were 3.5 and 5.

* Assisted by the joint program of the ONR and AEC.

SA5. Motion of an Ion in a Fixed Frequency Cyclotron. BERNARD L. COHEN, *Oak Ridge National Laboratory.*—*Horizontal motion:* A study is made of (1) the phase shift per gap crossing, (2) energy gain per gap crossing, and (3) radius as a function of energy. Mathematical expressions are obtained for contributions to (1) from magnetic field change, relativistic mass increase, "grouping" (a tendency to get into phase with the electric frequency), and electric field fall-off; and to (2) from electric field shape and acceleration across the gap. Equations for $r/\partial r$ and $[\dot{\theta}-(eH/mc)\dot{\theta}]$ are involved in (3) (these quantities are shown to perform strongly damped oscillations about zero). Combining (1), (2), and (3) allows calculation of the phase as a function of radius, and the results are shown in terms of the range of electric frequencies which will give transmission, as a function of dee voltage and cyclotron parameters. *Vertical motion:* Modifications of the focusing formulas found in the literature are presented. The complete vertical motion is computed; the displacement is characterized by an exponentially increasing portion which determines the fraction of the ion source current received in the high energy beam. *General:* Formulas are derived for the maximum energy obtainable in a fixed frequency cyclotron as a function of dee voltage, and for the minimum voltage required to obtain a given energy as a function of magnetic field shape.

SA6. Design and Operation Features of an R.F. Ion Source. C. D. MOAK, H. REESE, AND W. M. GOOD, *Oak Ridge National Laboratory.*—Following the general design described by Thoneman, Moffatt, Roaf, and Sanders,[1] an rf ion source has been developed which delivers over 1 ma of positive ions, 90 percent of which are protons. Modifications to Thoneman's source both increase the output current and simplify fabrication of the source to the close tolerance required for large currents. Performance data D_2, He, A, and Xe will be given.

[1] Thoneman, Moffatt, Roaf, and Sanders, Proc. Phys. Soc. (London) 61, 483 (1948).

SA7. Electron Capture in Betatron Orbits. E. C. GREGG, JR., *Case Institute of Technology.*—Through the instigation of a note by Wideroe, studies were made of the capture conditions in the Case betatron by magnetic perturbation with pulses ranging from 1 to 20μs and variable in amplitude. Such perturbations were tried in slope, field, and flux with no observable difference in effects. It was found that electrons were accepted only at the peak or on the trailing edge of the injection voltage pulse ($dV/dt\leq0$) and that the capture time is about 1μs. Further, the expected parabolic relationship between time and voltage was found to hold at capture. Attempts to capture for $dV/dt>0$ resulted in no output. Additional studies corroborated that capture efficiency rises with

injection current and then saturates. Deliberate azimuthal inhomogeneities were found to increase capture time (up to 4.5μs) but to reduce the total captured charge considerably. The above observations were repeated for various electron injection angles and the conditions for capture found to be the same as above. It appears that constancy or diminution of space charge ($dV/dt \leq 0$) is essential to capture and provides a coupling coefficient for resonant damping.

SA8. Van de Graaff Accelerator for 5.5-Mev Protons. D. M. ROBINSON, L. R. MCINTOSH, AND J. C. NYGARD, *High Voltage Engineering Corporation.*—Reliable operation at 5.5 million volts has been consistently obtained with a van de Graaff proton accelerator in recently completed performance tests. By using differential-pumping and acceleration tubes, having polished aluminum electrodes, whose internal diameter is tapered to the waist part way up the tube, and by pumping with mercury through optically-blocked dry-ice traps, the troublesome electron loading which has heretofore limited maximum voltage is pushed out of the working range of the tubes. The electrostatic generator is housed in a vertical steel pressure tank 8 feet in diameter and 23 feet high. At 5.5 Mev, the magnetically analyzed proton beam intensity is 6 microamperes with an energy homogeneity of ± 0.07 percent, after being deflected through 105 degrees. This stability is obtained with a corona load controlled by the Mass-II beam position. A comparable performance is obtained throughout the energy range 1–5.5 Mev. Although the tank was designed for 400 psi, optimum generator performance has been obtained at 250 psi, using a mixture of nitrogen and carbon dioxide. The above data were obtained without the use of an intermediate equipotential shell. Preliminary results with this shell point toward a small improvement in maximum voltage.

SA9. The Use of Radioactive Material for the Generation of High Voltages. E. G. LINDER AND S. M. CHRISTIAN, *Radio Corporation of America.*—An investigation has been made of the use of beta-emissive radioisotopes for generating high voltages. The voltage was obtained by supporting the beta-emitter on an insulated electrode in a vacuum and allowing it to charge itself by virtue of its electron emission. This method represents a direct conversion of nuclear energy into electrical energy. The apparatus and some associated problems will be described. The characteristics of such a generator will be discussed. Experimental results will be given. Using an emitter containing 0.25 curie of strontium 90, a voltage of 365 kilovolts was obtained.

SA10. High Current X-Ray Tube.* C. H. SHAW AND JACK A. SOULES, *Ohio State University.*—Production of long wavelength x-rays requires the application of relatively low voltage to the x-ray tube if considerable intensity of second-order radiation is to be avoided. To maintain the intensity at a satisfactory level the tube current should be increased accordingly, but in practice, a practical limitation owing to space charge is encountered. A focused beam oxide cathode developed by O. Heil[1] has been adapted to the production of long wavelength x-rays. The cathode is capable of about 500 ma emission at 2500 volts with an electron beam cross section of 3 mm². The beam spreads rapidly upon emergence, unless other provisions are made. A magnetic lens has been used to refocus the beam onto a conventional x-ray target approximately 15 cm from the cathode. Preliminary operation has yielded 180 ma emission current at 1500 volts cathode potential with 135 ma to the target in a focal spot 2 mm diameter. An auxiliary accelerating potential up to 8 kv has been used.

* This work supported by the ONR.
[1] Heil and Ebers, Proc. I. R. E. 38, 645 (1950).

SA11. 65-Mev Bremsstrahlung Spectrum.* RICHARD H. STOKES, *Iowa State College.*—The energy spectrum of the I.S.C. synchrotron x-radiation has been measured by observing the momentum distribution of pair electrons in a cloud chamber. The x-radiation produced in a 5-mil tungsten target was collimated and entered a 12-inch cloud chamber through a beryllium window. A single burst of radiation timed with respect to the cloud chamber expansion produced electron pairs in the air filling of the chamber. The pairs were deflected in a 2500 gauss field and photographed. Preliminary results show reasonable agreement with the Bethe-Heitler theory. Also, a value will be obtained for the number of quanta per unit solid angle at the center of the beam in the range 5–65 Mev, as correlated with readings of a Victoreen thimble chamber surrounded by lead $\frac{1}{4}$-inch thick.

* Work was performed in the Ames Laboratory of the AEC.

SA12. High Energy Bremsstrahlung and Pair Production.* J. W. DEWIRE AND L. A. BEACH, *Cornell University.*—The Bremsstrahlung spectrum from a $\frac{1}{2}$-mil tungsten target bombarded with electrons from the synchrotron has been measured with an electron pair spectrometer. The beam passes through $\frac{1}{16}$-inch aluminum, $\frac{1}{4}$-inch Lucite, and 8 feet of air before striking the thin gold radiator of the spectrometer. The shape of the spectrum is in good agreement with the Bethe-Heitler theory down to 30 Mev, the lowest point measured. The upper energy endpoint was determined to be 309 ± 5 Mev. The spectrum from a 40-mil tungsten wire shows essentially the same shape with possibly somewhat fewer photons near the maximum energy.[1] The sharing of energy between members of pairs produced in aluminum and gold by 270-Mev photon has also been observed. Preliminary results give agreement between the distributions from the two radiators but a somewhat larger contrast between equal and unequal sharing than predicted by the Bethe-Heitler theory. Further work is in progress to study possible instrumental effects on this result.

* Assisted by the joint program of the ONR and AEC.
[1] Powell, Hartsough, and Hill, Phys. Rev. 81, 213 (1951).

SATURDAY MORNING AT 9:45

Wardman Park, Continental Room

(D. J. HUGHES presiding)

Neutrons; Fission

T1. Direct Measurement of Gravity Acceleration of Neutrons.* A. W. MCREYNOLDS, *Brookhaven National Laboratory.*—Gravity acceleration of neutrons was measured directly by determining the free fall of a highly collimated beam from the Brookhaven reactor. Separation was measured between two beams of different velocity but defined by the same collimating system. Thermal neutrons, of velocity 4×10^5 cm/sec, were compared at 12.5 meters range with neutrons of 9×10^4 cm/sec

and less, filtered through BeO, and at 100 meters range with fast neutrons of velocity 6×10^8 cm/sec and greater, selected by inserting a cadmium absorber. Separations are of the order of 1–2 mm in both cases and agree within the experimental error of about 10 percent with the usual value of g.

* Research carried out under contract with the AEC.

T2. Energy Spectrum of Neutrons Produced in Light Elements by 385-Mev Protons.* W. F. GOODELL, JR., H. H. LOAR, AND R. P. DURBIN, *Columbia University.*—Measurements have been made of the energy distributions of neutrons produced in light elements by 385-Mev protons. The neutrons were produced inside the cyclotron and were collimated in the forward direction by a 4-inch pipe embedded in 6 feet of lead and concrete shielding. The neutrons were detected by measuring the difference in the number of recoil protons from polyethylene and carbon targets. Measurements were made at an angle of 45° in the laboratory system. The energies of the protons were determined by differential measurements of the ranges in copper. A defining telescope of proportional or scintillation counters was followed by an absorber and a 2-inch scintillation counter. The last counter was so desensitized as to detect only protons near the end of their range. Corrections were made for nuclear absorption and coulomb scattering in the absorber. The corresponding distributions of neutron energies were then calculated, assuming previously published $n-p$ scattering cross sections at 40, 90, and 270 Mev at 45°. Preliminary analysis of the data indicates a strongly peaked neutron energy distribution from beryllium and a less strongly peaked distribution from carbon. For a 2-inch beryllium target, the peak of the distribution lies near 310 Mev and has a half-width of approximately 100 Mev. The average flux over the peak at the detector was of the order of 100 neutrons/cm²/sec/Mev.

* Assisted by the joint program of the ONR and AEC.

T3. A Simplified Theory of Neutron Scattering and Capture. T. A. WELTON, *Oak Ridge National Laboratory.*—The elastic scattering of slow neutrons by nuclei is conveniently described by a single real phase shift. A simple differential equation for the energy variation of this phase shift is derived from first principles. Integration of this equation yields directly the usual Breit-Wigner one-level formula for elastic scattering. A more complete treatment seems to yield a series of resonances, approximately equally spaced in energy. The predicted spacing agrees quite well with experiment in at least one reliable set of measurements, but the existence of marked discrepancies in other cases casts strong doubt on the general validity of this expression for the level spacing. Neutron capture is treated by making precise the concept of the time spent inside the nucleus by the incident neutron. It is then assumed that during the time spent within the nucleus, the compound nucleus has a constant probability per unit time of radiating. There results a neutron capture cross section which has the same maximum value and width as that given by the Breit-Wigner formula. The details of the curve are different, and this point is receiving further investigation.

T4. Resonant Scattering of Thermal Neutrons. B. N. BROCKHOUSE, M. BLOOM,* AND D. G. HURST, *Chalk River Laboratory.*—The scattering of neutrons from the resonant absorbers cadmium, indium, samarium, and gadolinium has been investigated with a crystal spectrometer. An annular bank of BF_3 counters was used as detector. The counting rate N for a "thick" specimen was compared with the rate N_T for a "thin" sample of vanadium. The absence of coherent scattering in vanadium makes it a suitable standard. The ratio N/N_T is proportional to σ_{ss}/σ_a for the specimen, the constant of proportionality being determined from the geometry. For cadmium from 0.02 to 0.4 ev this ratio is given accurately by a Breit-Wigner formula with accepted constants and 6.5×10^{-12} cm as the potential scattering length in the interference term. The spin of the compound nucleus Cd^{114} is unity, in agreement with Beeman.[1] The spin of the compound nucleus In^{116} is four if σ_0 is taken as 26,000 barns. The spins of the target nuclei Sm^{149} and Gd^{157} are not known, but the signs of the spin changes and possible values of the original spins can be given.

* Now at University of Illinois.
[1] W. W. Beeman, Phys. Rev. 72, 986 (1947).

T5. Neutron Capture in Pb^{206}. B. B. KINSEY AND G. A. BARTHOLOMEW, *Chalk River Laboratory.*—Some recent measurements on the gamma-rays of neutron capture in Pb show that the simplicity of the spectrum from Pb^{207} is shared by Pb^{206}. The intensities of the gamma-rays at 6.73 and 7.38 Mev produced by neutron capture in Pb^{206} and Pb^{207}, respectively, have been compared using samples of ordinary lead and a radiogenic lead in which the concentration of Pb^{206} was 89 percent. The thermal neutron capture cross sections of our samples have been measured at the Atomic Energy Research Establishment, Harwell, England. From these results we find that the ratio of the gamma-ray intensities in the radiogenic lead (in which they are most easily measured) is equal to the ratio of the rates of neutron capture in the two isotopes. Since roughly one photon of 7.38 Mev is produced per neutron captured in Pb^{207}, it follows that the intensity of the 6.73-Mev gamma-ray is about one photon per capture in Pb^{206}.

T6. Fast Neutron Capture Cross Sections and Shell Structure.* D. J. HUGHES AND R. C. GARTH, *Brookhaven National Laboratory,* AND C. EGGLER, *Argonne National Laboratory.*—The capture cross section for one-Mev neutrons is a direct measure of the average level density in the compound nucleus at an excitation energy equal to the neutron binding plus one Mev. Previous cross section results[1] obtained with fission neutrons (effective energy one Mev) have shown clearly the increase in level density with atomic weight and the marked decrease in level density (associated with decreased neutron binding energy) at the nuclear shells. The measurements have been continued with special attention to nuclei near the complete shells. The level density for nuclei just above the 82 neutron shell is low but rises to normal at 90 neutrons. The low cross sections for several Ru and Mo isotopes indicate a hitherto unreported shell at 58 neutrons. Several isotopes with neutron number near 110 exhibit a normal level density. The explanation of the observed cross section variation involves both the single particle nuclear model (low binding for neutrons in excess of filled shells) and the statistical model (rapid variation of level density with excitation energy).

* Research carried out under contract with AEC.
[1] D. J. Hughes and D. Sherman, Phys. Rev. 78, 632 (1950).

T7. Low Energy Neutron Cross Sections of Bismuth.* H. PALEVSKY AND D. J. HUGHES, *Brookhaven National Laboratory,* AND C. EGGLER, *Argonne National Laboratory.*—The low energy scattering, absorption, and activation cross sections of bismuth are being measured in order to determine the properties of a bismuth mirror. Several noteworthy results, which have no special reference to mirrors, have been obtained from the measurements to date. The absorption cross section (at 2200 m/sec velocity), measured by the effect of bismuth on pile reactivity, is 30 mb, while the activation cross section (for the 5-day Bi^{210}) is only 15 mb. Chemical and spectroscopic analysis, as well as intense neutron irradiation, reveal no impurities in the various purified bismuth samples used. It is possible that the excess absorption leads to the long lived alpha-emitter ascribed by Neumann, Howland, and Perlman[1] to an isomeric state of Bi^{210}, although such a large cross section would imply an exceedingly long lived isomer ($\sim10^8$ years).

The inelastic as well as the spin dependent scattering is being measured with the Brookhaven slow chopper for neutrons of wavelength 6 to 23A. In this wavelength range the inelastic scattering departs widely from the proportionality to λ that is expected theoretically and that has been observed in several other materials.

* Research carried out under contract with AEC.
[1] Neumann, Howland, and Perlman, Phys. Rev. **77**, 720 (1950).

T8. The Neutron Resonance in V^{51} at 3300 ev. S. P. HARRIS, *Argonne National Laboratory.*—Using the high speed resonance region neutron velocity selector,[1] direct measurements have been made on the resonance in vanadium.[2,3] Hamermesh and Muehlhause give an energy of ~2700 ev for the V^{51} resonance from the correlation of cross-section values in the one-level Breit-Wigner formula. Velocity selector transmission curves indicate a strong dip at ~3300 ev, in good agreement with the value of Hamermesh and Muehlhause. Transmission curves for vanadium and for several other elements having resonances will be presented and a brief description of the machine will be given.

[1] W. Selove, Phys. Rev. **76**, 187A (1949).
[2] S. P. Harris and A. S. Langsdorf, Phys. Rev. **74**, 1216A (1948).
[3] M. Hamermesh and C. O. Muehlhause, Phys. Rev. **78**, 175 (1950).

T9. Internal Conversion of Neutron Capture γ-Rays. I. C. O. MUEHLHAUSE, *Argonne National Laboratory.*—Low energy internal conversion electrons from neutron capture γ-rays have been reported for Cd, Gd, and Br.[1] The work to be described in this paper was performed at Argonne Laboratory in April, 1948. At that time the author made a survey of strong neutron absorbers in an attempt to search for other examples of this phenomena. Thin films (~1 mg/cm²) of Cd, Gd, Sm, Eu, Dy, and Hg were placed in contact with a photographic plate and bombarded in a thermal neutron flux from the Argonne heavy water reactor. In each case an intense blackening of the plate resulted which could be removed by interposing a few mg/cm² of either Al or Be between the absorber and plate. This and other control experiments indicated a prompt soft charged radiation to be present in the capture process which was identified as an internal conversion electron. Absorption measurements of the radiation yielded electron energies of the order of 100 to 500 kev. Since in all the materials examined low energy electrons were found in abundance, it is concluded that low energy capture states having a long lifetime (~10^{-10} sec) are a common occurrence.

[1] T. H. Davies and S. Wexler, Brookhaven National Laboratory Report C-7, Conference on Chemical Consequences of Nuclear Transformations (1948).

T10. Internal Conversion of Neutron Capture Gamma-Rays. II. CARL T. HIBDON AND C. O. MUEHLHAUSE, *Argonne National Laboratory.*—Low energy neutron capture gamma-rays from Gd and Sm^{149} have been measured with a 180° focusing permanent magnet beta-spectrograph. A well-collimated beam of neutrons from the Argonne heavy water reactor passes through the spectrograph and irradiates a neutron absorber which is located in the usual source position. Internal conversion electrons from this absorber are focused on no-screen x-ray film. Several lines resulting from a Gd absorber are easily observed and are associated with two gamma-rays, one of 80 kev and another of 90 kev. The K, L_2, L_3, and M lines occur for the 80-kev gamma-ray and the K and L_3 lines for the one at 90 kev. A faint line always observable at a higher energy could not be associated with either of these two gamma-rays. If interpreted as the K-line of a third gamma-ray, the energy of this gamma-ray is 185 kev. Only one line from a Sm^{149} absorber is observed with this instrument, and if interpreted as a K-line, the gamma-ray has an energy of 341 kev.

T11. Paramagnetic Scattering of Neutrons by MnF_2 and MnO.* P. J. BENDT, L. J. RAINWATER, AND W. W. HAVENS, JR., *Columbia University.*—Ruderman[1] obtained experimental confirmation of paramagnetic neutron scattering and checked the free-ion integral form factor derived by Halpern and Johnson[2] by making neutron transmission measurements on MnF_2 and MnO. Shull *et al.* (ORNL 481) have confirmed the free-ion differential form factor and have studied magnetic reflections from MnO and other manganese compounds when these were cooled below their Curie temperature. The neutron scattering experiments to be described were for the purpose of studying the intermediate situation, when the magnetic ions are neither entirely uncoupled, nor rigidly locked in an antiferromagnetic array. In the analysis of the results, an attempt has been made to separate inelastic effects from coherent effects due to short-range ordering of the ion spins. The parameters which could be varied in this experiment were the angle of scattering, 18° or 33°; the neutron wavelength, 1 to 5.5 angstroms, determined by the Columbia Neutron Velocity Selector; the strength of the exchange coupling between Mn^{++} ions, which is stronger in MnO than in MnF_2; and the sample temperatures, between 107°K and 610°K.

* Supported in part by the AEC.
[1] I. W. Ruderman, Phys. Rev. **76**, 1572 (1949).
[2] O. Halpern and M. H. Johnson, Phys. Rev. **55**, 898 (1939).

T12. Long Period Delayed Neutrons. J. W KUNSTADTER, J. J. FLOYD, L. B. BORST, AND G. J. WEREMCHUK, *Brookhaven National Laboratory.*—The neutron density at a point in the Brookhaven reactor has been measured with indium foils as a function of time after a rapid shutdown. Neutrons of low yield and long half-life were observed after the decay of the groups of up to 55-second half-life previously reported.[1] Three groups of neutrons were found by a peeling-off process on data obtained after varying lengths of reactor operation time. The half-lives are about 3, 12, and 120 minutes, and the yields relative to the 55-second group are $1:3\times10^{-3}:10^{-7}:5\times10^{-8}$, with no correction for the unknown neutron energies. The limits of error are estimated to be 15 percent in the half-lives and 25 percent in the yields. No known fission product γ-rays are recorded which can give photo-neutrons or photo-fission with these characteristics.

[1] Hughes, Dabbs, Cahn, and Hall, Phys. Rev. **73**, 111 (1948). Sun, Charpie, Pecjak, Jennings, Nechaj, and Allen, Phys. Rev. **79**, 3 (1950).

T13. Velocity Distribution of Fission Fragments.* R. B. LEACHMAN, *Los Alamos Scientific Laboratory.*—The velocity distribution of fragments from the slow neutron fission of U^{235} has been obtained by time-of-flight measurements. Two well-defined peaks were found corresponding to the light and heavy fragment groups. When compared with the velocity distribution calculated from coincidence ionization data of fragments in argon,[1] the measured distribution indicates that in argon the energy-ionization ratios w_L and w_H of the most probable light and heavy fragments exceed w of uranium alpha-particles by factors of 1.05 and 1.12, respectively. On this basis, the average kinetic energy of fission is about 12 Mev greater than the 156 Mev[1] found by the customary conversion of ionization to energy by w of alpha-particles. The ratio $w_L/w_H=0.938$ determined from velocities is in reasonable agreement with the values 0.963 and 0.964 found by other methods.[2]

* Work performed under auspices of the AEC.
[1] D. C. Brunton and G. C. Hanna, Can. J. Research **A28**, 190 (1950).
[2] Knipp, Leachman, and Ling, Phys. Rev. **80**, 478 (1950).

SATURDAY MORNING AT 9:45

NBS, East Building

(E. U. CONDON presiding)

Physical Problems Solved by Computing Machines

U1. Crystal-Structure Computations on X-RAC. RAY PEPINSKY, *Pennsylvania State College.* (30 min.)

U2. Statistical Fields for Atoms. L. H. THOMAS, *Watson Scientific Laboratories.* (30 min.)

U3. Droplet Dynamics and Nuclear Fission. J. A. WHEELER AND D. L. HILL, *Los Alamos Scientific Laboratory.* (30 min.)

U4. Solution of X-Ray Diffusion Problems with the SEAC. L. V. SPENCER, *National Bureau of Standards.* (30 min).

U5. Formation of the Elements in the Expanding Universe. R. A. ALPHER AND R. C. HERMAN, *Johns Hopkins University.* (30 min.)

SATURDAY MORNING AT 9:45

Shoreham, Main Ballroom

(C. C. LAURITSEN presiding)

Invited Papers

V1. Meson Masses and the Energetics of Meson Decay. WALTER BARKAS, *University of California, Berkeley.* (30 min)

V2. *V*-Particles and Their Disintegration Products. R. B. LEIGHTON, *California Institute of Technology.* (30 min.)

V3. Precision Measurements with a New Mass-Spectrograph. S. A. GOUDSMIT, *Brookhaven National Laboratory.* (30 min.)

SATURDAY MORNING AT 9:45

Shoreham, West Ballroom

(G. C. WICK presiding)

Nuclear Theory, I

W1. Influence of Nuclear Size on X-Ray Fine Structure.* A. L. SCHAWLOW AND C. H. TOWNES, *Columbia University.*—Christy and Keller[1] calculated the fine structure constant, α, from the x-ray doublet separation L_{II}–L_{III}. When their value is corrected for the anomalous spin moment of the electron,[2] it gives $1/\alpha=137.11$, which is higher than the average of other accurate measurements (137.0435 ± 0.0007). One factor which was not considered in these calculations is the finite size of the nucleus. This reduces the binding energy of a $p_{\frac{1}{2}}$ electron more than that of a $p_{\frac{3}{2}}$ and so reduces the doublet splitting for a given value of α. The correction has now been calculated and is found to vary from 0.01 percent for $Z=60$ to 0.2 percent for $Z=95$. After applying this correction, the value obtained for $1/\alpha$ is 137.04 in good agreement with other determinations. Since the percentage correction varies very rapidly with Z it can be separated from other atomic effects. The available data is not as accurate as might be desired, but indicates such a variation. The effect is related to isotope shifts in optical spectra but measures the total change of electronic energies rather than differences between isotopes.

* Work supported by the AEC.

[1] R. F. Christy and J. M. Keller, Phys. Rev. 61, 147 (1942).

[2] H. A. Bethe and C. Longmire, Phys. Rev. 75, 306 (1949).

W2. Evaluation of the Metric for Liquid Drop Configuration Space. DAVID L. HILL, *Vanderbilt University.*—The successive shapes of a deforming liquid drop nuclear model define the trajectory of its system point in an n-dimensional configuration space defined by parameters such as the α_i's of the expression describing a cylindrical symmetric surface:

$$R(\mu)=a_0[1+\sum_{i=1}^{n}\alpha_i P_i(\mu)].$$

The deformation potential energy surface,[1] constructed in the corresponding $(n+1)$-dimensional space, enables us to determine this dynamical path for any initial motion, provided the metric of the configuration space is known. I shall display a procedure for evaluating the elements of the metric tensor by employing the connection between the parameters of the expansion for velocity of internal motion and the time variation of the shape coordinates α_i. We may then specify, for example, the path of steepest descent of the system point away from the saddle point of the energy surface, corresponding to that development of the nuclear surface which leads most directly from the shape of unstable equilibrium toward fission.

[1] N. Bohr and J. A. Wheeler, Phys. Rev. 56, 426 (1939); S. Frankel and N. Metropolis, Phys. Rev. 72, 914 (1947).

W3. Ionization Statistics. J. K. KNIPP, *Iowa State College.*—The ionization produced by electrons, protons, alpha-particles, and other atomic particles including fission fragments and recoiling atoms from nuclear decay can be described statistically in terms of the fundamental processes of a single atomic or molecular collision. The basic equations, which are the result of the application of the usual rules for the composition of probabilities, relate the probabilities of obtaining certain numbers of ion pairs to the corresponding probabilities after a single collision. For example, consider a gas particle in its own gas and suppose all collisions either cause ionization with energy loss ω^*, for which the probability is $Q_i(E)$, or give rise to recoil atoms of energy E^1, with the differential probability $Q(E, E^1)dE$. Then the probability $P(E, I)$ that a particle of energy E produce I ion pairs when stopped in the gas is readily described in terms of $Q_i(E)$ and $Q(E, E^1)$. The calculation of moments from the basic equations leads to integral equations for the average total ionization, mean square fluctuation, etc. Thus, for the example given, the average total ionization satisfies the equation

$$I(E) = Q_i(E)[I(E-\omega^*)+1] + \int_0^E dE^1 Q(E, E^1)[I(E-E^1)+I(E^1)].$$

The mean square fluctuation satisfies a similar equation.

W4. Excitation and Ionization by Electrons. T. EGUCHI AND J. K. KNIPP, *Iowa State College.*—An electron in its passage through a gas leaves the atoms and molecules in states of excitation, dissociation, and ionization. The number of atoms or molecules in a particular condition is subject to a statistical treatment wherein the fundamental processes are the collisions of the primary electron, and the ejected electrons, with the unexcited constituents of the gas. Were the solutions of the basic equations known, averages and mean square fluctuations could be calculated directly. Instead, nonhomogeneous integral equations are obtained for these quantities, the solutions of which are asymptotic to linear functions of the energy. The coefficients of the energy in the asymptotic expressions are simply related to the energy loss per excitation, energy loss per ion pair, deviations from poisson fluctuations, and other physically interesting parameters of the statistics. The constant terms in the asymptotic expressions are the excitation defects, ionization defects, etc. Explicit expressions which are obtained for certain of these quantities are rather insensitive to the exact form of the solutions of the integral equations.

W5. Range-Straggling Due to Ionization. H. W. LEWIS, *Institute for Advanced Study.**—The problem of range-straggling of a fast nonrelativistic heavy particle, due to ionization and excitation, has been re-examined to determine the region of validity of the usual gaussian approximation to the range distribution. This approximation may be expected to be less accurate than is commonly thought, for several reasons, of which the most cogent is illustrated by the following typical example: if a 100-Mev proton is stopped in aluminum, 35 percent of the variance (mean square dispersion) in range is provided by collisions in which it loses more than half the maximum energy it is possible to lose in a single event. The average number of such collisions is nine, which is not an extremely large number. Indeed, 20 percent of the variance arises from a single collision. Consequently, the central limit theorem of statistics, which requires that each even contribute a vanishing part of the variance, is inapplicable. An exact solution of the straggling problem, in a simplified model, will be discussed, along with the relation between this model and reality.

* On irregular leave from the University of California, Berkeley.

W6. On the Theory of Multiple Scattering.* GEORGE YEVICK, *Stevens Institute of Technology.*—The general integral-differential equation for the distribution function of a proton beam throughout a scattering material is converted into an integral equation by obtaining the Green's function (straight-line Green's function) for the differential part of the equation and considering the integral part as a source term. The integral equation is solved by iteration. As an initial trial function, the small-angle coulomb distribution function with energy loss obtained by Eyges[1] is used. One interprets this physically in the following way: the particles are smeared out over space in a manner given by the small-angle distribution, suffer a large angle nuclear or coulomb collision, and then travel in a straight line via the Green's function. The integrals must be solved in an approximate manner. For the case of finite domains of material a surface integral must be evaluated. It is also possible to convert Eyges' solution into a Green's function, which physically means that after a large angle scattering the particle is multiply small-angle scattered. The integrals, however, become rather lengthy to handle. The effect of absorption, which takes care of star production and inelastic scattering, can be treated by the above methods.

* A major portion of this work was done during the summer of 1950 at the Nevis Cyclotron Laboratory.

[1] L. Eyges, Phys. Rev. 74, 1534 (1948).

W7. Gamma-Ray Transmission through Finite Slabs.* GLENN H. PEEBLES, *Rand Corporation* (Introduced by M. S. PLESSET).—The transmission of photons through a plane slab of finite thickness but infinite extent is the sum of the transmissions with 0, 1, 2, etc., scatterings. If the transmission in the first few scatterings is known and comprises 50–60 percent of the total, then the total transmission can be estimated with accuracy adequate for most purposes. A process is described for calculating the transmission with $k+1$ scatterings when the transmission with k scatterings is known over sufficiently wide ranges of three parameters: slab thickness, incident energy, and incident direction. The magnitude of the task of developing the three variable system is offset by the amount of information gained. Estimates of the transmission for mono-energetic, mono-directional incident beams are given for slabs of lead and iron. Thickness ranges from 0 to 20 mean free paths, incident energy from 1 to 20 mc^2 and incident angle from 0 to 90°. One easily uses these estimates to find the transmission for beams whose photons are distributed continuously over incident energy and angle. Although the basic calculations are for lead and iron, they yield estimates of the transmission for many other materials.

* This work was supported in part by the AEC.

W8. Z-Dependence of the Cross Section for Capture of Photons by Nuclei. J. HEIDMANN, *Cornell University* (Introduced by H. A. BETHE).—Experiments on the emission of photo-neutrons have shown anomalies for light nuclei (Z from 8 to 20) consisting of fluctuations between even and odd nuclei and generally small cross sections. We have applied the theory of the compound nucleus to this problem for gamma-rays of 10 to 20 Mev. Owing to the high binding energy of the neutron, light nuclei are found to emit mainly protons. The so-called resonance observed in the formation of radioactive isotopes by gamma$-n$ reactions is explained by the competition by emission of two neutrons at the higher energies. To avoid assumptions on the energy dependence of the cross section, the theory is compared with experiments using 17-Mev photons from Li detected by BF_3 counters.[1] The measured cross section for light nuclei, Cu, and heavy elements with single isotopes is divided by the calculated number of neutrons emitted from the compound nucleus; the result is, within 25 percent, proportionate to Z, in agreement with theoretical expectation.

[1] McDaniel, Walker, and Stearns, Phys. Rev. 80, 807 (1950).

W9. On Nuclear Disintegration by Positron—K Electron Annihilation. S. C. CHEN AND R. D. PRESENT, *University of Tennessee.*—A positron with insufficient energy to excite or disintegrate a nucleus by collision may annihilate a K electron of an atom with subsequent excitation or disintegration of its nucleus. If the positron energy is close to threshold for the process, competition from two-quantum annihilation does not occur. The process is of first order and, apart from the occurrence of negative energy states, is the reverse of internal conversion. The cross section may be factored into a cross section for annihilation with emission of a photon converging on the nucleus times a probability for nuclear disintegration. The latter is essentially the ratio of the photo-disintegration cross section to the S-wave black-body absorption cross section $\pi\lambda^2$. The annihilation cross section in light elements has been calculated in the Born approximation using the retarded interaction corresponding to converging spherical waves of electric dipole radiation (the nucleus acts as a sink for these waves, in addition to conserving momentum). For large incident energy of the positron the difference between positive and negative energy states can be neglected and the cross section obtained by detailed balancing from the internal conversion coefficient. The cross section for disintegration of Be^9 is $\sim 10^{-31}$ cm^2 near threshold; for heavier nuclei it would be larger ($\sim Z^3$).

W10. A Note on Angular Distribution of Gamma-Radiation from 16-Mev C^{13*}. G. B. ARFKEN AND L. C. BIEDENHARN, *Oak Ridge National Laboratory.*—In the reaction $B^{11}(p, \gamma)C^{12}$ the 16-Mev crossover γ is observed to be isotropic, while the 12-Mev γ follows a $1+0.15\cos^2\theta$ distribution.[1] It appears to be a general result that if one has isotropic 2^L pole radiation from a state of spin J (magnetic substates m_J with random phase) and $L \geq J-\frac{1}{2}$, then all gamma-radiation from that state must be isotropic. The condition $L \geq J-\frac{1}{2}$ has been proven necessary and is sufficient in all cases considered here. This lemma applies to C^{12} and in general whenever the final nuclear state in the isotropic γ-transition has $J=0$ or $\frac{1}{2}$. The possibility of a small undetected anisotropy in the 16-Mev γ has been considered in detail. It is concluded that the 16- and 12-Mev γ's must come from different states of C^{12}.

[1] High Voltage Group, Oak Ridge National Laboratory (private communication).

W11. Wave Functions in Momentum Space. E. E. SALPETER, *Cornell University.*—The momentum-space wave functions for a nonrelativistic two-body problem with a phenomenological interaction potential satisfy a well-known integral equation. A general prescription is given for finding suitable trial wave functions, which depend on some adjustable parameters. Reasonable values for these parameters are found by iteration of the wave function for particularly simple values of the momentum. Successive approximations are then obtained for the wave functions by repeated iteration of the integral equation. The method outlined is similar to some methods used previously,[1] but is not based on a variational principle and is more suitable for numerical work. For the deuteron ground-state, using central Yukawa, exponential, and square well potentials, accurate momentum-space wave functions are being calculated in numerical form. The application of the method to scattering problems, and to a four-dimensional integral equation obtained in a relativistic treatment of the two-body problem, will be discussed.

[1] N. Svartholm, Thesis (Lund) 1945; B. A. Lippmann and J. Schwinger, Phys. Rev. 79, 469 (1950).

W12. Relativistic Theory of Interaction at a Distance Between Particles. L. H. THOMAS, *Watson Scientific Computing Laboratory.*—A nonrelativistic classical dynamical system with a finite number of degrees of freedom may be specified in terms of canonical variables by a hamiltonian function. If the system admits the newtonian group, the motion of the center of mass can be separated. If the hamiltonian separates for large values of certain variables, the system can be regarded as a system of particles, perhaps spinning, interacting at a distance. Using Lie theory we can extend such systems to admit the Lorentz group, and we have relativistic classical dynamical systems, in exactly the same variety as nonrelativistic systems. Separation of the center of mass motion is still possible. Particles in interaction do not have invariant world lines as the transformations involve all the variables, and the usual argument against the possibility of such systems does not apply. The contact transformations corresponding to change of Lorentz frame are of the form of extended point transformations in terms of variables that, for non-interacting particles, are physically momenta. The usual quantization can then be carried out. The transformations involve square roots, and the systems cannot in general be changed to wave equations similar to the Dirac equations for an electron.

W13. The Kinetic Energy Operator for the Nuclear Three-Body Problem. B. T. DARLING AND B. R. LINDEN,* *The Ohio State University.*—Darling's method[1] of separating rotational from radial motion by use of group operators has been applied to the three-body problem.[2] The coordinates chosen were those of the center of mass, the interparticle distances, and the infinitesimal rotations about the coordinate axes. The kinetic energy expression consists of terms involving only the radial distances and derivatives, terms quadratic in the angular momentum operators (similar, in form, to the asymmetric rotator), and mixed terms involving radial derivatives and angular momentum operators (coriolis terms). The pure radial term is equivalent to the Hylleraas[3] expression and is the only contribution to the kinetic energy for S states. With moving axes defined by taking the origin at the center of mass, the x axis through one of the particles, and the plane of the particles as the $x-y$ plane, pure radial equations were obtained by replacing the angular momentum operators by their matrix representatives. In these equations terms quadratic in the angular momentum matrices play the role of centrifugal forces.

* AEC Predoctoral Fellow.
[1] B. T. Darling, Doctoral Thesis, University of Michigan, 1939.
[2] B. R. Linden, Master's Thesis, Ohio State University, 1949.
[3] Z. Physik 54, 347 (1929).

W14. The Pure Radial Equations for Nuclear Three-Body Problem. B. R. LINDEN* AND B. T. DARLING, *The Ohio State University.*—The exact radial equations for the nuclear three-body problem have been determined under the assumption of a charge independent potential of the most general static exchange central interaction and a static non-exchange tensor interaction. The kinetic energy operator is that discussed in a previous paper[1] by the same authors. Only those S, P, and D states mix which have even K (the projection of orbital angular momentum along the body-fixed z-axis associated with the symmetric rotator function $\theta(L, M, K)$) as is predicted on the basis of parity. The eight radial wave functions satisfy a set of eight simultaneous differential equations. These equations seem to indicate that the states have the following order of decreasing magnitude: (a) the ^3S state, ψ_1, with spins antisymmetric for like particles; (b) the ^1S state, ψ_2, with spins symmetric for like particles; (c) the ^1D states with $K=\pm 2$; (d) the ^3D state with $K=0$; (e) the ^1P and ^3P states. The ^1D states are apparently determined mainly by ψ_2. It does not appear that the question of relative phases can be disregarded.

* AEC Predoctoral Fellow.
[1] See preceding abstract.

SATURDAY AFTERNOON AT 2:00

Shoreham, West Ballroom

(J. H. VAN VLECK presiding)

Nuclear Theory, II

WA1. Low Energy Photo-Meson Production in Hydrogen. S. D. DRELL, *Stanford University.*—Berkeley experiments indicate approximate equality of the π^0 and π^+ production cross sections. Calculations based on a weak coupling perturbation treatment of the meson-nucleon interaction predict π^0 production to be reduced by $\sim(\mu/M)^2$ relative to π^+ production for energies at which the Berkeley experiments are performed ($\sim$320 Mev). We avoid this perturbation approximation. With a Bloch-Nordsieck type canonical transformation we obtain a solution to the hamiltonian equation that involves no assumption concerning the largeness or smallness of $g^2/4\pi$. The approximations involved are neglect of nucleon recoil and treatment of spin and charge matrices as classical unit vectors. Handling the electromagnetic field by standard perturbation theory, we use this solution to calculate the matrix elements for photo-production. In evaluating the matrix elements we must use a finite source cutoff to compensate neglect of nucleon recoil. We obtain qualitative agreement with the observed equality of π^0 and π^+ production cross sections with a choice of $g^2/4\pi\sim1-2$ and of source radius of the order of a nucleon Compton wavelength. We also obtain an angular distribution and energy dependence for the production cross sections in accord with observation.

WA2. π^- Meson Reactions in Tritium. E. R. CAIANIELLO AND A. M. L. MESSIAH, *University of Rochester.*—It has been shown[1] that the π^- meson reactions in hydrogen and deuterium are sensitive to spin and parity of the π-meson. Qualitatively, the ratios can be predicted on the basis of angular momentum and parity selection rules. We have searched for similar selection rules in the reactions: (1) $\pi^-+H^3\rightarrow3n$ and (2) $\pi^-+H^3\rightarrow3n+\gamma$. No selection rules follow from the exclusion principle alone. However, if the ground-state space wave function of tritium is totally symmetric, reaction (1) is forbidden for scalar and pseudovector π^- mesons. The small non-symmetric contribution to the tritium wave function which may exist[2,3] does not alter this conclusion. Since reaction (2) is allowed for all meson fields, the relative probabilities of (1) and (2) should help decide between the pseudovector and pseudoscalar fields for the π-meson.[1]

[1] S. Tamor and R. E. Marshak, Phys. Rev. 80, 766 (1950).
[2] F. Villars, Helv. Phys. Acta 20, 476 (1947).
[3] R. L. Pease and H. Feshbach (private communication).

WA3. Pion Scattering with Exchange. M. L. GOLDBERGER, *University of Chicago.*—The reactions $\pi^-+P\rightleftarrows N+\pi^0$ and $\pi^++N\rightleftarrows P+\pi^0$ will be discussed on the basis of a simple model proposed by E. Fermi. The scattering processes with and without charge exchange are treated, using a formalism essentially identical to nuclear reaction methods of Wigner and Eisenbud.[1] It is assumed that outside a region of radius equal to the meson Compton wavelength there is either no interaction or only coulomb interaction between pions and nucleons. The inside problem is specified in terms of three parameters in the form of boundary conditions at the critical radius. The description is limited to low energy processes and is made entirely without meson theory. The lifetime of a π^- bound in a K orbit is computed. From this computation, an estimate of the strength of the coupling can be deduced. It is shown that charge exchange processes are improbable in both the very weak and very strong coupling limits. The above description is admittedly highly speculative but may provide a simple method of correlating experimental results without using detailed meson theories.

[1] E. P. Wigner and L. Eisenbud, Phys. Rev. 72, 29 (1947).

WA4. A Quantitative Analysis of the Impulse Approximation. G. F. CHEW, *University of Illinois,* AND G. C. WICK, *Carnegie Institute of Technology.*—The impulse approximation[1] is a generalization of Fermi's method for treating the scattering of slow neutrons by bound protons.[2] It extends the method to energies at which many partial waves may be scattered and takes into account a possible energy dependence of the two-body scattered amplitude. The general criterion for the validity of the impulse approximation has now been drived on the basis of an integral equation, and the order of magnitude of the accuracy can be determined. In particular, it can be shown that for 100-Mev neutrons scattered by deuterons, an accuracy of $\sim$15 percent is to be expected. For still higher energies, it becomes reasonable to apply the method to the interaction of nucleons with even more tightly bound nuclei.

[1] G. F. Chew, Phys. Rev. 80, 196 (1950).
[2] E. Fermi, Ricerca sci. VII–II, 13 (1936).

WA5. Nuclear Saturation and Magic Numbers in Terms of a Non-Linear Meson Theory.* L. I. SCHIFF, *Stanford University.*—Work reported earlier under the above title[1] has been extended with a better model for nuclear matter, in which a nucleon is embedded in a uniform meson source. Neutrons and protons are regarded as equal sources for a non-linear neutral scalar meson field, and a variation method is used. Two parameters that specify the single nucleon source strength, and one parameter that specifies the non-linearity of the meson field, are chosen so that the total energy (potential and kinetic) of nuclear matter has a minimum at the observed density and equal to 42 percent of the observed energy. The two-nucleon interaction in free space then has a short-range repulsive core, and has 45 percent of the observed strength (as measured by the square of the zero energy phase integral $f'(-V)^{\frac{1}{2}}dr$). When embedded in nuclear matter, this calculated two-nucleon interaction strength is reduced to 38 percent of its free space value. These results indicate that the theory is capable of accounting qualitatively for nuclear saturation and for the independent-nucleon model that leads to shell structure and magic numbers.

* Assisted by the joint program of the ONR and AEC.
[1] L. I. Schiff, Phys. Rev. 80, 137 (1950).

WA6. Short-Range Correlations in Nuclear Structure. KEITH A. BRUECKNER, *Institute for Advanced Study,* AND KENNETH M. WATSON, *University of California, Berkeley.*—It has been observed experimentally by Panofsky that the capture of Pi-mesons in deuterium[1] leads to a radio of non-radiative to radiative capture of seven to three, while in carbon the ratio is greater than two hundred to one. It is possible to show that the difference can be attributed almost entirely to the existence of stronger short-range correlations in nucleon positions in carbon than in deuterium. The explicit calculation involves an integral over the coordinates of the initial and final nuclei which may be simplified by application of an approximate closure rule to the wave functions of the final nuclei. Further simplifications can be made by introduction of the transition matrix leading to meson absorption, as de-

duced from the deuteron absorption experiments. The remaining integral is interpreted as representing the probability of finding in contact the two nucleons involved in the act of absorption. Comparison with experiment shows that this probability is much greater than the random probability based only on nuclear volume, or that deduced, for example, from a Fermi distribution. This effect is presumably due to the strong short-range nucleon-nucleon interaction.

[1] W. K. H. Panofsky, Phys. Rev. 81, 565 (1951).

WA7. Dipole Oscillator-Strength Sum Rules for Relativistic Systems. L. L. FOLDY, *Case Institute of Technology.*—The well-known Thomas-Reiche-Kuhn sum rule for electric dipole oscillator strengths has been very useful in studying the interaction of electromagnetic radiation with atoms and has more recently been applied to the analysis of the nuclear photo-effect. An analagous sum rule can be derived for the interaction of electromagnetic radiation with the meson field about a nucleon as well as to more general electromagnetic interactions with relativistic charged fields. In general, the oscillator-strength sum involves the expectation value of a space integral of the commutator of the operators for the charge density and current density for the system. For scalar and pseudoscalar meson fields, this reduces to the expectation value of the space integral of the absolute square of the meson potential. Ambiguities in the sum rules arise because of the presence of divergent expressions. It is believed that these difficulties will be eliminated when charge renormalization and convergence techniques, such as the use of regulators, are applied. Applications of the results may be made to such processes as photo-production of mesons, scattering of gamma-rays by nucleons, Delbruck scattering, and pair production by gamma-rays.

WA8. Matrix Elements of Beta-Decay. HENRY BRYSK AND EUGENE GREULING, *Duke University.*—In the expression for the transition probability of beta-decay

$$1/\tau = (G^2/2\pi^3)\,|M|^2 f(Z, W_0),$$

the function $f(Z, W_0)$ of the electron-neutrino field has been investigated in detail and calculated for the various interactions. The nuclear matrix elements $|M|$, however, have heretofore only been very crudely estimated, because the wave functions of the many-body problem involved could not be determined. Under the one-particle nuclear shell model, the task becomes feasible. Using the Dirac representation, we have derived the wave functions for a nucleon in a square-well potential, and from them computed the matrix elements for all allowed and first-forbidden and some higher forbidden interactions. The results obtained differ considerably from the previous assumptions as to relative order of magnitude of terms, and contributions are found to so-called "L-forbidden" transitions, since L is not a good quantum number in the dirac representation. Interpretations of specific cases will be presented.

WA9. An Alpha-Particle Model for Be^8 and C^{12}. RICHARD R. HAEFNER, *University of Minnesota.*—The interaction of two alpha-particles is represented by a square-well potential with the addition of a potential q^2/r^2 for separations of the centers of the particles less than r_0, and a pure coulomb potential for greater separations. The well depth is chosen to give a $^1S_0$ virtual state at 90 kev, center-of-mass energy. A resonance for the $^1D_2$ state is found near 3 Mev for $r_0 = 4.5 \times 10^{-13}$ cm for $q^2 = 30\hbar^2/2\mu$. The extensions of this model to the Li^8 beta-decay show good agreement with the data of Bonner *et al.* on the resulting alpha-particle spectrum. The comparison of the cross sections for alpha-alpha-scattering from this model and those using the phase shifts determined by Wheeler from the experimental data are in fair agreement when account of the poor geometry and large energy spread of the actual experiments is taken into account. Experiments with improved geometry and better energy definition for alpha-particle laboratory energies 4–7 Mev might show the $^5S_0$ level at 2.8 Mev[2] to be non-existent. Owing to the symmetry requirements on the wave function for a rigid model with alpha-particles at the vertices of an equilateral triangle, the first excited state of C^{12} for this model has even parity and two units of angular momentum. Associating this level With the excited state of C^{12} at 4.47 Mev, experimental evidence applicable to it will be discussed.

WA10. The Interpretation of Isomeric Transitions. STEVEN A. MOSZKOWSKI, *Argonne National Laboratory.*—Graphs of the theoretical half-life energy relation for nuclear isomeric transitions according to the recently developed theory of Blatt and Weisskopf[1] are shown. According to this theory, many isomeric transitions can now be assigned to magnetic 2^4 pole radiation, consistent with predictions from the Mayer[2] shell model. There are a number of isomeric transitions with half-lives of 1 second to 1 hour, which cannot be caused by magnetic 2^4 pole radiation. A possible explanation of these transitions for odd-A nuclides is that one of the states involved in the transition has a spin determined by the coupling of several odd nucleons, rather than by one odd nucleon. On this assumption, the transitions might be expected to be electric 2^3 pole. These short-lived isomeric states occur exactly for those nuclides for which one would expect "many-particle" levels, according to the shell model. Some difficulties associated with this explanation will be discussed.

[1] J. M. Blatt and V. F. Weisskopf (privately circulated notes to appear as part of a book on nuclear physics).
[2] M. G. Mayer, Phys. Rev. 78, 16 (1950).

WA11. Quantum States of Aggregation. PETER FIREMAN, *Columbian Carbon Company.*—Light waves of high frequency in approaching a metallic surface negatively charged consolidate, as it were, and strike the surface like corpuscles, forcing the emission of electrons. Viewing the whole process with an open mind, it suggests that the discontinuous waves, in encountering the metal surface, aggregate more closely while colliding with the atoms of the metal. In other words, we are confronted with the phenomenon of the light waves passing from one state of aggregation (waves) to another (corpuscles). On the other hand, electrons, true corpuscles, greatly confined while being forced through gratings, spread out freely on issuing from the gratings and form diffraction patterns after the manner of waves; another play of change of state of aggregation.

WA12. Eccentric Circular Orbits. GERTRUDE SCHWARZMANN.—Interpreting all corpuscle motion as compounded motion,[1] the electron spinning about its spin axis is supposed to revolve in an eccentric circle about its nucleus. Each axis of a rectangular coordinate system, the nucleus in its origin, divides the eccentric circle into two semicircles. In the two equal semicircles, wavelength 7.3/v cm and frequency $v^2/7.3$ sec^{-1} are conjoint to v, velocity of electron *and* electron wave.[1] In each unequal semicircle the operations arc/pi, $(\text{sector}/\frac{1}{2}\text{pi})^2$, 2 sector/arc yield the radii r_1, r_2, r_3, respectively, to which are conjoint the velocities v_1, v_2, v_3, respectively, (r_2 geometrical mean between r_1 and r_3). The radius vector sweeps at the rate $\frac{1}{2}v_2 \cdot r_2$, during period $r_1\text{pi}/v_2$, over the sector, while the electron, spinning at frequency $v_2^2/7.3$, describes the wavelength $7.3/v_1$, if the ground orbit is considered, wherein each semicircumference equals one wavelength.[1] Motion in eccentric circular orbits fulfills exactly the laws of classical physics, if modified by quantum and relativity theory, if the third radius is interpreted as radius vector and the inert electron mass as quantity of motion, hf/mv^2.[1]

[1] G. Schwarzmann, Phys. Rev. 72, 536 (1947); 744 (1947); 73, 1273, 1274 (1948); 75, 1334 (1949).

SATURDAY AFTERNOON AT 2:00

Shoreham, Main Ballroom

(W. F. G. SWANN presiding)

Counters and Counting Circuits

X1. Organic Scintillators.* R. C. SANGSTER† AND J. W. IRVINE, JR., *M.I.T.*—The scintillation-counting behavior and fluorescent spectra have been determined for a number of organic compounds from the homologous series based upon diphenyl, diphenylmethane, stilbene, and diphenylacetylene. The substances were carefully purified, primarily by adsorption and crystallization techniques. Fairly perfect, standardized crystals were prepared. Counting data were taken at 30°C and at −75°C using a Co-60 γ-ray source and an RCA C-7140 photo-multiplier. It is reproducible to within ±2 percent. In the given radiation field, a useful "efficiency" parameter is the discriminator voltage at which the counting rate has been reduced to one-half of that (extrapolated) for zero discrimination. The "phosphor absent" background parameter is less than 2 percent of that of anthracene. The parameters for different crystals of a given substance usually fall within ±3 percent of the mean value. Thermal coefficients range from slightly positive values to −3.5 percent per degree centigrade. Spectrographic data were obtained with an automatic-recording, grating spectrograph using a C-7140 photo-multiplier as the radiation detector. An attempt has been made to interpret the results to gain insight into the fundamental phenomena involved.

* The work described was supported in part by the AEC.
† AEC Predoctoral Fellow.

X2. Some Characteristics of Nonluminescent Cadmium Sulfide as a Gamma-Ray Counter. DAVID E. SOULE, *Northwestern University* (Introduced by J. H. ROBERTS).—Nonluminescent cadmium sulfide crystals with small internal strain and relatively large photo-conductivity exposed to radium gamma-rays were studied in a fast conduction counter circuit at room temperature. A negative space charge effect was observed resulting in a decrease of the count rate by a factor of about 6 and the crystal current by a factor of 1.26 during the total time of irradiation. An equilibrium value was reached after 2 to 3 hours. At this time the count rate increased linearly with increased applied potential (230 to 385 volts/cm). The differential pulse height distribution was approximately gaussian with a mean input pulse height greater than 36.5 microvolts and a root mean square deviation of 4.3 microvolts. An attempt is being made to fit a curve consisting of the theoretical count rate of secondary electrons *versus* their energy absorbed in the crystal (Compton effect contributing 95 percent of the total absorption for 1.8-Mev gamma-rays) to the above differential pulse height curve and to determine an approximate value for the schubweg.

X3. Pulse Height Spectrum Produced in NaI by Nuclear γ-Rays of Various Energies. W. M. GOOD, C. D. MOAK, G. P. ROBINSON, AND H. REESE, *Oak Ridge National Laboratory.*—Owing to its high efficiency and to its compactness, the NaI Scintillation Spectrometer has some obvious advantages over magnetic spectrometers for the study of γ-rays. The response of such a spectrometer to γ-rays of various energies is being studied by means of nuclear gamma-rays of known energies. The gamma-rays being studied include those from the reactions of $B^{11}+H^1 \rightarrow C^{12}+\gamma$ 16.70 Mev, $B^{11}+H^1 \rightarrow C^{12}+\gamma_1+12.12$ Mev $+\gamma_2+4.58$ Mev, $H^3+H^1 \rightarrow He^3+\gamma+5.48$ Mev, $H^3+H^1 \rightarrow He^4+\gamma+19.7$ Mev. The spectrometer is of the type described by others at ORNL[1] and consists of a NaI crystal, a multiplier tube, a linear amplifier and preamplifier, and a differential pulse height selector. At the present time, as the γ-ray energy gets higher, the spectra show a less and less well-defined peak in the pulse height spectrum corresponding to complete absorption of the positron, electron pair. At the moment, it is not clear that this is due to the size of the crystal.

[1] W. H. Jordan and P. R. Bell, Nucleonics **5**, 30 (1949).

X4. A Large Area Photo-Cathode Photo-Multiplier for Scintillation Counting.* P. W. DAVISON AND G. A. MORTON, *R.C.A. Laboratories.*—A number of applications of scintillation counters require a large phosphor crystal or screen. If the phosphor is absorbing or nonreflective, efficient optical coupling can only be obtained if the areas of the screen and multiplier photo-cathode are comparable. For this reason a multiplier photo-tube has been developed having a photo-cathode with an area of 95 cm². The tube has a diameter of 2½ inches and an over-all length of 8 inches. The cathode covers 180° of the cylindrical wall and extends for about half the length of the tube. The multiplier unit has ten stages and a gain of 10^6 under normal operating conditions. The properties of the tube will be described. As an illustration of one application of the tube, its performance as an alpha-particle counter with a large sensitive screen will be discussed.

* Work done under Navy BuShips contract.

X5. Response of Scintillation Counters to Heavy Particles.* C. J. TAYLOR,** M. E. REMLEY, W. K. JENTSCHKE, AND P. G. KRUGER, *University of Illinois.*—The response of anthracene, stilbene, and sodium iodide crystals in a scintillation detector to the type and energy of heavy charged particles incident on the crystals has been investigated. Deuterons and molecular hydrogen ions with energies of 1 to 11 Mev, protons of 1 to 5 Mev, and alpha-particles of 4 to 21 Mev were used. Aluminum absorbing foils were placed in the cyclotron beam to obtain the various particle energies incident on the crystals. Pulses were amplified with a Los Alamos Model 100 amplifier and analyzed with a twelve-channel pulse amplitude analyzer. Essentially gaussian distributions with a full width at half-maximum of six to eight percent were obtained for the higher energy particles. With the exception of protons and deuterons in sodium iodide, which gave linear response, plots of pulse height *vs* energy gave a nonlinear relation over a certain low energy region with a linear response being indicated provided the energy of the particle is large enough. There are indications that this nonlinearity is dependent on the ionization density of the incident particle.

* Assisted by the joint program of the ONR and AEC.
** Now at North American Aviation, Inc.

X6. Response of Scintillation Counters to Electrons.* W. K. JENTSCHKE, C. J. TAYLOR,† M. E. REMLEY, F. S. EBY, AND P. G. KRUGER, *University of Illinois.*—The investigation described in the preceding paper was extended to a study of the response of anthracene and sodium iodide crystals to electrons. Electrons of energies from 500 ev to 624 kev were used. The lower energy electrons (500 to 5000 ev) were obtained from a pulsed electron gun, fabricated in a special cathode-ray tube in which current was measured with a vibrating reed electrometer. Pulse heights were measured visually and photographically on a high speed oscilloscope. Higher energy electrons were obtained from internal conversions in radioactive sources, and the pulses were analyzed with a twelve-channel pulse

amplitude analyzer. Pulse height *vs* energy curves for anthracene show a nonlinear response below 100 kev in agreement with Hopkins,[1] while the sodium iodide curve is essentially linear, agreeing with the work at Stanford.[2] The dependence of the response on ionization density of both electrons and heavy particles will be discussed.

* Assisted by joint program of the ONR and AEC.
† Now at North American Aviation, Inc.
[1] J. I. Hopkins, Rev. Sci. Instr. **22**, 29 (1951).
[2] West, Meyerhof, and Hofstadter, Phys. Rev. **81**, 141 (1951).

X7. A High Efficiency Detector for Fast Neutrons.* H. L. Poss, C. E. Falk, and Luke C. L. Yuan, *Brookhaven National Laboratory*.—The effectiveness of a liquid scintillator for detecting fast neutrons has been investigated. Terphenyl-xylene solutions[1] enclosed in glass cells of various lengths mounted on RCA 5819 photo-multipliers were used. Integral bias characteristics with sharp cutoffs were obtained. The ratio of maximum pulse heights of Co^{60} γ-rays (1.2 Mev), to ThC″ γ-rays (2.6 Mev), and to 14-Mev neutrons is 1:1.4:2.4. Absolute detection efficiency for neutrons was determined by counting the α-particles from the $H^3(d, n)He^4$ reaction serving as the neutron source.[2] Efficiencies ranging from 6 percent to 25 percent were obtained with counters $1\frac{1}{4}$″ in diameter and 1″ to 6″ long. The effects of the optical coupling and reflecting surfaces on the pulse height distributions will be discussed.

* Work done at Brookhaven National Laboratory under the auspices of the AEC.
[1] Reynolds, Harrison, and Salvini, Phys. Rev. **78**, 488 (1950). H. Kallmann and M. Furst, Phys. Rev. **79**, 857 (1950).
[2] Hanson, Taschek, and Williams, Revs. Modern Phys. **21**, 635 (1950).

X8. Fast Neutron Detection Using Scintillation Counters.* John H. Neiler, George E. Owen, and A. J. Allen, *University of Pittsburgh*.—Scintillation counters are being employed to detect fast neutrons with good efficiency. Preliminary experiments to determine the ratio of gamma-counting rates to fast neutron rates indicate that the gamma-ray background in the shielded scattering laboratory of the University of Pittsburgh Cyclotron Building are negligible. These results were obtained from lead and paraffin absorption experiments. The design and results of preliminary experiments for a fast neutron coincidence spectrometer will be presented. This design indicates that resolutions of approximately 3 to 6 percent can be obtained with 10^{-8} coincidence per unit neutron flux at 1 Mev.

* Assisted by the joint program of the ONR and AEC.

X9. Differential Coincidence Counting Method.* Z. Bay, *The George Washington University* (Introduced by R. R. Meijer).—The amplitudes of the output pulses of a coincidence circuit depend on the time delays between the input pulses. Hence, using two identical coincidence circuits, we can perform differential measurements which yield a more accurate determination of short times (e.g., 10^{-10} sec) than is obtained with a single coincidence circuit. We branch the channels coming from the two detectors and apply one branch of each channel to a first coincidence circuit and the other two with an inserted time delay to a second. The difference of the amplitudes of the output pulses will then be dependent on time delays of the original pulses. It can be positive or negative and is zero only in a short time interval, generally much shorter than the resolving time of the coincidence circuits. The difference-output can be used, e.g., to close a gate circuit for the output pulses from one of the coincidence circuits, thus narrowing its delay curve. Preliminary experiments show that the resolving time of a coincidence circuit can be improved, in this manner, by about one order of magnitude, without essential loss in sensitivity; and, therefore, this method seems to be superior to the shorted line technique.

* Supported by the ONR and AEC.

X10. An Experimental Study of Dead-Time Errors in Counting Particles from Pulsed Sources.* C. H. Westcott and J. S. Greenberg, *McGill University*.—Counting losses due to dead-time effects may become serious when instantaneous effects from a synchro-cyclotron or other pulsed-output accelerator are studied. For a single counting channel, these effects have been computed;[1] but when coincidence techniques are used, the calculation of the errors becomes quite involved. To check the published calculations and to extend our knowledge to errors expected for coincidence arrangements, the problem is being studied experimentally with scaled-up time intervals. Instead of microsecond or shorter pulses used with proportional or scintillation counters, we use a polonium source placed behind a rotating shutter to give random-spaced counts within a pulse of duration of the order of milliseconds, and dead-times of the same order are introduced electronically. Coincident events superimposed on a noncoincident background can be studied with a mixer arrangement. The results obtained to date will be discussed in relation to the program for coincidence arrangements. While primarily intended to guide work with the McGill cyclotron, the interest of the problem is general and its relation to work elsewhere will be reviewed.

* Work supported by the National Research Council of Canada.
[1] C. H. Westcott, Proc. Roy. Soc. (London) **A194**, 508 (1948).

X11. Current Time Relationships for Single and Multiple Centered* Geiger Counter Pulses.† W. E. Ramsey, *Bartol Research Foundation*.—These measurements focus on the region from 10^{-8} to 10^{-6} second. For argon—ether and argon—butane, the current is constant while the sheath is being established, then varies inversely as the time while it moves outward to the cathode. Current and spreading velocity are both proportional to overvoltage. All pulses initiated by a single electron at a point are identical throughout their life history. The initial current in multiple centered discharges indicates the number of centers except for overlapping due to the spreading process. An improved form of a circuit previously described,[1] was used for these studies.

* A discharge initiated by more than one electron in the gas.
† Assisted by the joint program of the ONR and AEC.
[1] W. E. Ramsey, Phys. Rev. **57**, 1022 (1940).

Saturday Afternoon at 2:00

NBS, East Building

(Eric Rodgers presiding)

General Physics

Y1. Equilibrium Ultracentrifuge.* J. D. Ross, A. Robeson, and J. W. Beams, *University of Virginia*.—The ultracentrifuge rotor is suspended magnetically in a brass vacuum chamber (pressure less than 10^{-5} mm Hg). It is driven to running speed by an air turbine below the vacuum chamber which is connected to the rotor by a small shaft along the axis of rotation.

The shaft passes through vacuumtight oil glands in the chamber and is disconnected from the rotor when it attains operating speed. During the sedimentation experiment the rotor coasts freely and decelerates less than 0.1 revolution per sec per hour. Consequently, the rotor is free of "hunting," and its speed can be precisely determined. Also, since there is no shaft, the temperature is maintained at a known constant value by thermostating the chamber. The rotor is constructed of steel and Duralumin ST-14. It weighs 4.9 kg, and the center of the standard centrifuge cell is 65 mm from the axis of rotation. So far, schlieren methods have been used for measuring the concentration gradients in the cell, but a more precise interferometer method is under development. Although the apparatus was designed for determining molecular weights by the equilibrium method, it also may be used for the rate of sedimentation method.

* Supported by Navy Bureau of Ordnance, Contract NOrd-7873.

Y2. Electron Optical Field Mapping. A. VANBRONKHORST, L. MARTON, AND S. B. GARFINKEL, *National Bureau of Standards.*—In continuation of the study of quantitative measurements of small magnetic fields by the electron-optical shadow method,[1] it became desirable to determine empirically shadow deflection distance as a function of field strength. The basis of this investigation is the direct measurement, in the "equatorial" plane, of a magnetic field which has a high gradient and is of small enough physical dimensions to be viewed by a high resolution electron optical system. For this purpose a small electromagnet was made having spade-shaped pole pieces and a gap width variable from 0.05 to 0.025 inch. Using a rotating coil the field of this magnet was directly measured to an accuracy of ±0.2 gauss. Under the assumption of small electron deflection angles, an empirical relation between shadow deflection distance and field strength can be established. This serves as an independent check on any theoretical determination of deflection vs field strength.

[1] J. Appl. Phys. 20, 1258 (1949).

Y3. Electron Optical Bench. L. MARTON, M. M. MORGAN, D. C. SCHUBERT, J. R. SHAH, AND J. A. SIMPSON, *National Bureau of Standards.*—An electron optical bench has been built capable of utilizing up to three electron lenses and four independently adjustable apertures or test objects. All the lenses and apertures or test objects can be aligned and displaced with three degrees of freedom by means of controls located outside the vacuum system. Up to the present time the electron optical bench has been used exclusively for measurement of the optical constants of magnetic electron lenses. The accuracy obtained in preliminary measurements of focal length is discussed, as well as possible improvements in design and operation.

Y4. Dielectric Constants of Various Gases for 9470 Mc.* CLAYTON M. ZIEMAN, *Wabash College.*—Cavity comparator methods and a microwave refractometer[1] were used to measure the dielectric constants of dry air, O_2, H_2, CO_2, and dry air mixed with SO_2 for 9470 Mc and pressures from 2 up to 740 mm Hg. The results for dry air, O_2, and CO_2 agree closely with recently published values;[2] a tentative S.T.P. value of $(\epsilon-1)\times10^4$ for H_2 is 3.56. For dry air of partial pressure 634 mm Hg contaminated with various amounts of SO_2 of partial pressures 20 to 100 mm Hg, $(\epsilon-1)\times10^4$ increases from 4.36 to 5.43 at 25°C.

* Research supported by Research Corporation.
[1] George Birnbaum, Rev. Sci. Instr. 21, 169 (1950).
[2] Birnbaum, Kryder, and Lyons, J. Appl. Phys. 22, 95 (1951).

Y5. A High Speed Magnetic Storage System for Parallel Digital Computers. DONALD H. JACOBS AND MICHAEL MAY, *The Jacobs Instrument Company.*—The extremely high computing speeds which all-parallel computers can attain require a storage medium of correspondingly high speed. Such a medium must (for practical reasons) be very compact, very reliable, and consume very little power, in addition to having a short access time. A register satisfying these requirements has been constructed using small magnetic cores and new circuit techniques. This type of register is different in theory and use from the various magnetic storage devices developed for use with serial computers. This type of register employs one core of a nickel-iron oriented alloy per stored digit. This core is ¼" in diameter and ¼" wide, and is fabricated of 0.0004" thick tape. The register is of the parallel type, and all its contents can be transferred out in 2–4 microseconds. The register is very small and requires very little power. It comprises one core per digit, plus five subminiature tubes. These five tubes suffice for registers holding up to 40 digits. The register can transfer its contents into another register without the use of any auxiliary circuits. Each core is used to control a gate through which a transfer pulse passes, or not, depending on the state of magnetization of the core.

Y6. Maximum Safe Amplitude of Several Simple Mechanical Systems Vibrating at Resonant Frequency. PRESTON B. CARWILE, *Raytheon Manufacturing Company.*—Derivations are given for several simple bodies (slender bars and thin plates) and different types of vibration, under the condition that the tensile stress may not exceed the endurance limit at any point in the body. Among the cases treated is an unpublished study by Dr. Carlo Calosi of a circular plate of tapered thickness. A comparison of the results show that in the few cases treated and for a fixed resonant frequency, longitudinal resonance offers greater safe amplitude than flexural resonance. Furthermore, longitudinal resonance of an exponentially tapered bar offers the possibility of safe amplitude in excess of that ordinarily considered possible in either a uniform bar or plate of the same material.

Y7. On Polarization in Conductance Phenomena.* GEORGE JAFFE, *Louisiana State University.*—A theory of polarization in conducting media has been previously developed by the author based on the concept that some of the carriers are unable to discharge at the electrodes. The strong effects of polarization in crystals and semiconductors can thereby be explained quantitatively.[1] The theory may be extended to liquid media, electrolytes, and dielectrics, if it is assumed that the rate of discharge is proportional to the concentration of the relevant carriers at the boundary. The amount of polarization and the currents will depend on the ratio of the "discharge constant" to the diffusivity. The theory has been generalized in this direction for direct and for alternating applied voltages. Measurements on electrolytes were carried out under conditions where polarization effects are predominant, i.e., between parallel plates of relatively large area and small distance. The equivalent series resistances and capacitances were measured under varying conditions of frequency, concentration and plate distance. The results are in quantitative agreement with theory; however, it is necessary to assume a group of ions of unusually low mobility to account for the high values of capacitances observed (several microfarads per cm^3), and their frequency dependence.

* Work supported in its later phases by ONR.
[1] George Jaffe, Ann. Physik 16, 217–284 (1933). Final Report, Signal Corps Project 152 B.

Y8. A Concept of Active Surface. J. G. BARREDO, *University of Chicago.*—By using an oscillograph, it has been possible to record the polarization current of an electrode immersed in 1*N* KMO_4 and 0.1*N* NaOH solution. The increase in polarization and subsequent decrease in current passed by the electrode is recorded as function of time over a period of 1/250 sec. Using those data, and knowing the current in the static state of the system, it has been possible to define a new concept of

surface as follows:

$$\Sigma = K^{1/n} F^{-1} I^{1-1/n} t^{-1/n},$$

in which Σ is the value of the active surface of the electrode, F the faraday, I the current, t the time, K a constant, and n the number of particles which produce the elemental reaction over the electrode. This concept of surface embraces as a particular case the geometrical concept of surface, where all the points of the surface are equally active.

Y9. On Fluctuations in Thermodynamic Intensive Parameters.* RICHARD F. GREENE† AND HERBERT B. CALLEN, *University of Pennsylvania.*—The fluctuations in thermodynamic intensive parameters ("generalized forces") have relevance to the theory of linear irreversible processes, as well as having direct application to the description of thermodynamic equilibrium. The conventional statistical mechanical definition of the intensive parameters, however, is such that these parameters are rigorously constant and not subject to fluctuation. Despite this, the possibility of fluctuation is indicated by the intuitive notion of temperature, pressure, etc.; and, an analysis of the operational meaning commonly attached to these concepts requires that they be defined in such a way as to be capable of fluctuation. We have introduced a definition of the intensive parameters which is appropriate in this respect, and have computed the moments of the fluctuations of these parameters.

* Assisted in part by the ONR.
† John F. Frazer Fellow.

Y10. A New Interpretation of Entropy. MAX SOLOW.—The importance of entropy in thermodynamics and statistical mechanics cannot be overemphasized. The concept of entropy resulted from empirical considerations.[1] Using a method developed in communication theory,[2,3] the quantity $H = -\Sigma_i P_i \log_2 P_i$ can be interpreted for any ensemble as the average number of binary digits, b, necessary to designate a gross event with the probability P_i. From group theory b represents the degrees of freedom. Since this interpretation is true for all ensembles, it is true for H in statistical mechanics, hence for entropy in thermodynamics, and for H in information theory.[3] Thus, entropy is related to the complexity of an ensemble; biological systems can be ordered according to complexity and hence entropy. For irreversible processes the entropy of the universe increases and it becomes more complex. Thus, time is irreversible: its positive direction results in increasing complexity. From communication theory[3] the uncertainty of any experiment is caused by the degrees of freedom occupied by the observing mechanisms; thus nature is not necessarily uncertain.

[1] K. K. Darrow, Memorial to the classical statistics, Bell System Tech. J. 22, 108–135 (January, 1943).
[2] C. E. Shannon, *The Mathematical Theory of Communication* (The University of Illinois Press, Urbana, 1949).
[3] R. M. Fano, "The transmission of information," Research Lab. of Electronics, M.I.T., Tech. Rpt. 65.

Y11. Thermodynamics of Material Systems: a Theory of Catalysis. J. L. FINCK, *The J. L. Finck Laboratories.*—This paper is a continuation of the previous work of the author on thermodynamics.[1] Utilizing the concept of a *complete* system, which requires the complete definition of a system by n independent variables, the author points out that among these independent variables may be those describing the chemical composition, the degrees of transformation among the phases of the system, the degrees to which chemical reactions have taken place, and also quantities such as mechanical stress, electric and magnetic field intensities, and density. The velocity is also considered in that it enters the kinetic energy. All types of metastable states are included. An equation for the continuity of energy of a complete system is developed, and the concepts of isotropy and homogeneity are applied to the considerations of the activity of the system. The concept of boundaries is generalized, and this leads directly to a logical theory of catalysis. It is shown that there may be mechanical, electric, chemical, phase, and other types of boundaries: in fact, for a complete system there are n types of boundaries. For each boundary a gradient may exist which if not zero will excite activity involving a change of energy with time. It is therefore the function of heterogeneous catalysts, say, to introduce such gradients in the system. The concept of equilibrium is elaborated on, and it is shown that Guldberg and Waage's law of mass-action is but a very restricted and approximate statement of what actually occurs in the activity of a system. States in thermodynamic equilibrium are considered, and some relations are developed for systems in several phases and of one or more chemical components.

[1] J. Franklin Inst. 245, No. 4 (April, 1948); also, 245, No. 5 (May, 1948).

SATURDAY AFTERNOON AT 2:00

Shoreham, Terrace Room

(H. H. NIELSEN presiding)

Optical Spectroscopy

Z1. On a Modification of the Eagle Diffraction Grating Mounting. HARRY S. ROBERTSON AND JEAN A. POTVIN, *University of Miami.*—The conventional Eagle spectrograph mounting has among its advantages compactness and a wide wavelength range. As usually constructed, however, three independent adjustments (grating rotation, plate rotation, and distance from grating to slit) are necessary in order to change the range of the instrument. In addition, conversion from photographic to photoelectric recording is, at best, awkward. A simple coupling mechanism in the modified instrument automatically rotates the grating and the plate holder as the grating is moved along the axis, thereby reducing the number of controls to one, but leaving the instrument optically equivalent to the Eagle. The plate holder may now be replaced by a photo-tube, fixed to look always at the grating. Thus, if the lead screw governing the slit-to-grating distance be motor driven, the photo-tube may be set to scan the desired spectral range. As a final feature, a servomechanism can easily be devised, such that the recorder plots wavelength linearly.

Z2. Fine Structure in Some Infrared Bands of Methylene Halides. EARLE K. PLYLER AND W. S. BENEDICT, *National Bureau of Standards.*—The infrared absorption of CH_2ClBr, CH_2ClBr, and CH_2Br_2 has been studied with a high resolution grating spectrometer in the region 16–2.3 u. Using the saturated vapor in a cell 60 cm long, it was possible to resolve the fine structure corresponding to rotation about the least axis of inertia in three to five bands of each molecule. The resolved bands all are overtones and combinations of fundamental vibrations localized in the methylene radical, and hence ap-

pear at nearly the same frequencies for each molecule, and show no detectable isotope shift. Bands with Q branches (type C, B, symmetry) and without that feature (type B, A, symmetry) both appear. Application of combination relations to all bands of a given molecule yield rotational spacings of the ground state agreeing within 0.5 percent. The spacings, $[A''-(B''-C'')/2]$, are, respectively, for CH_2Cl_2, 0.961 cm^{-1}; CH_2ClBr, 0.902 cm^{-1}; and CH_2Br_2, 0826 cm^{-1}. The molecular dimensions cannot be uniquely determined from these data alone; but if tetrahedral angles are assumed, they lead to improbably low values of the C-Halogen distance, namely 1.69A for C-Cl and 1.82A for C-Br. If the Halogen-C-Halogen angle is increased to 112°, as found by electro diffraction,[1] the C-Cl distance is in perfect agreement with the electron diffraction value 1.759A, and C-Br becomes 1.899A in CH_2Br_2 and 1.906A in CH_2ClBr.

[1] L. O. Brockway, J. Phys. Chem. 41, 747 (1937).

Z3. Bands of C_2 and CN in Infrared Flame Spectra.* W. S. Benedict and Earle K. Plyler, *National Bureau of Standards.*—In the inner cone of the oxy-acetylene flame, as observed under high resolution using a 15,000-line grating spectrometer and lead sulfide cell, several bands appear between 1μ and 1.6μ. These have been identified as the (1, 0), (0, 0), and (0, 1) bands of the Phillips system of C_2 ($^1\Pi_u - {}^1\Sigma_g^+$), with origins at 9852, 8268, and 6441 cm^{-1}, and the (0, 0) and (1, 1) bands of the red system of CN ($^3\Pi - {}^3\Sigma$), with origins at 9117 and 8862 cm^{-1}. The rotational structure of the C_2 bands shows an intensity distribution characteristic of thermal equilibrium with an effective temperature near 2400°K.

* Supported in part by ONR.

Z4. The Infrared Dispersion of C_2H_2. R. L. Kelly, R. Rollefson, and B. Schurin, *University of Wisconsin.*—The index of refraction of C_2H_2 has been measured for wavelengths between 1 micron and 18 microns by the method described previously.[1] A dispersion formula has been found which fits the observed data in the visible and infrared regions, including the formula of Watson and Ramaswamy.[2] The dispersion formula contains the integrated absorption coefficient for the strong vibration-rotation bands. An interpretation of the results in terms of C−H bond moment is being attempted.

[1] R. Rollefson and R. Havens, Phys. Rev. 57, 710 (1940).
[2] H. E. Watson and K. L. Ramaswamy, Proc. Roy. Soc. (London) 156A, 144 (1936).

Z5. High Dispersion Measurements on ω_3 of $C^{14}O_2^{16}$ at 4.5μ. Alvin H. Nielsen and Robert T. Lagemann,* *The University of Tennessee† and Oak Ridge National Laboratory.*—A preliminary report on measurements currently being made on the infrared vibration-rotation spectrum of $C^{14}O_2^{16}$ will be given. Thus far, the fundamental, ω_3, has been resolved and its rotation-line frequencies determined. A prism-grating spectrometer utilizing a rocksalt monochromator and a 7200 lines-per-inch grating was employed in this investigation. The $C^{14}O_2^{16}$, made from 4.2 percent enriched $BaCO_3$, was contained at a pressure of 14 cm of mercury in an 8-cm long glass cell closed with rocksalt windows. Combination relations have been applied to the data and values of B_{000}, B_{031}, α_3, and the band center have been obtained. The expressions for the anharmonic constants X_{13}, X_{23}, X_{33} together with ω_3 as given by Dennison[1] have been adjusted with the appropriate reduced mass factor. Satisfactory agreement is achieved between the observed and calculated values of the constants.

* Emory University.
† A Frederick Gardner Cottrell Grant-in-Aid is gratefully acknowledged.
[1] D. M. Dennison, Revs. Modern Phys. 12, 175 (1940).

Z6. Comparison of the Near Ultraviolet Absorption Spectrum in the Gaseous State and in Solution for Benzene and Substituted Benzenes.* Carl A. Beck and Brother Bernard J. Jansen, S.M., *Catholic University of America.*—A study of the broadening effect in solution spectra is given for the electronic transition around 2600A for benzene, toluene, phenol, monochlorobenzene, and aniline. Assuming the same ratios of intensities in vapor as in solution respectively, the various vapor bands are broadened by giving each the same half-intensity breadth and the same percentage asymmetry. They are then added. Then, the resultant curve after shifting to the red, agrees reasonably well with that in solution. Results show that the broadening and shift is dependent only on the electronic transition, the kind of molecule and solvent.

* Aided by ONR contract.

Z7. Fluorescence of Benzotrifluoride and Para-Xylene in the Near Ultraviolet.* Mantrala L. N. Sastri and H. Sponer, *Duke University.*—The ultraviolet fluorescence spectra of benzotrifluoride and para-xylene were investigated in the vapor phase by using condensed sparks from Sn, Mn, Fe, and a mercury arc as exciting light sources. Excitation was chiefly into the strong absorption regions of a few main bands. Corning glass filters and organic filters were used to cut off the short wavelength end of the spark spectrum. Pressures varied from 1–20 mm Hg so that the spectra obtained represent "high pressure" fluorescence. It extends from 2640–2925A in benzotrifluoride and from 2620–3150A in p-xylene. The spectra were photographed in a medium Bausch and Lomb quartz spectrograph. The analysis is in agreement with that of the corresponding absorption spectra. Observed prominent ground state fundamental vibrations are for benzotrifluoride: 141, 338, 623, 1004 cm^{-1}; and for para-xylene: 388, 458, 648, 829, 1208 cm^{-1}. They occur in progressions and combinations.

* Supported by the ONR.

Z8. Calculation of Electronic Levels in Pyridine and the Isomeric Picolines.* Gertrud P. Nordheim[1] and H. Sponer, *Duke University.*—The molecular orbital method as first described by Wheland and Pauling[2] was used for calculating electronic levels in pyridine and the picolines. The change in charge distribution of the benzene ring caused by the nitrogen atom in pyridine is treated by introducing into the secular matrix a perturbation parameter δ_1, at the position of the N-atom and smaller perturbations $\delta_2 = \delta_4$ in the neighboring positions 2 and 6 of the ring. In the isomeric picolines an additional perturbation δ_3 is introduced in the appropriate position of the secular determinant. Bonding and anti-bonding single electron molecular orbitals were calculated and the transitions determined to the lowest excited levels. They are of symmetry B_1 and A_1. This level scheme is incomplete because the $2sp^2$ electrons of the nitrogen atom have not been included in the calculation. Also, the overlap integral has been neglected. The theoretical results will be compared with experimental values.

* Supported by the ONR.
[1] Died in 1949.
[2] G. W. Wheland and L. Pauling, J. Am. Chem. Soc. 57, 2086 (1935).

Z9. Calculation of Electronic Levels in Pyridine and the Isomeric Picolines Including Overlap.* P. O. Löwdin and H. Sponer, *Duke University.*—Pyridine and the isomeric picolines have been treated by the semi-empirical molecular orbital method described in the foregoing abstract, but now the overlap integrals have been included according to a method developed by one of us.[1] Not only the energy levels but even the charge densities are affected by the overlap. The theoretical results will be compared with experimental experience.

* Supported by the ONR.
[1] P. O. Löwdin, J. Chem. Phys. 18, 365 (1950).

Z10. Absorption Studies of the Vapors of the Isomeric Picolines in the Near Ultraviolet.* Joseph H. Rush† and

H. SPONER, *Duke University*.—Studies of the near ultraviolet absorption spectra of α-, β-, and γ-picoline vapor have been made in low and medium dispersion. Conclusive evidence is found for two electronic transitions in the vicinities of 35,500 and 38,500 cm^{-1}. The former transition gives rise to a system I of sharp bands resembling the spectrum of pyridine in the same region; the latter is represented by a diffuse system II, which resembles the spectra of some substituted benzenes and lies in the same region as the benzene group. The intensity of the diffuse system is markedly higher than that of the sharp system. Both systems exhibit the characteristics of allowed transitions. The diffuse system in β-picoline presents features which suggest superposition of still another system. The analysis of the spectra will be presented and the assignment of the electronic levels discussed. There is in pyridine the possibility of electronic states, in addition to those analogous to the benzene states, which may arise from the presence of nitrogen in the pyridine ring.

* Supported by the ONR.
† Present address: High Altitude Observatory of Harvard University and University of Colorado, Boulder, Colorado.

Z11. A Comparison of the Near Ultraviolet Absorption Spectra of Some Pyridine Derivatives in Various Solvents.* HAROLD P. STEPHENSON,† *Duke University* (Introduced by H. SPONER).—The near ultraviolet absorption spectra of picolinic acid, nicotinic acid, isonicotinic acid, α-picoline, β-picoline, γ-picoline, and α-chloropyridine have been measured in liquid solutions. It was observed that different solvents had different effects on the electronic transitions in the spectral region 2200–3000A. A Beckman Model DU spectrophotometer was used throughout to measure the following solutions: picolinic acid, nicotinic acid, and isonicotinic acid in water; α-picoline, β-picoline, γ-picoline, and α-chloropyridine in isooctane; all the compounds in 95 percent ethyl alcohol; and isonicotinic acid in 95 percent ethyl alcohol-water mixtures. Extinction coefficients ϵ have been calculated and have been used for a graphical determination of the oscillator strengths (f factors). α-chloropyridine shows anomalous behavior which apparently is related to chemical instability. Tables of results and graphs of the spectra will be presented and discussed.

* In part supported by the ONR.
† Shell Oil Company Fellow.

Post-Deadline Papers, if Any

SUPPLEMENTARY PROGRAMME

SP1. Cross Sections in the Feynman Quantum Electrodynamics.* MURRAY PESHKIN,† *Cornell University*.—The relation between cross sections and S matrix elements in the Feynman quantum electrodynamics follows from the equivalence of Feynman's formulation to the "standard" theory. An alternative approach, based on a familiar theorem from optics, is to normalize the scattering amplitudes by observing that the diagonal elements of S_{ba} are simply related to the total cross sections σ_a. This statement is identical to conservation of probability. To find the total cross section for an event to the lowest order in which it occurs, one writes down the S matrix element for the "closed" Feynman diagram, which consists of the original diagram joined to its reflection in the plane t=const. The expressions obtained converge except for infrared terms, and lead directly to invariant expressions for the cross sections. An explicit recipe will be given. This method has an interesting application to meson theories, where it is possible to limit the possible interaction forms directly from the S matrix by requiring that they must lead to positive cross sections. This criterion is analogous to the requirement of hermitian operators in order to obtain real eigenvalues in ordinary wave mechanics.

* To be given at the end of Session QA if time permits.
† Now at Northwestern University. This research was supported by the AEC predoctoral fellowship program.

Author Index to Papers Presented at the Washington Meeting

Achter, M. R. and R. Smoluchowski—N3
Adams, W. R. and Ernest Pollard—S4
Almqvist, E., K. W. Allen, J. T. Dewan, and T. P. Pepper—D2
Alpher, R. A. and R. C. Herman—U5
Amble, E.—H8
Anderson, H. L. and John Marshall—SA1
Appleyard, R. K.—S7
Arfken, G. B. and L. C. Biedenharn—W10
Armstrong, A. H., J. C. Allred, R. O. Bondelid, and L. Rosen—M9
Astin, A. V.—P1
Barkas, Walter—V1
Barile, Sam—R7
Barredo, J. G.—Y8
Bay, Z.—X9
Beck, Carl A. and Brother Bernard J. Jansen, S. M.—Z6
Belinfante, F. J. and J. S. Lomont—QA9
Beling, J. K., B. T. Feld, and I. Halpern—Q5
Bendt, P. J., L. J. Rainwater, and W. W. Havens, Jr.—T11
Benedict, W. S. and Earle K. Plyler—Z3
Bennett, F. D.—B8
Bergdolt, V. E., A. J. Greenwald, and D. B. Sleator—B5
Bergmann, Peter G.—QA5
Bestul, A. B. and H. V. Belcher—JA7
Biondi, Manfred A.—C3
Block, M. M., S. Passman, and W. W. Havens, Jr.—F1
Bohm, David and David Pines—N11
Boley, F. I. and L. J. Laslett—K7
Bostick, W. H., W. W. Striker, and M. F. Grover—C2
Boyd, G. E. and B. H. Ketelle—K8
Branch, G. M.—A4
Breckenridge, R. G. and W. R. Hosler—R9
Breit, G. and M. C. Yovits—QA1
Brockhouse, B. N., M. Bloom, and D. G. Hurst—T4
Brossel, J.—H9
Brueckner, Keith A. and Kenneth M. Watson—WA6
Bryak, Henry and Eugene Greuling—WA8
Buchdahl, Rolf and Lawrence E. Nielsen—JA6
Bullock, M. L., W. O. McMinn, V. K. Rasmussen, and M. B. Sampson—J6
Burke, W. H. and J. R. Risser—J2
Burson, S. B., K. W. Blair, H. B. Keller, and S. Wexler—Q1
Caianiello, E. R. and A. M. L. Messiah—WA2
Camac, Morton—F11
Canada, Robert and A. C. G. Mitchell—K12
Carlson, R. R.—D12
Carwile, Preston B.—Y6
Chamberlain, O., E. Segrè, and C. Wiegand—M8
Chen, S. C. and R. D. Present—W9
Chew, G. F. and G. C. Wick—WA4
Chodorov, M., A. Eldredge, E. L. Ginzton, W. W. Hansen, J. H. Jasberg, C. B. Jones, R. L. Kyhl, R. B. Neal, and P. A. Pearson—SA2
Codrington, R. S., F. McCaffrey, B. A. Mrowca, and E. Guth—JA1
Cohen, Bernard L.—SA5
Collins, T. L., Alfred O. Nier, and Walter H. Johnson, Jr.—RA1
Cook, R. K.—PA6
Coomes, E. A., E. G. Brock, and A. L. Houde—N9
Corben, H. C.—QA4
Corey, Robert B., Jerry Donohue, Kenneth N. Trueblood, and Kenneth J. Palmer—JA3
Cork, J. M., J. M. LeBlanc, A. E. Stoddard, W. J. Childs, C. E. Branyan, and D. W. Martin—Q2
Corson, Dale R.—M3
Craig, D. S., C. P. Browne, D. J. Donahue, R. M. Williamson, and R. E. Benenson—D7
Curtiss, J. H.—PA1
Dabbs, J. W. T. and L. D. Roberts—C6
Dannis, M. L.—E4
Darling, B. T. and B. R. Linden—W13
Dart, S. Leonard—S3
Davis, Marguerite and Ernest Pollard—S5
Davison, P. W. and G. A. Morton—X4
Dayton, B.—F12
de Besauregard, O. Costa—QA2
der Mateosian, E.—Q9
Deutsch, Martin—F13
DeWire, J. W. and L. A. Beach—SA12
de Witt, T. W.—EA3
Dexter, D. L.—R5
Dickinson, W. C. and D. C. Dodder—M5
Doede, Clinton M.—E7
Drell, S. D.—WA1
Eguchi, T. and J. K. Knipp—W4
Ehrenberg, W.—I2
Eirich, E. R. and H. F. Mark—JA8
Enge, H. A.—J8
Epstein, H. T. and Max A. Lauffer—S9
Erickson, R. A. and C. G. Shull—G6
Esterman, I. and J. R. Weertman—R10
Fairbank, Henry A., Charles A. Walker, and Clinton M. Doede—E8
Fano, U.—P3
Ferrell, R. A.—QA3
Ferry, J. D.—EA2
Finck, J. L.—Y11
Fireman, Peter—WA11
Fitzgerald, Edwin R. and Robert F. Miller—S1
Foldy, L. L.—WA7
Forster, Harriet H.—A7
Forster, M. J. and R. L. Anthony—E5
Fowler, J. L., J. E. Brolley, Jr., and E. J. Stovall, Jr.—D3
Fox, Francis E.—B2
Fox, T. G., Jr.—E1
Frieman, Edward and Lloyd Motz—D1
Fry, W. F.—F8
Fuller, E. G. and M. Wiener—D4
Galt, J. K.—G1
Gardner, I. C.—PA3
Geschwind, S., G. R. Gunther-Mohr, and C. H. Townes—H2
Glucksternn, R. and F. Rohrlich—M6
Goldberger, M. L.—WA3
Goldstein, Louis—QA10
Good, Myron L. and Frank R. Wrenn, Jr.—S10
Good, W. M., C. D. Moak, G. P. Robinson, and H. Reese—X3
Goodell, Jr., W. F., H. H. Loar, and R. P. Durbin—T2
Goudsmit, S. A.—V3
Graham, R. L. and R. E. Bell—Q6
Greene, Richard F. and Herbert B. Callen—V9
Gregg, E. C., Jr.—SA7
Groetzinger, Gerhart and Sam Barile—R6
Guild, W. R.—S6
Gyorgy, E. M. and R. H. Kingston—N6
Haefner, Richard R.—WA9
Hainer, R. M., M. Elaine Hungerman, and Gilbert W. King—H6
Hall, R. N.—R12
Hamilton, Donald R., W. P. Alford, and Leonard Gross—K1
Hammerle, W. G. and D. J. Montgomery—JA5
Harris, S. P.—T8
Harrison, F. B. and J. Warren Keuffel—F6
Havas, Peter—QA9
Hayakawa, S.—F9
Heckrotte, W. and L. Schecter—D9
Heidmann, J.—W8
Hibdon, Carl T. and C. O. Muehlhause—T10
Hill, David L.—W2
Hine, G. J.—M4
Hoffman, Marvin—K6
Holstein, T. and Ira B. Bernstein—C4
Hopkins, I. L.—JA4
Haieh, Yu-Chang and I. Bloch—R13
Huggins, Maurice L.—JA9
Hughes, D. J., R. C. Garth, and C. Eggler—T6
Hull, G. F., Jr. and J. W. Meyer—C1
Hull, M. H., Jr.—QA13
Hountoon, R. D.—P2
Israel, H. I., T. L. Harlor, and R. G. Wilkinson—Q4
Jaccarino, V. and J. King—H3
Jacobs, Donald H. and Michael May—Y5
Jaffe, George—Y7
Jensen, Erling N. and R. T. Nichols—K3
Jentschke, W. K., C. J. Taylor, M. E. Remley, F. S. Eby, and P. G. Kruger—X6
Johnson, M. H.—M2
Kahl, G. D. and F. D. Bennett—B7
Kanner, H. and F. L. Ribe—J13
Kegley, Cort L. and Henry E. Duckworth—RA3
Keim, C. P.—L1
Keller, H. B. and J. M. Cork—K13
Kelly, R. L., R. Rollefson, and B. Schurin—Z4
Kern, B. D., C. D. Moak, W. M. Good, and G. P. Robinson—J3
Keuffel, J. Warren and F. B. Harrison—F7
Kikuchi, Seishi—A8
Kingston, R. H. and E. M. Gyorgy—N5
Kinsey, B. B. and G. A. Bartholomew—T5
Kisliuk, P. and C. H. Townes—H7
Kittel, Charles—G5
Klema, Ernest D. and G. C. Phillips—J4
Knipp, J. K.—W3
Koester, L. J., E. Goldberg, S. G. Kaufman, F. P. Mooring, and D. Saxon—M12
Kouvelites, J. S., L. W. McKeehan, and F. J. Beck—G7
Krimm, S. and A. V. Tobolsky—E2
Kundu, D. N. and M. L. Pool—Q10
Kunstadter, J. W., J. J. Floyd, L. B. Borst, and G. J. Weremchuk—T12
Laughlin, J. S. and J. W. Beattie—S11
Leachman, R. B.—T13
Lehmann, William L. and Melvin Lax—QA11
Leighton, R. B.—V2

Lewis, H. W.—W5
——, W. W. Brown, D. O. Seevers, and E. W. Hones—A12
Linden, B. R. and B. T. Darling—W14
Linder, E. G. and S. M. Christian—SA9
Littauer, R. M. and D. Walker—F3
Löwdin, P. O. and H. Sponer—Z9
Malkus, Willem V. R.—B4
Mandeville, C. E. and E. Shapiro—K11
Markovitz, H., P. M. Yavorsky, R. C. Harper, Jr., L. J. Zapas, and T. W. DeWitt—S2
Marton, L., M. Morgan, D. C. Schubert, J. R. Shah, and J. A. Simpson—Y3
Marvin, R. S.—EA4
Mason, W. P., H. J. McSkimin, and R. M. Bozorth—N7
McClure, G. W.—F10
McCoubrey, A. O., D. Alpert, and T. Holstein—C5
McCue, J. J. G., J. A. Lovington, and W. M. Preston—J11
McMurdie, H. F.—PA4
McNally, J. R., Jr.—L2
McNish, A. G.—P6
McReynolds, A. W.—T1
Medicus, Heinrich A.—F5
Meggers, W. F.—P4
Merz, Walter J.—R2
Meyerhof, W. E., H. Roderick, and L. G. Mann—D11
Mihelich, J. W., M. Goldhaber, and Elizabeth Wilson—K9
Miller, B. L. and W. C. Porter—SA4
Miller, Charles E., Joseph E. Henderson, D. S. Potter, and J. Todd, Jr. —A13
Miller, D. W., Ben Petree, and C. H. Johnson—J1
Miller, S. L., A. Javan, and C. H. Townes—H1
Milligan, W. O., H. A. Levy, and S. W. Peterson—R3
Moak, C. D., H. Reese, and W. M. Good—SA6
Mooring, F. P., E. Goldberg, S. G. Kaufman, L. J. Koester, and D. Saxon —M11
Moszkowski, Steven A.—WA10
Motz, H. T.—K2
Moyer, B. J., R. Madey, R. H. Hildebrand, N. Knable, and R. Hales—F4
Muehlhause, C. O.—T9
Neiler, John H., George E. Owen, and A. J. Allen—X8
Nielsen, Alvin H. and Robert T. Lagemann—Z5
Nier, A. O. C.—L4
Nolle, A. W.—EA5
Nordheim, Gertrude P. and H. Sponer—Z8
Oberly, J. J.—R14
Offenbacher, Elmer L. and Herbert B. Callen—R4
Oleksa, Sophie, E. P. Ney, and C. L. Critchfield—A6
Osborn, R. K.—QA7
Packard, M. E. and J. T. Arnold—H10
Palevsky, H., D. J. Hughes, and C. Eggler—T7
Palmatier, E. D.—A3
Pearson, P. A., R. B. Neal, R. L. Kyhl, C. B. Jones, J. H. Jasberg, W. W. Hansen, E. L. Ginzton, A. Eldredge, and M. Chodorov—SA3
Peebles, Glenn H.—W7
Pellam, J. R.—P5
Pepinsky, Ray—U1
—— and William Cochran—R1
Peshkin, Murray—SP1
Peshkin, M. and A. J. F. Siegert—D5
Pines, David and David Bohm—N10
Plyler, Earle K. and W. S. Benedict—Z2
Pool, M. L. and D. N. Kundu—L3
Pope, N. K.—R8
Poss, H. L., C. E. Falk, and Luke C. L. Yuan—X7
Preston, W. M., J. J. G. McCue, W. D. Roseborough, Jr., and C. Goodman —J5
Pugh, Emerson M., N. Rostoker, and A. I. Schindler—G2
Ramsey, W. E.—X11
Reynolds, H. L., D. M. Ritson, and E. P. Woodruff—A1
Rigney, Carl J. and Lester I. Bockstahler—N8
Roberts, J. H. and H. M. Mann—D6
Roberts, L. D. and J. W. T. Dabbs—C7
Robertson, Harry S. and Jean A. Potvin—Z1
Robinson, Charles V.—Q11
Robinson, D. M., L. R. McIntosh, and J. C. Nygard—SA8
Rodeback, G. W. and J. S. Allen—K5
Rogers, John D. and Dudley Williams—H5
Ross, J. D., A. Robeson, and J. W. Beams—Y1
Ross, John S. and Kiyoshi Murakawa—RA6
Rostoker, N.—G4
Rothlein, B. J.—R11
Rush, Joseph H. and H. Sponer—Z10
Sack, H. S.—EA6
Salpeter, E. E.—W11
Salvini, G. and Geo. T. Reynolds—A11
Sangster, R. C. and J. W. Irvine, Jr.—X1
Sastri, Mantrala L. N. and H. Sponer—Z7
Savitt, J. and R. H. F. Stresau—B9
Sawyer, B., R. Smoluchowski, and R. W. Turner—G8
Schamberger, R. D.—M10
Schawlow, A. L. and C. H. Townes—W1
Schelbe, A.—I1
Scheidegger, A. E.—QA8
Schein, Marcel and J. J. Lord—A9
Schiff, L. I.—WA5
Schindler, A. I. and Emerson M. Pugh—G3
Schubauer, G. B.—PA5
Schwarzmann, Gertrude—WA12
Sette, Daniele—B1
Shapiro, M. M., M. Birnbaum, F. W. O'Dell, and B. Stiller—A10
Shaw, C. H. and Jack A. Soules—SA10
Shaw, T. M. and K. J. Palmer—JA2
Sheline, R. K., R. B. Holtzman, and C. Y. Fan—K4
Silverman, A. and M. Stearns—F2
Skinner, M. and C. Richman—M1
Slater, M.—S8
Sleator, D. B., V. E. Bergdolt, and F. D. Bennett—B6
Slutz, R. J.—PA2
Smoluchowski, R.—N1
Smoluchowski, R. and M. R. Achter—N2
Solow, Max—Y10
Sommer, H. and J. A. Hippie—RA5
Soule, David E.—X2
Spencer, L. V.—U4
Stanford, George S. and Henry E. Duckworth—RA2
Steffen, R. M. and D. M. Roberts—Q3
Stephenson, Harold P.—Z11
Stokes, Richard H.—SA11
Storm, Martin L.—QA14
Sun, K.-H., F. A. Pecjak, B. Jennings, A. J. Allen and J. F. Nechaj—J12
Sunyar, A. W. and M. Goldhaber—K10
Swann, C. P. and C. E. Mandeville—J9
Taylor, C. J., M. E. Remley, W. K. Jentschke, and P. G. Kruger—X5
Thomas, L. H.—U2, W12
Thompson, R. W., Hans O. Cohn, and R. S. Flum—A5
Ting, Yu, Thomas L. Weatherly, and Dudley Williams—H4
Tobolsky, A. V.—EA1
Tomboulian, D. H. and R. W. Johnston—N4
Tomlinson, E. P., H. W. Fulbright, and J. J. Howland, Jr.—Q7
Toops, Edward C., Frederick E. Steigert, and Milo B. Sampson—J7
Trees, R. E.—QA12
VanBronkhorst, A., L. Marton, and S. B. Garfinkel—Y2
Van Patter, D. M., A. Sperduto, and H. Enge—J10
Verbrugge, Frank and Robert L. Henry—H11
Vidale, M. and Marcel Schein—A2
Vreeland, John A. and Kiyoshi Murakawa—RA7
Walker, R. L. and R. B. Day—D10
Weir, C. E.—E3
Welton, T. A.—T3
Westcott, C. H. and J. S. Greenberg—X10
Wheeler, J. A. and D. L. Hill—U3
Williamson, R. M., C. P. Browne, D. J. Donahue, D. S. Craig and K. W. Jones—D8
Witmer, Enos E.—RA4
Work, Richard N.—E6
Yadoff, Oleg—N12
Yevick, George—W6
Yu, Ming Chen W. and Eugene Guth—M13
Zaffarano, D. J. and F. I. Boley—Q8
Zieman, Clayton M.—Y4
Zimmerman, E. J. and P. G. Kruger—M7
Zmuda, Alfred Joseph—B3